Hygrothermal Behavior of Interior Basement Insulation

by

Kohta Ueno

A thesis
presented to the University of Waterloo
in fulfillment of the
thesis requirement for the degree of
Master of Applied Science
in
Civil Engineering

Waterloo, Ontario, Canada, 2007

Author's Declaration

I hereby declare that I am the sole author of this thesis. This is a true copy of the thesis, including any required final revisions, as accepted by my examiners.

I understand that my thesis may be made electronically available to the public.

Kohta Ueno

Abstract: Hygrothermal Behavior of Interior Basement Insulation

An uninsulated basement can contribute a significant fraction of a building's total heating load: insulating the basement can provide significant energy savings. In addition, the desire of homeowners to maximize usable space has resulted in the finishing of many basements. However, traditional interior basement wall insulation assemblies and finishes have resulted in a large number of moisture-related failures of these wall systems, including mold, decay, and poor thermal performance.

This thesis involves the experimental and analytical investigation of the hygrothermal behavior of interior insulated basement walls. The experimental portion involved the hygrothermal monitoring of twelve interior basement insulation assemblies in two field locations (Huntley, IL, and Kitchener, ON). These assemblies included various insulated stud wall configurations, rigid foam insulation configurations, and insulation roll blankets. At the Huntley site, the walls were run under normal conditions during the first year, to determine baseline performance. In the subsequent years, controlled wetting events introduced equal amounts of liquid water to the assemblies, and the drying response was measured. At the Kitchener site, the walls were installed during the first year of house operation, capturing the effect of built-in construction moisture on assembly performance.

The measured boundary conditions from field monitoring were then used in one-dimensional hygrothermal simulations. Validation simulations were performed, followed by extrapolations that varied interior conditions, exterior climate, and assemblies.

None of the monitored walls experienced conditions that would be considered a moisture-related failure, but monitored data and simulations indicated which walls have higher and lower risks. The data demonstrated that the concrete basement wall will be a source of moisture throughout the year; this was even seen with a concrete wall that had dried for two years before wall installation. Analysis of basement wall boundary conditions shows that usually, drying to the interior is the only available path for the majority of the assembly. Another conclusion was that air leakage plays a large role in the behavior of assemblies: performance could not be predicted simply by the permeability of the assembly, or its least permeable layer.

Wintertime condensation was not found to be a problem in the monitored walls, with or without an interior vapor control layer. One important reason for this behavior was that temperatures of the above-grade portion of the wall were much warmer than predicted by hygrothermal simulations of a one-dimensional wall section, demonstrating the two-dimensional thermal effects of coupling to the ground. This results in a much lower risk for wintertime condensation.

Measurements demonstrated summertime inward vapor drives at the above-grade portions of the walls; condensation was seen in walls with an interior polyethylene vapor barrier, and correlated to an inward thermal gradient. Simulations showed that this issue is likely in climates with a significant cooling load (i.e., inward thermal gradient); therefore, locations with negligible cooling loads, such as Edmonton, Vancouver, or St. John's, are unlikely to have these problems.

Insulated stud frame walls with and without polyethylene were compared; both walls had moisture levels within acceptable limits. The non-polyethylene wall had higher wood framing moisture

contents at the above-grade section in winter, but within safe limits. The polyethylene wall showed generally wetter behavior, demonstrating the effect of eliminating drying to the interior.

This research suggests that vapor control at the lower portion of the basement wall is unnecessary. These locations experience temperatures that are similar to geographic locations that require no vapor control layer. The monitored data shows that an impermeable layer at this location reduces drying and results in longer periods of elevated humidity at the concrete-insulation interface. Simulations showed that performance at the lower portion of the wall improves with increasing vapor permeability of interior layers. Furthermore, simulations of ventilating the basement with exterior dewpoint air showed negligible accumulation, which could dry in the winter. Instead of a vapor barrier, this result suggests an air barrier might be all that is required to prevent condensation.

Future suggested research includes improved validation of hygrothermal simulations and continued monitoring of the Kitchener site, followed by disassembly and examination of the assemblies at the conclusion of the research.

Acknowledgements

Any research project of this scope is, by necessity, a collaborative effort. This thesis is no exception: I can only hope that I am giving adequate credit where it is due.

My advisor, Dr. John Straube, was instrumental in my decision to come to the University of Waterloo to pursue a graduate degree in the field of building science. His collegial guidance, knowledge, and humor made me conclude that the decision was a good one. I can gratefully say that I now feel that I have a thorough grounding in much of the underlying science in the field of building science.

Dr. Joseph Lstiburek of Building Science Corporation has been my mentor for close to a decade now; he is singularly responsible for bringing me into this field and shepherding me forwards. It was wonderful to have such generous encouragement and support from both him and his wife and business partner, Betsy Pettit.

Mr. Christopher Schumacher has been my frequent collaborator on all of the research that is the core of this thesis, as well as many other projects. He has been exceedingly generous with his time while working on the experimental facets of this thesis—brainstorming, design, setup, troubleshooting, and analysis–perhaps even to the detriment of his own work. The second set of eyes and reality checks that he brought to the project were invaluable.

Mr. Aaron Townsend at Building Science Corporation was my coworker and sounding board for much of the Huntley site work. In our field research, analysis, and writing together, he was a major asset to the project who kept me intellectually honest on more than one occasion. He should also receive the credit for the design and implementation of the Huntley site wetting system, an important facet of that experiment.

I was fortunate to have the able assistance of my colleagues at the University of Waterloo's Building Engineering Group: Mr. Jonathan Smegal, Mr. Christopher Black, Mr. Graham Finch, and Ms. Rachel Smith.

I would like to thank my thesis readers, Dr. Achilles Karagiozis and Dr. Eric Soulis, for their generosity with their valuable time and their excellent constructive criticism.

This research would not have been possible without funding and support for the field research portions. The Chicago-area project was funded by Dow Chemical Corporation and the Department of Energy's Building America Program. Use of the test site and generous logistical assistance were provided by Pulte/Del Webb Corporation. The Kitchener basement site research was funded by Canada Mortgage and Housing Corporation, and the test site was kindly made available by its homeowner, Tony Mohr.

I would like to thank my parents, for their financial and moral support in pursuing this graduate degree. Finally, my widely scattered friends were my lifeline and connection to the community that I left behind in Boston. With their kindness and correspondence from all over the continent, they helped fight the isolation that I felt moving away from my home of over a decade, and helped me keep a measure of sanity throughout the darkest hours of this degree.

Table of Contents

Chapter 1 Introduction 1
1.1 Background 1
1.2 Objectives 2
1.3 Approach 2
Chapter 2 Background and History 4
2.1 Background Information 4
2.1.1 Definitions and Nomenclature 4
2.1.2 Functional Role of the Basement 6
2.2 Historical Background 9
2.2.1 Regional Distribution of Basements 9
2.2.2 Basements as Finished Space 10
2.2.3 Insulation of Basements 11
2.2.3.1 Historical Overview 11
2.2.3.2 Structural and Frost Heave Concerns 12
2.2.3.3 Historical Development of Basement Insulation Assemblies 13
2.2.3.4 Construction Reference Literature 15
2.2.3.5 Code Requirements 16
2.2.3.6 Implications and Conclusions 17
Chapter 3 Thermal and Moisture Physics of Basements 19
3.1 Heat Loss from Basements 19
3.2 The Below Grade Environment 21
3.2.1 Ground Temperature Behavior 21
3.2.2 Soil Thermal and Moisture Properties 22
3.3 Basement Interior Temperature and Humidity Conditions 25
3.4 Psychrometric Relationship of Boundary Conditions 30
3.5 Moisture Transport in the Foundation Environment 31
3.5.1 Bulk Water Flow 31
3.5.2 Capillarity/Liquid Transport 33
3.5.3 Air Transported Moisture 35
3.5.4 Vapor Diffusion 36
3.5.5 Comparisons between Transport Mechanisms 38

3.5.6 Moisture Storage 41
3.6 Moisture Failure Modes 44
3.6.1 Summertime Condensation on Lower Wall 44
3.6.2 Wintertime Condensation or Frost on Upper Wall 45
3.6.3 Inward Vapor Drives 46
3.6.4 Moisture Accumulation in Single Polyethylene Systems 47
3.6.5 Moisture Accumulation in Double Polyethylene Systems 48
3.7 Implications for Foundation Detailing 49
3.7.1 Recommended Foundation Drainage Details 50
3.7.2 Advantages of Exterior Insulation of Foundations 51
3.7.3 Vapor Barriers on Lower Portion of the Basement Wall 54
3.7.4 Recommended Details for Interior Insulation 56
Chapter 4 Literature Survey 59
4.1 Analysis and Modeling Research 59
4.1.1 Swinton and Karagiozis (1995) 59
4.1.2 Timusk and Pressnail (1997) 60
4.1.3 Cheple and Huelman (2001) 61
4.2 Experimental Research/Field Surveys 62
4.2.1 Robert W. Anderson and Associates (1989) 63
4.2.2 Canada Mortgage and Housing Corporation (1999) 64
4.2.3 Goldberg and Huelman (2001) 65
4.2.4 Goldberg and Aloi (2002) 66
4.2.5 Goldberg and Farkas (2004) 70
4.2.6 Goldberg and Gatland (2006) 73
4.2.7 Zuluaga et al. (2004) 75
Chapter 5 Experimental Setup 78
5.1 Huntley, Illinois Site 78
5.1.1 Site and house description 78
5.1.2 Test Wall Descriptions 79
5.1.2.1 Stud frame walls (Walls 1 and 2) 80
5.1.2.2 Foam plastic insulation walls (Walls 3 and 4) 81
5.1.2.3 Composite walls (Walls 5 and 6) 81

5.1.2.4 Other walls (Walls 7 and 8) 82
5.1.3 Instrumentation Package 83
5.1.4 Installation of Test Walls 87
5.1.4.1 General Installation Details 87
5.1.4.2 Test Panel Installation Details 88
5.1.5 Wetting System 96
5.2 Kitchener, Ontario Site 97
5.2.1 Site and house description 97
5.2.2 Test Walls 98
5.2.3 Instrumentation Package 99
5.2.4 Test Panel Installation Details 103
Chapter 6 Results: Huntley Site 108
6.1 Soil Sensors 108
6.1.1 Soil Temperature Behavior 108
6.1.2 Soil Moisture Behavior 112
6.2 Interior and Exterior Boundary Conditions 116
6.3 Wall Behavior in Normal Conditions 119
6.3.1 Temperature Behavior 119
6.3.2 Wall Data Availability and Wall Dewpoint Behavior 123
6.3.3 Stud frame walls (Walls 1 and 2) 125
6.3.4 Foam plastic insulation walls (Walls 3 and 4) 129
6.3.5 Composite walls (Walls 5 and 6) 133
6.3.6 Other walls (Walls 7 and 8) 136
6.3.7 Overall Hygrothermal Comparison 138
6.3.8 Seasonal Condensation Risks 140
6.4 Wall Behavior with Wetting System 142
6.4.1 Interpretation of Wetting Events (Recovery Time) 143
6.4.2 Stud frame walls (Walls 1 and 2) 145
6.4.3 Plastic foam-based walls (Walls 3, 4, 5, and 6) 149
6.4.4 Other walls (Walls 7 and 8) 153
6.4.5 Overall Interpretation of Wetting Events 154
6.5 Wall Disassembly and Inspection 156

6.5.1 Single Polyethylene (Panel 1) and Double Polyethylene (Panel 2) 156
6.5.2 Foil-faced Polyisocyanurate (Panel 3) 159
6.5.3 XPS (2”/50 mm) (Panel 4) 160
6.5.4 XPS w. fiberglass (Panel 5) and XPS w. Cellulose (Panel 6) 161
6.5.5 Rigid fiberglass with PA-6 (Panel 7) 163
6.5.6 Perforated Roll Blanket (Panel 8) 164
6.5.7 Fiberglass Brown Staining 164
Chapter 7 Results: Kitchener Site 167
7.1 Interior and Exterior Boundary Conditions 167
7.2 Soil Sensors 168
7.2.1 Soil Temperature Behavior 168
7.2.2 Soil Moisture Behavior 171
7.3 Monitored Wall Behavior 172
7.3.1 Temperature Behavior 172
7.3.2 Wintertime Condensation 174
7.3.3 Summertime Condensation 176
7.3.4 Accumulation Within the Insulation Assembly 178
7.3.5 Framing Moisture Content 182
7.4 Field Visit Disassembly 184
7.4.1 Frame-Polyethylene Wall Disassembly and Inspection 185
7.4.2 Frame-Latex Paint Wall Disassembly and Inspection 186
7.4.3 Moisture Content Measurements 189
7.4.4 Roll Blanket Inspection 191
7.4.5 XPS Wall Inspection 191
Chapter 8 Hygrothermal Modeling 193
8.1 Validation Simulations 194
8.1.1 Above-Grade Validation Simulations 194
8.1.1.1 Boundary Conditions 194
8.1.1.2 Assembly Initial Conditions 194
8.1.1.3 Test Assembly Details 196
8.1.1.4 Temperature Comparison Between Model and Monitored Data 197
8.1.2 Below Grade Validation Simulations 203

8.1.2.1 Boundary Conditions 203
8.1.2.2 Assembly Initial Conditions 203
8.1.2.3 Test Assembly Details 205
8.1.2.4 Simulation Results and Analysis: Mid Height 205
8.1.2.5 Simulation Results and Analysis: Lower Height 208
8.2 Extrapolation Simulations 210
8.2.1 Above Grade Simulations for Kitchener Site 210
8.2.2 Condensation Layer Diagnostic Tool 213
8.2.2.1 Development of the Condensation Layer 213
8.2.2.2 Sample Use of the Condensation Layer 214
8.2.2.3 Condensation Layer Response in Kitchener Above-Grade 216
8.2.3 Boundary Conditions for Extrapolations: Exterior 218
8.2.3.1 Above Grade Boundary Conditions 218
8.2.3.2 Below Grade Boundary Conditions 220
8.2.4 Boundary Conditions for Extrapolations: Interior 220
8.2.5 Above-grade Extrapolations 222
8.2.5.1 Toronto Simulations 222
8.2.5.2 Vancouver Simulations 225
8.2.5.3 St. John's Simulations 228
8.2.5.4 Edmonton Simulations 228
8.2.6 Below-grade Extrapolations 230
8.2.6.1 Simulations Using Kitchener Boundary Conditions 230
8.2.6.2 Simulations Using Edmonton Simulated Boundary Conditions 235
8.2.6.3 Simulations Using High Summertime Interior Relative Humidity 239
8.3 Conclusions from Extrapolation Simulations 242
8.3.1 Above Grade Simulations 242
8.3.1.1 Wintertime Condensation Issues 242
8.3.1.2 Summertime Condensation Issues 243
8.3.2 Below Grade Simulations 245
8.3.3 Other Concerns and Observations 246
Chapter 9 Conclusions and Recommendations 249
9.1 Analysis of Installed and Monitored Assemblies 250

9.2 General Observations 251
9.2.1 Air Leakage 251
9.2.2 Modeling Correlation 252
9.2.3 Wetting System Response 252
9.3 Wintertime Condensation 252
9.4 Summertime Inward Vapor Drive 254
9.5 Vapor Control on Below Grade Walls 254
9.6 General Recommendations for Basement Assemblies 256
Chapter 10 Recommendations and Future Work 258
10.1 Proposed Wall Assemblies 258
10.1.1 Thin Foam Composite Wall 258
10.1.2 Hybrid Roll Blanket 258
10.2 Further Research Needs 259
Appendices 261
Appendix A Sensors and Data Collection Equipment 261
Huntley, Illinois Site 261
Kitchener, Ontario Site 261
Appendix B Development and Calibration of Wood Surrogate Sensors 272
Background 272
Plug Sensor Geometry 273
Plug Sensor Calibration and Time Constant 274
Wafer Sensor Geometry 276
Wafer Sensors: Calibration 277
Wafer Gravimetric Adsorption and Desorption Measurement 279
Hygrothermal Simulation of Wafer Sensor Response 281
Wafer Sensors: Field Comparison to Relative Humidity Sensors 285
Conclusions 289
Appendix C Development and Commissioning of Wetting System 290
Wetting Equipment and Installation 290
Commissioning 291
Appendix D Vapor Permeability Testing 293
Procedure 293

Results 294
Sample Post-Test Conditions 296
Equipment 296
Appendix E Foil-faced Polyisocyanurate Permeability Experiment 297
Introduction 297
Experimental Setup 297
Results 299
Conclusions 301
Appendix F Wood Moisture Content Measurements in Cellulose Wall 303
Appendix G Data Collection Timeline 306
Huntley, Illinois Site 306
Kitchener, Ontario Site 307
Bibliography 308

List of Figures

Figure 2.1: Common foundation types (Carmody et al. 1991) 4
Figure 2.2: A schematic of the building enclosure, with the basement enclosure highlighted 5
Figure 2.3: Parts and nomenclature of the basement enclosure 6
Figure 2.4: United States Map of Frost Penetration Depths (Inches) (PHRC 1997) 10
Figure 2.5: Percentage of houses with basements, by US Census Region (DOE-EIA 1999) 10
Figure 2.7: Interior basement insulation detail (Crocker 1974) 14
Figure 2.8: Interior basement insulation detail (CHBA 2001) 14
Figure 2.9: Roll blanket insulation, full-height 15
Figure 2.10: Roll blanket insulation, half-height 15
Figure 2.11: DOE Proposed Map of Climate Zones (Briggs et al. 2002) 17
Figure 3.1: Heat flow from below-grade surfaces (ASHRAE 2005) 20
Figure 3.2: Fraction of basement heat loss vs. depth in meters (Boileau and Latta 1968) 20
Figure 3.3: Monthly ground temperatures, Ottawa, ON (Hutcheon and Handegord 1995) 22
Figure 3.4: Monthly temperature variation with soil depth, St. Paul, MN (Bligh 1975) 22
Figure 3.5: Apparent thermal conductivity vs. moisture content for various soils (ASHRAE 2005) 23
Figure 3.6: Monitored data for a Grayslake, IL development house 26
Figure 3.7: Grayslake, IL interior and exterior dewpoints 27
Figure 3.8: Vernon Hills, IL interior and exterior dewpoints 27
Figure 3.9: Interior above-grade and basement temperature conditions (Ruest 1993) 28
Figure 3.10: Interior above-grade and basement dewpoint conditions (Ruest 1993) 29
Figure 3.11: Psychrometric relationships of basement wall boundary conditions 30
Figure 3.12: Common bulk water problems for basements (Rose 1997) 32
Figure 3.13: Path of capillary rise through footing (Lstiburek 2006) 35
Figure 3.14: Examples of air transported moisture in basements (Lstiburek 2006) 36
Figure 3.15: Condensation potentials in an insulated basement wall (above-grade portion) 36
Figure 3.16: IEA Annex 24 Data: vapor permeability of concrete vs. water content (Rose 2005) 38
Figure 3.17: Moisture transport rates of diffusion vs. air transport (Lstiburek 2004) 39
Figure 3.18: WUFI comparison of capillarity and vapor diffusion 40
Figure 3.19: WUFI simulation equilibrium moisture content of concrete 41
Figure 3.20: Typical sorption isotherm of a hygroscopic material (Straube and Burnett 2005) 42
Figure 3.21: IEA Annex 24 Data: sorption and desorption isotherm for concrete (Rose 2005) 42

Figure 3.22: Mold growth on upper portion of basement wall 45
Figure 3.23: Mold growth at insulated rim joist of basement 45
Figure 3.24: Moisture accumulation and mold growth in single polyethylene wall 47
Figure 3.25: Moisture accumulation behind polyethylene; high MCs in framing 49
Figure 3.26: Surface mold at interface of fiberglass batt and polyethylene 49
Figure 3.27: Protection of foundation from precipitation and ground moisture (Lstiburek 2006) 50
Figure 3.28: Temperature gradients through walls with interior (left) and exterior (right) insulation (Garden 1969, taken from Hutcheon and Handegord 1995) 51
Figure 3.29: Exterior foundation insulation using draining rigid fiberglass board 52
Figure 3.30: Exterior foundation insulation using extruded polystyrene and drainage mat 52
Figure 3.31: Above grade protection of exterior insulation & dimensional adjustments (Lstiburek 2006) 53
Figure 3.32: Thermal bridging at masonry shelf with exterior insulation (Lstiburek 2006) 53
Figure 3.33: Comparison of basement lower wall temperature and monthly average outdoor temperatures 55
Figure 3.34: Interior basement insulation using extruded polystyrene foam (Lstiburek 2006) 58
Figure 3.35: Interior basement insulation using permeable spray foam (Lstiburek 2006) 58
Figure 4.1: Simulation results, Swinton & Karagiozis (1995) 60
Figure 4.2: Internally insulated wall from Timusk and Pressnail (1997) 61
Figure 4.3: Concept (5), from Huelman and Cheple (2001) 62
Figure 4.4: Concept (6), from Huelman and Cheple (2001) 62
Figure 4.5: Wood stud frame drying responses to controlled leak (CMHC, 1999) 64
Figure 4.6: Owens Corning basement test (Goldberg and Aloi 2002) 67
Figure 4.7: Removable test panel at upper position (Goldberg and Aloi 2002) 67
Figure 4.8: Water mass in removable panels, below grade/mid-height (Goldberg and Aloi 2002) 67
Figure 4.9: Water mass in removable panels, above grade/upper height (Goldberg & Aloi, 2002) 69
Figure 4.10: Installation of Icynene insulation (Goldberg and Farkas 2004) 70
Figure 4.11: Removable test panels (Goldberg and Farkas 2004) 70
Figure 4.12: Removable Icynene panel weight gain; mid height (Goldberg and Farkas 2004) 71
Figure 4.13: Removable Icynene panel weight gain; upper height (Goldberg and Farkas 2004) 72
Figure 4.14: Example of worst condensation seen on PA-6 vapor retarder (Goldberg and Gatland 2006) 75

Figure 4.15: Deterioration of wall-side waterproofing coating (Goldberg and Gatland 2006) 75
Figure 5.1: Front elevation of Huntley test house 79
Figure 5.2: Rear elevation of Huntley test house 79
Figure 5.3: Aerial view of Huntley test house 79
Figure 5.4: Rear oblique Huntley test house 79
Figure 5.5: Wall 1 (2x4 frame with polyethylene interior) 80
Figure 5.6: Wall 2 (2x4 frame w. polyethylene interior & exterior) 80
Figure 5.7: Wall 3 (Foil-faced polyisocyanurate (1.5") 81
Figure 5.8: Wall 4 (Extruded polystyrene (2") w. gypsum wall board) 81
Figure 5.9: Wall 5 (Extruded polystyrene (1") w. 2x4 frame, fiberglass) 82
Figure 5.10: Wall 6 (Extruded polystyrene (1") w. 2x4 frame, cellulose) 82
Figure 5.11: Wall 7 (Rigid fiberglass (2") with polyamide film) 82
Figure 5.12: Wall 8 (Fiberglass roll blanket (3") with perforated facer) 83
Figure 5.13: Section and sensor layout for Huntley site walls 1, 2, and 3 85
Figure 5.14: Section and sensor layout for Huntley site walls 4, 5, and 6 86
Figure 5.15: Section and sensor layout for Huntley site walls 7 and 8 86
Figure 5.16: Boring for soil sensor installation, Huntley site 87
Figure 5.17: Data collection system at Huntley site 87
Figure 5.18: THERM model, showing assembly components 88
Figure 5.19: THERM model, showing thermograph results 88
Figure 5.20: T and T/RH sensor at concrete 89
Figure 5.21: Concrete wall upper form extension out of plane 89
Figure 5.22: Lateral air sealing at Walls 1 and 2 (stud frame walls) 90
Figure 5.23: Instrumentation package at lower location of stud frame walls (Wall 2) 90
Figure 5.24: Instrumentation package at middle location of stud frame walls (Wall 2) 90
Figure 5.25: Instrumentation package at upper location of stud frame walls (Wall 2) 90
Figure 5.26: Caulk sealing and expanding foam at Wall 3 concrete 91
Figure 5.27: Installation of temperature/RH sensor in foam board (Wall 3) 91
Figure 5.28: Installation of furring strips and foam at wall 4 91
Figure 5.29: Completed assembly (side view) of wall 4 91
Figure 5.30: Installation of XPS board at wall 6 with powder actuated fasteners 92
Figure 5.31: Installed cellulose insulation in wall 6 92

Figure 5.32: Installation of cellulose insulation in wall 6 93
Figure 5.33: Top air sealing detail and foam wedge at wall 5 93
Figure 5.34: Installation of PA-6/rigid fiberglass material (wall 7) 93
Figure 5.35: Lateral air sealing and joint sealing at wall 7 93
Figure 5.36: Installation of 2x2s at wall 8 94
Figure 5.37: Completed installation of wall 8 94
Figure 5.38: Schematic layout of test panels in Huntley 95
Figure 5.39: Composite photo of test panels in Huntley (prior to wall 7 installation) 95
Figure 5.40: Schematic of wetting system 96
Figure 5.41: Front elevation of Kitchener test location 97
Figure 5.42: Floor plan of test basement, showing test wall locations 97
Figure 5.43: Kitchener test site, showing proximity of adjacent house 98
Figure 5.44: Kitchener test site, with projected line from adjacent house 98
Figure 5.45: Orientation of Kitchener test house and surroundings 98
Figure 5.46: Location of test walls at Kitchener site, pre-installation 98
Figure 5.47: Section and sensor layout for Kitchener site walls 102
Figure 5.48: Relative position of soil sensors at Kitchener site 103
Figure 5.49: Gypsum soil block, wood plug sensor, and temperature sensor in soil installation 103
Figure 5.50: Location of soil sensor hole 103
Figure 5.51: Existing rim joist condition at Kitchener site 104
Figure 5.52: Evidence of rim joist moisture damage at Kitchener site 104
Figure 5.53: Test panel openings at Kitchener site 105
Figure 5.54: Installation of XPS wall at foundation step down 106
Figure 5.55: Air sealing at perimeter of stud frame walls 106
Figure 5.56: Air sealing at top plate of frame walls 106
Figure 5.57: Sensors at upper location of stud frame wall 106
Figure 5.58: Sensors at middle location of stud frame wall 107
Figure 5.59: Sensors at lower location of stud frame wall 107
Figure 5.60: Test panels at Kitchener site (pre-drywall); approximate grade level shown 107
Figure 6.1: Soil temperatures for representative year (January 2005-February 2006) 108
Figure 6.2: Daily average soil temperatures at center stack (2005) with exterior temperature 109
Figure 6.3: Hourly soil temperatures at center stack (winter detail) with exterior temperature 110

Figure 6.4: Hourly Argonne Laboratory soil temperatures (winter detail) with exterior temperature 111
Figure 6.5: Hourly soil temperatures at center stack (summer detail) with exterior temperature 112
Figure 6.6: Soil matric potentials at Huntley site (2004-2006) 113
Figure 6.7: Historical monthly average rainfall data for Huntley 114
Figure 6.8: Monthly rainfall data at Argonne National Laboratory weather station 114
Figure 6.9: Center stack soil matric potentials and rainfall data (2004-2006) 115
Figure 6.10: Center stack soil matric potentials and rainfall data (2005 detail) 116
Figure 6.11: Interior and exterior temperature (daily average values) 117
Figure 6.12: Interior and exterior temperature & relative humidity (daily average values) 118
Figure 6.13: Interior and exterior dewpoint conditions at Huntley site (daily average values) 119
Figure 6.14: Concrete above-grade surface temperatures (July 2006) 120
Figure 6.15: Bay near Wall 8, showing shading on above-grade portion of concrete 120
Figure 6.16: Temperatures at concrete-insulation interface at grade (interior side); June-July 2006 120
Figure 6.17: Bay interior near Wall 8, showing incomplete blocking/air leakage location 121
Figure 6.18: Temperatures at concrete-insulation interface at grade (interior side); December 2006-January 2007 121
Figure 6.19: Thermal profile (summertime) down height of wall 1 122
Figure 6.20: Upper, mid-height, and lower concrete temperatures, with exterior T 123
Figure 6.21: Interior dewpoint, stud bay dewpoint, and concrete temperature (upper location) 124
Figure 6.22: Interior dewpoint, stud bay dewpoint, and concrete temperature (mid-height) 124
Figure 6.23: Interior dewpoint, concrete temperature (mid-height), exterior T and dewpoint 125
Figure 6.24: Single and double poly dewpoint (upper location), with interior DP 126
Figure 6.25: Single & double poly dewpoint (mid-height location), with interior DP 127
Figure 6.26: Single & double poly insulation/concrete interface dewpoint & RH, w. interior DP 128
Figure 6.27: Gap in air seal at the top of panel 1 129
Figure 6.28: Panel 1 top connection sealed with builders' tape 129
Figure 6.29: Polyiso mid-insulation and concrete/insulation interface dewpoint, w. interior DP 130
Figure 6.30: Foam seal at top of wall; note gap in foam at tape measure. 131
Figure 6.31: Caulk air seal around the perimeter and at form board extension intersection 131
Figure 6.32: Polyiso upper insulation-to-concrete interface dewpoint and RH, with interior DP 131
Figure 6.33: 2” XPS concrete/insulation interface dewpoint, with interior DP 132
Figure 6.34: XPS+fiberglass concrete/insulation interface dewpoint, with interior DP 133

Figure 6.35: XPS+cellulose concrete/insulation interface dewpoint, with interior DP 134
Figure 6.36: Stud bay dewpoints for XPS+FG (5) and XPS+cell (6) walls, upper location 134
Figure 6.37: Upper and lower stud bay dewpoints before and after drywall/paint installation 135
Figure 6.38: PA-6 and roll blanket concrete/insulation interface dewpoint, with interior DP 136
Figure 6.39: Roll blanket lateral seal failure in October 2003 137
Figure 6.40: Roll blanket lateral seal condition in June 2004 137
Figure 6.41: Roll blanket dewpoint in late 2006, with interior dewpoint 138
Figure 6.42: Mid-height concrete interface dewpoint for all panels, with interior DP 139
Figure 6.43: Mid-height concrete interface relative humidity for all panels 140
Figure 6.44: Dewpoint comparison to concrete wall surface temperatures (2004) 141
Figure 6.45: Dewpoint comparison to concrete wall surface temperatures (winter detail) 141
Figure 6.46: Dewpoint comparison to concrete wall surface temperatures (spring/summer detail) .. 142
Figure 6.47: Interior and exterior temperature & relative humidity (daily average values) 143
Figure 6.48: Wall to interior Δ dewpoint; non-wetted year (2004), daily average values 144
Figure 6.49: Wall to interior Δ dewpoint; wetted year (2006), daily average values 145
Figure 6.50: September 2005 wetting event dewpoint response, stud frame walls, 130 days 146
Figure 6.51: September 2005 wetting event relative humidity response, stud frame walls, lower stud bay 147
Figure 6.52: January 2006 wetting event dewpoint response, stud frame walls, 220 days 147
Figure 6.53: January 2006 wetting event dewpoint response, stud frame walls mid-height 148
Figure 6.54: September 2005 wetting event dewpoint response, foam-based walls 149
Figure 6.55: January 2006 wetting event dewpoint response, foam-based walls 150
Figure 6.56: September 2005 wetting event relative humidity response, foam-based walls 151
Figure 6.57: January 2006 wetting event relative humidity response, foam-based walls 151
Figure 6.58: Psychrometric comparison of September 2005 and January 2006 wetting events for 2" XPS wall 152
Figure 6.59: September 2005 wetting event dewpoint response, other walls 153
Figure 6.60: January 2006 wetting event relative humidity response, other walls 154
Figure 6.61: Concrete-insulation mid-height dewpoint; full length of experiment; all walls 155
Figure 6.62: Upper portion of wetting plume in single polyethylene wall (panel 1) 157
Figure 6.63: Lower portion of wetting plume in single polyethylene wall (panel 1) 157
Figure 6.64: Water beads on polyethylene at double polyethylene wall (panel 2) 158

Figure 6.65: Water beading at fiberglass batt in double polyethylene wall (panel 2) 158
Figure 6.66: Sill plate of double polyethylene wall (panel 2) 158
Figure 6.67: Close up of double polyethylene sill plate 158
Figure 6.68: Wetting plume in foil-faced polyisocyanurate wall 159
Figure 6.69: Wetting plume in 2” XPS wall 160
Figure 6.70: Concrete interface side of insulation, showing wire tracks 160
Figure 6.71: Craters or burrows on exterior face of XPS insulation (upper panel only) 160
Figure 6.72: Wetting plume in 1" XPS + fiberglass (left) and XPS + cellulose (right) walls 162
Figure 6.73: Wetting plume in rigid fiberglass/PA-6 wall 163
Figure 6.74: Wetting plume in perforated roll blanket wall 164
Figure 6.75: Initial condition of interior of fiberglass (panels 1 and 2), September 2003 165
Figure 6.76: Small brown stains in June 2004; double polyethylene wall (panel 2) 165
Figure 6.77: Brown stains on interior of fiberglass (panel 1), July 2006 165
Figure 6.78: Brown stains on interior of fiberglass (panel 2), July 2006 165
Figure 6.79: Brown stains in XPS/FG (panel 5), July 2006 166
Figure 6.80: Concrete interface of rigid fiberglass in PA-6 wall (panel 7) 166
Figure 7.1: Interior and exterior temperature & relative humidity (daily average values) 167
Figure 7.2: Interior and exterior dewpoint conditions at Huntley site (daily average values) 168
Figure 7.3: Soil temperatures for Kitchener site, with exterior air temperature 169
Figure 7.4: Soil temperatures for UW weather station, with air temperature (1998-2001) 170
Figure 7.5: Soil temperatures for UW weather station, with air temperature (winter 1998-1999) 170
Figure 7.6: Soil matric potentials (front stack) for Kitchener site 171
Figure 7.7: Soil moisture content "plug" sensor data for Kitchener site 172
Figure 7.8: Concrete-insulation interface temperature, upper location, with maximum daily solar .. 173
Figure 7.9: Thermal profile down height of frame walls in September 2006; outdoor T ~12-14° C. 174
Figure 7.10: Thermal profile down height of polyethylene-frame wall in January 2007; outdoor T~ -8 to -9° C 174
Figure 7.11: Exterior view of basement window, for vertical reference to brick ledge 174
Figure 7.12: Interior view of basement window, for vertical reference, compared to test panels 174
Figure 7.13: Monitored data: relative humidity at concrete-insulation interface; above-grade 175
Figure 7.14: Moisture content wafer response, interior side, above grade, with exterior T 176
Figure 7.15: Taping of perimeter studs, and faces of inner studs (at staple holes) 178

Figure 7.16: Tape only covers exposed portion of edge studs; could not apply at buffer panels..... 178
Figure 7.17: Relative humidity, concrete-insulation interface, mid-height (daily avg. values) 179
Figure 7.18: Wafer moisture content, concrete-insulation interface, mid-height (daily avg. values) 180
Figure 7.19: Dewpoint at concrete-insulation interface, mid-height, with interior DP 181
Figure 7.20: Wafer moisture content, concrete-insulation interface, lower height 182
Figure 7.21: Framing moisture content for upper portion of stud walls..... 183
Figure 7.22: Framing moisture content for lower portion of stud walls..... 184
Figure 7.23: Frame-polyethylene wall after drywall removal 185
Figure 7.24: Upper moisture content wafer..... 185
Figure 7.25: Close up; mold growth was seen on both sides 185
Figure 7.26: Brown staining at inboard side of upper portion of left-hand test bay stud 186
Figure 7.27: Brown staining at inboard side of upper portion of right-hand test bay stud..... 186
Figure 7.28: Interior face of mid-height wafer 186
Figure 7.29: Exterior face of mid-height wafer 186
Figure 7.30: Frame-latex paint wall after drywall removal..... 187
Figure 7.31: Exterior face of drywall in frame-latex paint wall 187
Figure 7.32 Close-up of upper portion of drywall exterior face..... 187
Figure 7.33: Upper wafer 187
Figure 7.34: Upper left side stud of test bay 188
Figure 7.35: Upper right side stud of test bay 188
Figure 7.36: Mid-height concrete-insulation interface wafer, interior side..... 189
Figure 7.37: Mid-height concrete-insulation interface wafer, exterior side 189
Figure 7.38: Moisture meter measurements of the test bay stud, parallel to MC pins 190
Figure 7.39: Measurement of bottom plate 190
Figure 7.40: Upper portion of roll blanket wall..... 191
Figure 7.41: Close up of the upper wafer 191
Figure 8.1: Moisture content profiles through concrete thickness (exterior=left; interior=right) 195
Figure 8.2: Gypsum wallboard permeability data (painted and unpainted) from Kumaran (2002) ... 196
Figure 8.3: Daily average dewpoint (upper portion) comparison of Kitchener walls 197
Figure 8.4: Upper height concrete temperature, monitored vs. model (full year) 198
Figure 8.5: Upper height concrete temperature, monitored vs. model (winter detail) 198
Figure 8.6: Upper height concrete temperature, monitored vs. model (summer detail)..... 199

Figure 8.7: Concrete ΔT as % of overall wall ΔT (winter detail); monitored vs. model..... 200
Figure 8.8: Detail of the above-grade monitoring location 200
Figure 8.9: Air, soil (150 mm), and concrete interface temperatures (winter detail) 201
Figure 8.10: Vertical temperature gradient in frame-latex wall 202
Figure 8.11: Measurement of concrete-insulation interface temperatures 202
Figure 8.12: Concrete moisture content; parametric drying studies (exterior=left; interior=right).... 204
Figure 8.13: Concrete moisture content; initial conditions for simulation (exterior=left; interior=right)205
Figure 8.14: Monitored data: mid-height RH sensors at concrete-insulation interface..... 206
Figure 8.15: Monitored data: mid-height wafer sensors (calculated RH) at concrete-insulation interface 206
Figure 8.16: Simulation data: mid-height RH at concrete-insulation interface..... 207
Figure 8.17: Monitored data: lower-height RH at interface and mid-batt..... 208
Figure 8.18: Simulation data: lower-height RH at interface and mid-batt 209
Figure 8.19: Simulation data: relative humidity at concrete-insulation interface, above-grade..... 211
Figure 8.20: Monitored data: relative humidity at concrete-insulation interface; above-grade 211
Figure 8.21: Simulation data: upper-height relative humidity at interior interface..... 212
Figure 8.22: Monitored data: upper-height wafer sensors (calculated RH) at interior interface..... 213
Figure 8.23: Sorption isotherm for WUFI imaginary condensation layer..... 214
Figure 8.24: Simulation relative humidity at concrete-insulation interface, above grade portion 215
Figure 8.25: Simulation relative humidity at concrete-insulation interface, winter detail 215
Figure 8.26: Simulation condensation layer moisture content, upper location 216
Figure 8.27: Concrete-insulation interface condensation layer MC, Kitchener data, above grade 217
Figure 8.28: Vapor barrier condensation layer MC, Kitchener data, above grade..... 217
Figure 8.29: Monthly average temperatures for climate locations (Environment Canada data)..... 219
Figure 8.30: Comparison of monitored and climate average monthly temperatures for Waterloo 219
Figure 8.31: Summary of interior conditions (temperature and RH) with Waterloo exterior T..... 221
Figure 8.32: Interior conditions, shown as temperature and dewpoint (° C)..... 221
Figure 8.33: Condensation layer MC, Toronto AG, low RH 223
Figure 8.34: Condensation layer MC, Toronto AG, mid RH..... 223
Figure 8.35: Condensation layer MC, Toronto AG, high RH 223
Figure 8.36: Toronto AG condensation layer hours over 500 g/m2..... 223
Figure 8.37: Interior cavity side condensation layer MC, Toronto AG, mid RH..... 224

Figure 8.38: Roll blanket isopleth at concrete-insulation interface, “mid” humidity 225
Figure 8.39: Latex paint-gypsum isopleth at concrete-insulation interface, “mid” humidity 225
Figure 8.40: Condensation layer MC, Vancouver AG, mid RH 227
Figure 8.41: Condensation layer MC, Vancouver AG, high RH 227
Figure 8.42: Vapor barrier cond. layer MC, Vancouver AG, mid RH 227
Figure 8.43: Edmonton AG condensation layer hours over 500 g/m2 228
Figure 8.44: Condensation layer MC, St. John’s AG, low RH 229
Figure 8.45: Condensation layer MC, St. John’s AG, mid RH 229
Figure 8.46: Condensation layer MC, St. John’s AG, high RH 229
Figure 8.47: St. John’s AG condensation layer hours over 500 g/m2 229
Figure 8.48: Interior dewpoint extrapolation conditions, and lower wall temperature 231
Figure 8.49: Condensation layer accumulation for lower location, “high” relative humidity 232
Figure 8.50: Roll blanket isopleth at concrete-insulation interface, “mid” humidity 232
Figure 8.51: No vapor control isopleth at concrete-insulation interface, “mid” humidity 232
Figure 8.52: Concrete water content, "low" humidity conditions 233
Figure 8.53: Concrete water content, "high" humidity conditions 234
Figure 8.54: Interior dewpoints and lower wall T for Edmonton extrapolation 235
Figure 8.55: Accumulation at storage layer, Edmonton extrapolation, "low" humidity 236
Figure 8.56: Accumulation at storage layer, Edmonton extrapolation, "mid" humidity 236
Figure 8.57: Dewpoint degree hour differences between concrete & interior conditions 237
Figure 8.58: Concrete water content, "low" humidity conditions 238
Figure 8.59: Interior dewpoint, lower wall temperature, and Edmonton exterior dewpoint 239
Figure 8.60: Exterior dewpoint and lower wall temperature from Kitchener data 240
Figure 8.61: Results of Kitchener simulation with elevated summertime interior humidity 240
Figure 8.62: Exterior dewpoint and lower wall temperature from Huntley data 241
Figure 8.63: Minneapolis AG condensation layer hours over 500 g/m2 243
Figure 8.64: Vapor barrier condensation layer MC, Minneapolis above grade, mid RH 244
Figure 8.65: Roll blanket and double polyethylene interface condensation layer MC and RH 247
Figure A.1: Average sorption isotherm for wood (Straube and Burnett 2005) 272
Figure A.2: Close-up of completed sensor 273
Figure A.3: Schematic cross section of sensor (dimensions in mm) 273
Figure A.4: Sensors in 100% humidity calibration enclosure 274

Figure A.5: Plug sensor response after placement in humidity enclosure 274
Figure A.6: Plug sensor response after removal from humidity enclosure 275
Figure A.7: Plug sensor response to water immersion test and drying 276
Figure A.8: Close-up of completed sensor 277
Figure A.9: Close-up of completed sensor 277
Figure A.10: Schematic of wafer sensor (dimensions in mm) 277
Figure A.11: Wafer sensor response after placement in humidity enclosure 278
Figure A.12: Wafer sensor response after removal from humidity enclosure 278
Figure A.13: Wafer stock in 100% humidity calibration enclosure 279
Figure A.14: Wafer stock in 100% humidity calibration enclosure with balance 279
Figure A.15: Gravimetric adsorption response of wafers 280
Figure A.16: Gravimetric desorption response of wafers 280
Figure A.17: NTNU pine moisture content response to 50-100% and 50-99% RH cycling 281
Figure A.18: Detail of NTNU pine adsorption/desorption response 282
Figure A.19: IBP softwood moisture content response to 50-100% and 50-99% RH cycling 282
Figure A.20: Sorption isotherms for IBP softwood and NTNU pine 283
Figure A.21: Moisture-dependent permeability data for IBP softwood and NTNU pine 284
Figure A.22: Modified IBP softwood moisture content response to 50-100% RH cycling 284
Figure A.23: Adsorption and desorption response of modified isotherm NTNU pine material 285
Figure A.24: RH sensor and MC wafer in brick space cavity at UW test facility 286
Figure A.25: RH sensor and MC wafer in brick space cavity 286
Figure A.26: BEGHut brick space wafer moisture content data 286
Figure A.27: BEGHut brick space relative humidity data 287
Figure A.28: BEGHut relative humidity vs. moisture content, with sorption isotherm 287
Figure A.29: Mid-height sensors in Kitchener basement 288
Figure A.30: Kitchener site relative humidity vs. moisture content, with sorption isotherm 288
Figure A.31: Schematic of wetting system 290
Figure A.32: Injector, for size reference and as installed 290
Figure A.33: Holes were drilled at the same elevation in each wall 291
Figure A.34: Reservoirs and pump and manifold housing 291
Figure A.35: Pump housing 291
Figure A.36: Commissioning 292

Figure A.37: Sample edges wrapped with foil tape 293
Figure A.38: Sample sealed to container lid with foil tape 293
Figure A.39: Testing at 20° C/50% RH in climate-controlled test laboratory 294
Figure A.40: Testing at elevated humidity levels in environmental chamber 294
Figure A.41: Vapor permeability measurements for materials from walls P7 and P8 295
Figure A.42: Mold growth on water side of P8 perforated facer sample 296
Figure A.43: Detail of mold growth, showing water "matting" at one end 296
Figure A.44: View of the 2' square polyisocyanurate specimens 298
Figure A.45: View of access port cut into center of each specimen 298
Figure A.46: Diagram of polyisocyanurate specimens 298
Figure A.47: Temperature during final week of experiment 299
Figure A.48: Relative humidity during final week of experiment 300
Figure A.49: Dew point during the final week of experiment 300
Figure A.50: Relative humidity data from Huntley site (Thermax and 1" XPS + fiberglass walls) .. 302
Figure A.51: Original installation of MC pins (unpainted) 303
Figure A.52: MC pin painting with non-conductive coating, 10/04 303
Figure A.53: Wrapping pins with electrical tape, 9/05 304
Figure A.54: Framing moisture content measurements in XPS-cellulose wall 304
Figure A.55: Holes drilled into test stud for sub-surface MC measurements 305
Figure A.56: Handheld moisture meter measurement of cellulose insulation 305

List of Tables

Table 2.1: General category of functions (from PHRC 1997) 7
Table 3.1: Soil matric potentials and moisture conditions 24
Table 3.2: Relationship between relative humidity and suction pressure values (Rose 2005) 25
Table 3.3: Summary of interior temperature & humidity surveys 30
Table 4.1: Vapor control combinations tested (Goldberg and Huelman 2001) 65
Table 4.2: Assemblies tested (Goldberg and Farkas 2004) 69
Table 4.3: PA-6 Wall assemblies tested (Goldberg & Gatland 2006) 72
Table 4.4: Wall assemblies tested in Zuluaga et al. (2004) 74
Table 5.1: Summary list of test walls at Huntley site 80
Table 5.2: Summary of sensors at Huntley site 84
Table 5.3: Summary list of test walls at Kitchener site 99
Table 5.4: Summary of sensors at Kitchener site 101
Table 6.1 (repeated): Soil matric potentials and moisture conditions 113
Table 7.1: Moisture content measurements of frame walls 190
Table 8.1: Climate data for extrapolation locations 218
Table 8.2: Interior humidity conditions used in extrapolation simulations 220
Table A.1: Commissioning test results 292
Table A.2: Vapor permeability results for polyamide-6 with laminated perforated facer (P7) 294
Table A.3: Vapor permeability results for perforated vinyl facer (P8) 295

Chapter 1
Introduction

1.1 Background

Basements are a common type of foundation used in residential and commercial construction. It has been estimated that 90 to 95% of Canadian houses and low-rise apartments are built on basements (BETT 1984, 1985). Basements are used as the majority of foundations in the Northeast and Midwest regions of the United States (DOE Energy Information Administration 1999).

Traditionally and historically speaking, basements have not been considered habitable space (i.e., "cellars"), instead being used for storage (e.g., food, fuel such as coal) and mechanical equipment. High interior moisture levels, lack of temperature control, and even incidental flooding were accepted conditions for these spaces. However, given the demand for maximizing available living space in houses in the past 50 years, basements have increasingly been finished and used as conditioned occupied space, with commensurate demands for a comfortable environment. A survey of the northeast indicated that 40% of basements have been finished, to some degree (PHRC 1997).

The oil crisis of the 1970s raised the importance of energy efficiency in the public consciousness. Both homeowners and government agencies made efforts to increase the energy efficiency of buildings in response to this situation, due to the rising cost of space conditioning (e.g., heating fuel). This was often achieved by installation of higher efficiency mechanical equipment and/or better controls, increasing insulation levels of walls, roofs, and windows, and increasing airtightness. However, the basement was often ignored during this weatherization work. Heat losses through the basement have been estimated in the range of 10-30% of a house's total heat loss (BETT 1985, Beausoleil-Morrison 1997, Swinton & Kesik 2005): controlling this heat loss is important for reducing overall energy use, especially when the remainder of the house has been weatherized.

One solution to basement heat loss is to insulate the floor joist cavities between the first floor and the basement, in an attempt to create a thermal barrier. However, the air barrier between the first floor and the basement is typically minimal to nonexistent, due to mechanical penetrations and chaseways. Ductwork and mechanical equipment are often located in the basement; duct leakage and waste heat can be recaptured by connecting the basement to the above-grade space. Therefore, the best practice under most circumstances is to include the basement in the conditioned space, and to insulate the basement walls; the increase in conditioned or semi-conditioned square footage is an added benefit.

Houses built before the 1950's rarely had insulation on below grade walls (Cheple and Huelman 2001). Basement wall insulation became more common in the 1980s, most notably in Canada and the colder regions of the United States, such as Minnesota, where it was eventually required by building codes. But with this increasing use of basement wall insulation came reports of moisture-related failures due to accumulation of water within insulation systems, and accompanying deterioration, such as mold growth or wood decay.

Exterior insulation of basement walls has a substantial body of research supporting its use (BETT 1982). This practice eliminates or reduces many problems seen with basement insulation, and is considered a superior solution by most of the building science community. However, this technique has not been widely adopted in practice; issues that prevent acceptance include the difficulty of protecting the exposed above-grade portion of the insulation, insect or pest control, detailing of brick veneers, and construction sequencing.

As a result, many builders choose to insulate basements on the interior. However, many of the insulation assemblies used in the field (and/or mandated by building codes) have been linked to moisture-related failures. One problem is that unlike exterior basement insulation, there is not a large body of research on interior insulation. The common assemblies are often the result of an iterative process responding to failures. There are assemblies that have been demonstrated to have low vulnerability to moisture related problems, but they are not widely adopted due to higher first cost.

As interior basement insulation is used in greater numbers of houses, high-risk assemblies are likely to experience a fraction of failures that might well prove to be intolerable. This provides a strong reason to pursue research that increases understanding of interior basement insulation, and to develop more effective solutions.

1.2 Objectives

One objective of this research was to improve understanding of the hygrothermal behavior of interior basement wall insulation, in order to inform the design of assemblies with reduced risks of moisture-related failure. First, several field-installed assemblies were monitored: the performance of these walls was compared against each other, and observations could be related to phenomena reported in practice, and in the published literature.

In addition, computer hygrothermal modeling was used to simulate a selection of the test walls, and extrapolation simulations in several geographic locations were run based on these models. The goal was to gain additional insight into interior basement insulation systems, including walls not included in the field testing.

1.3 Approach

This thesis is divided into the following nine chapters (not including this introduction).

A review of the history of basement insulation and problems that have resulted in its installation is presented in Chapter 2, “Background and History.” The below grade environment exhibits particular thermal and moisture behaviors; the environment’s interaction with basement walls and the impact on enclosure design is examined in Chapter 3, “Thermal and Moisture Physics of Basements.” Chapter 4, “Literature Survey,” summarizes the body of research on basement insulation that extends back to the 1970s, including both hygrothermal simulations and multiple field experiments.

The main body of this thesis research was the monitoring and sensor data analysis of full-scale basement wall interior insulation systems at two field sites, which were located in Huntley, IL (outside of the Chicago area) with eight test walls, and Kitchener, ON (outside of the Toronto area),

with four test walls. The experimental setup for both sites, including wall selection, installation process, and monitoring equipment setup, is covered in Chapter 5, "Experimental Setup." Data and interpretation of results are presented for the two sites, respectively in Chapter 6 ("Results: Huntley Site") and Chapter 7 ("Results: Kitchener Site").

Finally, computer hygrothermal models were run on the assemblies installed at the Kitchener site; the results were compared to the monitored data. Extrapolation models with different exterior climates (three Canadian weather locations) and interior climates (humidity levels) were run and analyzed. Wall assemblies that were not installed at the Kitchener site were also simulated, in order to gain a better understanding of some proposed basement insulation assemblies. These results are presented in Chapter 8, "Hygrothermal Modeling."

In the conclusions (Chapter 9), the results of field monitoring and simulations are compared. The implications of this research for interior basement insulation enclosure design and some recommended assemblies are presented in Chapter 10, "Recommendations and Future Work."

Information is presented in the appendices on instrumentation and data collection equipment, development of sensors specific to this project, and secondary experimental projects that contributed to this research.

Chapter 2

Background and History

To provide a framework for the presentation of this thesis research, this chapter defines the basement portion of the building enclosure and its nomenclature, and examines its functional role. This is followed by an examination of the movement towards the use of a basement as an insulated, conditioned, and sometimes-finished space, as well as the history of basement insulation, and the associated building code requirements.

2.1 Background Information

2.1.1 Definitions and Nomenclature

The foundation connects the structure of a building to the ground, thus providing physical support. Some common types of foundations are shown in Figure 2.1 (Carmody et al. 1991): the full or deep basement, the crawl space, and the slab on grade.

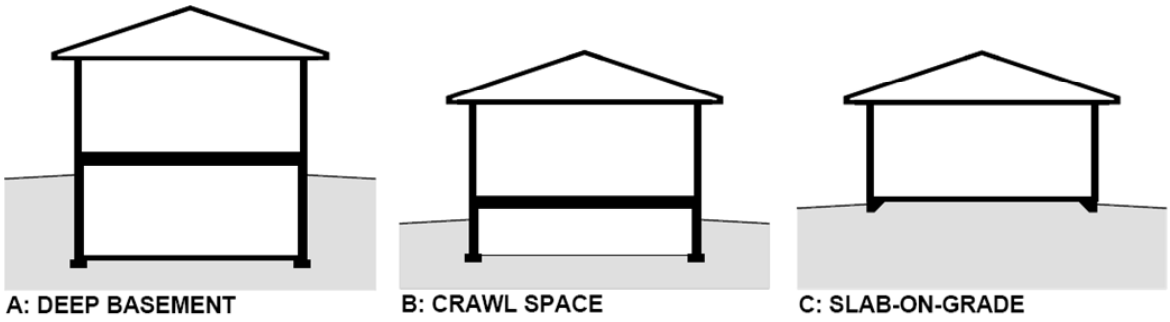

Figure 2.1: Common foundation types (Carmody et al. 1991)

The basement is the focus of this thesis; it is differentiated from the crawl space principally by its height (i.e., depth into the ground)—a basement typically has a ceiling height that allows its use as walkable floor area. Code definitions of a basement typically rely on location of the space with respect to ground level; for instance, the International Building Code (International Code Council 2006) defines a basement as follows: "That portion of a building that is partly or completely below grade plane. A basement shall be considered as a story above grade plane where the finished surface of the floor above the basement is: 1. More than 6 feet (1829 mm) above grade plane; or 2. More than 12 feet (3658 mm) above the finished ground level at any point."

There are many similarities between the construction of a conditioned basement and a conditioned (i.e., non-ventilated) crawl space. However, there are issues unique to the insulation of basements (as opposed to crawl spaces), due to the depth of the foundation and the use of the space for habitation.

The building enclosure, shown in a schematic from Straube and Burnett (2005) in Figure 2.2, is defined as the portions of the building that separate the interior from the exterior. The drawing below includes

interior spatial separators: these are not included in the definition of the building enclosure. The specific functions of the building enclosure are covered in more detail in the following section.

The building enclosure is composed of several components, as shown by the list in that figure. The basement portion of the building enclosure is highlighted; it includes the floor of the basement (item 1) and the foundation wall system (item 2). The basement enclosure separates the interior space from the exterior air or soil.

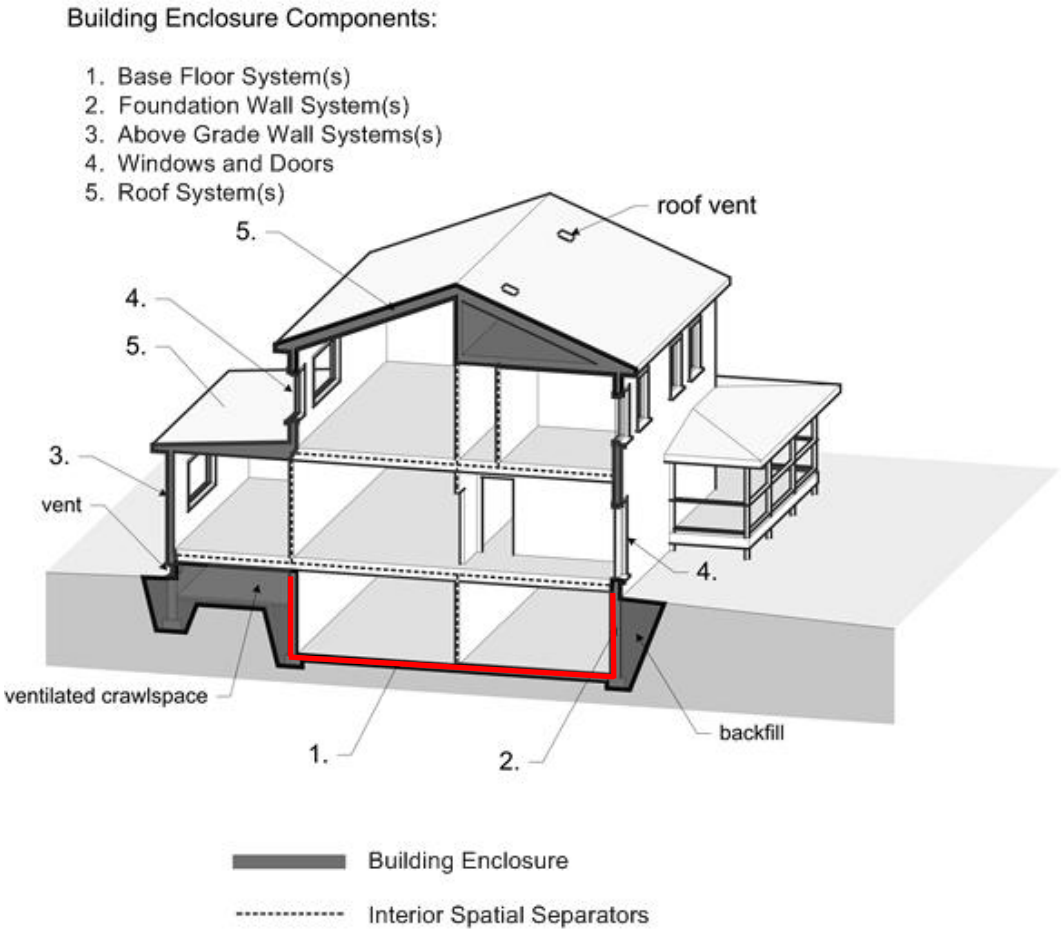

Figure 2.2: A schematic of the building enclosure, with the basement enclosure highlighted

The basement enclosure is examined in more detail in Figure 2.3, with explanations of its parts and nomenclature. The basement wall is exposed to two different conditions: above grade (i.e., exterior weather conditions), and below grade (i.e., soil). It rests upon a footing, which distributes the structural load on the underlying soil. A floor slab completes the bottom of the building enclosure.

The sill plate and rim joist (or rim closure) connect the foundation wall to the above-grade structure; for functional purposes, the rim joist area is usually included as a part of the basement building enclosure.

Some common components of the basement enclosure are shown in that figure. Moisture control is a critical function of this portion of the enclosure: at the basement wall, the dampproofing, exterior draining material, and footing drain (drain tile) all are tied to this function. Similarly, the subslab polyethylene vapor barrier and drainage material provide moisture protection for the floor slab, and the sealant/bond break provides a connection between the basement wall and floor components. All of these assembled components should be considered integral parts of the building enclosure, including items such as the compacted gravel field under the slab, or the free-draining backfill.

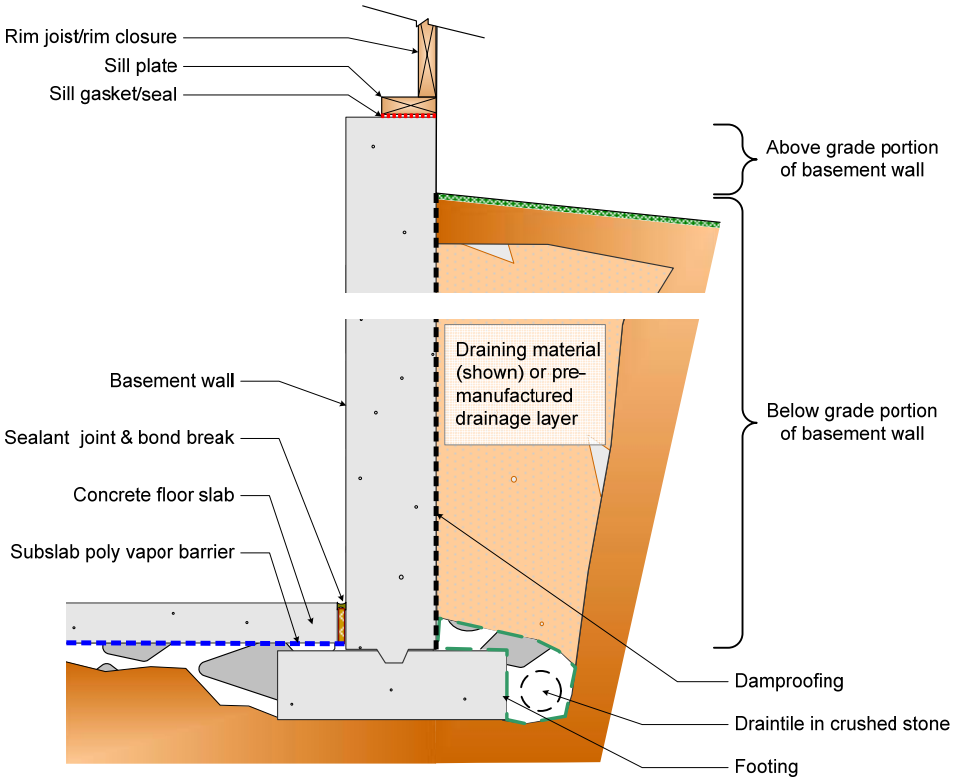

Figure 2.3: Parts and nomenclature of the basement enclosure

2.1.2 Functional Role of the Basement

A hierarchy of the physical functions of the building enclosure is presented in Straube and Burnett (2005), which is more specific than the description of the enclosure as an "environmental separator," breaking down its functions as follows:

- **Support:** the enclosure must addresses the structural loading from interior and exterior environments, the enclosure itself, and the building's live and dead loads.
- **Control:** the enclosure must regulate the loads due to separating the interior and exterior environments. This aspect encompasses the classic "environmental separator" items such as heat, air, and moisture, as well as other items such as sound or access.

- **Finish:** the exposed interior and exterior surfaces of the enclosure need to provide aesthetic/visual and weathering/wear characteristics that will meet the required functions and loads.

In addition, the enclosure is often used to fulfill a fourth set of functions related to the building's functional requirements:

- **Distribute:** the enclosure is sometimes used to distribute services or utilities such as electricity, water, gas, or air for space conditioning (HVAC).

This framework can be used to examine the roles of the basement: the Pennsylvania Housing Research Center (1997) completed this analysis, as shown in Table 2.1. It lists the specific loads that the enclosure will face, divided into groupings of primarily support, primarily control, and primarily finish functions. It indicates the primary, secondary, and tertiary importance these loads have on the function categories of support, control, and finish (interior and exterior).

It should be noted that the distribution function is not included in this analysis. Unfinished basement walls have a minimal, if any, distribution function. Finished basements include distribution of services in the enclosure, but that aspect is not examined here.

Table 2.1: General category of functions (from PHRC 1997)

Primary significance	●	Secondary significance	●	Tertiary significance	○

Specific Loads	**Finish (interior)**	**Support**	**Control**	**Finish (exterior)**
Primarily Support-Related				
Gravity – Dead (assembly, etc.)		●		
Gravity – Live (people, snow, etc.)		●		
Wind		●		●
Ground Movement (seismic, settlement, etc.)		●		
Explosion		●		
Rheological (creep, shrinkage, etc.)		●		○
Impact (vehicles, missiles, people, etc.)	●	●		●
Fire		●		

Primarily Control-Related				
Heat (thermal, etc.)		○	●	
Air (pressure, movement, leakage, etc.)		○	●	
Moisture (built-in, precipitation, etc.)		○	●	○
Smoke	●		●	
Solar radiation (incident, reflected, etc.)		●	●	○
Chemical attack/atmospheric (acid rain, etc.)			●	○
Particulate matter (dust, VOCs, etc.)			●	●
People (wear and tear, etc.)	○		●	●
Insects, birds, animals (termites, rodents, etc.)	●		●	
Light (natural, incandescent, fluorescent, etc.)	●		●	
Sound	○		●	○
Primarily Finish-Related				
Visual – local	●			●
Visual – contextual	●			●

A similar type of functional role analysis was also presented in Swinton and Kesik (2005).

The basement needs to support and accommodate the structural loads of the above-grade house, as well as lateral pressures from ground/soil pressures. The most important control functions include control of moisture, heat, and insects/pests.

Moisture sources include exterior loadings (precipitation, soil moisture, groundwater), construction moisture (in particular, the loading due to site-cast concrete), and interior loadings (water vapor). The basement must be protected from exterior moisture loads, which can be substantial. Approaches include grading and drainage, dampproofing of the exterior of the basement wall, and use of exterior drainage layers; they will be examined in more detail in a later section. Construction moisture must be allowed to dry out, while simultaneously avoiding damage to interior finishes, if any. Interior moisture vapor can create problems when it condenses on cold surfaces, such as the upper portion of the concrete wall in wintertime; the assembly must prevent accumulation and/or allow sufficient drying to avoid damage to any finishes.

Basement walls perform the function of controlling heat flow if the basement is included in the building enclosure. It is a common practice to attempt to exclude the basement from the building enclosure, by placing insulation in the ceiling of the basement/first floor, creating a thermal barrier at that location. However, the air barrier between the first floor and the basement is typically minimal to nonexistent, because of mechanical penetrations and chaseways. This is exacerbated by HVAC ductwork in the basement: duct leakage results in air communication between the above-grade and basement space, both due to direct leakage and building pressurization/depressurization from these leaks. Furthermore, mechanical equipment is often located in the basement: in heating-dominated climates, inclusion of the basement recaptures losses from equipment. Therefore, insulation of basement walls is considered to be

best practice under normal circumstances. The addition of basement wall insulation reduces energy consumption and increases comfort.

Due to the generally airtight nature of poured concrete or concrete block (typical basement wall materials), control of air is an ancillary concern. Exceptions are control of soil gases (typically from junctions between the wall and floor, or from the cores of concrete block) or air exfiltration/infiltration at the rim joist and sill plate areas.

Insect control, specifically of termites and carpenter ants, is an especially important control function, since the basement enclosure is in contact with the ground. Subterranean termites maintain their colonies in the ground, and travel between the ground and the above-grade structure, building mud tunnels to reach the wood portions. The field of termite control is beyond the scope of this chapter; avenues of attack can include entry through cracks and joints, as well as via plastic foam insulation board in contact with the ground.

The focus of this thesis is the moisture and thermal control aspects of the basement enclosure: the addition of insulation and/or finishes to basement can either solve or exacerbate moisture control issues.

2.2 Historical Background

2.2.1 Regional Distribution of Basements

A building foundation must have footings below the local frost line, in order to prevent damage due to frost heaving. The United States map of frost penetration depths is shown in Figure 2.4; it shows that in most of the Northeast and the northern portions of the Midwest, frost depths of 1.3-1.5 m (50-60”) or deeper are common. Of course, actual frost depths are a function of local soil conditions, moisture levels, and type of surface cover. But assuming these values, and given that foundations are typically exposed 150-300 mm (6-12”) above grade, the total height of 1.4 to 1.8 m (56-72”) is close to the height required for a basement foundation. Given the builder’s opportunity to profit by offering additional space, the decision to excavate for a full basement is a common practice for areas where frost penetration depths are more than about 30 or 40”.

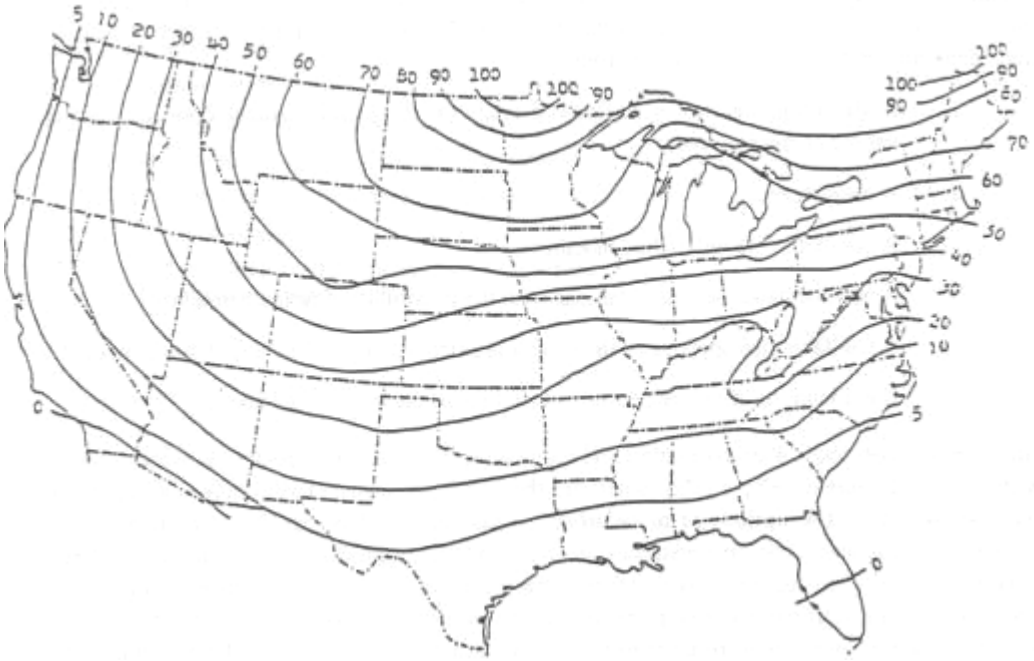

Figure 2.4: United States Map of Frost Penetration Depths (Inches) (PHRC 1997)

Basements are the most common type of residential foundation (~80%) in the Northeast and Midwest United States Census Regions (DOE Energy Information Administration 1999); this information is shown in Figure 2.5. Basements are much less common in the warmer regions (South and West regions), where slabs on grade and crawl spaces dominate. Roughly 90 to 95% of Canadian houses and low-rise apartments are built on basements (BETT 1984, 1985). Northern Europe has a relatively cold climate, with a similar prevalence of basements or cellars.

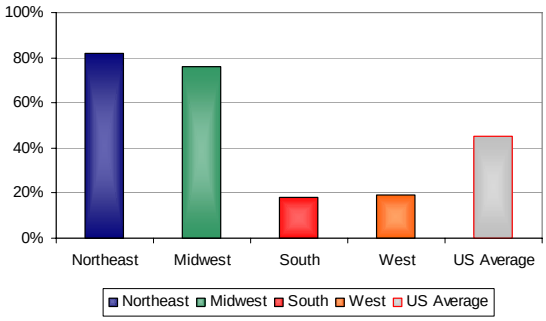

Figure 2.5: Percentage of houses with basements, by US Census Region (DOE-EIA 1999)

2.2.2 Basements as Finished Space

The purpose of the basement has been evolving over time; they were historically used as non-habitable spaces (i.e., "cellars") used for storage (e.g., food, fuel such as coal) and mechanical equipment, especially when such equipment consumed significant space and generated heat and noise. High interior moisture levels, lack of temperature control, and even incidental flooding were accepted conditions for these spaces. However, given the demand for maximizing available living space in houses, basements

have increasingly been finished and used as conditioned occupied space, with commensurate demands for a comfortable environment.

One account of the reason for the greater use of basements as conditioned space comes from Rogers (1938): a boiler manufacturer (American Radiator Company) in the 1920s tried to distinguish its product with an attractively painted red jacket. In order to capitalize on this aesthetic difference, they created publicity material showing activity and furnishings in the basement. By the time of the author's account, the "basement recreation room" was a popular modification.

This trend was also noted in the literature in the 1960s: NRC's Division of Building Research (currently the Institute for Research in Construction), published a Canadian Building Digest that gave recommendations for moisture control and finishing of residential basements (Crocker, 1961).

A proprietary survey described by PHRC (1997) indicated that in the northeast, 40% of basements have been finished, to some degree, and that 25% of homeowners planned to expand into the basement as living space. In addition, the survey noted that half of the basement finish installations occur within the first five years of occupancy, with 80% within ten years.

Production builders and developers often shy away from finishing basements, because basements have historically been a source of moisture-related problems. Providing a finished space, with a warranty of performance and comfort, can increase exposure to complaints and callbacks. In addition, basement square footage is not included in real estate area calculations, which makes the value of this space less apparent to the homebuyer. Builders even avoid a basic drywall covering of the basement walls, because it implies a finished or semi-finished space, which then generates a code-mandated requirement for services such as electrical outlets. In addition, construction sequencing of the trades is often difficult with basement finishing (McDermott 2001).

As a result, basements are often left unfinished, despite the opportunity to upsell the added option, and the job of finishing has historically been left to the homebuyer or renovation contractors. However, more recently, some production builders have adopted strategies and building assemblies to manage their risks for finishing basements, and sell finished basement space as a premium option, passing along the cost of the upgraded assemblies to the homebuyer.

2.2.3 Insulation of Basements

This section addresses the history of the insulation of basement walls, including the timeline of its adoption and the types of assemblies used. The scientific and technical discussion is provided in Chapter 3: Thermal and Moisture Physics of Basements. The following subsections deal with the inclusion of basement insulation in the construction reference literature, and building code references to basement insulation.

2.2.3.1 Historical Overview

Homes built before the 1950's rarely had insulation on below grade walls (Cheple and Huelman 2001). One early appearance of basement wall insulation in the North American technical literature was

Canadian Building Digest 161 (“Moisture and Thermal Considerations in Basement Walls”) (Crocker, 1974). Even at that early date, the building science community noted the need for basement insulation, as stated by Crocker: “The heat loss from the heated but uninsulated basement of an otherwise well-insulated typical frame bungalow may be 25 per cent or more of the total heat loss from the house. There is no question of the value of insulating the walls of a heated basement.” In addition, that document states that insulating on the exterior of the basement has the advantage of reducing condensation risks.

The insulation of basement walls started to be implemented in some volume in the late 1970's and early 1980's, in response to the energy crisis. This was typically seen among lower-volume builders who were emphasizing energy-efficient construction. Canadian studies from 1981 and 1983 indicate that approximately 30% of the surveyed basements were insulated (BETT 1982), which included both new and existing construction.

Basement insulation came into more common use in Canada with the R-2000 program, a program created in 1982 by the Canadian Home Builders’ Association / HUDAC (Housing and Urban Development Association of Canada), to improve energy efficiency in housing. The program guidelines called for full-height basement insulation. The R-2000 program had the effect of “raising the bar” for residential construction, resulting in adoption of many of its improvements into typical construction practices.

2.2.3.2 Structural and Frost Heave Concerns

During the beginning of the implementation of foundation insulation, strong concerns were raised that the addition of insulation would reduce heat loss through basement walls, thus causing problems. Predicted dangers included an increased risk of frost heaving (frost penetration to the footings), adfreezing (adhesion freezing and uplift of buried structures above the frost line), freeze-thaw damage to the structure, and damage due to differential thermal expansion.

To respond to these concerns, a study (BETT 1984) surveyed 157 building officials and approximately one hundred building specialists, to find cases where an insulation retrofit caused or exacerbated basement problems. Potential problem cases were examined in more detail with follow-up interviews and analysis. Problems could not generally be ascribed to the insulation retrofits per se: damage to the structure were caused by issues such as poor exterior drainage (in particular, frost heaving damage), poor detailing of the rim joist space (resulting in condensation), and poor air barrier detailing. No evidence was found that the reduction in heat flux was the cause of this damage.

Pressnail and Timusk (1987) examined the adfreezing issue in more detail; analysis demonstrated that adfreezing is a function of freezing direction or thermal gradient, with problems occurring when the freezing front progressed towards the foundation component. A heated structure—even if insulated—creates a thermal gradient in the opposite direction, eliminating adfreezing risk. In contrast, unheated structures, which do not release heat outwards, can be vulnerable to adfreezing: this is evidenced by adfreezing of foundation piers, porches, and unheated garages.

2.2.3.3 Historical Development of Basement Insulation Assemblies

The building research in the 1980s tended towards examination of exterior basement insulation, including work with manufacturers of rigid fiberglass insulation (Fiberglass Canada), polystyrene foam (Dow), and steel basement system manufacturers (Dofasco).

A snapshot of energy-efficiency building practices from the mid 1980s can be found in the *R-2000 Builders' Manual* (CHBA 1984). Most of the basement wall insulation details show exterior insulation; a detail for preserved wood foundations is also presented. Despite the technical merits and reduced risks of exterior insulation, as found in previous research, the lower costs of interior insulation resulted in the inclusion of a detail. It appears that this detail was added without the extensive research or modeling done on exterior insulation. This detail shows, from exterior to interior: the concrete wall, a "moisture barrier" (shown as polyethylene or some other sheet membrane), fiberglass batt insulation in a wood frame wall, an interior polyethylene air/vapor barrier (AVB), and gypsum board. This assembly limits drying of the freshly placed concrete, as acknowledged by the accompanying text from the Guide: "If this technique is to be used, the foundation should be allowed to cure as much as possible before insulating and sealing."

Further examples of interior basement insulation with two layers of polyethylene (or similar) can be found in several sources. One of the earliest is in Crocker (1974), as shown in Figure 2.6. This document acknowledges that the above-grade and below-grade portions of the wall face different boundary conditions, and should therefore be detailed in different ways. The assembly details, and the logic behind them, are as follows:

- A "moisture barrier" is placed on the concrete wall, from grade level down to the slab, in order to protect the interior finish from moisture sourced from the damp earth. Recommended materials were asphalt emulsion, cutback asphalt, or polyethylene.
- Insulation is only installed from the top of the wall to 1-½ to 2 feet below grade, given that this location has the greatest heat loss (as demonstrated in section 3.2 "Thermal Interaction of the Basement and the Below-Grade Environment").
- An interior vapor barrier is shown on the upper portion of the wall. A layer of polyethylene is not explicitly specified: the document states that the vapor barrier facer on fiberglass batt insulation is adequate (typically Kraft paper).

The influence of this assembly can be seen in modern day details of interior basement insulation, such as the one presented in *The Canadian Homebuilders' Manual* (CHBA 2001), as seen in Figure 2.7. This detail has several important changes: the moisture barrier is explicitly shown as sheet polyethylene (still extending from grade to the floor); the insulation and interior vapor barrier are both full-height; and as a result, the above grade and below grade portions of the wall are treated in the same way.

The Ontario Building Code (1997 Edition, updated 2005) essentially specifies this assembly in Section 9.13 (Dampproofing, Waterproofing and Soil Gas Control). In addition to specifying exterior dampproofing to grade, interior dampproofing is required from the basement floor to grade, "where a separate interior finish is applied to a concrete or unit masonry wall which is in contact with the soil, or

where wood members are applied to such walls for the installation of insulation or finish…" (Section 9.13.3.3. Interior Dampproofing of Walls). It specifies a permeance less than 170 ng/(s·m^2·Pa) or 3 Imperial perms. However, it appears that in practice many interior basements are finished contrary to this code requirement.

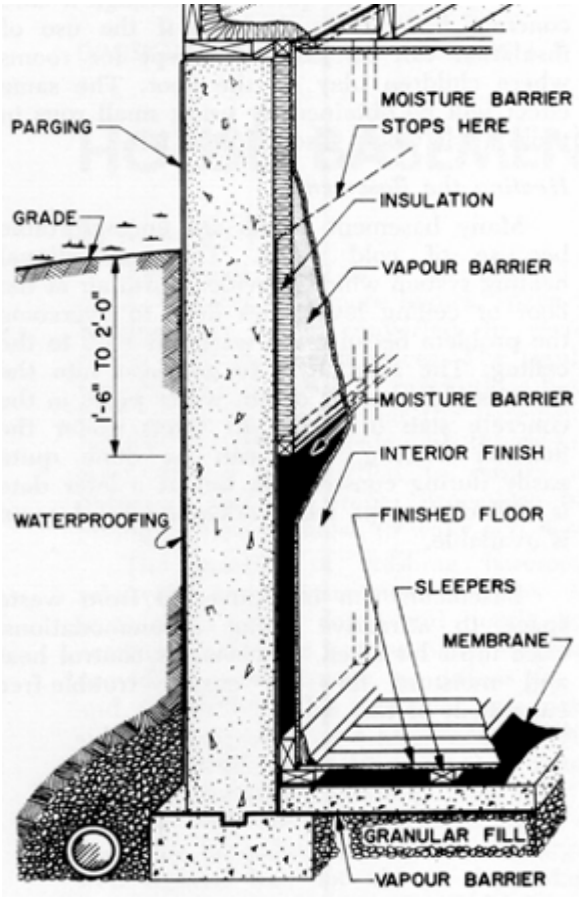

Figure 2.6: Interior basement insulation detail (Crocker 1974)

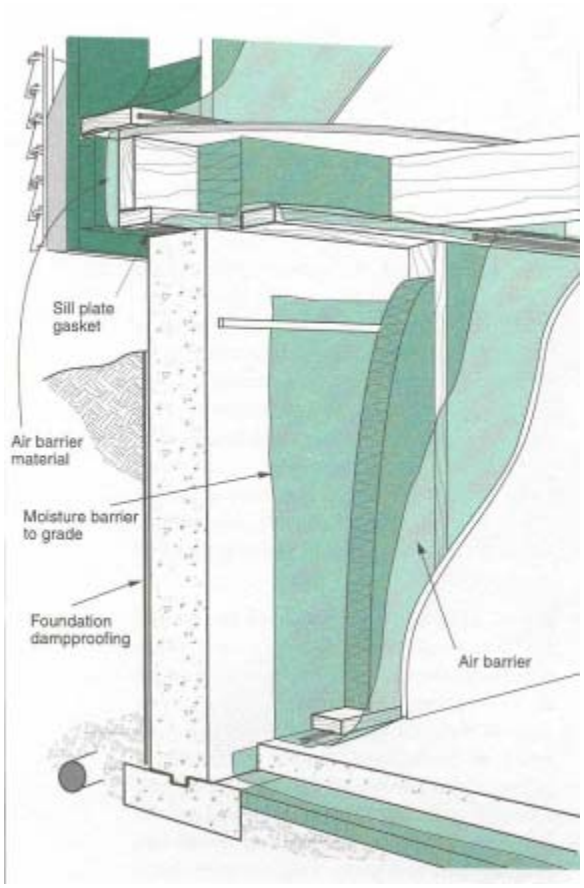

Figure 2.7: Interior basement insulation detail (CHBA 2001)

This detail has been common since the mid 1980s; the building science community initially expressed some wariness due to the limited drying available with impermeable layers on both sides. However, the general consensus was that the limited drying to the exterior in the above grade portion would probably be adequate (Lstiburek 2006).

The state of Minnesota used several iterations of interior basement insulation designs over time. The first variant was a fiberglass batt insulated stud frame wall, with a layer of polyethylene only on the interior as an air and vapor barrier. This version appears to simply transpose a cold-climate above-grade wall assembly to the below-grade space. Problems were seen with this assembly, which had little or no research to support it. Cheple and Huelman (2001) note that there is no scientific literature (with one

exception, detailed later) supporting the installation of interior insulation/finishes without using some moisture protection between the concrete and the insulation.

As a result, an assembly with polyethylene on both sides of the insulated stud frame assembly was adopted; this was basically the adoption of the CHBA detail (Figure 2.7), including the "moisture barrier" run up to grade. This wall was also alternately installed with the "moisture barrier" run up the full height of the wall, which had the net effect of reducing the drying potential of this assembly.

Another common basement insulation system that is currently used is known as a "roll blanket": it is a 1.2 m (4 foot) wide roll of fiberglass insulation with an interior facer (polyethylene, polypropylene, or reinforced foil), and is attached either directly to the concrete or to wooden furring strips. It can be installed either full height (Figure 2.8) or half-height (Figure 2.9). Moisture accumulation problems have occurred with this material; manufacturers have responded by producing a roll blanket with a permeable perforated facer.

Figure 2.8: Roll blanket insulation, full-height

Figure 2.9: Roll blanket insulation, half-height

The unperforated roll blanket is used in Ontario; it appears that it renders the exterior-side "moisture barrier" unnecessary due to the clause: "where a separate interior finish is applied to a concrete or unit masonry wall which is in contact with the soil…" It seems that the interior polyethylene is not deemed to be a "separate interior finish": to wit, its components are not as moisture-vulnerable as wood framing and drywall.

Literature begins to identify several moisture-related failures of interior insulation systems by the mid 1980s, when basements began to be insulated in greater numbers. This was particularly pronounced in the single and double polyethylene assemblies, which are detailed in 3.6.4 and 3.6.5. The physics behind the various failures mentioned above will be examined more closely in Chapter 3: Thermal and Moisture Physics of Basements

2.2.3.4 Construction Reference Literature

Several construction references can be used to gauge the acceptance or market penetration of basement insulation. *Architectural Graphic Standards (Tenth Edition)* (American Institute of Architects 2000)

often reflects the common practice and detailing for a given era. It shows construction details (including waterproofing details) for masonry block and site-cast concrete foundations, as well as details for insulated preserved wood foundations. However, those details in the main portion of the reference do not include insulation of foundations. Details are included later, in Chapter 18 (Energy and Environmental Design) showing external and internal foundation insulation, based on information by the National Research Council of Canada (NRCC) from 1980 onwards.

ASHRAE Handbook of Fundamentals included basement wall insulation details for the first time in the 1997 edition (ASHRAE 1997); no details were provided prior to that date. Those details were adapted from Lstiburek and Carmody (1996).

2.2.3.5 Code Requirements

This discussion is not meant as an exhaustive list of building and energy code requirements for basement insulation, but more of a survey, to understand the degree of acceptance. By 1989-90, several codes were revised to recommend foundation insulation in climates of 1400 or more heating degree days (HDD 18°C, or 2500 HDD 65° F) (Carmody et al. 1991).

In the United States, in general, it appears that the requirement for basement wall insulation varies between states, and even by local jurisdiction. For example, two states that require basement insulation are Minnesota and Wisconsin. The Minnesota code (Chapter 1322 Residential Energy Code, 2006 Draft Version) requires RSI-0.9 to 1.8 (R-5 to R-10 Imperial) basement wall insulation. The Wisconsin Energy Code (Chapter Comm 22 Energy Conservation 2003), Table 22.20 requires basement wall insulation of RSI 1.9 to 3.3 (R-11 to R-19 Imperial), depending on climate zone within the state. In contrast, the adjacent state of Illinois does not require basement insulation.

The Ontario Building Code will transition into a requirement for near full-height basement insulation of R-2.1 (R-12 Imperial) in 2008; the current requirement is for half-height insulation, at a minimum of RSI 1.4 (R-8 Imperial).

The current 2006 International Energy Conservation Code (IECC) (International Code Council 2006) requires basement wall insulation for climates with higher heating loads: insulation is specified for US Department of Energy (DOE) Climate Zones 4-8 (Briggs et al. 2002), or 2000 HDD base 18° C (3600 HDD base 65° F) and higher, as shown in Figure 2.10. This code requires either RSI-1.8 (R-10 Imperial) continuous insulation (e.g., sheet foam or spray foam), or RSI-2.3 (R-13 Imperial) framing cavity (stud bay) insulation.

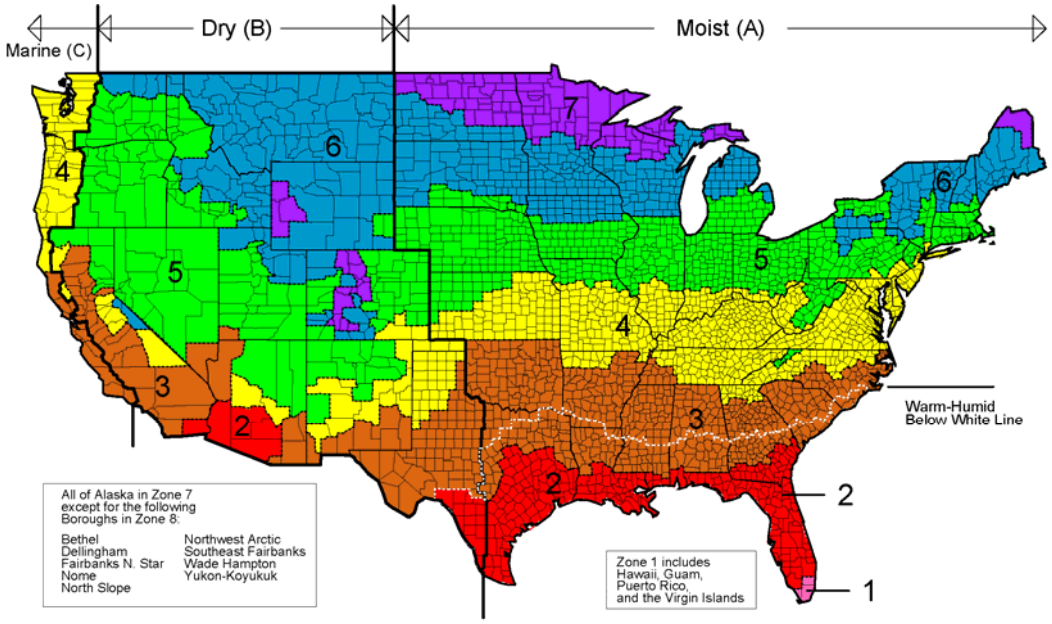

Figure 2.10: DOE Proposed Map of Climate Zones (Briggs et al. 2002)

2.2.3.6 Implications and Conclusions

Overall, the historical record of basement interior insulation assemblies shows a lack of systematic research to support their design; instead, it has been an iterative process responding to failures when they occur in the field. The situation is summarized by several authors below:

> In the last fifteen years, almost every imaginable combination of moisture and energy control has been suggested. Unfortunately, there is a lack of published field research supporting these methods. In short, we don't have a substantial published body of hard experimental evidence indicating which methods work. (Cheple and Huelman 2001)

> Most envelope systems used in Canadian house construction have evolved into present-day practice through a sequence of improvements based on trial and error. When a particular system and its materials become recognized (often marked by a reduction in the overall cost of construction, including cost of 'errors' or call-backs) the approach becomes mainstream practice. (Swinton and Kesik 2005)

> The chief cause of problems is solutions. (Eric Sevareid, American Journalist, 1912-1992)

The consequences of similar future behavior may go beyond further assembly failures in the field—Yost & Lstiburek of Building Science Corporation (2002) provides a warning on the use of some common risk-prone systems:

> Continued use of these approaches by the home building industry will likely lead to a disaster of unprecedented proportions and may result in the construction of energy efficient homes being set back a generation.

As more building energy codes around North America specify basement insulation, an assembly that has a consistent risk of failure will become obvious with its use in a large number of houses. Given this danger, the consequences are dire enough that there is a strong reason to pursue rigorous research in developing more effective interior basement insulation solutions.

Chapter 3
Thermal and Moisture Physics of Basements

The environmental loadings on basement walls provide the boundary conditions that should govern their design. This chapter first examines heat loss from basements, in order to understand the priorities when insulating basement walls. This is followed by an explanation of the temperature and humidity conditions of the below-grade environment, and the interaction between basement walls and this environment. Interior conditions are the other boundary condition for basement walls; a survey of basement data is presented with analysis. The psychrometric relationship between these two boundary conditions is then examined.

Since wetting and drying is the critical parameter for the failure or success of interior basement insulation systems, the next section covers the basics of the various modes of moisture movement and storage, and their relative importance and magnitude.

The remaining sections connect this background information to its implications for basement wall assembly performance and design. The first portion examines historical interior basement insulation failures, connecting them with the relevant moisture phenomena. The final section provides a synthesis of the background material and historical failures, explaining recommended basement details and interior insulation assemblies.

3.1 Heat Loss from Basements

An understanding of heat loss from basements is needed to understand the reasons for basement wall insulation. A thorough treatment of the calculation of below grade heat losses is beyond the scope of this thesis, and is a subject that has been studied at length by many other researchers with substantial field research and mathematical rigor. Deru (2003) provides a review of the relevant literature. There have been many models of ground temperatures coupled with heat loss through foundations; Beausoleil-Morrison (1997) provides an excellent summary of the research to that date. Some models, such as BASECALC (Beausoleil-Morrison & Mitalas 1995), are geared more towards predicting seasonal heat flows for energy modeling. Others (Deru 2002) are three-dimensional finite-element models, and appear to be intended as high-end research tools, requiring detailed inputs of soil conditions.

However, only a basic understanding of heat flow from below-grade structures is necessary to understand the intent of and priorities for basement insulation. Figure 3.1 from *ASHRAE Handbook of Fundamentals* (ASHRAE 2005) shows the path that heat loss from the foundation walls takes through the ground. Heat flows in a radial path from the basement to the surface; the longer the path, the greater the insulation provided by the soil. As a result, in the below grade wall, the greatest heat loss occurs in the upper portions. Figure 3.2 shows calculated heat loss (assuming homogenous soils) from various horizontal bands of the foundation wall from Boileau and Latta (1968); their results show close to 40% of the heat loss occurring in the top 0.3 m (1 foot) of the below-grade portion.

Of course, the greatest heat loss occurs in the above grade portion of the wall, as would be expected by the insulating value provided by the soil.

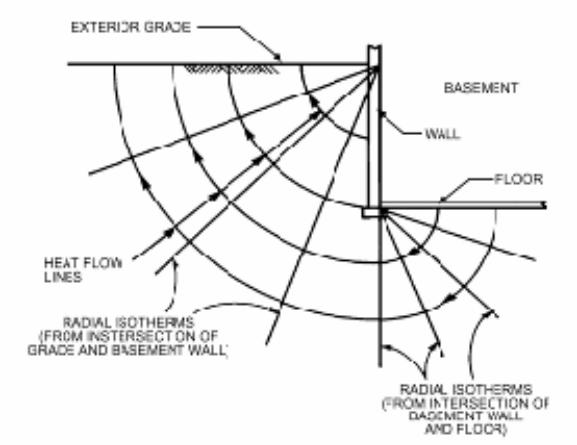

Figure 3.1: Heat flow from below-grade surfaces (ASHRAE 2005)

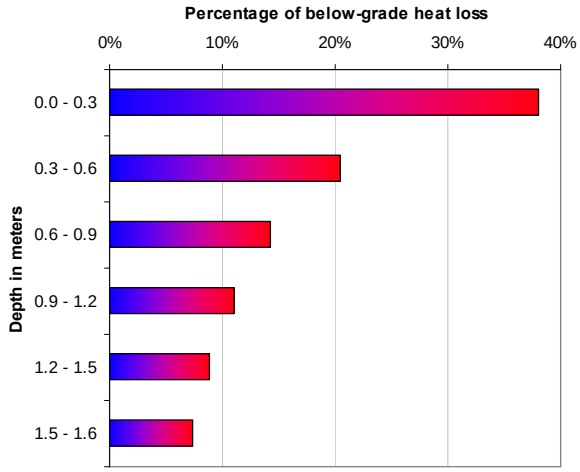

Figure 3.2: Fraction of basement heat loss vs. depth in meters (Boileau and Latta 1968)

Heat losses through the basement have been estimated in the range of 10-30% of a house's total heat loss (BETT 1985, Beausoleil-Morrison 1997, Swinton & Kesik 2005): controlling this heat loss can significantly reduce overall space conditioning energy use. This is especially true in modern energy efficient houses, which reduce the heat loss through the above-grade portion of the enclosure by measures such as better-insulated roofs, windows, walls, and increased airtightness. These measures would therefore increase the relative contribution of an uninsulated basement. This trend was already noted by the mid 1970's (Crocker 1974); some suggested that this weatherization of the above-grade enclosure increases the contribution of an uninsulated basement to 50% of the total heating load (Carmody et al. 1991). Of course, the actual heat loss through the below-grade structure is a function of the local soil conductivity, climate, and interior conditions of the basement.

The R-value of an uninsulated concrete wall is very low: assuming conductivity values of 1.4 to 2.6 W/m·K, a typical 8" thick wall is in the range of RSI 0.08-0.15 (R-0.44 to R-0.82 Imperial). The conductivity of concrete is higher than typical soil conductivities (0.8-0.9 W/m·K), and is comparable to the higher conductivity/wetter soils shown in Figure 3.5. One implication of the high conductivity of concrete is that insulation can have a tremendous effect: a typical code value of RSI 1.8 (R-10 Imperial) is a tenfold increase in insulating value.

A topic often discussed when dealing with foundation insulation is whether it is worthwhile to insulate the full height of the wall. As noted in Figure 3.2, the majority of the heat loss occurs in the upper portion of the wall. A complete study would require an economic analysis of fuel and insulation costs, as well as varying the climate loading; an example of this analysis can be found in BETT (1982). They noted that economic payback was only justified in some climates using half-height insulation. However, some points should be noted: the deep ground temperature in heating-dominated climates will always be below interior setpoint levels (~20° C/68° F). Therefore, the foundation walls will be a heat sink throughout the year. Some point out the benefit of this passive cooling during the summer. There is a benefit to this free cooling in warm weather; however, an examination of the economics of heating vs. cooling in a heating-dominated climate shows that the heating costs dominate strongly.

One final concern is the effect of bulk movement of water through soil on foundation thermal losses. Hagentoft and Claesson (2006) note that previous research has shown that horizontally flowing groundwater has a minimal role in heat losses. Their current research shows that vertical percolation of precipitation through soil has a negligible effect on basement heat loss, assuming regular precipitation levels and permeable soils. However, the same cannot be said for bulk water (misdirected from drainage), as opposed to percolation through the soil. For instance, a roof downspout connected to the foundation footing drains can cause a notable increase in basement heat loss during the heating season (BETT 1982), although this effect is ameliorated by the installation of basement insulation.

3.2 The Below Grade Environment

3.2.1 Ground Temperature Behavior

The temperature of the ground varies with depth and with time: the temperature distribution is due to the periodic variation of seasonal temperatures and the thermal mass of soil. The surface is roughly in equilibrium with seasonal air temperature, while the deep ground temperature is approximately constant. The depth at constant temperature is a function of variables such as the annual climate swing and the thermal diffusivity (ratio of thermal conductivity and volumetric heat capacity) of the soil. This deep ground temperature is typically 2-6° C above the mean annual air temperature (Hutcheon and Handegord 1995).

Shallow depths exhibit greater seasonal temperature variations, while greater depths exhibit a smaller seasonal amplitude swing. Although the surface of the soil shows diurnal temperature swings, these variations are damped out at shallow depths, on the order of 0.3 m (1 foot).

In addition, as depth increases, temperatures show a phase shift: for example, at a depth of 8 m, ground temperatures are highest during the coldest air temperatures (January-February). As another example, the temperature at 1.6 m (5.3 feet) only reaches its minimum in early spring (April), even though the minimum air temperature occurs two months earlier. The resulting temperature distributions with depth are presented in two forms in Figure 3.3 (Ottawa, ON, from Hutcheon and Handegord 1995) and Figure 3.4 (St. Paul, MN, from Bligh 1975). Both of these plots are for ground in open fields undisturbed by heat loss from a basement.

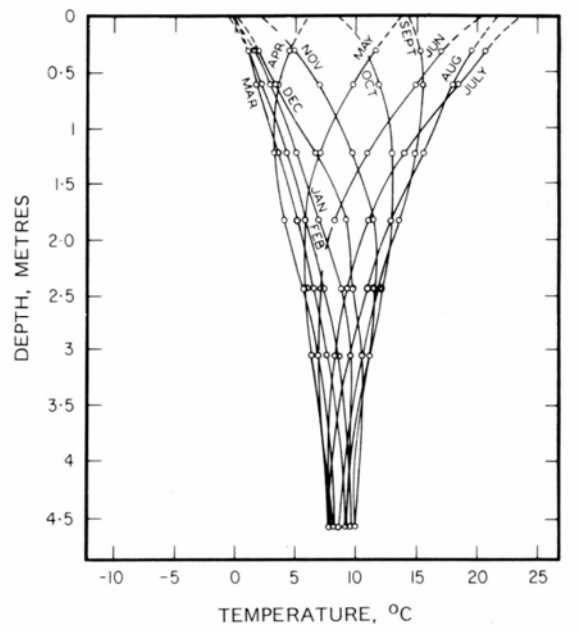

Figure 3.3: Monthly ground temperatures, Ottawa, ON (Hutcheon and Handegord 1995)

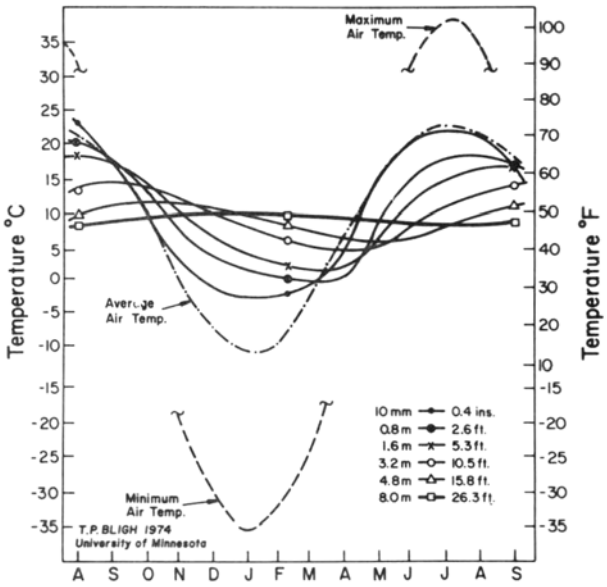

Figure 3.4: Monthly temperature variation with soil depth, St. Paul, MN (Bligh 1975)

3.2.2 Soil Thermal and Moisture Properties

The thermal conductivity of soil is a strong function of its moisture content: going from dry soil to saturated soil can increase conductivity by a factor of ten (Deru 2002). This increase is due to greater thermal contact between grains due to the adsorbed moisture layer, the presence of a conducting continuous liquid phase (at high moisture contents), and latent heat transfer via evaporation-condensation cycles. Other soil properties are functions of moisture content as well: going from dry to wet soil can triple the heat capacity value.

Soil thermal conductivity is also a function of the soil characteristics, such as the proportion of sand, soil, clay, and organic components. However, in practice, the characteristics of soil at a given site or building are seldom available as inputs for the calculation of heat flows around foundations. Therefore, a rigorous analysis of soil conductivity is not warranted: instead, a survey of the typical range of conductivity values is presented.

A wide range of conductivity values is found in ASHRAE (2005) (see Figure 3.5): the drier range is ~0.5-1.2 W/m·K, and some saturated soils have conductivity values up to 2.8 W/m·K. Various sources provide some guidance on expected or typical soil conductivities. Straube and Burnett (2005) give values for earth, dry to damp, of 0.8 to 2.0 W/m·K. The software package BASECALC (Beausoleil-Morrison 1995) gives default values for "normal," "high conductivity (wet)," and "permafrost" soils. The "normal" values are 0.80 W/m·K above the basement slab (presumably lower density, excavated and backfilled), and 0.90 W/m·K below the slab (presumably higher density and undisturbed).

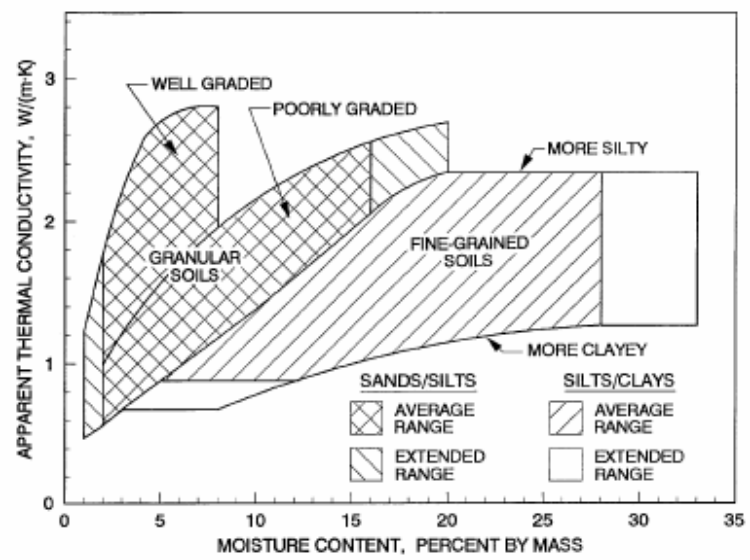

Figure 3.5: Apparent thermal conductivity vs. moisture content for various soils (ASHRAE 2005)

In almost all cases, the soil, and therefore the exterior boundary condition of a foundation wall, will be at 100% relative humidity. This is stated in works on heat and moisture transfer in soils (DeVries 1975), as well as design recommendations for basements (Crocker 1974).

This 100% RH boundary condition is corroborated by the basics of soil moisture content measurement. In the agricultural sciences, soil water dynamics are expressed in the term 'water potential' (Ψ), using units of pressure (e.g., bar, mm of water head, Pascals). One form of water potential is the matric potential, Ψ_M, or suction pressure, which expresses how strongly water is drawn into soil. This measurement can be related to the soil moisture content (although it varies with soil type).

As a point of information, total water potential Ψ_T is the sum of pressure potential (Ψ_P), matric potential (Ψ_M, or suction pressure/capillary suction), solute potential (Ψ_S, caused by a solute concentration gradient), gravitational or head potential (Ψ_Z), and any other potentials operating in the system (e.g., electrical, temperature).

Free water has a zero matric potential; it is in equilibrium with saturated soil (at 0 bar), and will not be drawn into that soil. However, free water has a higher potential than unsaturated soil, and will therefore be drawn up by soil in that condition. Matric potential ranges with respective soil conditions are shown below in Table 3.1

Table 3.1: Soil matric potentials and moisture conditions

Measurement	Soil Condition (from wetter to drier)
0.0 bar	Soil is saturated
0.0 to –0.33 bar	Free water drainage (-0.33 = "field capacity")
-0.33 to –15 bar	"Available water" (plants can obtain water from soil)
-0.6 bar	Typical boundary condition for making decision to irrigate soil
-15 bar	"Wilt point" (plants can no longer extract water from soil)
-31 bar	Air dry state for soil with air at 100% RH
-10,000 bar	Oven dried soil

Some of these conditions require more detailed explanation: saturation is the filling of all free pores in the soil. Soil that has been saturated and allowed to drain in air (so that water is only held in by surface tension) is at its "field capacity," so any measurement of –0.33 bar or lower indicates that the soil is free-draining. At the "wilt point," plants can no longer extract adequate water from the soil to remain turgid. Finally, the "air dry" state of soil (only hygroscopically bound water) is in equilibrium with a 100% RH environment.

These values show that the soil is at 100% RH at any condition of –31 bar or higher. Given that plants often grow around foundations (requiring a much higher moisture content of –15 bar), it implies that in almost all cases, the soil will be at 100% RH.

The Kelvin equation provides similar information: this equation relates the reduction in vapor pressure over a curved meniscus. By using the Kelvin equation on water (treating it as an ideal gas), a relationship can be drawn between suction pressure (equivalent to matric potential) and the relative humidity, as done in Rose (2005):

$$\ln \phi = \frac{P}{\rho_w R_w T} \qquad \text{(Eq. 3.1)}$$

where ϕ is the relative humidity

P is the suction pressure

ρ_w is the density of water

R_w is the ideal gas constant for water vapor, and

T is the absolute temperature

The resulting values are shown in Table 3.2, which demonstrates that even at the noticeably dry condition of the "wilt point" (-15 bar), the relative humidity of the soil is approximately 99%. These results do not exactly match the table values (of –31 bar = 100% RH), coming closer to 98% RH instead. However, given the difficulty and uncertainty of measuring extremely high relative humidity levels (~99%), and the asymptotic behavior shown in the Kelvin equation when approaching 100% RH, this correspondence seems reasonable.

Table 3.2: Relationship between relative humidity and suction pressure values (Rose 2005)

RH (%)	Atmospheres	MPa	bar
20	2167.0	221.0	2210.0
50	933.3	95.2	951.8
80	300.4	30.6	306.4
90	141.9	14.5	144.7
95	69.1	7.0	70.5
98	27.2	2.8	27.7
99	13.5	1.4	13.8
99.9	1.3	0.1	1.4
99.99	0.14	0.01	0.14
99.999	0.013	0.001	0.013

3.3 Basement Interior Temperature and Humidity Conditions

The interior temperature and humidity conditions of the basement space provide the interior boundary conditions for basement walls and insulated assemblies. A rigorous treatment of interior humidity design loads are beyond the scope of this thesis: TenWolde and Walker (2001) demonstrate a methodology to generate interior humidity levels based on climate, interior loads, ventilation, and other variables.

Building Science Corporation collected data from 1997 through 1998 on nine houses in the Chicago area: they were new energy-efficient (US EPA/DOE Energy Star level) construction: one and two-story, single family detached houses of 1340 to 3240 square feet. The houses were built on either full basements, or partial basements attached to conditioned and insulated crawl spaces. The four houses at the Grayslake, IL subdivision had insulated basements (full-height vinyl-faced fiberglass blankets), while the five houses in Vernon Hills, IL, had uninsulated basements. Blower door testing on the houses showed an average airtightness of 2.7 ACH 50 (air changes per hour at 50 Pa test pressure), ranging from 2.0 to 3.5 ACH 50 (i.e., relatively airtight construction).

Monitored data included:

- Air temperature and humidity of the central return of the HVAC system (hourly averages)
- Air temperature of the basement (hourly averages)
- Hourly runtime fraction of the heating, cooling, and domestic hot water systems

This data was examined to provide some insight on temperature conditions of the basement space, relative to the above-grade space; other information can be gleaned from the monitored data as well. For instance, although the relative humidity of the basement was not directly monitored, a hypothetical humidity can be calculated, assuming that the above-grade and below-grade air is well mixed and at the same dewpoint. Furthermore, temperature and dewpoint conditions were compared with hourly weather data collected from the Argonne National Laboratories weather station.

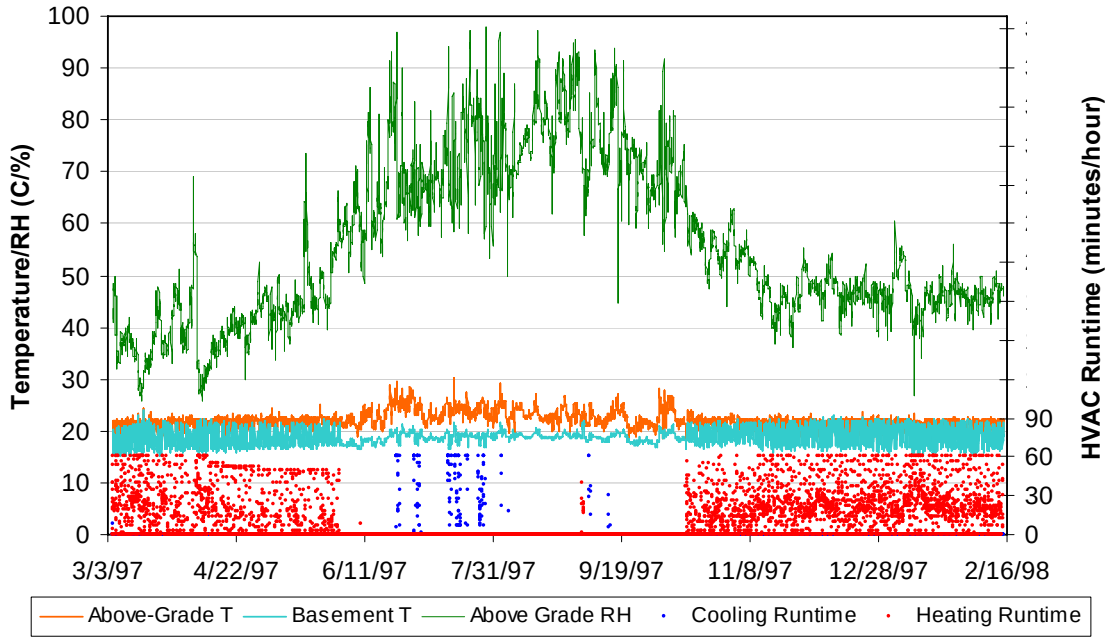

Figure 3.6: Monitored data for a Grayslake, IL development house

The house in Figure 3.6 demonstrates some patterns that are typical in the monitored data. The basement ran consistently cooler than above-grade setpoint, with an average difference of roughly 3° C in the wintertime, and 4.5° C in the summertime. The homeowner only used the cooling system intermittently in the summertime, resulting in relatively high above-grade temperatures (often 25-30° C). This implies that windows were typically operated for cooling, which would result in similar interior and exterior dewpoints. Summertime relative humidity was typically in the 60-90% range; wintertime humidity was 30-50% during the first winter (1997) and 40-50% in the second winter. The above-grade and basement temperatures are relatively stable during the summer, but there is substantially greater inter-hour swing during the seasons when the heating system is run.

In surveying the other Grayslake, IL houses, they also show lower temperatures in the basements than in the above-grade space. In the wintertime, this difference is on the order of 2-3° C, and in summertime, 2.5-4.5° C. The uninsulated basement houses in Vernon Hills, IL had wintertime differences of 3-5° C, and summertime differences of 2.5-5° C. Although there are many variables in determining the relationship between the temperatures of the two spaces, including setpoint, use of the HVAC system, number of basement HVAC registers, etc., it is seen that the uninsulated basements showed notably colder temperatures, on average, than the insulated basements, in the winter (with a higher indoor-outdoor ΔT). Overall, basement temperatures are in the 18-22° C range in the summer, and 16-21° C range in the winter in the Grayslake houses. In the Vernon Hills houses, summertime temperatures are 19-22° C, and wintertime temperatures are 16-19° C.

The interior dewpoint (from the above-grade HVAC return) was graphed with the exterior dewpoint, to determine correspondence, if any (Figure 3.7 and Figure 3.8). Note that the Vernon Hills, IL data only covers a limited period.

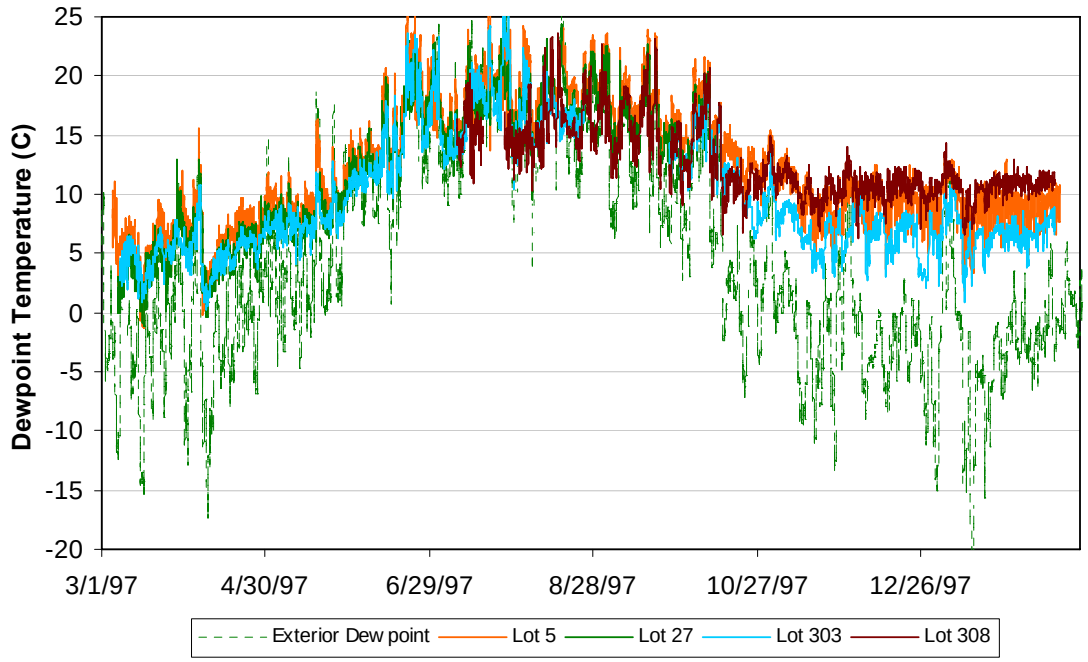

Figure 3.7: Grayslake, IL interior and exterior dewpoints

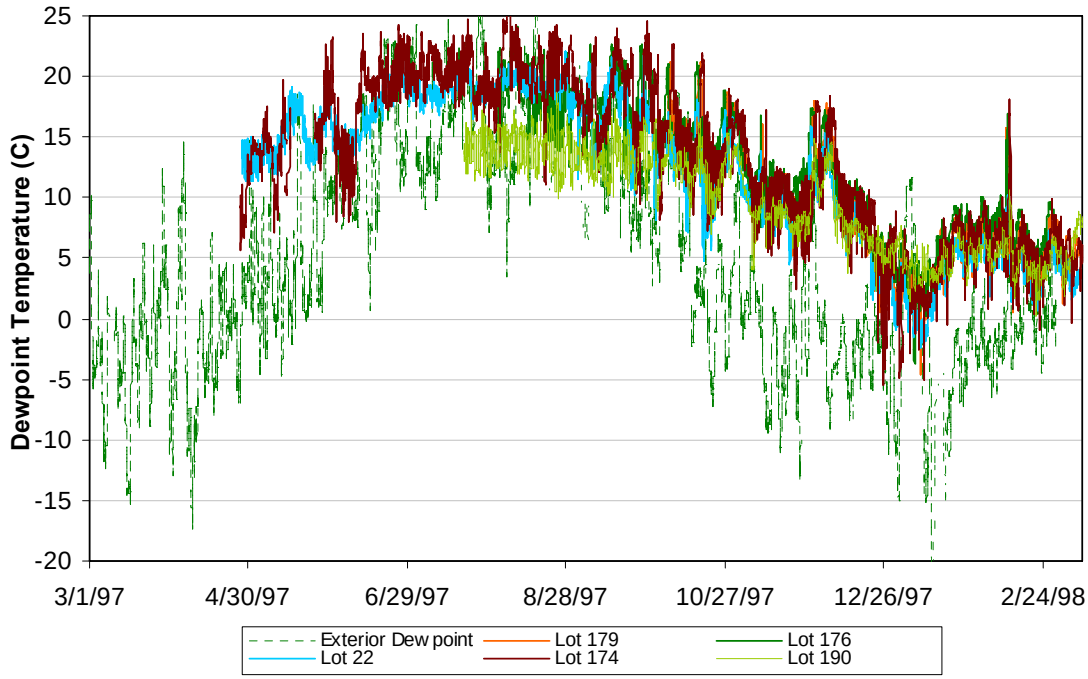

Figure 3.8: Vernon Hills, IL interior and exterior dewpoints

Several points of interest are found in this data. First, the summertime interior dewpoint is almost identical to exterior, with one exception (Vernon Hills Lot 190). This shows (as confirmed by the HVAC

system runtime data) that the use of ventilation and windows is dominant among these houses for summertime cooling. The exception (Lot 190) shows consistent use of the cooling system over the summer, resulting in interior dehumidification.

In the winter, interior dewpoints are largely in the 0-10° C range in the Vernon Hills houses, averaging 5° C. Assuming a typical interior temperature of 20° C, this is a relative humidity of under 40%. In contrast, in the interior dewpoints are higher in the Grayslake houses, typically in the 5-12° C range. The highest dewpoint (Lot 308) has an interior relative humidity consistently running at 50%: this clearly shows the use of a humidifier.

This information provides some indication of interior humidity levels, but does not show the basement dewpoint in a definitive manner. However, if the above-grade and basement dewpoint are assumed to be equal (i.e., well-mixed air in the house), a relative humidity can be calculated. If these values are used, very high humidities are found in many of these basements during the summer: from 90% RH to above saturation. It is not known whether these high humidities are actually occurring: it is quite possible that mixing between the spaces is low, and/or the concrete is adsorbing moisture and thus lowering humidity levels. But it does raise the possibility that some of the high humidity linked with basements might be a function of high summer dewpoints combined with the low temperatures of basements.

In addition to the BSC data, a 50-house cross-Canada study completed by Ruest (1993) examined the relationship of basement and above-grade interior conditions. Temperature and humidity were measured in the basement and the above grade space, at a single visit in the winter, in houses across five provinces (British Columbia, Manitoba, Nova Scotia, Ontario, and Quebec). The temperatures of the two spaces are plotted against each other in Figure 3.9.

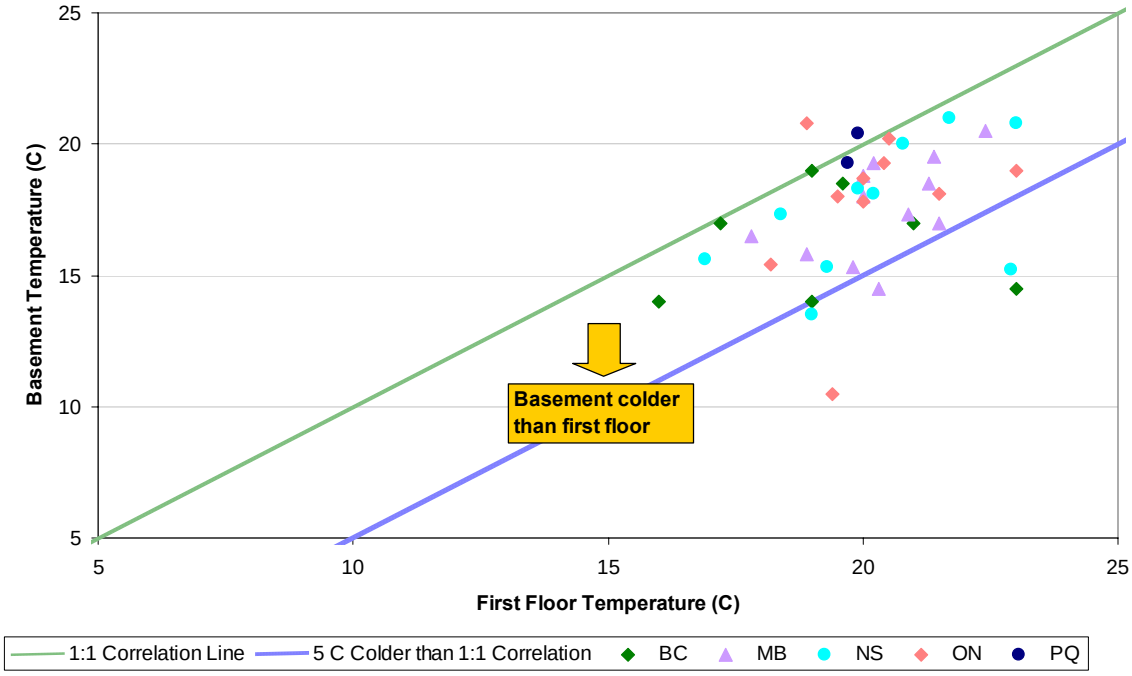

Figure 3.9: Interior above-grade and basement temperature conditions (Ruest 1993)

Two lines are superimposed on the plot for reference: 1:1 correspondence (identical temperatures above grade and in the basement), and basement 5° C colder than 1:1. The data clearly shows that basements are typically colder than above grade, and that most measurements fall within 5° C of above-grade temperature. There is no clear pattern discerning the data from the various provinces.

The dewpoint temperatures were plotted against each other in a similar manner, in Figure 3.10; a 1:1 correspondence line is plotted on that graph. The figure is set up so that basements drier than the first floor are below this correspondence line.

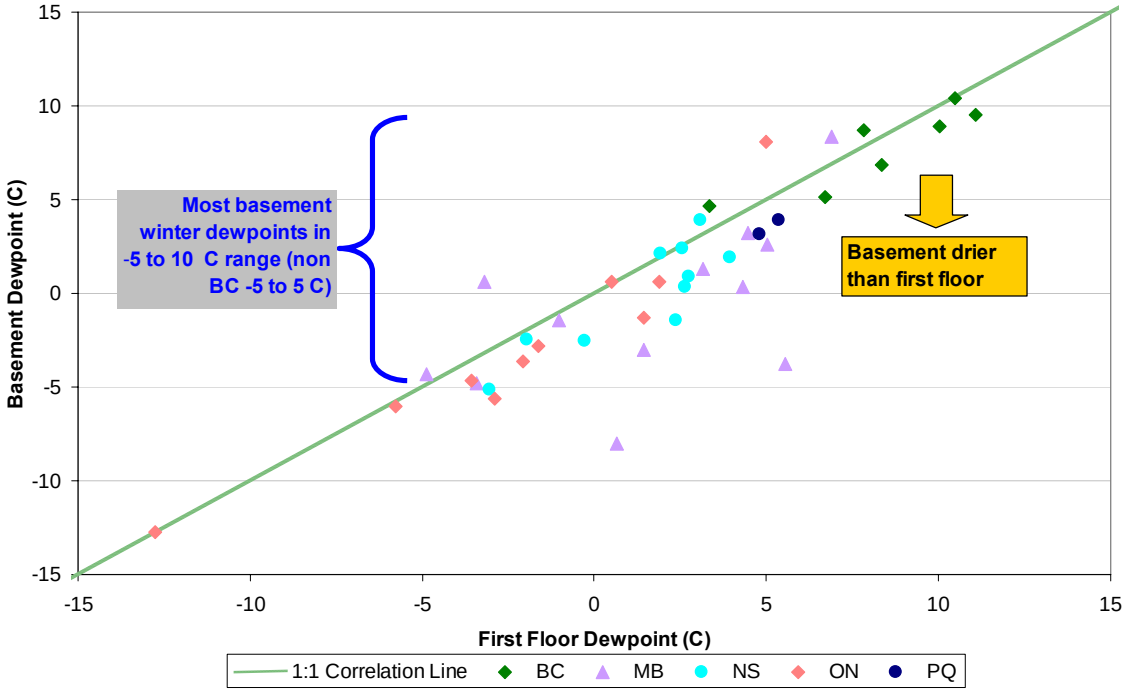

Figure 3.10: Interior above-grade and basement dewpoint conditions (Ruest 1993)

Interior dewpoints are mostly in the –5 to 10° C range (both above and below grade); one noticeable pattern is that if the BC houses are omitted, most of the data is in –5 to 5° C range. This reflects the marine climate of BC, which is mild and at a relatively high humidity (higher exterior wintertime temperatures result in higher exterior dewpoints).

Second, basement dewpoints are usually close to above-grade conditions, but typically slightly drier. This might seem odd, given the reputation basements have for dampness. However, this can be explained by normal house operation and construction. Wintertime stack effect will tend to draw air into the house from the lower portions, and it will leave at the upper portions (ceiling/roof). The rim joist and sill plate-to-foundation wall intersection are normally leaky locations, so air will be drawn first into the house at that location, into the basement. Therefore, the basement will have the highest ventilation rate with cold dry air, and a minimal interior generation rate; therefore, in wintertime, it will have a lower dewpoint than above grade.

The critical parameters of these two studies are summarized in Table 3.3 below.

Table 3.3: Summary of interior temperature & humidity surveys

	Above grade/ basement ΔT	Wintertime interior dewpoint	Summertime interior dewpoint
Grayslake, IL	2-3° C winter 2.5-4.5° C summer	5-12° C	12-23° C
Vernon Hills, IL	3-5° C winter 2.5-5° C summer	0-10° C	12-23° C
Ruest Cross-Canada, BC	0-5° C winter	5-10° C	n/a
Ruest Cross-Canada, non-BC	0-5° C winter	-5-5° C	n/a

3.4 Psychrometric Relationship of Boundary Conditions

Given the interior and exterior temperature and humidity boundary conditions described above, their relationship can be summarized on a psychrometric chart (see Figure 3.11).

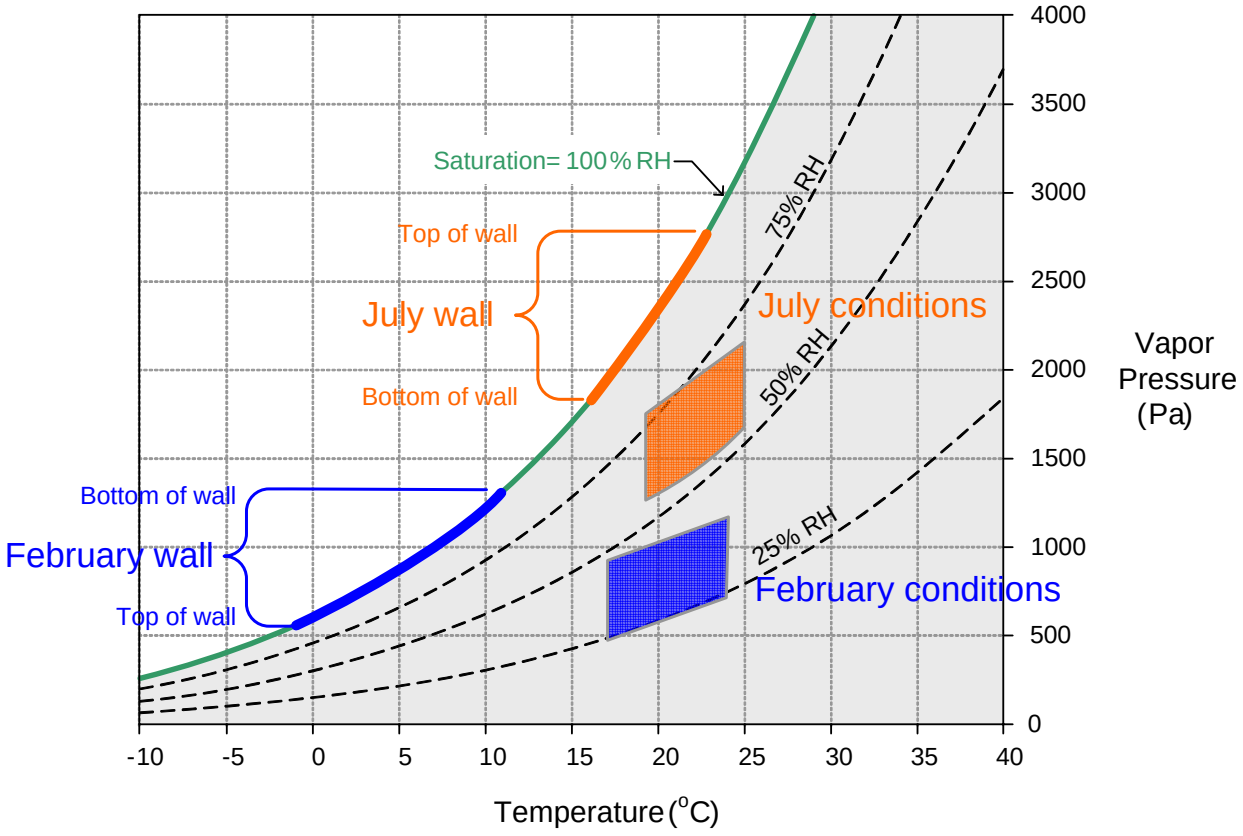

Figure 3.11: Psychrometric relationships of basement wall boundary conditions

The psychrometric chart shows dry bulb temperature (in °C) on the horizontal axis, and the absolute moisture content of air (in vapor pressure, Pa) on the vertical axis. Typical indoor and outdoor below grade (soil) conditions for winter and summer in a heating-dominated climate are shown on the chart.

Specific values would depend on local climate, indoor conditions, and soil properties: this graphic is meant to show some of the general psychrometric relationships.

Some typical conditions for interior air in winter (February) and summer (July) are shown: obviously, February is colder and at a lower relative humidity (i.e., following the general pattern of exterior dewpoint). The conditions of the soil adjacent to the foundation are shown along the saturation (100% RH) line, given soil moisture conditions discussed in Section 3.2.2. The soil temperatures are colder in February than in July: the top of the wall is coldest in winter, and the warmest in summer.

With this presentation, it is simple to determine the available drying direction based on vertical position of boundary conditions, which reflect the absolute moisture content of the air. It demonstrates that the water vapor drive is always inwards except at top of wall in winter, depending on relative humidity of interior.

The interior relative humidity could be raised enough to cause an outwards gradient, where the air would wet the wall, in either season. For instance, increasing interior humidity to 50% in winter while maintaining the same dry bulb temperature range would increase the outwards drive at the top of the wall, and the air and the wall would be roughly in equilibrium at the bottom of the wall. However, this condition would require continual winter humidification, and could be considered an unreasonable loading for normal construction practice, as it would likely result in visible window condensation.

If the interior humidity in the summer is raised, the drying direction will still mostly be inwards (i.e., interior air dries the wall), except at the bottom of the wall. The results of this set of conditions are described in section 3.6.1.

3.5 Moisture Transport in the Foundation Environment

Most failures of interior basement insulation systems are due to the movement and accumulation of moisture in the system. Therefore, an understanding of the relevant modes of moisture transportation is needed to determine risks and appropriate countermeasures when designing these assemblies.

The modes of moisture transportation examined here, in rough order of significance, are bulk water flow, capillarity, air-transported moisture, and vapor diffusion. Capillarity and vapor diffusion are interrelated portions of moisture transport in porous media, and are dealt with in greater detail in Kunzel (1995) and Straube & Burnett (2005). This is followed by a comparison of selected moisture transport mechanisms, and a discussion of moisture storage in porous media (specifically concrete).

3.5.1 Bulk Water Flow

The intrusion of bulk liquid water is typically the transport mechanism with the highest deposition rate. Almost limitless volumes of water can be provided in the worst case: in basements, catastrophic floods from exterior or interior sources are bulk water events. Bulk water can cause damage to interior finishes and insulation systems, mold and microbial growth, high humidity levels, and if visible, will be immediately viewed by the occupants as a failure. The major sources include groundwater, precipitation/surface sourced moisture, and interior leaks.

The level of the groundwater table varies with topography, soil drainage characteristics, and season (typically highest in late fall or early spring due to precipitation peaks). Residential basements are typically constructed with perimeter drainage, such as French drains or weeping tile, placed in granular drainage material at the level of the footings. These sub-surface drains act to locally reduce the water table to their level. This collected water must be drained to daylight (i.e., to exterior at a lower level than the footing), or otherwise collected to a sump and pumped out. If these drainage mechanisms are not in place, the foundation system will need to resist hydrostatic head of accumulated water—a very risky proposition.

Precipitation, or surface sourced moisture, is a common and significant moisture loading for basement walls. Bulk water leaks due to surface moisture can often be diagnosed by their correlation in time with rain events. Note that this moisture can take many paths, including some that will not be immediately obvious, as shown in Figure 3.12. However, the clear recommendation is to redirect runoff water concentrated by the roof away from the house, and to shed water away from the building on the ground with proper grading.

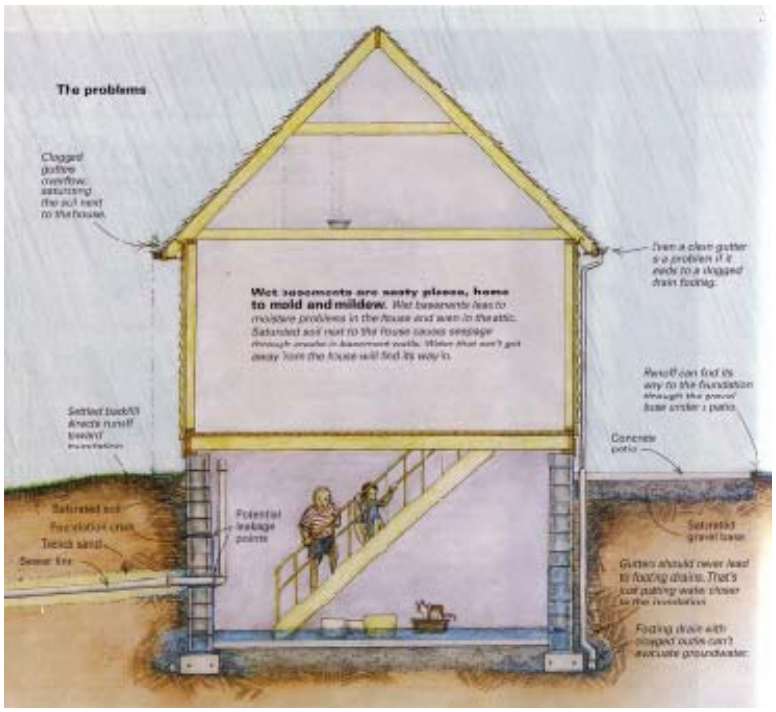

Figure 3.12: Common bulk water problems for basements (Rose 1997)

Many sources (Crocker 1974, CMHC 1992, Rose 1997) list common moisture paths linked to surface/precipitation water, such as:

- Improper grading: backfill is often inadequately compacted; settling over time redirects surface water towards the house.
- Lack of, disconnected, or inadequate eavestroughs and downspouts: this system is designed to redirect concentrated runoff water from the roof away from the house; an inadequate system will deposit this concentrated water adjacent to the foundation.

- Missing or clogged footing drains: as mentioned above, this system drains water from the base of the foundation, preventing buildup of hydrostatic head against the foundation wall. In addition, connecting the downspouts to the footing drain system adds an exceptionally large load at a very vulnerable point.
- Window wells: clogged or improperly constructed window wells will collect bulk water and direct it towards the foundation.
- Snowmelt water: collected snow adjacent to the house will create a significant loading during spring melts.
- Subsurface paths: an impermeable surface adjacent to the house, such as a patio, walkway, or driveway, can direct water away from the house on the surface, but allow it to travel towards the foundation if the underlying gravel bed is not graded or drained correctly.
- Service trenches: pipes and conduits are typically buried in free draining sand or gravel; this can provide a path for precipitation water to accumulate and enter the basement at the service penetration.
- Cracks in foundation walls: macroscopic cracks, cold joints, and penetrations through cast concrete or concrete block walls will often provide entry points for bulk water if it is present in the adjacent soil.

Interior flooding from sources such as plumbing leaks warrant little mention, due to their obvious cause and solution. But anecdotal information from the insurance industry suggests basement floods are very common: on the order of 50% of basements flooding to a depth of 25 mm (1 inch) over their lifetime. The likelihood of these failures provides a reason to recommend details that keep moisture-sensitive materials and finishes away from floor level.

The importance of controlling bulk water is demonstrated by the results of a 1996 CMHC study of mold in finished basements. The survey of approximately 400 basements showed that moisture problems were linked more with bulk water issues rather than issues related to interior relative humidity levels or specific wall finishing practices. These problems included items mentioned above, such as incorrect downspout location, window well flooding, cracks/leaks in the foundation, plumbing leaks, and grading problems. Similar results were found in a smaller, 42-house study in Minnesota (Robert Anderson & Associates 1989).

There are strong secondary reasons to reduce the saturation of the soil adjacent to the foundation, in addition to the risk of bulk water leakage. The presence of liquid water in the soil in contact with the foundation wall increases moisture available for subsequent transport by capillarity and vapor diffusion (see below). Furthermore, as mentioned in Section 3.2.2, dry soil is less thermally conductive. Finally, frost heave damage requires both freezing conditions and saturated soils; eliminating the saturated soils close to the foundation minimizes this risk.

3.5.2 Capillarity/Liquid Transport

To investigate capillarity as a moisture transport mechanism in the foundation system, it is necessary to define the topic more precisely. Capillary suction is the force that draws liquid water, on a macroscopic

scale, into cracks and openings (e.g., water wicking upwards into the overlap of clapboard siding), or on a microscopic scale, into porous materials (e.g., a brick in contact with water). The suction force is inversely proportional to the size (or average size) of the opening or pore. As will be discussed below, liquid absorption into porous materials can provide a high rate of moisture transport.

Note that capillarity through macroscopic cracks is not the focus of this section: visible "weeping" of cracks of this type is water flow driven by gravity (which overpowers capillarity in cracks once their width exceeds about 0.1 mm) and hence would be grouped with bulk water flow, for the purpose of this discussion.

Capillary flow is liquid water driven by differences in suction pressure, while vapor diffusion is the movement of free water vapor molecules driven by differences in vapor pressure. Within a porous material such as concrete, both mechanisms can be acting simultaneously, often when the material is at high moisture contents. A third mechanism, adsorbed flow or surface diffusion, drives adsorbed water from high RH to low RH within a material. The complex interaction of these three mechanisms explains why the apparent vapor permeance of porous materials (such as concrete or wood) increases at higher RH (which is equivalent to higher moisture contents).

The mathematical relationships describing capillary flow are complicated, given that there are multiple processes are acting in parallel and in series. Water flow through fully saturated porous media is described reasonably well by Darcy's law, in which the flow is a function of hydraulic conductivity (a material property that is in turn a function of temperature, due to its effect on the viscosity of water), and the pressure gradient. However, in reality, the pores of a material are seldom completely filled with water, so it must be described as unsaturated flow. As a result, empirical measurements are used, describing the water uptake of an initially dry material with a simplified form of Darcy's equation (as described in Straube and Burnett 2005)

$$m_w = A \cdot \sqrt{t} \qquad \text{(Eq. 3.2)}$$

where m_w is the mass of the water absorbed per unit area (kg/m^2)

A is the water absorption coefficient ($kg/m^2\ s^{0.5}$ or $kg/m^2\ hr^{0.5}$), and

t is time (s or hr)

Note that capillary condensation will occur within small pores in environments with relative humidity levels below 100%, as quantified by the Kelvin equation. However, these mechanisms are not significant to flow in basements, and hence are not the focus of this section.

One example of capillary flow is the transport of groundwater from soil via the foundation footing and through the wall (see Figure 3.13). The footing is cast on compacted soil, as opposed to free-draining fill, and the bottom of the footing is typically below the level of the perimeter drain. Therefore, any liquid water present in the drainage system will be in capillary contact with the footing. Even if the soil were not saturated, if the suction pressure in the concrete is less than that of the soil, moisture will flow from the soil to the concrete. Moisture in the wall can then be transported to the interior space, assuming evaporation occurs at that surface.

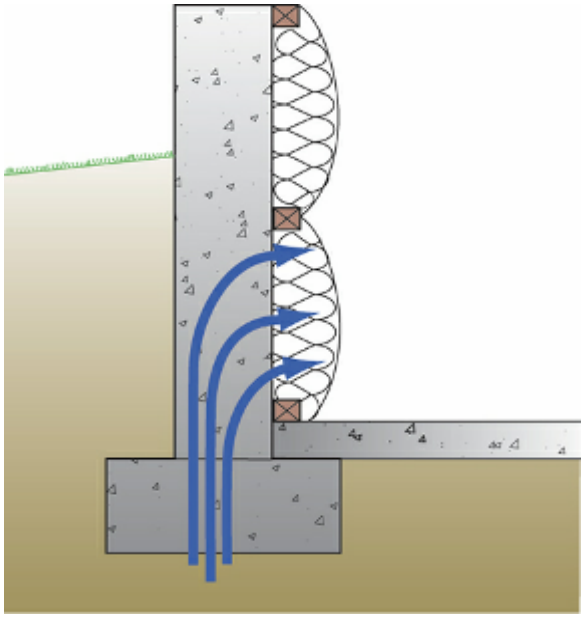

Figure 3.13: Path of capillary rise through footing (Lstiburek 2006)

3.5.3 Air Transported Moisture

Air can carry sufficient water (in vapor form) that movement of air can be a substantial source of moisture transport. Air movement occurs in building applications driven by pressure differences caused by natural forces (stack effect, wind, convective looping in cavities), and/or mechanical systems (pressurization or depressurization by HVAC systems).

The rate of moisture transported by air movement is a function of the airflow rate, and the moisture level of that air:

$$m_W = \frac{M_W}{A} = \rho_{air} \cdot W \cdot Q_{air} \qquad \text{(Eq. 3.3)}$$

where m_W is the rate of water vapor advection (kg/s),

W is the humidity ratio (kg water vapor to kg or air), and

Q_{air} is the volumetric flow rate of the air (m^3/s).

One example of air-transported moisture in basements would be the movement of 100% relative humidity air from the subslab gravel field into the basement due to stack effect. Another would be leakage of interior air into the insulation cavity; both examples are illustrated in Figure 3.14.

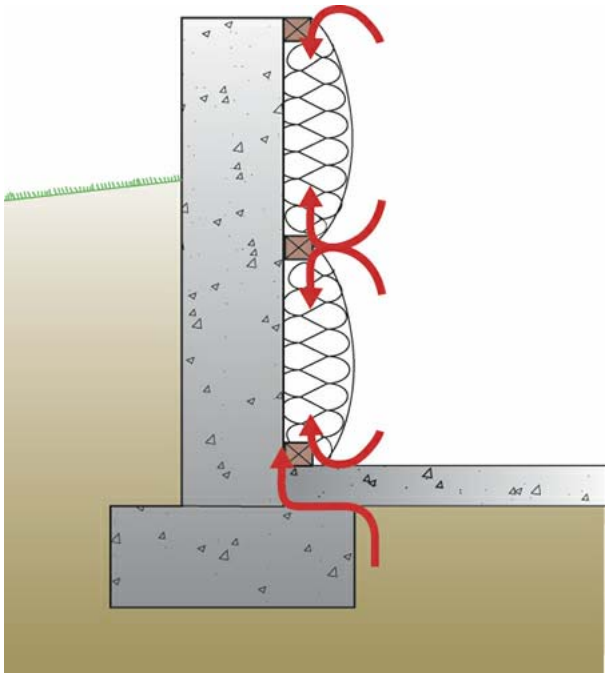

Figure 3.14: Examples of air transported moisture in basements (Lstiburek 2006)

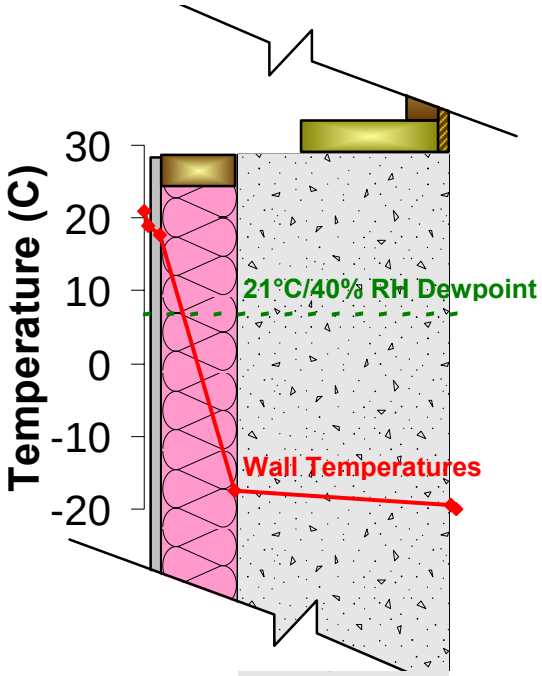

Figure 3.15: Condensation potentials in an insulated basement wall (above-grade portion)

The mechanism of interstitial condensation (i.e., condensation within the assembly cavity) via air leakage is demonstrated in Figure 3.15. Assuming indoor and outdoor temperatures of 21° C and –20° C, respectively, the temperature distribution through the wall is roughly as shown in the illustration. The majority of the temperature drop occurs across the insulation; therefore, the concrete-insulation interface is at a cold temperature (-19.5° C, close to exterior).

Interior air conditions of 21° C and 40% relative humidity have a dewpoint temperature of 7° C (as shown in the figure by the green dashed line). The concrete-insulation interface is below the dewpoint of this air, so a leak of interior air into the cavity would result in condensation at the interface.

Note that this type of condensation could be caused by either air transported moisture or vapor diffusion. One key point of interest is a comparison of the transport rate of these two mechanisms, as detailed in Section 3.5.5.1.

3.5.4 Vapor Diffusion

Vapor diffusion is the transport of moisture in the vapor state along a concentration gradient. Vapor permeability (μ, perms or ng/(s·m·Pa)) is the material property that characterizes the ease with which vapor can move through a material, as described in the one-dimensional version of Fickian diffusion:

$$\frac{dw_x}{d\theta} = -\overline{\mu} \cdot A \cdot \frac{dP_w}{dx} \qquad \text{(Eq. 3.4)}$$

where w_x is the quantity of water vapor (ng) moving in the x-direction

θ is unit time (s)

$\overline{\mu}$ is average vapor permeability (ng/(s·m·Pa))

A is the unit area (m^2)

P_w is the water vapor pressure difference (Pa), and

x is distance in the x-direction

It is generally the slowest mechanism of moisture transport, as discussed in section 3.5.5.

Most materials used in basement assemblies have well characterized vapor diffusion properties (vapor permeability); however, concrete warrants some additional discussion. ASHRAE (2005) lists concrete permeability at 4.7 ng/(s·m·Pa); Straube & Burnett (2005) gives a range of 2 to 6 ng/(s·m·Pa). Assuming a 0.20 m (8 inch) concrete wall, this gives permeance values of 23 ng/(s·m^2·Pa), or 0.4 Imperial perms for the ASRHAE value, and 9.8-30 ng/(s·m^2·Pa) or 0.2-0.5 Imperial perms for Straube & Burnett.

It is well known that the vapor permeability of concrete is a strong function of the water to cement (w/c) ratio. This is due to the fact that an increase in w/c ratio increases porosity. Specifically, the volume fraction of concrete gel pores (extremely small pores, <10 nm in diameter) remains constant, but the fraction of capillary pores (larger, interconnected pores) increases with w/c ratio. Since vapor diffusion occurs in the air-filled pore space in a porous medium, the reason for the vapor permeability / water to cement ratio relationship should be quite clear.

IEA (International Energy Agency) Annex 24 provides some data for the vapor permeability of concrete as a function of w/c ratio and moisture content (Figure 3.16, from Rose 2005). It shows that permeability is a strong function of water content: it varies over two orders of magnitude as water content is increased from 0.015 to 0.07 kg/kg (or 1.5 to 7% MC by weight). To put this upper limit of water content in context, we can assume a concrete density of 2200 kg/m^3, which gives a volumetric water content of 154 kg/m^3. The porosity of concrete is on the order of 0.18 (18% pore space, volumetrically), so this water content is close to full saturation of the concrete. As another reference point, moisture content of "damp" concrete is in the 1-5% range (20-110 kg/m^3). Therefore, it is likely that the extremely high permeability values shown in the graph would no longer be the case for in-service cured concrete.

Unfortunately, the w/c ratio is given only in relative terms (high/medium-high/medium-low/low), as opposed to specific mix ratios. Assuming the labeling is correct ("cement ratio" is meant to describe water to cement ratio), it demonstrates the increase in permeability with greater w/c ratio.

Note that the graph is presented in kg/(s·m·Pa). The 2 to 6 ng/(s·m·Pa) cited in Straube and Burnett (2005) is equal to 2 to 6E-12 kg/(s·m·Pa), which matches the drier to mid portions of the graph.

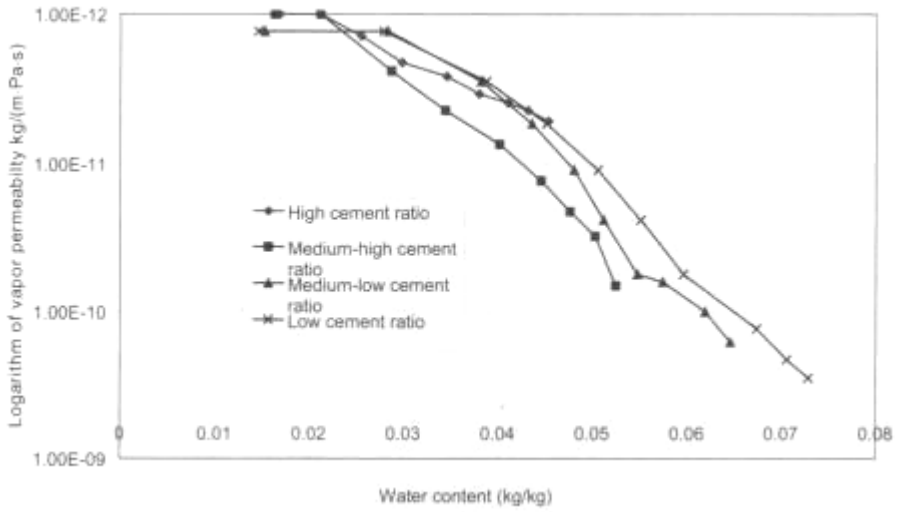

Figure 3.16: IEA Annex 24 Data: vapor permeability of concrete vs. water content (Rose 2005)

3.5.5 Comparisons between Transport Mechanisms

Comparing the rates of these transport mechanisms is of fundamental importance in determining the success or failure of building assemblies: if the influx exceeds the outflow over time, moisture will accumulate in the assembly, and failure is likely. In most cases, to dry out an assembly, a moisture transportation method with an equal or faster rate to the wetting rate is required. Removing moisture with a slower method than its ingress method is unlikely to succeed. For example, it is unlikely that a bulk water event could be dried out using only vapor diffusion, unless exceptional measures are taken (e.g., commercial drying equipment providing heated ultra low-humidity air). Therefore, an assembly should be designed with the likely wetting mechanism and rate in mind, and with the ability to dry proportional to that for wetting.

3.5.5.1 Air Leakage and Vapor Diffusion

In common building applications, air transport can move moisture at a rate an order of magnitude or more faster than vapor diffusion. Straube (2005) notes that air leakage is linked to common moisture-related enclosure failures, rather than diffusion (e.g., wintertime air leakage condensation in interstitial cavities). An example given by Lstiburek (2004) compares the transport rate of diffusion through a sheet of painted gypsum wallboard with air leakage through a 650 mm^2 (1 in^2) hole at a moderate (~3 Pa) pressure difference, assuming the same interior conditions. In that example, air leakage moves two orders of magnitude more water than vapor diffusion over the course of a season (1/3 of a quart, or 0.33 liter vs. 30 quarts or 28 liters).

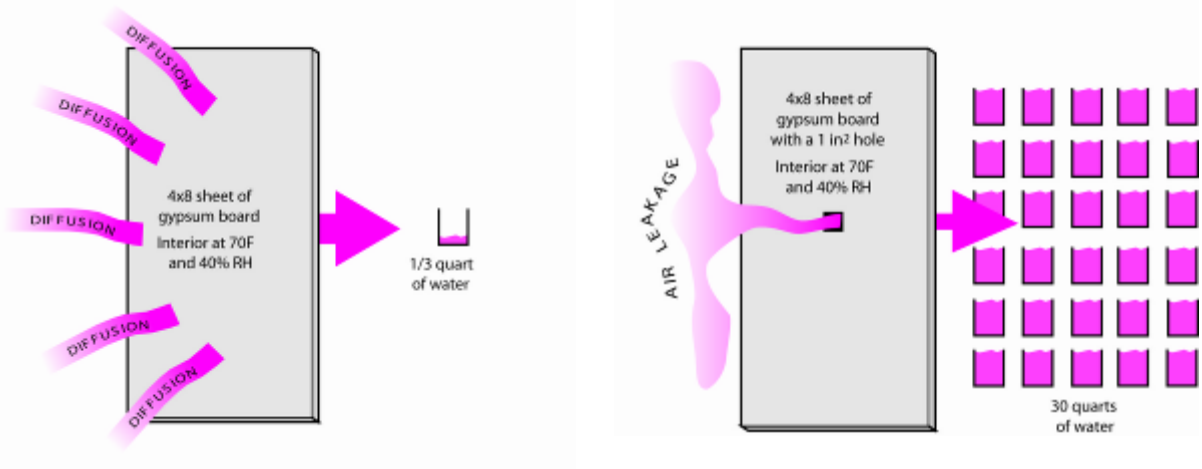

Figure 3.17: Moisture transport rates of diffusion vs. air transport (Lstiburek 2004)

As another example, TenWolde and Carll (1998) note that very low permeance materials can often be bypassed and therefore rendered ineffective by air leakage. A 1 perm vapor retarder could be considered to have an equivalent moisture transport rate as airtightness levels specified for typical air infiltration barriers, or an ELA (equivalent leakage area) of 0.003 $in.^2/ft^2$ (2×10^{-5} m^2/m^2) at 0.5 Pa, which is the maximum ELA for a continuous air infiltration barrier (ASHRAE 2005). In contrast, a 0.1 perm vapor barrier (e.g., polyethylene) would require an unreasonable level of airtightness to effectively not be bypassed (an ELA of 0.0003 $in.^2/ft^2$ (2.1×10^{-6} m^2/m^2) or less at 0.5 Pa).

3.5.5.2 Capillary Transport and Vapor Diffusion

In order to gain some understanding of the relative magnitudes of liquid capillarity and vapor diffusion as water transport mechanisms in concrete, simulations using WUFI (a one-dimensional hygrothermal model) were conducted. WUFI is described in detail in Chapter 8.

A section of concrete (0.5 water to cement ratio, from the default WUFI database) 0.2 m (8 inches) thick was simulated, with several steady-state weather files to provide boundary conditions for both sides. The simulated conditions are listed below. The exterior side is meant to represent the boundary conditions in the soil. Water vapor pressure (P_w) is shown next to the boundary conditions, where relevant.

1. Exterior: 20° C, continuous liquid exposure, 100% relative humidity
   Interior: 20° C, 50% relative humidity
   10 mm rain/hour was used in simulation to provide continuous liquid exposure
2. Exterior: 20° C, 100% relative humidity (P_w = 2326 Pa)
   Interior: 20° C, 50% relative humidity (P_w = 1163 Pa; ΔP_w = 1163 Pa)
3. Exterior: 10° C, 100% relative humidity (P_w = 1221 Pa)
   Interior: 10° C, 50% relative humidity (P_w = 611 Pa; ΔP_w = 611 Pa)
4. Exterior: 10° C, 100% relative humidity (P_w = 1221 Pa)
   Interior: 20° C, 50% relative humidity (P_w = 1163 Pa; ΔP_w = 58 Pa)

The first case is meant to demonstrate the effect of liquid capillarity. The remaining three cases show the effect of vapor diffusion: case 2 demonstrates isothermal conditions at 20° C, case 3 at isothermal conditions at 10° C. Case 4 is meant to reflect a more realistic condition of a relatively cool (10° C) soil environment, and a warmer conditioned interior space.

The simulation was run for a sufficient number of years to achieve steady-state conditions. Note that the required length of time varied depending on the case: the "rain" case reached steady state conditions after one year, while some of the diffusion cases required 10 to 20 years.

The results below are shown in Figure 3.18; the graph uses the metric of water flux, in kg/m^2·year. All of the cases resulted in inward water flow.

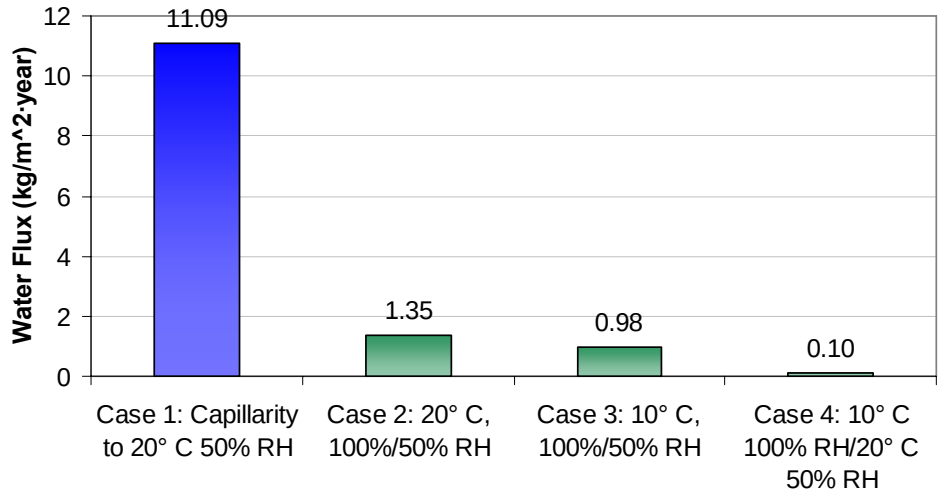

Figure 3.18: WUFI comparison of capillarity and vapor diffusion

An additional simulation was run, similar to case 1 (rain/liquid water), but with capillary moisture transport turned off in the numerical calculation options. This resulted in a very low water flux or transport rate (0.20 kg/m^2·year): this shows the importance of capillary transport, even in the cases involving no liquid water boundary conditions (cases 2, 3, and 4).

The simulation shows that liquid capillarity is a much more powerful moisture transfer mechanism than diffusion: almost an order of magnitude greater than a similar situation with only vapor diffusion. Diffusion rates are roughly, but not exactly, proportional to the vapor pressure gradient across the concrete: case 3 has half the vapor pressure gradient of case 2, but shows 75% of the vapor flow.

These rates can be used to estimate the rate of moisture supply to a house by capillarity and diffusion through unfinished concrete basement walls. We will assume a 30 by 40 foot (9.1 m x 12.2 m) basement with 8-foot (2.4 m) high walls, and use the two calculated rates for the entire height of the wall (an overestimate). The calculated rates are 3.2 liters/day for the capillarity case, and 0.4 liters/day for vapor diffusion only case. These rates can be compared to moisture production rates of the occupancy/activities of a family of four, at 10-15 liters/day, or that of a person (body evaporation only), at 0.75 (sedentary) to 1.2 (average) liters/day (Straube and Burnett 2005).

This suggests that if liquid transport can be eliminated (by a capillary break between the wall and the soil or footing) the moisture loading from a basement will have a small effect on interior moisture levels. Limiting capillarity should therefore be the highest priority to control basement-sourced humidity. However, water vapor transmission can still result in moisture accumulation within interior insulation assemblies, especially when impermeable interior finishes are used, limiting drying to the interior.

The equilibrium moisture content through the thickness of the concrete is plotted in Figure 3.19; the exterior condition is on the left-hand side of the graph.

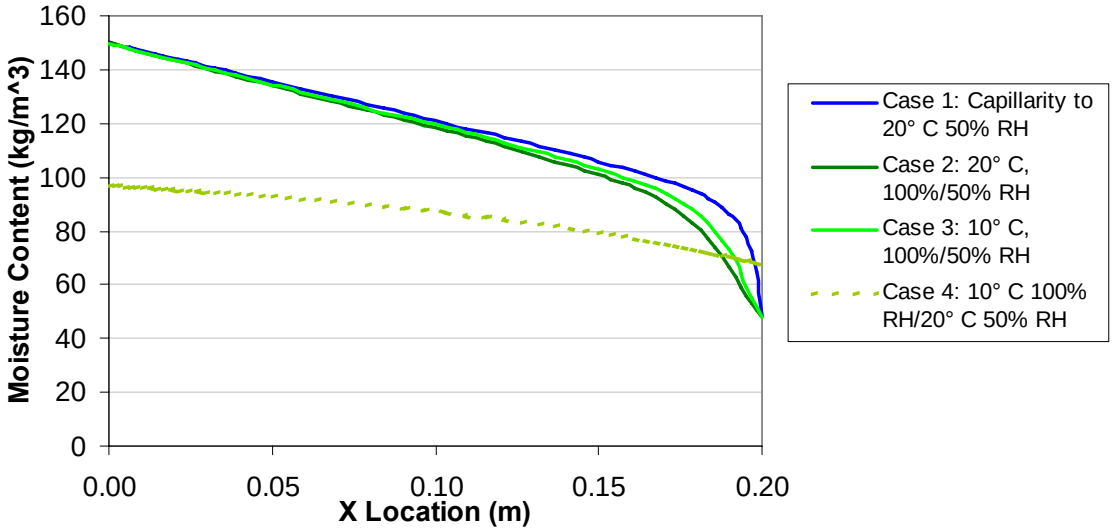

Figure 3.19: WUFI simulation equilibrium moisture content of concrete

Interestingly, this graph shows that cases 1, 2, and 3 have similar moisture profiles. However, case 4, with the extremely low vapor pressure gradient across the material, shows a much lower equilibrium moisture content through the thickness. Note that case 4 is the only one with a temperature gradient across the thickness; cases 1-3 are all at isothermal conditions.

Future work should include similar simulations using approximated properties for concrete more typically used for basement construction (e.g., 0.7 w/c, Swinton & Karagiozis 1995), in order to determine the effect of this increased permeability on overall transfer rates. Both vapor permeability and capillarity of concrete increase with higher w/c ratios; the combined effect of these two phenomena is unknown.

3.5.6 Moisture Storage

3.5.6.1 Sorption/Desorption Storage in Porous Materials

Porous materials can store moisture in the adsorbed state (i.e., molecularly bound to the interstitial surfaces). The response of a material's moisture content to relative humidity conditions at a fixed temperature is known as the sorption or desorption isotherm, as shown in Figure 3.20.

As would be expected, as humidity rises, the moisture content of the material increases; however, it is not a simple linear relationship. The reason for this is that several interrelated mechanisms are working in combination; this is covered in more detail in Straube (2005) and Kunzel (1995). Note that two curves are shown: the sorption (gaining moisture) and desorption (releasing moisture) responses are not identical, resulting in a hysteresis response.

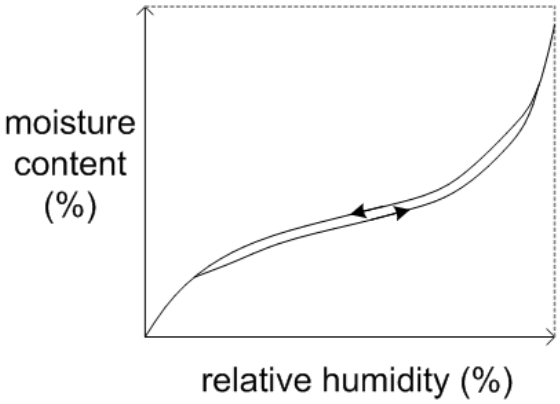

Figure 3.20: Typical sorption isotherm of a hygroscopic material (Straube and Burnett 2005)

The sorption isotherm for concrete is shown in Figure 3.21; it also shows the strong effect of sorption/desorption hysteresis in this material.

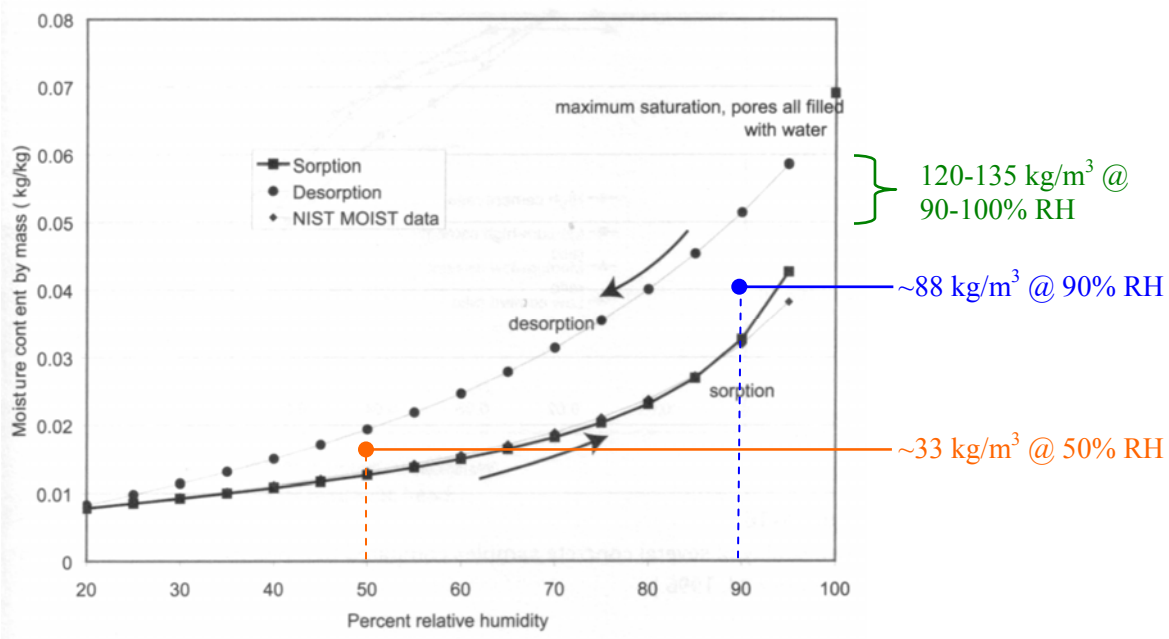

Figure 3.21: IEA Annex 24 Data: sorption and desorption isotherm for concrete (Rose 2005)

The implication of this behavior is that concrete can store a significant amount of moisture by adsorption, when exposed to high relative humidity conditions. For instance, at 50% RH, assuming an average value of 0.015 kg/kg, this is a volumetric moisture content of 33 kg/m^3. At 90% RH, at 0.04

kg/kg, 88 kg/m^3 is stored in the concrete. This is equal to approximately 18 kg/m^2 (0.5 gallons/sf) for a 0.2 m (8") thick concrete wall. As a point of comparison, the moisture-holding capacity of air at saturation (i.e., 100% RH) at 20° C is orders of magnitude less, at 17 g/m^3, or 0.017 kg/m^3.

3.5.6.2 Condensation and Surface Tension Storage

In building assemblies, condensation is often considered a failure or at least a danger point; condensation on an interstitial surface was discussed in section 3.5.3. Porous materials with storage capacity tend to safely store moisture until the surface attains equilibrium with 100% RH, at which point visible condensation occurs. In contrast, non-porous materials such as glass, metal, and polymers have no storage capacity and hence show condensation when the dewpoint exceeds the surface temperature. In terms of the danger of microbial and mold growth, moisture in its adsorbed state has a lower risk than liquid water; this was clearly demonstrated by Doll (2002) and Black (2006). These and other researchers have noted that mold growth in common building materials occurs much more readily in the presence of even a small amount of liquid water, rather than at high relative humidity conditions.

Although the moisture storage capacity of concrete can increase the moisture "forgiveness" of an assembly, it can also pose some risks. The built-in construction moisture of fresh concrete is at or near its saturation value, which is a substantial amount of water. A reasonable estimate would be 175 kg/m^3 for fresh 0.5 w/c concrete; after initial curing some, of the water remains chemically bound in the concrete from the hydration process (~60%/~100 kg/m^3), while a portion remains in the capillary pores, even after months of curing (10-20%, or 20-35 kg/m^3). This gives a total of 120-135 kg/m^3, or 0.05-0.06 kg/kg (in the 90-100% RH range on the desorption curve, see Figure 3.21). Unless provisions are made to allow the drying of this water, construction moisture can damage assemblies.

In addition to storage of moisture by adsorption, some liquid storage can take place on a surface due to surface tension, after condensation occurs. Ideally, this condensation would be stored temporarily, and then re-evaporated over the course of a season, without causing damage to the assembly. The German DIN Standard 4108-3 Section 3.2.1 (Deutsches Institut für Normung 1999) gives some recommended limits for safe storage of condensation:

- In wooden wall construction, the amount of condensation water must not exceed 1 kg/m^2.
- In order to prevent water running down or dripping condensation arising on contact surfaces of layers that cannot absorb water, the amount of condensation water must not exceed 0.5 kg/m^2 (e.g. contact surfaces of fiber insulation, or air layers on the one hand with damp-proof or concrete surfaces on the other).

These values can provide limit states for evaluating risks in hygrothermal simulations. Research by Smegal (2006) has shown that these limits are generous: drainage begins from smooth hydrophobic surfaces such as polyethylene at levels of as little as 60 g/m^2, and from textured acrylic stucco surfaces at levels of about 150 to 200 g/m^2. The DIN values likely include some storage in the insulation or framing, not just surface tension storage.

3.6 Moisture Failure Modes

With the technical understanding presented above, we can describe some common historic interior basement insulation moisture failures, and the underlying physics. The failures examined here are summertime condensation on the lower wall, wintertime condensation on the upper wall, spring or summertime inward vapor drives, and moisture accumulation in single and double polyethylene systems.

Bulk water events are not addressed as an independent failure mode here. There are some cases where it might be difficult to conclusively determine the source of moisture, e.g., initial construction moisture, condensation, or bulk water leakage. However, several of the failed assemblies have a limited ability to dry, and this is the underlying cause of the failure, regardless of moisture source.

3.6.1 Summertime Condensation on Lower Wall

As discussed in section 3.2.1, the thermal mass of the soil causes a phase shift between outdoor temperatures and below-grade temperatures. As a result, the lower part of the basement wall sees its lowest temperatures in early spring, as seen in Figure 3.4. This is also a time of year when the exterior dewpoint is rising; interior dewpoint roughly follows exterior in most houses, especially those cooled by window ventilation (see section 3.3 Basement Interior Temperature and Humidity Conditions).

As a result, there is a danger of condensation occurring on the lower portions of the concrete wall or floor slab, especially if the basement is ventilated with outside air during this period. This problem is exacerbated by insulation: the wall temperatures are colder than they would be if the wall were left uninsulated. Also, condensation would be worst at the corners, which have the greatest heat loss to the soil, and the lowest radiative heat gain from the interior. Wall areas with reduced air circulation, such as behind stored boxes and furniture, would be similarly affected.

To some degree, this problem is controlled by the ability of concrete to safely adsorb and store moisture; hence it is made worse with the use of impermeable finishes, such as vinyl composition tile on the floor slab.

Anecdotal evidence points to air leakage from the interior to the interstitial space (e.g., as shown in Figure 3.14) as the main cause; this is strongly supported by the higher moisture transport rate of air movement (see section 3.5.5.1).

The location of this failure mode means that it can easily be confused with bulk water leakage through the wall. When diagnosing this failure, the temporal correspondence with weather events is an important diagnostic tool. Bulk water events will, of course, tend to follow rain events. In comparison, condensation events can match up to sudden rises in exterior temperature that have matching dewpoint increases. Ventilating the basement with outside air can cause this problem; running the air conditioner can have a similar effect, as the operation mixes the air in the above grade space with that in the basement. This occurs even if there are no intentional vents in the basement ductwork because of the leakiness of sheet metal basement duct systems.

The occurrence of this phenomenon has been documented as far back as Rogers (1938):

> …[foundation walls and floors] should be protected against internal dampness due to condensation of moisture from warm humid air on the cooler masonry in contact with earth. Such condensation is often as much the cause of dampness in basements as actual leakage. … This trouble appears most frequently during mild rainy spring weather when the ground is still cold and the air warm and humid. Its coincidence with warm rains has led many owners to mistake condensation for subsoil leakage.

In response to these problems, Rogers recommends insulation material that prevents contact between the cold surfaces and interior air, such as hair felt or cork. Other alternatives include creating details that assume condensation will occur, and drain this condensate without harming finishes.

3.6.2 Wintertime Condensation or Frost on Upper Wall

As mentioned in section 3.4, the vapor pressure gradient will be outwards at the upper (but still below grade) portion of the foundation wall during the winter, especially when the interior is humidified. The above-grade portion of the wall is even colder, and has a greater temperature gradient in winter. The surface of the concrete will therefore be a likely place for condensation of interior moisture, since the majority of the temperature drop across an insulated basement wall occurs at the insulation layer. This is the reasoning behind specifying a vapor diffusion retarding layer at the interior side of these basement insulation systems.

An example of this failure is shown in Figure 3.22, taken in a basement in Iowa (photos courtesy of Building Science Corporation, 2004).

Figure 3.22: Mold growth on upper portion of basement wall

Figure 3.23: Mold growth at insulated rim joist of basement

The wall system is (from interior to exterior) concrete wall, fiberglass batt in wood framing, polyethylene vapor barrier, and gypsum drywall. It is important to note that the mold damage is concentrated on the upper portion of the wall and at the window well. The large plume of mold is located

at the wiring penetration at the top plate of the stud bay, suggesting that air leakage is the culprit, as opposed to vapor diffusion, which would create a more uniform pattern on the concrete surface. There does not seem to be any air sealing materials placed between the stud frame and the concrete wall; the fiberglass batt placed at this junction provides minimal airflow resistance.

However, research by Goldberg and Farkas (2004) demonstrated that at high interior dewpoint temperatures and low exterior temperatures, moisture/frost accumulation can take place at the interface between the insulation and the concrete purely by vapor diffusion, with a sufficiently vapor-open interior insulation material (see Chapter 4: Literature Survey).

Figure 3.23 shows further mold damage from the same basement, at the insulated rim joist. In this case, the cold condensing surface is the rim closure board; it appears that the rim joist was insulated without either a vapor retarder or an air barrier; either transport mechanism could explain the mold growth. This problem can be effectively solved by cutting, fitting, and air sealing XPS foam blocking into the rim joist space, or by insulating with XPS on the exterior of the rim joist.

3.6.3 Inward Vapor Drives

Many building science researchers have observed that when absorptive claddings are wetted and exposed to an inward thermal gradient (especially by solar heating), an extremely high inward vapor pressure gradient can result. If an assembly combines this with an impermeable interior-side vapor barrier (e.g., polyethylene), moisture can accumulate within the assembly—even in heating-dominated climates, which have an outward vapor drive for most of the year. This problem can be ameliorated by reducing the absorption of the cladding, adding or increasing ventilation drying behind the cladding, decreasing the permeability of sheathing behind the absorptive cladding, or increasing the permeability of the interior layer.

This phenomenon has been observed in above grade walls as far back as the 1960s: test hut work by the National Research Council's Division of Building Research showed condensation and decay in southwest facing walls with polyethylene. More recent examples include Straube & Burnett, et al. (2004) and Lstiburek (2004).

The above grade portions of basement assemblies with a single layer of polyethylene on the interior (e.g., the roll blanket wall, as described in Chapter 2, under “Historical Development of Basement Insulation Assemblies”) are susceptible to this phenomenon as well: the concrete wall is typically at a high moisture content, and warm exterior conditions will result in an inward vapor pressure gradient. This problem is manifested as condensation on the exterior side of the polyethylene (visible from the interior if clear polyethylene is used); if the vapor drive is of sufficient intensity and duration, it will result in rundown and accumulation or drainage of this condensation. Condensation typically occurs during spring or summer, and is worst during the first cooling season, due to the moisture stored in freshly placed concrete. Note that the methods used above-grade to ameliorate inward vapor drives (such as adding ventilation or decreasing sheathing permeability) are not readily available in basements.

This problem was examined and modeled by Swinton & Karagiozis (1995), their work, which includes two-dimensional modeling and design recommendations, is examined in more detail in Chapter 4.

3.6.4 Moisture Accumulation in Single Polyethylene Systems

The interior insulation assemblies of interest here include the roll blanket and stud wall with polyethylene; they both have an impermeable layer on the interior side. This material is specified ostensibly as an air and vapor barrier, to (for instance) protect the wall from condensation of interior moisture on the concrete surface during the winter. However, as demonstrated in section 3.4, the drying direction of the basement wall assembly is primarily to the interior: an impermeable layer on the interior removes the ability to dry in this direction almost entirely.

There can be many actual causes of failure in this assembly, including stored construction moisture, trapped condensation, or bulk water leakage. As a caveat, it would be unreasonable to claim that all of these assemblies would have been able to dry with the omission of the polyethylene, especially in the case of bulk water leakage. However, a sufficiently low deposition or moisture emission rate can be safely dried to the inside through a permeable interior finish, without damaging that material. Possible consequences of the removal of the vapor retarding layer from the bottom portion of the insulated wall are discussed in section 3.7.3.

Figure 3.24: Moisture accumulation and mold growth in single polyethylene wall

Some builders have experienced problems with these assemblies and have reacted by changing their construction practices to reduce their risks. These practices essentially negate or bypass the interior low permeance layer, allowing drying. For instance, some builders cut off the bottom 150 mm (6”) of the roll batt material, in an effort to allow drainage of any accumulated moisture (Zuluaga et al. 2004). This also has the effect of allowing air convection in the assembly (and the resulting wetting and drying) at the lower part of the wall; this is covered in more detail in Chapter 4: Literature Survey.

In addition, some builders install the stud wall system spaced off the concrete wall by approximately 25 mm (~1”); this is done to allow straight wall framing against an imperfectly formed wall (Zuluaga et al. 2004). It also prevents direct contact between the vulnerable wood framing and the potentially wet concrete. However, it often has the secondary effect of creating an air space behind the insulated wall system. If the junction between the framing and the concrete wall is not air sealed, it can allow communication between interior air and this space. If the interior dewpoint is below the dewpoint at the lower portion of the wall, as suggested by the psychrometric relationships, this can be a path for drying.

3.6.5 Moisture Accumulation in Double Polyethylene Systems

As described in Chapter 2 ("Historical Development of Basement Insulation Assemblies"), the interior insulation assembly using polyethylene on both sides of an insulated stud wall was developed to protect the vulnerable portions of the frame wall from moisture sourced from the damp soil and/or the concrete. The outer layer of polyethylene was typically referred to as a "moisture barrier," and was either run up only to grade, or full height.

However, a notable number of moisture accumulation failures have occurred with this assembly; these started to be noted in the builder and building science community during the 1990s. Many practitioners no longer favor this assembly; for instance, Lstiburek issued errata to his *Moisture Control Handbook* (1996) in 2002, where he recommends against this assembly. Also, Goldberg (2002) added an author's note to a document originally published in 2000, stating:

> The dual vapor retarder configuration specified in the Minnesota building code for new construction (rule 7672.0600, consisting of a warm-side (interior) full-height vapor retarder and a "moisture barrier" (undefined) from floor to grade on the wall side) is shown by the data in this report to be prone to failure since, in the critical condensation zone at top of the wall, the code configuration functions as a single interior retarder with all the attendant consequences demonstrated in this report. Therefore (if a minor speculation may be allowed), the presence of the below-grade wall side retarder may actually exacerbate matters by reducing the drying potential to the outside compared with the situation when using a single interior retarder alone. This supports the anecdotal reports of the service failures of the MN code configuration.

Photos provided by Paul Ellringer of Tamarack Technologies Incorporated show the types of failures seen in this assembly. Figure 3.25 shows accumulation of moisture behind the concrete side "moisture barrier;" in addition, there are high moisture contents and mold growth in the framing. Figure 3.26 shows surface mold at the interface between the fiberglass batt and the interior vapor barrier.

Figure 3.25: Moisture accumulation behind polyethylene; high MCs in framing

Figure 3.26: Surface mold at interface of fiberglass batt and polyethylene

There are several failure mechanisms at play in these problems:

- First and foremost, by putting impermeable materials on both sides of the vulnerable wood framing/fiberglass portion of the wall assembly, if moisture enters the stud space, drying will occur at a slow or negligible rate. This is especially true with the exterior side moisture barrier run full height.
- The lower portion of the concrete wall can dry only to the interior; with a completely impermeable material placed directly against the concrete, moisture can build up to the point of condensation, as seen in the photo. In most typical construction details, if this occurs, the moisture would drain to the interior.
- If the wall is built with the exterior-side moisture barrier only to grade, it is still vulnerable to moisture gain from inward solar drives (as described in section 3.6.3). With the lack of drying, the problem is compounded. If the moisture barrier is run full height, the condensation will occur on the exterior side of the polyethylene and run down the wall.
- The concrete's moisture safe storage and buffering capacity is eliminated by the use of the moisture barrier against the concrete. This can result in greater condensation either at the bottom or the top of the wall, depending on season.

3.7 Implications for Foundation Detailing

The information provided here can be synthesized to provide an overall picture of how a basement should be built and insulated. The topics presented here are recommended foundation drainage details, the advantages of exterior insulation of foundations, the use of vapor barriers on the lower parts of the basement wall, and finally, recommended details for interior insulation.

3.7.1 Recommended Foundation Drainage Details

The focus of this thesis is the interior insulation of basement walls, so it might be considered a digression to deal with bulk drainage. However, given the importance of controlling bulk water, as described in section 3.5.1, it is worthwhile to provide a brief discussion of the vital details that cannot be ignored. Also, there is substantial interplay between these bulk water details and the environmental loading of the foundation walls, such as the loading of liquid water in the soil.

Rose (2005) provides a good philosophical approach to how surface runoff should be controlled and redirected away from the house:

> A soil surface is a roof. Rather, water is managed on the soil surface in much the same way that water is managed on a roof. To design a soil surface for rainwater management, think of that soil surface as a roof. The designer should know what to keep dry—the soil in contact with the foundation—and where the water should be delivered.

An illustration from Lstiburek (2006) provides a guide to some of the essential foundation drainage details, as shown in Figure 3.27. Some points that should be emphasized include:

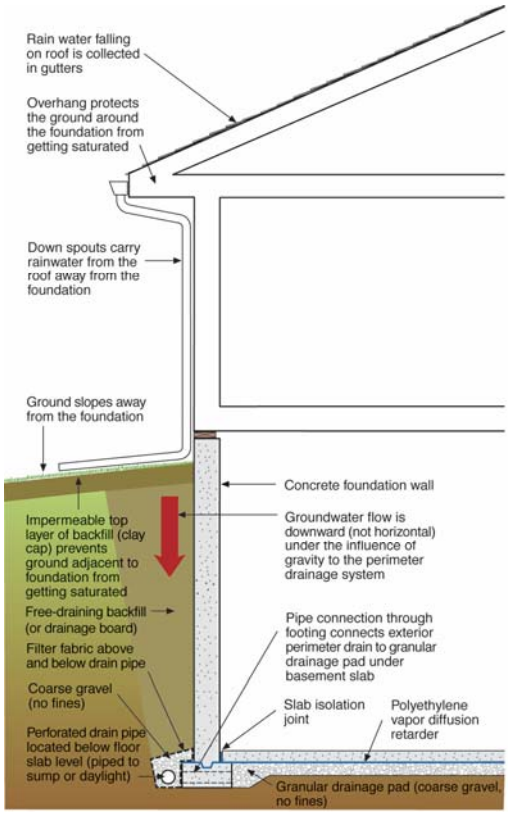

Figure 3.27: Protection of foundation from precipitation and ground moisture (Lstiburek 2006)

- The rainwater from the roof is collected and carried away from the house by gutters and downspouts; this concentrated water has a high potential to cause problems if not handled properly
- Proper grading is used to redirect surface water away from the house
- An impermeable backfill cap, such as clay or paving, cuts surface absorption of water and therefore reduces saturation of soil around the foundation
- Free draining backfill or drainage board keeps liquid water out of contact with the foundation wall; this can prevent liquid capillarity through the wall, which can transport much higher rates of moisture than vapor diffusion
- The footing drain is embedded in coarse gravel and wrapped with filter fabric, to prevent clogging with fines
- The footing drain is below the floor level to prevent liquid contact with the bottom of the slab, and piped to daylight or a sump.

One detail shown but not called out on this diagram is a capillary break over the top of the footing, where it comes in contact with the foundation wall. This is shown later in Figure 3.34 and Figure 3.35. The importance of this detail is obvious when the effect of liquid capillary water uptake is compared with other transport mechanisms (section 3.5.5.2): the connection from the bottom of the footing to the wall provides an effective moisture transport path (see Figure 3.13) if a capillary break is not used.

Exterior dampproofing of the concrete wall to grade is not shown on this detail, as in Figure 3.34 and Figure 3.35. Note that dampproofing should not be confused with waterproofing: the former is not meant to withstand hydrostatic head. Instead, it is intended to reduce vapor diffusion into the concrete from the soil, and to provide a capillary break.

Many of these details have long been recommended by the building science community; however, industry has often failed to incorporate them into standard practice, due to pressures to minimize initial cost, and perhaps a lack of understanding of the implications of omitting certain portions of these assemblies.

3.7.2 Advantages of Exterior Insulation of Foundations

The general concept of insulating on the exterior of the structure has many advantages for durability, moisture control, and the prevention of thermal bridging; this was noted in Canadian Building Digests 50 (Hutcheon 1964) and 120 (Garden 1969). Makepeace and Dennis (1998) promoted these same principles with their PERSIST ("Pressure Equalized Rain Screen Insulated Structure Technique") construction method.

The fundamental advantage is due to the thermal gradient through the assembly, as shown in Figure 3.28. The majority of the temperature drop is across the insulation, so with exterior insulation, the structure (concrete wall in the figure below) is close to interior temperatures. In contrast, with interior insulation, the interface between the insulation and the concrete will see a wide seasonal swing. These conditions require the isolation of this surface from the interior with air and vapor barriers for moisture control, as described in section 3.5.3.

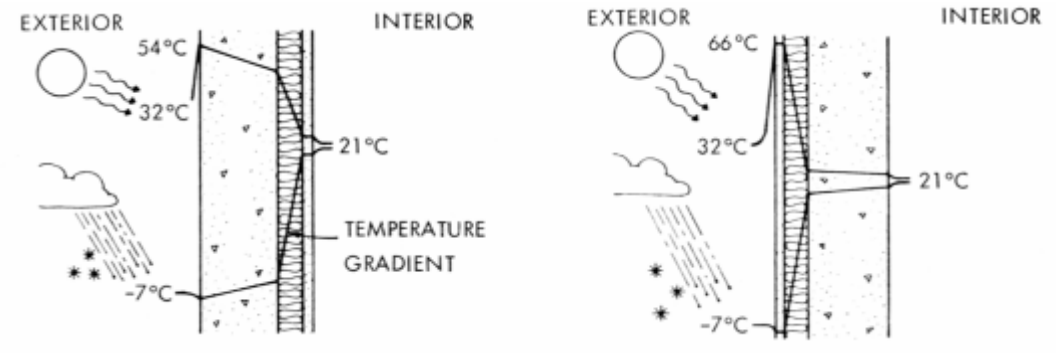

Figure 3.28: Temperature gradients through walls with interior (left) and exterior (right) insulation (Garden 1969, taken from Hutcheon and Handegord 1995)

These principles can be applied to foundation walls. Looking at the historic failures of interior insulation (section 3.6), we see that the concrete surface is akin to a dangerous "third rail" to be avoided

and protected against. With exterior insulation, this danger is mostly removed: wintertime and summertime condensation on the concrete wall would be minimal with the modified thermal gradient. Also, given the small ΔT across the concrete, inward vapor drives are no longer an issue; since there is no need for an interior vapor retarder, the construction moisture of the concrete would be free to dry to the interior.

Secondly, exterior insulation provides a drainage plane and capillary break at the interface with the soil. Conventional construction practice typically backfills with soil available on site, relying on dampproofing to sufficiently reduce vapor and capillary conduction through the concrete. Drainage relies on the continuity of this dampproofing, and is dependent on the drainage characteristics of the soil backfill.

In contrast, exterior insulation provides a robust capillary break between the soil and concrete; the physical separation completely eliminates capillary conduction, especially given that the insulation materials are typically hydrophobic. The insulation provides drainage at its exterior surface and at the interface of the insulation and the concrete (e.g., through the unintentional space, or less importantly, through drainage channels), or within the insulation itself (e.g., an intrinsically draining medium such as rigid fiberglass) (Swinton et al. 1999).

Examples of exterior insulation are shown in Figure 3.34 (draining rigid fiberglass board) and Figure 3.35 (extruded polystyrene/XPS and drainage mat). Other materials used as exterior foundation insulation include expanded polystyrene (EPS), spray polyurethane foam, and mineral fiberboard.

Figure 3.29: Exterior foundation insulation using draining rigid fiberglass board

Figure 3.30: Exterior foundation insulation using extruded polystyrene and drainage mat

The European and Canadian building science communities have long emphasized the advantages of exterior foundation insulation; they have generated a significant body of research on this field. However, exterior insulation has only gained limited acceptance in practice. There are several reasons for this lack of market penetration.

One recurring difficulty is the protection of the above-grade portion of the insulation, as shown in Figure 3.31. The insulation must be continued above grade for thermal continuity; if it stopped at grade, a thermal bridge will result, even with interior insulation corresponding to the missing portion.

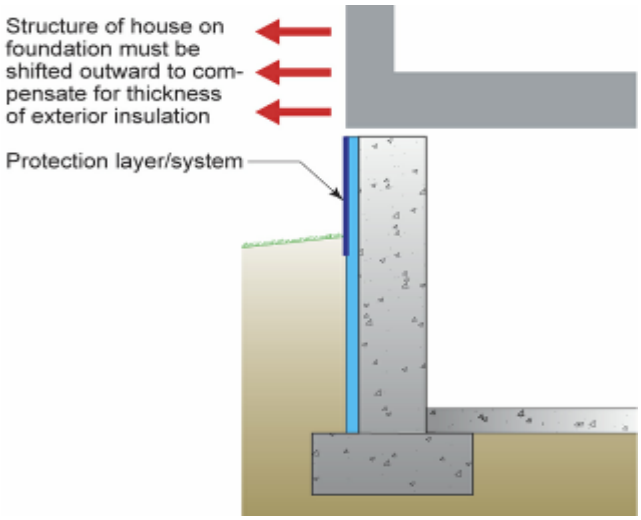

Figure 3.31: Above grade protection of exterior insulation & dimensional adjustments (Lstiburek 2006)

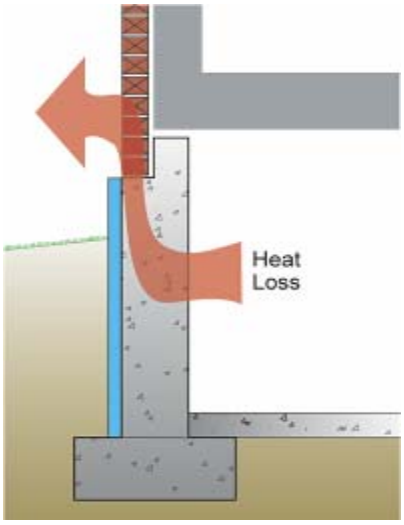

Figure 3.32: Thermal bridging at masonry shelf with exterior insulation (Lstiburek 2006)

Several materials have been used for this exterior protection, including mortar parging, cement board, sheet metal, and plastic extrusions. However, this material must stand up to both physical abuse (e.g., landscaping equipment) and partial burial in soil, with direct capillary contact. The difficulty and expense of solving this problem has hampered the use of this system.

A second problem is also illustrated in Figure 3.31: the increased overall dimensions of the foundation force a change in the dimensions of the above-grade structure for proper alignment.

Insect control is a strong issue with exterior insulation, especially in the southern United States. The insulation provides a direct pathway from the ground to the wood above-grade structure that cannot be easily inspected. Some solutions have included foam insulation with insect repellant properties, and various insect shields; however, this issue remains an obstacle to adoption.

Figure 3.32 illustrates another issue with exterior insulation: when a brick veneer with a cast-in shelf is used, a thermal bridge is created. Several solutions have been proposed, including a metal brick shelf angle, a high compressive strength foam thermal break, or a “stub wall” cast outside of the insulation. However, none of these details have gained wide acceptance.

Another problem is construction sequencing: the insulation can only be installed after the removal of the forms but before backfilling takes place.

A final concern with interior insulation of basement is that summertime condensation low on the wall (see 3.6.1) might still be a factor, due to the thermal mass of the concrete. This incidence of this problem would be rare compared to interior-insulated basements, since the concrete is decoupled from the close to constant temperature thermal mass of the soil. However, it could occur, under certain setpoint conditions and interior dewpoints.

3.7.3 Vapor Barriers on Lower Portion of the Basement Wall

Most of the interior insulation details used in practice incorporate a vapor retarder or vapor barrier (typically polyethylene) for the full height of the wall; this is a requirement in building codes as well. However, as noted by the psychrometric relationships of boundary conditions in section 3.4, the lower portion of the foundation wall dries primarily to the interior, which is prevented by a vapor barrier. Granted, the above-grade and higher below-grade portions of the basement wall have an outward vapor pressure gradient in winter, given sufficient interior relative humidity, so some type of vapor retarding layer is necessary, although it is functionally needed more as an air barrier than a vapor barrier.

It is interesting to note the use of a uniform insulation assembly for the full height of the wall, despite the contrasting boundary conditions with height. This might be necessary for ease of construction in a production setting: treating these two areas differently would require two different assemblies, and a horizontal air barrier separation to prevent communication between the portions.

The reason for a vapor retarding layer is to prevent condensation and moisture accumulation on a cold interstitial surface; the critical parameters for success or failure are the temperature of the surface (and therefore, the exterior temperature) and the interior dewpoint. To provide an extremely basic analysis using readily available data, several below-grade temperature profiles were compared with monthly average temperatures of several climate locations in Figure 3.33. The below grade temperature profiles were soil temperatures for St. Paul, MN, from the plot by Bligh (1975), at a depth of 1.6 m (5.3 feet), and monitored data from the lower portion of a basement wall at the Huntley, IL, and Kitchener, ON experimental sites. These locations are in DOE Climate Zone 6, 5, and 6 "equivalent" respectively. We see that the minimum temperatures are 1° C, 9° C, and 10° C respectively.

Monthly average temperature data was examined to find locations with similar profiles. Washington, DC (in Zone 4) and Savannah, GA (in Zone 2, borderline Zone 3) were selected; they have monthly minimum temperatures close to the two below-grade conditions. Note, however, that although the minimum temperatures are similar, the maximum monthly temperatures are much higher in these city weather profiles. The colder condition of the below-grade environment means that there is a relatively low drying potential available in the summer (i.e., less "energy in the system"). However, assuming saturated soil and concrete conditions, it also implies that the vapor pressure gradient will not be as high as in the above grade situation, i.e., the situation that causes summertime inward vapor drives. In addition, the below-grade temperatures show the phase shift effect caused by the thermal mass of the soil.

Savannah, GA, the milder of the climates, is in a climate zone that the 2006 International Residential Code and 2006 International Energy Conservation Code have accepted as not needing a vapor barrier (International Code Council 2006). Washington DC, in Zone 4, has a recommendation from Lstiburek (2004) for only a Class III vapor retarder, which is between 57 and 570 ng/(s·m^2·Pa) (1.0 and 10 Imperial perms). Therefore, the use of a layer of 3.5 ng/(s·m^2·Pa) (0.06 Imperial perm) polyethylene is far less permeable than either required or desired.

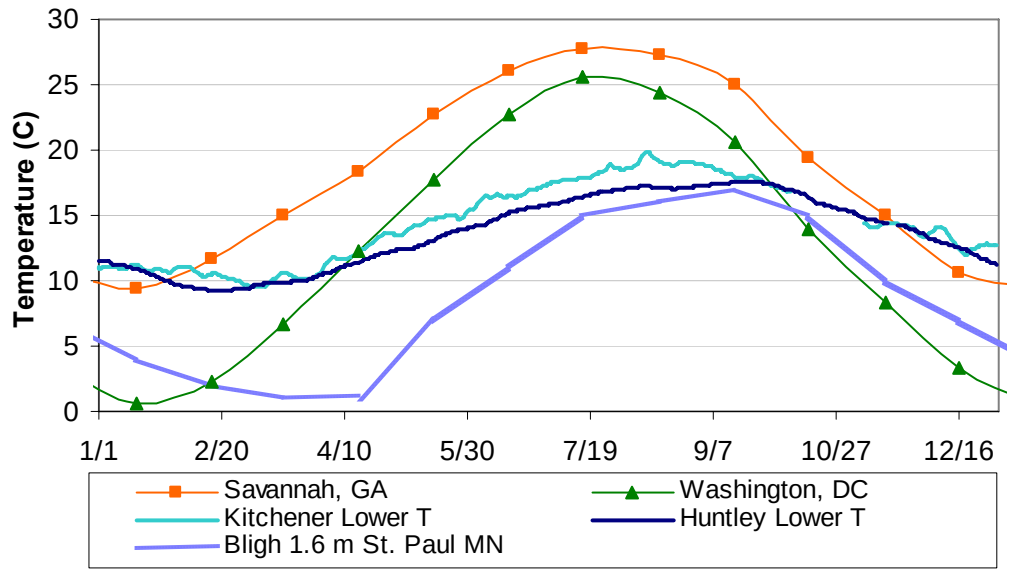

Figure 3.33: Comparison of basement lower wall temperature and monthly average outdoor temperatures

Note that this analysis is quite conservative: the above-grade cases (monthly average temperature data) actually have a greater chance of condensation. First, the above-grade data is monthly average temperatures, while the underground temperatures are continuous profiles. Data from above grade walls has demonstrated that condensation and high moisture contents correspond with sharp drops in outdoor temperature; these events are completely averaged out in monthly data, creating a much less stringent temperature profile. Second, above-grade vapor retarder recommendations are typically made for the worst-case scenario of wood or steel frame walls. Concrete basement walls have a tremendous moisture buffering capacity, which is not accounted for here.

On the other hand, one effect of the phase shifting of soil temperatures is that the coldest period will occur during the early spring. This period is coincident with rising exterior dewpoint temperatures; in contrast, wintertime minimum temperatures are associated with low outdoor dewpoints. As a result, since interior dewpoints follow exterior conditions, it reduces the conservatism of this analysis.

A building science researcher (Huelman 2006) has questioned whether all vapor control can or should be eliminated from the below-grade portion of the wall. He cites the example of carpets on basement slabs, which have long been recognized as a source of mold and dust mites: it is an insulating material without a vapor control layer, and is at a similar temperature and moisture regime as the bottom of the wall.

This question does not lend itself to a facile response: one point demonstrating why an insulated lower basement wall without a vapor control layer would not experience these problems is the location of the air barrier. In a carpet, the least air permeable layer is basically the carpet backing, on the bottom or cold side of the assembly. Interior air can travel freely through the carpet fibers, and condense (or reach high RH) on the lower surface. In contrast, the types of assemblies envisioned here would have an air barrier on the interior side, preventing this air communication. Secondly, carpet may be a more amenable

substrate for microbial growth, both in terms of its structure and composition, as well as its application as a horizontal surface in occupied space: its retain dust, food and skin particles, and bulk water spills.

This comparison is not meant as a comprehensive or conclusive analysis by any means. Instead, the intent is to roughly relate experience with above grade walls to the below grade conditions. But we can see that there is a weak case, at best, for an impermeable layer to the interior. It is noted that colder climates and/or highly conductive soils could lower the temperatures found at the below grade wall. Concrete block walls that experience thermal looping could also reduce the concrete surface temperature.

Although the use of an impermeable layer for condensation control below grade might be questionable, there are some more compelling reasons for using a vapor impermeable (or at least hydrophobic) layer on the exterior of the insulation:

- As described in Chapter 2, the use of a "moisture barrier" on the exterior side of the assembly protects vulnerable portions such as wood framing from moisture vapor sourced from the concrete or the soil.
- This moisture barrier provides some measure of protection from incidental bulk liquid water events from the exterior, draining these incidental leaks away from vulnerable parts of the assembly. Ideally, it should be set up to drain this water into the sub-slab gravel field, as per Timusk and Pressnail (1997). If it is simply set up to drain to the interior space, it will provide an indication to the homeowner of a problem, but would damage interior floor finishes and furnishing.
- A vapor barrier would control moisture ingress from the concrete and/or soil, for humidity control of the interior space, as discussed in Cheple and Huelman (2001). The magnitude of the moisture generation rate and its implications were discussed in section 3.5.5.2).

However, in all of these cases, the impermeable layer should be installed outboard of the insulation system, thus protecting the vulnerable components of the assembly. In addition, use of an impermeable material such as polyethylene at the concrete-insulation interface eliminates the storage available in the concrete, thus increasing chances of summertime condensation on the lower wall. The first and last reasons are a function of amount of moisture released from concrete/soil into the assembly or interior.

The next step in determining optimum permeability characteristics for this surface would be hygrothermal modeling. This more rigorous analysis will account for thermal mass, moisture storage/sorption, the effect of several interior moisture levels, and the effect of various levels of vapor control.

3.7.4 Recommended Details for Interior Insulation

A final piece of background information is two interior basement insulation details from Lstiburek (2006) that have been demonstrated in the field to be robust and resistant to moisture damage. As stated in section 3.7.2, exterior insulation of foundations has many advantages, but many builders do not find this solution practical.

The assemblies shown here have higher initial costs but lower risks, compared to those that are intended to simply meet code minimum requirements. They have been shown to be quite constructible:

they are being deployed by production builders when homeowners opt for a finished basement option. It is interesting to note, however, that despite the superior performance of these premium assemblies, they would not be acceptable to some building codes.

Both of these assemblies use exterior bulk drainage details as shown in Figure 3.27; since they have already been described in section 3.7.1, no further explanation will be made.

Figure 3.34 shows a basement wall using an extruded polystyrene (XPS) and insulated stud bay interior insulation system; expanded polystyrene (EPS) would also be an acceptable substitution. The foam plastic insulation material is installed against the concrete and air sealed at the interface at top, bottom, and penetrations. In addition, the seams are taped or otherwise air sealed. The intent of these measures is to use the foam board as an air barrier between the concrete and the interior air. This treatment is continued onto the horizontal surface of the concrete wall, which has similar condensation risks. Inboard of this layer, a frame wall with insulation is installed; sill seal material is used under the bottom plate to provide a capillary and thermal break. Gypsum drywall must be installed on the inboard side to provide an ignition barrier for the foam; vapor permeable latex paint is specified for the interior finish. The stud frame wall provides a space to run electrical and plumbing services.

The key to this wall is its use of XPS or EPS foam: air impermeable insulation materials with some vapor permeability (Class II or III vapor retarders; 5.7 to 570 ng/(s·m^2·Pa), or 0.1 to 10 Imperial perms). This material prevents wintertime condensation on the upper wall, as well as summertime condensation on the lower wall. It allows some drying of the concrete: at 57 ng/(s·m^2·Pa) (1.0 Imperial perm) XPS has more than an order of magnitude greater permeability than polyethylene at 3.5 ng/(s·m^2·Pa) (0.06 Imperial perm). However, XPS is impermeable enough that it cuts moisture transport from inward vapor pressure gradients above grade, and there is no impermeable material on the interior to collect condensation. Instead, the fiberglass batt and latex-painted drywall are quite permeable, and pass the limited moisture through without damage. Finally, the foam plastic insulation materials are intrinsically hydrophobic and more moisture tolerant than vulnerable assemblies such as wood stud frames. They will not be damage by sustained high relative humidity levels at the interface with the concrete, and they can even withstand some incidental liquid water wetting.

Figure 3.35 shows a basement wall using spray foam insulation applied directly to the inside surface of the concrete; an uninsulated steel stud frame wall on the interior provides a finish surface and a space to run services. It is similar to the XPS wall in that the concrete surface is isolated from the interior by an air impermeable, semi vapor permeable insulating material, resulting in protection from any of the condensation scenarios mentioned above.

Lstiburek notes that in both of these assemblies, the greater the permeability of the foam, the greater drying is available to the interior. He suggests a maximum thickness of 51 mm (2”) of XPS foam; 102 mm (4”) of EPS, 76 mm (3”) of closed cell urethane foam, and 254 mm (10”) of open cell low density foam, to allow for some drying by vapor diffusion.

One of the options, open cell foam, is quite vapor permeable (1400 ng/(s·m^2·Pa) or 24 Imperial perms) in a two-inch thickness; however, this is not an issue with summertime inward vapor pressure gradients because there is no impermeable layer to capture condensation, and it passes through the assembly. The concern with this product is thin applications in cold climates at the above grade portion of the wall.

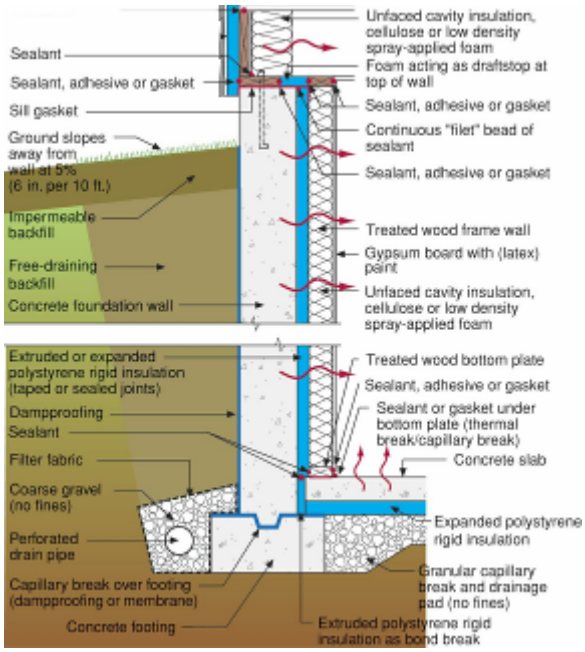

Figure 3.34: Interior basement insulation using extruded polystyrene foam (Lstiburek 2006)

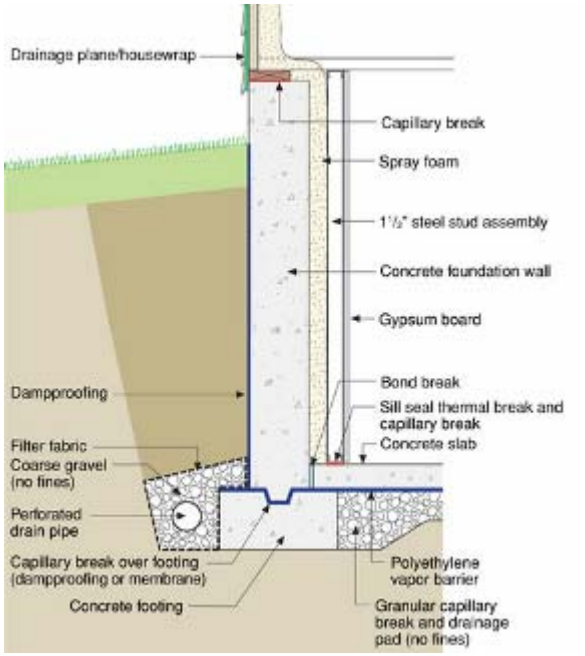

Figure 3.35: Interior basement insulation using vapor permeable spray foam (Lstiburek 2006)

Chapter 4

Literature Survey

Although there is a substantial body of literature cited in the previous chapter, research with a specific focus on the interior insulation of basements is only a subset of that work. The literature here is divided into two portions: analysis and modeling research, and field surveys and experimental work; it dates from the late 1980s through today.

4.1 Analysis and Modeling Research

The research described here includes both analysis and design recommendations from physics first principles and hygrothermal computer modeling of basement problem situations.

4.1.1 Swinton and Karagiozis (1995)

"Investigation of Warm Weather Condensation in New and Insulated Basement Walls"

This work, conducted at NRC-IRC, examines the spring- and summertime inward vapor drive problem as described in Chapter 3 (Section 3.6.3). The researchers hypothesized that a two-dimensional vapor diffusion mechanism was at work: both the inward vapor drive, and vertical vapor movement due to the temperature gradient. They examined several field cases; it was notable that the problem was seen in both a half-height insulated basement (previous researchers had thought that full-height insulation was a component of this problem), and in a retrofitted installation (on a 30-year old concrete block wall; i.e., not a construction moisture issue).

Several interior insulation assemblies were simulated in a two-dimensional hygrothermal model. In addition, other parameters such as basement temperature/relative humidity and solar gains were varied. The test assemblies were, from exterior (concrete side) to interior:

- **A1:** Fiberglass insulation only (no vapor retarders on either side)
- **B3, B4, & B6:** Fiberglass insulation, polyethylene (baseline condition causing problems)
- **B1 & B2:** Building paper, fiberglass insulation, polyethylene
- **A2 & B5:** Building paper, fiberglass insulation, building paper

The results are summarized in a graph showing moisture accumulation over the course of a summer (May though mid-June) in Figure 4.1. It demonstrates that B3 (the baseline case) experiences the highest accumulation, followed by B6 and B4 (same assembly, but with warmer basement temperatures, creating a smaller thermal gradient across the wall).

In contrast, the assemblies with building paper on the concrete side (B1, B2, B5) show much lower accumulation, indicating the benefit of moderate vapor control to the exterior of the assembly. The driest is B5 (building paper on both sides): it controls inward vapor drives, but allows the greatest drying to the interior of accumulated moisture.

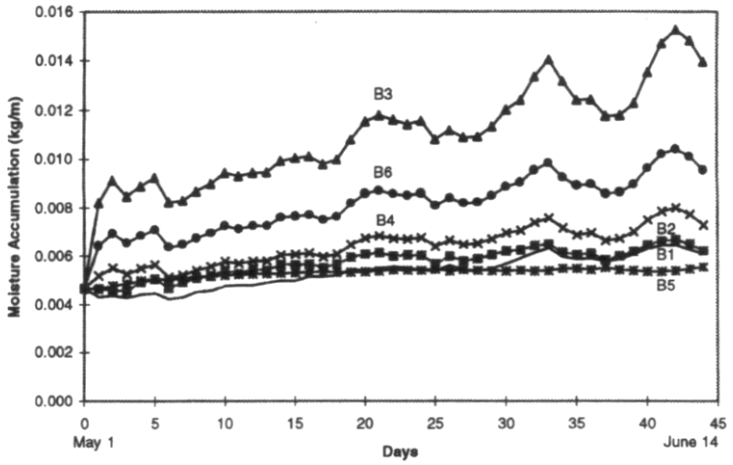

B3 Poly interior; 15° C int.
B6 Poly interior; 21° C int.
B4 Poly interior; 25° C int.

B2 Building paper & poly w/o solar gains
B1 Building paper & poly w. solar gains

B5 Building paper both sides

Figure 4.1: Simulation results, Swinton & Karagiozis (1995)

Full-year simulations were also run on two cases: fiberglass only (no vapor retarders), and building paper on both sides. Although the fiberglass-only wall had low moisture levels in summer, wintertime condensation on the cold upper concrete occurred. In comparison, the building paper (both sides) assembly showed consistent low moisture levels, and was considered the most promising assembly by the researchers.

4.1.2 Timusk and Pressnail (1997)

"Another Look at Interior-Insulated Basement Wall"

The researchers present extensive background on soil moisture and thermal conditions; this thesis is indebted to their presentation of the basic underlying physics. They point out that a water vapor diffusion membrane is unnecessary on the wall at a depth of a few hundred millimeters (4-8") below grade or deeper. The storage ability of the concrete makes this vapor diffusion membrane unnecessary. Summertime adsorption of interior moisture vapor by a concrete wall colder than interior dewpoint is proposed as a passive dehumidification system; this moisture could be released in winter, providing needed humidification.

Based on these physics, they propose an interior basement insulation assembly designed with the knowledge that the above and below grade portions face different conditions, as shown in Figure 4.2. The assembly is a stud frame with fiberglass batt insulation and gypsum board, with horizontal blocking in the stud bays to create an air barrier between the upper and lower portions. The upper portion is as per the CHBA detail (see Figure 2.8), with an exterior moisture barrier to grade and an interior vapor retarder full height. The lower portion has no vapor retarders, with only gypsum board to the interior. Note that strips of XPS foam are used at to isolate the vulnerable wood framing from the cool damp concrete surface, creating "thermal studs."

The researchers also recommend the use of a gap at the edge of the floor slab, to allow drainage of incidental condensation to the sub-slab drainage field. The air barrier to the interior is provided by a seal between the bottom plate and the floor slab.

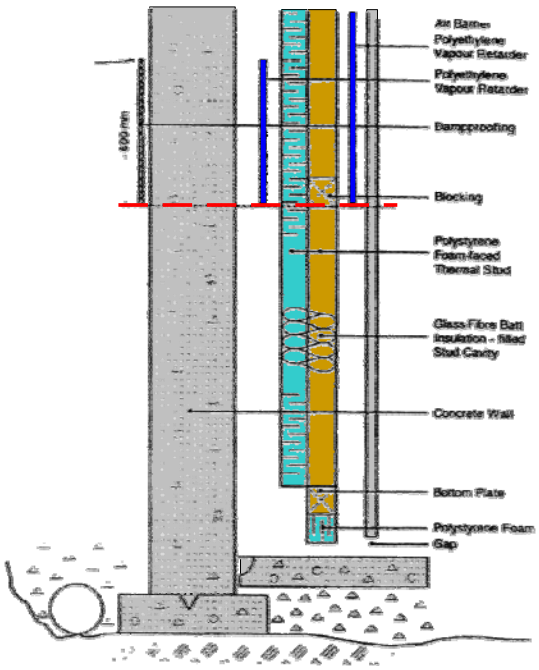

Figure 4.2: Internally insulated wall from Timusk and Pressnail (1997)

While this assembly addresses many of the problems caused by these boundary conditions, this detail is complex enough that it is unlikely to be built. For instance, the horizontal blocking and use of polystyrene foam might be problematic.

In addition, this assembly is still vulnerable to inward vapor drives at the above-grade section, given the lack of an exterior vapor retarder above grade. Finally, the dampproofing is omitted in the below-grade portion, in order to enhance dehumidification capacity of the concrete. Although this effect will occur, it leaves the exterior of the concrete vulnerable to liquid capillary uptake, if exterior drainage does not keep liquid water away from the wall surface.

4.1.3 Cheple and Huelman (2001)

"Why We Need to Know More About Basement Moisture"

These researchers from the University of Minnesota conducted a literature survey of basement moisture research, and proposed six assemblies that manage moisture risks. The authors emphasize the role of the basement as a moisture source within the house, resulting in high interior relative humidity levels, and risks of condensation and mold growth. They provide some background on the structural and health implications of high moisture levels, as well as moisture transport mechanisms. They also present field diagnostic procedures and tools to assess the feasibility of converting an existing basement into finished space.

Of the six assemblies, the first three, while providing excellent solutions to historic moisture problems, would unfortunately be unlikely candidates for low-cost implementations that would meet

energy codes. These options were (1) exterior insulation (2) no insulation (with permeable interior finishes) and (3) a completely sealed interior-side waterproof/vapor impermeable barrier, with provision for drainage behind the system into the sub-slab gravel (i.e., full negative-side waterproofing). Some type of vapor control would be needed inboard of the insulation layer, in order to prevent condensation on the waterproof/vapor impermeable barrier. This last method is acknowledged to be expensive; in addition, an adequate air seal must be installed between the drainage space and the interior to ensure indoor air quality.

Concept (4) is the use of interior insulation with highly vapor permeable but airtight interior finishes. High wintertime humidities would present the risk of condensation or frost on the upper wall surface, as described in Chapter 3 (Section 3.6.2). The authors emphasize the need for interior dehumidification with this system, due to the moisture loading through the basement walls. In addition, they present their opinion that this system should only be used with "dry foundations and wall systems," due to that potential moisture source.

Concept (5), as shown in Figure 4.3, is a variant of the assembly presented by Timusk and Pressnail (see Figure 4.2); this version includes exterior semi-rigid fiberglass draining insulation, from the footing to grade.

Concept (6), as shown in Figure 4.4, addresses specific problems with concrete block foundation walls: convective transport or thermal looping within the cores of the block, resulting in increased heat loss. The solution presented is to insulate on the exterior from the top of the wall to some distance below grade, and as an option, to add a horizontal skirt of insulation, similar to frost-protected foundations. However, this approach still has the problem of requiring protection for the exterior insulation above grade.

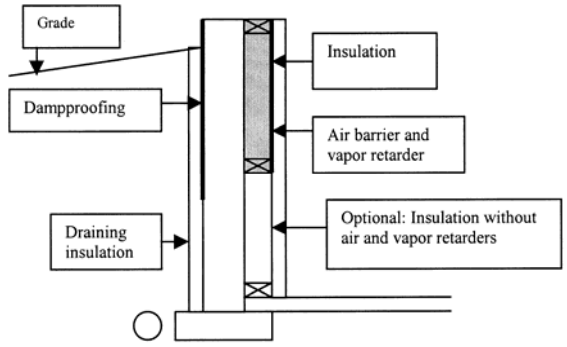

Figure 4.3: Concept (5), from Huelman and Cheple (2001)

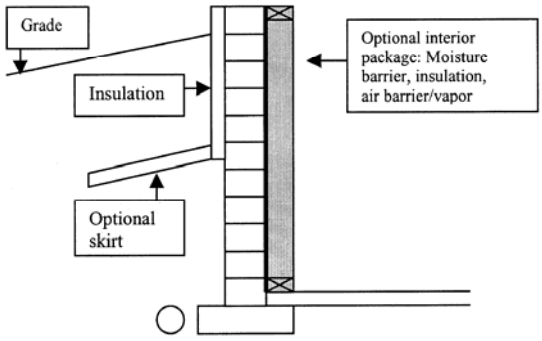

Figure 4.4: Concept (6), from Huelman and Cheple (2001)

They conclude with a list of research needs for hygrothermal behavior of below-grade spaces.

4.2 Experimental Research/Field Surveys

Research on interior insulation of basement walls in the field is described here. A substantial and continuing body of research has been conducted by Goldberg of the University of Minnesota Buildings Foundation Research Program (from 2001 through 2006). Although this research was not

published in the peer-reviewed literature, some of the experimental data is available electronically, making it well suited for secondary analysis.

4.2.1 Robert W. Anderson and Associates (1989)

"Final Report: A Survey of Moisture in Minnesota Home Interior Foundation Wall Insulation "

Robert W. Anderson and Associates (1989) performed a field survey of 42 houses in the Minneapolis/St. Paul area for the Energy Division of the Minnesota Department of Public Service. Goals included determining the prevalence of long-term moisture damage to interior basement insulation systems, as well as correlations between moisture damage and construction details, the presence or quality of vapor barriers, and interior relative humidity.

The researchers inspected all the basements in April 1989, and then reinspected sixteen of the basements in June 1989, to measure contrasting summer conditions. The houses were recently constructed (up to four years old); basement walls included cast concrete and block construction. The researchers measured moisture content of wood framing of the interior insulation assemblies, and interior humidity conditions. Insulation cavities and framing were visually examined for damage; the inspection also looked at evidence of bulk water drainage/leakage problems, and the condition/presence of a vapor barrier. The installation of the polyethylene vapor barrier (on 38 of the 42 basements) was classified as "excellent," "good," or "poor" (i.e., from "air sealed" to having "many tears and rips").

In the April inspection, the researchers found no evidence of moisture damage, mold, or elevated wood moisture content in 40 of the 42 basements. The two basements with elevated moisture levels (22-24% MC) and observable mold had evidence of bulk water leakage through foundation cracks. In the June inspection, three additional foundations showed damp insulation cavities at the bottom of the walls; this was also attributed to inadequate drainage. In addition, one block foundation showed evidence of inward vapor drive, in the form of beads of moisture on the exterior side of the polyethylene at the above-grade portion.

The wood moisture content measurements were largely in the safe range; little correlation was seen between MCs and interior relative humidity levels. As would be expected, higher MC levels were seen in the summer inspection.

Basement wall temperatures were measured in April; lower concrete wall surfaces were largely in the 7-13° C (45-55° F) range.

There was no correlation between the quality and/or presence of a vapor retarder and framing moisture content; walls without polyethylene had moisture content levels similar to those with polyethylene, in both April and June. In addition, the authors noted that polyethylene impedes the drying of incidental wetting (such as leakage due to improper drainage or capillarity), and suggested that it might be better to omit this layer. They therefore concluded that the presence of the polyethylene vapor barrier has little benefit for reducing moisture damage in the insulation cavities.

4.2.2 Canada Mortgage and Housing Corporation (1999)

"Basement Walls that Dry Quickly"

This research was conducted by Forest and Ackerman at the University of Alberta; they compared ten basement interior insulation systems by introducing water to the assemblies and measuring their drying responses. Two types of wetting events were imposed on the walls: a controlled leak behind the panel, and a short-term flood to a depth 100 mm (4") above the slab. The drying response was measured by periodic disassembly and inspection, plus moisture content measurements with a handheld meter.

Seven of the tested walls were stud frame with fiberglass batt insulation and polyethylene: five wood and two steel stud. Variants were constructed with options such as the use of a concrete-side moisture barrier (polyethylene), raising the bottom plate 19 mm (3/4") off the slab, and using a non-paper faced drywall alternative.

The remaining three walls were proprietary systems that were not based on conventional stud frame & fiberglass insulation construction. One used draining extruded polystyrene foam with polyethylene, and the drywall alternative as the interior finish; the second used rigid fiberglass panels in a plastic frame, and the third used a conventional wood stud frame with spray polyurethane foam insulation and the drywall alternative as the interior finish.

The results for the controlled wetting of the wood frame walls are shown in Figure 4.5 below; the legend reflects the vertical order found on the graph.

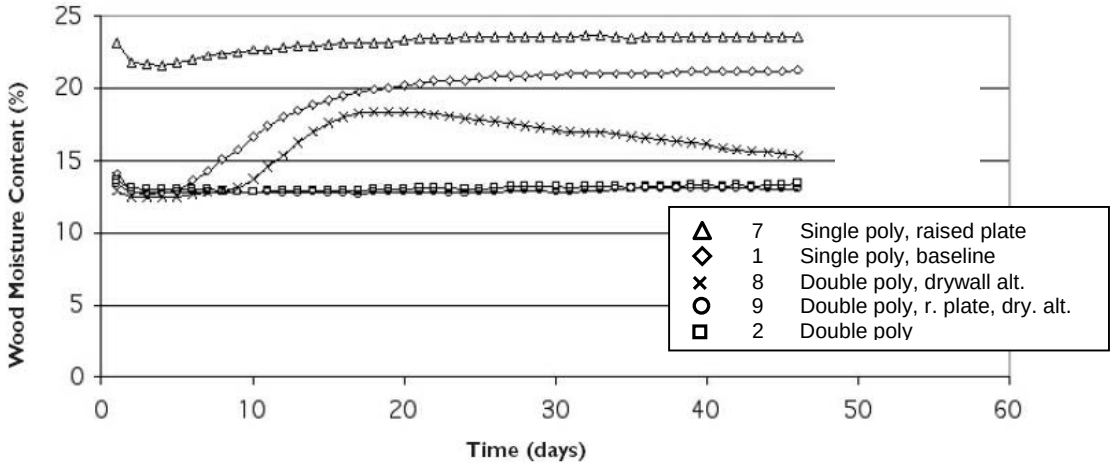

Figure 4.5: Wood stud frame drying responses to controlled leak (CMHC, 1999)

The researchers found that the "double poly" assemblies (i.e., with an exterior side moisture barrier) were protected from controlled leaks: the water ran down the exterior side of the polyethylene and into the basement. This is noted by their flat response (walls 9 and 2), or by a quick decline in moisture content (wall 8; likely drainage of moisture from the cavity). In comparison, the single poly walls retained moisture for a sustained periods; this is possibly due to the moisture storage of the concrete, which is closely connected to the stud bay.

In the flooding test, the conventional stud frame walls (including the "double poly" assemblies) all showed long periods with sustained elevated moisture levels.

In comparison, in both of these tests, the proprietary wall systems showed low retained moisture levels and/or quick drying. The only caveat was that the humidity in the gap between the concrete and the extruded polystyrene had sustained high humidity levels, which could be conducive to mold growth.

Overall, the researchers found that no visible mold growth was found over the course of their experiment, only water staining. One conclusion was that the conventional stud walls all retain too much moisture to withstand substantial leaks or flooding.

4.2.3 Goldberg and Huelman (2001)

"Cloquet Residential Research Facility: Rim Joist and Foundation Insulation Project Final Report"

Goldberg, of the University of Minnesota Buildings Foundation Research Program, tested several stud frame and fiberglass batt interior basement insulation wall assemblies with a variety of vapor control strategies in a test basement facility. In addition, rim joist vapor retarders were examined as a variable. Test wall combinations were as follows:

Table 4.1: Vapor control combinations tested (Goldberg and Huelman 2001)

Interior vapor retarder	Exterior moisture barrier	Moisture barrier height
Polyethylene, full height	Polyethylene	Full
Polyethylene, full height	Polyethylene	To grade
Polyethylene, full height	None	n/a
Kraft batt facing, full height	Polyethylene	Full
Kraft batt facing, full height	Polyethylene	To grade

Other variables included orientation (north and south) and foundation wall (block and cast concrete).

Unfortunately, interpretation of Goldberg's results is made difficult by the use of relatively unconventional terminology ("degree of saturation," and "condensation plane location ratio"). The former term appears to be equivalent to the relative humidity at a given surface, assuming a certain dewpoint. The latter term seems to indicate a misunderstanding of the actual mechanisms of condensation; the author appears to believe that condensation occurs at a discrete plane within the insulation batt space, and then migrates to the surface where condensation actually occurs. Condensation requires a surface with sufficient thermal mass to absorb the latent heat of vaporization, and typically occurs at a surface with a substantial change in vapor permeability, thus the appearance of condensation on the interior side of sheathing or the exterior side of polyethylene. However, she does characterize the mechanisms of summertime inward vapor drive in the various assemblies in a manner consistent with the understanding discussed earlier.

Although there is a complete set of data presented, it is shown with all data for a given wall type on a single graph, making performance comparisons between walls difficult.

This report recommended the adoption of the double vapor retarder assembly (first assembly listed in Table 4.1). However, this recommendation is followed by a 2002 addendum, which notes problems with this assembly in a "wet basement" or "superficially dry" basement walls (as described in Chapter 3, Section 3.6.5). The author offers interior insulation with polystyrene foam and a concrete-side moisture barrier as a viable alternative. Based on earlier discussions, the need for the polyethylene is questionable, and more likely to exacerbate problems.

The author also recommends the use of RSI 1.8 (R-10 imperial) exterior foam insulation at the rim joist, with an empty joist bay cavity, in order to minimize moisture accumulation at the rim closure.

4.2.4 Goldberg and Aloi (2002)

"Owens Corning Basement Insulation System Experimental Evaluation Project"

Goldberg evaluated an Owens Corning proprietary interior basement insulation and finishing system at the same basement facility, against concrete block walls. This system uses 64 mm (2.5") rigid fiberglass insulation panels with a vapor permeable polyolefin air barrier material on the interior surface. The panels are attached to the wall by PVC tee channels nailed to the concrete (see Figure 4.6). Several variants were tested:

- The system as designed, with no vapor retarder
- The system with an exterior-side moisture barrier (between insulation and concrete)
- The system with an interior-side vapor barrier (on interior side of insulation)

In addition to temperature and humidity measurements, the researchers installed removable panels that could be periodically weighed to measure moisture accumulation in the insulation. These panels were located at a high position (above grade), and mid-height in the panel (midway between grade and slab) (see Figure 4.7).

Figure 4.6: Owens Corning basement test (Goldberg and Aloi 2002)

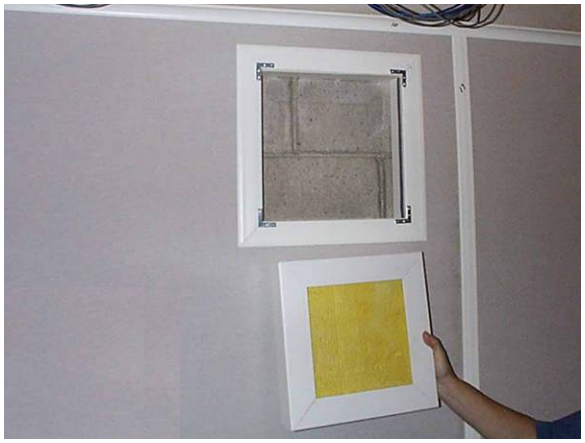

Figure 4.7: Removable test panel at upper position (Goldberg and Aloi 2002)

Like previous work, a complete data set is published, but comparison between individual test panels is difficult with that presentation. However, the record of moisture accumulation in the removable panels provides an excellent metric of overall performance.

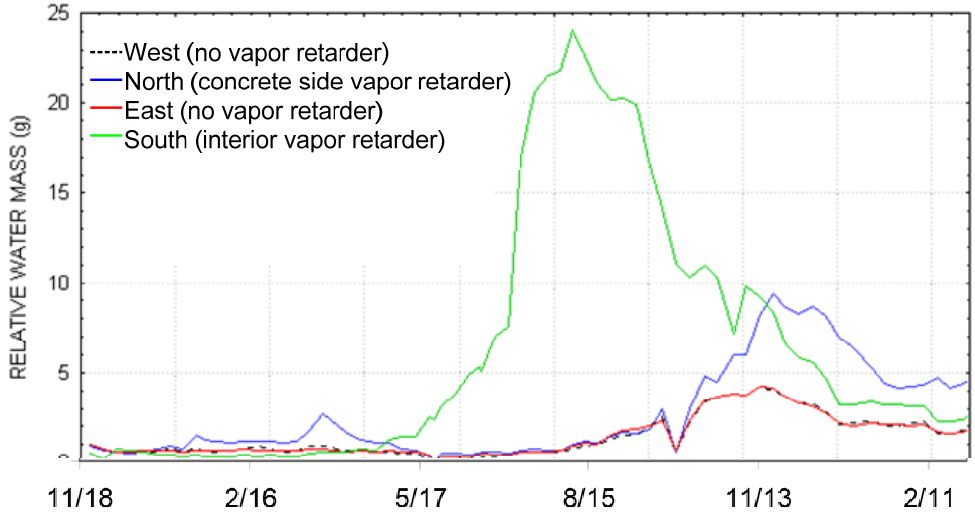

Figure 4.8: Water mass in removable panels, below grade/mid-height (Goldberg and Aloi 2002)

Figure 4.8 shows the water mass in the removable panels at the mid-height (below grade) location. All panels show minimal accumulation through the winter; conditions were 20°, 35-45% RH (5-8° C dewpoint). Moving into the summer, the assembly with the vapor retarder on the interior shows a sharp spike in moisture content, and then dries going into the winter. Given the orientation, it seems likely that this is an attenuated version of inward vapor drive, especially because no dampproofing is applied to the exterior of the foundation.

As the temperature gradient shifts outwards going into the fall and second winter, the north, east, and west walls gain moisture. However, the concrete side vapor retarder (north) wall shows a greater rise: this is likely due to the removal of concrete's storage capacity by the polyethylene, compared to the no vapor retarder walls. The interior dewpoint during the second winter were similar to the first winter, at 6-11° C (14° C and 60-80% RH). The difference is likely caused by colder exterior conditions: online weather data backs this claim, although exterior temperature records are not included in the research.

It is notable that the as-designed panels (no vapor retarder) consistently show the driest behavior throughout the entire monitoring period at the mid-height location.

In comparison, the water mass in the upper position removable panels is shown in Figure 4.9. The no vapor retarder (north) panel shows the greatest weight gain the first winter, but the identical panel on the south side is the driest. It is unfortunate that the effects of orientation and assembly design are combined in this experiment, as it impedes direct comparisons in performance. The difference is likely from the temperature difference between orientations; the colder north side would experience the greatest condensation or frost buildup on the above-grade portion of the wall.

Moving into the summer, the interior-side vapor barrier (west) panel shows a tremendous rise in moisture content; it is graphed on a separate axis, peaking at 375 g, compared to a maximum of 25 g in other panels. This clearly demonstrates inward vapor drive in the above-grade portion of the wall. In comparison, the no vapor retarder panels are letting moisture pass through to the interior, and the concrete side vapor retarder assembly prevents inward vapor drive from entering the fiberglass.

In the second winter, the north side no vapor barrier panel gains the greatest amount of moisture, peaking at 25 g. To put this gain in perspective, it can be compared with the DIN 4108-3 standard (Deutsches Institut für Normung 1999) for maximum allowed condensation, at 0.5 kg/m^2 for nonabsorbent surfaces, and 1 kg/m^2 for absorbent surfaces. This weight gain over a 0.093 m^2 (1 square foot) panel is 0.27 kg/m^2; the photographic record suggests this moisture is being stored within the structure of the fiberglass as opposed to condensing on a surface.

The no vapor retarder (south) wall shows less accumulation than the concrete side vapor retarder (east) wall in the second winter. It is unknown if this is due to the reduced moisture storage in the "moisture barrier" wall, or because of orientation effects.

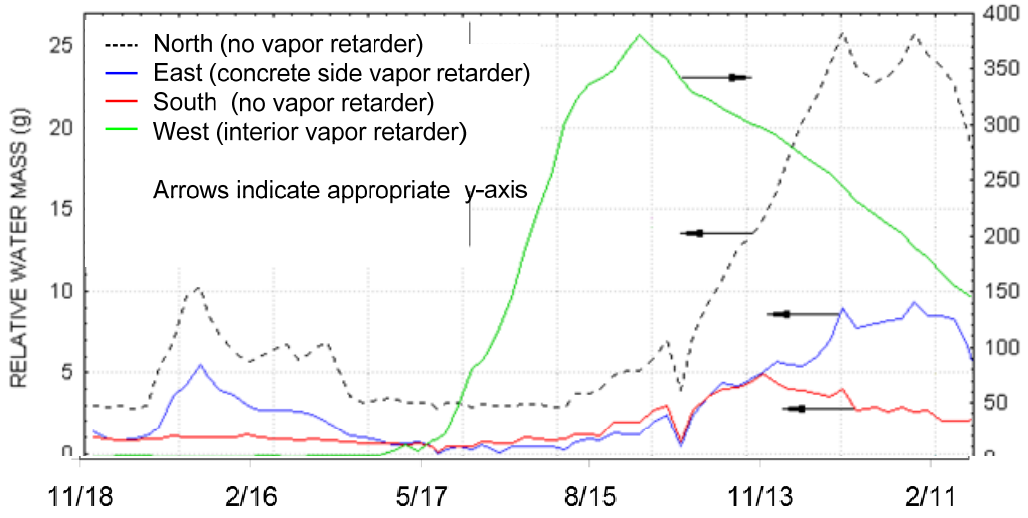

Figure 4.9: Water mass in removable panels, above grade/upper height (Goldberg & Aloi, 2002)

Photos and descriptions from the wintertime disassembly at the conclusion of the experiment provide insight into the overall performance of the walls. On the no vapor retarder walls, there was a small amount of incidental condensation on the fiberglass-block interface and some condensation on the impermeable plastic track, at the above-grade portion. The block showed some darkness, suggesting dampness and storage of moisture in the concrete. The wall with the "moisture barrier" (polyethylene on the concrete side) had visible condensation and rundown on the above-grade portion; some portions of the insulation were waterlogged, and rust was visible on the nails attaching the track. The wall with the vapor barrier on the interior side had some damp portions, and strong brown discoloration on the surface of the fiberglass, especially at the top of the wall.

From this data, it appears that the system with permeable surfaces (as designed) has the best overall performance; the only question is whether or not the condensation seen during winter disassembly would re-evaporate safely, resulting in no net moisture accumulation.

Goldberg uses these results to promote the double vapor barrier configuration, noting the failure of both single vapor barrier versions; however, a 2002 addendum notes the problems with the impermeable assembly. She concludes that the vapor permeable Owens Corning system provides thermal protection and does not accumulate moisture. However, she notes that it does not control vapor entry into the basement, thus necessitating dehumidification—a potential obstacle for regulatory approval.

4.2.5 Goldberg and Farkas (2004)

"Icynene Foundation Insulation Project"

In this project, Goldberg and Farkas compared a variety of vapor control strategies using open cell spray polyisocyanate foam (Icynene) in wood and steel stud framed walls inboard of a concrete block foundation (Figure 4.10). Inspection ports were cut in the foam insulation, to allow observations of interstitial conditions and weighing of the sample, as shown in Figure 4.11. The vapor barrier combinations are shown in Table 4.2 a given "quadrant" or corner of the test basement has test panels on both orthogonal orientations.

Table 4.2: Assemblies tested (Goldberg and Farkas 2004)

Description & location	Interior side vapor retarder	Exterior (concrete side) vapor retarder
No vapor retarder NW Quadrant	None (drywall only or exposed)	None
Wall-side vapor retarder NE Quadrant	None (drywall only or exposed)	Trowel-applied waterproofing + poly or polyethylene full height
MN Code (both sides) SE Quadrant	Polyethylene	Polyethylene to grade or polyethylene full height
Interior vapor retarder SW Quadrant	Polyethylene	None

Figure 4.10: Installation of Icynene insulation (Goldberg and Farkas 2004)

Figure 4.11: Removable test panels (Goldberg and Farkas 2004)

One weakness in the experimental design was the use of corner bays as experimental bays: they are not directly comparable to bays in the middle of the wall. The corners will be colder and wetter during the heating season; this fact was demonstrated in Goldberg's previous research. In addition, as in earlier experiments, wall assemblies are scattered on all four orientations, further complicating comparison between walls.

Similar to previous work, there is a complete presentation of data, but not a focused set of graphs to back up specific arguments by showing relative performance of walls. Again, graphs of weight gain in the removable panels provide a comparison of the walls. Raw data was processed and replotted here in Figure 4.12 and Figure 4.13: they plot weight change as a percentage of the sample weight.

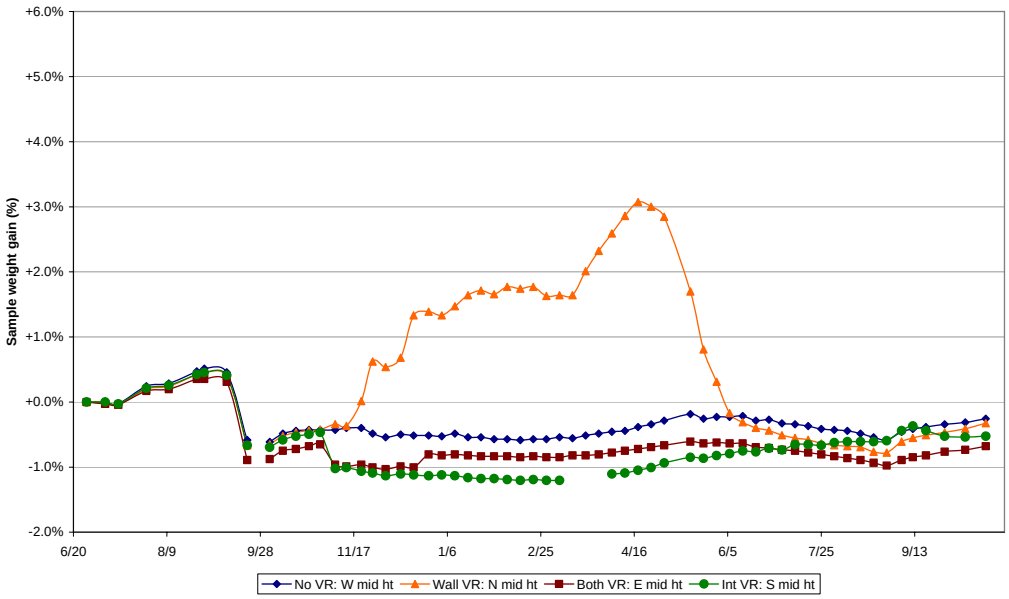

Figure 4.12: Removable Icynene panel weight gain; mid height (Goldberg and Farkas 2004)

The mid-height panels have relatively stable moisture uptake behavior; the panel with the concrete-side vapor retarder shows a moisture gain through the winter, peaking at 3%; this can be explained by the elimination of storage in the concrete block. In addition, this panel is on the north side, which is the worst-case orientation. The remaining panels are drier than their initial state, which is expected behavior: water/steam is the blowing agent for this insulation, so construction moisture would be released over time.

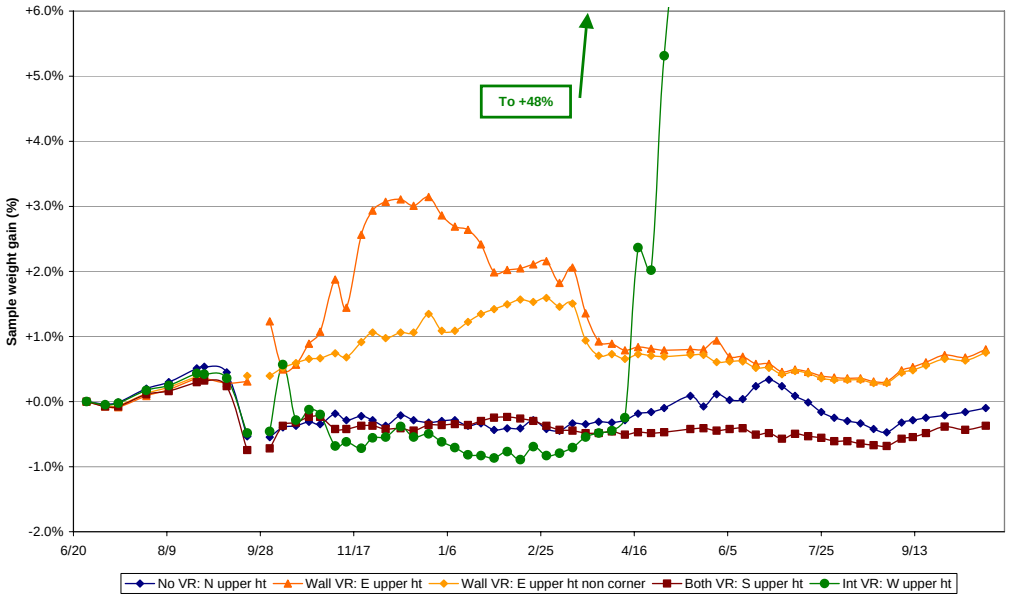

Figure 4.13: Removable Icynene panel weight gain; upper height (Goldberg and Farkas 2004)

The weight change for the upper height panels shows much more dynamic behavior. Again, the concrete-side vapor retarder wall shows a weight gain during the winter: it is interesting to note that the gain is worse for the corner panel (Wall VR: E upper ht) compared to the mid-wall panel (Wall VR: E upper ht non corner); both panels have the same orientation. This difference is likely due to the colder corner, which would result in greater condensation or accumulation.

The largest weight gain is in the interior-side vapor retarder wall (Int VR: W upper ht). In early spring, moisture content climbs sharply: it reaches a peak value of 48% gain by mid-September, and then starts to slowly drop. This is a clear demonstration of inward vapor drives trapped by the impermeable polyethylene in this assembly. It shows the magnitude of this above-grade inward vapor pressure gradient, relative to the other driving forces. The no vapor retarder configuration (No VR: N upper ht) shows a slight rise in moisture content, but dries out in the fall.

Disassembly at the conclusion of the project was also useful to compare the walls; this was done in the fall (October). At the removable panels, the only visible moisture accumulation was at the interior vapor retarder wall, as would be expected by data shown in Figure 4.13. There was some darkening or dampness observed on the concrete surface in the north-facing no vapor retarder wall. This was followed by removal of the gypsum board and inspection of the surfaces. In the wall with poly on both sides, but only to grade on the exterior, condensation was noted on the interior-side vapor barrier. This demonstrates inward vapor drive entering at the exposed above-grade portion, and become trapped in the assembly.

It is worth noting that in the assemblies with no vapor barrier, the exterior side of the gypsum board showed no damage; this indicates that any moisture vapor driven inwards was safely passed through without accumulation. However, these assemblies were on the north and west orientations, which are not the worst case.

In addition, the no vapor barrier wall was run into the following February; disassembly then showed some frost accumulation occurring within the outer layer of the Icynene.

The author concluded that a wall with permeable foam insulation (such as Icynene) without vapor retarders had no net moisture accumulation, condensate rundown, or visible mold growth. Both of the assemblies that had polyethylene on only one side showed some accumulation and condensation, with an interior vapor retarder giving the worst performance. The double polyethylene assembly showed some condensation within the cavity; the author ascribes this to lateral leakage from the adjacent wall. This demonstrates the lack of drying available in this assembly.

It should be noted that this Icynene research is an interesting case study because the material eliminates airflow as a transport mechanism, and only shows diffusion. These results show that diffusion can transport enough moisture to cause frost accumulation within the insulation when run at a condition such as 20° C/40% RH or 18° C/50% RH (+6 to 7° C dewpoint). It was not determined conclusively if this would safely be stored and re-evaporated over the spring. As a reference point, the 89 mm (3.5") of Icynene used here has a permeability of 1380 ng/(s·m^2·Pa) or 24 Imperial perms.

4.2.6 Goldberg and Gatland (2006)

"Polyamide-6 Based Interior Foundation Insulation System: Experimental Evaluation"

In this research, Goldberg and Gatland tested interior basement insulation assemblies that included a vapor control material with permeability that varies as a function of relative humidity. As humidity increases, the permeability of the membrane increases. This material is a 0.05 mm (2 mil) polyamide-6 (PA-6) nylon film marketed under the name MemBrain™ by CertainTeed; it is known colloquially as a "smart vapor retarder." This material has permeability that can change between 43-700 ng/(s·m^2·Pa) or 0.8-12 perms, dry/wet cup. Other materials tested were a trowel-applied elastomeric waterproofing coating (a bitumen- and solvent-free, latex rubber-based cold vulcanizing material; 4.6 ng/(s·m^2·Pa) or 0.08 Imperial perms), and Kraft-faced fiberglass batts. Kraft paper also responds to ambient relative humidity similarly to PA-6, but with a much smaller change in permeability (17 to 34-240 ng/(s·m^2·Pa) dry cup/wet cup, or 0.3 to 0.6-4.2 perms) (ASHRAE 2005).

Table 4.3: PA-6 Wall assemblies tested (Goldberg & Gatland 2006)

Interior finish	Interior vapor control	Insulation	Exterior moisture barrier	Orientation & location
Gypsum board or none	PA-6	Fiberglass batt	—	East, south (including corners)
Gypsum board or none	PA-6	Fiberglass batt	PA-6	North corner, east (including corner)
Gypsum board or none	PA-6	Fiberglass batt	Elastomeric waterproofing	North, east
None	Kraft facing	Fiberglass batt	—	North, south

Although the selection of assemblies reflects polyethylene-based assemblies used in practice (i.e., vapor or moisture barriers on one side or both sides), it appears that the second assembly does not

reflect the best use of PA-6, knowing its properties. Specifically, using PA-6 as a "moisture barrier" against the concrete will result in accumulation behind the membrane until a higher relative humidity is reached; it will then become more permeable, allowing moisture to enter the stud bay. In other words, it would do little to protect against inward vapor drives at the top of the wall, or moisture sourced from the concrete/soil. In the first and third assemblies, the PA-6 layer is being used in its expected role as an interior-side vapor retarder. As with earlier research, orientation and corner effects are mixed with the use of various assemblies, complicating interpretation of results.

During the examination and monitoring of the walls during the experiment, interesting behavior was noted in walls experiencing summertime inward vapor drive. Although the PA-6 walls showed high relative humidity conditions on the interior side of the stud bay (i.e., where condensation was expected to happen; levels at or near 100%), little condensation actually occurred. An example of worst-case condensation is shown in Figure 4.14. Polyethylene walls being run concurrently showed substantial condensation on the equivalent surface. The incidental condensation noted in the PA-6 walls was able to dry; by wintertime, it was at dewpoint levels lower than the interior. Goldberg concludes from the data that a system using a PA-6 vapor retarder on the interior side (with no exterior moisture barrier/"water separation plane" has acceptable performance, with no net accumulation of moisture and no noted mold activity.

During the winter, the walls with PA-6 on the interior side showed some frosting and condensation; however, it was unclear if this was due to vapor transport or air bypass at the removable test panels. The frosting pattern (at the perimeter of the panels) suggests air leakage as the mechanism.

The Kraft-faced batts had similar performance to the PA-6 walls; Goldberg argues that it had better hygrothermal performance. However, a minimal difference is seen in the data; a larger difference appears to be due to the effect of different orientations (east vs. north). Goldberg also noted wetting of the paper facing during the experiment, raising the possibility of mold growth, although none was observed over the length of the experiment (slightly over one year).

Vapor pressure measurements showed that the liquid-applied dampproofing applied to the interior side of the concrete greatly reduced or eliminated moisture gain from inward vapor drives in the above-grade portion of the wall. However, the hydrophobic nature of the coating results in greatly increased wintertime condensation and rundown; frost and condensation were observed during inspections. In comparison, bare concrete block has the storage capacity, reducing liquid water condensation.

The liquid-applied dampproofing showed some delamination or bubbling on the above-grade portion on the north-side test wall, as shown in Figure 4.15. This may be damage due to extended condensate exposure, or perhaps damage due to frost exposure. As a latex-based coating, it would be vulnerable to re-emulsification in a wet (liquid water) alkaline environment, as would be caused by extended condensation. It is unlikely that the delamination is due to inward vapor gradients, given that the north wall least likely to experience this problem, and it was not seen on the east exposure.

Figure 4.14: Example of worst condensation seen on PA-6 vapor retarder (Goldberg and Gatland 2006)

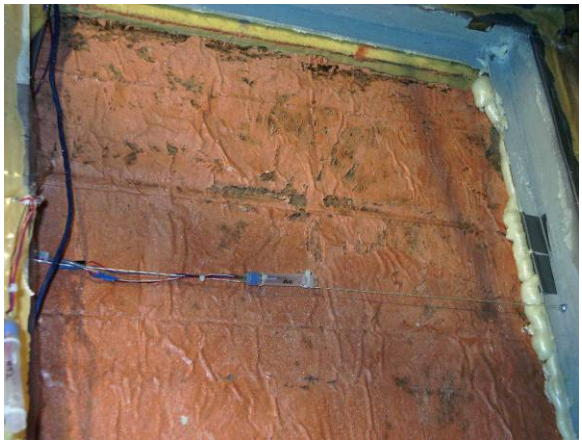

Figure 4.15: Deterioration of wall-side waterproofing coating (Goldberg and Gatland 2006)

The wall built with PA-6 on both sides of the assembly showed performance equivalent to the wall with PA-6 only on the interior. This was the expected behavior, since the inward vapor drives would render the exterior-side PA-6 highly permeable (as noted above).

Those walls with PA-6 on the concrete side (as a "moisture barrier") also showed condensation collecting between the membrane and the concrete block during the final disassembly in wintertime (February), especially on the upper portions of the wall. This is roughly expected behavior: the interior conditions create an outwards vapor gradient at the top portion; at the cold interface between the insulation and PA-6, the relative humidity is high. Therefore, the permeability of the membrane increases, and the moisture reaches the concrete surface and condenses.

4.2.7 Zuluaga et al. (2004)

"Field Performance of Different Interior Basement Insulation Systems"

These researchers from Steven Winter Associates performed long-term monitoring on eight interior basement insulation assemblies in an unoccupied model house in the Chicago, IL area. The tested insulation systems could be divided into three categories: rigid plastic foam boards, fiberglass roll blankets, and wood stud frame with fiberglass insulation. The assemblies are summarized in Table 4.4, below.

Table 4.4: Wall assemblies tested in Zuluaga et al. (2004)

Category	Description	Notes
Rigid foam	1.5" polyisocyanurate	Impermeable foil facers (Class I)
Rigid foam	2" EPS (expanded polystyrene)	Gypsum board applied for fire protection
Roll blanket	Nonperforated facer	Class I vapor retarder facer, cut 6" above slab
Roll blanket	Perforated facer	Class III vapor retarder facer, cut 6" above slab
Stud frame	Encapsulated fiberglass batt	Frame 1" from concrete; no gypsum board
Stud frame	Kraft-faced fiberglass batt	Gypsum board interior; frame 1" from concrete
Stud frame	Unfaced fiberglass batt	Gypsum board interior; frame 1" from concrete

The two roll blankets walls were built with a 150 mm (6”) gap at bottom, which is a builder practice described in Chapter 3 (Section 3.6.4); this results in an imperfect air barrier for the bottom section of the insulation. The stud walls were framed 1” away from the concrete wall, creating an air space at the interface location.

The results were recorded over the course of approximately two years: both winters had a very low interior dewpoints (-10 to 5° C), but two different summer conditions were imposed. The first summer was run at a relatively low dewpoint, while the second summer had a high dewpoint (~15° C); this was accomplished by running a cold setpoint the first summer, and a warmer one the second summer. Results were presented in the form of monthly average water vapor pressure (absolute air moisture content) for the interior air, and the interface between the concrete and the insulation at high, middle, and low locations.

The results of the two rigid foam insulation systems were compared. The polyisocyanurate showed high vapor pressures behind the foam board at the upper and middle location; this can be ascribed to an inward thermal (and vapor) gradient combined with the impermeable insulation. In winter, interior and interface vapor pressures were similar. In contrast, the vapor pressures behind the EPS wall run roughly parallel to but higher than interior vapor pressures; this is considered the effect of the permeable interior insulation, in rough equilibrium with interior. No moisture spike was seen in the first summer (as in the polyisocyanurate wall), demonstrating the permeability of this system. The authors concluded that the behavior of these two walls was vapor diffusion dominated.

In the stud frame/fiberglass walls, all three had vapor pressure conditions almost identical to interior, at all three heights. The encapsulated batt was slightly wetter than interior in the first summer, but only by a small margin. These three systems had very different permeability values: the difference was ascribed to air bypass movement through the 1” space behind the walls. The gap between the top of the frame wall and the concrete had minimal air sealing, with only fiberglass batt stapled at that location.

In the roll blanket walls, the various wall heights showed varied responses. The lower height sensor closely matched interior vapor pressures; this was ascribed to the air communication to the interior at the cut off bottom portion of the blanket. In contrast, the nonperforated upper and middle locations showed high summer vapor pressures, indicating the inward vapor drive, while the analogous perforated wall locations had a minimal rise. The perforations increased permeability enough to reduce the summer moisture accumulation. In the second winter, the bottom of the blanket was air sealed against the concrete; this resulted in higher vapor pressures in the nonperforated assembly, showing the greater drying ability of the perforated blanket.

One point noted was that with sufficiently low interior dewpoints/vapor pressures, the various forms of air bypass seen in the roll batt and stud frame walls can provide drying. However, at higher interior dewpoints, it can result in condensation on the concrete wall surface.

The authors ascribe several phenomena to vertical diffusion through the concrete wall. While a vertical gradient definitely does exist, the magnitude of this transport mechanism is not conclusively demonstrated or calculated. This vertical diffusion through concrete is questionable, given that the

vapor permeability of concrete (4.7 ng/(s·m·Pa) or 3.2 perm-inch) is several orders of magnitudes smaller than the value of still air or fiberglass batt insulation (172 ng/(s·m·Pa) or 120 perm-inch) (ASHRAE 2005).

Chapter 5
Experimental Setup

To provide more and better quality data as well as to investigate assemblies different than those already tested, a field experimental program was undertaken. Field data was collected at two sites: one was located approximately 56 km (35 miles) west of Chicago, in Huntley, Illinois, United States. The second was located in Kitchener, Ontario, Canada, approximately 100 km (60 miles) west-southwest of Toronto. Huntley is in a DOE Zone 5 climate with 3851 heating degree days base 18° C (6933 HDD 65° F). Kitchener is in the equivalent to DOE Zone 6, having 4288 heating degree days base 18° C (7719 HDD 65° F).

There are eight test walls at the Huntley site, and four at the Kitchener site. Data was recorded at the Huntley site from January 2004 through January 2007, and at the Kitchener site from September 2005 onward.

5.1 Huntley, Illinois Site

5.1.1 Site and house description

The test house is a model house built by a production builder; it is a single-story, three bedroom, 2256 square foot house with a full basement (see Figure 5.1). The basement walls are nine-foot tall 254 mm (10”) cast concrete with spray-applied dampproofing (may be either a solvent-based or an emulsified water-based asphalt coating) on the exterior to grade. Downspouts are directed away from the house with splash blocks, and grading is sloped away from the house on all sides; bulk water is directed away from the foundation. The house was unoccupied for the duration of this experiment. The house had been completed and space conditioned for approximately two years before the installation of the test walls (November 2001 casting; September 2003 installation); therefore, construction moisture was not a significant loading of the experimental assemblies.

Figure 5.1: Front elevation of Huntley test house

Figure 5.2: Rear elevation of Huntley test house

The interior insulation test walls are placed on the rear orientation of the house (see Figure 5.2): it is a long, straight wall, and faces southwest (see Figure 5.3). The ground changes elevation, sloping downwards from the house, on the right-hand side rear corner (see Figure 5.4).

Figure 5.3: Aerial view of Huntley test house

Figure 5.4: Rear oblique Huntley test house

The basement was uninsulated and unfinished before the start of this experiment. The domestic hot water heater, HVAC system, and sheet metal ductwork are all located in this space. A normally closed door at the base of the stairwell separates the basement from the main space.

5.1.2 Test Wall Descriptions

A total of eight test walls were installed in the test basement: they are summarized in Table 5.1 below. They can be divided into four groups: stud frame walls (Walls 1 & 2), foam plastic insulation walls (Walls 3 & 4), composite foam-stud frame walls (Walls 5 & 6), and several other walls that do not fall into these categories (Walls 7 & 8). In the following sections, the walls details are shown in plan.

Table 5.1: Summary list of test walls at Huntley site

Wall #	Wall Description	Wall assembly (exterior to interior, from concrete)
1	2x4 frame with polyethylene interior	2x4 studs 16" o.c. with R-13/RSI 2.3 fiberglass batt insulation, 6 mil polyethylene film
2	2x4 frame w. polyethylene interior & exterior	6 mil polyethylene film; 2x4 studs 16" o.c. with R-13/RSI 2.3 fiberglass batt insulation; 6 mil polyethylene film
3	Foil-faced polyisocyanurate (1.5")	Foil-faced polyisocyanurate (1.5"/38 mm; R-10/RSI 1.8) attached using proprietary PVC plastic channel†
4	Extruded polystyrene (2") w. gypsum wall board	Extruded polystyrene (2"/50 mm; R-10/RSI 1.8); 1x2 furring strips 16" o.c. with airspace; ½" gypsum wall board
5	Extruded polystyrene (1") w. 2x4 frame, fiberglass	Extruded polystyrene (1"/25 mm; R-5/RSI 0.9); 2x4 studs 16" o.c. with R-13/RSI 2.3 fiberglass batt insulation; spun-bonded polyolefin housewrap or ½" gypsum wall board‡
6	Extruded polystyrene (1") w. 2x4 frame, cellulose	Extruded polystyrene (1"/25 mm; R-5/RSI 0.9); 2x4 studs 16" o.c. with R-13/RSI 2.3 damp-spray cellulose insulation; spun-bonded polyolefin housewrap or ½" gypsum wall board‡
7	Rigid fiberglass (2") with polyamide film	Semi-rigid fiberglass board (2-3/8"/60 mm; R-10/RSI 1.8); 2 mil polyamide film and laminated perforated scrim facer
8	Fiberglass roll blanket (3") with perforated facer	Fiberglass roll blanket (3"/76 mm; R-11/RSI 1.9) 4' wide; perforated vinyl facer; 2x2 wood attachment

R-value in $ft^2 \cdot °F \cdot h/Btu$; RSI value in $K \cdot m^2/W$

†: Later in the experiment, the foam board was directly applied to the concrete wall, removing the plastic channels.

‡: The walls were originally installed with spun-bonded polyolefin housewrap at as interior air barrier. This was changed later in the experiment to gypsum wallboard, painted with latex paint.

5.1.2.1 Stud frame walls (Walls 1 and 2)

The two stud frame walls discussed in Chapter 3 (Sections 3.6.4 & 3.6.5) were both tested in this research; they were built with 2x4 framing (16" o.c.) and unfaced fiberglass batts; Wall 1 has a 6 mil polyethylene sheet on the interior side of the stud wall; Wall 2 has 6 mil polyethylene sheet on both the interior and exterior sides.

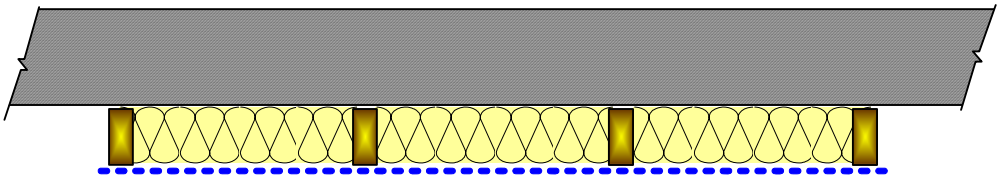

Figure 5.5: Wall 1 (2x4 frame with polyethylene interior)

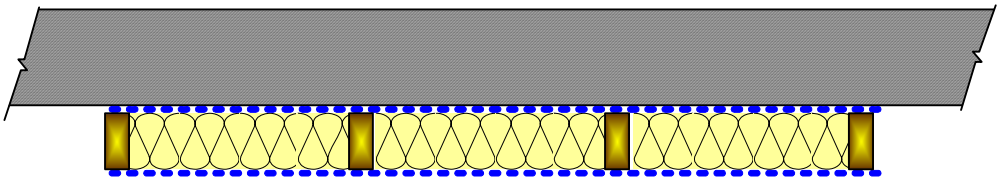

Figure 5.6: Wall 2 (2x4 frame w. polyethylene interior & exterior)

5.1.2.2 Foam plastic insulation walls (Walls 3 and 4)

Wall 3 uses 1-½" thick foil-faced polyisocyanurate insulation, attached to the concrete basement wall using manufacturer-supplied two-piece PVC plastic tee channels. Later in the experiment, the foam board was directly applied to the concrete wall, using caulk and concrete fasteners, removing the plastic channels.

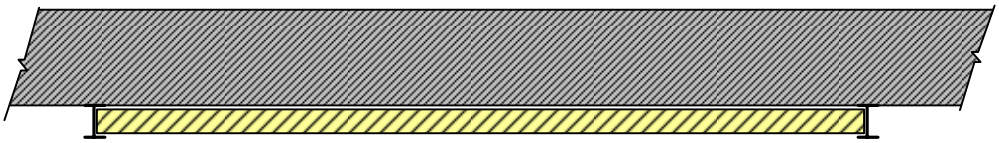

Figure 5.7: Wall 3 (Foil-faced polyisocyanurate (1.5")

Wall 4 has 2" thick extruded polystyrene (XPS), attached to the concrete basement wall with fasteners through 1x3 furring strips, 16" o.c. To provide code-required fire protection, gypsum wallboard was attached to the furring strips.

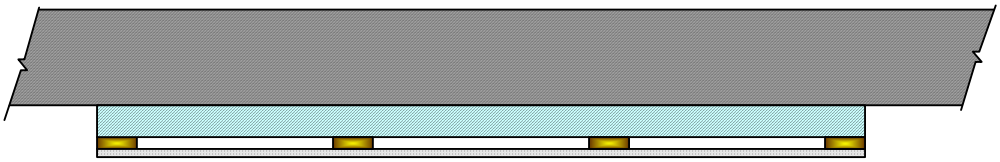

Figure 5.8: Wall 4 (Extruded polystyrene (2") w. gypsum wall board)

5.1.2.3 Composite walls (Walls 5 and 6)

Two variants of the insulation system recommended by Lstiburek (2006), as discussed in Chapter 3 (Section 3.7.4) were tested. These walls combine XPS and a 2x4 frame wall: these assemblies have high resistance to moisture damage, high R-value, and the ability to dry; however, this wall has a higher first cost than most other solutions. Both walls consist of one inch of XPS directly against the concrete wall, followed by a 2x4 stud wall, cavity insulation, and spun-bonded polyolefin (SBPO) housewrap used as an air barrier. Wall 5 uses fiberglass batt insulation in the stud bays; Wall 6 uses damp-spray cellulose. The reason for the use of cellulose insulation was to examine the moisture storage effects of this material in this below-grade application, in comparison to the fiberglass batt baseline.

A high permeability spun-bonded polyolefin (SBPO) housewrap was initially installed (instead of a finish material such as gypsum board, as would be required by code for fire protection) to demonstrate the effect of free vapor flow into and out of the cavity. Later in the experiment, the SBPO layer was replaced with ½" gypsum drywall, painted with latex paint.

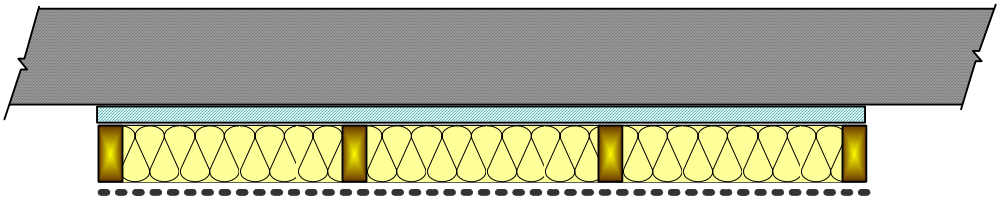

Figure 5.9: Wall 5 (Extruded polystyrene (1") w. 2x4 frame, fiberglass)

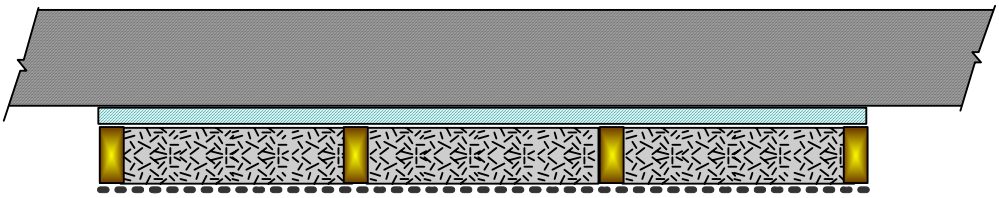

Figure 5.10: Wall 6 (Extruded polystyrene (1") w. 2x4 frame, cellulose)

5.1.2.4 Other walls (Walls 7 and 8)

Two final insulation systems were tested. Wall 7 is a semi-rigid fiberglass board with a polyamide-6 (PA-6) film and a laminated perforated scrim facer. The film is a variable-permeance vapor retarder; at low relative humidities, the permeance is low (<57 ng/(s·m^2·Pa)/1 perm dry cup @ 25% RH;, and at high relative humidities, the permeance is high (> 570 ng/(s·m^2·Pa)/10 perms wet cup @ 75% RH). The material is colloquially known as a "smart vapor retarder" (SVR). The perforated scrim is required for fire protection, and is on the interior side.

The vapor permeability of the combined laminated materials was tested; the results are shown in Appendix D: Vapor Permeability Testing. The results are consistent with the published data on the PA-6 material, combined with a semi-vapor permeable perforated scrim.

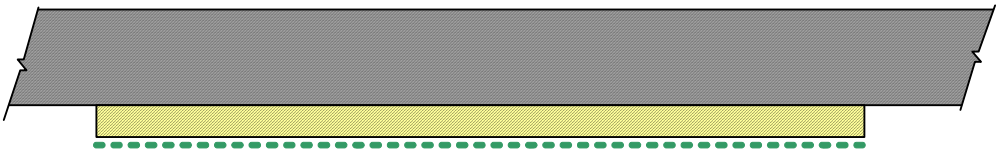

Figure 5.11: Wall 7 (Rigid fiberglass (2") with polyamide film)

Wall 8 is a 4' wide fiberglass roll blanket with a perforated polypropylene facer, and represents standard practice in many areas of the United States. As mentioned in Section 2.2.3.3, the perforations are intended to reduce moisture accumulation behind the batt.

The vapor permeability of the perforated facer was tested as well (see Appendix D); it is a vapor permeable (>570 ng/(s·m^2·Pa)/10 perms) material that shows little response to changing relative humidity conditions. The permeance changes from 720 ng/(s·m^2·Pa)/13 perms dry cup (25% RH) to 790-850 ng/(s·m^2·Pa)/14-15 perms wet cup (75% RH).

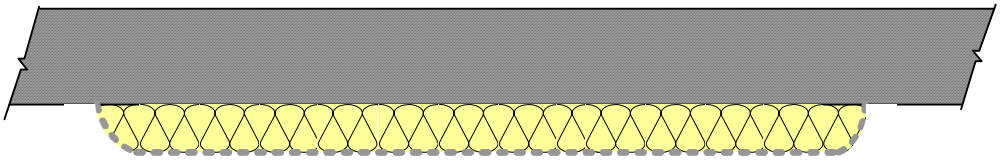

Figure 5.12: Wall 8 (Fiberglass roll blanket (3") with perforated facer)

5.1.3 Instrumentation Package

The test panels were instrumented with temperature (T), relative humidity (RH), and electric resistance-based wood moisture content (MC) sensors, using methodology described in Straube et al (2002). Specifications for sensors used at this site are shown in Appendix A: Sensors and Data Collection Equipment. In addition, wood surrogate moisture content sensors similar to Duff gauges (a.k.a. “wafers”) were installed; the development and calibration of these sensors is described in Appendix B: Development and Calibration of Wood Surrogate Sensors.

The sensor package in each test panel varied according to wall construction, with additional sensors added at noteworthy locations. This layout is shown in Table 5.2, below, and illustrated in Figure 5.13, Figure 5.14, and Figure 5.15.

In all walls, the temperature of the interface between the concrete wall and the insulation was recorded at upper (~100"/2.54 m above finish floor), middle (~50"/1.27 m A.F.F.) and lower (~8"/0.2 m A.F.F.) heights. The upper location is roughly at the level of the exterior grade. A temperature sensor was also installed at the interface between the insulation and the interior finish material (polyethylene, SBPO, or perforated facer), at mid-height. In addition, relative humidity was recorded at the middle height at the concrete-insulation interface. Sensors were installed along the centerline of each test panel, to minimize edge effects.

In the test panels with stud framing (1, 2, 5, and 6), additional sensors were used. Temperature and relative humidity sensors were installed mid-thickness in the stud bay insulation at upper, middle, and lower heights. In addition, the moisture content of a single vertical stud was measured at four locations: at the upper and lower heights, on the exterior and interior sides (3/8"/10mm from the edges of the stud).

In the non-stud framing walls, sensors were added at locations of interest. For instance, in the polyisocyanurate foam and PA-6/rigid fiberglass, and roll blanket walls, a temperature/relative humidity sensor was installed mid-thickness in the insulation layer at mid height. In the 2” XPS wall, moisture content was measured in the wood furring strips.

Moisture content wafers were installed late in the recording of data; they were used in the stud frame polyethylene walls (1 and 2), and the PA-6 wall (7). They were installed at locations intended to capture moisture accumulation from wintertime condensation (high on exterior side of insulation), summertime condensation (low on exterior side), and spring/summertime inward vapor drives (high on interior side of insulation).

Sensor location	1: Single poly stud wall	2: Dbl. poly stud wall	3: Polyiso w, foil facers	4: 2" XPS w. furring strips	5: XPS + fiberglass	6: XPS + cellulose	7: SVR w. fiberglass bd	8: Perforated roll blanket
Concrete temperature high	▲	▲	▲	▲	▲	▲	▲	▲
Concrete temperature mid	▲	▲	▲	▲	▲	▲	▲	▲
Concrete temperature low	▲	▲	▲	▲	▲	▲	▲	▲
T/RH concrete interface, mid	●	●	●	●	●	●	●	●
T/RH insulation, high	●	●			●	●		
T/RH insulation, mid	●	●	●[1]		●	●[2]	●	●
T/RH insulation, low	●	●			●	●		
Interior finish/VB temperature	▲	▲	▲	▲	▲	▲	▲	▲
Framing T/MC high (in & out)[3]	■	■			■	■		
Framing T/MC low (in & out)[3]	■[4]	■[4]			■	■		
Framing T/MC furring strip				■				
MC wafer low exterior side	◪[5]	◪[5]					◪[5]	
MC wafer high exterior side	◪[5]	◪[5]					◪[5]	
MC wafer high interior side	◪[5]	◪[5]						

Table 5.2: Summary of sensors at Huntley site

Several points should be noted in the sensor table above:

1. This temperature/relative humidity sensor was originally placed mid-thickness in the polyisocyanurate foam. However, it was later moved to the interface between the insulation and the concrete at the upper height location; this was done at the same time the insulation board was reinstalled in a direct-applied air sealed manner (see section 5.1.2.2). The sensor layout shown in Figure 5.15 reflects the final configuration.
2. In the XPS-cellulose wall, the single temperature/relative humidity sensor mid-thickness in the stud bay was replaced with two sensors, at inboard and outboard. This was done because of the hygric storage capacity of cellulose insulation; accumulation of stored moisture can cause higher vapor pressures (absolute moisture contents) on one side of the assembly, unlike vapor permeable and non-storing insulations such as fiberglass.
3. Moisture content and temperature sensors were located in a vertical stud, at the inboard and outboard sides, 9 mm (3/8") from the faces of the studs. Sensors at these locations can demonstrate a moisture gradient forming through the thickness of the wall.

4. During the experiment, these moisture content and temperature sensors were shifted from the vertical stud to the middle of the sill plate in these panels. Similarly to the original installation, the sensors were placed at the inboard and outboard sides.
5. The moisture content wafers were a later addition to the monitoring package. Originally, condensation gauges (similar to resistance-based leaf wetness sensors) were installed in these channels. However, little useful information was returned from the condensation gauges, so they were replaced with these wafer sensors.

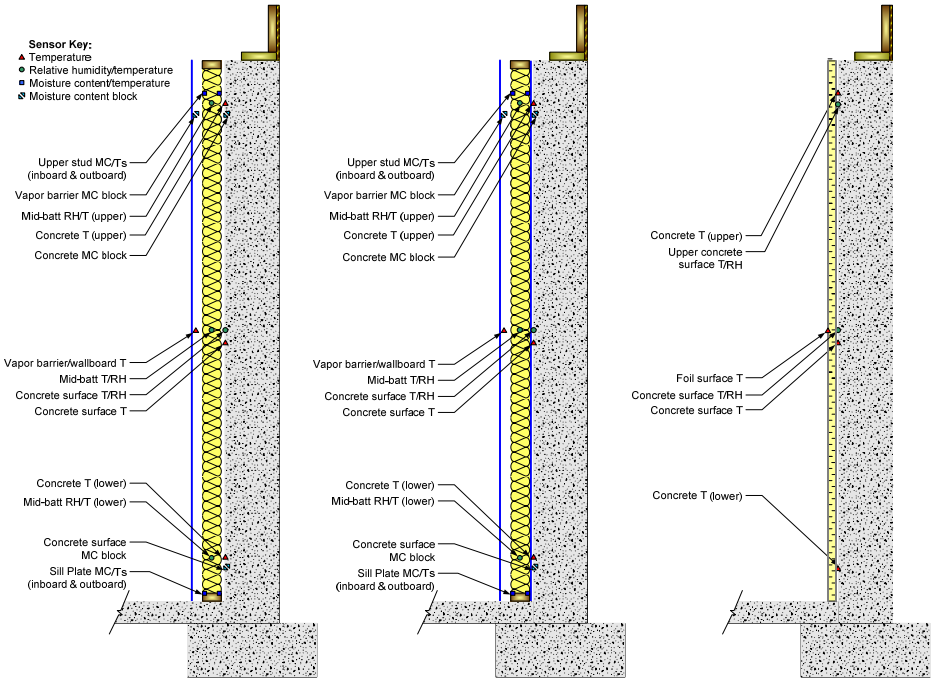

Figure 5.13: Section and sensor layout for Huntley site walls 1, 2, and 3

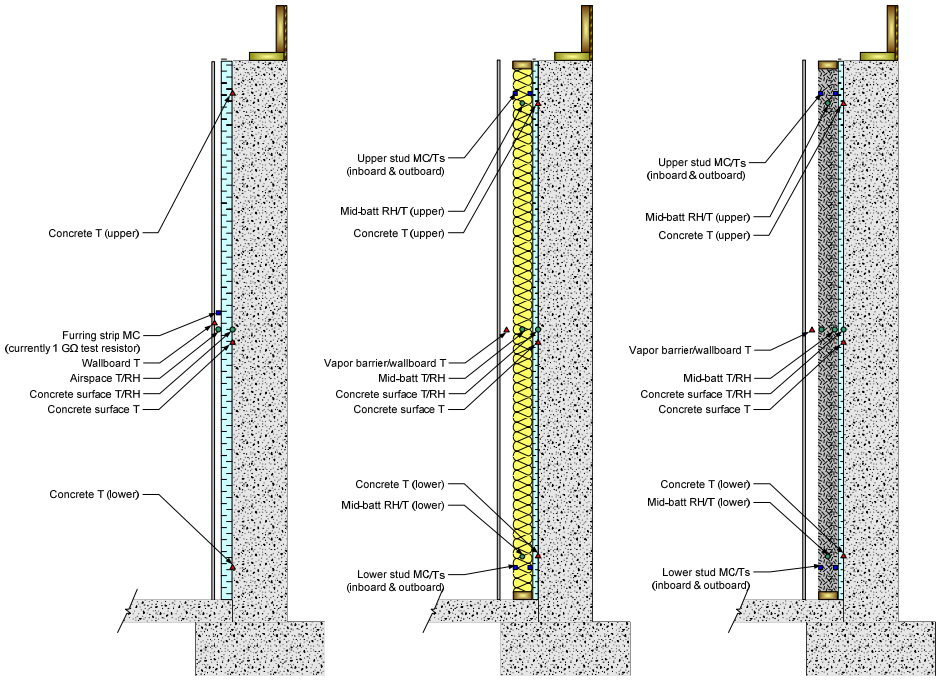

Figure 5.14: Section and sensor layout for Huntley site walls 4, 5, and 6

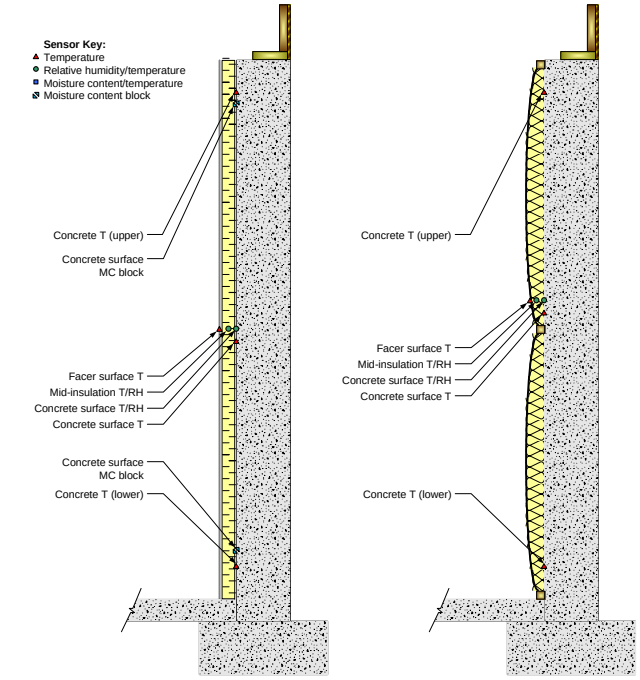

Figure 5.15: Section and sensor layout for Huntley site walls 7 and 8

In addition to the wall panel sensors, several environmental conditions were monitored. Interior and exterior temperature and relative humidity were recorded, the interior at two locations.

Soil conditions were measured, to obtain boundary conditions for the below-grade portions of the walls. Temperatures and water matric potentials (relative wetness) were measured at three lateral locations approximately two feet away from the test wall: installation is shown in Figure 5.16, and positions relative to the test walls are shown in Figure 5.38. Water potentials were measured using Delmhorst gypsum soil blocks (see Appendix A), which provide soil water potential as a function of electric resistance. These sensor packages were installed at three depths (6"/150 mm, 12"/300 mm, and 36"/900 mm), for a total of nine locations.

Hourly data was recorded by a Campbell Scientific CR10X-2M Measurement and Control System, as shown in Figure 5.17 (see Appendix A). Data was retrieved via periodic remote modem downloads; occasional gaps are seen, due to either sensor or logging system failures.

Figure 5.16: Boring for soil sensor installation, Huntley site

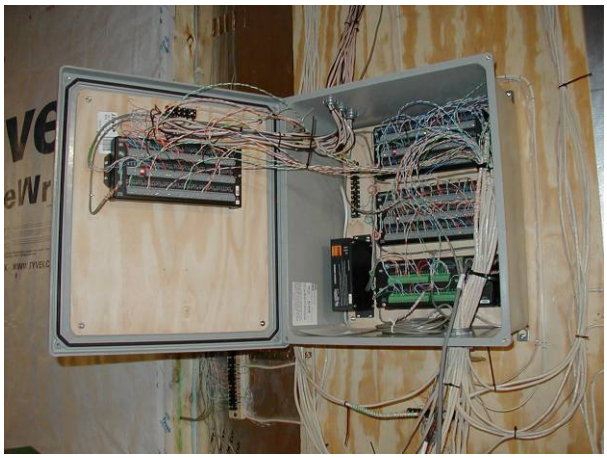

Figure 5.17: Data collection system at Huntley site

5.1.4 Installation of Test Walls

A timeline for installation of test walls and equipment is presented in Appendix G.

5.1.4.1 General Installation Details

The installation and instrumentation of walls at the Huntley site was completed in September of 2003. Some details were required to ensure optimized and comparable test conditions between the panels. For instance, there were several non-uniform conditions along the rear wall shown in Figure 5.38: two cantilevered bay windows, a cast concrete porch, and the corners of the basement. The bay windows could not be avoided, so panel pairs that required direct comparison (such as 1 &2, and 5 & 6) were installed at non-bay locations.

The data collection system was installed in a “buffer” panel at the porch, and the corners were not used for experimental panels, being covered with buffer panels. Foil-faced polyisocyanurate (1” thick), directly applied to the concrete, was used as buffer material. Buffer panels were installed between dissimilar test walls, to provide thermal and moisture isolation. These panels also provide a place to locate the instrumentation connection terminals.

One concern was the thermal effect of the mixture of buffer and test panels: to understand these effects, a two-dimensional static thermal model (THERM) was run on the distinct basement panels, assuming an outdoor (soil) temperature of 10° C (50° F), and an indoor setpoint of 20° C (68° F). The modeled assembly and test results are shown in Figure 5.18 and Figure 5.19, respectively.

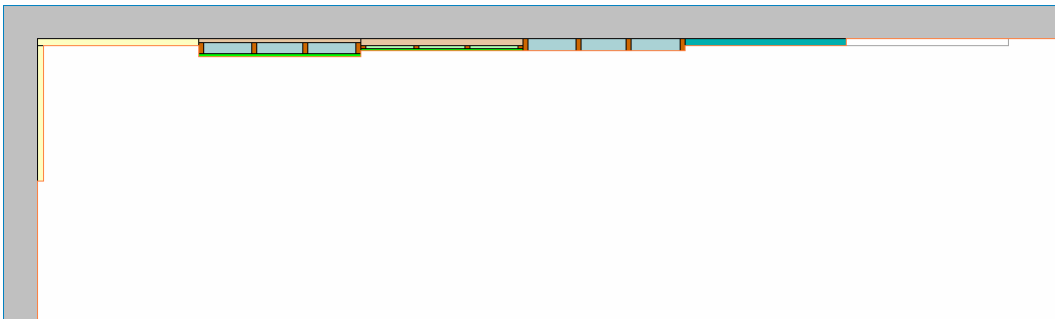

Figure 5.18: THERM model, showing assembly components

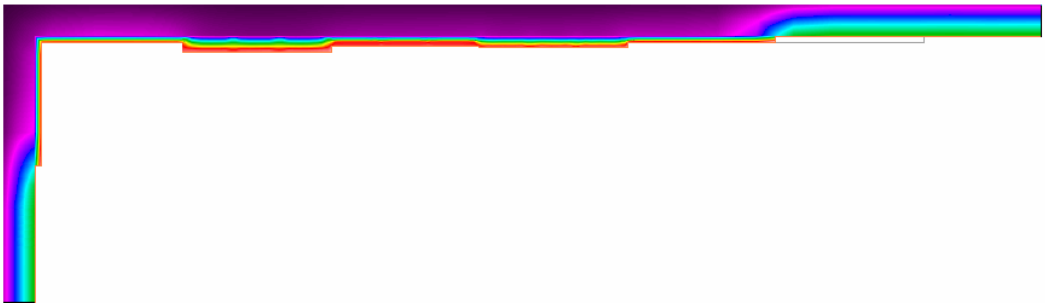

Figure 5.19: THERM model, showing thermograph results

These results show that although there are different thermal conditions behind the buffers and the test panels, these differences are small at the center of the 4’ wide test panels.

Only the rear orientation of the basement was insulated (with test panels and buffer panels). The remaining orientations of the basement remained uninsulated.

The rim joist spaces in the basement were not addressed or instrumented in this project; they were left as per the builder’s standard practice, with Kraft-faced batts friction-fit into the joist space.

5.1.4.2 Test Panel Installation Details

The following section has details on the installation and instrumentation of the test walls. All walls had temperature sensors low/middle/high; these were attached to the surface of the concrete with caulk, and the wire was attached to the concrete with small pieces of foil tape. The temperature/ relative humidity sensors located at the interface between insulation and concrete has a noticeable thickness, and requires some space at walls. Therefore, a divot was carved in the concrete to create this space. Both of these details are shown in Figure 20.

The nine-foot tall basement walls required the use of a one-foot tall extension form at the top of the walls. This extension was not maintained in plane during casting: it typically bends to the exterior by

12-25 mm (1/2” to 1”), as shown in Figure 5.21. This provided some difficulties in finishing the top detail of the interior insulation assemblies, and air sealing; these types of problems are not uncommon in practice.

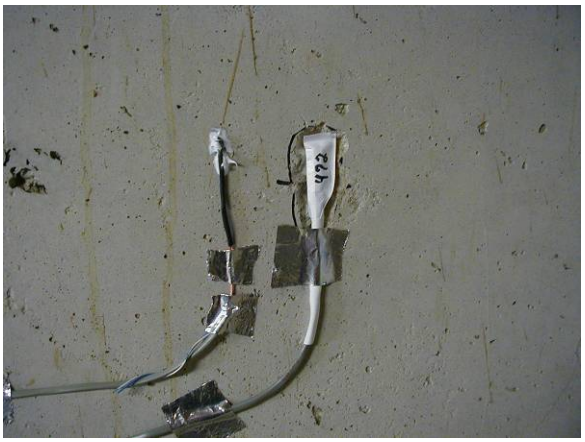

Figure 5.20: T and T/RH sensor at concrete

Figure 5.21: Concrete wall upper form extension out of plane

At walls 1 and 2 (stud frame with polyethylene) the walls were laterally air sealed with expanding foam (as shown in Figure 5.22), to simulate the effect of a long unbroken section of wall. However, the joint between the top plate and concrete was not sealed at the beginning of the experiment. This was done to mimic typical practice seen in the field: although an air seal is recommended at this top plate-concrete intersection, it is seldom implemented. Later in the experiment, however, this interface was sealed with expanding foam. The framing has a capillary break (polyethylene foam sill seal) below the bottom plate and is pushed tight to the concrete wall. The instrumentation installed in these walls is shown in Figure 5.23, Figure 5.24, and Figure 5.25, for lower, middle, and upper locations, respectively.

The polyethylene on the interior side was taped with builders’ tape to the face of the stud, to complete the air seal. In the “double poly” (both sides) wall, the exterior side polyethylene was run full height; one continuous piece of polyethylene was used for interior and exterior sides, run under the bottom plate.

Figure 5.22: Lateral air sealing at Walls 1 and 2 (stud frame walls)

Figure 5.23: Instrumentation package at lower location of stud frame walls (Wall 2)

Figure 5.24: Instrumentation package at middle location of stud frame walls (Wall 2)

Figure 5.25: Instrumentation package at upper location of stud frame walls (Wall 2)

In wall 3 (foil-faced polyisocyanurate), the plastic attachment track system creates a small air gap between the insulation and the concrete, between 1/8 and 1/4" (3-6 mm) wide, even when the plastic tee cap is installed tightly. Partway into the experiment, the junction between the top of the foam insulation board and the concrete was sealed with expanding foam. However, later disassembly showed that this air seal was incomplete. During the last portion of this research, the plastic tracks were removed, and the foam insulation was directly applied to the concrete using caulk and concrete fasteners. Caulk was applied around the perimeter and at the junction to the top form extension to ensure a good air seal (see Figure 5.26).

A temperature/relative humidity sensor was installed mid-thickness in the insulation board by cutting a pocket out of the board from the exterior face, as shown in Figure 5.27. The sensor was installed, and sealed with foil tape.

Figure 5.26: Caulk sealing and expanding foam at Wall 3 concrete

Figure 5.27: Installation of temperature/RH sensor in foam board (Wall 3)

At wall 4 (2" XPS), the furring strips were attached at 410 mm (16") o.c., using concrete screws (see Figure 5.28). This attachment method resulted in the foam being held tightly against the concrete wall, with little chance of air leakage, despite the lack of other air sealing measures. Unpainted gypsum drywall was attached to the furring strips at the interior; the vented cavity space was well connected to the interior. Due to the 9-foot tall walls, two pieces of foam board were required; the joint was placed between the "lower" and "middle" sensor locations, to minimize the effects of this seam. The joint was sealed with builders' tape on the interior face.

Figure 5.28: Installation of furring strips and foam at wall 4

Figure 5.29: Completed assembly (side view) of wall 4

Walls 5 & 6 (XPS with stud frame/insulation) were the most involved in construction, due to the combination of stud framing and foam board. In wall 6 (XPS + cellulose), the foam was attached to the concrete with powder-actuated fasteners (see Figure 5.30), and the stud frame erected inboard. No air sealing measures were taken laterally or at the top between the frame and the foam, due to scheduling constraints of cellulose damp-spray installation. The cellulose installation is shown in Figure 5.31 and Figure 5.32.

In contrast, in wall 5 (XPS + fiberglass), the foam was installed and then wedged tightly against the concrete, to conform to the uneven wall profile (see Figure 5.33). The joint between the foam and stud bay cavity was then sealed using expanding foam, both at the sides and the top. The difference in the installation method is a likely explanation for some of the differences in behavior seen in these walls.

Like walls 1 and 2, the wood framing has a capillary break (sill sealer) below the bottom plate, and the interior air barrier (spun-bonded polyolefin housewrap) was sealed to the face of the frame with builders' tape.

Figure 5.30: Installation of XPS board at wall 6 with powder actuated fasteners

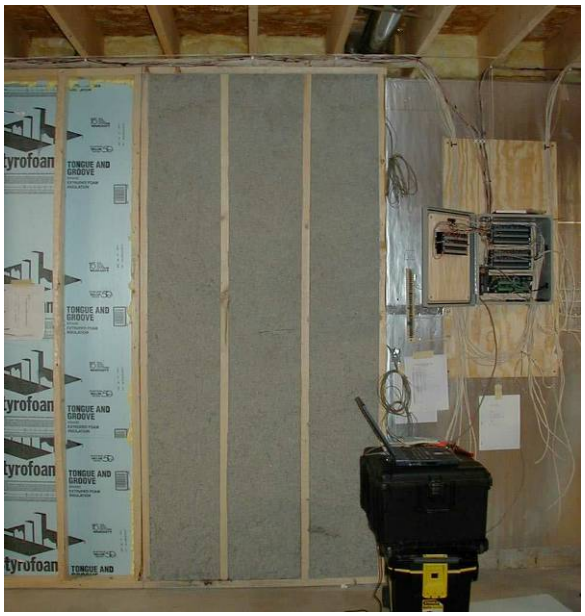

Figure 5.31: Installed cellulose insulation in wall 6

Figure 5.32: Installation of cellulose insulation in wall 6

Figure 5.33: Top air sealing detail and foam wedge at wall 5

The material for wall 7 (PA-6 facer and perforated scrim attached to rigid fiberglass) was shipped after the initial installation; this wall was commissioned in January of 2004. The material was attached tightly to the concrete wall with concrete screws and nylon washers. The horizontal joint between panels and the vertical side joints were sealed with foil tape; the lateral joints were sealed to the adjacent buffer panels. Although no special effort was made to air seal the system at top and bottom, semi-rigid fiberglass is of a high enough density that airflow through the insulation would be minimal.

Figure 5.34: Installation of PA-6/rigid fiberglass material (wall 7)

Figure 5.35: Lateral air sealing and joint sealing at wall 7

Wall 8 it is attached to the concrete wall by installing 2x2 at the bottom, middle, and top of the wall, attached with powder actuated tool pins to the concrete. The vinyl flanges of the rolls were then stapled to the 2x2s. The lateral joints were sealed to the buffer panels with builders' tape; the horizontal joints were left untaped. However, the vertical joints failed routinely, and air leakage is likely. It was upgraded over time, using foil tape and staples; the latter sealing methods were more successful.

Figure 5.36: Installation of 2x2s at wall 8

Figure 5.37: Completed installation of wall 8

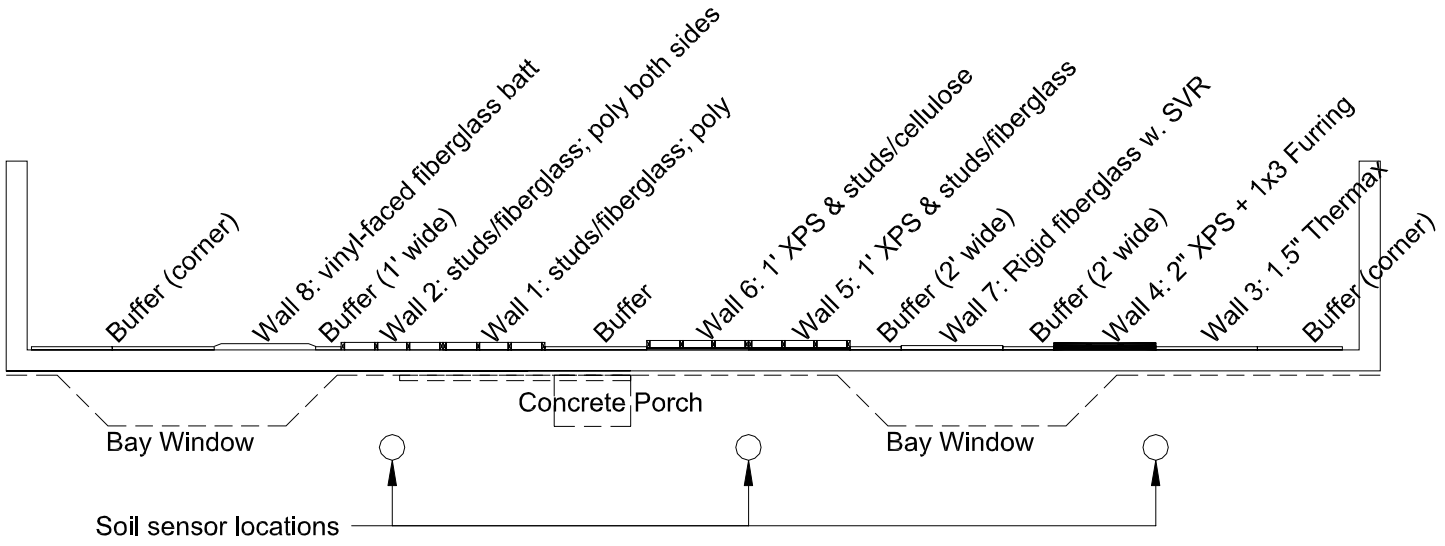

Figure 5.38: Schematic layout of test panels in Huntley

Figure 5.39: Composite photo of test panels in Huntley (prior to wall 7 installation)

5.1.5 Wetting System

A system that introduces controlled amounts of water into the test panels was installed to evaluate the drying behavior of the wall assemblies; it was operated in the second year of the experiment. The technical details of this wetting system and the calibration procedure are described in Appendix C: Development and Commissioning of Wetting System. To summarize, this wetting system has a water injector at each test panel, fed by a logger-activated relay-controlled pump. The goal was to equally wet all walls simultaneously; field calibration showed discharge rates within ±10% of the average. The injector assembly is a small-diameter brass tube with a small, drilled opening; it was fed through the insulation assembly into a shallow (¼") hole drilled into the concrete wall, as shown in Figure 5.40. The injector was located approximately 2.4 m (95") above finish floor, at the panel centerline. The intent was to simulate a water event originating at the concrete wall, such as a leak or condensation, or the drying of construction moisture.

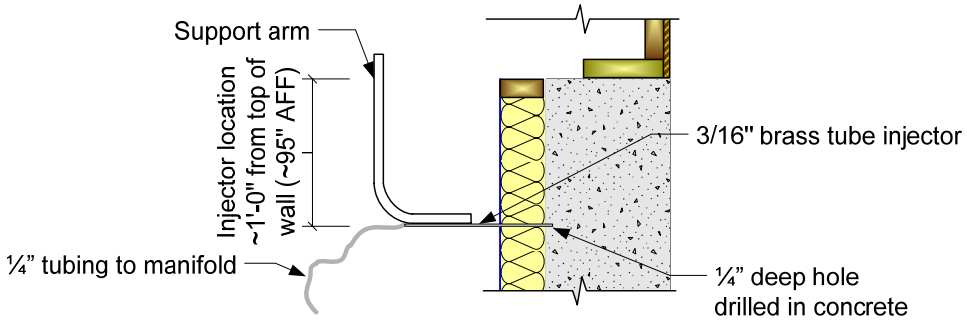

Figure 5.40: Schematic of wetting system

5.2 Kitchener, Ontario Site

5.2.1 Site and house description

The test site is a two-story, 2444 square foot, 4 bedroom, 2.5 bathroom production house with a full basement (see Figure 5.41 and Figure 5.42). It is located on a lot that slopes downwards to the rear; the back of the basement is a walkout condition. The foundation wall steps down from full height at the front to walkout at the rear. The test walls are located on the right-hand side of the house, towards the front, before grade slopes away too drastically. The test walls are installed to either side of a basement window.

The house is occupied by a family of three. The basement is unfinished; code-compliant roll blanket insulation is installed on the upper half of the wall at the front of the basement. At and around the rear walkout, insulation in stud framing (with a polyethylene vapor barrier) and roll blanket is used to insulate the wall full height. The HVAC and hot water systems are located in the basement.

Figure 5.41: Front elevation of Kitchener test location

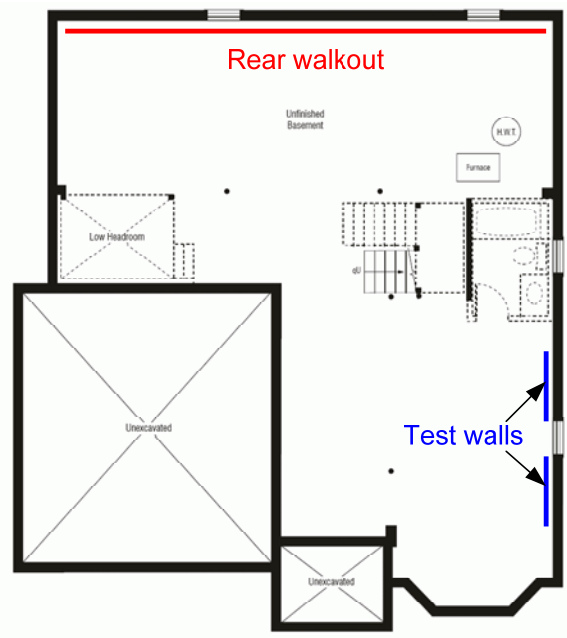

Figure 5.42: Floor plan of test basement, showing test wall locations

There is an adjacent house on the right hand side; it is located 2.8 m (9 feet) away from the test house, and the front of the adjacent house is slightly set back from that of the test house (see Figure 5.43 and Figure 5.44).

The test walls face roughly southeast, as shown in Figure 5.45. The interior wall height is 2.36 m (7’9”), from the finish floor (slab) to the bottom of the first floor framing.

The house was built in winter 2004-2005, and occupied in late June 2005, so construction moisture loading in these walls was significant.

Figure 5.43: Kitchener test site, showing proximity of adjacent house

Figure 5.44: Kitchener test site, with projected line from adjacent house

Figure 5.45: Orientation of Kitchener test house and surroundings

Figure 5.46: Location of test walls at Kitchener site, pre-installation

5.2.2 Test Walls

Four test walls were installed in the test basement: they are summarized in Table 5.3 below. There is one foam plastic insulation wall (Wall 1), a roll fiberglass blanket (Wall 2), and two stud frame-based walls (Walls 3 & 4). The type of illustrations used in section 5.1.2 would be redundant here, and are not included.

One goal of this portion of the research at this site, which was sponsored by Canada Mortgage and Housing Corporation, was to study the role of an impermeable layer such as polyethylene in wall

construction (in both above-grade and below-grade wall assemblies). Therefore, two assemblies compared side-by-side were stud frame insulated walls with gypsum board, constructed with and without polyethylene.

Table 5.3: Summary list of test walls at Kitchener site

Wall #	Wall Description	Wall assembly (exterior to interior, from concrete)
1	Extruded polystyrene (2") w. gypsum wall board	Extruded polystyrene (2"/50 mm; R-10/RSI 1.8); 1x2 furring strips 16" o.c. with airspace; ½" gypsum wall board
2	Fiberglass roll blanket (3") with polyethylene facer	Fiberglass roll blanket (3"/76 mm; R-11/RSI 1.9) 4' wide; polyethylene facer; fastened directly to concrete
3	2x4 frame with polyethylene and gypsum board	2x4 studs 16" o.c. with R-13/RSI 2.3 fiberglass batt insulation, 6 mil polyethylene film, ½" gypsum wall board with latex paint
4	2x4 frame with painted gypsum	2x4 studs 16" o.c. with R-13/RSI 2.3 fiberglass batt insulation, ½" gypsum wall board with latex paint

R-value in $ft^2 \cdot °F \cdot h/Btu$; RSI value in $K \cdot m^2/W$

Wall 1 is basically identical to wall 4 from the Huntley site, with 50 mm (2") extruded polystyrene foam, direct applied to the concrete, and attached with concrete screws through 1x2 furring strips. Gypsum board (½") is installed as an interior finish and ignition barrier. This wall is meant to demonstrate best practice; it is an assembly that Lstiburek (2002) points out as having good performance.

Wall 2 is the builder's standard practice basement insulation material (unperforated polyethylene-faced fiberglass roll blanket), installed full height. The half-height installation was left in place, and an additional section was moved from the adjacent upper portion to the bottom half. This material was attached to the concrete wall using a metal termination strip with masonry nails.

Wall 3 is a stud frame (2x4) wall, with unfaced fiberglass batt insulation, a polyethylene vapor barrier on the interior side, and ½" gypsum wallboard painted with latex paint. This assembly does not meet the Ontario code requirements (as mentioned in Chapter 2, Section 2.2.3.3), as it lacks a "moisture barrier" (layer of 170 $ng/(s \cdot m^2 \cdot Pa)$/3 perms or less) between the concrete and the insulation/vulnerable wood elements and finishes. However, this assembly is the one used by most homeowners and/or remodellers to finish basements, and allows direct comparison of a wall with and without polyethylene.

Wall 4 is similar to wall 3, except that the layer of polyethylene is removed. Interior vapor resistance in the assembly is provided by the latex paint.

5.2.3 Instrumentation Package

As at the Huntley test site, the test panels were instrumented with temperature (T), relative humidity (RH), electric resistance-based wood moisture content (MC) sensors, and wood surrogate moisture content sensors ("wafers"). The sensor setup is summarized in Table 5.4.

In all walls, the temperature of the interface between the concrete wall and the insulation was recorded at upper (~73"/1.85 m above finish floor) and lower (~16"/0.4 m A.F.F.) heights. The upper

location is roughly at the level of the exterior grade. A temperature & relative humidity sensor was installed at the middle height (~46"/1.17 m A.F.F.) at the concrete-insulation interface.

Additional temperature/relative humidity sensors were added in walls of particular interest. The roll blanket wall had a sensor at the upper location, to capture inward vapor drive phenomena. The two stud walls had sensors at high, middle, and low locations mid-thickness in the stud bay.

In all walls except the XPS wall, a temperature sensor was installed mid-height at the interface between the insulation and the interior finish material (polyethylene or drywall). This was installed to capture the likelihood of condensation on this surface, given the dewpoint of the cavity space.

In the stud frame walls, the moisture content of a single vertical stud was measured at four locations: at the upper and lower heights, on the exterior and interior sides (3/8"/10mm from the edges of the stud). These were measured 150 mm (6”) from the top or bottom of the wall.

Finally, moisture content surrogate sensors (“wafers”) were installed at several points in the panels. They provided some redundancy to the relative humidity sensors in challenging high-humidity environments; they also compensated for the limited number of humidity measurements available with this specific data collection setup. In addition, the moisture storage of the wafer sensor provides a good picture of seasonal moisture accumulation. Although these sensors have a very slow response time (150-200 hours to respond to 50%-100% step change), this is not an issue when capturing slower seasonal patterns.

Wafers were installed at the lower location in the XPS and roll blanket wall, and at the middle location in all walls, to provide comparisons of moisture accumulation between the walls. In addition, wafers were used at the upper location in all walls, to provide indication of accumulation of inward vapor drives. These were located to the exterior of the least vapor permeable layer: the XPS (wall 1), polyethylene (walls 2 and 3), or drywall (wall 4).

Sensor location	1: 2” XPS w. furring strips	2: roll blanket	3: single poly stud wall	4: no poly stud wall
Concrete temperature high	▲	▲	▲	▲
Concrete temperature low	▲	▲	▲	▲
T/RH concrete interface, mid	●	●	●	●
T/RH insulation, high		●	●	●
T/RH insulation, mid			●	●
T/RH insulation, low			●	●
Interior finish/VB temperature		▲	▲	▲
Framing T/MC high (in & out)			■	■
Framing T/MC low (in & out)			■	■
MC wafer low exterior side	▨	▨		
MC wafer mid exterior side	▨	▨	▨	▨
MC wafer high exterior side	▨			
MC wafer high interior side		▨	▨	▨

Table 5.4: Summary of sensors at Kitchener site

Sensors were installed along the centerline of each test panel, to minimize edge effects. Layouts are shown in Figure 5.47 below; the two stud walls have identical sensor layouts, so only one figure is shown.

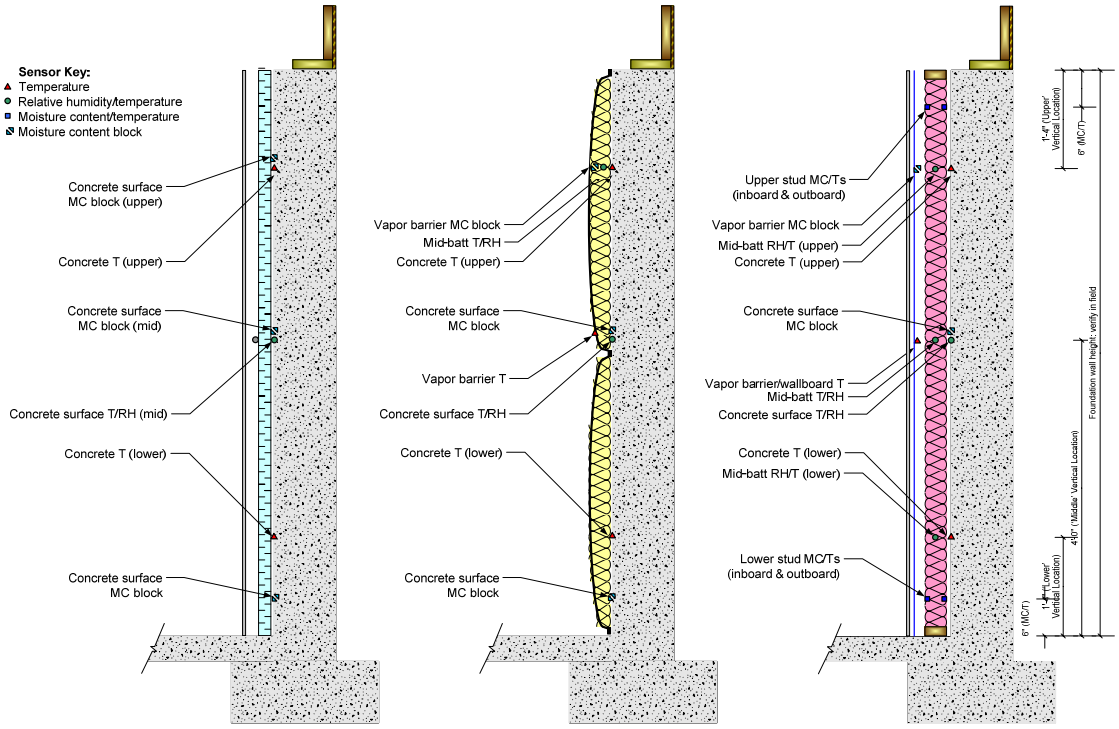

Figure 5.47: Section and sensor layout for Kitchener site walls

As with the Huntley site, interior and exterior temperature and relative humidity were recorded; interior conditions were measured at two locations. Soil conditions were measured as well, to obtain boundary conditions for the below-grade portions of the walls. Soil sensors recorded temperatures, water matric potentials (with soil gypsum blocks), and moisture content using wood "plug" sensors (similar to "wafer" sensors; see Appendix B). Measurements were taken at two lateral locations approximately two feet away from the test wall: positions relative to the test walls are shown in Figure 5.48; installation is shown in Figure 5.49 and Figure 5.50. These sensor packages were installed at three depths (6"/150 mm, 12"/300 mm, and 36"/900 mm), for a total of six locations.

Hourly data was recorded by a Campbell Scientific CR1000 Measurement and Control System; data was retrieved via downloads conducted during site visits.

A timeline for installation of test walls and equipment is presented in Appendix G.

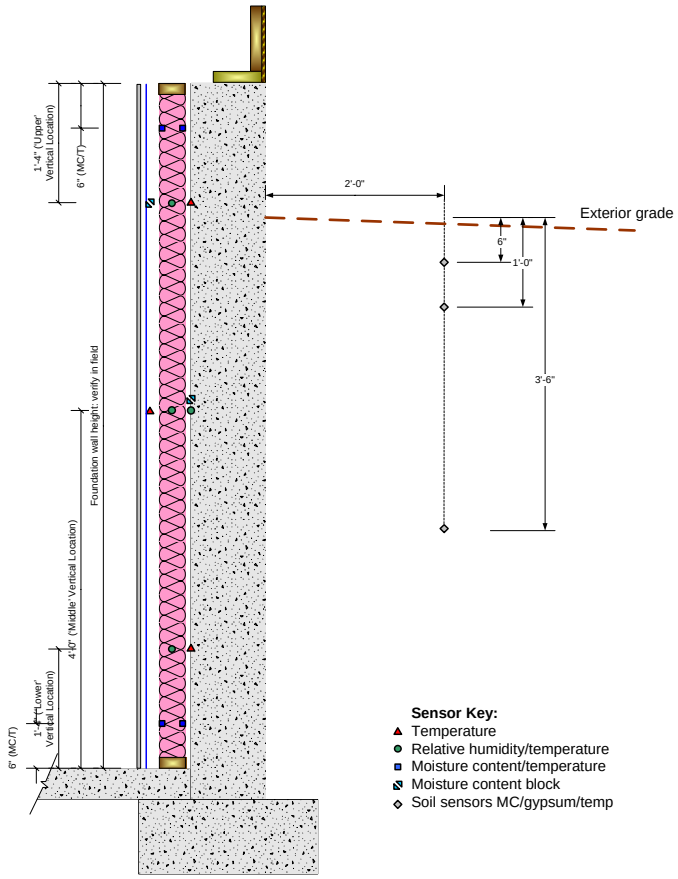

Figure 5.48: Relative position of soil sensors at Kitchener site

Figure 5.49: Gypsum soil block, wood plug sensor, and temperature sensor in soil installation

Figure 5.50: Location of soil sensor hole

5.2.4 Test Panel Installation Details

The installation and instrumentation of walls at the Kitchener site was completed in August of 2005. Like the Huntley site, existing conditions required special detailing to minimize their effects on the test. For instance, the sheltering and shading provided by the adjacent house, as well as the sloping ground, results in different exposure conditions for the front and rear walls.

On the exterior, the basement walls are treated with spray-applied dampproofing to grade, which is then covered with an HDPE (high density polyethylene) plastic “dimple mat” drainage and protection board; the top termination of this board can be seen in Figure 5.50.

The space available for test panels was limited; locations on either side of a basement window were used, as shown in Figure 5.42. Due to space constraints such as the window, the corner of the basement, and the foundation step down, full 1.2 m (48”) wide panels could not be installed; 0.81 m (32”) wide panels were used instead. In the framed walls, the center bay was maintained at 16” o.c., and the guard bays were compressed to fit into the opening.

During the initial disassembly of the existing walls, some evidence of moisture accumulation was noted at the rim joist, as shown in Figure 5.52; note that in Figure 5.51, the polyethylene facer of the roll blanket is continued from the foundation wall up to the rim joist. This moisture damage could be bulk leakage, or it could be redistribution of moisture accumulated from inward vapor drives. There was some discoloration of the fiberglass roll blanket, suggesting the occurrence of this inward drive.

Figure 5.51: Existing rim joist condition at Kitchener site

Figure 5.52: Evidence of rim joist moisture damage at Kitchener site

The layout of the test walls is shown in Figure 5.53, including the data collection equipment and the basement window. The leftmost panel was built at a foundation step down; since the XPS wall was the least critical for the CMHC study, it was installed at this location. The two frame walls required a direct comparison against each other; therefore, providing equivalent exposure was critical. The right-most walls had the greatest solar and rain exposure, so the frame walls were placed there. The roll blanket wall was located in the remaining panel opening.

The panels were separated by 3” wide 2” thick XPS separator: they provided thermal and moisture isolation, as well as locations for the wiring connection panels. The black material at the top of the concrete wall (as seen in Figure 5.53) is housewrap that is used as a rim joist air barrier closure: it wraps around the rim joist, under the sill plate (mudsill), and down the top of the concrete wall.

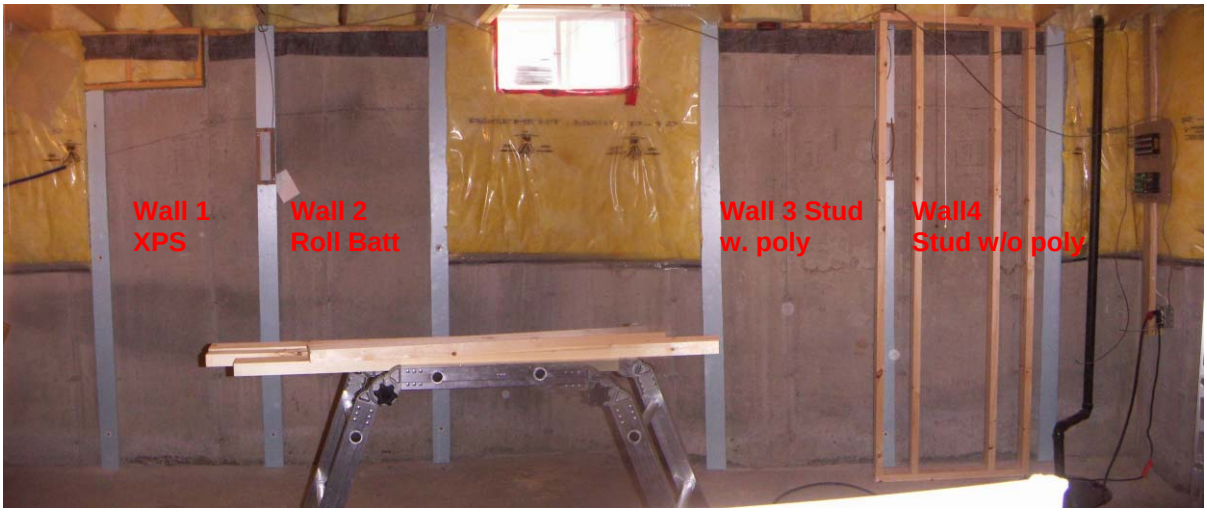

Figure 5.53: Test panel openings at Kitchener site

The installation of the XPS wall (Wall 1) is shown in Figure 5.54. Two-foot wide pieces were installed horizontally, and held in place with furring strips attached with concrete screws. The roll blanket wall (Wall 2) was installed with materials used in the original installation; the panel was air sealed to the panel separators using builders' tape, to mimic the effect of a long continuous wall.

The frame walls were installed with a polyethylene foam sill seal below the bottom plate. The frame was installed directly plumb but against the concrete wall; contact between the two occurred at some points. The gap between the frame and concrete was sealed with expanding foam at top, side, and bottom, as shown in Figure 5.55 and Figure 5.56.

Figure 5.54: Installation of XPS wall at foundation step down

Figure 5.55: Air sealing at perimeter of stud frame walls

Figure 5.56: Air sealing at top plate of frame walls

Figure 5.57: Sensors at upper location of stud frame wall

The sensor installation for the frame walls is illustrated in several photos: at the upper location (Figure 5.57: stud MC/T, upper concrete T, mid-batt T/RH, upper wafer), middle location (Figure 5.58: middle wafer, concrete-side T/RH, mid-batt T/RH, GWB T), and lower (Figure 5.59: stud MC/T, lower concrete T, mid-batt T/RH).

Figure 5.58: Sensors at middle location of stud frame wall

Figure 5.59: Sensors at lower location of stud frame wall

The completed installation, pre-drywall, is shown in Figure 5.60; approximate grade level is shown.

Figure 5.60: Test panels at Kitchener site (pre-drywall); approximate grade level shown

Chapter 6

Results: Huntley Site

The data from the Huntley site is covered and analyzed in four sections: the data from the soil sensors, the interior and exterior boundary conditions, the response of the walls under normal conditions, and the response of the walls to the use of the wetting system. In addition, the walls were inspected during field visits and final disassembly; the observations are presented in a final section.

6.1 Soil Sensors

The sensors used to provide soil boundary conditions were described in Chapter 5; they included measurements of temperature and soil matric potential (water content). They were placed at three vertical "stacks" at three depths (6"/150 mm, 12"/300 mm, and 36"/900 mm), for a total of nine measurement locations. These vertical stacks were referred to as SE (southeast), SC (south central) and SW (southwest) locations.

6.1.1 Soil Temperature Behavior

Temperatures were recorded for the full length of the experiment; there was minimal variation between years; a representative year (January 2005-February 2006) is plotted below in Figure 6.1; daily average values are shown.

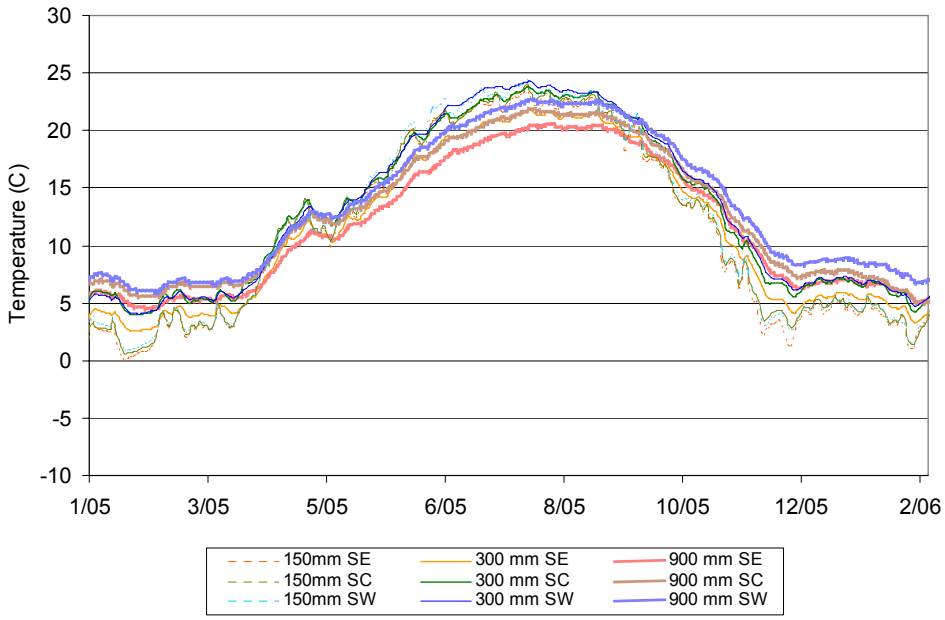

Figure 6.1: Soil temperatures for representative year (January 2005-February 2006)

Several behavior patterns similar to those predicted in the literature can be seen. First, the shallowest (150 mm/6") sensors show the greatest day-to-day variations, while these variations are

more damped out at the 300 mm (12”) and 900 mm (36”) depths. The temperatures show seasonal changes, with the deepest temperatures showing some phase shifting. The deepest temperatures are the warmest in winter, and the coolest in summer, due to the thermal mass of the soil. These trends can be seen more clearly in the plots of the center stack alone, shown in Figure 6.2.

It is difficult to make comparisons between the temperatures at the three horizontal locations or stacks. All of the shallow temperatures show practically identical behavior, but the deepest sensors (900 mm) show some consistent differences. The southwest sensor is consistently warmest, and southeast coldest, with the center one between the two. This might be a function of the local topography or soil conditions/conductivity.

The constant deep ground temperature for a given location can be estimated from the monthly average air temperatures plus 2 to 6° C (Hutcheon and Handegord 1995). Using the historical weather data for Huntley, this calculation yields values of 11 to 15° C. The average of the top and bottom of the sinusoidal values at 900 mm gives 14° C, which falls within the estimated range.

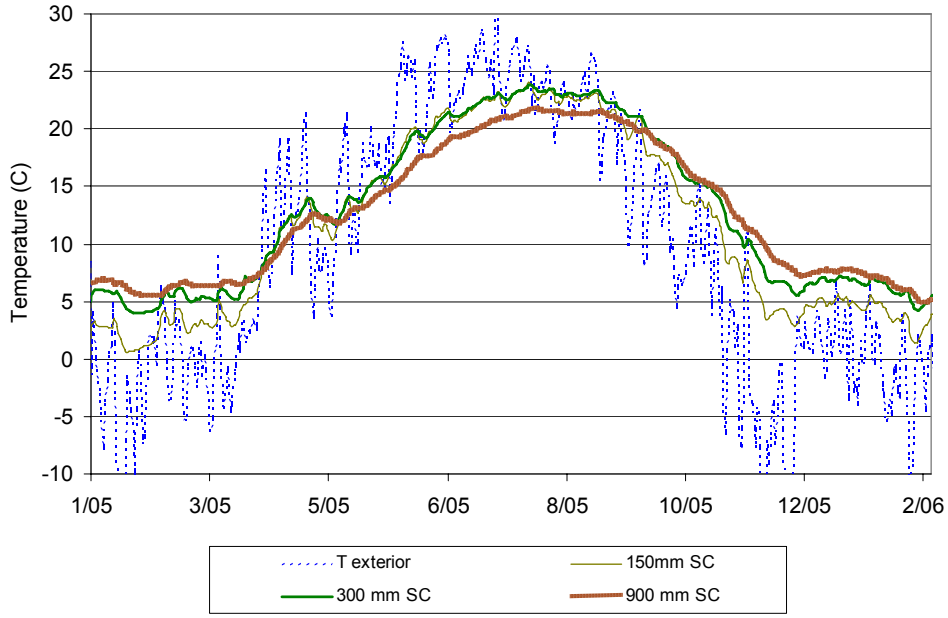

Figure 6.2: Daily average soil temperatures at center stack (2005) with exterior temperature

Further insight is gained by isolating one set of plots (the center sensor stack, in Figure 6.2), and superimposing the daily average outdoor temperature. This shows the response of the soil to weather patterns: shifts in temperature are reflected in the ground temperatures with some lag and damping, with greater damping and lag at greater depths. In addition, the phase shifting behavior with depth can be seen more clearly in this plot. The annual amplitude swing (i.e., variation over the season) is reduced at greater depths, showing the insulating effect of the soil.

It is notable that the temperatures come close to freezing at the shallowest depths but do not go below freezing. This was examined in more detail in Figure 6.3, which focuses in on the coldest three-week winter period in the data shown in Figure 6.2.

The temperatures at the shallowest depth come close to freezing, but do not go below freezing, even following sustained periods averaging roughly –13° C. This behavior was seen consistently over several years; it is likely due to the latent heat of fusion. Essentially, the soil may be "protected" from freezing by the amount of energy needed to freeze the water contained in the soil.

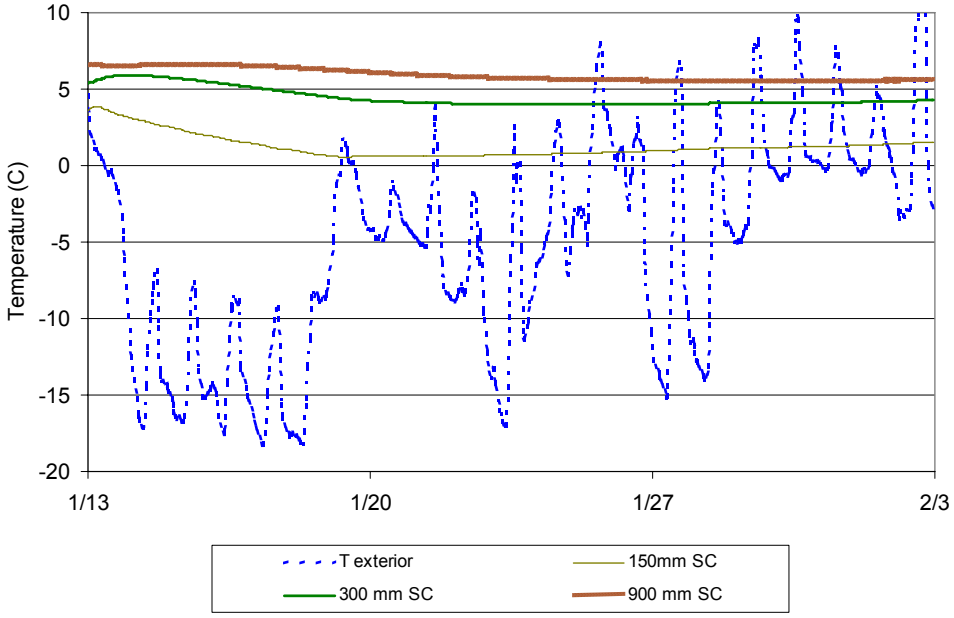

Figure 6.3: Hourly soil temperatures at center stack (winter detail) with exterior temperature

To determine if this effect might be a local anomaly, additional data was found and analyzed.

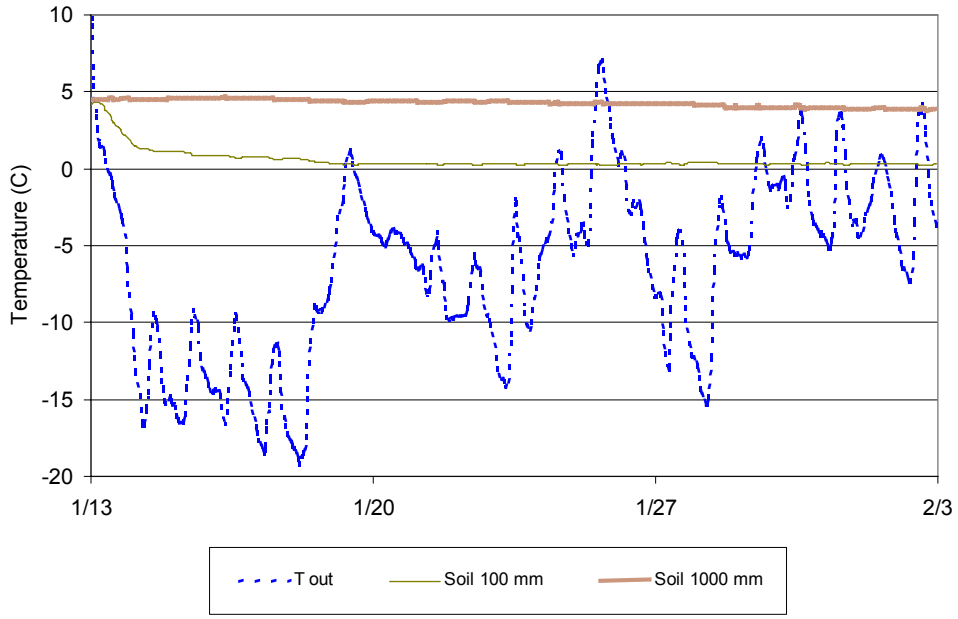

Figure 6.4: Hourly Argonne Laboratory soil temperatures (winter detail) with exterior temperature

Soil temperature data from a weather station at a nearby site (Argonne National Laboratory, in Lemont, IL, roughly 80 km/50 miles southeast of Huntley) was plotted in Figure 6.4 for the same time period, to see if the similar behavior was seen. This data also removes the effect of any heat loss from a building: this weather station is located in an isolated field. The data for soil at 100 mm (as opposed to 150 mm) shows that temperatures stay above the freezing point despite sustained cold temperatures, reinforcing the interpretation reached above. In both plots, the deeper soil temperatures are warmer than the surface (100 or 150 mm) temperatures, staying in the 4-6° C range during this cold period.

In addition, the ground temperature data found in the literature (Hutcheon and Handegord 1995 and Bligh 1975) shown in Figures 3.3 and 3.4 has similar behavior. Temperatures at all but the shallowest depths remain above freezing through the winter.

A detail plot of the three hottest summer weeks of 2005 in Huntley is shown in Figure 6.5. As seen in Figure 6.2, the deepest temperatures remain the coolest. In addition, the shallow (150 mm) sensor shows daily variations of 1° C, while the daily air temperature amplitude was on the order of 15-20° C. At a depth of 300 mm, all daily variation is damped out: it is notable that any diurnal temperature variation is eliminated at 300 mm or 1 foot below grade. In addition to the strong damping of daily variations, the shallow sensor also shows a phase shift of slightly less than 12 hours from the exterior temperatures.

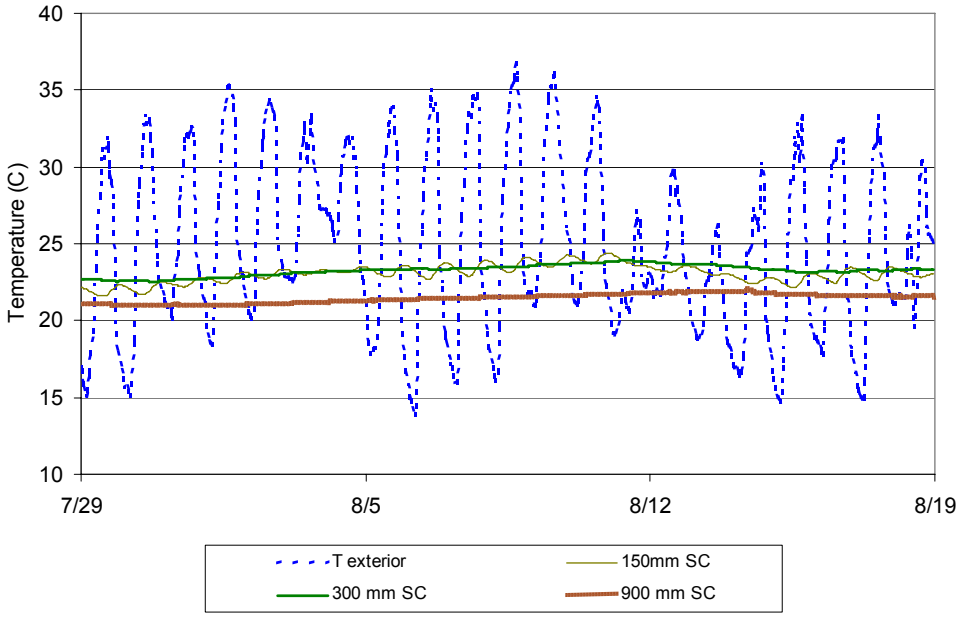

Figure 6.5: Hourly soil temperatures at center stack (summer detail) with exterior temperature

6.1.2 Soil Moisture Behavior

Soil matric potentials were measured using gypsum electrical resistance blocks at nine locations. As mentioned in Chapter 3 (Section 3.1.2), the matric potential scale equates zero with the soil being in equilibrium with liquid water (i.e., saturation). Therefore, negative values show greater suction (i.e., attraction force to water), or dryness.

The data from the gypsum soil blocks showed a great deal of rapid variation: the unfiltered data is close to unreadable, showing rapid excursions between very dry and moderately wet conditions. It is likely that these measurements reflect electrical noise or other measurement issues: soil, especially at a depth of 900 mm, should not exhibit such rapid changes. Therefore, after examining of the data, the measurements were filtered by eliminating values less than –1 and calculating daily averages; the results are shown in Figure 6.6, over the full course of the experiment. Relative wetness or dryness of the soil is indicated by the arrows on the graph.

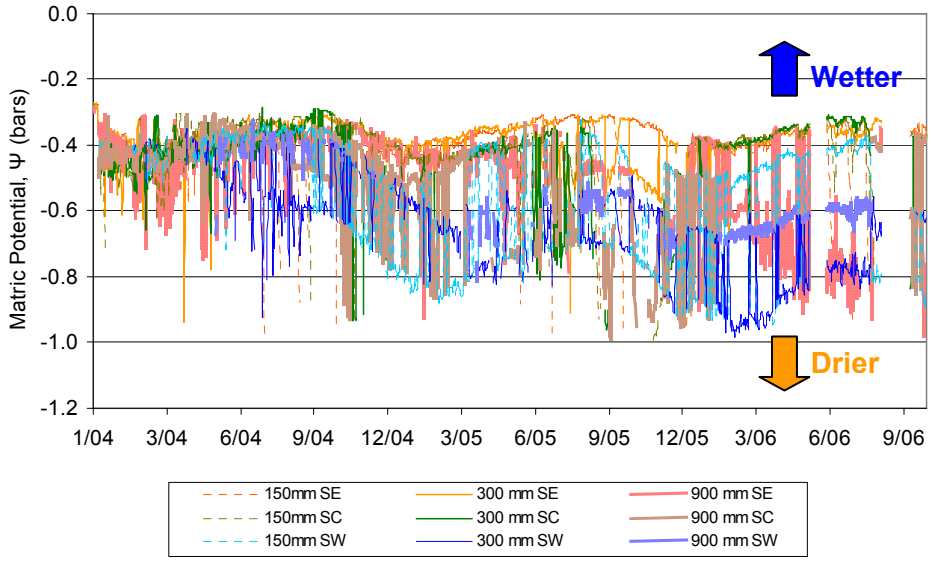

Figure 6.6: Soil matric potentials at Huntley site (2004-2006)

Even with this filtering, there is still a substantial amount of noise or scatter. However, some basic trends can be discerned from this plot. First, the majority of the reliable data falls between approximately –0.3 and –1.0 bar. These results can be compared to the moisture conditions presented in Table 6.1: the soil remains below the "field capacity" value (i.e., water would drain freely by gravity from soil wetter than this level). In other words, the measurements do not indicate saturated/soaking conditions; the soil is free draining. Some sensors indicate a level of soil dryness that would require irrigation (below –0.6 bar). However, there is some question to the accuracy of these measurements, given the suddenness of the variations, followed by returns to previous values.

Table 6.1 (repeated): Soil matric potentials and moisture conditions

Measurement	Soil Condition (from wetter to drier)
0.0 bar	Soil is saturated
0.0 to –0.33 bar	Free water drainage (-0.33 = "field capacity")
-0.33 to –15 bar	"Available water" (plants can obtain water from soil)
-0.6 bar	Typical boundary condition for making decision to irrigate soil
-15 bar	"Wilt point" (plants can no longer extract water from soil)
-31 bar	Air dry state for soil with air at 100% RH
-10,000 bar	Oven dried soil

Some of the behavior of the gypsum blocks might be attributed to known issues for these sensors, as described in the documentation (see Appendix A): they have a typical longevity of one to two years, and are damaged by saline or acidic soils, and by freezing temperatures. In addition, the literature notes that blocks below the frost line may not maintain full contact with the soil over seasonal cycling. These problems could explain why some sensors show substantially drier

measurements over time: reduced contact with soil would result in higher resistance, and thus drier measurements.

A second trend noted in Figure 6.6 is the annual sinusoidal variation: the soil becomes wetter over the summer, and drier in the winter. This reflects the seasonal rainfall pattern, as shown in Figure 6.7, using historical weather data for Huntley.

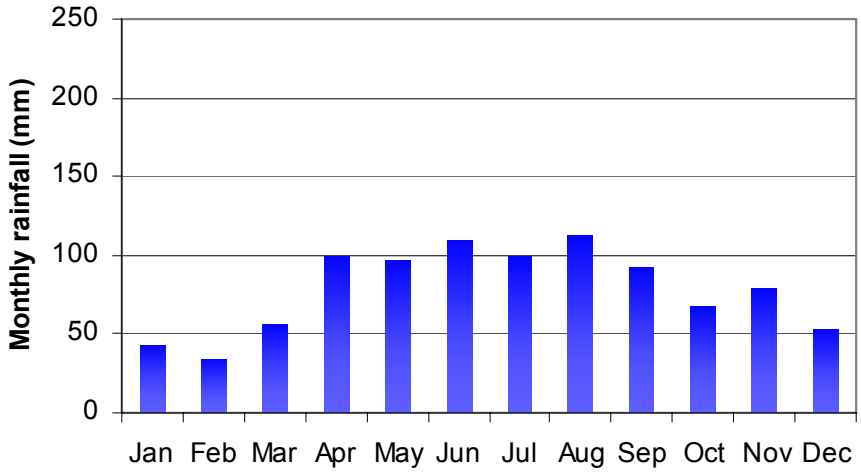

Figure 6.7: Historical monthly average rainfall data for Huntley

The rainfall data for the Argonne National Laboratory weather station for the monitoring period was similarly plotted in Figure 6.8, to see if correlations could be made between rainfall and soil matric potential measurements. However, no clear relationship could be discerned.

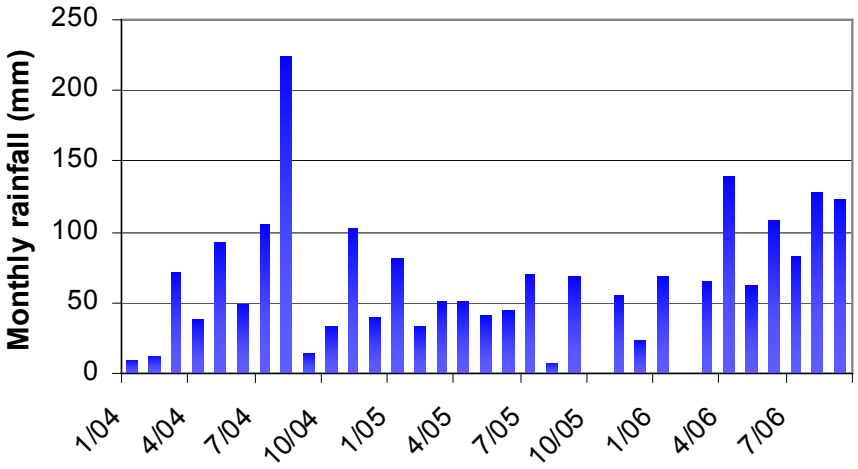

Figure 6.8: Monthly rainfall data at Argonne National Laboratory weather station

Given the difficulty of interpreting graphs showing all nine sensors, the results were culled to a single stack of three sensors, as shown in Figure 6.9, for the full timescale. Rainfall data was plotted to determine whether a response to individual rain events could be discerned in the soil sensors. It is possible that there is some correlation with the shallowest sensor and rainfall patterns, but there is no consistent or repeatable behavior pattern.

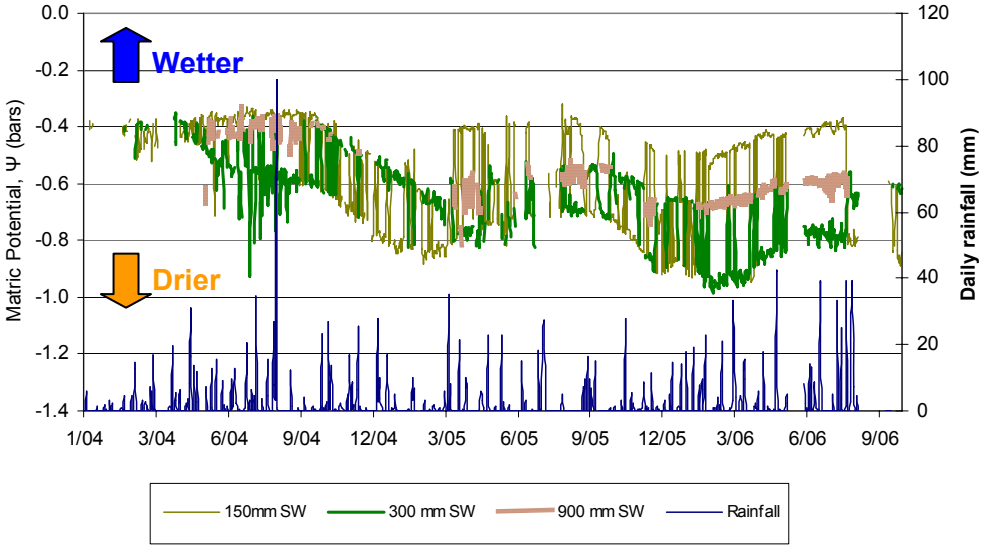

Figure 6.9: Center stack soil matric potentials and rainfall data (2004-2006)

Figure 6.10 is a close-up of the 2005 data; it appears that soil wetness does not necessarily match rain events. It should be noted that there is sprinkler irrigation at this site; the soil wetness might be dominated by operation of this system.

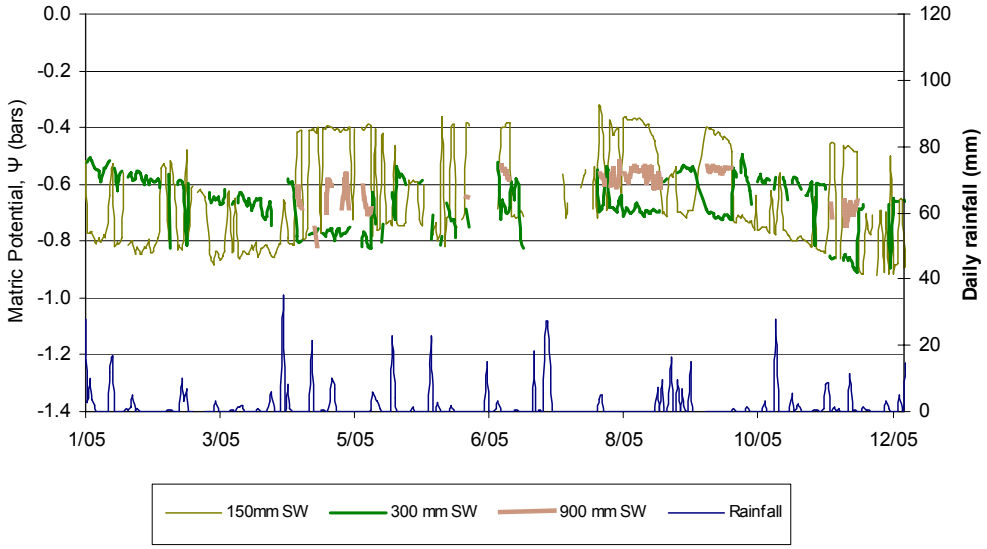

Figure 6.10: Center stack soil matric potentials and rainfall data (2005 detail)

Overall, correlation between matric potentials and individual rain events was not seen: this suggests that an immediate humidity spike in the test walls after rain wetting in this basement would be due to a bulk water bypass (e.g., a gap at the foundation wall or downspout connected to footing drain), instead of water draining through the soil. Soil wetness varies seasonally, but does not seem to correspond to rain events.

It was difficult to discern consistent and believable behavior patterns between the various depths and lateral locations. For instance, one "stack" was not notable drier or wetter than the others; consistent behavior was not seen at a given depth.

6.2 Interior and Exterior Boundary Conditions

Indoor and outdoor temperature conditions are shown in Figure 6.11 for the three-year monitoring period. Basement interior conditions were not explicitly controlled; setpoint was maintained on the main floor of the house (above grade conditions were not monitored). Wintertime and summertime extreme temperatures varied year to year; typical wintertime interior temperatures were in the range of 13-15° C (55-60° F) summer conditions were approximately 17-19° C (63-66° F).

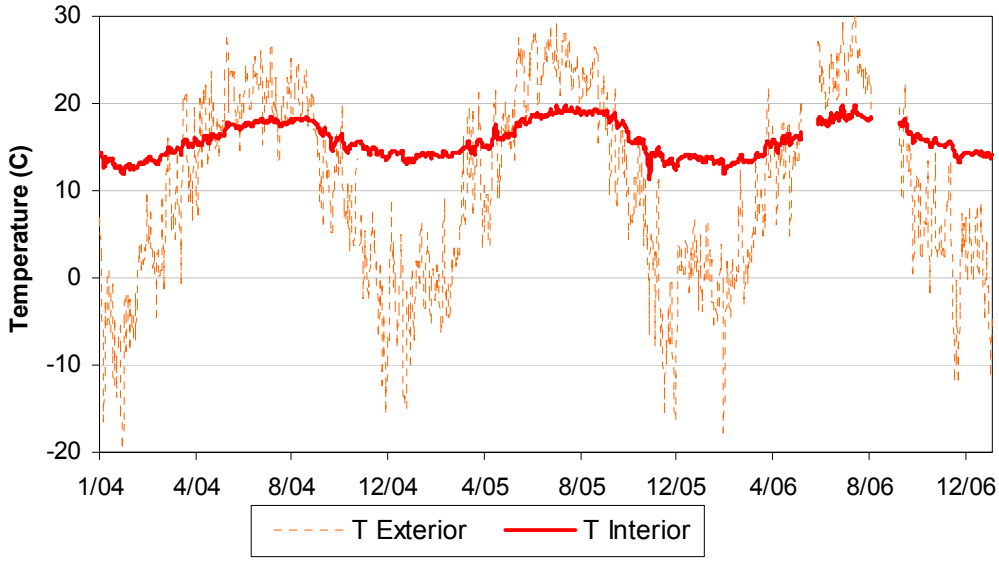

Figure 6.11: Interior and exterior temperature (daily average values)

These wintertime temperatures are distinctly cooler than those monitored in the nine-house Chicago-area sample described in Chapter 3 (Section 3.4): they were in the range of 16-21° C (compared to 13-15° C at Huntley). As a model house, the space conditioning of the basement would be of minimal concern, so it is possible that the HVAC runs to the basement were dampered off or minimized. Secondly, the basement walls were uninsulated except at the test walls (one elevation). Third, field observations suggested that air infiltration to the basement was relatively high.

The summertime temperatures were also colder than those monitored at the Chicago-area houses, which were in the range of 18-22° C (compared to 17-19° C at Huntley). The Huntley was a model house, so the air conditioning was run through the entire summer; in comparison, the Chicago area houses were often cooled using window ventilation.

Interior and exterior relative humidity for the monitored period are shown in Figure 6.12, with temperature data. Humidities were in the 20-40% RH range during the winter, and 60-80% RH during the summer. As a comparison point, in the Chicago houses, summertime relative humidity was typically in the 60-90% range; wintertime humidity was 30-50% during the first winter, and 40-50% during the second winter.

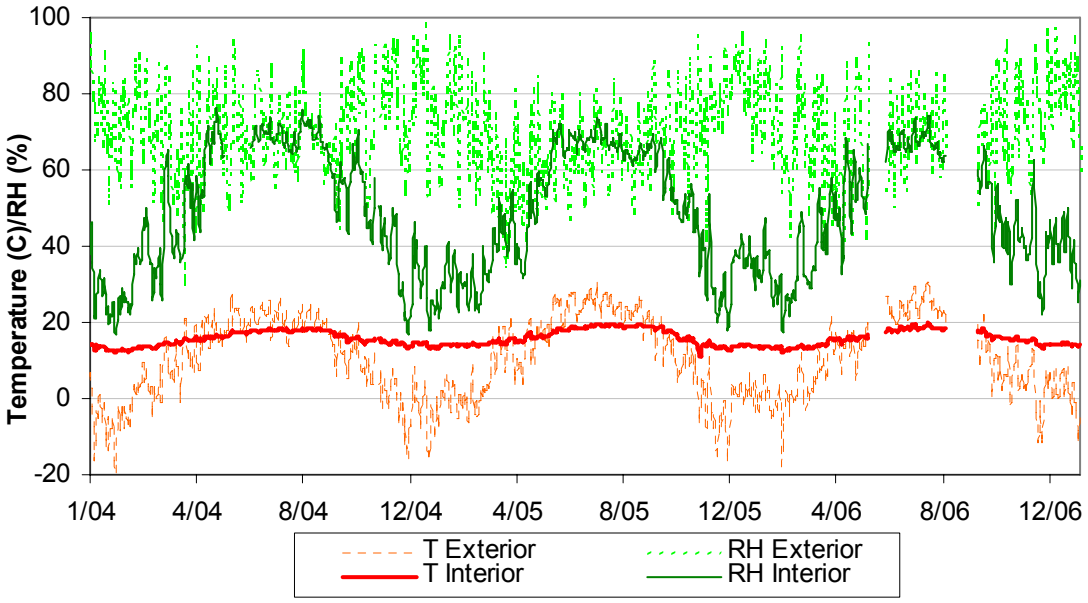

Figure 6.12: Interior and exterior temperature & relative humidity (daily average values)

However, this comparison does not provide much information, due to the difference in temperatures; therefore, dewpoint temperatures for the Huntley site are plotted in Figure 6.13. The interior dewpoint follows the pattern of exterior dewpoint, but is lower than exterior in summer (reflecting the dehumidification of the air conditioning system), and higher than exterior in winter (reflecting airtightness, and desorption from interior finishes and materials).

Wintertime dewpoints were in the –10 to 0° C range, reflecting very dry conditions: at 20° C, these conditions would be equivalent to 12-26% RH. In comparison, the Chicago houses had higher dewpoints, in the 0-10° C range (5-12° C in one development), and the Ruest data showed Canadian basement dewpoints in the –5 to 5° C range. The dry winters are expected behavior given that the Huntley site is an unoccupied model home, with no interior moisture generation sources such as cooking, cleaning, or showering.

Summertime dewpoints peaked at approximately 13° C. In the Chicago houses, summertime dewpoint was often identical to that of the exterior, showing the effect of window ventilation cooling; this would have put summertime dewpoints in the 15-20° C range.

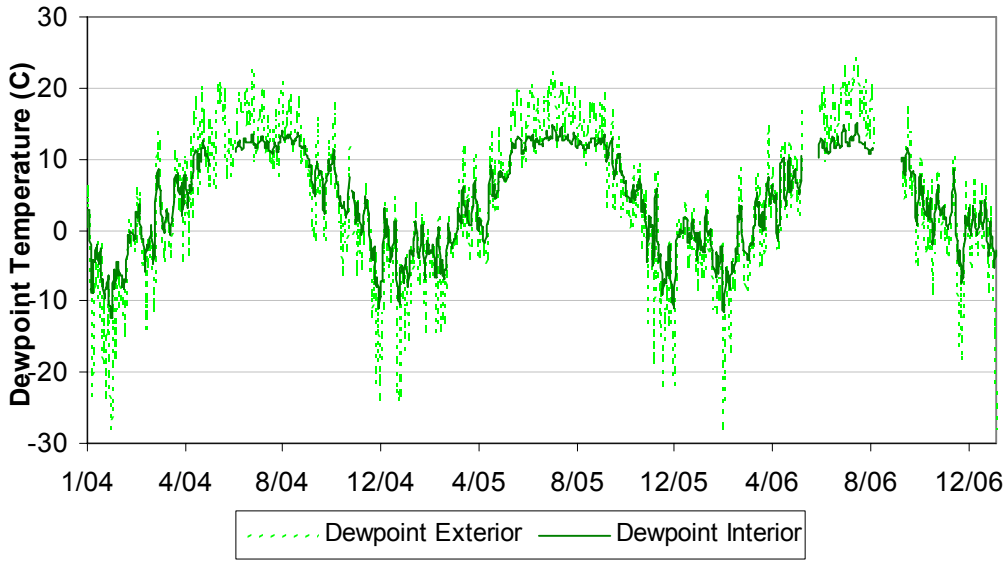

Figure 6.13: Interior and exterior dewpoint conditions at Huntley site (daily average values)

Overall, interior conditions were cooler and dryer, both winter and summer, than the interior conditions from the survey of nine Chicago-area houses and the Canadian Ruest data.

6.3 Wall Behavior in Normal Conditions

The behavior of the walls without the operation of the wetting system was first examined: this is primarily the first year of data (January 2004 through February 2005). Some additional data is available after the drying of the last wetting event (January 2006); modifications were made to some walls, and comparisons can be made with earlier behavior.

The analysis first covers the temperature behavior of these walls; if there are differences between the test panels, the hygrothermal results should be interpreted with that data in mind. The walls will be examined in similar sets, and then their performance will be compared. Analysis and comparisons will use temperature, relative humidity, dewpoint (computed from T and RH), and some wood moisture content data.

6.3.1 Temperature Behavior

Although efforts were made to place test panels in positions that would result in similar exposures, some features of the house resulted in differential conditions. An important factor was the rear bays that are cantilever framed out from the straight wall foundation. One effect was the shading of the walls beneath. Therefore, infrared temperature measurements were taken along the exposed portion of the concrete foundation wall, during a field visit in July 2006, at 4 PM. Outdoor temperature was 31-32° C; conditions were mostly sunny with some clouds. Measured temperatures are shown in Figure 6.14.

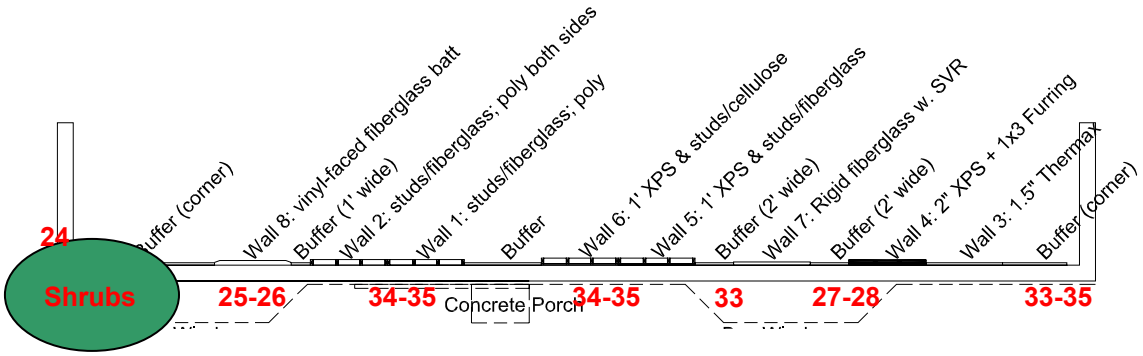

Figure 6.14: Concrete above-grade surface temperatures (July 2006)

Further measurements were taken around the non-experimental sides of the house, to gauge the effects of solar exposure on above-grade temperatures. The east (left) side of the house, which was in the shade by the afternoon, was at 25-26° C, except at the garage (26-27° C). The west (right) side was at 28-30°, except behind the shrubbery at the corner.

It was therefore concluded that solar exposure creates a noticeable temperature difference at the above-grade wall portions of the wall in summertime. This is demonstrated in the plot of the temperature at the concrete-insulation interface at the upper location (Figure 6.16). The solar exposed walls (1 and 6) show markedly higher temperatures, and sharper daily peaks than the shaded walls (7 and 8). The peak differences are roughly 4° C. Note that these selected walls are the extreme cases: walls 7 and 8 are noticeably cooler than the remaining walls; the remaining six walls are clustered near the warmer walls.

Figure 6.15: Bay near Wall 8, showing shading on above-grade portion of concrete

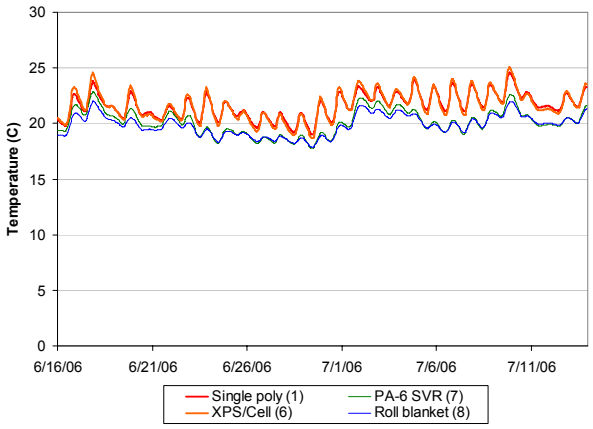

Figure 6.16: Temperatures at concrete-insulation interface at grade (interior side); June-July 2006

A similar examination was conducted for winter; it also showed temperature differences between the walls. During field visits, a second reason for this temperature difference was observed. At the cantilever bays, there was no air barrier in the joist bay between the interior and the cantilever space (Figure 6.17), and the air barrier at the cantilever (to exterior) is very poor, due to access/detailing difficulties. As a result, there is a substantial cold air leak at the cantilever bays; this was noticeable

while standing several feet away from the wall. Stack effect will tend to draw exterior air into the house at this location (bottom). This air infiltration tends to cool the upper portion of the concrete wall, as reflected in the data (Figure 6.18). Maximum temperature differences were roughly 4° C.

Figure 6.17: Bay interior near Wall 8, showing incomplete blocking/air leakage location

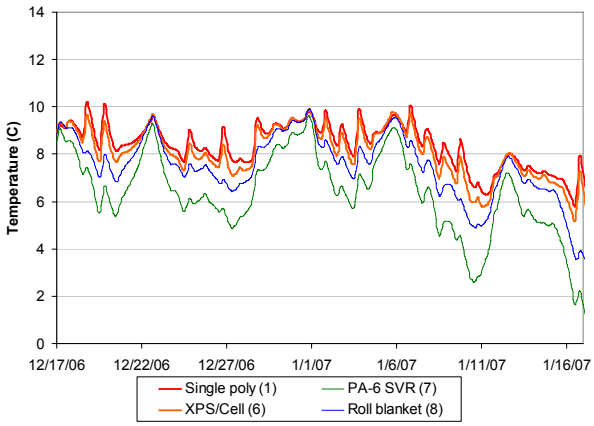

Figure 6.18: Temperatures at concrete-insulation interface at grade (interior side); December 2006-January 2007

Daily mean temperatures over the course of the year were examined: this data showed that walls 7 and 8 are noticeably cooler than the remaining walls. However, at mid height of the wall (below grade), all concrete surface temperatures are ±1° C or less; also, this measurement does not factor in the effect of the different R-values of the assemblies (which should be small, given the small ΔT across insulation). At the lowest depth, the concrete wall conditions are virtually identical (±0.5° C), except for wall 3 (polyisocyanurate), which shows consistently colder wintertime temperatures.

Therefore, it was concluded that the walls are thermally comparable, except for the above-grade portions of walls 7 and 8 (rigid fiberglass with PA-6, and roll blanket). In addition, the consistent thermal anomaly at wall 3 (polyisocyanurate) warrants further investigation.

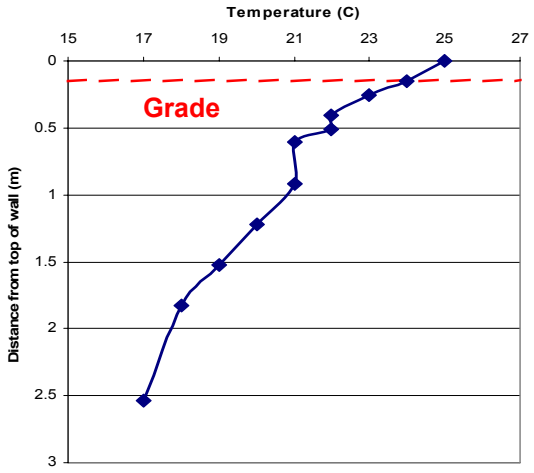

In addition to comparing the walls, during a summer field visit, the vertical thermal profile of the wall was taken, as shown in Figure 6.19. This was done in wall 1 (single polyethylene), immediately after removing the batt insulation from the wall during disassembly. Outdoor temperature was 35° C at that time.

The temperatures show behavior expected from the literature: a sharp change in temperature with depth at the top of the wall, and a more gradual drop in temperature going further down the wall.

Figure 6.19: Thermal profile (summertime) down height of wall 1

The temperature behavior of the concrete wall with depth is worth examining in closer detail, over the course of the year, as plotted in Figure 6.20. The daily average temperatures at the interface between the concrete wall and the insulation system are shown at upper, mid-height, and lower locations; exterior temperature is shown as well. Data from the single polyethylene test panel (wall 1) is shown, but all walls had similar behavior patterns.

The temperatures show seasonal swing similar to outdoor temperature, but with greater damping at increasing depth. The upper location is roughly at grade, and shows the similar day-to-day spikes, but with some damping, while the mid-height and lower location show much more damped behavior. In addition, as predicted by literature, the temperatures show greater phase shift with depth: the lower location only reaches its peak by late September, while air temperatures peaked in August.

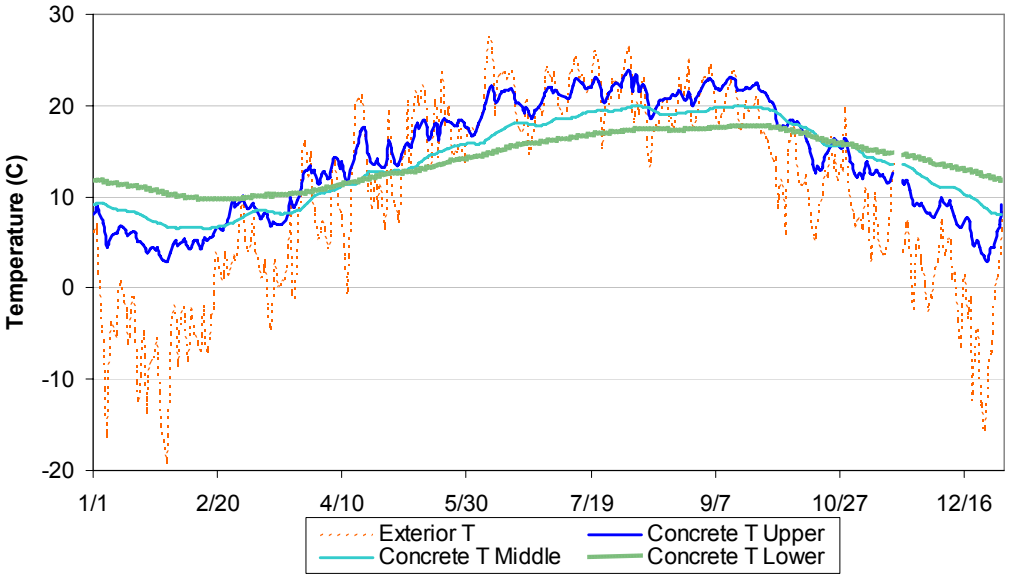

Figure 6.20: Upper, mid-height, and lower concrete temperatures, with exterior T

6.3.2 Wall Data Availability and Wall Dewpoint Behavior

As mentioned earlier, temperature, relative humidity, dewpoint (calculated from T and RH), and wood moisture content are used to understand wall behavior. However, it should be noted that there is a limited amount of useful moisture content data, due to some logger issues: this was solved during a field visit in October 2006. Also note that moisture content measurements were not corrected for species: the framing lumber was unspecified SPF (spruce-pine-fir), so no single species correction could be applied.

The dewpoint provides a very useful metric for analysis of wall behavior. First, as a measurement of absolute water content in the air, it can provide a comparison of moisture conditions in locations with different temperatures, such as the interior air and within the stud bay cavity. Second, it can be compared to surface temperatures, such as the concrete or polyethylene, to provide an indication of condensation risk and/or severity. Third, as an indication of absolute moisture content, it provides the direction and magnitude of the gradient driving moisture flow. However, this does not remove the importance of relative humidity. RH values (when combined with temperature) provide threshold conditions for biological activity, such as mold growth.

One item noted in interpreting wall behaviors was the relationship of interior dewpoint, the dewpoint inside the wall assembly, and the concrete wall temperatures. All of these measurements move in parallel when plotted together, as shown in Figure 6.21 and Figure 6.22, which show these values for the single polyethylene wall (interior vapor barrier only; wall 1).

The hourly data shows that all three respond in parallel to day-to-day spikes or drops. Note that the response is more smoothed at mid-height, as discussed in section 6.3.1, while the upper location shows greater variation. However, given that the dewpoint in the stud bay is a critical metric for wall

failure, finding the dependency of its behavior can provide some insight into how these walls are wetted and dry.

For instance, the stud bay dewpoint could be influenced by interior dewpoint due to air leakage or vapor diffusion (in the walls with permeable interior finishes). Alternately, a hygroscopic component with substantial storage, like the concrete wall, would tend to maintain the local relative humidity close to a fixed point while the temperature varies. A wall that links the stud bay with the concrete surface (such as the single polyethylene wall here) would be influenced by the concrete temperature.

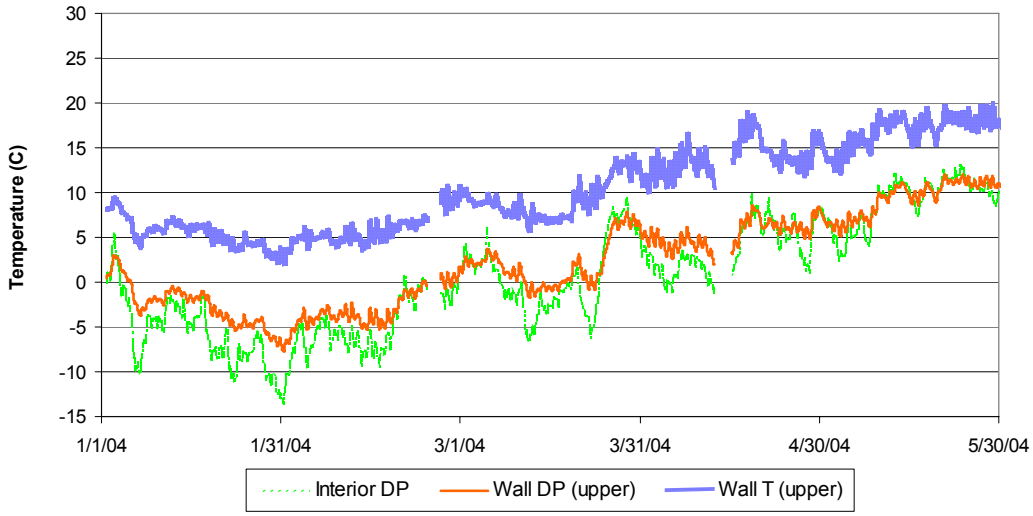

Figure 6.21: Interior dewpoint, stud bay dewpoint, and concrete temperature (upper location)

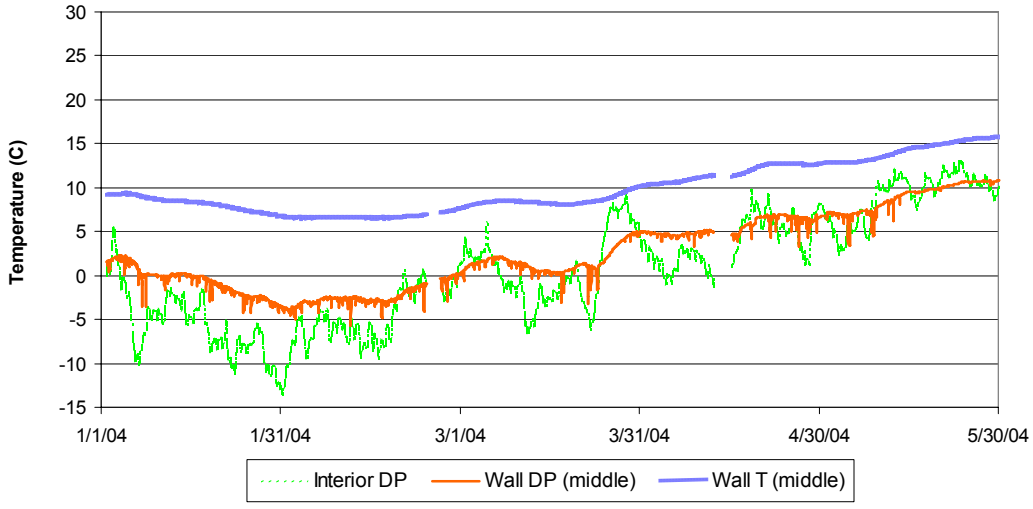

Figure 6.22: Interior dewpoint, stud bay dewpoint, and concrete temperature (mid-height)

To understand the dependencies, the interior dewpoint and mid-height concrete temperature were plotted with the driving forces of exterior temperature and dewpoint in Figure 6.23. It is clear that

interior dewpoint is set mostly by exterior dewpoint, which in turn is linked to the exterior temperature (i.e., exterior RH falls mostly within a band of 60-80% throughout the year). The concrete wall temperature at mid-height parallels outside temperature, but with a phase shift.

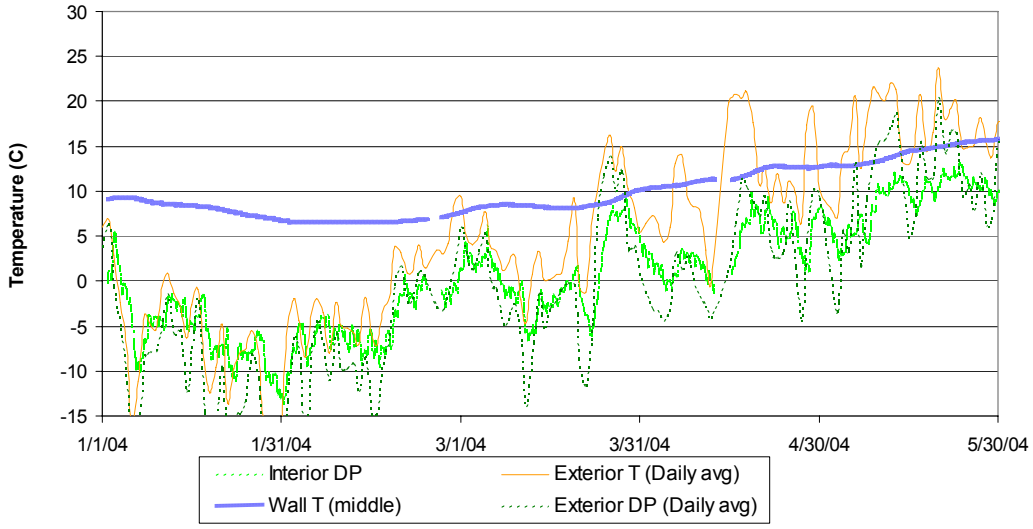

Figure 6.23: Interior dewpoint, concrete temperature (mid-height), exterior T and dewpoint

Therefore, returning to the graph of the mid-height wall behavior (Figure 6.22), the stud bay dewpoint follows the peaks and valleys of the wall temperature, as opposed to the interior dewpoint (or exterior temperature). However, at the upper height (Figure 6.21), it is difficult to conclusively ascribe the behavior to either force.

6.3.3 Stud frame walls (Walls 1 and 2)

These two walls demonstrate the effect of the presence or absence of a second layer of polyethylene at the concrete-insulation interface as a "moisture barrier." Note that this layer was run full-height in this wall.

The walls were compared using dewpoint temperatures within the assembly, first at the upper location (Figure 6.24). Although the profiles are similar, the single poly wall is drier (lower dewpoint) than the double poly wall in both winters, but is wetter in the summer. This can be explained with the moisture physics of these assemblies mentioned earlier. During the winter, the double poly assembly eliminates any drying to the exterior due to its low permeability (roughly 3 ng/Pa·s·m^2, or 0.06 Imperial perms for poly, vs. 19 ng/Pa·s·m^2, or 0.3 Imperial perms for concrete). The exterior polyethylene "moisture barrier" also removes the moisture storage capacity of the concrete.

But in the summer, there is some inwards vapor drive: the double poly wall is isolated from this source, while in the single poly wall, this moisture can enter the stud bay cavity. However, it should be noted that this was not a very strong inwards vapor drive: summertime humidity in the stud bay

peaks at roughly 70% in mid-batt; no condensation would have occurred on the interior polyethylene. As noted earlier, this wall had been drying for two years before the installation of these assemblies.

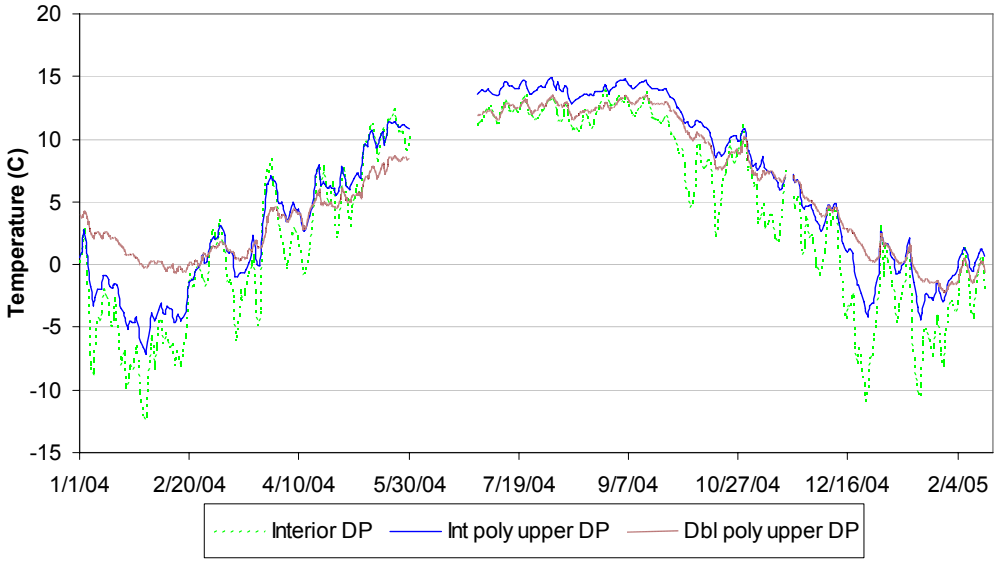

Figure 6.24: Single and double poly dewpoint (upper location), with interior DP

In the mid-height location, a similar pattern is seen (Figure 6.25). It is notable that the single poly wall shows steadier moisture behavior than the double poly wall: this is likely due to the damping effect of the hygrically massive concrete wall, coupled to the stud bay.

It may seem odd to ascribe the higher summertime dewpoint of the single poly wall to inwards vapor drive, at the below-grade (mid-height) location. However, the temperature at this location rises seasonally: given the 100% RH boundary condition of the soil and the near-100% RH condition of the interior of the concrete, this results in moisture entry into the stud bay. Note, however, that the concrete-insulation interface is not at 100% RH in this wall, so concrete surface temperature is not equal to the dewpoint.

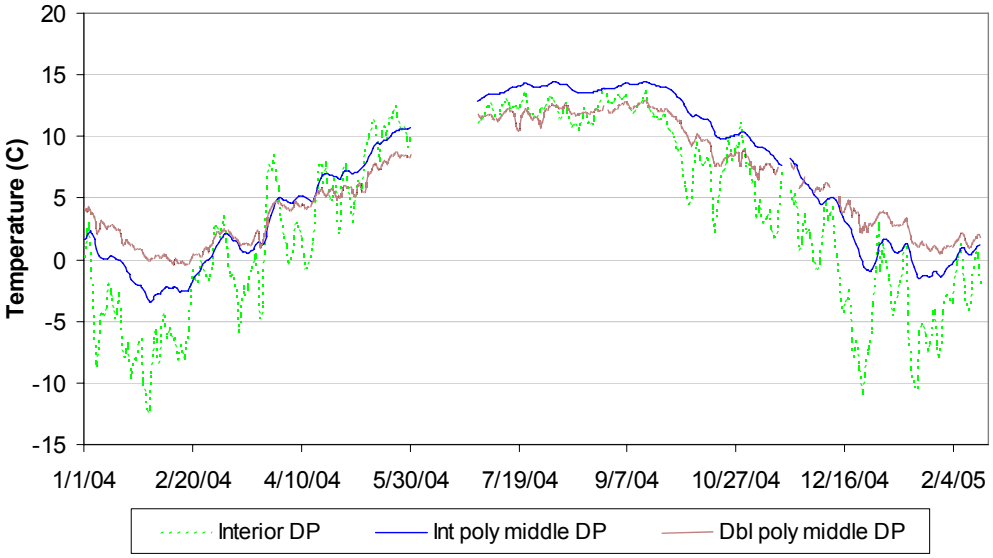

Figure 6.25: Single & double poly dewpoint (mid-height location), with interior DP

The lower location has a similar relationship between the stud bay dewpoints.

As a final dewpoint comparison, the measurements at the interface between the concrete wall and the insulation were compared in Figure 6.26. In the single poly wall, the sensor at this location had a virtually identical dewpoint to the mid-stud sensor, due to the minimal vapor resistance of the fiberglass batt. In the double poly wall, this sensor was sandwiched between the concrete and the outer "moisture barrier" polyethylene.

This plot shows that substantial moisture accumulates on the exterior of the outer layer of polyethylene; this interface is intended to accumulate moisture, to protect the stud bay and vulnerable wood framing.

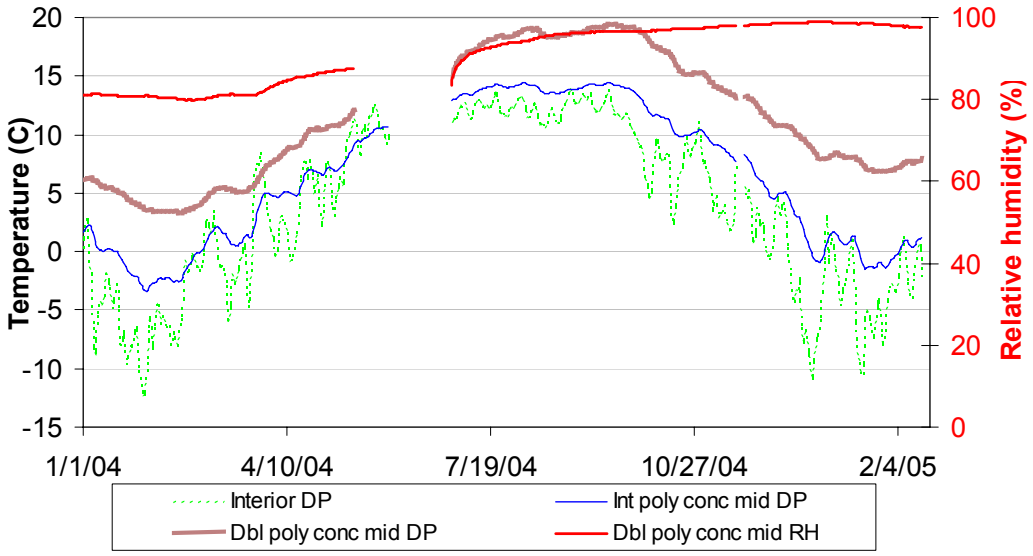

Figure 6.26: Single & double poly insulation/concrete interface dewpoint & RH, w. interior DP

The relative humidity at this location is also plotted in Figure 6.26: it shows that the humidity approaches saturation over the summer, and remains close to that level through the winter. Note that this even occurs in a concrete wall that has been drying for approximately two years. These would be conditions conducive to mold growth: this suggests the importance of isolating this interface from the interior air. However, minimal nutritive value is available at this interface between concrete and polyethylene, although accumulated dust/dirt could provide a substrate.

Wood framing moisture content measurements were examined as well; they indicated little difference between these two walls. The single poly wall shows marginally but consistently lower moisture content (9% vs. 10%), but this is below the reliable resolution of the system. Both moisture content measurements are well within the safe range for wood framing.

In the single polyethylene wall (panel 1), the air seal between the top of the framing and the concrete wall went through several stages. It was originally constructed unsealed, as per typical builder practice. Expanding foam was used to seal this joint in September 2005 (see Figure 6.27), and when the walls were opened in July 2006, this seal was refined with builders' tape (see Figure 6.28).

Figure 6.27: Gap in air seal at the top of panel 1

Figure 6.28: Panel 1 top connection sealed with builders' tape

Unfortunately, the effect of the first air sealing could not be discerned, because the wetting system was run on the same trip that this repair was completed. The data at the time of the second air sealing (using builders' tape) showed no effect.

6.3.4 Foam plastic insulation walls (Walls 3 and 4)

The foil-faced polyisocyanurate and 50 mm (2") extruded polystyrene walls are the next set compared; surprisingly, they showed very different behaviors, so results are shown on separate plots.

The dewpoint measurements of the polyisocyanurate panel are shown in Figure 6.29 for the sensor mid-thickness in the foam (foil taped into cut pocket) and the sensor at the interface between the insulation and concrete. Both show similar responses: they remain very close to interior dewpoint, with the latter sensor practically indistinguishable from interior dewpoint.

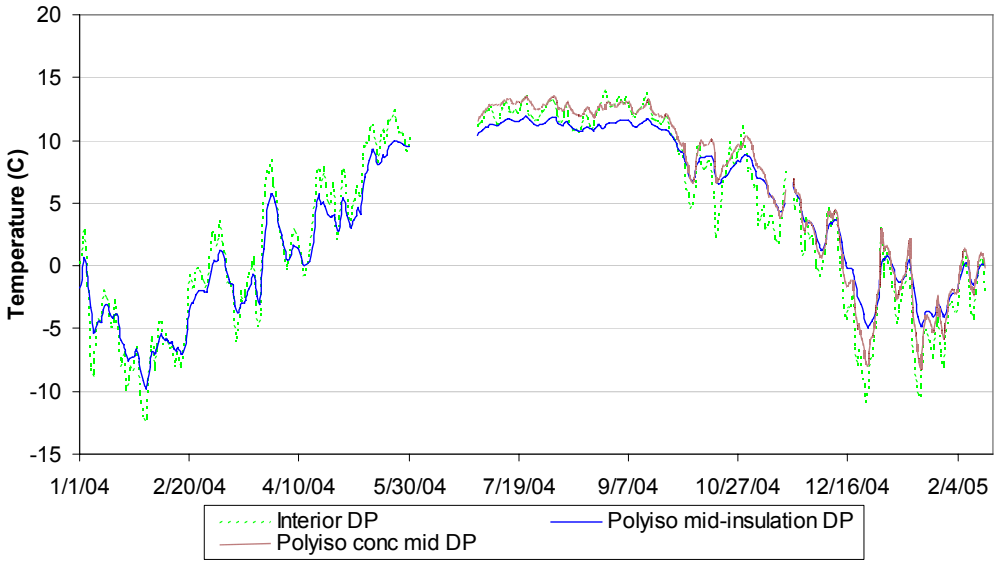

Figure 6.29: Polyiso mid-insulation and concrete/insulation interface dewpoint, w. interior DP

These results were initially confusing, as the insulation board has two vapor impermeable foil facers, and should show a much smaller response to interior dewpoint, as well as moisture accumulation behind the board sourced from the concrete and/or soil. Initial theories included causes such as perforation of the interior-side foil facer due to the finish texturing, or lateral diffusion through the open edges of the insulation board. A benchtop experiment was performed by Aaron Townsend of Building Science Corporation, to examine the permeability behavior of foil-faced polyisocyanurate, as shown in Appendix E: Foil-faced Polyisocyanurate Permeability Experiment.

The conclusion was that lateral vapor diffusion through the foil-faced polyisocyanurate is relatively slow (consistent with published values, given the long distance that would be required for lateral vapor transport across the panel), and that the polyisocyanurate material is very hygroscopic, keeping relative humidity steady over wide temperature swings.

Subsequent field visits demonstrated that the plastic channels used to install the insulation panel result in a gap of 3 to 9 mm (1/8" to 3/8") between the panel and the concrete; it is apparent that interior air can communicate freely with this space. This was true even after the installation of expanding foam at the top interface of the insulation and the concrete in late 2005 (see Figure 6.30). In addition, the sensor installed mid-thickness in the panel has an inadequate air seal, despite the lack of visible installation deficiencies: it could communicate with the air gap space. The hygric mass of the concrete and the polyisocyanurate results in the damping seen in the sensor response (relative to interior dewpoint).

In July 2006, after running this assembly in this configuration with an air gap, the panel was reinstalled in an air sealed manner, with no gap behind the board. Caulk was used at all edges of the board, and an additional bead of caulk was run below the 1' form extension at the top of the wall that

bows outwards (creating an additional gap), as shown in Figure 6.31. The board was attached directly to the foundation wall with concrete screws and washers.

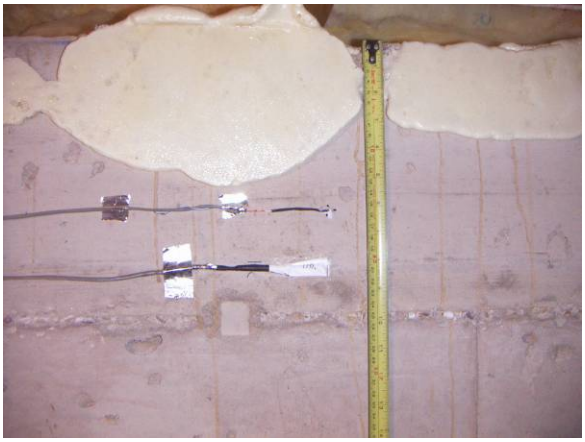

Figure 6.30: Foam seal at top of wall; note gap in foam at tape measure.

Figure 6.31: Caulk air seal around the perimeter and at form board extension intersection

Since the RH sensor installed in the middle of the insulation board only provided information on the effectiveness of the foil tape seal at the "pocket," it was removed and reinstalled in a different location. It was moved to the upper part of the wall (roughly at grade), at the interface between the concrete and insulation, as shown in Figure 6.30. This sensor placement is intended to capture moisture accumulation behind the foil-faced insulation board, as well as possible inwards vapor drives. Results of this reconfiguration are shown in Figure 6.32.

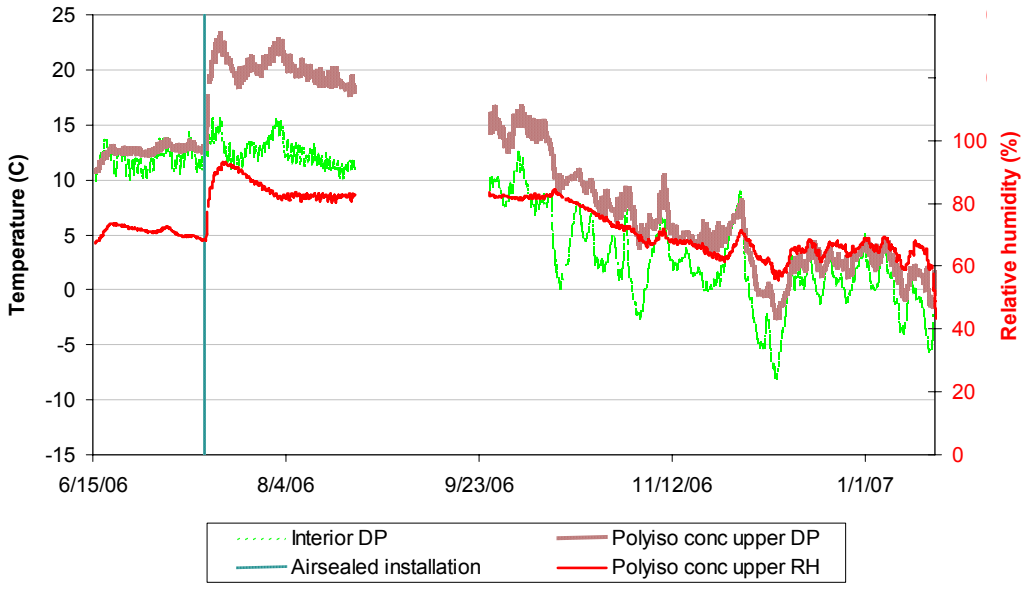

Figure 6.32: Polyiso upper insulation-to-concrete interface dewpoint and RH, with interior DP

This change of installation configuration caused a sudden rise in relative humidity at the upper interface, peaking at 93%, before declining with the seasonal shift. This demonstrates accumulation of moisture at the impermeable interface. A similar accumulation occurs at the mid-height, but it is much less pronounced, with relative humidity remaining below 80% at all times.

The humidity levels behind the polyisocyanurate do not rise or remain nearly as high as the double polyethylene wall (see Figure 6.26), even though the permeability values of the foil facer and polyethylene are comparable. The reason for this difference is not clear; the air seal at the perimeter of the polyisocyanurate board was more carefully detailed than the outer polyethylene "moisture barrier."

The extruded polystyrene foam wall results are shown in Figure 6.33, showing the dewpoint and relative humidity at the interface between the insulation and concrete at mid-height. Note that this was the only relative humidity sensor of interest in this wall: a T/RH sensor was placed in the furring air space, but it only showed temperature and dewpoint conditions identical to interior.

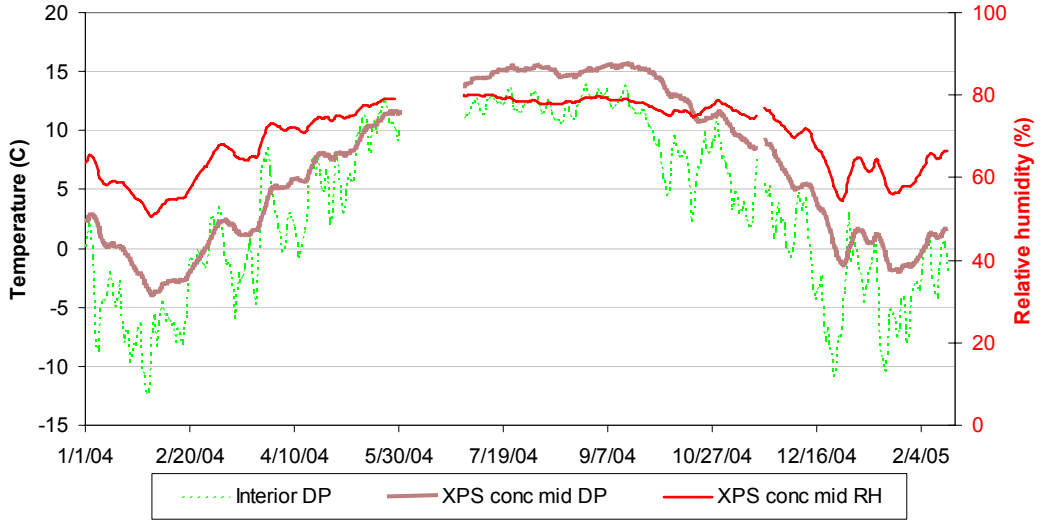

Figure 6.33: 2" XPS concrete/insulation interface dewpoint, with interior DP

The dewpoint behavior behind the insulation follows the seasonal temperature/dewpoint pattern, but shows some moisture accumulation at the exterior of the insulation. Dewpoint remains above interior levels for most of the year, like the corresponding sensor in the double polyethylene wall. However, the accumulation behind the assembly much is lower: relative humidity peaks at 80% in the summer, compared to close saturation in the double poly wall. This occurs because the permeability of the XPS is an order of magnitude greater than polyethylene: 28 ng/Pa·s·m^2 (0.5 Imperial perms) for 50 mm/2" XPS vs. 3 ng/Pa·s·m^2, (0.06 Imperial perms) for polyethylene. Although 80% RH is considered a danger level for mold growth (ASHRAE 2006), Doll (2002) and Black (2006) have demonstrated that this may be an overly conservative threshold. In any event, layers with vapor permeance of over 28 ng/Pa·s·m^2 (0.5 Imperial perms) can be expected to maintain interface RH levels of 80% or lower.

Moisture content measurements of the furring remained at completely safe conditions throughout the year.

6.3.5 Composite walls (Walls 5 and 6)

These test panels combined 25 mm (1") of extruded polystyrene with an insulated stud frame wall, the only difference being stud bay insulation material (fiberglass in wall 5; cellulose in wall 6). Instrumentation was placed at the interface of the concrete and the XPS (at mid-height), and within the stud bay (at low, mid-height, and high locations).

The concrete/XPS interface dewpoint and relative humidity for the XPS-fiberglass wall are shown in Figure 6.34. They are similar to the results seen in the 2" XPS wall (panel 4), as shown in Figure 6.33, except that the moisture peak during the summer is not as high. For instance, the relative humidity in wall 5 peaks at approximately 75%, while the 2" XPS peaks closer to 80%. The XPS foam, in both cases, allows the controlled release of moisture from the concrete.

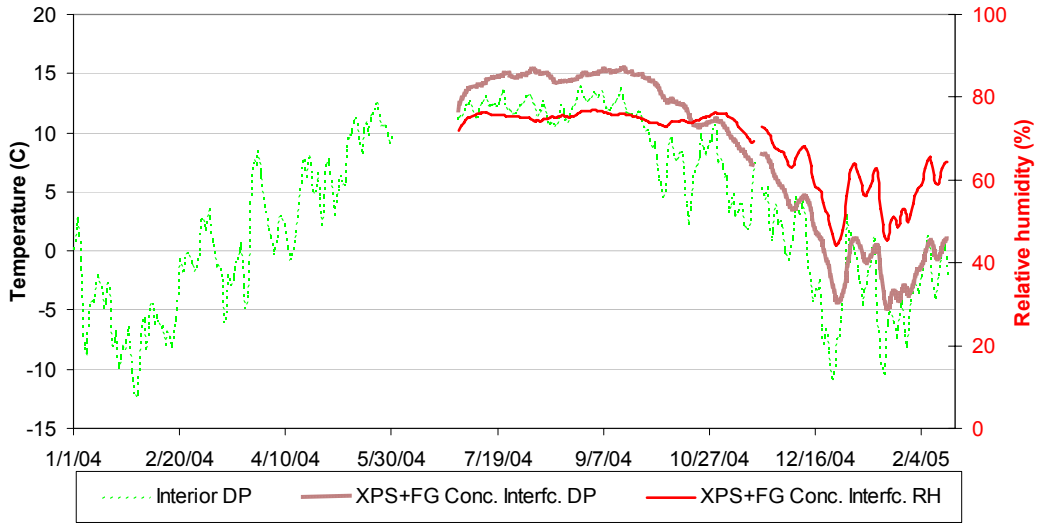

Figure 6.34: XPS+fiberglass concrete/insulation interface dewpoint, with interior DP

The matching plot for the cellulose wall is shown in Figure 6.35: it behaves similarly for most of the year, and the stud bay insulation material does not appear to make a difference. However, the dips in dewpoint/relative humidity at the end of the year are not identical; smaller changes are seen in the cellulose wall. This may simply be a function of the installation details of the XPS, as described in Chapter 5 (Section 5.1.4.2).

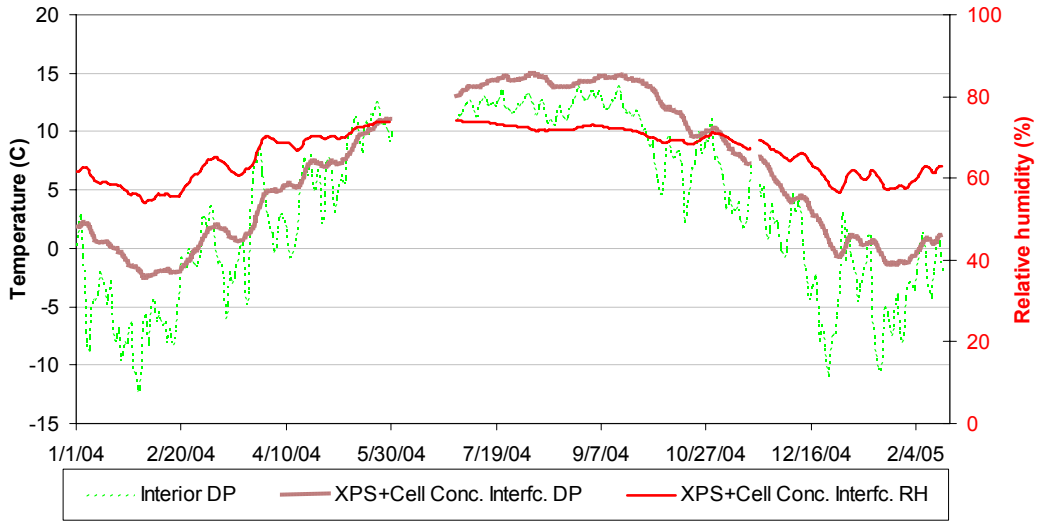

Figure 6.35: XPS+cellulose concrete/insulation interface dewpoint, with interior DP

The dewpoints of the stud bay at the upper location are shown in Figure 6.36, for both walls. Both walls have dewpoints almost identical to interior; this is expected behavior, given the high permeance of the spun bonded polyolefin (SPBO, Tyvek) layer used as an air barrier. Note that the cellulose wall shows a damped response, demonstrating the effect of the hygric mass of the insulation. The fiberglass insulation, in contrast, has minimal moisture storage. This behavior can be seen very clearly in plots of hourly data (not included here). Diurnal variations in stud bay relative humidity were almost completely damped out in the cellulose wall.

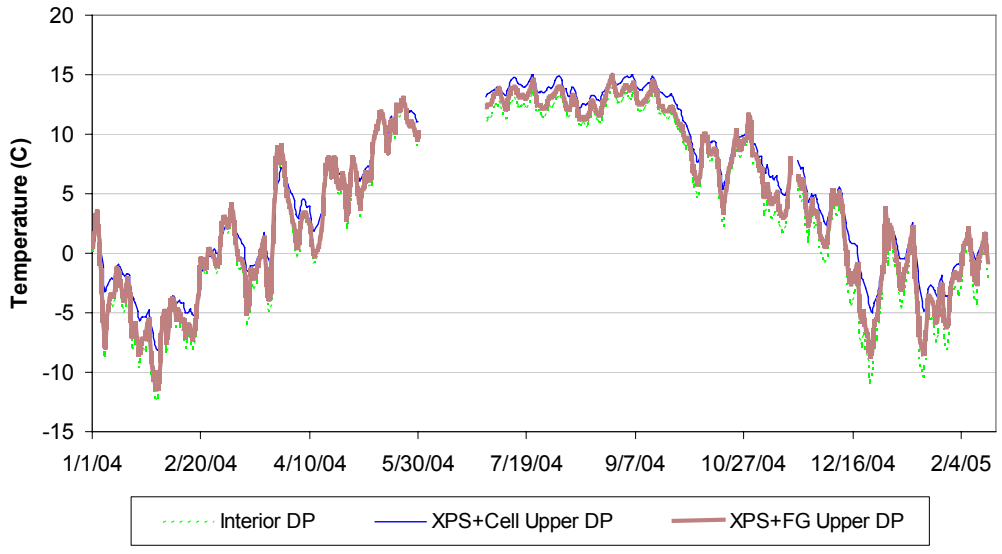

Figure 6.36: Stud bay dewpoints for XPS+FG (5) and XPS+cell (6) walls, upper location

The analogous plots of stud bay dewpoint at the mid-height and lower location show similar results and are not included.

In July 2006, the SBPO layer was replaced with ½" gypsum drywall, painted with latex paint (two coats). The effect of the installation is shown in Figure 6.37; there is a spike in the stud bay dewpoints in both walls, due to the drying of the water-based latex paint. The cavity dewpoints then remain slightly higher than interior, and have a smaller daily amplitude. However, note that the vertical scale is zoomed in relative to previous plots, and this difference is still quite small. This is the expected behavior from the interior finish being changed from SBPO, at 3300 ng/Pa·m·s^2 (58 Imperial perms) to latex paint on drywall, at 210-1100 ng/Pa·m·s^2 (4-19 Imperial perms) (dry and wet cup ranges).

Both before and after this change, the stud bay relative humidity levels remain below 80%.

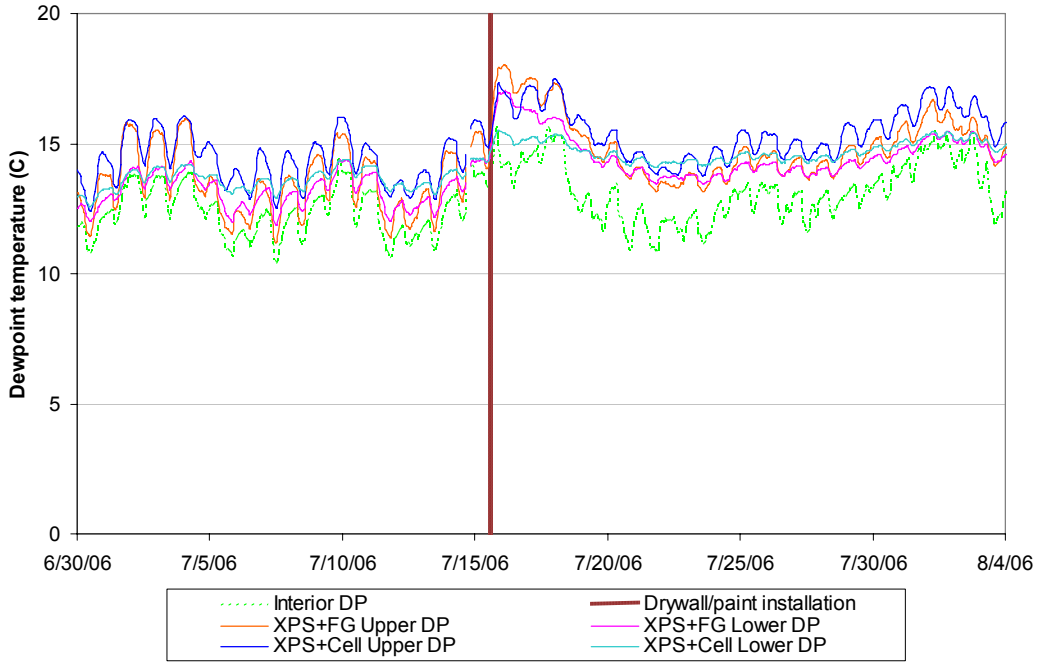

Figure 6.37: Upper and lower stud bay dewpoints before and after drywall/paint installation

These plots demonstrate that the XPS foam isolates the stud frame walls from the concrete moisture source, but allows controlled drying. Unlike the double poly wall, which shows moisture accumulation to saturation, the relative humidity is limited by this drying.

In the XPS-fiberglass wall, the moisture content measurements at the stud showed safe conditions throughout the year, with measurements in the 8-12% range. Moisture content measurements in the XPS-cellulose wall indicated a summertime rise to over 20%; however, it was later discovered that this behavior was due to the conductivity of cellulose insulation, due to the borate salts added to the insulation to enhance fire, pest, and mold resistance. Successful isolation of the pins from the insulation material resulted in similar moisture content measurements to the XPS-fiberglass wall, in the 8-10% range. This phenomenon is documented in Appendix F: Wood Moisture Content Measurements in Cellulose Wall.

6.3.6 Other walls (Walls 7 and 8)

The remaining walls are the rigid fiberglass with a "smart vapor retarder" ("SVR") PA-6 facer, and the fiberglass roll blanket with a perforated facer. The dewpoint measurements of these two walls at the interface between the insulation and the concrete are shown in Figure 6.38. Each wall had two T/RH sensors: one at this interface, and the other mid-thickness in the insulation. Given the lack of vapor resistance between these two locations and their proximity, the dewpoint results from these two measurements were virtually identical, so only one set will be plotted.

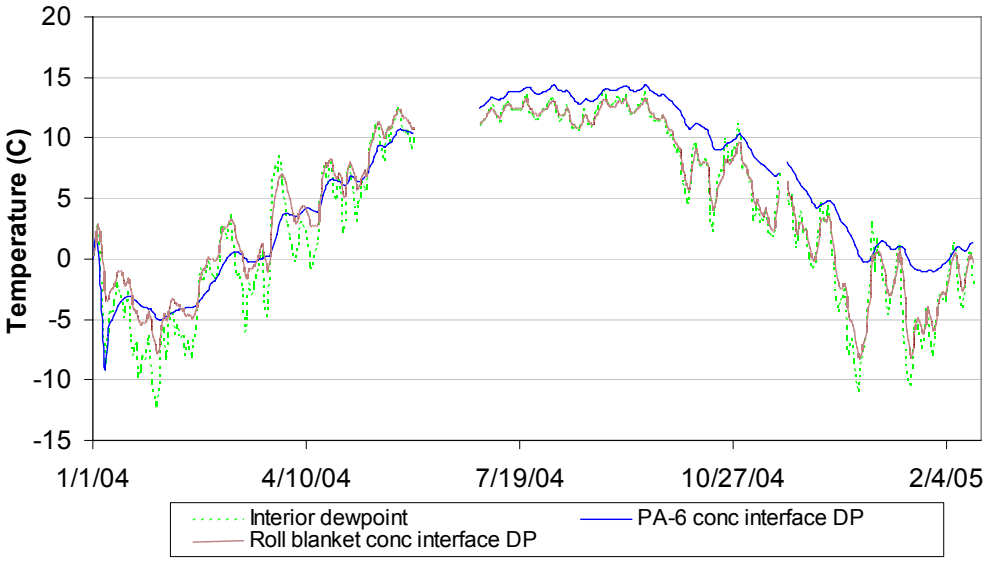

Figure 6.38: PA-6 and roll blanket concrete/insulation interface dewpoint, with interior DP

The PA-6 (SVR) wall (panel 7) shows behavior similar to the XPS walls (panels 4, 5, and 6): a relatively steady dewpoint, roughly following seasonal swings, but slightly above interior for most of the year. The relative humidity at the interface between the insulation and concrete peaked at 75%, which is well within safe limits.

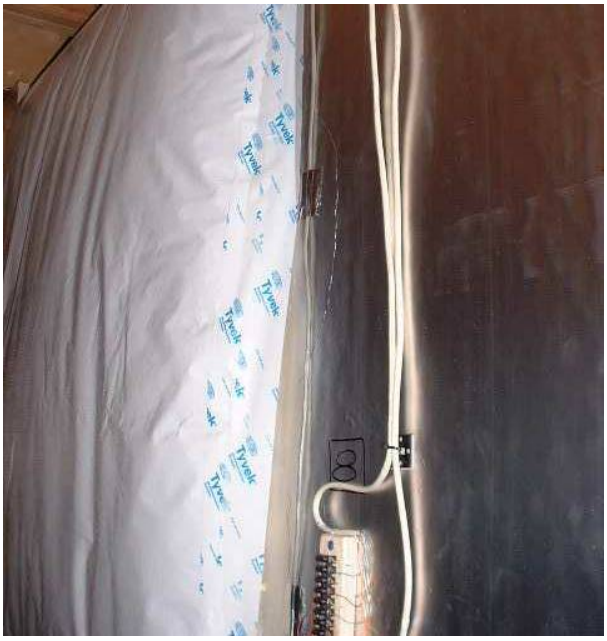

Figure 6.39: Roll blanket lateral seal failure in October 2003

Figure 6.40: Roll blanket lateral seal condition in June 2004

In contrast, the roll blanket wall (panel 8) shows dewpoint levels that are practically identical to interior dewpoint. There is some damping, likely due to the hygric storage of the concrete. As mentioned in Chapter 5 (Section 5.1.4.2) the vertical seals at the edges of the panels were problematic, failing over time as shown in Figure 6.39. However, later repairs using mechanical fasteners to reinforce the tape (as shown in Figure 6.40) proved to be more durable.

It is difficult to say conclusively from the 2004-2005 data whether this behavior was due to air leakage or vapor permeability of the facer. The roll blanket facer is quite permeable, as measured in Appendix D: Vapor Permeability Testing, at 700-1040 ng/Pa·m·s^2, or 12-18 Imperial perms; therefore, results could be explained by either mechanism.

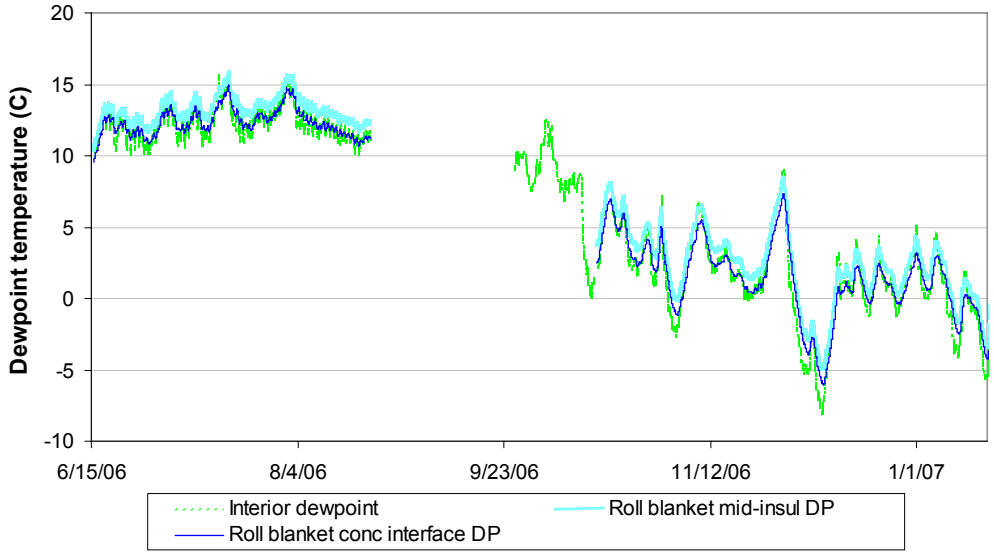

Figure 6.41: Roll blanket dewpoint in late 2006, with interior dewpoint

The dewpoint measurements in the roll blanket wall for 2006-2007 are shown in Figure 6.41; the quality of air seal of the wall had been improved by that point. The two dewpoints inside the wall still track interior conditions closely (but with some slight lag and offset), suggesting that vapor diffusion through the permeable facer dominates the behavior.

As noted in section 6.3.1, these walls had lower temperatures at the upper portion than the remaining test panels; as a result, they would experience less inwards vapor drive, and have greater risk of wintertime condensation. However, at mid-height, temperatures are close to identical.

6.3.7 Overall Hygrothermal Comparison

One useful comparison is to plot the same sensor type and location in all of the test panels, thus providing an indication of their relative performance. The only sensor which was common to all walls was the temperature/relative humidity at the interface between the concrete wall and the insulation system, at mid-height. The dewpoint measured by this sensor for all walls is shown in Figure 6.42.

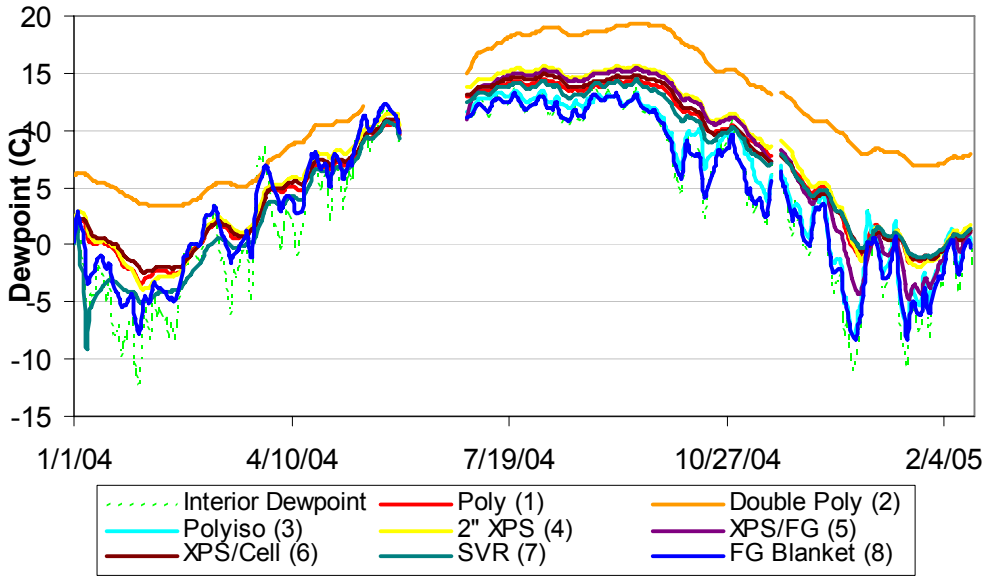

Figure 6.42: Mid-height concrete interface dewpoint for all panels, with interior DP

It basically summarizes the results from the previous sections, and provides a comparison. Two walls have dewpoints close to interior conditions: the polyisocyanurate (panel 3, due to the air gap behind the panel) and the perforated facer roll blanket (panel 8, either due to air leakage, or vapor diffusion through a permeable facer). The double polyethylene wall (panel 2) shows an elevated dewpoint relative to other walls. The remaining walls (single polyethylene, 2" XPS, 1" XPS w. fiberglass or cellulose, and PA-6 SVR) fall between these extremes, and have essentially similar behavior to each other. Similar patterns were seen in the 2006-2007 data.

It could be argued that in the double polyethylene wall, the dewpoint in the stud space (mid-height) should be graphed instead; as shown in Figure 6.25, it is similar to the single polyethylene wall, but with a higher dewpoint in winter, and a lower dewpoint in summer.

These results can also be graphed in terms of relative humidity, which is the critical metric for microbial activity; as shown in Figure 6.43. Again, the polyisocyanurate and roll blanket walls show mostly dry behavior (similar to interior dewpoint), and the double polyethylene wall shows humidity levels increasing to saturation (100%). The remaining walls are scattered between these extremes; the 2" XPS wall shows higher relative humidities, given the slow vapor diffusion through the insulation. The single polyethylene and PA-6 SVR wall show some of the drier behaviors: this is somewhat surprising, given the low permeability of the polyethylene vapor barrier. However, as mentioned earlier, a low permeance material can be bypassed by air leakage, such as the unsealed joint at the top of the wall.

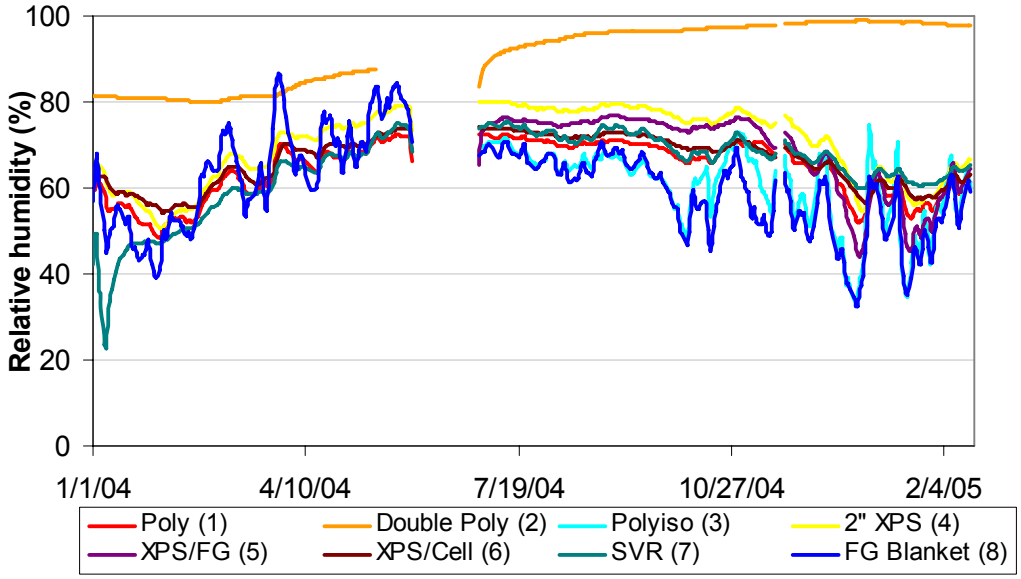

Figure 6.43: Mid-height concrete interface relative humidity for all panels

The humidity of the interface between the concrete and the insulation is determined by the combination of transportation mechanisms acting at that surface. When this interface is well connected to interior air (panels 3 and 8), it can dry to the dewpoint of that air. Therefore, dry interior conditions allow drying of those walls. If the interface has minimal transport to the interior, such as at the double polyethylene wall, moisture accumulates behind the assembly. Walls that fall between these ranges have performance between these extremes.

6.3.8 Seasonal Condensation Risks

In Chapter 3 (Section 3.6), several interior insulation failures modes were discussed that involve condensation of interior moisture on the concrete wall surface. These included condensation at the top of the wall in the winter (i.e., analogous to above-grade wintertime interstitial condensation), and condensation at the bottom of the wall in spring or summer (due to thermal lag effects and rising exterior dewpoints).

A useful comparison is to show the temperatures at the top and bottom portions of the concrete wall with respect to interior and exterior dewpoints (as shown in Figure 6.44), to gauge the risk of condensation. As noted in Figure 6.20, the upper portion of the wall shows more variable temperatures, and the lower portion shows a damped response.

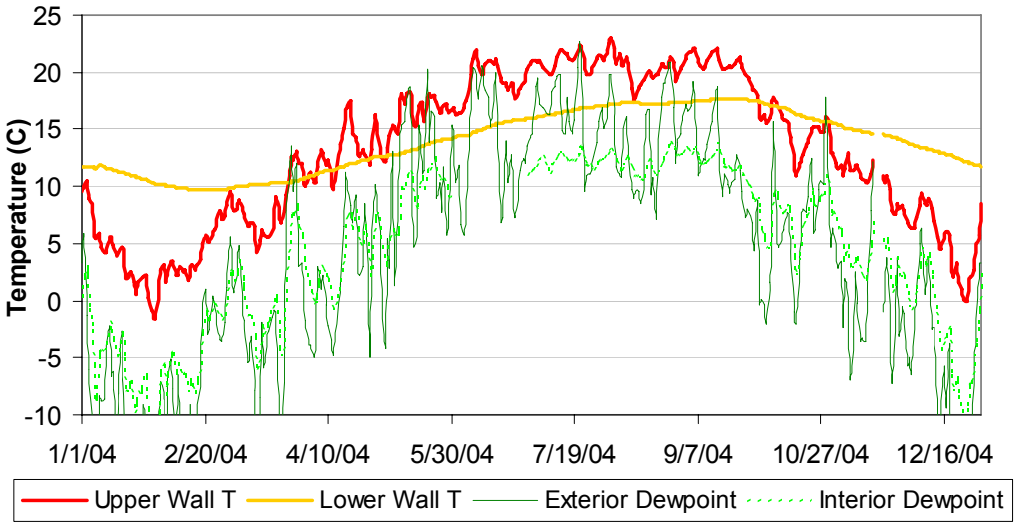

Figure 6.44: Dewpoint comparison to concrete wall surface temperatures (2004)

The plot shows that at the interior dewpoint conditions of the test house, there was no chance of condensation at either top or bottom of the wall (i.e., winter or summer). The low interior dewpoint stays below concrete surface temperatures. However, the exterior dewpoint rises above the lower concrete wall temperature: if the basement were ventilated with exterior air during the summer, condensation could result.

A close-up of three winter months is shown in Figure 6.45, comparing temperatures to higher dewpoint conditions.

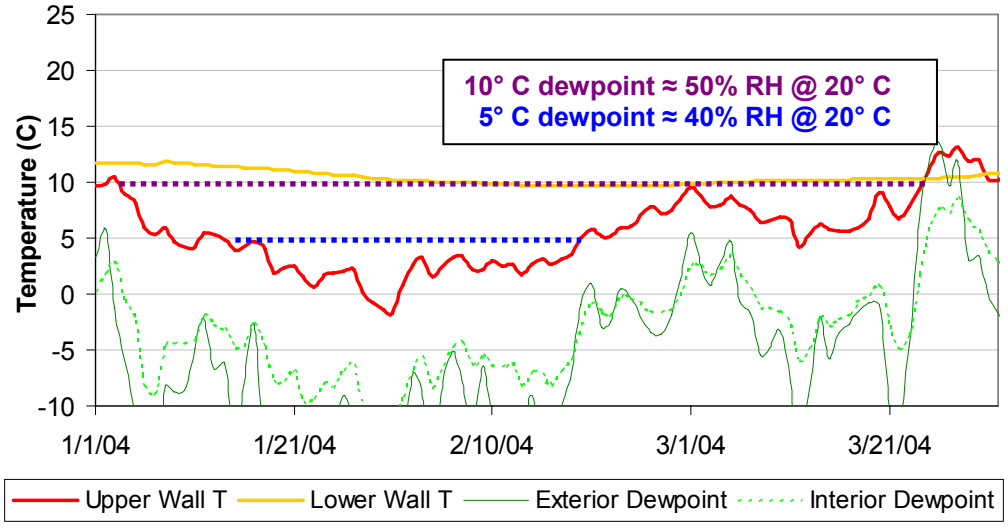

Figure 6.45: Dewpoint comparison to concrete wall surface temperatures (winter detail)

It shows the lack of risk due to the low (-10 to 0° C) dewpoints run in the basement. However, in the Chicago-area houses, interior dewpoints (above grade) were in the 0 to 10° C range; the relative

risk of these conditions is shown by the dotted blue and purple lines. At a dewpoint of 5° C (equivalent to 40% RH at 20°C), there are several weeks of condensation risk; at a 10° C dewpoint (equivalent to 50% RH at 20°C), this rises to almost the entire three-month period. In addition, the severity of the condensation risk can be considered proportional to the "integral" of the difference between interior dewpoint and surface temperature: this captures both the length of time and severity of condensation (horizontal and vertical axes). This shows that the condensation impact of a 10° C dewpoint is several times worse than a 5° C dewpoint.

A four-month detail of summer conditions is shown in Figure 6.46; the upper wall temperature is omitted for clarity.

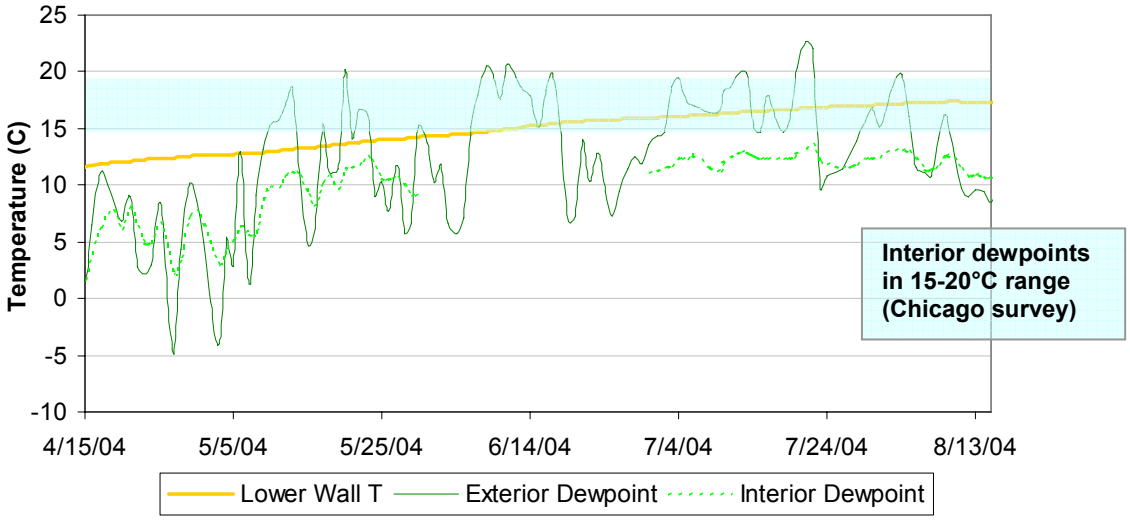

Figure 6.46: Dewpoint comparison to concrete wall surface temperatures (spring/summer detail)

The Chicago area survey houses had summertime dewpoints in the 15-20° C range, reflecting the use of window ventilation to provide cooling. When that range is plotted, it shows that condensation at the lower portion of the wall can result from ventilating the basement with exterior air in late summer.

One discussion point comes back to the issue of the permeability of the insulation assemblies. Several of the driest systems had very high vapor permeability (or effective permeability due to air leakage). The previous plots show that these systems might have problems at higher interior dewpoints.

6.4 Wall Behavior with Wetting System

Four distinct wetting events were triggered in February, April, and September of 2005, and January 2006; they are shown in a graph of temperature and humidity conditions below (Figure 6.47). Two of these wetting events are examined in more detail: the September 2005 wetting, and the January 2006 wetting. They are compared to see if there is any substantial difference between periods of falling

(September 2005) or rising (January 2005) interior and exterior dewpoints and temperatures. The September 2005 wetting was allowed to dry over the course of five months to January; the January wetting was examined out to mid-August. A total of 0.1 gal/400 ml per panel was applied in each wetting.

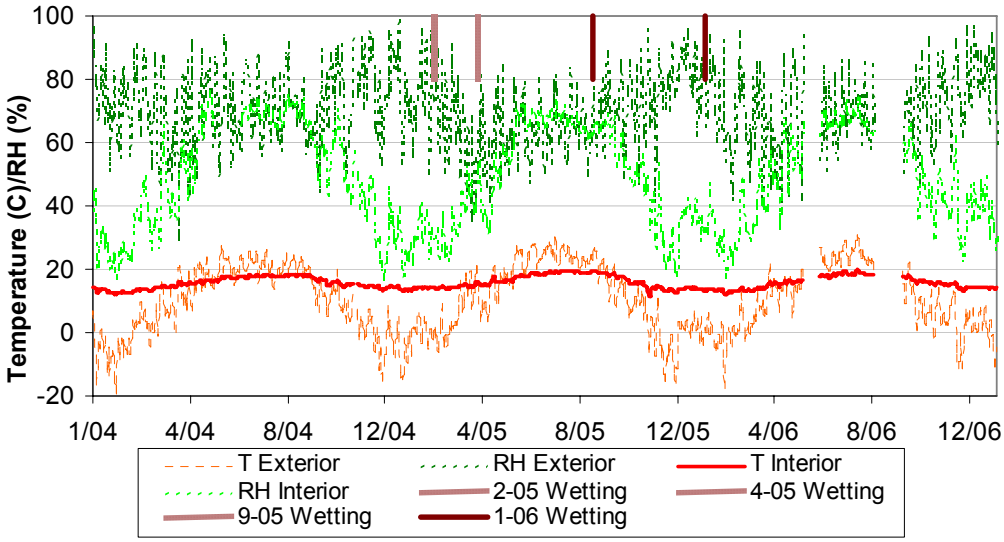

Figure 6.47: Interior and exterior temperature & relative humidity (daily average values)

6.4.1 Interpretation of Wetting Events (Recovery Time)

One difficulty in interpreting these wetting events is deciding what constitutes "dry" or "wet" conditions—i.e., determining when a wall has "recovered" from the wetting event. In the non-wetted year, most walls showed dewpoints consistently above interior conditions, due to the vapor retarding properties of the interior insulation and finish systems, and the moisture sourced from the concrete wall. This fact is demonstrated in a plot of the difference (Δ) between interior dewpoint and the concrete-insulation interface dewpoint for the non-wetted year (2004) in Figure 6.48.

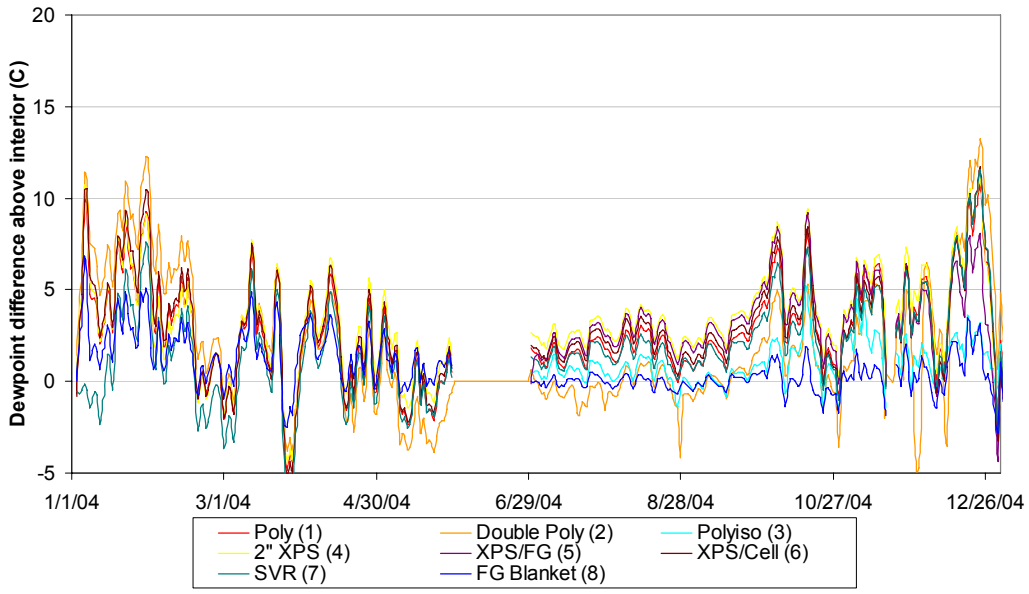

Figure 6.48: Wall to interior Δ dewpoint; non-wetted year (2004), daily average values

A positive value on the graph shows a wall dewpoint above interior (i.e., wetter than interior). In the double poly wall (panel 2), the stud space dewpoint was graphed instead of the concrete-insulation interface. This was done because the wetting event introduced water into the stud space in this wall, not at the concrete layer.

The rise in Δ dewpoint in the fall and winter is due to falling interior dewpoints, which are the result of falling exterior temperatures/dewpoints. The concrete is desorbing stored moisture and coming into equilibrium with the drier interior conditions, but this process is slowed by the impermeable or semi-permeable interior insulation assembly.

In comparison, the dewpoint differences for the year that included a single wetting event (2006) are shown in Figure 6.49. It shows the large spike in dewpoint difference after the wetting event; this difference drops over time. Again, the stud space dewpoint is plotted in the double polyethylene wall.

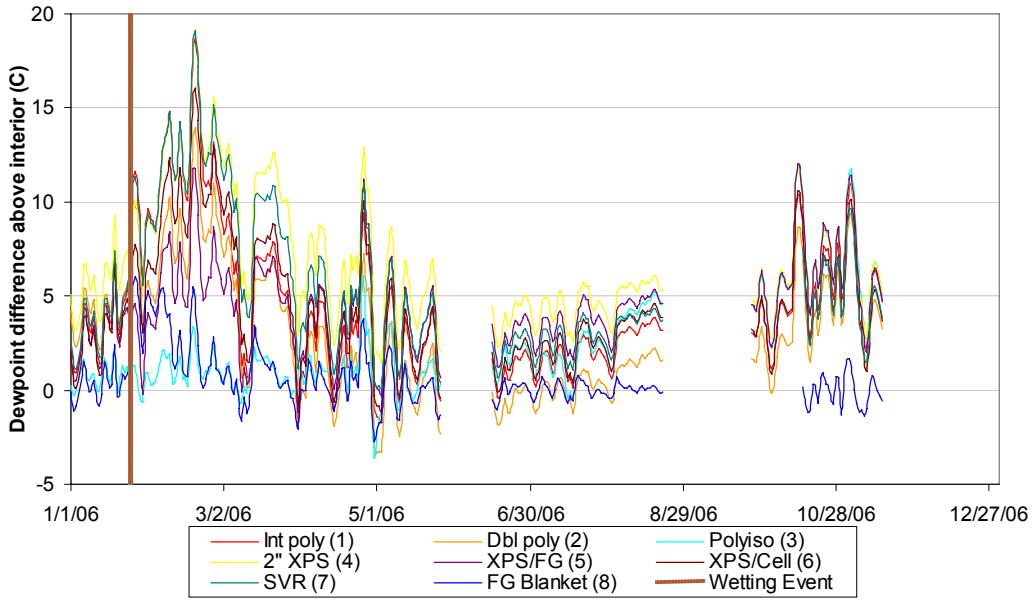

Figure 6.49: Wall to interior Δ dewpoint; wetted year (2006), daily average values

Some walls clearly recover by spring to mid-summer, showing dewpoints close to interior conditions, such as the double polyethylene wall (panel 2), the polyisocyanurate wall (panel 3), and the fiberglass blanket wall (panel 8). Other walls show dewpoints that are arguably above their non-wetted year conditions: approaching or over 5° C, vs. 0-4° C Δ dewpoint. It should be noted, however, that there were three wetting events prior to the January 2006 event. Also, the dewpoint difference spikes at the end of the year (October) are similar to patterns seen in the non-wetted year.

Note that this technique is a rather imperfect metric: for instance, the jump in dewpoint difference in late February reflects the decline of interior dewpoint due to cold outdoor conditions, while the dewpoint remains mostly steady within the walls. This behavior is shown in plots of individual sets of walls during the January wetting event, such as Figure 6.52.

In conclusion, it appears that it is difficult to conclusively declare a wall "dried to original conditions;" therefore, other metrics will be used to analyze the wetting system results. For instance, the performance of similar walls will be compared relative to each other, and behavior with respect to danger thresholds (such as relative humidity) will be examined.

6.4.2 Stud frame walls (Walls 1 and 2)

As mentioned earlier, the wetting system was set up to inject water at the interface of the concrete and insulation (in the single polyethylene wall, panel 1), or within the stud bay (in the double polyethylene wall, panel 2). This was done because historical failures often involve the accumulation of moisture between the two layers of polyethylene; in comparison, wetting at the concrete interface at this wall would simply result in rundown and drainage behind the exterior "moisture barrier" polyethylene (as demonstrated by CMHC 1999).

The results for the September and January wetting events are shown in terms of dewpoint in Figure 6.50 and Figure 6.52; the sensors at the upper and lower stud bay locations are plotted, and interior dewpoint are included for reference.

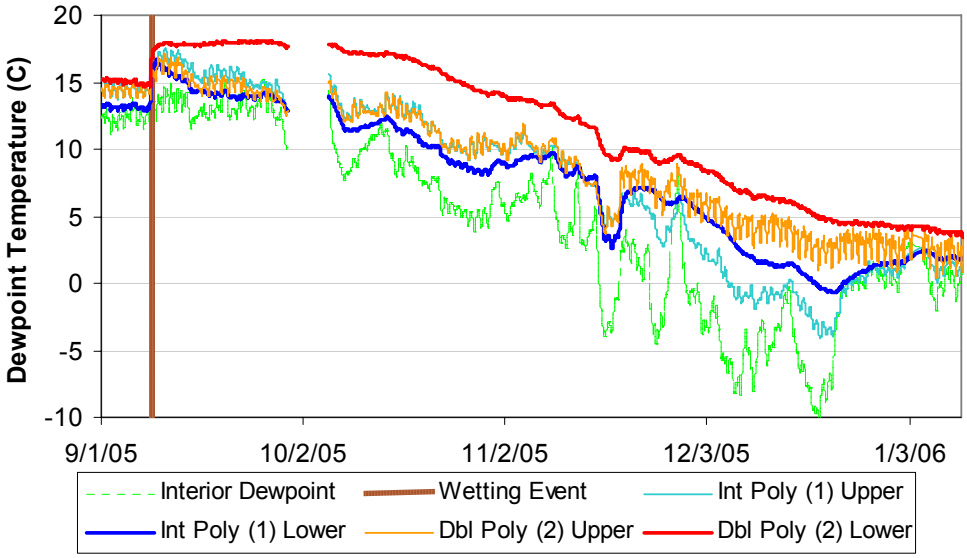

Figure 6.50: September 2005 wetting event dewpoint response, stud frame walls, 130 days

In the September event (Figure 6.50), at the upper level sensors, both walls show a dewpoint spike: the two walls quickly converge to similar levels. Going into the winter, the dewpoint at this upper level sensor rises higher in the double polyethylene walls. This is similar to the non-wetted behavior, and is due to the greater storage and/or permeability to outside available in the bare concrete surface in the single polyethylene wall.

In contrast, the sensors at the lower location show different behavior. The double polyethylene wall has sustained elevated dewpoints, while the single polyethylene wall dries to levels similar to the upper height sensor. This appears to demonstrate the limited drying available in the double polyethylene wall. The reason for this spatial difference is addressed in the disassembly of the walls (section 6.5).

This wetting event is shown in terms of relative humidity in Figure 6.51; only the lower height RH sensors are graphed. The double polyethylene wall has sustained relative humidities in the 90%+ range, while the single polyethylene wall quickly dries down to roughly the 70% level. The behavior of the former puts it at much greater risk of mold growth within the cavity.

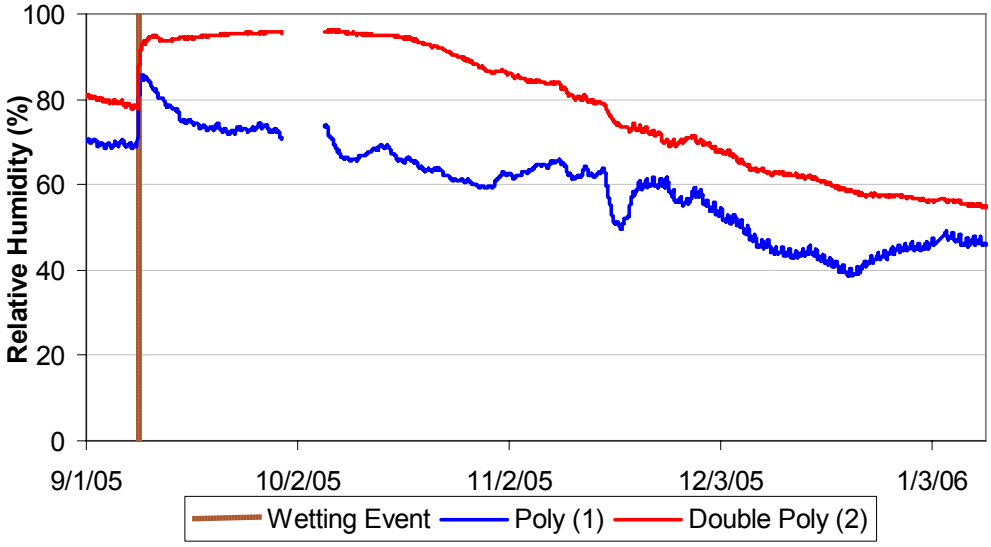

Figure 6.51: September 2005 wetting event relative humidity response, stud frame walls, lower stud bay

The dewpoint results of the January 2006 wetting event are shown in Figure 6.52; note that the timescale is much larger, at roughly 220 days, compared to 130 days in Figure 6.50. This was done to see if there are any longer-term effects.

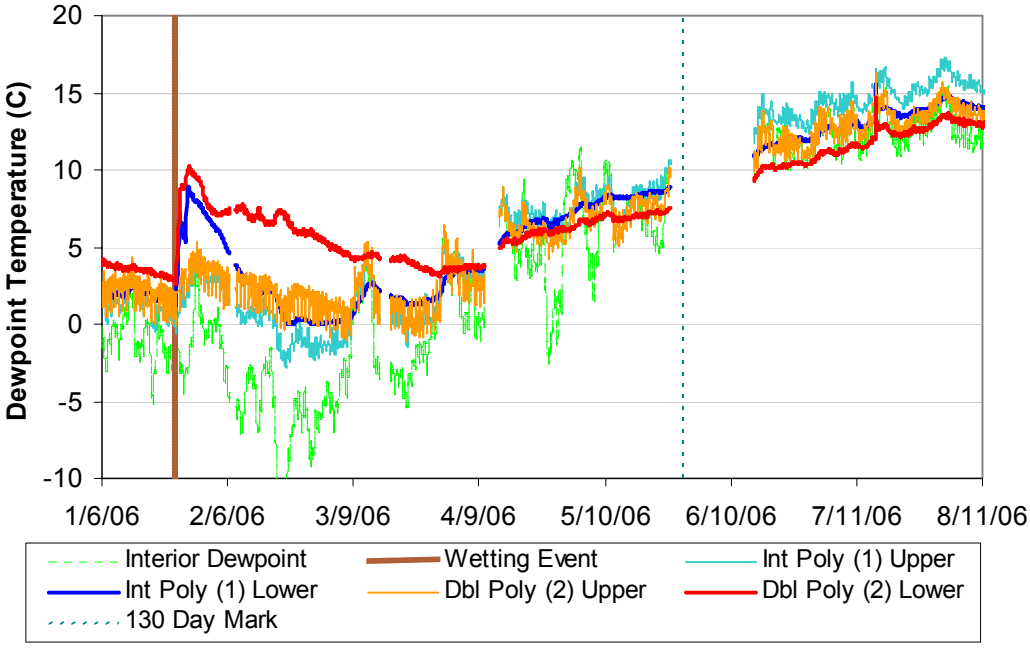

Figure 6.52: January 2006 wetting event dewpoint response, stud frame walls, 220 days

A similar response to the September 2005 event is seen; the upper sensors show quick drying, while at the lower location, the double polyethylene wall dries slower due to lower permeability.

Relative humidities were at less risky levels (compared to Figure 6.51): the single polyethylene wall peaked at 80% RH, and the double polyethylene at 85%; both dropped quickly to safer levels.

By mid to late summer, the behavior patterns are similar to those seen during non-wetted periods: the upper single polyethylene wall shows the highest dewpoints, due to some inward vapor drive. The lower single polyethylene wall shows a higher dewpoint than the lower double polyethylene, possibly due to moisture sourced from and/or stored in the concrete.

However, apparently contradictory data is shown in Figure 6.53: the single polyethylene wall shows sustained higher dewpoints, relative to the double polyethylene wall, and dries slower.

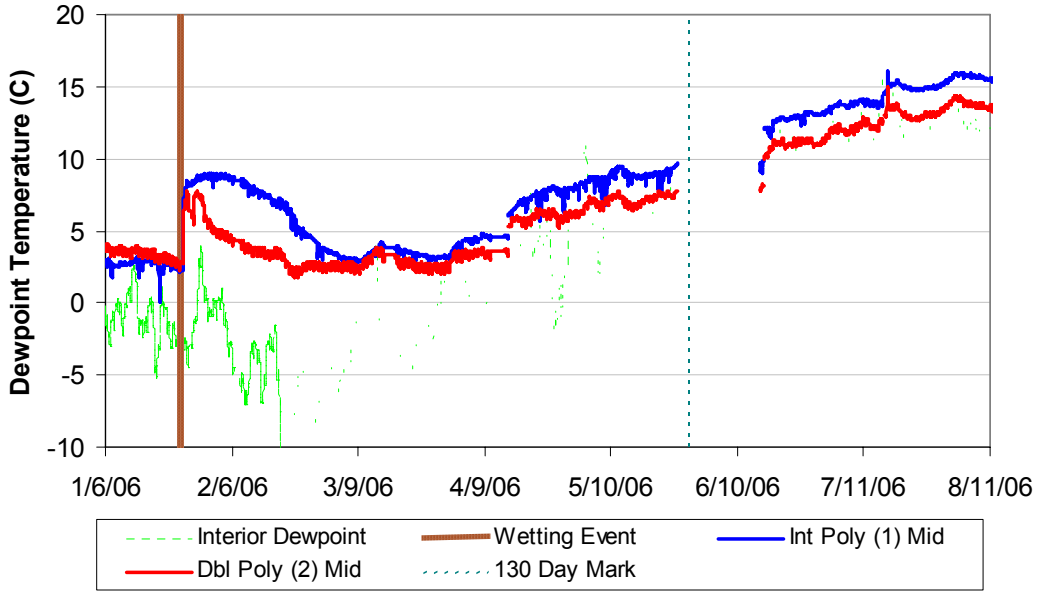

Figure 6.53: January 2006 wetting event dewpoint response, stud frame walls mid-height

This might be explained by the likely wetting behavior of the two walls, as discussed in section 6.5.1. In the single polyethylene wall, water is introduced at the concrete surface, then runs down the interface, and is absorbed by the concrete. This results in a wetting "plume" than runs down the concrete from the injector, and remains wet.

In contrast, in the double polyethylene wall, the water is introduced at the exterior layer of polyethylene, which eliminates the moisture absorption and storage of the concrete. Since the polyethylene has no storage, the water to drains down the surface, with some minimal absorption into the fiberglass batt insulation.

These wetting differences would cause the results shown above: the wetting plume in the single polyethylene wall would dry slowly compared to water quickly draining out of the wall system in the double polyethylene wall. The high dewpoints seen in the double polyethylene wall lower sensor are the result of drainage to the bottom of the cavity, and/or storage in the sill plate, as shown in Figure 6.66 and Figure 6.67. It could be argued that the initial moisture load in these two walls was not as identical as the ideal case.

The wood moisture content measurements did not show a noticeable response to any of these wetting events, and are not presented.

6.4.3 Plastic foam-based walls (Walls 3, 4, 5, and 6)

The dewpoints of the plastic-foam based walls (3/polyisocyanurate; 4/2" XPS; 5/1" XPS + fiberglass; 6/1" XPS + cellulose) are shown for the September 2005 (Figure 6.54) and January 2006 (Figure 6.55) wetting events. In all cases, the dewpoint at the concrete-insulation interface at mid-height was measured; the second graph has a longer timescale (220 days vs. 130 days).

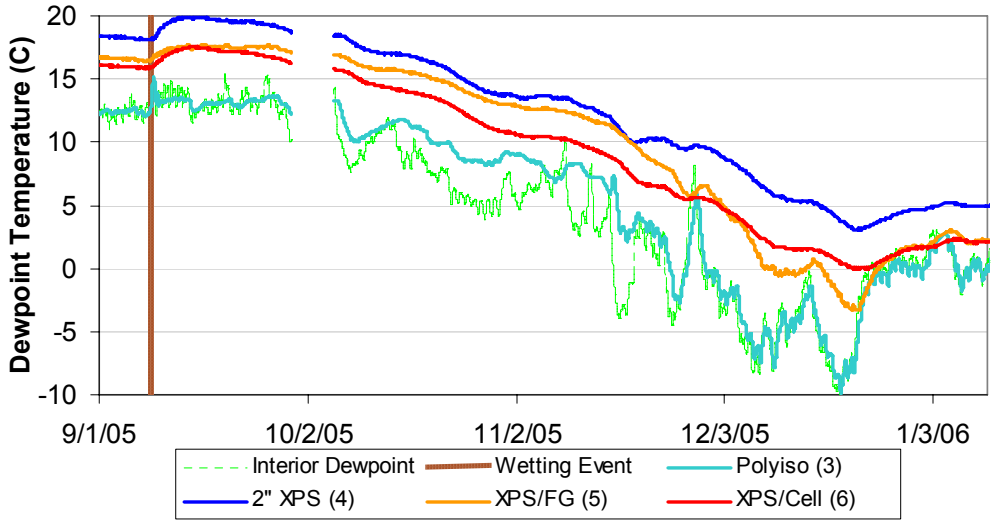

Figure 6.54: September 2005 wetting event dewpoint response, foam-based walls

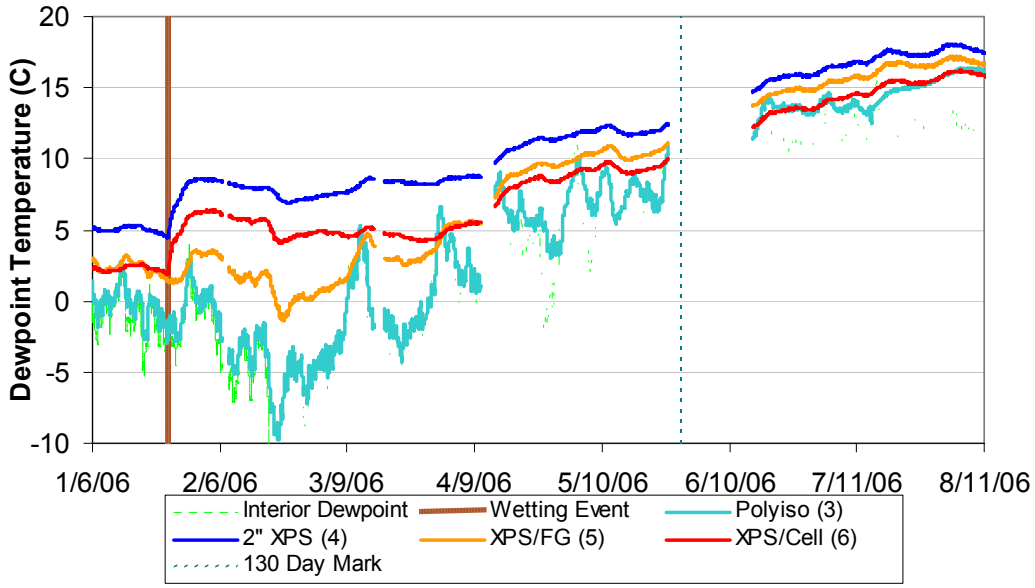

Figure 6.55: January 2006 wetting event dewpoint response, foam-based walls

In both cases, the polyisocyanurate wall showed a small dewpoint spike and stayed close to the interior dewpoint, due to the air leakage to the cavity behind the insulation, as mentioned in section 6.3.4. The behavior is likely due to a combination of drainage of bulk water and ventilation drying. Water staining at the floor slab was observed at the center of the wall (wetting system location), indicating water running out of the system. Like the double polyethylene wall, it appears that the initial moisture dosing between walls is not identical. Ventilation drying has been shown to occur in gaps as small as 1 mm (Smegal 2006), so drying at this gap of 3-9 mm seems likely.

The extruded polystyrene (XPS) walls (4, 5, and 6) show a gradual rise in dewpoint after the wetting event (showing absorption and/or distribution at the concrete), followed by a drop over time relative to interior conditions. The 2" XPS wall (panel 4) shows the greatest rise, and the slowest drying, as would be expected from "dry year" results. The two 1" XPS walls (panels 5 and 6) both show patterns similar to the 2" XPS, but with quicker drying, due to the higher permeability of 1" XPS (63 ng/Pa·s·m^2, or 1.1 Imperial perm, vs. 31 ng/Pa·s·m^2, or 0.6 Imperial perm).

The two 1" XPS walls were originally expected to show similar (if not identical) responses, given that the most permeable layer is the same. However, they show differing responses, and they also show inconsistent relative behavior in the two wetting events. In the September event, the cellulose wall dries faster, while the opposite is true in the January event. This is likely a function of the construction details of the panels; the installation of the XPS was different in the two walls due to construction sequencing issues. The difference in the wetting response is discussed in section 6.5.

The results of these two wetting events are also graphed in terms of relative humidity in Figure 6.56 and Figure 6.57, to gauge the relative risks of microbial growth.

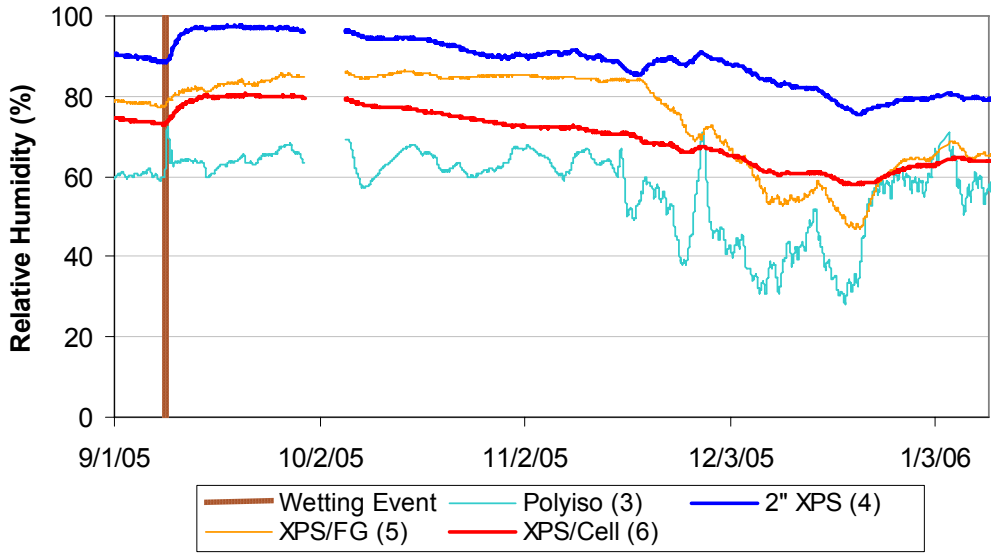

Figure 6.56: September 2005 wetting event relative humidity response, foam-based walls

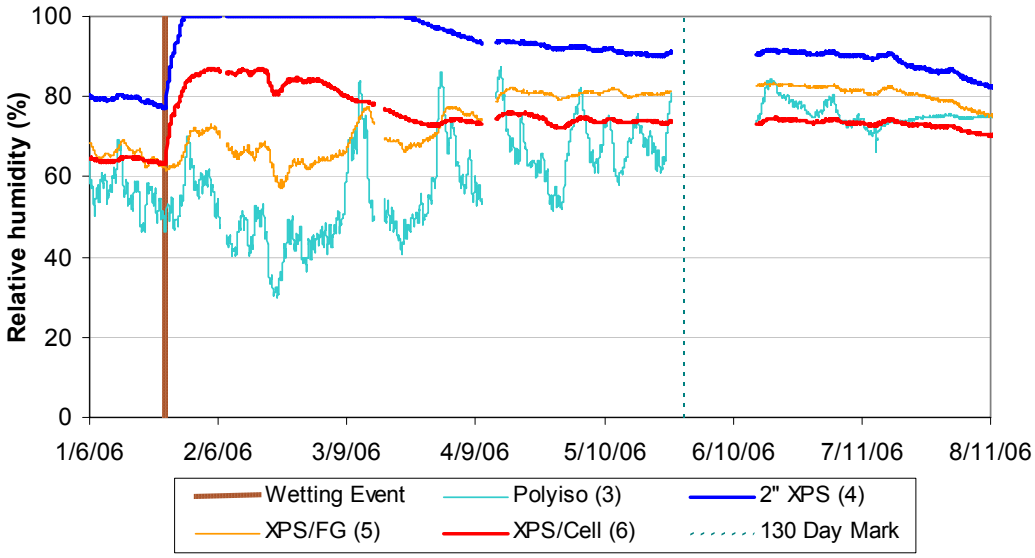

Figure 6.57: January 2006 wetting event relative humidity response, foam-based walls

Like the dewpoint response, the 2" XPS wall shows the highest relative humidity levels, and the longest sustained levels over 90-100% RH. In comparison, the other walls experience only moderate (if any) amounts of time over 80% RH.

There is a clear difference between the two wetting events: the January 2006 event stays at 100% RH for roughly 50 days in February and March, while in the September 2005 event, values peaked at 98% and then declined to roughly 90% RH in the same amount of time. The results can be explained by temperature conditions at this interface: the temperature and humidity conditions during these two events are represented on a psychrometric chart in Figure 6.58. Conditions are graphed for the 425

hour (18 day) periods after peak relative humidities are reached: September 12-29, 2005 and March 18-April 4, 2006.

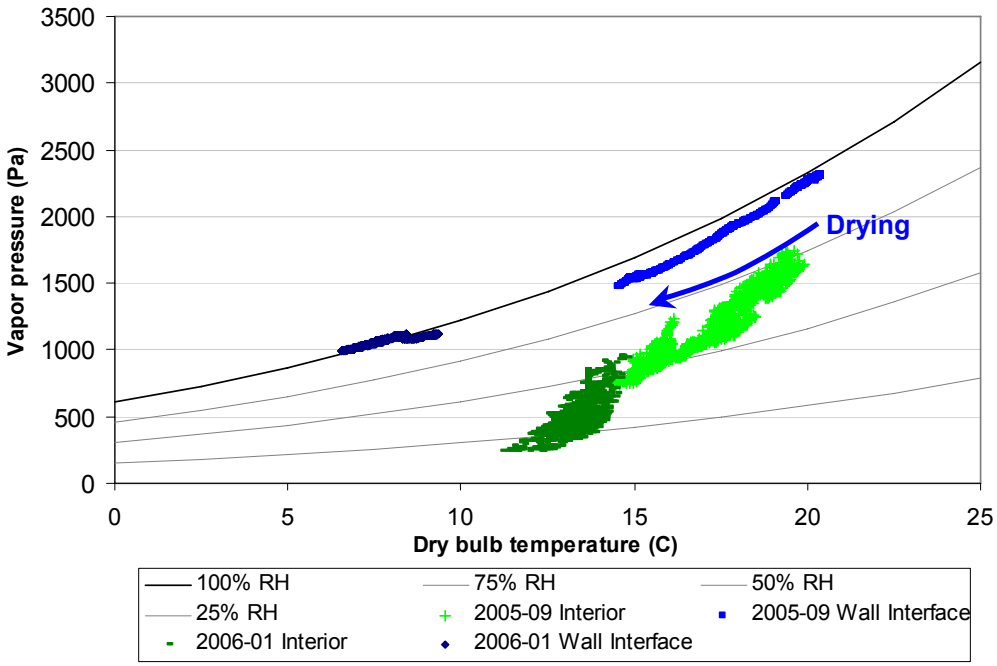

Figure 6.58: Psychrometric comparison of September 2005 and January 2006 wetting events for 2" XPS wall

In the September 2005 wetting event, conditions start at roughly 98% RH and 20° C; the temperature drops through September. Simultaneously, the dewpoint and relative humidity drop, as indicated by the curved arrow. Interior conditions are dryer than the wall; drying is also available to the outside (dewpoints in the 10-20° C range; not graphed).

In contrast, the January 2006 wetting event occurs in winter: even at the earth-sheltered mid-height sensor, temperatures are much colder (7-9° C). As a result, less drying energy is available, and drying occurs very slowly. This happens even though the interior conditions are drier than the saturated cold wall, and exterior dewpoints are below interior (-10 to 10° C, not graphed). It should be noted that at these conditions, mold growth would be somewhat inhibited by the low temperature range.

In light of these results, one further point should be noted on the installation of the 2" XPS wall. The regular schedule of fasteners through the furring strips results in a relatively "tight" interface with little or no air gap at the concrete. This construction minimizes drainage and ventilation drying, and maximizes the storage of injected water.

In addition to the conditions at the interface between the concrete and the insulation system, the relative humidity and wood moisture content conditions in the stud bays of panels 5 and 6 (XPS with fiberglass or cellulose) were examined. No response to either wetting event was evident; instead, stud bay dewpoints remained similar to interior conditions. This demonstrates that the semi-permeable

XPS board protects the vulnerable wood framing and insulation from moisture introduced at the concrete.

6.4.4 Other walls (Walls 7 and 8)

The behavior of the final set of walls, the PA-6 ("smart vapor retarder") wall (panel 7) and perforated facer roll blanket (panel 8) is shown for the September wetting event in Figure 6.59. The January 2006 event is not plotted, given that behavior was quite similar.

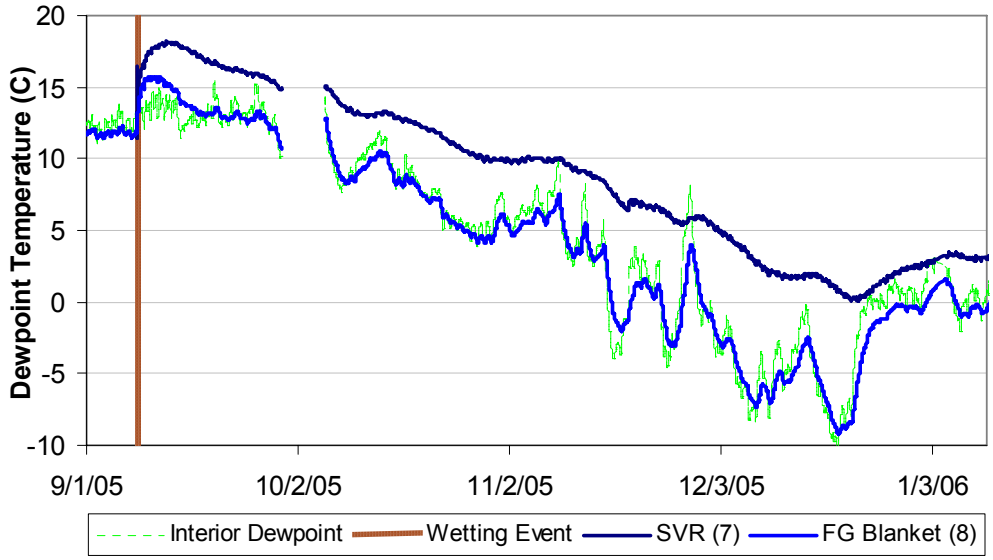

Figure 6.59: September 2005 wetting event dewpoint response, other walls

In the roll blanket wall, there is a small rise in dewpoint, followed by quick drying to interior dewpoint conditions. As discussed in section 6.3.6, this might be ascribed to either air leakage, the high permeability of the facer material, or both.

In contrast, in the PA-6 (SVR) wall, there is a larger rise in dewpoint, and levels remain above interior conditions for extended periods, similar to the behavior of the XPS walls. This effect is shown in terms of relative humidity for the January 2006 wetting event (see Figure 6.60); like the 2" XPS wall (panel 4), relative humidity levels stay at 100% for an extended period of time.

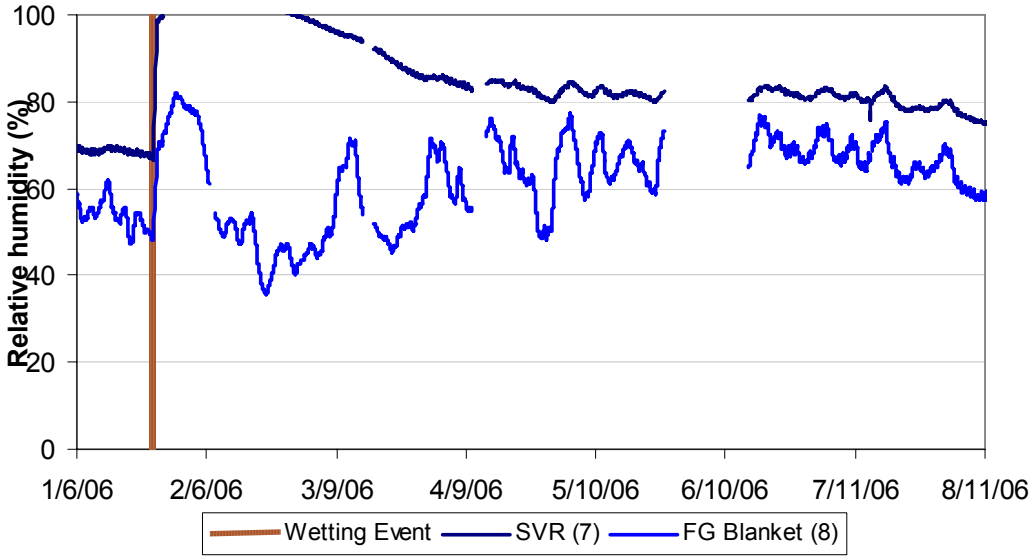

Figure 6.60: January 2006 wetting event relative humidity response, other walls

In contrast, during the September 2005 wetting, the humidity peaked at 90% and quickly fell (similar to the 2" XPS wall); this again indicates the slow drying that occurs during the winter. However, it was surprising that the PA-6 wall showed drying rates similar to the panel 4, given the difference in permeance values. A 2" thickness of extruded polystyrene has a permeance of 31 ng/Pa·s·m^2, or 0.6 Imperial perms, while the PA-6 material with the perforated facer should have permeance in the range of 450-650 ng/Pa·s·m^2, or 8-11 Imperial perms (assuming RH levels of 75-85% at the facer). Once again, this might be a function of how water was distributed within the wall from the injection nozzle (drainage and storage in the concrete). In addition, the lateral seals at this wall were vapor and air tight for the length of the experiment (sealed to the polyisocyanurate buffers).

6.4.5 Overall Interpretation of Wetting Events

The overall performance of the walls with and without the wetting system can be seen in dewpoint plot in Figure 6.61. Comparing the wetted and non-wetted performance on a large timescale, it appears that these wetting events had little effect on the overall seasonal patterns. As a reference point, it should be remembered that the fiberglass roll blanket (panel 8) had a dewpoint almost identical to interior. These were wetting events of 0.1 gal/400 ml per panel; an actual bulk water leak would probably cause repeated wetting on a more regular basis than these planned wetting events.

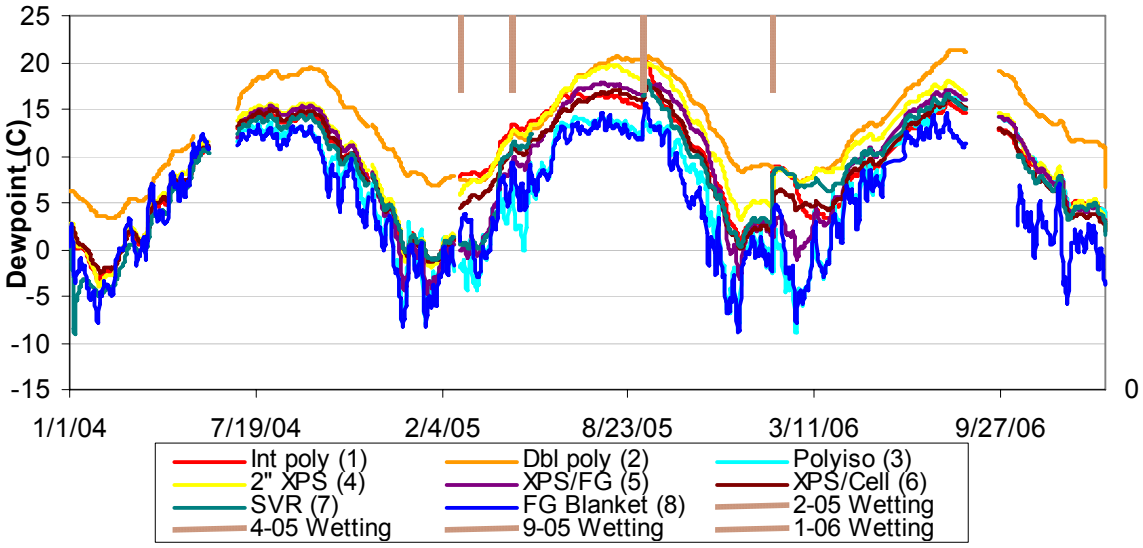

Figure 6.61: Concrete-insulation mid-height dewpoint; full length of experiment; all walls

In the initial design of this experiment, the performance of the interior insulation systems was expected to be dominated by the permeance of the assembly. However, the non-wetted year demonstrated that the in-service behavior combines effects of the assembly as a whole, including construction detailing and the effects of air bypass (as also seen in Zuluaga et al. 2004). The wetting events showed yet another complicating factor when comparing these walls: bulk water flow out of the systems varied between walls, causing differences in the net amount of water introduced to each panel. In addition, the location of the wetting plume relative to the sensors might had an effect on results, as covered in section 6.5. Therefore, the observed drying behavior reflects both the retained moisture from the wetting event and the drying ability of the insulation assembly.

This non-uniform moisture dosing was also seen in work by CMHC (1999): in their research, there were some walls with almost identical construction that had strongly different wood moisture content responses to a controlled wetting event. It seems likely that similar issues, such as uneven rundown, might have caused these results. This suggests that future basement wall wetting research should use an apparatus designed to wet walls evenly and avoid water rundown, as described by Van Straaten (2003).

Overall vapor permeability of the assembly did play a role in the relative drying of some of these panels. For instance, the 2" XPS wall (panel 4) dried much more slowly and had higher sustained relative humidity levels, compared to the 1" XPS walls (panels 5 and 6). In addition, the double polyethylene wall appeared to show slow drying relative to the single polyethylene wall, given the interpretation provided in section 6.4.2. However, an assembly that was expected to allow substantial drying in service (the PA-6/rigid fiberglass wall, panel 7) showed a response similar to a wall with low permeability (2" XPS, panel 4); the reason for this behavior is unclear.

Understanding the drying behavior of the walls is vital to predicting the likelihood of moisture-related damage in interior insulation systems. For instance, a system that quickly releases its moisture by drainage is unlikely to suffer damage in itself, but in a finished basement with moisture-sensitive

materials, it would raise the risk of damage to those materials. A system that retains moisture for long periods would protect interior finishes, but results in layers of the assembly remaining at a high humidity. This is of great importance if that layer contains moisture-sensitive materials, such as a wood framing. It is of lower importance—but not negligible—if those layers are not moisture sensitive, such as concrete or polystyrene insulation. Although those materials are not mold-sensitive in themselves, microbial growth can occur on surface dust at the interface, given sufficient moisture, temperature, and time.

Sustained high relative humidity levels were seen in the January 2006 wetting event, in the 2" XPS wall and the PA-6 wall (panels 4 and 7), demonstrating the seasonal effects of drying potential. Moderately elevated humidity levels were seen in the 1" XPS walls. The double polyethylene wall also showed sustained high humidity levels at the lower sensor location, especially at the September 2005 wetting event.

6.5 Wall Disassembly and Inspection

During the field visit on July 14-15, 2006, the stud frame walls were partially disassembled, in order to change sensor configurations and to examine the condition of the moisture-sensitive components of the walls (wood studs and insulation). This inspection was done roughly six months after the last wetting event, so no residual moisture was observed.

During the decommissioning of the experiment on January 18-19, 2007, all walls were disassembled and inspected. The wetting system was run immediately prior to disassembly, to demonstrate and visualize the wetting pattern in the wall.

This section combines results from both field inspections, broken down by wall type.

6.5.1 Single Polyethylene (Panel 1) and Double Polyethylene (Panel 2)

The observations during the second trip made the wetting difference between these two walls very clear. In the single polyethylene wall, a wetting "plume" ran below the nozzle on the concrete wall. As it ran down the wall, it shifted out of plumb, due to concrete surface features, and split into multiple streams (see Figure 6.62). The path of the wetting ran directly behind the temperature/relative humidity sensor at the concrete-insulation interface. This would result in a disproportionately strong and lengthy response to wetting events from this RH sensor. Running the system at roughly the interval used in previous wetting events, the water was absorbed by the concrete surface before it hit the sill plate (Figure 6.63). Little water was observed trapped by surface tension in the fiberglass batt.

The wall was disassembled and examined for evidence of moisture damage in the framing and fiberglass. No mold growth or damage was noted: it was limited to brown staining on the interior face of the fiberglass (discussed in section 6.5.5).

Figure 6.62: Upper portion of wetting plume in single polyethylene wall (panel 1)

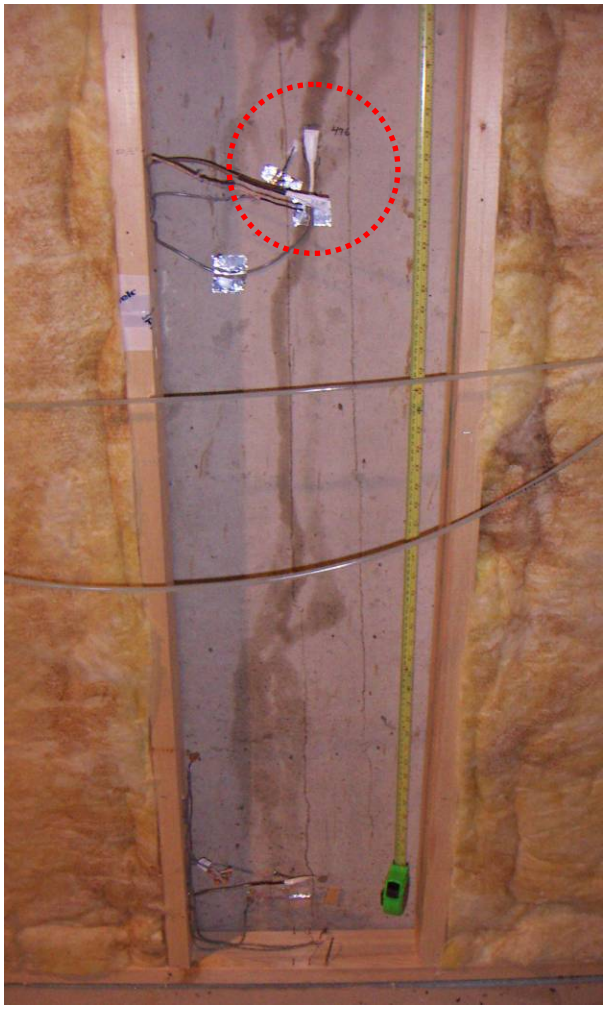

Figure 6.63: Lower portion of wetting plume in single polyethylene wall (panel 1)

In contrast, in the double polyethylene wall, the wetting system introduced water at the interface between the outer "moisture barrier" polyethylene and the fiberglass batt; it was not in contact with the concrete. The water quickly ran down this interface, along the hydrophobic polyethylene, with negligible accumulation, as seen in Figure 6.64. There was water retained in the fiberglass batt, as seen in Figure 6.65.

The water ran to the sill plate, and accumulated mostly at its underside, where it was trapped by the polyethylene. The upper surface of the plate only had minor discoloration, but the underside (especially the exterior edge) had very high moisture contents, and some mold growth.

Based on water staining patterns around the base of the wall, it appears that water ran out the corners of the polyethylene, and pooled on the floor. This pattern was not seen at the single polyethylene wall.

Figure 6.64: Water beads on polyethylene at double polyethylene wall (panel 2)

Figure 6.65: Water beading at fiberglass batt in double polyethylene wall (panel 2)

Figure 6.66: Sill plate of double polyethylene wall (panel 2)

Figure 6.67: Close up of double polyethylene sill plate

The conditions behind the polyethylene in panel 2 were close to 100% RH for most of the experiment; however, no mold growth was seen at this interface. Dirt/dust and insect bodies had collected at this cavity, but no odors or problems were noted.

Moisture contents were measured with a handheld Delmhorst meter in both walls in the July 2006 trip (uncorrected values stated here). In the single polyethylene wall, all moisture contents were in the 9-10% range, except for the upper face of the sill plate, which was 12-13%.

In the double polyethylene wall, the studs and top plate were at 9-10%; the upper face of the sill plate was in the 10-12% range (12% towards the center). Both of these results are basically consistent with the logger MC measurements (9% typical for panel 1, 9-11% for panel 2). However, as mentioned above, the underside of the sill plate had a very high moisture content (off scale high; over 30% MC), due to the recent wetting event.

6.5.2 Foil-faced Polyisocyanurate (Panel 3)

Figure 6.68: Wetting plume in foil-faced polyisocyanurate wall

The foil-faced polyisocyanurate wall showed very limited wetting responses; this was ascribed to bulk water drainage and ventilation drying in the cavity at the concrete-insulation interface.

The wetting pattern is a reasonable match to this behavior: the wetting plume contacts a concrete form seam, and immediately runs straight down, draining out of the wall. Again, a small surface feature plays a dominant role in the shape of the wetting pattern.

In previous visits, evidence of water pooling was seen at the base of this wall.

6.5.3 XPS (2”/50 mm) (Panel 4)

Figure 6.69: Wetting plume in 2” XPS wall

This wall showed extended periods at high relative humidity, especially after the wintertime wetting event. The panel was installed “tight” against the concrete, with concrete screws at a regular fastening schedule. Therefore, it was believed that water was “sandwiched” at this interface, instead of draining out of the system.

The wetting pattern is shown at the left; the wetting plume ran straight down until it hit the instrumentation wires, and then ran laterally out of the panel. This would result in a fairly large concentration of wetting near the relative humidity sensor. However, the wetting plume did not directly impinge on the sensor, as in the single polyethylene wall.

No actual mold growth was in evidence at this interface; however, dust and dirt that had collected behind the panel was “mud-like” after the wetting. The tightness of the installation is reflected by the wire “tracks” seen on the exterior side of the insulation (Figure 6.70).

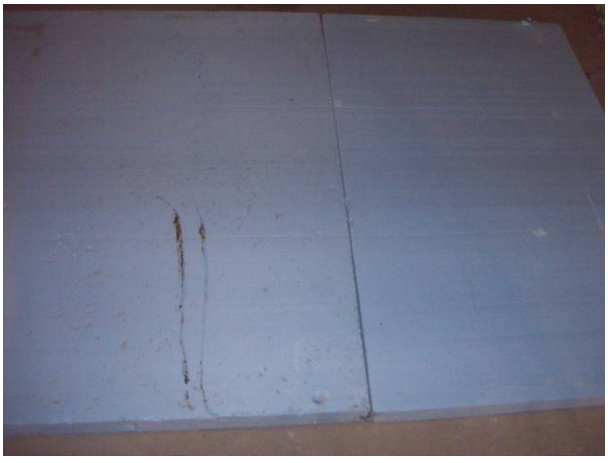

Figure 6.70: Concrete interface side of

Figure 6.71: Craters or burrows on exterior

insulation, showing wire tracks **face of XPS insulation (upper panel only)**

The exterior side of the insulation also revealed craters that appeared to be burrowed or chewed by insects or other pests (Figure 6.71). They were only seen on the upper panel. A large number of dead "pill bugs" (*Armadillidium vulgare*) were seen in most of the assemblies. These creatures are limited to damp environments: the observed damage corresponds to the wetting pattern (only seen in upper panel; wetting plume leaves the wall before hitting the lower panel).

6.5.4 XPS w. fiberglass (Panel 5) and XPS w. Cellulose (Panel 6)

These two walls had close to identical specifications, yet showed different responses to wetting events. In the September 2005 wetting, the walls had a similar initial response, but the XPS-cellulose wall dried faster. In the January 2006 wetting, the cellulose wall showed a larger initial jump in dewpoint, and took longer to recover than the fiberglass wall.

The wetting patterns provide some insight into the response, but do not completely answer questions.

Figure 6.72: Wetting plume in 1" XPS + fiberglass (left) and XPS + cellulose (right) walls

Neither wetting plume hits the T/RH sensor at the concrete/insulation interface. In the XPS-fiberglass wall, the wetting pattern follows a surface crack in the concrete, sending a portion of the water away from the centerline, to the right. Also, arguably, the crack provides additional surface area for water absorption. In contrast, the XPS-cellulose wetting plume runs straight down, and appears to drain out of the wall more easily. This could be ascribed to the installation of the XPS; in the fiberglass wall, the foam was tightly "wedged" against the concrete before stud bay insulation. In the cellulose wall, this gap was left loose.

No mold growth was observed at the concrete-XPS interface. The "burrowing" (possible insect/pillbug activity) seen in the 2" XPS wall was not observed in panels 5 and 6.

6.5.5 Rigid fiberglass with PA-6 (Panel 7)

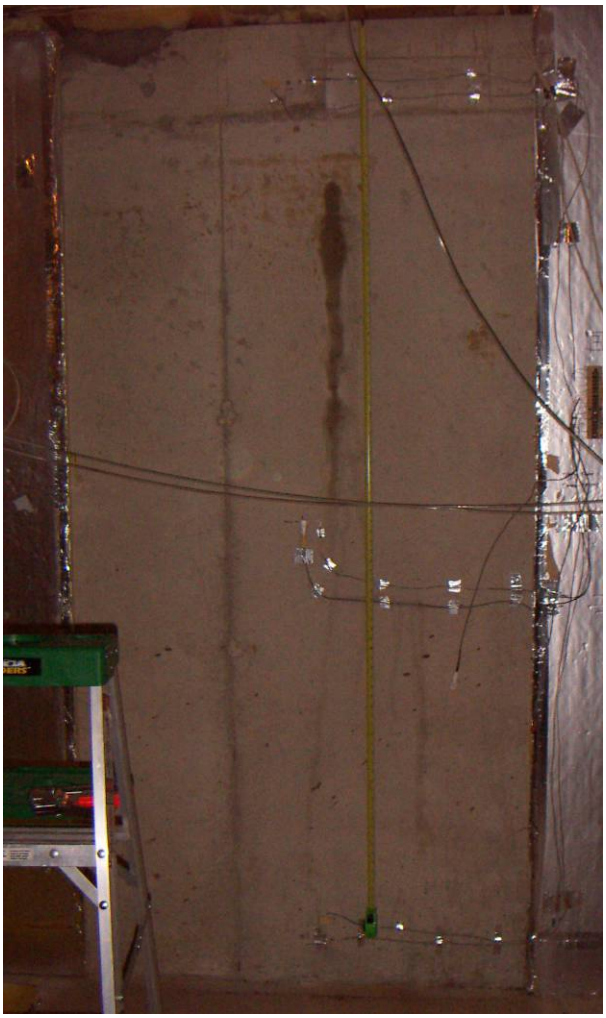

Figure 6.73: Wetting plume in rigid fiberglass/PA-6 wall

The rigid fiberglass/PA-6 wall had a very strong response to wetting events, with a large initial moisture spike, and slow drying (equivalent to the 2”/50 mm XPS wall).

The wetting pattern does not provide exceptional insight, except for the fact that it runs straight down (but misses the T/RH sensor). The lack of drainage or lateral movement out of the panel suggests that the moisture was fully absorbed by the concrete at each wetting event, providing a long-lasting moisture source.

There was minimal staining of the exterior side of the rigid fiberglass, as seen in Figure 6.80; no mold growth was observed, despite sustained high humidity levels.

6.5.6 Perforated Roll Blanket (Panel 8)

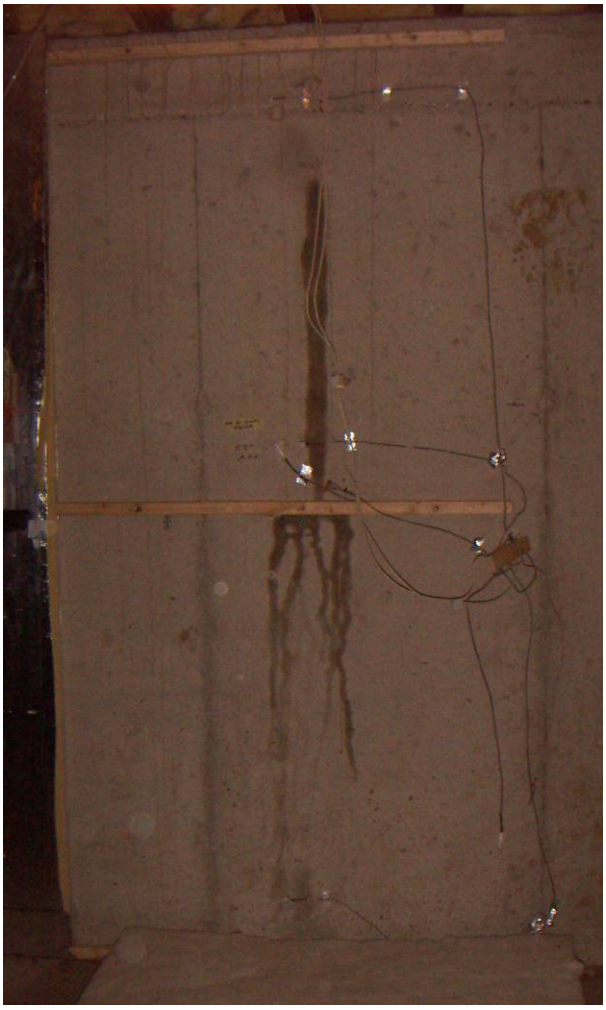

Figure 6.74: Wetting plume in perforated roll blanket wall

This wall was characterized by a very quick recovery from wetting events, with wall cavity dewpoints almost identical to interior conditions.

The wetting plume ran straight down from the injector until hitting the horizontal 2x2 furring at mid-height (below the T/RH sensor). At that point, the water ran behind the furring, and split into multiple rivulets.

No damage or mold growth was noted in the fiberglass insulation, or on the wood furring.

6.5.7 Fiberglass Brown Staining

The progress of the brown staining of the fiberglass batt walls was photographed over time; the initial installation condition is seen in Figure 6.75, and some small stains were noted in June 2004, prior to the installation of the wetting system (Figure 6.76).

By the time of wall disassembly in July 2006, brown staining on the interior side of the fiberglass was pronounced, as seen in Figure 6.77 (single polyethylene), Figure 6.78 (double polyethylene), and Figure 6.79 (XPS and fiberglass). This staining was mostly seen on the interior face; a similar stain was seen on the exterior face in one bay of the XPS-fiberglass wall.

The pattern is arguably the worst in the double polyethylene wall, with visible staining in all stud bays. However, if this is a moisture-related phenomenon, it is surprising that it was seen in the XPS-fiberglass wall, given the low stud bay dewpoints and lack of condensing conditions. On the other hand, the correspondence between the brown staining and the wetting system location in panel 5 suggests a relationship. The possibility of some air-transport phenomenon has not been conclusively dismissed. The chemistry of this staining is unknown; it is likely a water-based reaction with the organic binders used in the fiberglass batts.

In the PA-6/rigid fiberglass wall, no similar brown staining was noted at the fiberglass surface in contact with the concrete (Figure 6.80). No brown staining was observed in the white roll blanket fiberglass. This could be a function of either moisture exposure, or different binder chemistry between the materials.

Figure 6.75: Initial condition of interior of fiberglass (panels 1 and 2), September 2003

Figure 6.76: Small brown stains in June 2004; double polyethylene wall (panel 2)

Figure 6.77: Brown stains on interior of fiberglass (panel 1), July 2006

Figure 6.78: Brown stains on interior of fiberglass (panel 2), July 2006

Figure 6.79: Brown stains in XPS/FG (panel 5), July 2006

Figure 6.80: Concrete interface of rigid fiberglass in PA-6 wall (panel 7)

Chapter 7

Results: Kitchener Site

In this chapter, the data from the Kitchener site is covered and analyzed in four sections: the interior and exterior boundary conditions, the data from the soil sensors, the monitored behavior of the walls, and observations made during a field visit, which can be correlated to the monitored data.

7.1 Interior and Exterior Boundary Conditions

Indoor and outdoor temperature and humidity conditions are shown in Figure 7.1 for seventeen months of monitoring, from September 2005 through January 2007. Basement interior temperatures held very steady, both winter and summer, averaging 19° C. These conditions fall within the range of the Chicago-area nine-house survey.

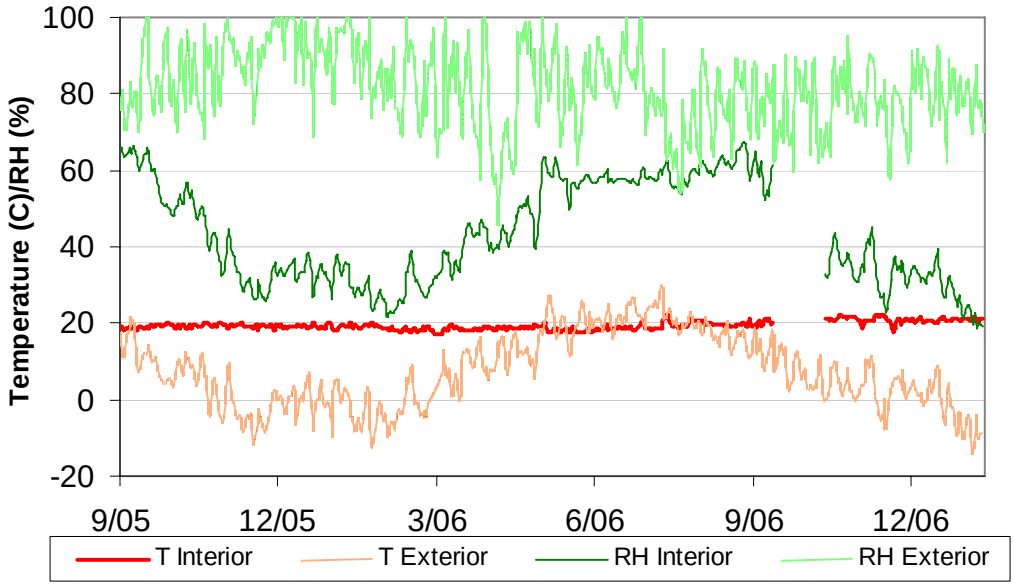

Figure 7.1: Interior and exterior temperature & relative humidity (daily average values)

Wintertime humidities were in the 20-40% RH range, and summertime in the 55-65% RH range. The interior moisture conditions are plotted in terms of dewpoint temperature in Figure 7.2. As in previous research, interior dewpoint follows the pattern of exterior dewpoint, but is lower than exterior in summer (reflecting the dehumidification of the air conditioning system), and higher than exterior in winter (reflecting interior generation, airtightness, and desorption from interior finishes and materials).

Wintertime dewpoints were in the –5 to 5° C range, which matches the range measured by Ruest (1993), and is drier than the Chicago survey (0-10° C). This is likely a function of the colder Canadian climate. Summertime dewpoints were in the 10-15° C range, which is drier than the Chicago survey data (15-20° C range, due to ventilation cooling).

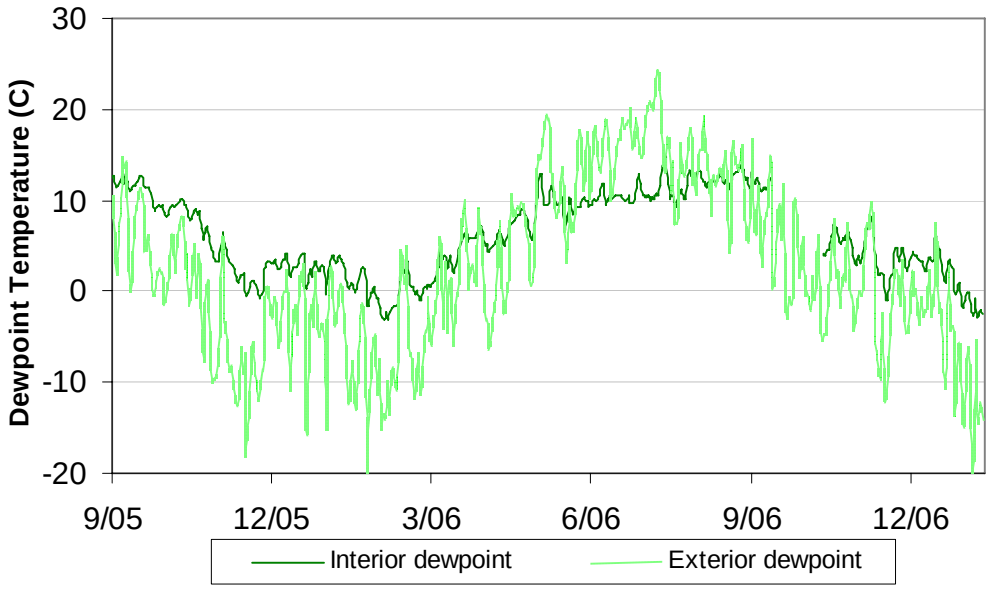

Figure 7.2: Interior and exterior dewpoint conditions at Huntley site (daily average values)

7.2 Soil Sensors

Soil boundary condition measurements included temperature, soil matric potential (water content), and moisture content using wood "plug" moisture content sensors (see Appendix B: Development and Calibration of Wood Surrogate Sensors). Sensors were placed at two vertical "stacks" at three depths (6"/150 mm, 12"/300 mm, and 36"/900 mm), for a total of six measurement locations. Vertical stacks were located in front of the "front" and "rear" sets of test panels, and are identified as such.

7.2.1 Soil Temperature Behavior

Daily average soil temperatures are plotted with exterior temperature in Figure 7.3. Similar patterns to the Huntley data are seen: the deepest measurements are more damped and have a smaller amplitude; and even at a depth of 150 mm/6", soil temperatures do not drop below freezing, despite sustained periods below 0° C. Diurnal variations were completely damped out at a depth of just 6"/150 mm in the wintertime. In the summer, daily amplitudes were 1-2° C at that depth. The front measurements were consistently warmer than the rear measurements (likely due to differential solar exposure due to shading by the adjacent building), but measurements at a given depth were typically within less than 1° C of each other.

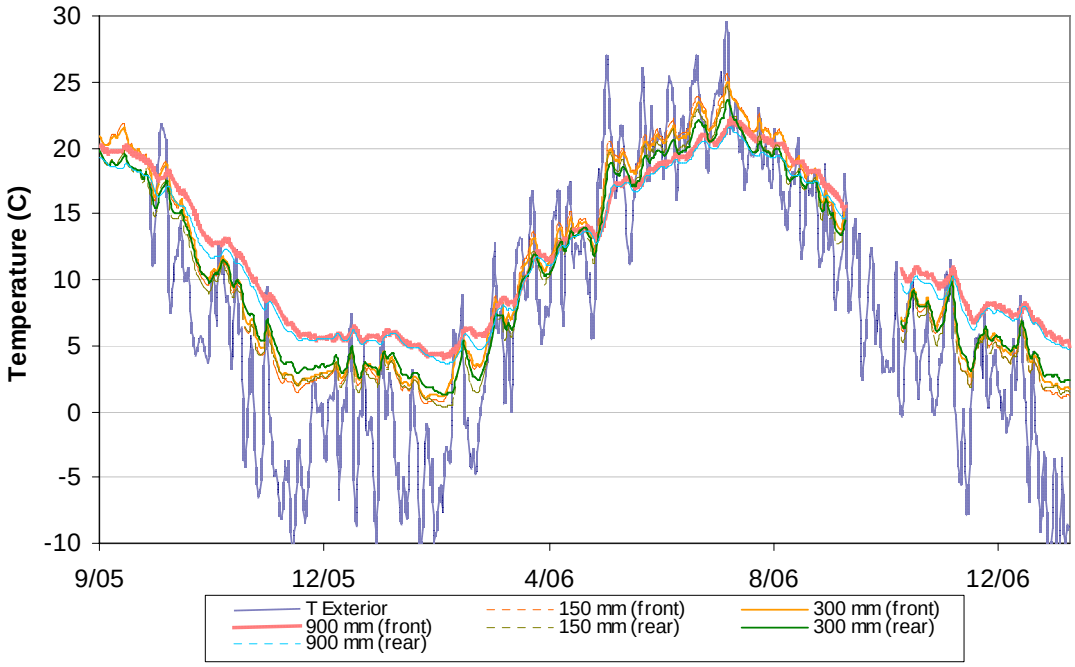

Figure 7.3: Soil temperatures for Kitchener site, with exterior air temperature

Like the Chicago-area site, a weather station that measured soil temperatures was available near the Kitchener test site. The University of Waterloo (Waterloo, ON) weather station measures air temperature, as well as soil temperatures at 50, 100, and 150 mm; it is located in an open field, so results are not influenced by heat loss from a basement. The daily average values for 1998-2001 are shown in Figure 7.4; despite extended periods below freezing, soil temperatures typically have minimum values of just above or below freezing. At 150 mm (6 inches) depth, the soil temperatures remain above freezing throughout the winter; this is seen in the detail of winter 1999-1998 (Figure 7.5).

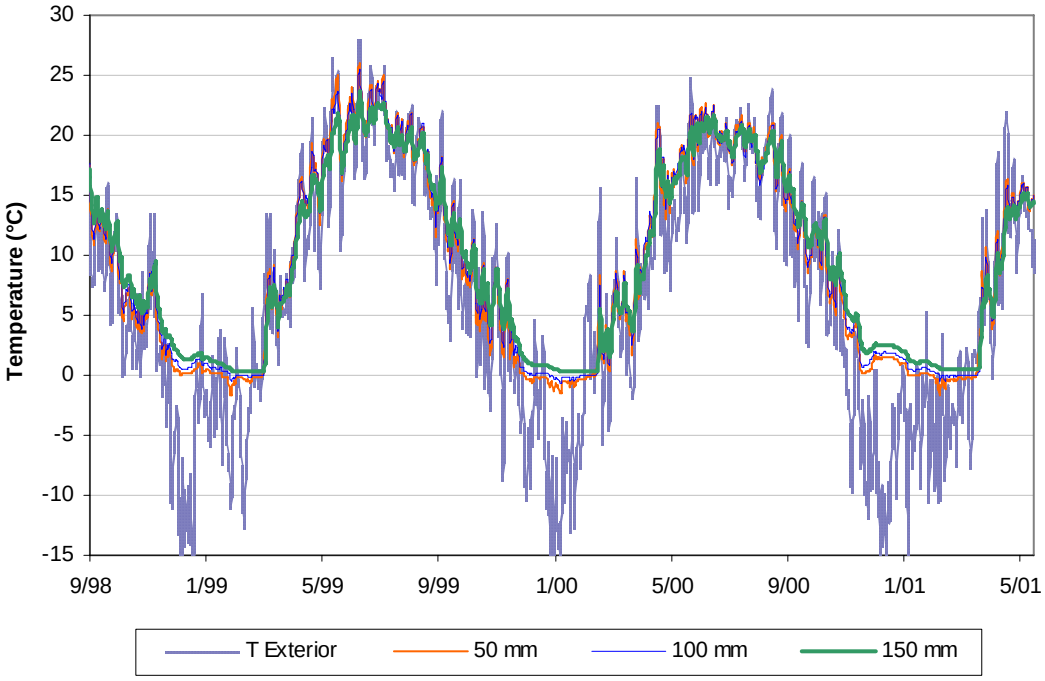

Figure 7.4: Soil temperatures for UW weather station, with air temperature (1998-2001)

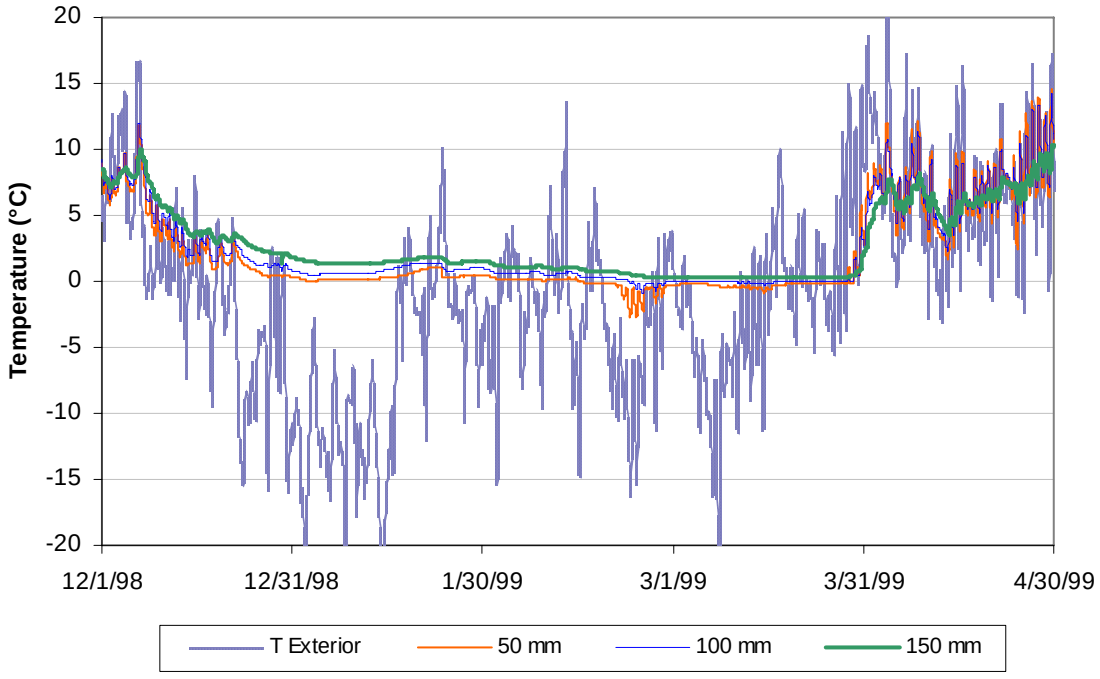

Figure 7.5: Soil temperatures for UW weather station, with air temperature (winter 1998-1999)

7.2.2 Soil Moisture Behavior

Soil moisture conditions were measured with gypsum soil blocks and wood "plug" moisture content surrogate sensors in parallel. The gypsum blocks were only used on the "front" three locations; "plug" sensors were used in all six locations. Gypsum block results are shown in Figure 7.6; "plug" sensors are shown in Figure 7.7; both plots show rainfall data for the monitored period.

The gypsum blocks have relatively inconclusive results; conditions seem to be somewhat drier than in Huntley. Matric potentials never go above "field capacity" (-0.33), showing that the soil is free draining. This might be expected, given that the soil around the foundation appeared to be hard clay surface, covering free-draining sand. Similar to the Huntley site, little correspondence could be found between measurements and rainfall data.

The calibration of the wooden "plug" sensors gave moisture contents of 25-28% in a 100% RH chamber; 11% is roughly equivalent to 50% RH. Measurements in the 25-28% range or higher were expected, given literature data on soil conditions; however, data showed measurements above and below these conditions. It is unclear whether these are measurement anomalies or reflections of real conditions; given that gypsum block data does not show exceptionally dry soil, it appears that these are mostly measurement artifacts. The initial drop in moisture content might be drying of the moisture introduced during the installation process; the sensors were encased in mud, as per gypsum block procedures.

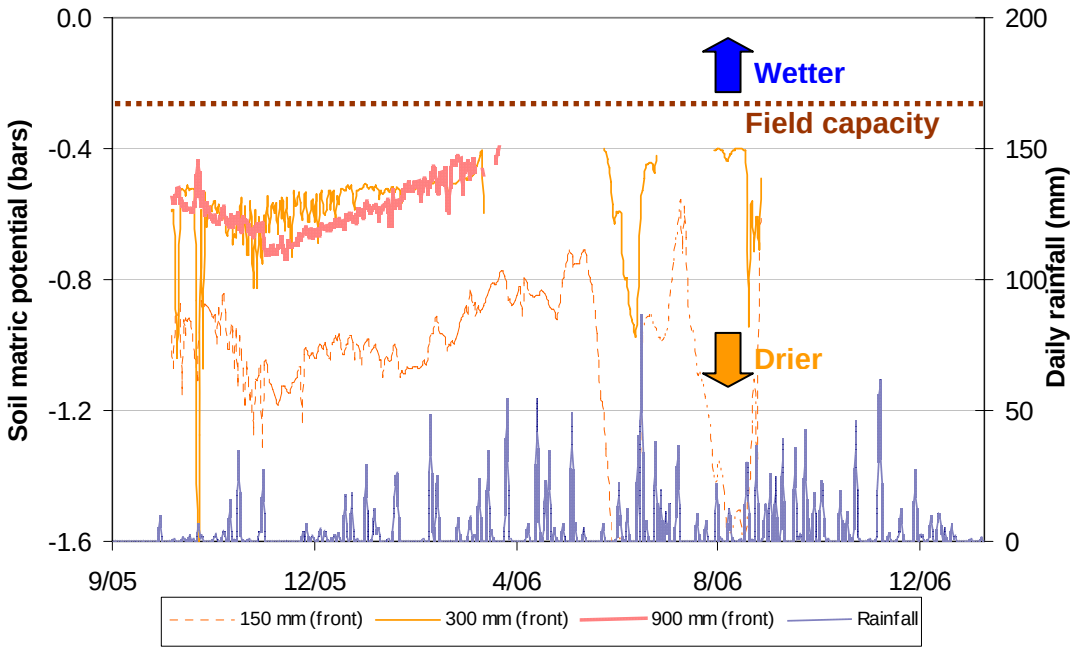

Figure 7.6: Soil matric potentials (front stack) for Kitchener site

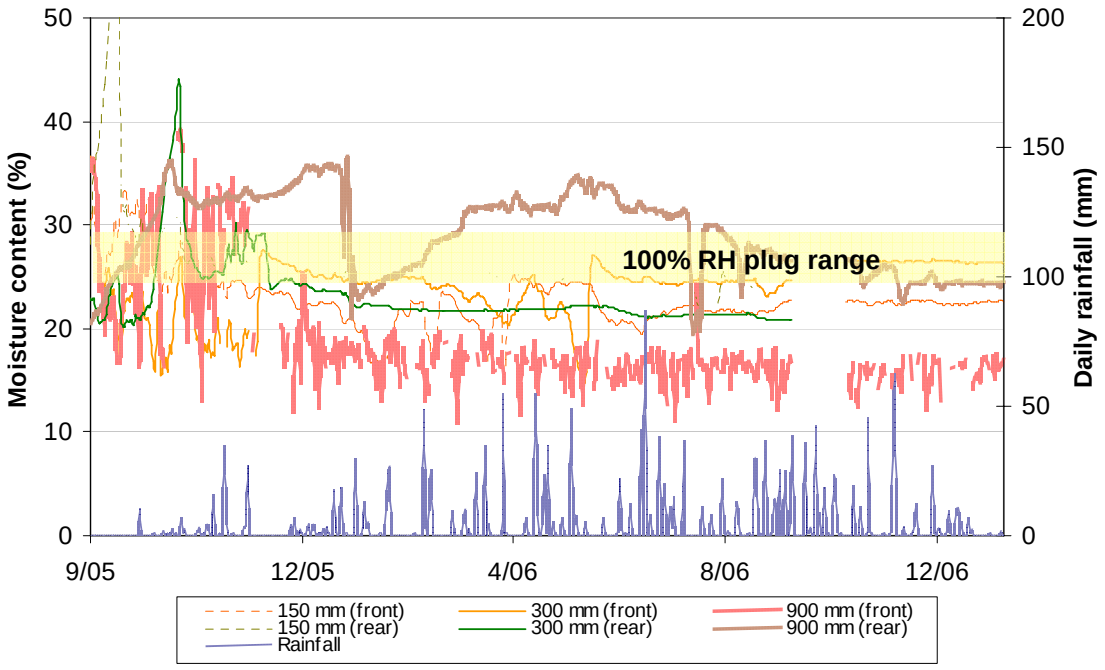

Figure 7.7: Soil moisture content "plug" sensor data for Kitchener site

7.3 Monitored Wall Behavior

The four walls were compared using temperature, relative humidity, dewpoint (calculated from T and RH), wood moisture content, and moisture content "wafer" sensors.

The analysis was broken down into several portions. First, the temperature behavior of the walls was compared. The next topic was wintertime condensation or frost accumulation at the concrete-insulation interface at the upper portion of the wall. This problem is due to movement of moisture (via vapor diffusion, or air transport if there is an incomplete air barrier) from the interior to that interface. Second, in the spring and summer, inward vapor drive can cause condensation on the exterior side of the polyethylene vapor barrier at the upper part of the wall. A concern in all seasons is the accumulation of moisture within an interior insulated assembly at the below grade portions of the wall. Finally, the wood moisture contents are compared in the two frame walls.

7.3.1 Temperature Behavior

Although efforts were made to place test panels in positions that would result in similar exposures, shading from the adjacent house resulted in differential conditions. This can be seen in a detail of wintertime temperatures at the concrete-insulation interface, at the top of the wall (roughly at grade), in Figure 7.8.

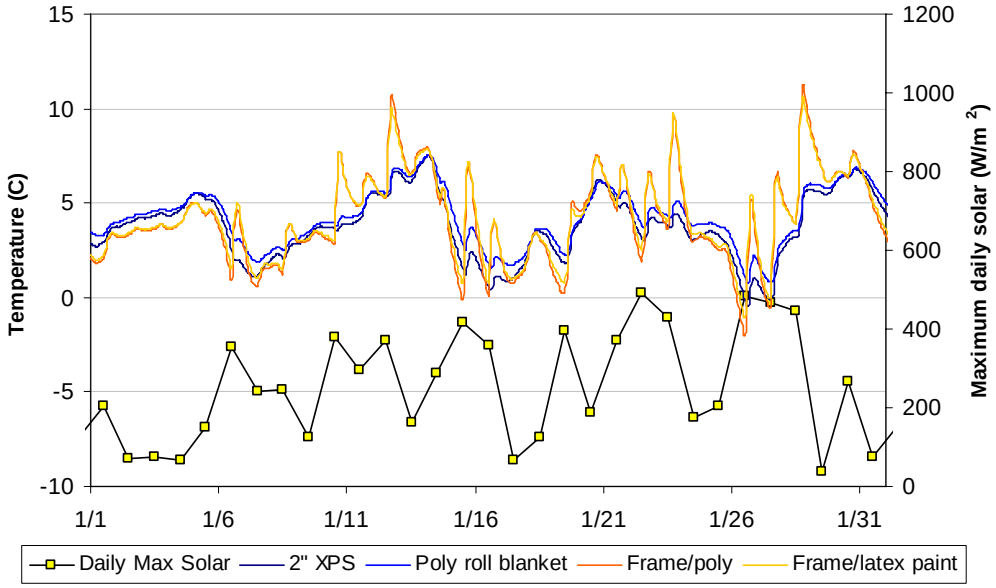

Figure 7.8: Concrete-insulation interface temperature, upper location, with maximum daily solar

The wall temperatures fall into two sets: the rear (XPS and polyethylene roll blanket) walls, which were shaded by the adjacent house, and the front (frame/polyethylene and frame/latex) walls, which were more exposed. The front frame walls show higher daytime temperature peaks (up to ~5° C difference); this behavior can be linked to solar exposure. On days with low (~200 W/m^2) maximum daily solar radiation, the walls have similar temperatures. Also, the front (frame) walls sometimes show colder nighttime temperatures; this may be due to night sky radiation and/or greater wind exposure.

Although the temperature ranges are noticeably different, the emphasis in the following will be on comparing thermally comparable pairs of walls.

In addition to comparing the walls, vertical thermal profiles were measured in the fall (September 2006) and winter (January 2007), as shown in Figure 7.9 and Figure 7.10. In the fall measurements, there is a consistent 1° C difference between the above-grade portions of the two walls. This was caused by changing temperatures over time (measurements were taken approximately an hour apart), and the limited resolution of the infrared thermometer (1° C). The top of the wall shows a 2° C jump from the main above-grade portion. This is due to the thinner concrete wall and air space at the brick ledge (see Figure 7.11 and Figure 7.12). Below grade, the temperature gradually increases until 500 mm below grade, where the concrete wall temperature remains constant with depth.

The winter measurements only cover the upper portion of the wall; the temperatures strongly show the effect of the brick ledge. The significance of this wintertime measurement will be explored in more detail in Chapter 8: Hygrothermal Modeling.

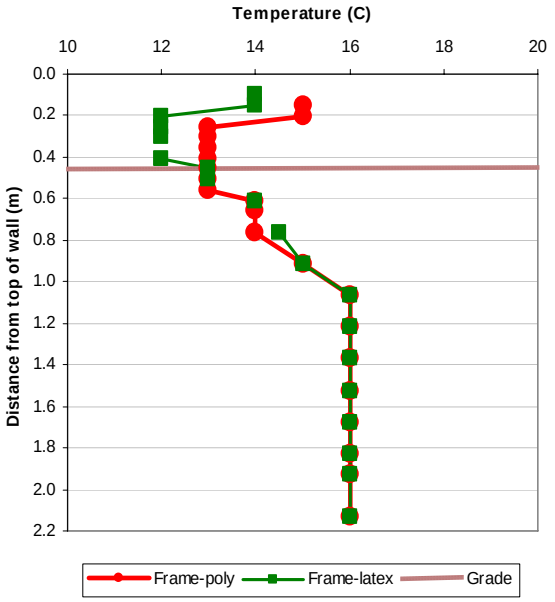

Figure 7.9: Thermal profile down height of frame walls in September 2006; outdoor T ~12-14° C

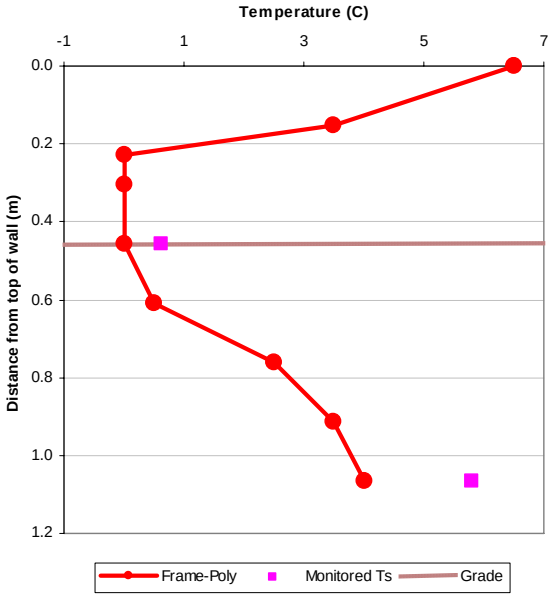

Figure 7.10: Thermal profile down height of polyethylene-frame wall in January 2007; outdoor T~ -8 to -9° C

Figure 7.11: Exterior view of basement window, for vertical reference to brick ledge

Figure 7.12: Interior view of basement window, for vertical reference, compared to test panels

7.3.2 Wintertime Condensation

This issue is examined by plotting the relative humidity at the interface between the concrete and the insulation (see Figure 3). The sensor is located at the upper part of the wall (roughly at grade), mid-thickness in the batt insulation. The plotted relative humidity values are calculated based on the

dewpoint at the sensor location, and the temperature of the concrete surface. The vapor resistance of batt insulation is very low, so this is a reasonable assumption for the purpose of this calculation. In the XPS wall, no RH sensor was available at that location; however, a moisture content wafer was placed at the concrete-insulation interface. Based on previous calibration data and a standard sorption isotherm for wood (Straube and Burnett 2005), a curve fit was used to provide estimated relative humidity values in the XPS wall.

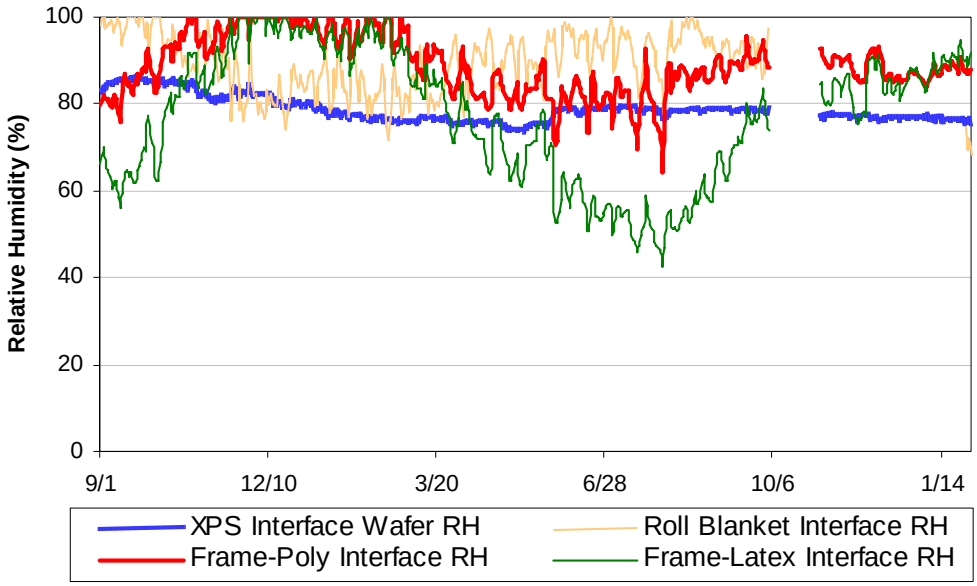

Figure 7.13: Monitored data: relative humidity at concrete-insulation interface; above-grade

The data show that two of the walls (frame/polyethylene and frame/latex paint) both experience high relative humidity during the first winter at the concrete-insulation interface. In contrast, the roll blanket wall has lower wintertime humidities (80-90%), but rises to the 90-100% RH range during the following summer. These results indicate that in terms of wintertime condensation issues, both the frame/polyethylene and frame/latex paint wall seem to be at risk. It is notable that the frame-polyethylene behaves more like the frame-latex paint wall in the wintertime, rather than the roll blanket. This behavior is examined in more detail in the following section (7.3.3); several reasons are proposed there.

During the spring and summer, the frame/latex paint wall is the driest, dropping to 50-60% RH, while the frame/polyethylene only drops to roughly 80%. The roll blanket has the highest summertime humidities; this is explored in the following section. These results show that inward drying is available in the more permeable frame/latex paint wall: during the summer, it is the driest wall. Also, it is notably drier during the first summer (start of monitoring), compared to the frame/polyethylene wall (which does not allow any inward drying).

During the entire monitoring period, the XPS wall maintains a stable RH, close to 80%. This behavior might partially be an artifact of the measurement: it is calculated from the wafer sensor,

which has a long response time (on the order of a week; see Appendix B: Development and Calibration of Wood Surrogate Sensors).

7.3.3 Summertime Condensation

This problem was examined by plotting the conditions at the insulation-polyethylene (or insulation-gypsum board) interface, where condensation would occur at the upper part of the wall. Although this could also be done in terms of calculated relative humidity (as per the wintertime plot), more informative results are produced by plotting the moisture content of the "wafer" sensor, which was actually placed at this interface (see Figure 7.14). Exterior temperature is also plotted in that graph.

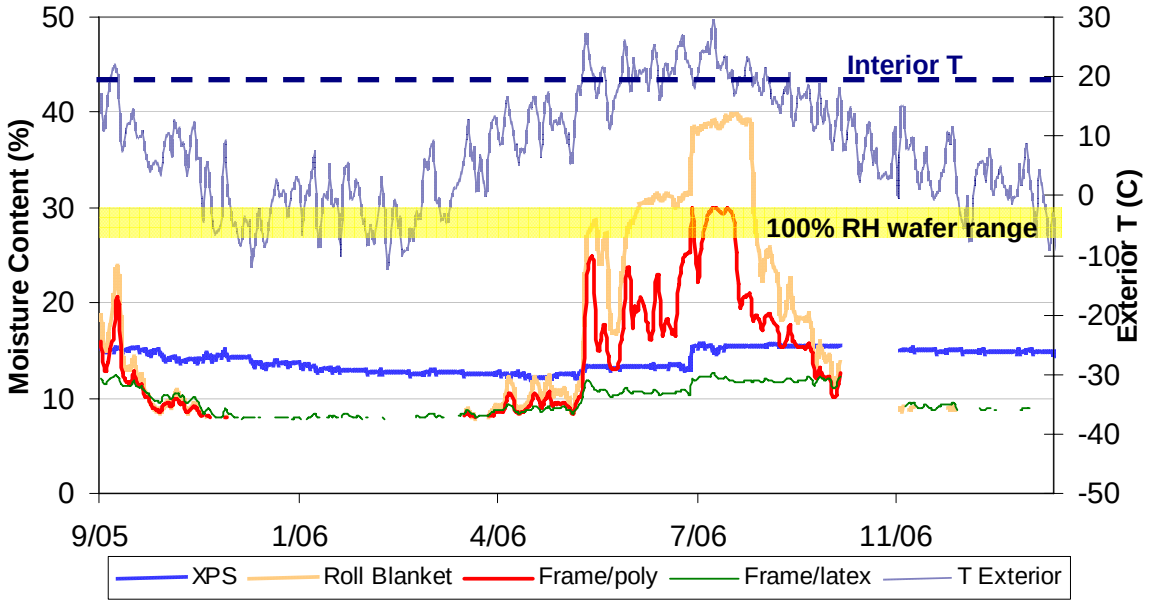

Figure 7.14: Moisture content wafer response, interior side, above grade, with exterior T

The graph clearly shows the inward vapor drive described in the background chapter: during the late spring and summer, the moisture content of the wafer rises sharply. The roll blanket wall shows the greatest rise in moisture content (peak at 40% MC), followed by the frame/polyethylene wall (peaks near 30%). Laboratory calibration of the wafers showed that 100% RH roughly corresponds to 25-30% MC, but moisture content could be driven higher by immersion in liquid water. The roll blanket data indicates condensation and the presence of liquid water for a sustained part of the summer.

The pattern of moisture accumulation at the wafer is tied to outdoor temperature, as indicated by the matching spikes; this is reasonable given that inward vapor drives are proportional to the temperature of the saturated layer (concrete). The interior temperature is roughly plotted on the graph; the wetting of the wafer is tied to an inward temperature gradient. When the exterior temperature cools below interior temperature (as in fall 2005, and mid-June 2006), the moisture content drops. This change in thermal gradient results in a reversal of the moisture gradient direction.

The roll blanket and frame/polyethylene walls do not behave identically, even though in a one-dimensional section through the insulation, they are identical. The roll blanket wall has much greater accumulation; this occurs even though it receives less solar exposure than the frame/polyethylene wall.

Several factors might be acting alone or in combination. First, unlike the roll blanket, which has a continuous layer of polyethylene sealed to the concrete on all sides, the frame/polyethylene wall is made of discrete components that are air sealed to create an assembly. Although best efforts were made to create an air seal on all sides, it is still possible that small incidental air leakage exists.

Second, the presence of wood framing results in a great increase in moisture storage capacity. The storage capacity of the wood studs was calculated for a shift of relative humidity from 50% to 97% RH, the difference was 32 to 116 kg/m^3. This is a relatively conservative estimate, given the sharp rise in the sorption isotherm near 100%. This was compared in the storage available in air at 20°C, with the same humidity shift. Assuming a 16" stud spacing, a stud has over 1000 times the moisture storage capacity as the air in the adjacent stud bay. Even if only a portion of the stud stores moisture during seasonal flows, it still strongly changes the behavior of the assembly.

Third, the framing was air sealed, but not vapor sealed at the sides and top of the frame/ polyethylene wall. Although vapor diffusion through 1-½" (38 mm) of wood is low (0.26-3.6 perms/15-205 ng/Pa·m·s^2; Straube and Burnett 2005), the permeability of polyethylene is so low that this vapor "flanking" could result in a noticeable change in the overall permeability of the assembly. Note that this effect is disproportionately large in this test installation, given the large exposed framing fraction.

The first and third items were addressed during a field visit in January 2007; the exposed portions of the perimeter studs were covered with builders' tape (see Figure 7.15). Unfortunately, the buffer panels prevented complete taping of the edge studs (see Figure 7.16). The top was not taped, as per normal practice. A second layer of tape was installed to link the vertical edges of the polyethylene with the tape on the side of the stud, completing the air seal at the lateral joints.

Figure 7.15: Taping of perimeter studs, and faces of inner studs (at staple holes)

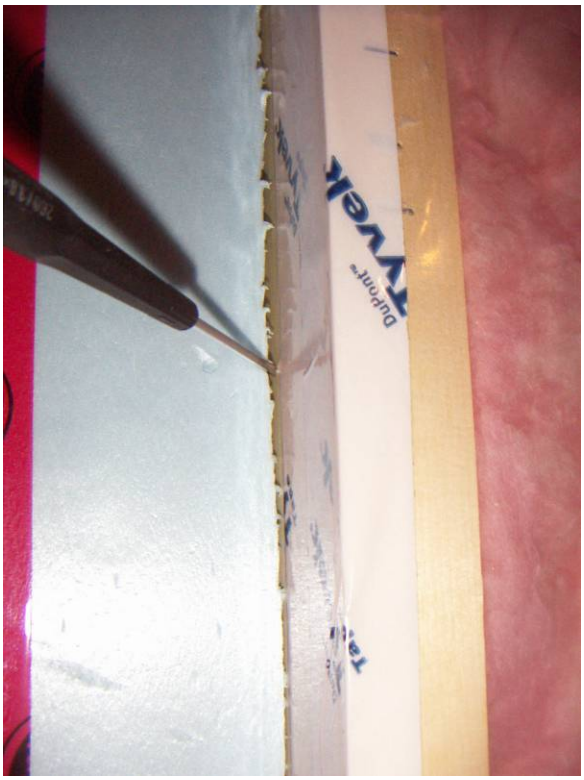

Figure 7.16: Tape only covers exposed portion of edge studs; could not apply at buffer panels

In contrast to the frame/polyethylene wall, the frame/latex paint wall does not show this sharp rise in moisture content during the summer. Although there is a slight jump with the onset of warm weather, moisture content peaks at roughly 12%, which is well within the safe range for wood. This indicates that the inward vapor drive passes through the gypsum board and latex paint, and does not accumulate in the cavity.

The XPS wall shows a much more stable wafer moisture content, remaining close to 15% throughout the year, which is equivalent to the 80% RH level seen in Figure 7.13.

7.3.4 Accumulation Within the Insulation Assembly

Another concern is the accumulation of moisture within the insulation assembly, resulting in high humidity and conditions favorable for mold growth. There is a high risk, given exterior conditions (100% RH, and the presence of liquid water in the below-grade environment) and construction moisture of the concrete. These risks are assessed for these walls using relative humidity, dewpoint, and wafer sensor measurements.

A relative humidity sensor was located at the concrete-insulation interface, at mid-height in all four walls; the results are plotted in Figure 7.17. However, the sensor in the frame/polyethylene wall

failed due to prolonged exposure to high RH, so relative humidity was calculated from the dewpoint of the stud bay and the surface temperature, similar to the method used in Figure 7.13.

The plot shows that moisture accumulation roughly corresponds to the vapor resistance of the assembly. The polyethylene roll blanket shows the highest sustained RH levels: near saturation in fall, spring, and summer, dropping to ~80-90% RH in winter. The frame/polyethylene wall shows calculated RH levels higher than the XPS wall, but not quite as high as the roll blanket; reasons for the difference in behavior were discussed in section 7.3.3. The XPS wall has vapor permeability an order of magnitude higher, and shows RH levels consistently in the 80-90% range (until sensor failure in October 2005). The frame/latex paint wall has permeability an order of magnitude higher than XPS, and shows the lowest humidity levels, indicating drying of the assembly to the interior.

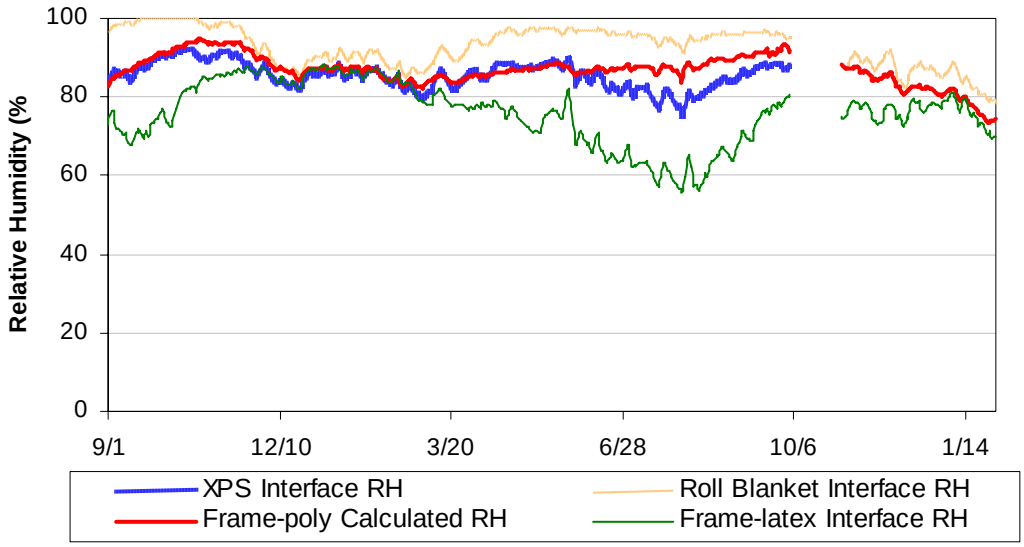

Figure 7.17: Relative humidity, concrete-insulation interface, mid-height (daily avg. values)

All of these interface relative humidity measurements were doubled by wafer sensors; they are plotted together in Figure 7.18 to verify the relative humidity relationship shown in Figure 7.17. The relative order of the walls and seasonal patterns remain essentially the same: the roll blanket is consistently wettest, the frame-latex paint driest, and the remaining walls between the two.

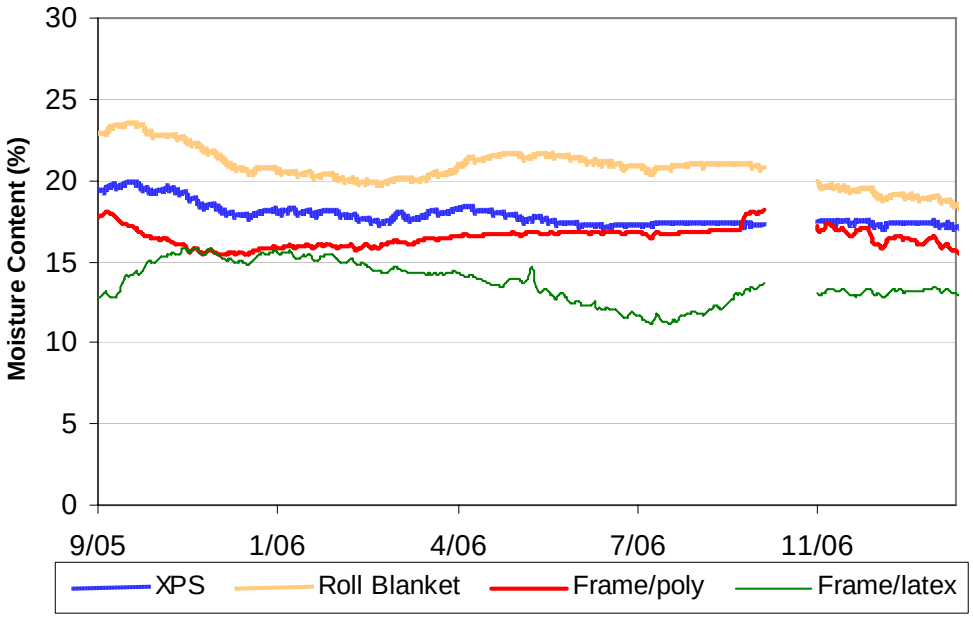

Figure 7.18: Wafer moisture content, concrete-insulation interface, mid-height (daily avg. values)

The results from the T/RH sensors are plotted in terms of dewpoint in Figure 7.19, similar to the plots comparing the Huntley assemblies. The stud bay RH is again substituted for the concrete-insulation interface RH sensor in the frame/polyethylene wall. The walls were thermally similar at mid-height, so the relative wetness/dryness is the same as in the relative humidity plot (Figure 7.17). Interior dewpoint is plotted as well; it demonstrates that drying to the interior is always available.

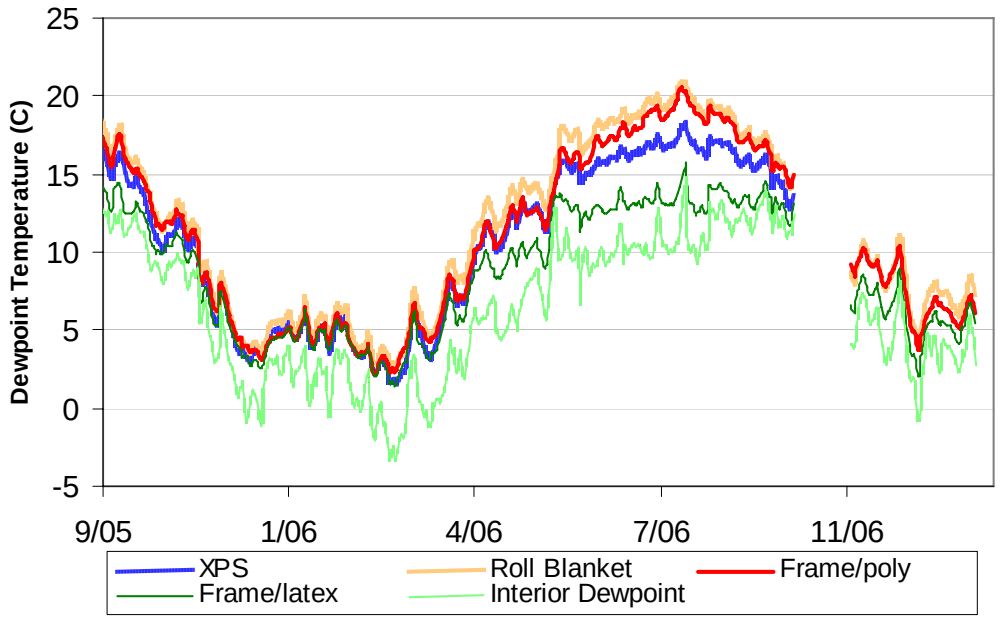

Figure 7.19: Dewpoint at concrete-insulation interface, mid-height, with interior DP

Moisture content wafers were also placed at the concrete-insulation interface at the lower portion of the wall; the results are plotted in Figure 7.20. Sensors were only installed in the XPS and roll blanket walls. However, the roll blanket sensor was incorrectly connected until a field visit in October 2006.

The XPS moisture contents are in the 20% range; this is roughly equivalent to 90% RH, which is a level that causes some concern. The small amount of roll blanket data indicates even wetter conditions than the XPS wall, as would be expected given the lower permeability of polyethylene. These results suggest that construction moisture or exterior-sourced moisture at the lower portion of the wall can be a concern with lower permeability materials that inhibit drying. The condition of the wafers should be examined during disassembly/decommissioning of these walls, to gauge this risk.

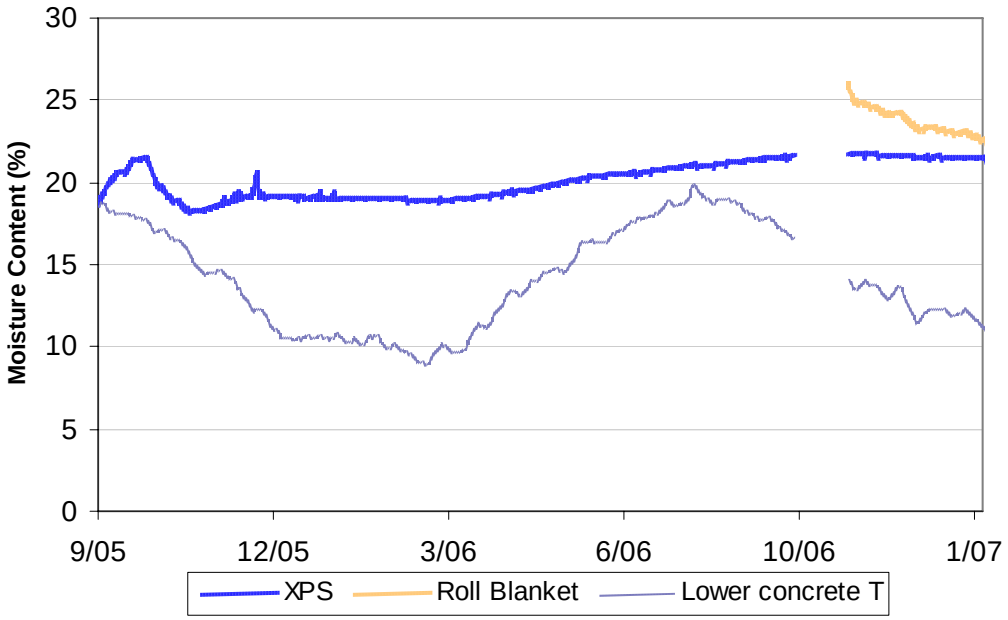

Figure 7.20: Wafer moisture content, concrete-insulation interface, lower height

7.3.5 Framing Moisture Content

The summertime inward vapor drive described in section 7.3.3 resulted in indications of condensation at the polyethylene. However, when assessing the risk of a wall assembly, the danger is not necessarily condensation *per se*, but mold growth and damage to moisture-sensitive portions of the wall, such as the framing. Therefore, moisture content measurements of the framing were compared, to see if they approached danger levels.

The moisture content of the framing at the upper portion of the wall is plotted in Figure 7.21. Moisture contents were measured at the inboard and outboard edges of the stud (3/8" or 9 mm from the faces). The summertime increases in the frame/polyethylene wall are seen at the interior side, similar to the moisture content wafer; however, peaks are roughly 17% MC, which is still in the safe range (albeit on the high side). A larger response is seen on the interior side, as would be expected, although a jump is observed on the exterior side. Like the wafer, accumulation patterns correspond to an inward temperature gradient, as shown by the plotted exterior temperature.

A similar rise in wintertime moisture content is seen at the outboard side of the frame/latex paint wall; again, the MC remains within the safe range (15% peak). The moisture content of the frame/latex paint wall at the inboard side remains the driest throughout the year; the permeable interior finish allows drying to the interior.

Overall, moisture contents at all of these upper framing locations presented little concern for mold growth: although there are seasonal rises, they are below danger levels. Furthermore, based on over a year of data, these cycles appear to be stable.

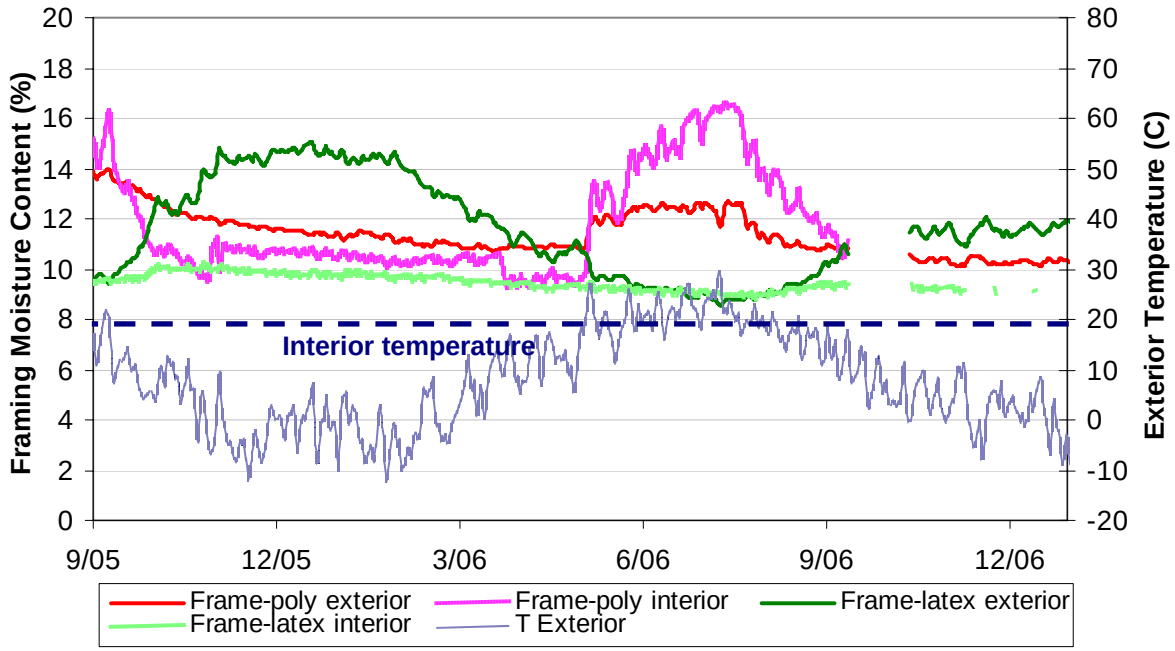

Figure 7.21: Framing moisture content for upper portion of stud walls

The moisture contents of the framing at the lower part of the walls are plotted in Figure 7.22. The measurements were in the 9-14% range; again, these levels present little concern for mold growth. One pattern was that the frame/polyethylene moisture contents were consistently higher than the frame/latex paint wall. The frame/polyethylene MCs rise and fall seasonally, in parallel with the temperature of the concrete at that height. The frame/latex paint wall has flatter moisture content behavior.

Figure 7.22: Framing moisture content for lower portion of stud walls

It should be noted that a vapor control layer (i.e., polyethylene) at this lower height is, if anything, detrimental. It results in greater moisture accumulation in the framing, although only by a small amount. There is no indication of wintertime accumulation due to the lack of vapor control. This is the expected behavior described in the technical background section; it is due to the temperature range seen at this portion of the wall (~10-20° C at concrete-insulation interface).

7.4 Field Visit Disassembly

In late September 2006 (after the first year of operation), some of the walls were disassembled and inspected for evidence of mold growth or other moisture-related damage. Spatial distribution of moisture content in the framing was measured with a handheld Delmhorst BD-10 electrical resistance-based meter.

In the frame/fiberglass/polyethylene wall, data showed condensation at the upper portion of the wall (albeit less severe than the roll blanket); the moisture content wafer also showed mold growth. However, the framing did not show notable mold growth: damage was limited to a small amount of brown spotted discoloration of the stud at the interior edge. Handheld moisture content measurements were in the 12-14% range for most of the framing; the members at the exposed perimeter (top plate and edge studs) were at 9-10% MC.

In the frame/latex paint wall, there was no visible staining or mold growth on the insulation, framing, or wafers. Moisture contents were in the 9-11% range throughout the wall, which was drier than the frame-polyethylene wall. One concern with omitting a polyethylene layer in assemblies is that inward vapor drives might cause mold growth on the back of the drywall, due to accumulation at

that location. Monitored data showed that there was negligible accumulation; a visual inspection of the exterior side of the drywall showed no damage, discoloration, or mold growth.

The roll blanket and extruded polystyrene walls were not disassembled; this will be done at the conclusion of the experiment. However, the clear polyethylene of the roll blanket wall allowed some observation of interstitial conditions. During the summer monitoring, this wall showed substantial condensation at the polyethylene: the upper moisture content wafer had noticeable mold growth. In addition, there was some brown discoloration of the fiberglass insulation.

7.4.1 Frame-Polyethylene Wall Disassembly and Inspection

Initial inspection after removing the drywall showed no moisture damage on the drywall or the fiberglass insulation; no condensation was seen on the polyethylene vapor barrier. The only notable observation was the mold growth on the upper moisture content wafer, on the interior side (Figure 7.24 and Figure 7.25).

Figure 7.23: Frame-polyethylene wall after drywall removal

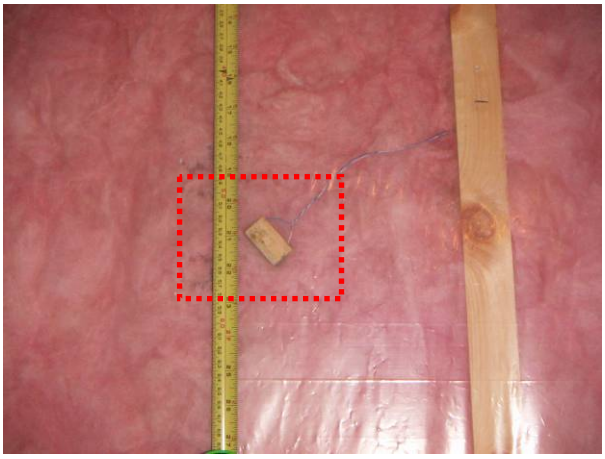

Figure 7.24: Upper moisture content wafer

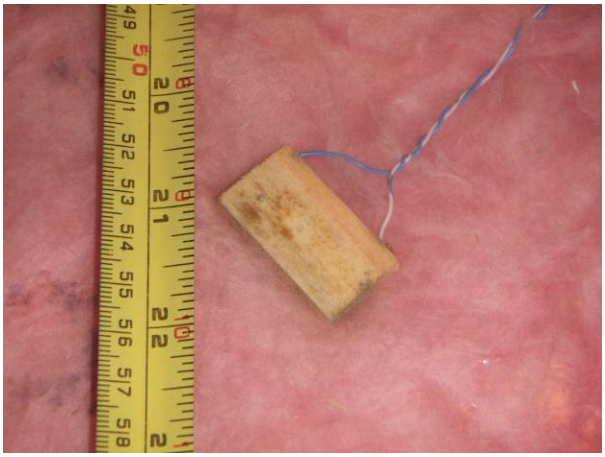

Figure 7.25: Close up; mold growth was seen on both sides

After removing the polyethylene, a small amount of brown spotted staining was found on the upper (above-grade) portions of the studs, on the inboard side (Figure 7.26 and Figure 7.27). This staining or growth was superficial/surface in nature.

The mid-height wafer showed no mold growth or moisture damage on the inboard face, but a slight amount of brown spotted staining on the exterior face (Figure 7.28 and Figure 7.29). Peak moisture content was roughly 18%.

Figure 7.26: Brown staining at inboard side of upper portion of left-hand test bay stud

Figure 7.27: Brown staining at inboard side of upper portion of right-hand test bay stud

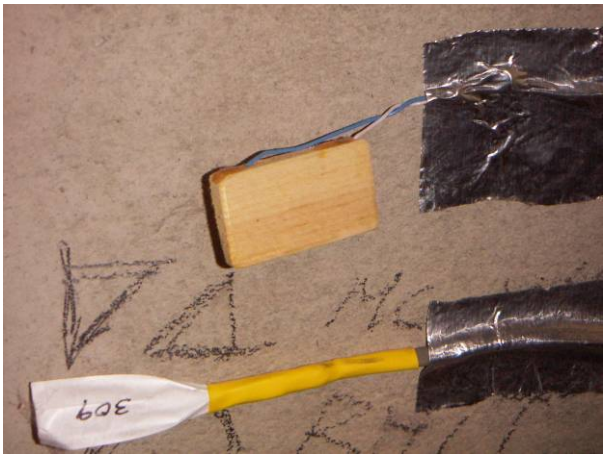

Figure 7.28: Interior face of mid-height wafer

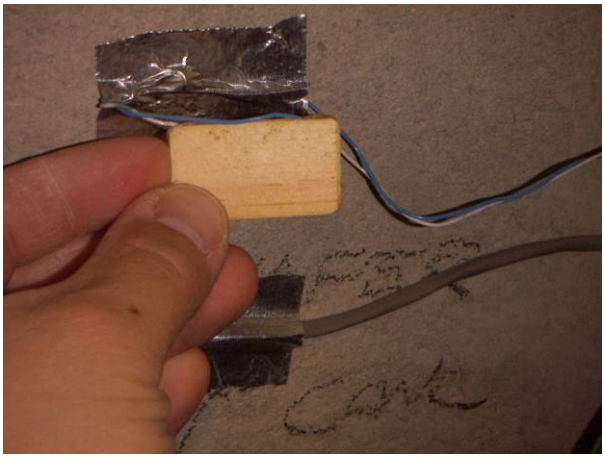

Figure 7.29: Exterior face of mid-height wafer

The quality of the air seal between the stud frame and concrete was inspected; it appears to be intact on all sides.

7.4.2 Frame-Latex Paint Wall Disassembly and Inspection

The initial inspection after removing the drywall showed no moisture damage to the fiberglass insulation or the drywall. As mentioned earlier, a common concern when a sheet vapor barrier is removed is the potential for moisture damage at the exterior face of the drywall, but the results shown

in Figure 7.31 and Figure 7.32 indicate that moisture passes through without causing harm. The circles visible in Figure 7.31 are dust/flash photographic artifacts.

Figure 7.30: Frame-latex paint wall after drywall removal

Figure 7.31: Exterior face of drywall in frame-latex paint wall

Figure 7.32 Close-up of upper portion of drywall exterior face

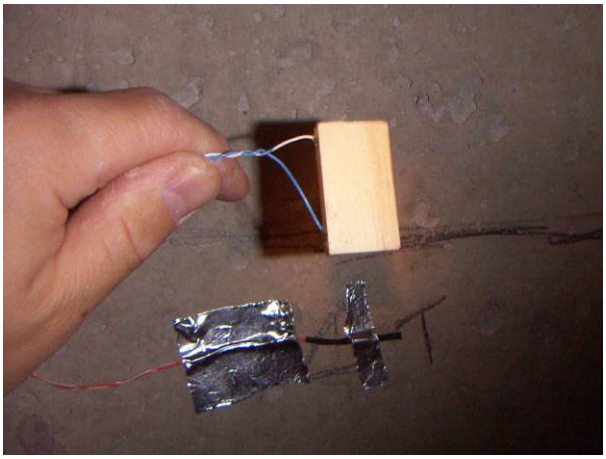

Figure 7.33: Upper wafer

No evidence of mold growth was seen on either face of the upper wafer sensor, as shown in Figure 7.33.

The upper portions of the frame were examined for mold or moisture damage (Figure 7.34 and Figure 7.35); none was seen, and the remainder of the frame also showed no moisture damage.

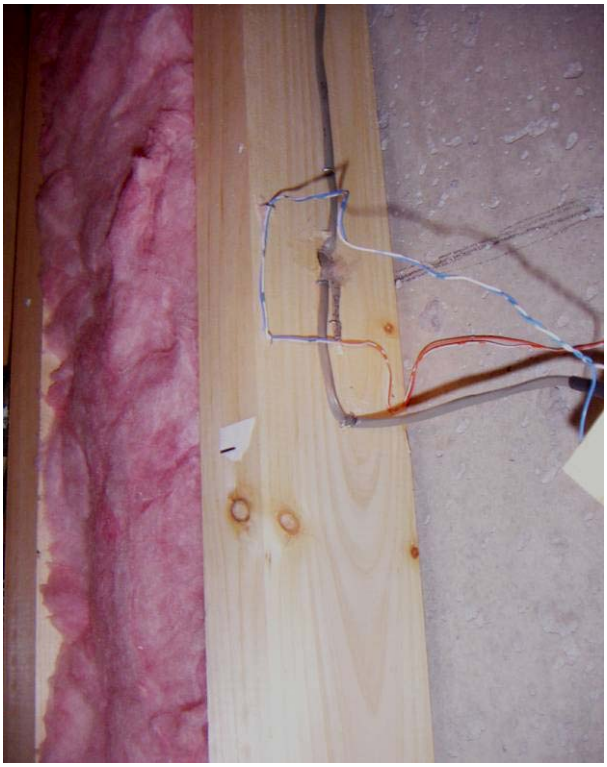

Figure 7.34: Upper left side stud of test bay

Figure 7.35: Upper right side stud of test bay

The middle-height concrete-insulation interface wafer showed no mold evidence on the interior side; there was a slight amount of brown spotted staining on the exterior face.

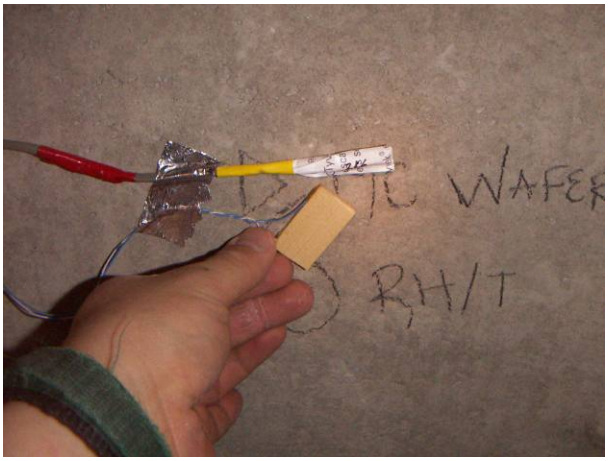

Figure 7.36: Mid-height concrete-insulation interface wafer, interior side

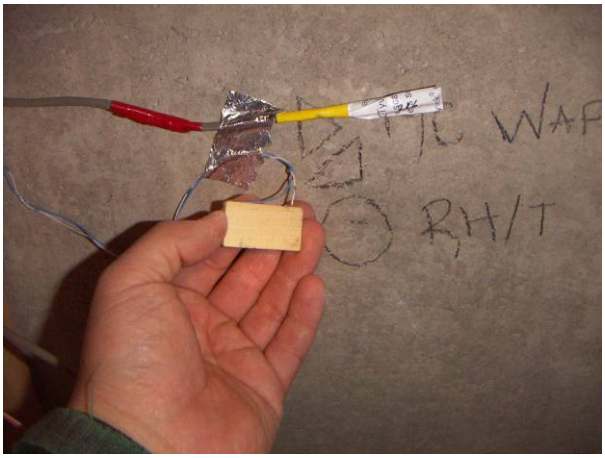

Figure 7.37: Mid-height concrete-insulation interface wafer, exterior side

The air seal on the perimeter of the frame was inspected; as per the polyethylene wall, it was intact and continuous.

7.4.3 Moisture Content Measurements

A handheld moisture meter was used to examine the spatial variation of moisture content (MC) measurements of the wood frames (Figure 7.38 & Figure 7.40); results are shown in Table 7.1 below.

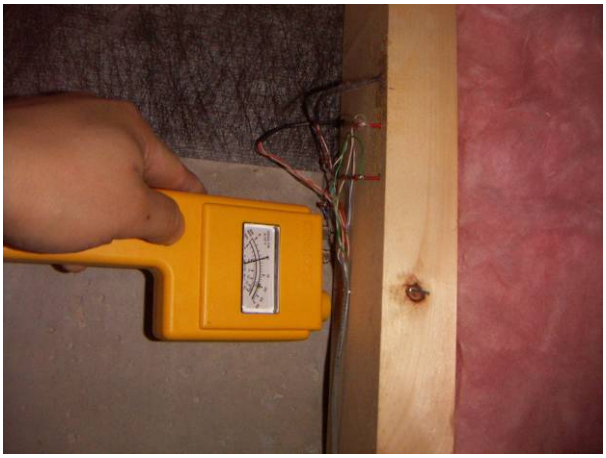

Figure 7.38: Moisture meter measurements of the test bay stud, parallel to MC pins

Figure 7.39: Measurement of bottom plate

Table 7.1: Moisture content measurements of frame walls

MCs at P3 Poly Wall 2006-09-22 ~9:30 AM		**MCs at P4 No Poly Wall 2006-09-22 10:30 AM**	
Location	**Reading**	**Location**	**Reading**
Stud 60" AFF		Stud 60" AFF	
@ foundation	14%	@ foundation	9%
@ mid	12%	@ mid	9%
@ interior	12%	@ interior	9%
Bottom plate		Bottom plate	
@ foundation	14%	@ foundation	11%
@ mid	13%	@ mid	10%
@ interior	13%	@ interior	9%
Wafer @ concrete		Wafer @ concrete	
Interior side	13%	Interior side	9%
Exterior side	14%	Exterior side	10%
Wafer @ poly		Wafer @ GWB	
Interior side	9%	Interior side	9%
Exterior side	9%	Exterior side	9%
Top plate		Top plate	
@ foundation	10%	@ foundation	9%
@ mid	10%	@ mid	9%
@ interior	9%	@ interior	9%
Outer stud, upper location		Outer stud, upper location	
@ foundation	10%	@ foundation	10%
@ interior	10%	@ interior	9%
		Outer stud, lower location	
		@ foundation	11%
		@ interior	9%

Note that these are all small variations in moisture content that are within the safe storage limits of wood. This presentation is meant more to show differences in behavior between the two walls with the distribution of moisture levels in the framing. Some notable points included the following. First,

the polyethylene wall shows consistently higher moisture contents than the latex paint wall, typically on the order of 13-14% MC vs. 9-11% MC.

There is typically a small but measurable moisture gradient through the thickness of the framing members; the highest moisture contents are found at the exterior (concrete) side.

In the frame/polyethylene wall, the outer perimeter framing members (top plate, outer perimeter studs) show markedly lower moisture content than the test bay studs or bottom plate. These frame members are exposed to interior conditions on one side: as a result, they have moisture levels similar to the frame/latex paint wall (9-10% MC).

7.4.4 Roll Blanket Inspection

The roll blanket wall was not disassembled, due to the disturbance that would result to the wall, and the lack of framing members to measure with a moisture meter. Evidence of moisture accumulation in upper batt was seen in the form of some discoloration of insulation, visible through the polyethylene. The upper moisture content wafer had visible mold on the exterior surface. This appears to be a limited amount of damage, given the amount of condensation indicated by monitoring.

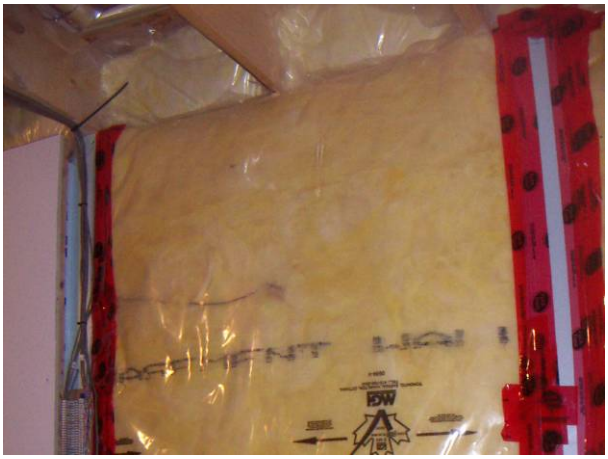

Figure 7.40: Upper portion of roll blanket wall.

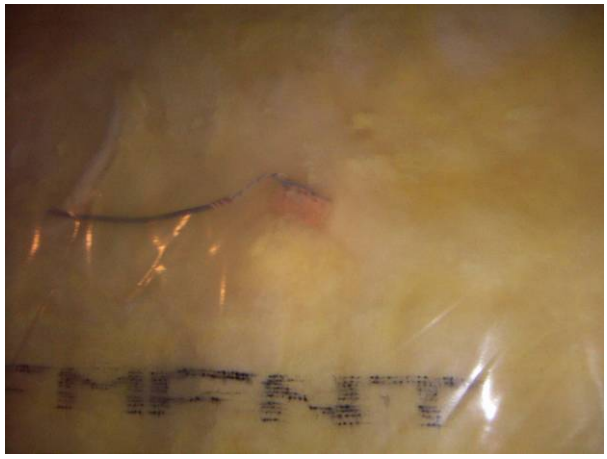

Figure 7.41: Close up of the upper wafer

The moisture content of the wafer was measured through the polyethylene at 9% MC; monitored data (corrected for species) was closer to 13%. The pinholes were sealed with builder's tape.

7.4.5 XPS Wall Inspection

The 2" XPS wall was not disassembled, due to the difficulty of the procedure, the disturbance that would result to the wall, and the lack of framing members to measure with a moisture meter. A full disassembly and inspection will occur at the final decommissioning at the conclusion of the experiment; the presence or absence of mold on the wafers is of particular interest.

Chapter 8
Hygrothermal Modeling

Computer modeling of the basement wall assemblies was done using WUFI® Pro 4.1, a commercially-available one-dimensional hygrothermal simulation package. This simulation has been validated against experimental data by many researchers (Karagiozis et al. 2001, Künzel 1998a, Künzel 1998b, Straube & Schumacher 2003) in applications that include roofs, walls, and foundations.

The assemblies installed in the Kitchener test basement and simulated in this work were as follows:

1. 2"/50 mm extruded polystyrene foam, furring strips, and gypsum drywall with latex paint (referred to as "XPS")
2. Full-height fiberglass roll blanket with polyethylene facer (referred to as "roll blanket")
3. 2x4 stud frame with fiberglass batt, polyethylene, and gypsum drywall with latex paint (referred to as "stud frame polyethylene")
4. 2x4 stud frame with fiberglass batt and gypsum drywall with latex paint (no polyethylene) (referred to as "stud frame no polyethylene" or "stud frame latex paint")

One issue was noted in planning the models: in a one-dimensional hygrothermal model such as WUFI, the roll blanket and stud frame polyethylene wall are basically identical, except for any minor different in R-value due to the gypsum drywall. However, in experimental data, these two walls were markedly different. Apparently, the three-dimensional aspects of the assembly had some effects that are not accounted for in the one-dimensional representation (e.g., lower effective permeance of the assembly, etc.).

The modeling approach was divided into two major steps: validation and extrapolation.

In validation, the assemblies from the test basement were modeled and compared to monitored data; simulation parameters were tuned to provide closer correspondence. To run these simulations, it was necessary to generate boundary conditions for several heights in the assembly, since exterior wall conditions vary above and below grade. The "low", "middle," and "high" (i.e., above-grade) monitoring locations were simulated, to match instrumentation data. Comparisons of temperature, relative humidity and dewpoint, and condensation potentials were used to calibrate the model. The correspondence between simulations and data was not strong; general patterns were often similar, but exact behavior was not matched. This was ascribed to the effects of two-dimensional geometry, not captured in the one-dimensional simulations.

With this caveat in mind, extrapolations with different exterior and interior climates were run and analyzed. Three exterior climates in Canada were simulated; the interior climate was varied as well (relative humidity level). Finally, wall assemblies that were not installed at the Kitchener site were simulated in order to gain a better understanding of some alternate basement insulation assemblies.

8.1 Validation Simulations

The validation simulations are broken into two sections: the above-grade and below-grade portions. It was necessary to create both boundary conditions (exterior and interior), and starting moisture levels for the assembly. Results from initial models were used to iteratively tune these input conditions. Then, the results were compared with monitored data. When a lack of correspondence was found, possible reasons for this difference were proposed, and the applicability of simulation results was examined.

8.1.1 Above-Grade Validation Simulations

8.1.1.1 Boundary Conditions

The uppermost portion of the wall is exposed to above-grade conditions, as reflected by exterior air temperature and relative humidity measurements taken at the Kitchener site. However, additional weather data (rainfall, wind, and solar radiation) is required to create a climate file for a WUFI simulation. Therefore, weather data from Building Engineering Group exposure facility (BEGHut) was substituted to generate these conditions; this weather station is roughly 15 km (9 miles) northwest of the Kitchener site. Comparison of temperatures at the two sites shows close correlation, suggesting weather patterns are sufficiently similar.

Interior boundary conditions were provided by measured data. Conditions were relatively dry throughout the year, due to a combination of low moisture generation, ventilation with exterior air (winter), and/or running of the air conditioner (summer). Interior relative humidity was in the 25-35% range in wintertime, which was equivalent to a dewpoint in the 0-5° C range; summertime humidity levels were approximately 60%, or a 10° C dewpoint (interior temperatures were cooler than 20° C).

A southeast-facing wall was used in the validation runs, matching the test setup. The rain exposure of the test walls is not well characterized: the adjacent building shields the side of the house, but the effect varies between the test panels. Although the test walls are close to the ground (low exposure), they might be subject to splashback of rain that comes off the building and hits the ground. As a first estimate, WUFI default values of R1=0.0 and R2=0.07 (short building up to 10 m) were used. This is roughly equivalent to a rain deposition factor (RDF) of 0.32, which is in line with exposures seen at the bottom of the wall (RDF<0.35, Straube 2005). Solar short-wave absorptivity (α) was set to 0.6, which is the value given for "concrete, rough" (ASHRAE 2005); long-wave emissivity (ε) was set to 0.9. No additional coatings or surface transfer coefficients were specified.

8.1.1.2 Assembly Initial Conditions

Unlike lighter framed wall assemblies, the built-in construction moisture of a basement wall is a significant source for in-service problems. Therefore, characterizing this moisture load (and its distribution) is necessary to simulate performance. Starting with an initial moisture content of 175 kg/m^3 (free water in fresh concrete, according to WUFI documentation), the wall was allowed to dry in WUFI with the described boundary conditions. Note that this is a conservative approach that

underestimates the drying of the concrete, as the building would not have been dried in and conditioned for that full period.

Figure 8.1 shows some moisture profiles generated under various drying conditions and periods; the exterior side is the left, and interior right. The initial moisture content is shown by the red dotted line (175 kg/m^3); the equivalent relative humidity (via the sorption isotherm in material properties) is indicated by shading. Unless noted otherwise, the wall had no interior finishes during drying.

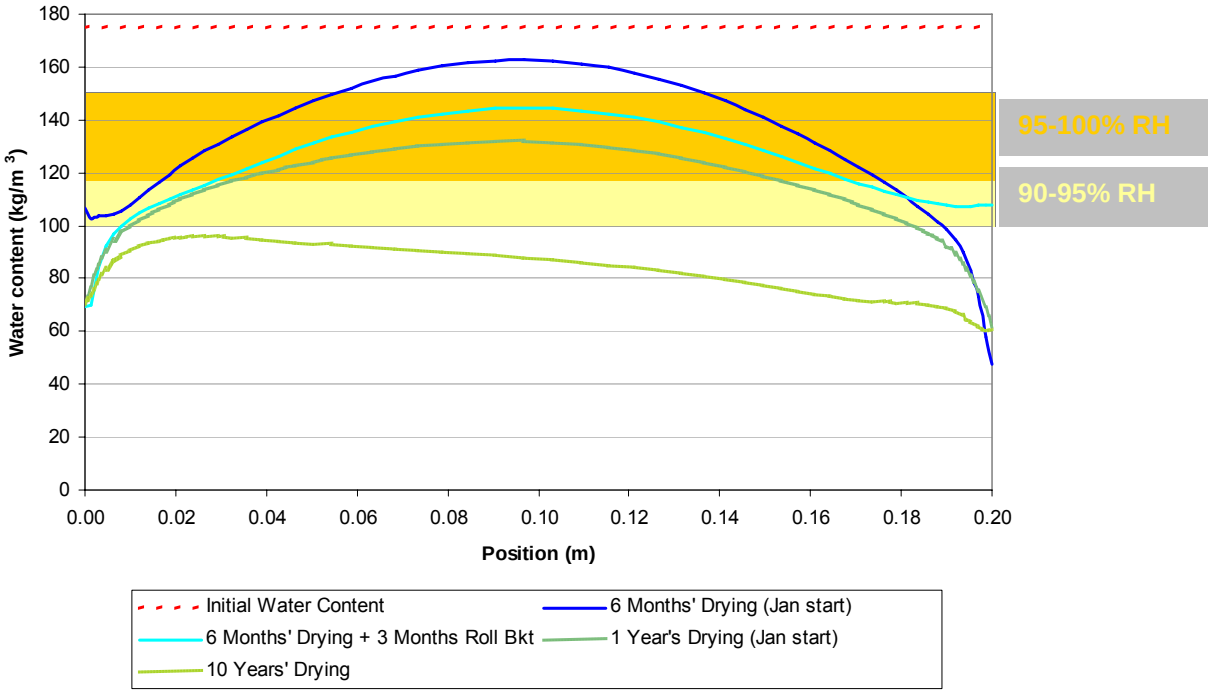

Figure 8.1: Moisture content profiles through concrete thickness (exterior=left; interior=right)

The plot shows that drying occurs to both interior and exterior, even though the wall is exposed to rain. However, drying progresses relatively slowly: even after a year, the majority of the wall's thickness is above 90% RH. This shows that the construction moisture loading can be significant, even after a year of drying. After ten years' of drying, the wall has dried below 90% through its thickness; however, based on additional simulations, it appears that little drying will occur below this level. The asymmetric drying profile at 10 years is due to the fact that rain moisture is introduced at the exterior side, and dries to the interior.

In initial simulations, the profile of six months' drying (January-June) of unfinished wall was used. Simulations of test walls showed a small humidity rise in the insulation cavity at the beginning of the year (September-October), followed by a much larger one at the end of the year (August-September). In contrast, in monitored data, these spikes were of comparable size. It was realized that the roll blanket insulation was applied to the upper part of the wall during the construction process, inhibiting drying to the interior. Therefore, a simulation was run with six months of uncovered wall (January-June), followed by three months with the roll blanket in place (July-September). The resulting profile is shown above: the high humidity front "advances" inwards through the concrete when an

impermeable material is placed inboard of the wall. This modification produced moisture "spikes" of similar magnitude for the two summer/fall seasons.

8.1.1.3 Test Assembly Details

After completion of this setup, simulation of the test walls could begin. One-dimensional simplifications of three assemblies were simulated: 50 mm (2") extruded polystyrene (Wall 1), the fiberglass roll blanket with polyethylene (Wall 2), and the framed 2x4 wall with fiberglass insulation, gypsum board, and latex paint (Wall 4). Most of these materials are already well characterized in WUFI; however, the latex paint was simulated as a separate layer with a vapor diffusion resistance factor (VDRF) that varied with relative humidity, instead of a fixed one (i.e., specifying a interior vapor resistance s_d-value). NRC-IRC data (Kumaran 2002) for "painted" and "unpainted" gypsum board was compared; the painted sample was gypsum wallboard with one coat primer and two coats of latex paint. The net difference in permeance between these the painted and unpainted data was calculated, as shown in Figure 8.2. These values were then made into a 1 mm fictitious layer in WUFI, and applied to the interior side of gypsum board ("interior gypsum board" from ASHRAE TRP 1018); this material has performance very similar to the NRC-IRC data. This approach retains the moisture storage properties of the gypsum board; it also models the vapor resistance of the latex paint at its correct location, at the innermost layer.

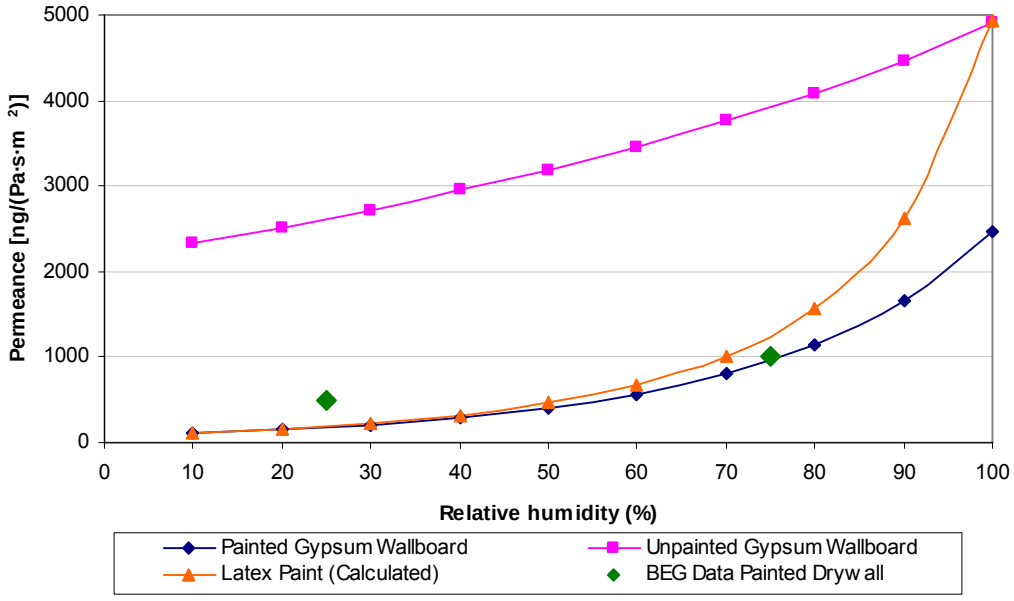

Figure 8.2: Gypsum wallboard permeability data (painted and unpainted) from Kumaran (2002)

However, it should be noted that Building Engineering Group is taking permeability measurements of similar latex paint/gypsum board samples (also plotted in Figure 8.2). Preliminary results are showing slightly different results: wet cup (75% average RH) measurements are in the 1000 ng/(s·m^2·Pa) or 18 perm range, which match NRC-IRC's data. However, dry cup measurements are approximately 400-600 ng/(s·m^2·Pa) (7-10 perms), compared to the 150-200 ng/(s·m^2·Pa) (2.6-3.5

perm) values stated in the literature. Further testing is still in progress; after completion and vetting of these results, they may be applied to simulations.

As a final note, the difference in monitored performance seen between the roll blanket wall and the stud frame/polyethylene wall is worth examining here. The dewpoint at the upper portion of the wall (daily average data) is plotted for the roll blanket, the stud frame with polyethylene, and the stud frame with gypsum/latex paint in Figure 8.3. The performance of the stud frame-polyethylene wall seems to lie between that of the other two walls, changing between seasons (closer to the roll blanket in the summertime, and latex-gypsum in wintertime).

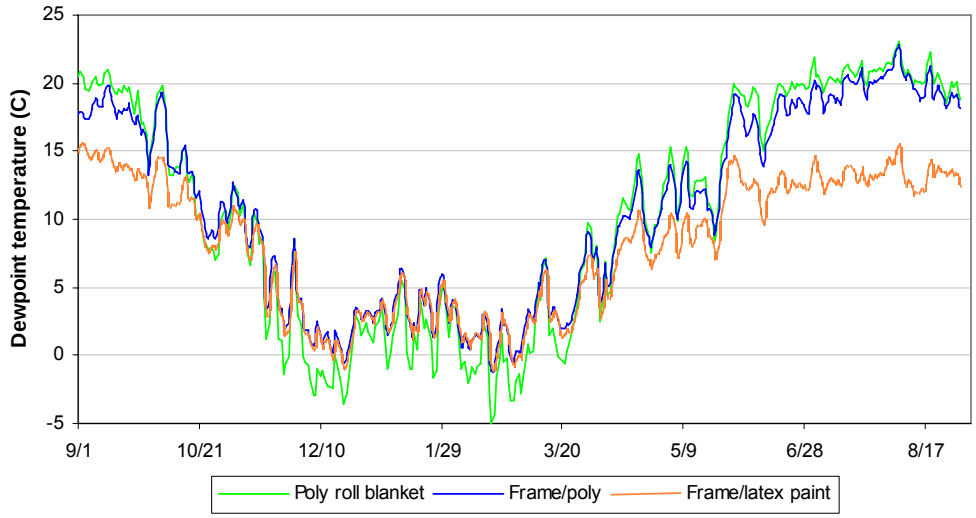

Figure 8.3: Daily average dewpoint (upper portion) comparison of Kitchener walls

There are several possible reasons for this difference. First, although strong efforts were made to air seal the stud frame-polyethylene wall, leakage is more likely in an assembly composed of discrete parts, compared to the "monolithic" roll blanket. Second, the frame-polyethylene wall has wood framing within the cavity (unlike the roll blanket), which provides some hygric storage mass.

Finally, vapor diffusion laterally through the framing members might play some role. The diffusion through the framing is low, given both material properties of wood and its area relative to the face of the wall. However, the permeance through polyethylene is low enough that the wood can provide a noticeable contribution. Using the range of 0.58-7.8 ng/(s·m·Pa)) for wood, this lateral flanking could result in an increase between double and fifteen times the vapor transmission through the polyethylene. Note that the test wall is assembled with an unusually high ratio of exposed framing (32" wide wall, side studs exposed): this effect would be much lower in field-installed walls.

8.1.1.4 Temperature Comparison Between Model and Monitored Data

The first step in validating simulations against data is to compare corresponding temperatures; the thermal performance is often captured more accurately than moisture performance. In the monitoring package, there are sensors located at the "upper" location, which is roughly at exterior grade height. The temperature at the interface between the concrete wall and the interior insulation at this upper

location was compared. Figure 8.4 shows the comparison between monitored and modeled temperatures; the dewpoint temperature in the wall cavity is also included for reference. That plot shows a lack of correspondence between the pattern and range of these temperatures: the modeled temperature is less damped and shows greater extremes than the monitored data. This behavior is most clear during the winter: a detail for November through January is shown in Figure 8.5. Monitored winter temperature minimums are in the 2° C range, while modeled data indicates lows of –8° C.

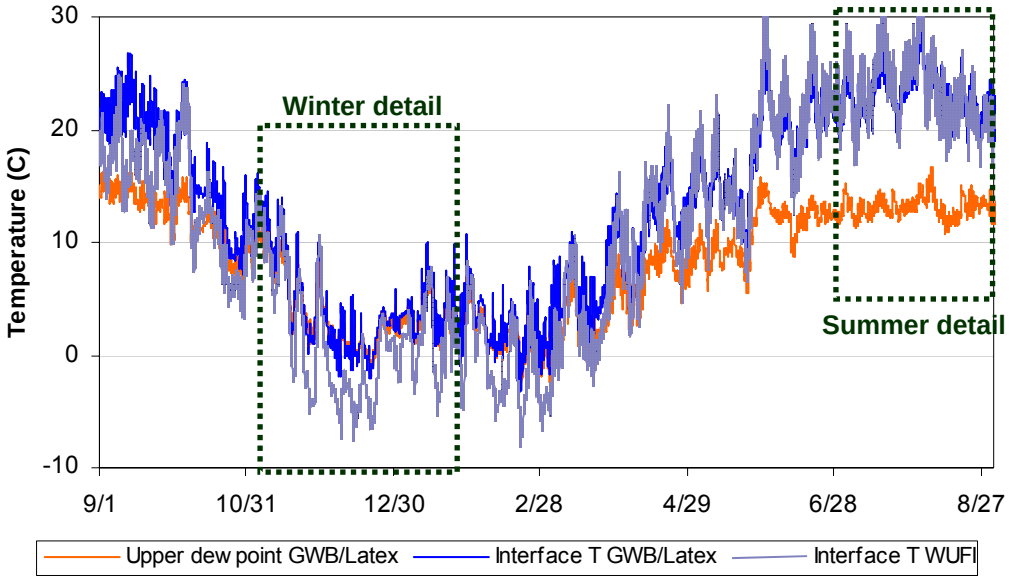

Figure 8.4: Upper height concrete temperature, monitored vs. model (full year)

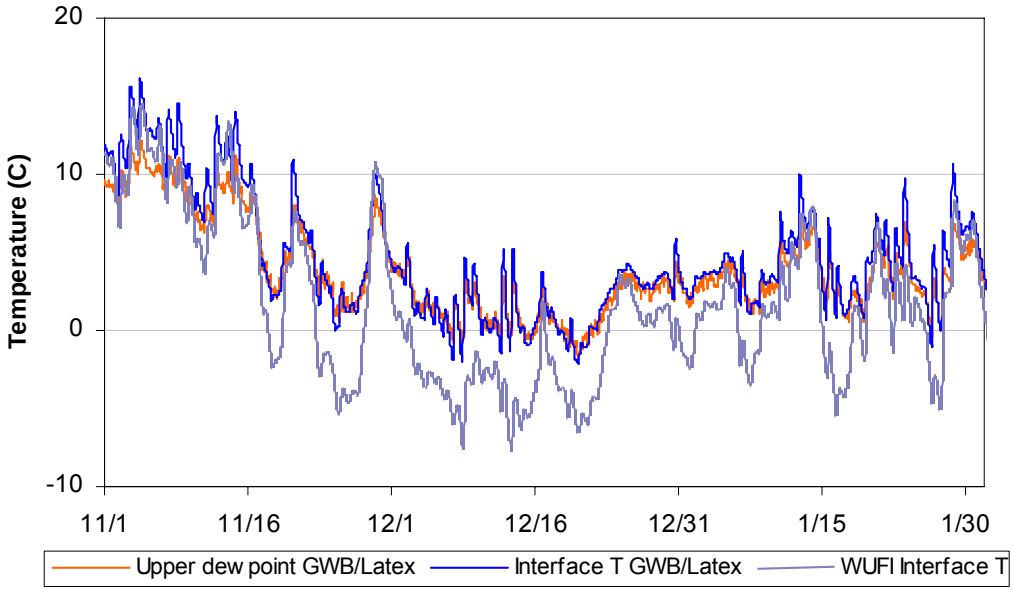

Figure 8.5: Upper height concrete temperature, monitored vs. model (winter detail)

The disagreement between the monitored data and the simulation in summertime is much smaller, as shown in Figure 8.6; the largest mismatches are on the order of 2-3° C, typically during daytime peaks. The monitored data for the framed walls (frame/polyethylene and frame/latex paint) are a close match to the model, while the remaining walls (roll blanket and XPS) show disagreement due to the shading from the adjacent house. In addition, the closer correspondence between monitored and simulated data may be due to the smaller ΔT operating across the wall.

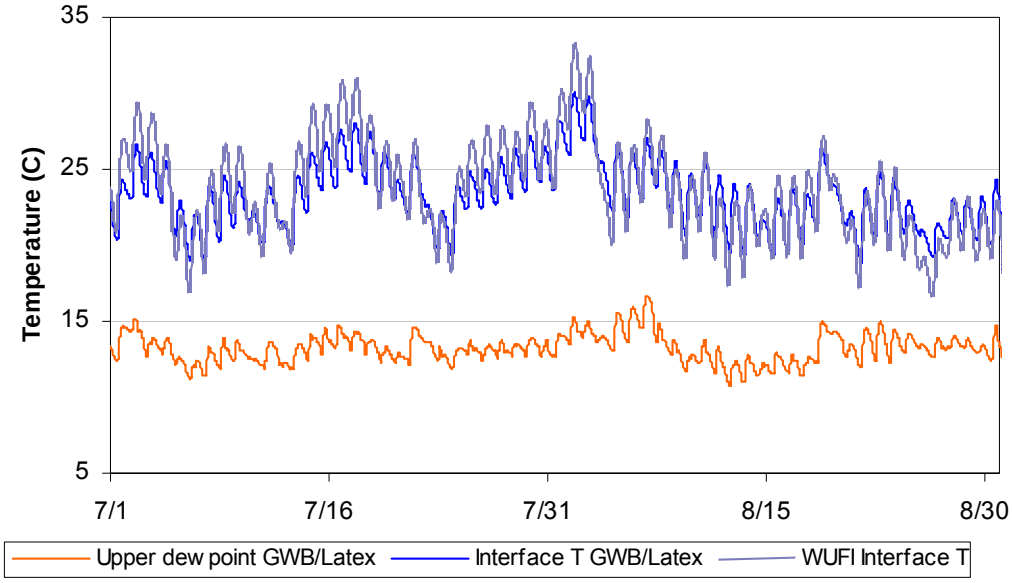

Figure 8.6: Upper height concrete temperature, monitored vs. model (summer detail)

The reason for the strong mismatch between monitored data and simulation (particularly in winter) was examined in more detail. The first approach looked at the possibility that the assembly thermal conductivities (U values) were not set properly; for instance, the insulation might have been compacted or wet, or the concrete drier (and therefore more insulative) than modeled.

The U values of the concrete and fiberglass insulation were used to calculate the relative contributions to the overall R-value of the assembly; these fractions give the temperature drop (ΔT) across each component of the assembly, and therefore the interface temperature under static conditions. According to these calculations, 3-6% of the overall ΔT occurs through the concrete, with the remainder in the fiberglass insulation (for a full analysis, see Section 8.1.2.1)

Then, this contribution of concrete to the overall ΔT was graphed for both the monitored data and the model, as shown in Figure 8.7. There is a great deal of scatter, due to the effects of thermal mass and solar gain. However, the modeled data is centered on the 3-6% range, as predicted by the static calculation. In contrast, the monitored data seems centered on the 20-30% range, which is much too large to be explained by variations in component U values.

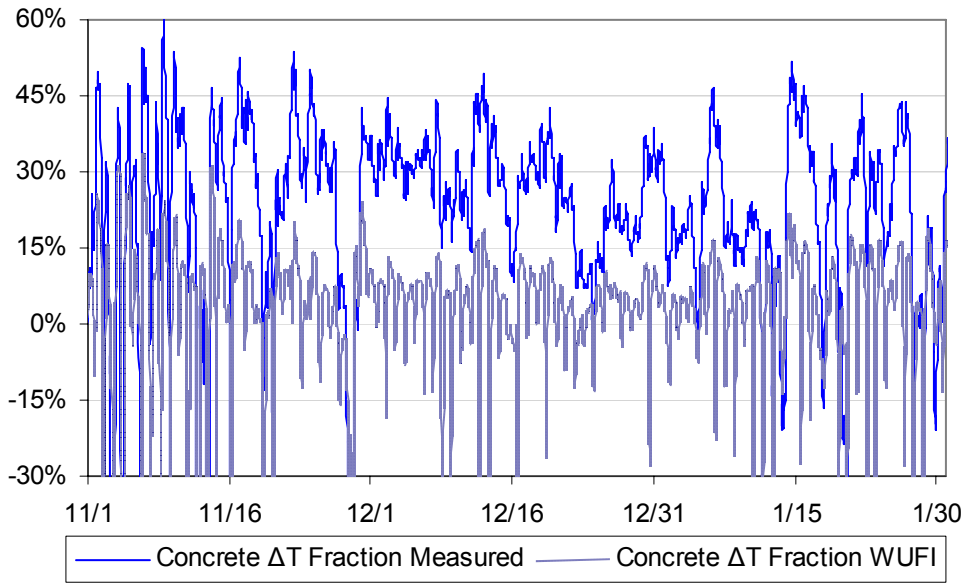

Figure 8.7: Concrete ΔT as % of overall wall ΔT (winter detail); monitored vs. model

Instead, the likely conclusion is that the exterior conditions recorded in weather data do not reflect the temperature difference that is operating across the wall. Looking at the details of the wall assembly at this location, it seems likely that two-dimensional effects are significant (see Figure 8.8). Since the temperature sensor is roughly at grade level, the above-grade and below-grade environments both have an effect. Furthermore, the details at the rim joist, such as the brick ledge and the transition to the insulated wooden framing, result in further thermal anomalies. Finally, the aspect ratio of the wall at this location does not favor a one-dimensional simplification; a taller above-grade portion would be a better candidate. Only a small portion of this wall is reflected by the one-dimensional simplification, so two-dimensional effects seem quite likely.

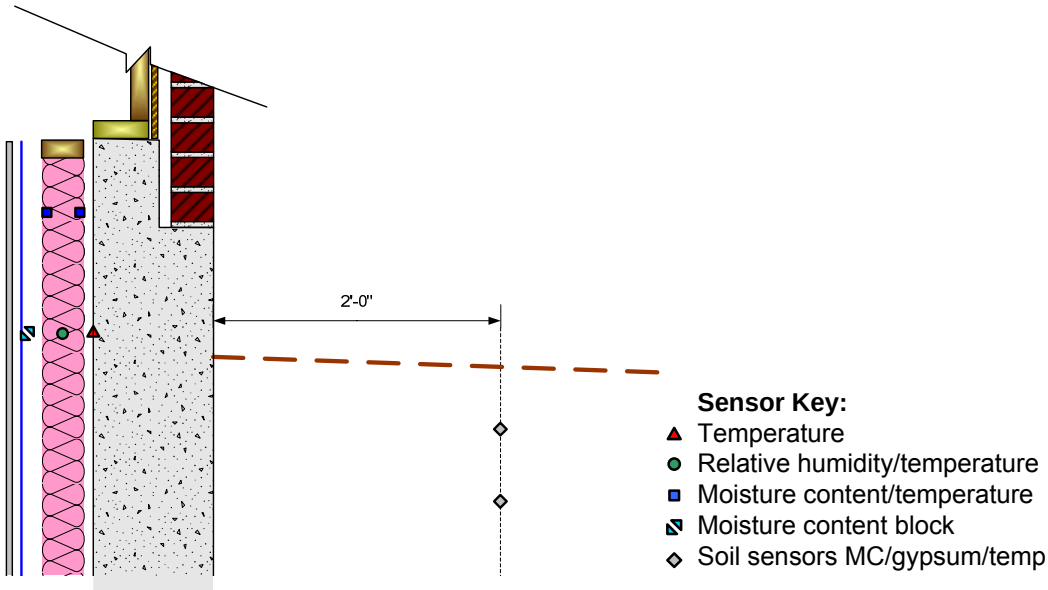

Figure 8.8: Detail of the above-grade monitoring location

Further evidence of two-dimensional effects can be found by plotting the soil temperature at the 150 mm (6") depth with the wall interface temperature and exterior air temperature, as shown in Figure 8.9. The interface temperature tracks much more closely to the shallow soil temperature than the exterior air temperature. In fact, a closer approximation to the concrete interface temperature can be made using a weighted average of the air and soil temperatures ("Weighted Shaded T").

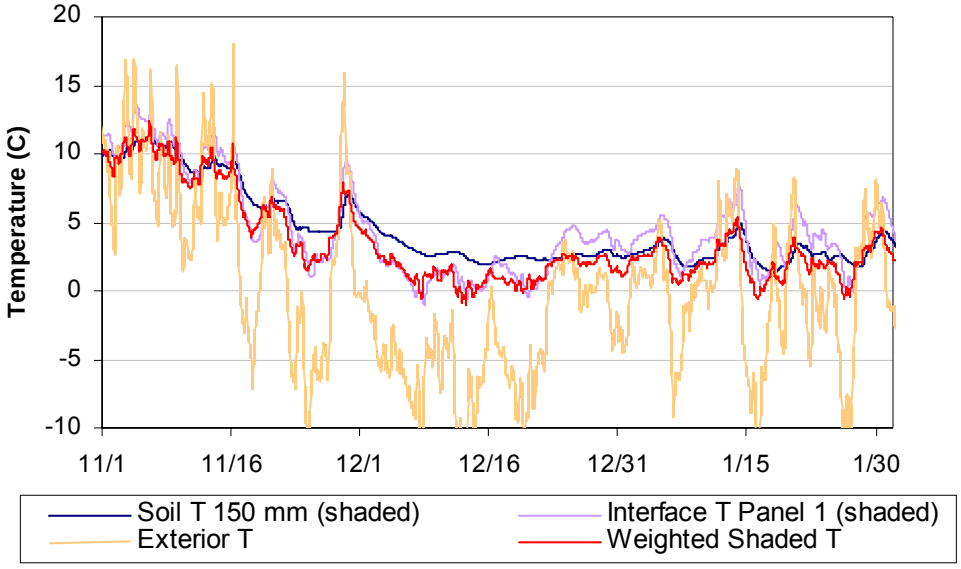

Figure 8.9: Air, soil (150 mm), and concrete interface temperatures (winter detail)

However, this level of extrapolation becomes increasingly difficult to justify. For instance, if this temperature were used as an exterior air temperature, this would require generation of modified exterior relative humidity, rain, and solar radiation levels, thus adding rather questionable boundary conditions.

Another question is whether the specific placement of the temperature sensor (at grade level) causes this poor correspondence when using above-grade boundary conditions. For instance, it seems possible that the upper portions of the above-grade concrete wall are closer to modeled behavior (i.e., colder in winter). First, dewpoint behavior shows that this is unlikely. The dewpoint in an assembly cavity with high vapor permeability (e.g., fiberglass batt) tends to be "pulled down" to the lowest temperature that the cavity is exposed to, when coupled to a hygrically massive material such as concrete. Therefore, if the upper parts of the wall are much colder, the dewpoint should reflect this effect. As shown in Figure 8.5, the dewpoint falls somewhat below the concrete surface temperature, but not by a large margin—nowhere near the –8° C lows seen in the simulation.

Secondly, a vertical temperature gradient of the wall was taken during a wintertime (late January 2007) field visit to the experimental site, as detailed in Chapter 6. Temperatures were measured using an infrared thermometer, from the top of the wall to the "mid-height" location, as shown in Figure 8.10 and see Figure 8.11. Exterior temperature was in the –8-9° C range during these measurements.

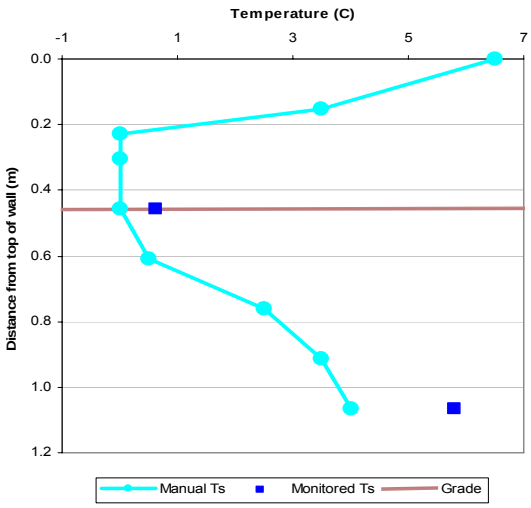

Figure 8.10: Vertical temperature gradient in frame-latex wall

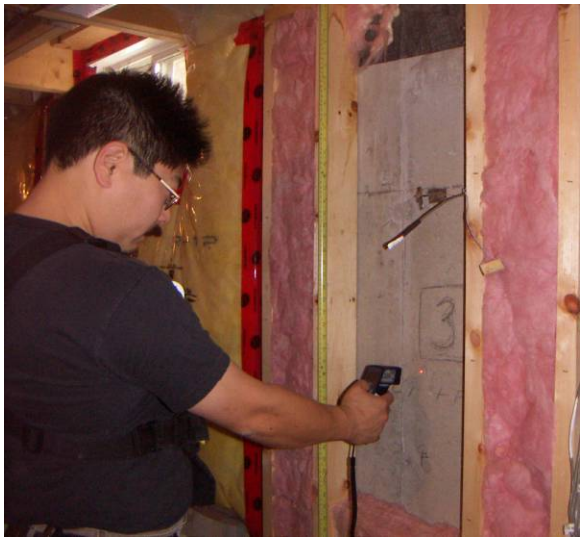

Figure 8.11: Measurement of concrete-insulation interface temperatures

Similar to the monitored data, a large portion of the ΔT (-8 or 9° C exterior; 20° C interior) occurs through the concrete. Also, the uppermost portions of the concrete-insulation interface are warmer (not colder) than the monitored T. This is likely due to the insulative effects of the brick airspace, as shown in the Figure 8.8. The U-value of 1" of still air (the brick drainage/ventilation space) is 1.2 $W/m^2 \bullet K$, while 8" of concrete is an order of magnitude greater at 7-13 $W/m^2 \bullet K$. Ventilation of the airspace will reduce its insulating value, but the overall relationship still stands.

The data for a Chicago-area basement site was similarly examined; it also showed higher wintertime temperatures at the concrete-insulation interface than would be predicted by a one-dimensional model. This basement had an even smaller portion exposed above grade (150-200 mm/6-8") than the Kitchener basement.

This lack of temperature correspondence at the above-grade portion makes the goal of validation and calibration of the simulation difficult. However, these simulations can still serve some use. A taller exposed above-grade section is more likely to have temperatures closer to the simulation. The resulting colder concrete-insulation interface temperature would be more challenging for wintertime condensation. Therefore, the simulation may be able to provide some insight for these worst-case extremes, even if they were not experienced at the experimental site. Modeling of these assemblies (using the Kitchener site data) is thus presented under the extrapolation modeling section.

8.1.2 Below Grade Validation Simulations

Like the above-grade validation simulations, the below-grade simulations required the development of boundary conditions and initial conditions.

8.1.2.1 Boundary Conditions

Soil temperatures were measured at multiple depths outside of the basement; the intent was to create exterior below-grade boundary conditions from this data. However, as shown in Figure 8.8, the soil measurement locations do not line up directly with the wall monitoring locations. In addition, no soil sensors were placed at a depth matching the "lower" wall position. Therefore, an alternate approach to creating exterior boundary conditions was used.

The temperature at the interior concrete surface (the interface between the insulation and concrete) was measured at all three monitoring heights (low, middle, high), parallel to other wall measurements. Given the low insulating value of the concrete, it seemed likely that the temperature on the interior of the concrete would be similar to the temperature at the exterior. Therefore, the relative R-values of the concrete and insulation were compared; the fractional contributions determine the temperature drop across each component. The concrete wall and RSI-2.3 (R-13 imperial) batt insulation were compared. Using thermal conductivity values for concrete of 1.4 to 2.6 W/m·K, the temperature drop across the concrete should be 3-6% of the total ΔT. Given this small contribution, it appears that this approach will provide reasonable results. Since temperatures at the deepest "lower" locations varied on the order of 1-2° C between walls, 3-6% of the ΔT across a wall would be smaller than this variation. In addition, at the below grade monitoring locations, the diurnal variations have been completely damped out; this should allay concerns of inaccuracies due to the thermal mass of the concrete.

The exterior below-grade relative humidity was set to a constant 100%. No rain was included in these climate files, which would have been used to simulate liquid water wetting from poor drainage, incomplete dampproofing, or other capillary sources.

Like the above-grade wall, it seems possible that two-dimensional effects might reduce the accuracy of the simulation: for instance, the lower location could be affected by thermal bridging at the floor slab and/or footing. The fact that the temperature gradient varies continually with height is also a concern.

8.1.2.2 Assembly Initial Conditions

Like the above-grade wall, the starting moisture content of the concrete had to be estimated, due to the moisture load it adds to the assembly. Drying simulations were run, using the below-grade boundary conditions. First, several parametric simulations were run to determine the effects of some extrapolations beyond the monitored walls, as shown in Figure 8.12.

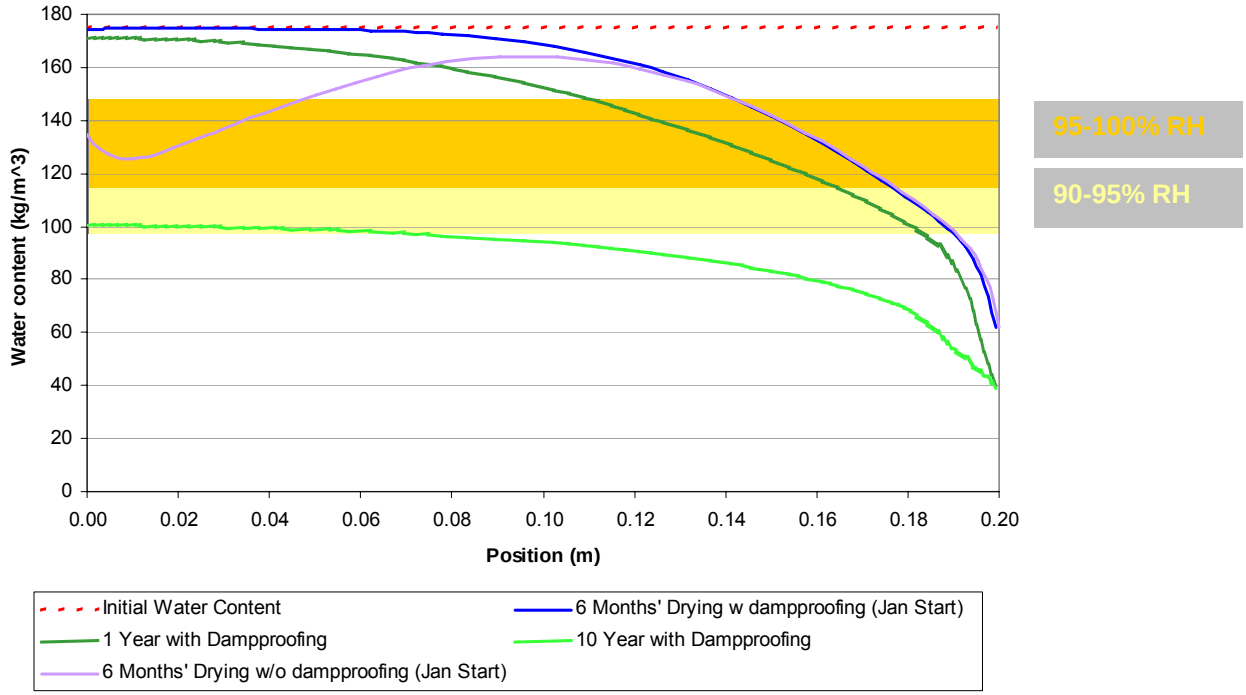

Figure 8.12: Concrete moisture content; parametric drying studies (exterior=left; interior=right)

Initially the wall (at mid height) was dried for six months, one year, and ten years. Like the above grade wall, after six months, the majority of the wall is still over 90% relative humidity; this is still the case after a year of drying. After ten years, the wall has largely dried below this level.

Due to the dampproofing layer, all drying is to the interior; as an alternative run, this initial drying was done with the dampproofing removed. This simulation shows drying to the exterior, which seems counterintuitive, given that the exterior is at 100% RH. However, there is a thermal gradient across the wall (interior is warmer than exterior); this creates a vapor pressure gradient that results in the outwards drying. Note that this is by no means a recommendation for the elimination of dampproofing. The effect of liquid water as a boundary condition was not included in these simulations; without dampproofing, any liquid water due to poor drainage, clogged footing drains, etc., would result in wetting of the concrete from the exterior, and a significant moisture loading.

The moisture profiles used as initial conditions for the simulations are shown in Figure 8.13. At the "middle" height of the wall, the roll bag insulation was installed before installation of the test walls; the effects are shown ("6 Months' Drying + 3 Months' Roll Blanket"): the higher concrete moisture levels redistribute towards the interior side, since that interface is no longer in equilibrium with dryer interior conditions. At the lower location, no insulation was installed before the test walls, so the profile for nine months of drying was used.

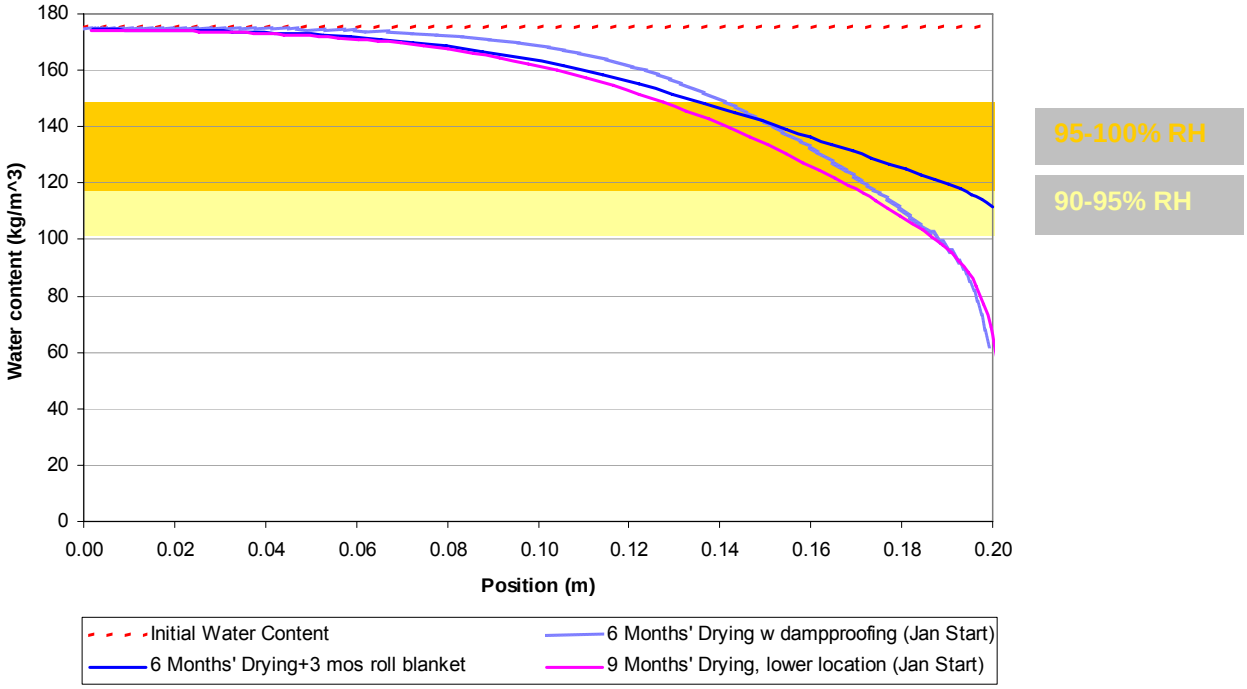

Figure 8.13: Concrete moisture content; initial conditions for simulation (exterior=left; interior=right)

8.1.2.3 Test Assembly Details

The simulated test assemblies were identical to their above-grade counterparts, except for the addition of dampproofing to the exterior of the concrete. Dampproofing options used in industry include cutback asphalt and asphalt emulsion products; in both cases, a 1/16" (1.6 mm) coating is recommended in manufacturer's specifications. Therefore, a 1/16" layer of cutback asphalt was simulated; *ASHRAE Fundamentals* (2005) gives a value of 8 ng/(s·m^2·Pa) or 0.14 perms.

The wall assembly, as simulated, did not include the use of the dimple mat drainage board. Since liquid water capillarity from the exterior was not simulated, it should not make any difference. Furthermore, simulating the air space would decrease accuracy of the boundary conditions generated by concrete interface temperatures.

In the simulation, transfer coefficients were set for below-grade conditions: the exterior temperature was directly coupled to the wall's exterior surface, without a heat transfer coefficient (i.e., "Basement" condition); no coatings or special transfer coefficient were used.

8.1.2.4 Simulation Results and Analysis: Mid Height

After running simulations, the simulation results were compared with monitored data. Due to the setup of the boundary conditions, temperature correspondence was high. The critical metric for moisture performance, however, is relative humidity. The monitored relative humidity data at the mid-height location, at the concrete-insulation interface, is shown in Figure 8.14.

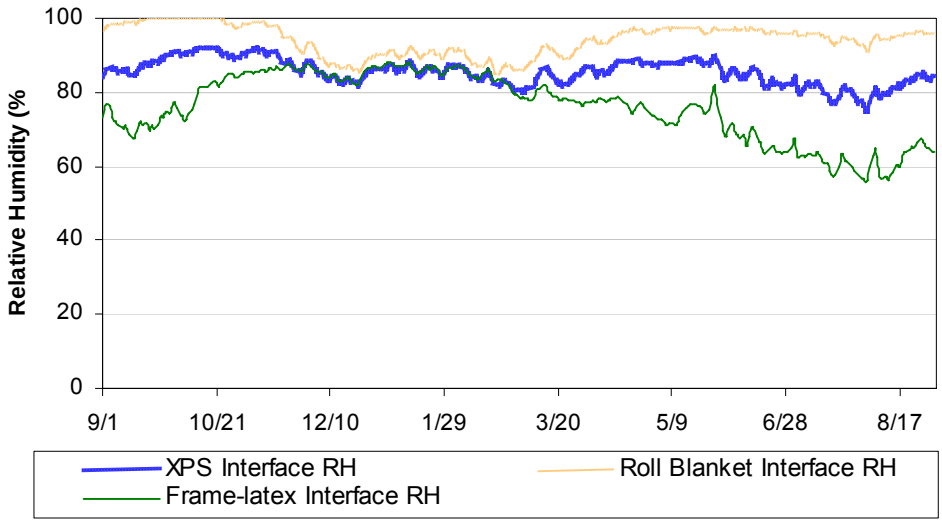

Figure 8.14: Monitored data: mid-height RH sensors at concrete-insulation interface

Behavior patterns are briefly described here, to see if they are matched in the model. The roll blanket, being the least permeable, has the consistently highest relative humidity levels. The interface is near saturation in fall, spring, and summer, dropping to ~90% RH in winter. The XPS wall shows moderately steady behavior, in the 80-90% RH range. And the fiberglass stud/latex paint wall has the driest behavior; it is at its peak during winter when the concrete wall is coldest. These three assemblies are generally ordered (wettest to driest) in the order of least permeable to most permeable.

There are moisture content surrogate sensors ("wafers") at the same location as these relative humidity sensors (concrete-insulation interface, mid height). The moisture content measurements can be related to relative humidity using the sorption isotherm for wood (Straube and Burnett 2005); the resulting data (using a curve fit) is plotted in Figure 8.15.

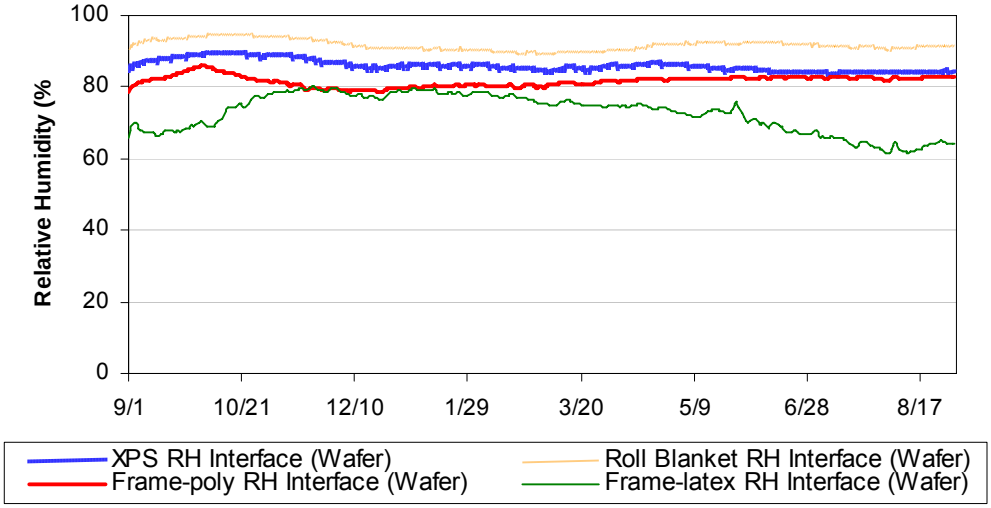

Figure 8.15: Monitored data: mid-height wafer sensors (calculated RH) at concrete-insulation interface

The wafer data shows a reasonable correlation with the relative humidity behavior shown in Figure 8.14 (such as the relative order and annual curve shape), but with slightly lower values and less response to transient changes. Note that this plot also includes wafer data for the frame-polyethylene wall, which was unavailable in the RH data. Also, similar to the data shown in Figure 8.3, the frame-polyethylene wall shows behavior between the roll blanket and frame-latex walls.

The corresponding data from the simulation is shown in Figure 8.16. The two low-permeance systems (roll blanket and XPS) behave very differently than the monitored data. In the simulation, relative humidity levels quickly rise to the 95-100% range for both of these walls, and stay at that level for most of the year. In contrast, the monitored data shows humidity levels of 85-100% for the roll blanket, and 80-90% for the XPS. The fact that the monitored data is drier than simulation has several possible explanations: perhaps, despite best efforts, there is some air leakage or communication from the interior space to the concrete-insulation interface. Given the relative humidity levels during the test year, this would result in drying of the assembly. Second, the possibility of vapor diffusion "flanking" through the edge framing of the panel was discussed above; this would also cause drying. Finally, it is possible that more drying of the concrete occurred before the installation of the insulation than simulations would indicate. The significant influence of the sorption isotherm in the high RH range also makes the simulations highly sensitive to the material property data input. Needless to say, all of these RH levels are high and cause for concern.

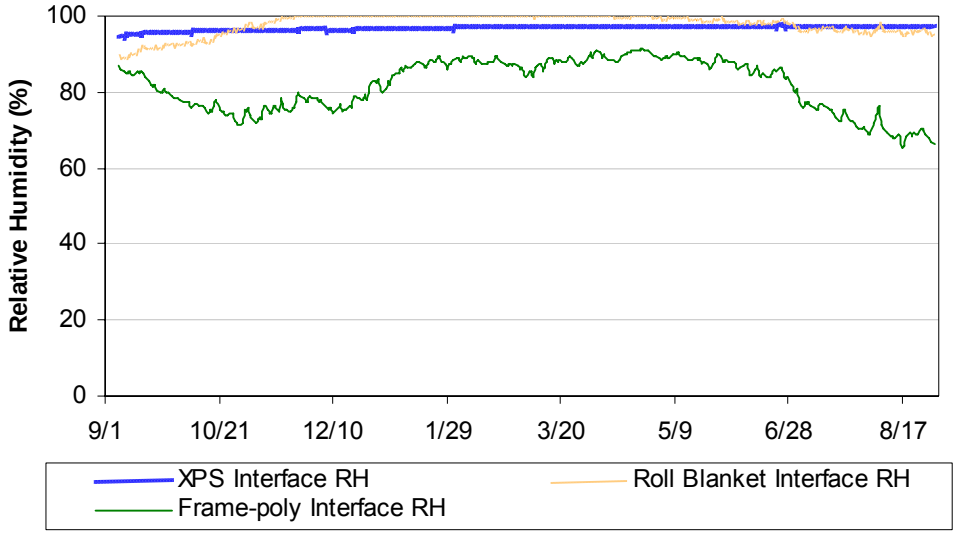

Figure 8.16: Simulation data: mid-height RH at concrete-insulation interface

The lack of correlation for the roll blanket wall is understandable, given the work of TenWolde and Carll (1998). They note that a very low permeance material (such as polyethylene) can effectively be bypassed by a very small air leak, as discussed in Chapter 3. Creating an air barrier system that would prevent this bypass would require an "extraordinary level of airtightness," well beyond the levels achievable in construction. Since these simulations did not account for airflow, no air bypasses the polyethylene layer and therefore it is fully effective at limiting water vapor flow.

The latex paint wall shows slightly better correspondence; the test wall operates a roughly similar humidity regime as that shown in the simulation. However, the peak values are not coincident; in the

monitored data, the large rise occurs in early winter, while in the simulation, it occurs in mid-winter, and remains at high levels through the spring. A possible explanation may come from dry-cup permeance values of latex paint; as mentioned earlier, preliminary test by Building Engineering Group show higher permeance values than the published literature. This difference would allow greater outwards vapor diffusion (and thus wetting of the assembly) during the winter. This could explain the earlier rise seen in the monitored data.

8.1.2.5 Simulation Results and Analysis: Lower Height

A similar examination was made for the data at the lower wall location; however, correlations were hampered by the limited data available in the field monitoring. Lower-height relative humidity sensors were only installed in the frame walls (polyethylene and latex paint), and moisture surrogate "wafer" sensors were installed in the XPS and roll blanket walls. However, the roll blanket "wafer" sensor did not return valid data until a modification made during a recent field visit. The monitored data is shown in Figure 8.17.

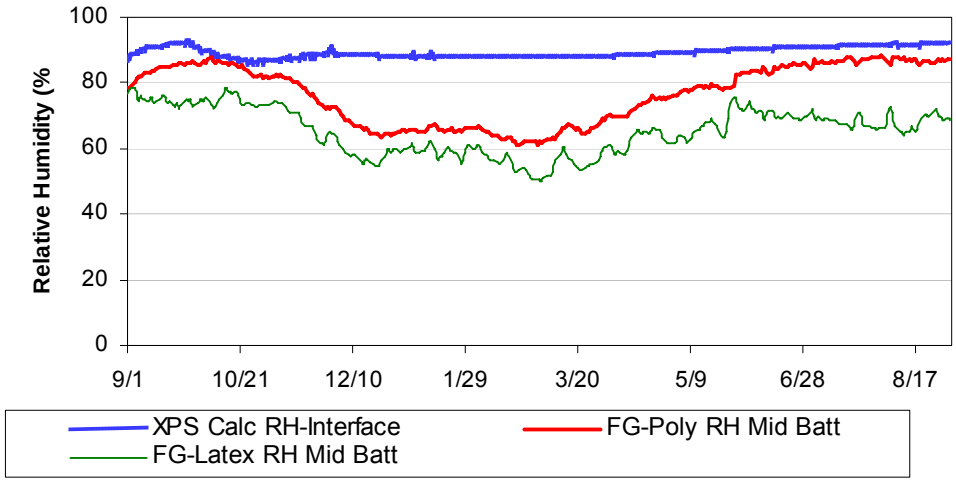

Figure 8.17: Monitored data: lower-height RH at interface and mid-batt

Note that this graph plots data from two different wall locations: the concrete-insulation interface (in the XPS wall), and mid-thickness in the batt (in the frame walls). The corresponding simulated data is shown in Figure 8.18.

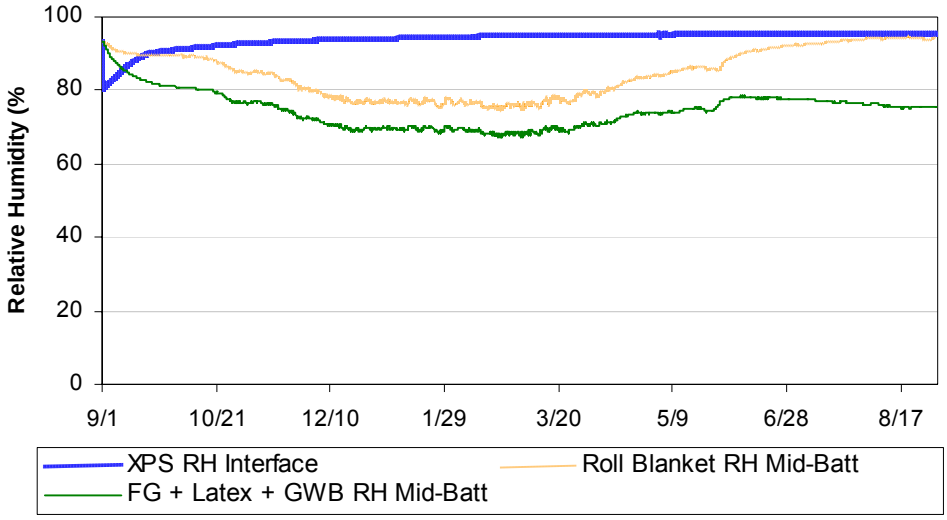

Figure 8.18: Simulation data: lower-height RH at interface and mid-batt

Again, the simulation captures the relative relationships between the relative humidity in the assemblies, but there is less accuracy in the absolute magnitudes. Note that unlike the "middle" height work, the roll blanket simulation is being compared to data from the framed wall with polyethylene.

In both the polyethylene and gypsum wallboard/latex paint simulations, the difference in performance can be explained by reasons stated earlier. The frame/fiberglass/polyethylene wall showed some evidence of moisture storage or bypass of the vapor control material, either by air leakage, flanking diffusion, or a drier initial state of the assembly.

Despite the marginal overall correspondence between monitored data and simulations, in all cases, the simulation shows higher humidity levels than in reality. Therefore, the simulation shows more challenging conditions in the assembly than experienced in reality, which means the simulation could be used as a conservative worst-case version of the situation.

8.2 Extrapolation Simulations

The extrapolation simulations use the walls developed earlier with different interior and exterior conditions. Given the lack of temperature and humidity correspondence between the validation simulations and experimental results, the value of these extrapolations might be questioned. Specifically, the above-grade simulations showed significantly lower concrete-insulation interface temperatures than measured results, and the below-grade simulations captured relative moisture behavior between walls, but not absolute magnitudes. However, as discussed in 8.1.1.4, the above-grade simulations provide a worst-case result for wintertime condensation. The below-grade simulations can be used to gauge relative risk between assemblies; however, judging absolute risk of failure would be rather tenuous.

Two topics are discussed before proceeding with the full complement of simulations. First, due to the lack of temperature correspondence between the Kitchener site data and simulations, the runs using site data are presented here under extrapolations. Second, in analyzing the results, it was useful to develop an indicator of likelihood of condensation and/or rundown of moisture accumulation at an interface, due to the strong effects of liquid water on mold growth. Specifics on incorporating this tool into the simulation and interpretation of results are discussed.

Extrapolations are divided into the above-grade and below-grade simulations; exterior weather locations used included Toronto, ON, Vancouver, BC; St. John's, NL; and Edmonton, AB. Various interior relative humidities were simulated, including "low," "mid," and "high" loadings. Finally, assemblies not tested at the Kitchener site were simulated. They included "bounding" conditions (i.e., no interior vapor control), and some materials currently used for interior basement insulation (perforated facer roll batt, Kraft paper-faced batt).

8.2.1 Above Grade Simulations for Kitchener Site

Due to the lack of temperature correspondence between simulations and monitored data at the above-grade portion of wall, these simulations are presented as extrapolations. However, there were some similarities noted between the simulations and monitoring, when channels were available.

A comparison of relative humidities at the interface between the concrete and insulation is shown in Figure 8.19 (simulated data for roll blanket and fiberglass/GWB/latex paint) and Figure 8.20 (monitored data for roll blanket, fiberglass/poly, and fiberglass/GWB/latex paint). This interface is of particular interest because it is the likely location for wintertime condensation.

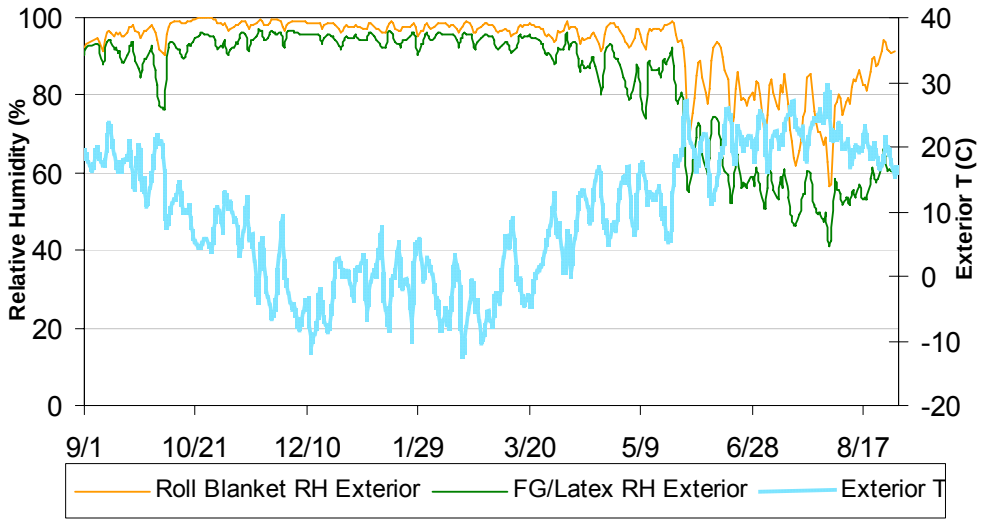

Figure 8.19: Simulation data: relative humidity at concrete-insulation interface, above-grade

A caveat must be noted for the monitored data: this is a calculated relative humidity value, based on the dewpoint temperature measured at the middle of the insulation, and the temperature of the concrete surface. As the vapor resistance of batt insulation is very low, this is a reasonable assumption for the purposes of this calculation.

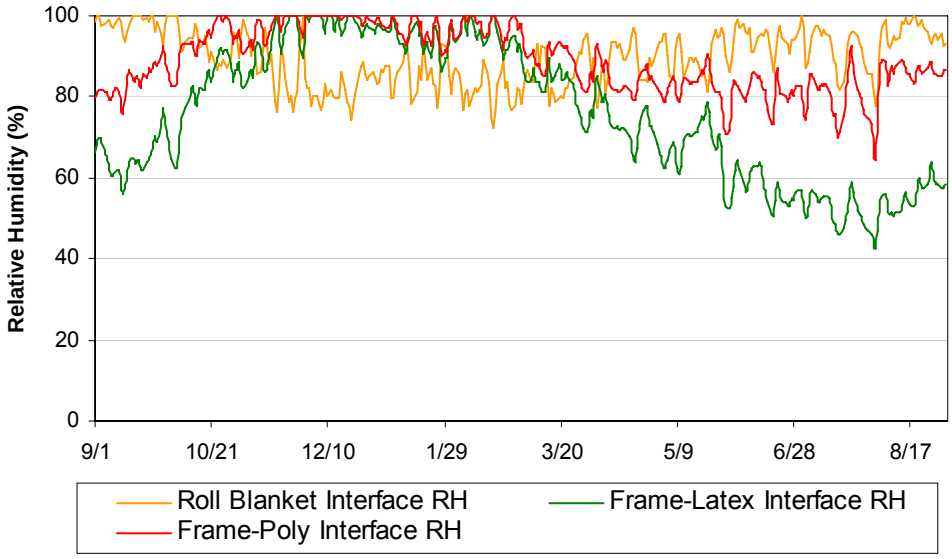

Figure 8.20: Monitored data: relative humidity at concrete-insulation interface; above-grade

Overall, relative humidity correspondence is relatively low, as would be expected by the lack of temperature correspondence. In the simulation, the polyethylene (roll blanket) and latex paint walls both show extended periods at high (90%+) relative humidity; this continues through the spring, until the temperature gradient shifts inward (mid-May). At that point, both relative humidity levels drop, and the latex paint wall shows lower humidity than the polyethylene wall, since it allows drying to the interior.

In contrast, the monitored data for the two frame walls shows a shorter period of high wintertime RH, dropping in mid-March. This can likely be ascribed to the warmer temperatures seen at this interface, due to the two-dimensional effects mentioned earlier. In the winter, the roll blanket wall has humidity levels substantially lower than the simulated wall (~80-90% RH, vs. 90%+ RH). At the end of the winter, the latex paint wall RH falls (like the simulation); however, the polyethylene-based walls (roll blanket and frame-poly) remain at higher levels.

Similar plots are shown for relative humidity at the interface between the insulation and the interior vapor control layer (polyethylene, or exterior face of gypsum board), to show the possibility of summertime condensation due to inward vapor drives. The interface between the concrete and XPS is also included in these plots. In the test walls, moisture content wafers were placed at these locations; therefore, a plot showing calculated relative humidity is shown for comparison. This metric introduces a fair amount of error; however, it is useful for examining high humidity conditions. The simulated data is shown in Figure 8.21, and the monitored (wafer) data in Figure 8.22.

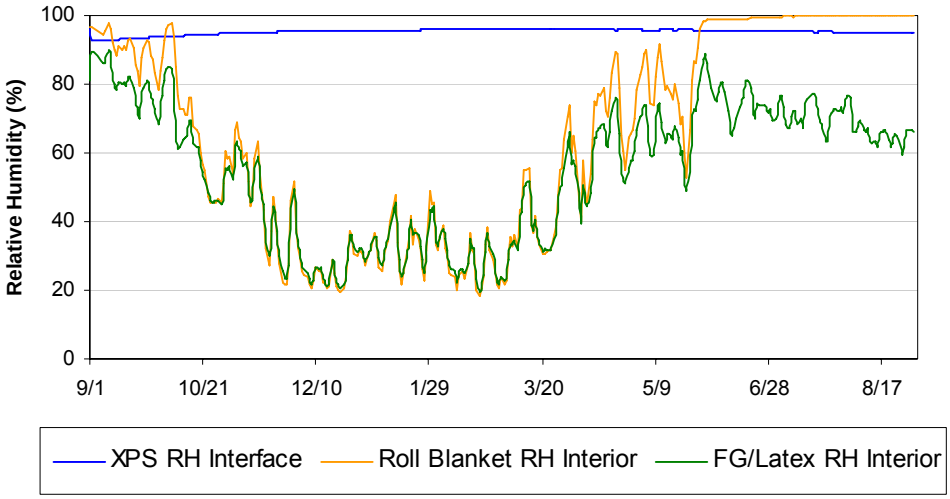

Figure 8.21: Simulation data: upper-height relative humidity at interior interface

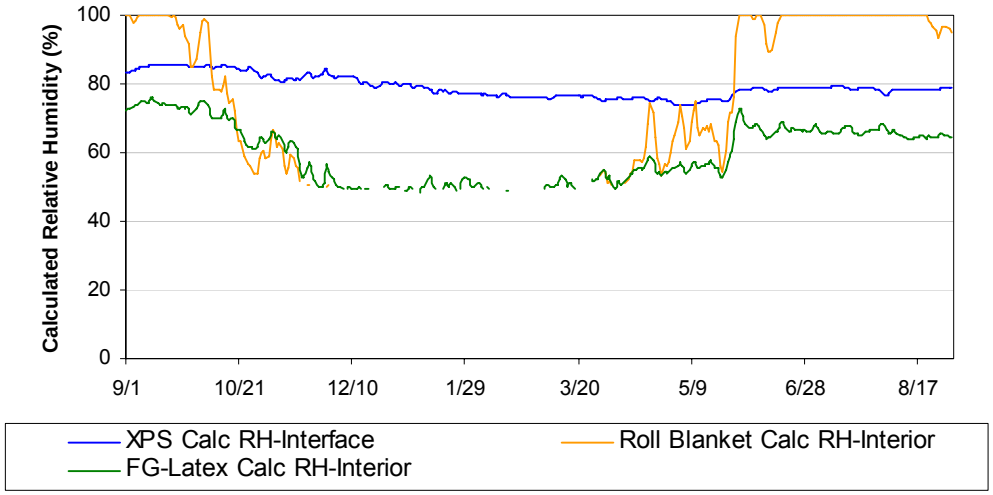

Figure 8.22: Monitored data: upper-height wafer sensors (calculated RH) at interior interface

These summertime comparisons seem to be a slightly closer match than the previous comparisons. Like the comparison between simulated and monitored data at the below-grade portion of the wall (Sections 8.1.2.4 and 8.1.2.5), the XPS wall has higher sustained RHs in the simulation. The summertime plots of the roll blanket and fiberglass/latex paint walls have similar patterns: summers with high relative humidity are seen in the roll blanket wall, while the latex paint wall allows drying.

However, the simulation has much lower relative humidity levels during the winter. Again, this can be explained by the lower temperatures seen at the concrete in the simulations (relative to monitored data). The cold concrete will "pull down" the dewpoint in the fiberglass insulation, resulting in humidity levels in the 20-40% range.

Overall, similar behavior patterns are seen between the simulation and monitored data; however, the lack of temperature correlation impedes the direct validation of the model.

8.2.2 Condensation Layer Diagnostic Tool

8.2.2.1 Development of the Condensation Layer

Although the risk threshold for the onset of mold growth is typically stated as 80% RH or higher, more recent research has shown that mold growth is greatly intensified by the introduction of liquid water (Doll 2002, Black 2006). Therefore, measuring the occurrence of condensation and duration of wetting is useful to determine relative risks of assemblies.

Second, although condensation may momentarily occur, it can be safely stored in the assembly and then released in more favorable conditions. This type of storage has been quantified by the German DIN 4108 Standard (Deutsches Institut für Normung 1999), which specifies maximum condensation levels in the design of wall assemblies, based on the limits of storage at the interface before rundown of liquid water occurs. The standard allows maximums of 500 g/m^2 for non-absorptive materials, or 1000 g/m^2 for absorptive materials (e.g., wood sheathed walls). As discussed in Chapter 2, these

limits may be quite generous, especially when compared with measurements of liquid water stored by surface tension on non-absorptive surfaces such as polyethylene film and acrylic plastic (Smegal 2006). These measurements showed storage levels of 35-65 g/m^2. It is likely that the DIN standard includes other forms of storage, such as surface tension within fiberglass batt insulation, and adsorption or absorption in the wall materials.

With this limit in mind, a useful criterion to estimate the risk of a wall assembly is to determine the maximum condensation seen in the simulation, and to compare it with this limit. This was done in WUFI by creating a fictitious "condensation layer" material, based on cellulose insulation, but with a very steep moisture storage function (sorption isotherm); the storage at 100% RH was set to the condensation limit. This fictitious layer was specified as 1 mm thick, which simplified setup, given the equivalence between 500 g/m^2 and 500 kg/m^3 at this thickness.

The remaining properties were set to minimize the impact of this layer on the simulation. The diffusion resistance factor (DRF, [-]) was set to 0.5 (twice as permeable as a layer of "still air," similar to the "Air Layer" materials in the WUFI database). The specific heat was set to a small figure (100 J/kg·K). All of the remaining hygric extensions (material properties) were left blank.

No.	RH [-]	Water Content [kg/m³]
1	0,0	0,0
2	0,35	0,1
3	0,65	0,2
4	0,8	1,0
5	0,9	10,0
6	0,95	15,0
7	0,99	20,0
8	1,0	500,0

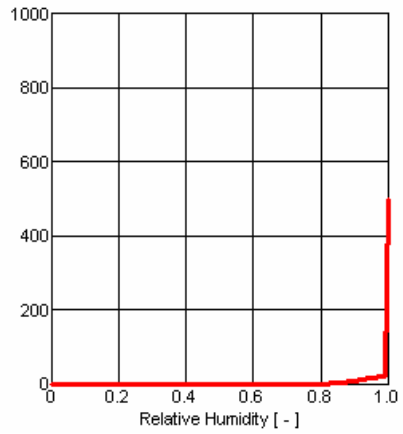

Figure 8.23: Sorption isotherm for WUFI imaginary condensation layer

This material was incorporated in simulations at interfaces likely to have condensation, based on monitored data.

8.2.2.2 Sample Use of the Condensation Layer

A sample use of this condensation layer is shown in the figures below, which examine the relative humidity at the interface between the concrete and insulation at the upper portion of walls with roll blanket insulation, fiberglass/latex paint, and no vapor control (but no air transport/bypass). In the whole-year plot (Figure 8.24), the high wintertime humidity levels are difficult to read.

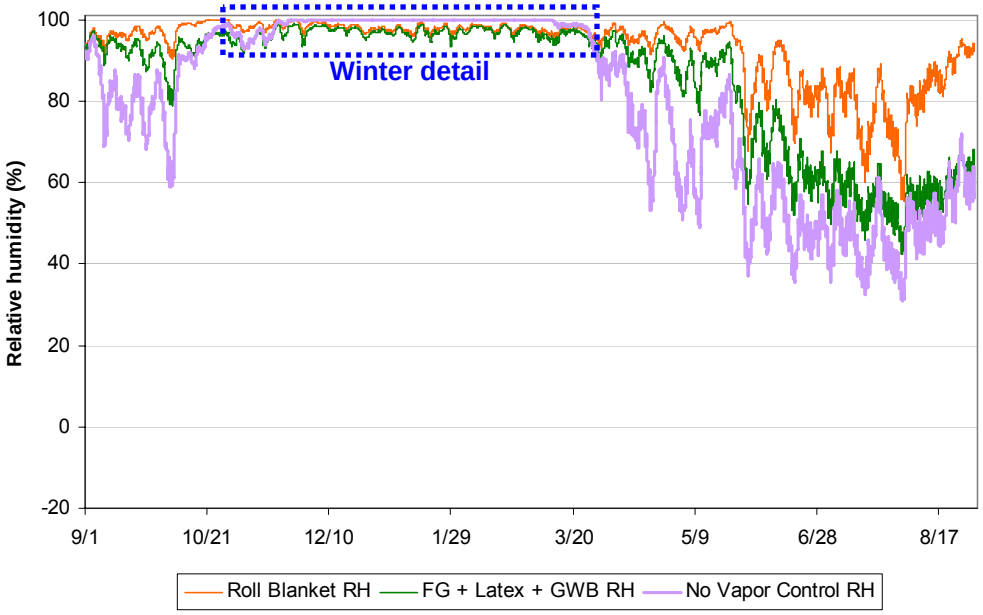

Figure 8.24: Simulation relative humidity at concrete-insulation interface, above grade portion

Greater resolution can be seen in the winter detail (Figure 8.25): it shows that the "no vapor control" wall remains at 100% RH for much of the winter, while the other walls vary between 95-99% RH. Although this suggests that condensation is occurring at the "no vapor control" wall, it does not give an indication of the magnitude of the accumulation.

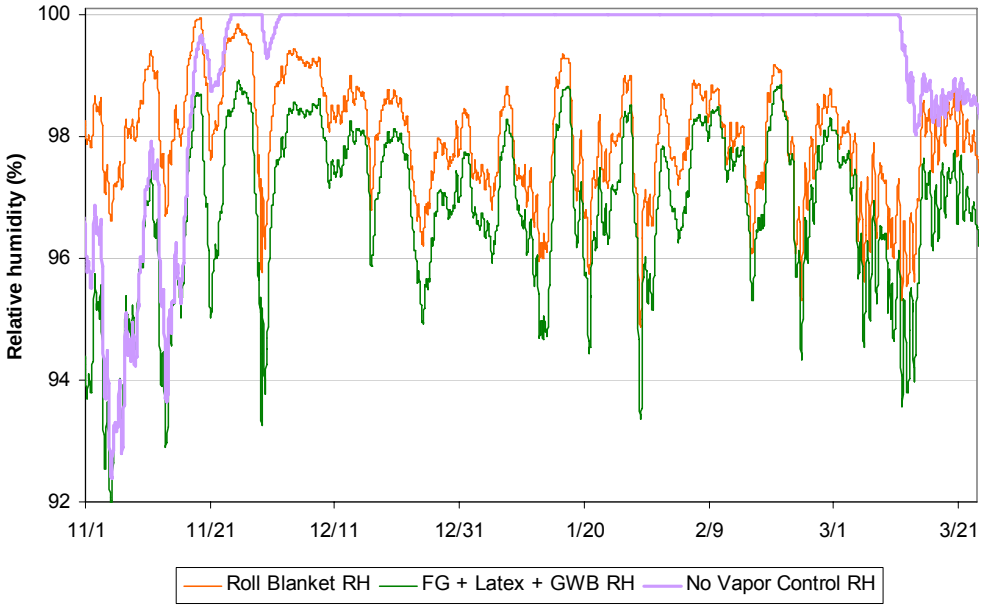

Figure 8.25: Simulation relative humidity at concrete-insulation interface, winter detail

The relative performance of these walls is much more clear when the moisture content of the condensation layer is plotted in Figure 8.26 below; the accumulation can be compared with the 500 g/m^2 limit used in the DIN 4108 standard. Exterior temperature is plotted for reference.

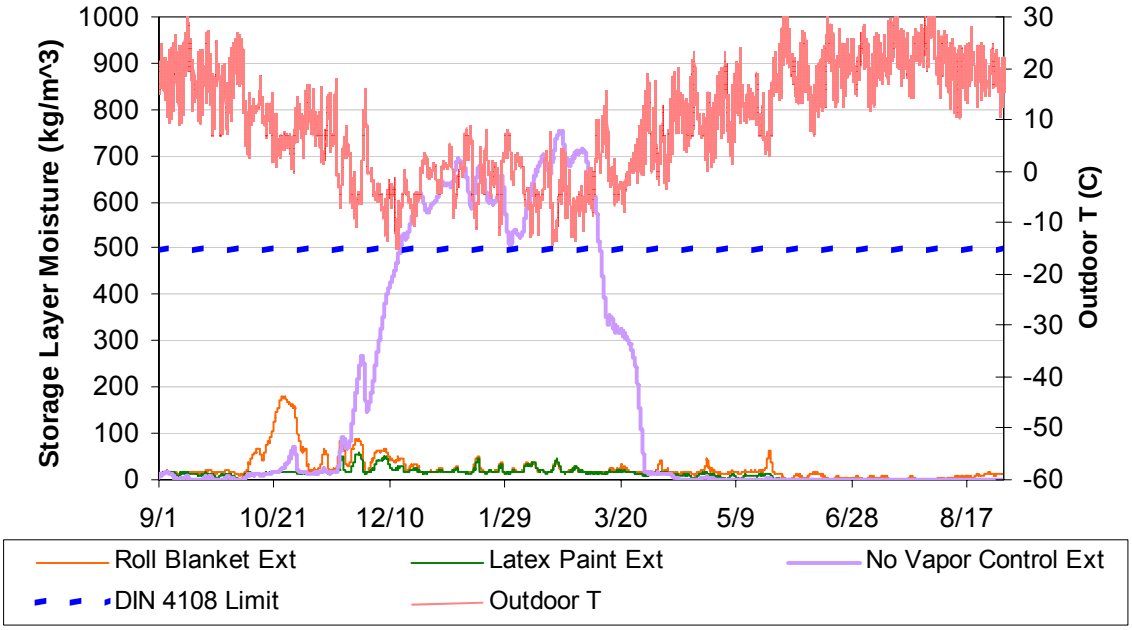

Figure 8.26: Simulation condensation layer moisture content, upper location

The results indicate a significant accumulation of wintertime condensation at the concrete-insulation interface in a wall without any interior vapor control; this amount exceeds the rundown storage limit of the layer. This representation also shows the fast drying of this layer in the spring.

The small spikes seen in late October can be explained as well. In the roll blanket (polyethylene) wall, some moisture accumulated in the insulation space at the end of the fall, due to the inward vapor gradient. This spike is due to the drop in temperatures seen at the concrete interface, at the onset of winter. A similar but smaller spike is seen in the "no vapor control" wall, corresponding to the extended period of cold weather in early November.

8.2.2.3 Condensation Layer Response in Kitchener Above-Grade

As mentioned in Section 8.1.1.4, the simulated temperatures did not match the monitored data at the above-grade portions of the Kitchener model. However, this was noticeably worse for the winter portion of the simulation; the summer data was a closer match. Therefore, the simulated condensation layer was run in the Kitchener above-grade model, to try to correlate predicted accumulation levels with the effects seen in the data and in disassembly.

First, the winter (i.e., worse correlation) data was plotted (Figure 8.27); it shows little accumulation, even though the concrete-insulation interface is noticeably colder than reality. Note the moisture content spike in late October in the roll blanket wall; this is likely due to moisture that has accumulated in the insulation space at the tail end of the summer, which is shifted to the exterior by the change in temperature gradient. Neither the latex paint nor the roll blanket wall show

condensation over the rundown limit in this simulation, which matches observations made during disassembly.

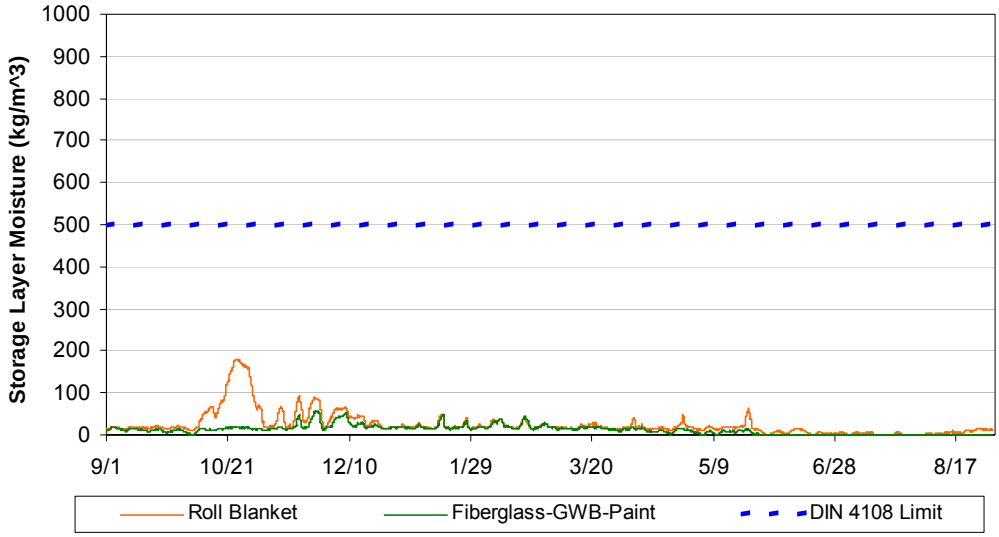

Figure 8.27: Concrete-insulation interface condensation layer MC, Kitchener data, above grade

This is followed by a plot of the accumulation at the condensation layer located between the insulation and either the polyethylene or the interior side of the gypsum board (Figure 8.28). The first summer is dry for both walls; however, during the second summer, the polyethylene roll blanket shows accumulation that exceeds the DIN 4108 limit, peaking over 900 g/m^2. This matches monitored data and disassembly observations: the moisture content wafer at this location in the roll blanket wall clearly showed the presence of liquid water, well over the 100% RH level.

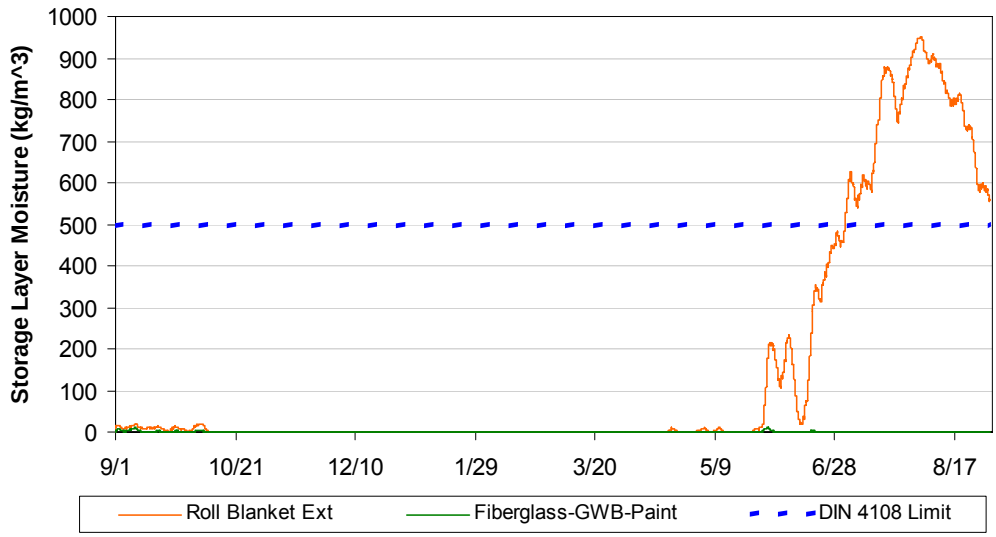

Figure 8.28: Vapor barrier condensation layer MC, Kitchener data, above grade

8.2.3 Boundary Conditions for Extrapolations: Exterior

8.2.3.1 Above Grade Boundary Conditions

The exterior conditions used for extrapolation simulations were several representative Canadian climates, which included Vancouver, BC; St. John's, NL; and Edmonton, AB. A summary of the Environment Canada is shown in Table 8.1 and Figure 8.29 below; the graph includes the historical data for Waterloo, ON.

Although the weather can be quickly compared in the monthly average graph, the patterns should be briefly described. Vancouver, BC represents a maritime coastal climate, and has both temperate winters and summers. St. John's, NL is a northern Maritime climate, and has winters roughly equivalent to Waterloo; however, it has greater rainfall (1500 mm vs. 900 mm), and cooler summers. Edmonton, AB represents a cold plains climate; it has significantly colder winters than Waterloo, and cooler summers. As shown by the cooling degree data, all three of these climates have almost no cooling loads (80 CDD 18° C or less).

In addition, three other climates (Toronto, ON, Montreal, QC, and Minneapolis, MN) are shown in Table 8.1 for reference. The average Environment Canada data for Toronto is similar to the monitored year in Waterloo, and the Montreal and Minneapolis data are included for later use.

Table 8.1: Climate data for extrapolation locations

	HDD 18° C	CDD 18° C	Average T (°C)	Average T vs. Monitored T Avg.
Waterloo (monitored year)	3558	349	9.2	
Waterloo, ON	4288	338	6.7	-2.5
Vancouver, BC	2926	80	10.1	+0.9
Saint John's, NL	4881	58	4.7	-4.5
Edmonton, AB	5708	51	2.4	-6.8
Toronto, ON	3570	359	9.2	-0.1
Montreal, QC	4891	158	5.0	-4.2
Minneapolis, MN	4376	388	7.5	-1.8

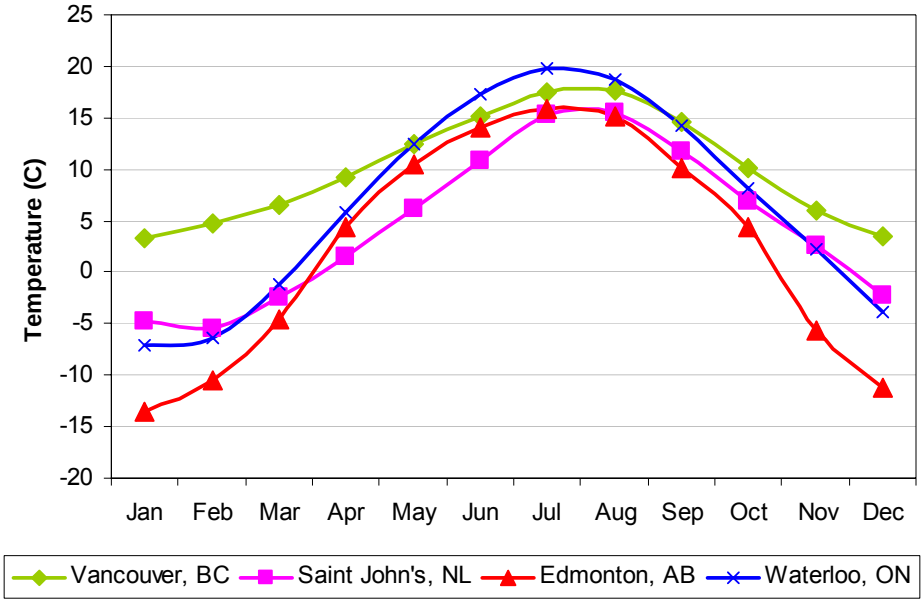

Figure 8.29: Monthly average temperatures for climate locations (Environment Canada data)

The historical data is compared with BEGHut weather conditions in Table 8.1 and Figure 8.30; the experimental year was warmer than average, especially in January 2006.

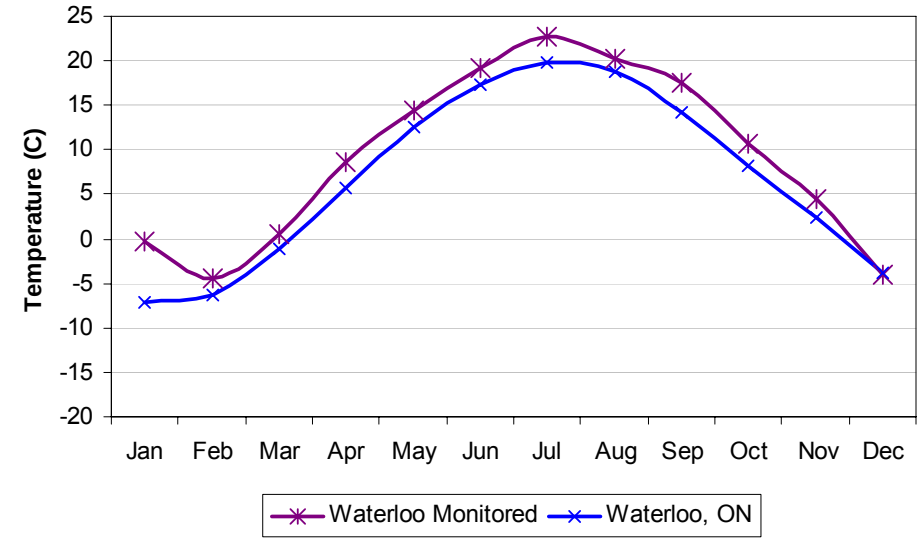

Figure 8.30: Comparison of monitored and climate average monthly temperatures for Waterloo

Next, it was necessary to choose simulation parameters to provide worst-case conditions. Risk of wintertime condensation at the upper portion of the wall is related to the temperature of the concrete surface, which in turn is linked to the exterior temperature. The worst-case conditions would be north facing or with no solar exposure; in locations with a "warm" and "cold" weather year (Edmonton, Vancouver, Toronto), the "cold year" was chosen.

Summertime inward vapor drives are related to the temperature of the saturated material, and thus, they are tied to exterior temperatures and orientation. Therefore, the highest solar exposure (south orientation) and the "warm" year climate file were used in these simulations. Simulation work by Swinton and Karagiozis (1995) demonstrated the worst vapor drives on the south orientation in a Montreal climate, but problems still occurred on the north orientation. One matter of curiosity is whether sufficiently cool summers will render inward vapor drive problems negligible or not.

8.2.3.2 Below Grade Boundary Conditions

The extrapolation boundary conditions for the below grade portions of the wall pose some issues: soil temperatures are not only a function of outdoor temperature, but also the soil's thermal diffusivity (ratio of thermal conductivity and volumetric heat capacity), and therefore soil composition and moisture content. Since there are too many unknowns to give definitive soil conditions, the following approach was used to do some form of geographic extrapolation.

The constant deep ground soil temperature is typically 2-6° C above the mean annual air temperature (Hutcheon and Handegord 1995); the monitored data from the Kitchener site follows this general trend. The sinusoidal temperature variation at 900 mm soil depth is centered at roughly 12° C, and the lower wall at roughly 14° C, which is within the range of 9° C (average annual temperature, Table 8.1) + 2 to 6° C. Therefore, for geographic extrapolation, the temperature profile at the lower concrete interface was offset by the mean annual temperature difference (between locations), and used as the exterior condition. However, this does not address the amplitude of the seasonal sinusoidal pattern, which would be a function of the annual climate swing and soil conditions.

These boundary conditions lend themselves to a simple initial analysis before proceeding with hourly hygrothermal models, which is to compare the concrete surface temperatures with interior dewpoints. If the surface temperature never exceeds dewpoint, there is no chance of condensation. However, even if this is the case, it is worthwhile to run hygrothermal modeling to demonstrate relative drying rates between assemblies.

8.2.4 Boundary Conditions for Extrapolations: Interior

Interior boundary conditions were also varied in the extrapolation simulations: relative humidity was the significant experimental variable. Sinusoidal annual humidity profiles were created to provide "low," "middle," and "high" humidity loadings, as shown in Table 8.2 and Figure 8.31.

Table 8.2: Interior humidity conditions used in extrapolation simulations

	Low Humidity: 30% low/60% hi	Mid Humidity: 40% low/60% hi	High Humidity: 50% low/65% hi
Waterloo, ON	●	●	●
Vancouver, BC		●	●
Saint John's, NL	●	●	●
Edmonton, AB	●	●	

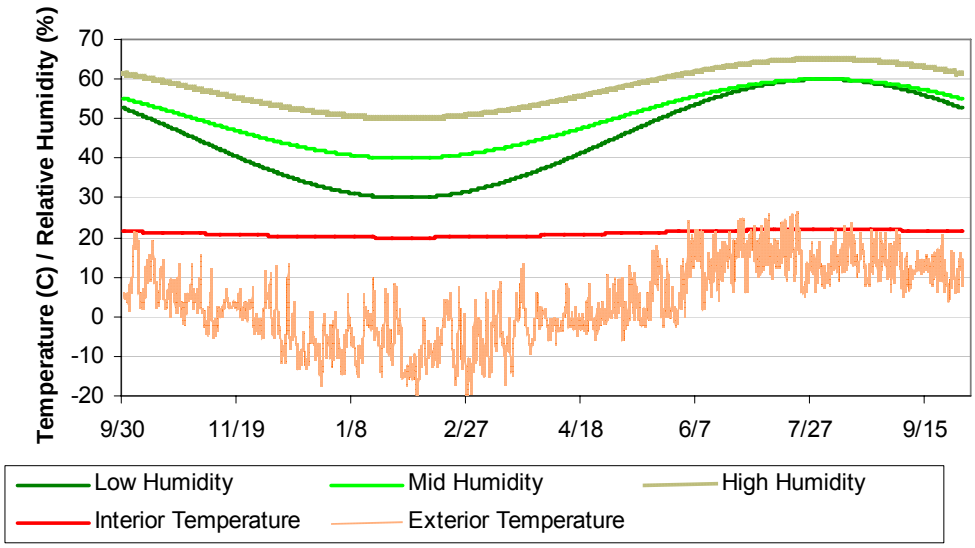

Figure 8.31: Summary of interior conditions (temperature and RH) with Waterloo exterior T

Not all humidity profiles were not used in all locations, as shown in Table 8.2. The Vancouver coastal climate is expected to have relatively high wintertime interior dewpoints, due to climate patterns, low ventilation rates, and high occupancy. Edmonton has very cold winters, resulting in low wintertime dewpoint temperatures (thus the elimination of the "high" humidity condition).

These interior humidity profiles are shown in terms of dewpoint in Figure 8.32. Interior temperature varies sinusoidally over the year from 20 to 22° C.

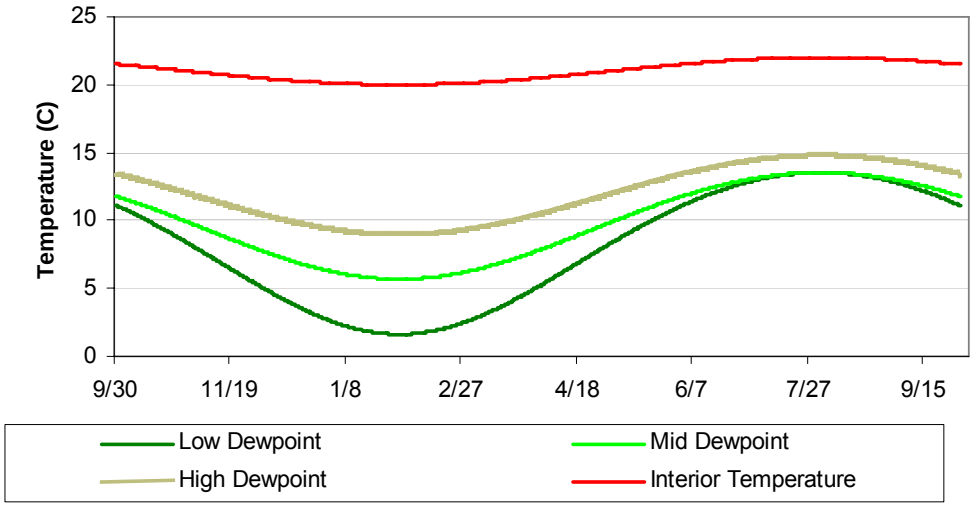

Figure 8.32: Interior conditions, shown as temperature and dewpoint (° C)

These interior conditions were compared to previous measurements. The Ruest et al. (1993) measurements of basement wintertime dewpoints across Canada were mostly in –5 to 5° C range (corresponding to "low" humidity conditions or drier). The exception was dewpoints in British Columbia, which were mostly in the 5-10° C range ("mid" to "high" humidity conditions).

Interior wintertime dewpoints collected by Building Science Corporation in the Chicago area were centered on the 5-8° C range, but with variations up above 12° C and down to near 0° C. The majority of the data is similar to the "mid" and "high" humidity ranges. It is worth noting, however, that these were recently constructed houses in their first season of occupancy. Summertime dewpoint data indicated that window ventilation was used for cooling in most houses; this resulted in dewpoints in the 15-20° C range, with peaks above this level. This is higher than the summertime interior conditions to be used in the simulations (13-15° C dewpoint).

8.2.5 Above-grade Extrapolations

At the above-grade portion of the wall, simulations were run for the three climate locations, as well as for Toronto. Toronto weather was used instead of Waterloo data for two reasons: a "cold" year and "warm" year were available, and being a larger population center, it might provide greater perceived applicability.

In addition to the three materials used in the Kitchener test basement, four other assemblies were simulated. As a bounding condition, a wall with fiberglass insulation and no interior vapor control was used. WUFI does not account for the bulk air transport that would occur through low-density insulation, but it does show the effect of vapor diffusion through this permeable material. Second, in the United States, the roll blanket material is available with a permeable perforated polypropylene facer attached the fiberglass. This facer has been tested by Building Engineering Group (as detailed in Appendix D), giving values of 720 ng/(s·m^2·Pa)/13 perms (dry cup) to 790-850 ng/(s·m^2·Pa)/14-15 perms (wet cup). Third, a fiberglass batt with a Kraft facer was simulated as well; the variable permeability of this material was simulated, ranging from 17 ng/(s·m^2·Pa)/0.3 perms (dry cup) to 34 ng/(s·m^2·Pa)/0.6 perms (wet cup). Finally, in some simulations, a bare uninsulated concrete wall was used as a comparison.

8.2.5.1 Toronto Simulations

The first set of simulations examined the risk of wintertime condensation at the above-grade portion of the wall. As mentioned earlier, these simulations are conservative, given the warmer temperatures seen at the concrete in the monitored data, due to two-dimensional effects. Five materials were compared: the roll blanket (polyethylene), the fiberglass batt with gypsum board and latex paint, fiberglass with Kraft paper, fiberglass with the perforated facer, and no interior vapor control. The XPS wall was not included in these graphs: early simulations indicated superior performance compared to these cavity walls even at the worst conditions; success of this assembly in the field is evidence that the simulation captures the behavior correctly.

The accumulation at the fictitious condensation layer is shown for these walls under "low" (Figure 8.33), "mid" (Figure 8.34), and "high" (Figure 8.35) humidity conditions; the DIN 4108 500 g/m^2 threshold is shown on the graphs as a proposed pass/fail criterion.

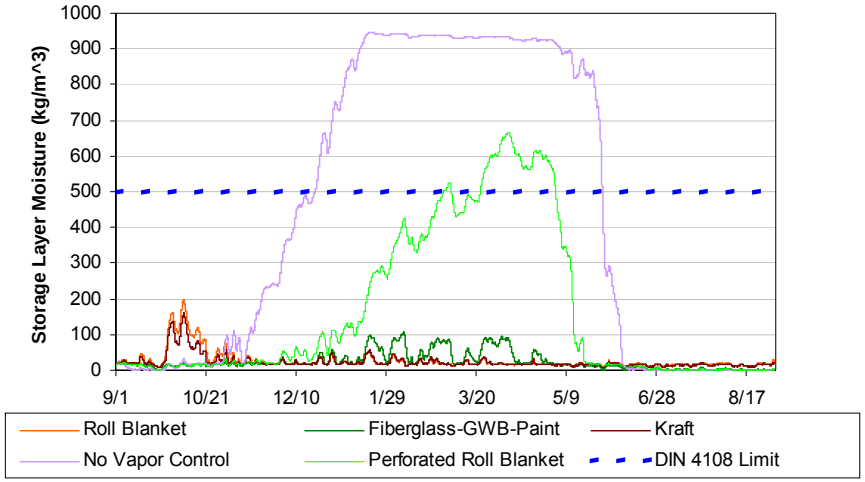

Figure 8.33: Condensation layer MC, Toronto AG, low RH

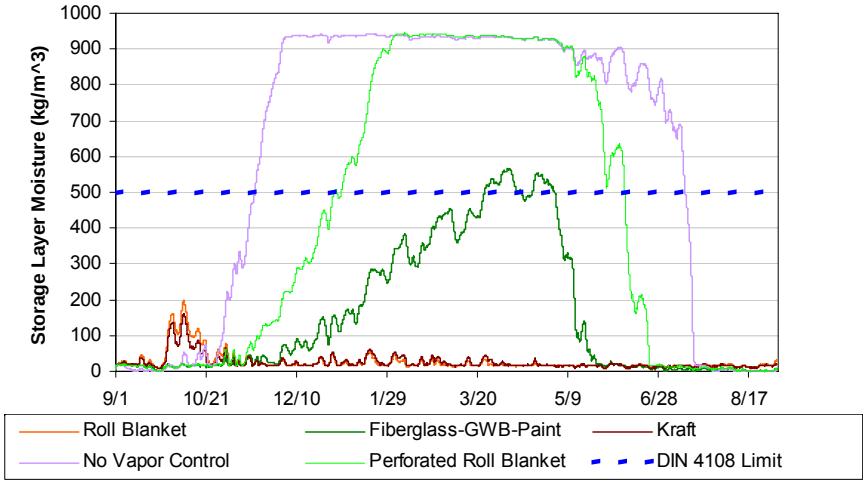

Figure 8.34: Condensation layer MC, Toronto AG, mid RH

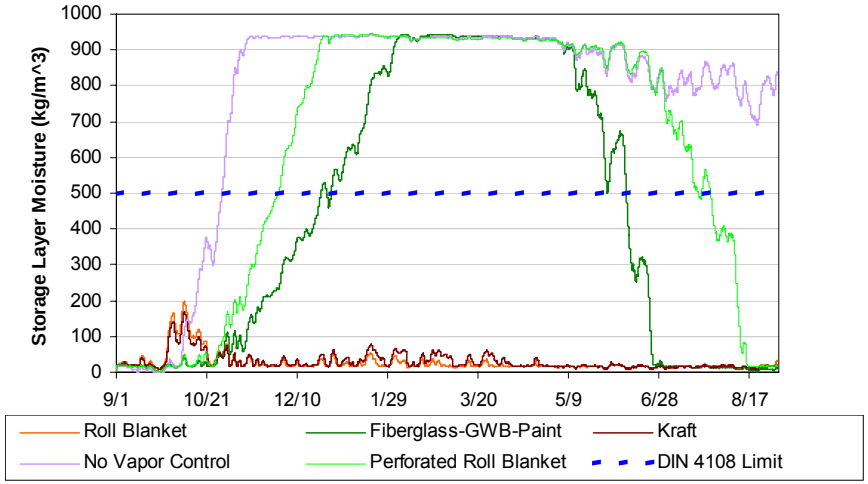

Figure 8.35: Condensation layer MC, Toronto AG, high RH

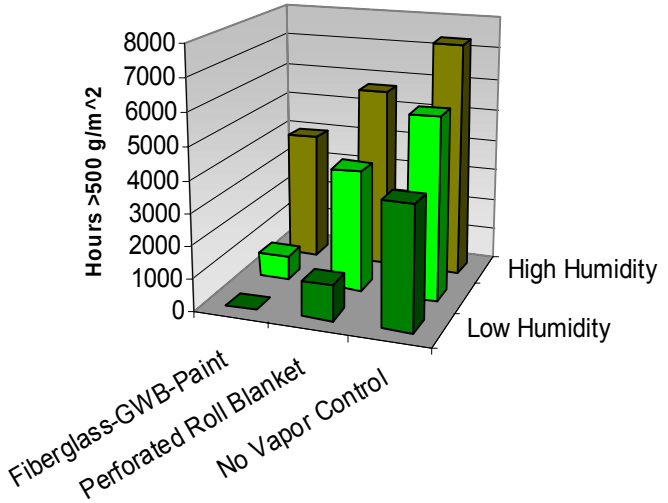

Figure 8.36: Toronto AG condensation layer hours over 500 g/m^2

The results show consistent patterns: the walls with polyethylene or Kraft paper, which are classified as vapor barriers (less than 57 ng/(s·m^2·Pa)/1 perm), have consistently safe behavior, with little condensation. The more permeable walls show behavior that becomes worse in the order of their permeability (from least to most): latex paint, perforated facer, and no vapor control. Also, increasing interior humidity causes increasing failures, starting with the most permeable. For instance, at low humidity conditions, the latex paint wall shows little accumulation, while the perforated facer and no vapor control walls show accumulation over 500 g/m^2. At higher humidity conditions, the performance of these permeable walls grows worse; at high humidity conditions, even the latex paint wall has significant time over 500 g/m^2 during the winter. Note that under high humidity conditions, the "no vapor control" wall is unable to dry the accumulated moisture in the following spring/summer, indicating a seasonal increase in moisture content (i.e., "ratcheting"). This high humidity condition would be expected to cause air leakage and condensation damage in wall and roof assemblies of many houses in this climate.

These results are summarized in Figure 8.36, showing the increase in hours over the condensation limit with increasing permeability, and with increasing interior humidity.

Another phenomenon simulated here was the inward vapor drives causing condensation on the exterior side of the polyethylene, in the roll blanket wall. The simulations compared the performance of the roll blanket, a Kraft-faced batt, and fiberglass/gypsum board/latex paint. A condensation layer was placed on the exterior side of the vapor control layer; the resulting moisture accumulation levels are shown in Figure 8.37. Again, the XPS wall showed no sign of this issue, and is not included in these plots. It clearly shows the condensation that would occur in late summer at this location in the polyethylene wall; the Kraft paper wall shows some accumulation, but below the rundown threshold. The more permeable latex paint-fiberglass assembly shows no accumulation. Note that the inward vapor drive failure shown here may be worse than the wintertime accumulation due to assembly geometry: the condensation would run down the impermeable polyethylene surface and accumulate. In contrast, in the winter situation, moisture accumulation would be absorbed into the concrete as it ran down the wall—specifically, at the below-grade portions that did not accrue condensation.

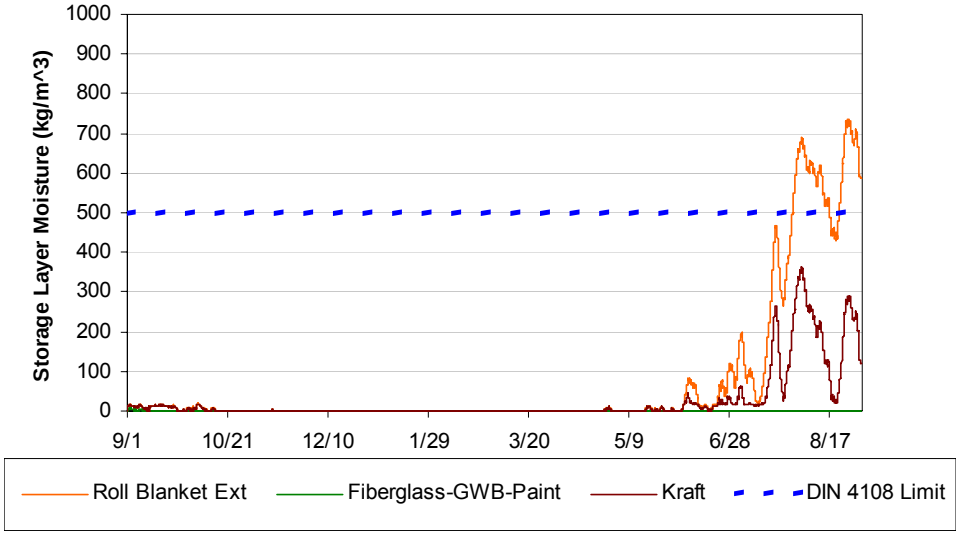

Figure 8.37: Interior cavity side condensation layer MC, Toronto AG, mid RH

Another way to compare these walls is to show the temperature and humidity conditions (isopleths) at a given monitoring location; the conditions at the concrete-insulation interface for the roll blanket and fiberglass-latex paint walls are shown in Figure 8.38 and Figure 8.39, respectively. These are the results for the "mid" humidity condition; note that the y-axis changes between these plots.

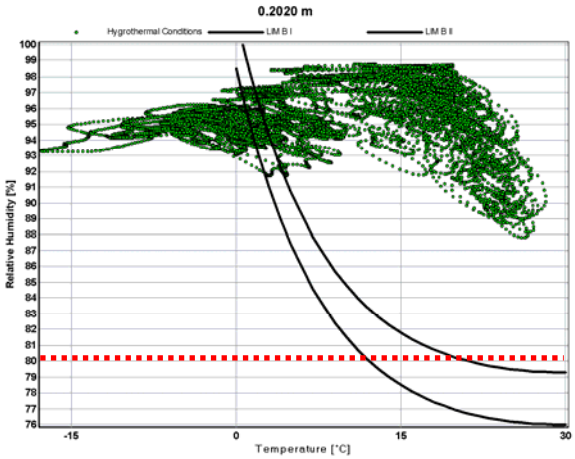

Figure 8.38: Roll blanket isopleth at concrete-insulation interface, "mid" humidity

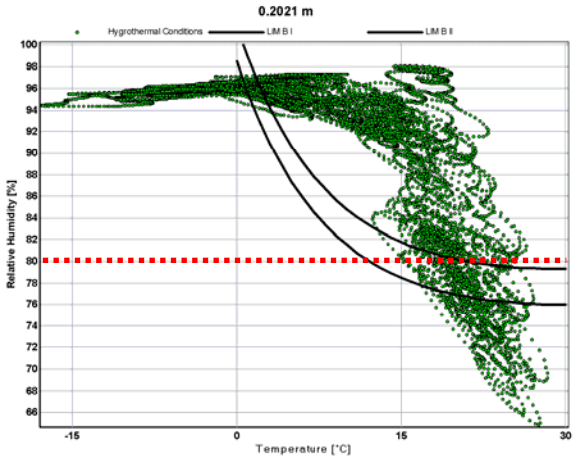

Figure 8.39: Latex paint-gypsum isopleth at concrete-insulation interface, "mid" humidity

These plots indicate that this interface has extended periods at high RH. The proposed ASHRAE Standard 160P (2006) defines mold growth failure when the RH exceeds 80% RH (shown by dotted red line) for one month. All of these walls fail this metric; however, the vulnerability of the assembly components should be accounted for. For instance, the XPS wall has materials at the high humidity interface with minimal nutrient value for mold growth, compared to wood studs in the frame walls.

Sedlbauer (2004) proposed a system of Lowest Isopleth for Mold (LIMs) curves for various building material substrates, indicating risk conditions for mold growth. They included the LIM_{Bau} I level (biodegradable materials such as wallpaper, plasterboard) and the LIM_{Bau} II level (porous substrates such as mineral building materials and some woods). These two curves are shown in Figure 8.38 and Figure 8.39: both of these walls show significant portions of the year above the LIM_{Bau} II level. Although these limits are known to be generally conservative, these isopleths indicate the risk of placing moisture-sensitive materials such as wood framing at this location.

8.2.5.2 Vancouver Simulations

Vancouver has mild winters (3.3° C average January temperature, vs. –4.2° C for Toronto); therefore, wintertime condensation was expected to be a smaller problem. This proved to be the case, as shown for "mid" (Figure 8.40) and "high" (Figure 8.41) interior humidity levels. The latex paint-fiberglass wall gives reasonable performance at "mid" humidity, but exceeds the rundown limit at "high" humidity. The other two permeable options (perforated facer and no vapor control) both exceed the limit at the "high" level. As per the Toronto simulations, the XPS walls showed no signs of moisture risks, and are not included in these results, or following geographic extrapolations.

The magnitude of inward vapor drive was also examined in these simulations. It appears that the lack of a cooling load results in less accumulation at the polyethylene than in Toronto: values peaked near 200 g/m^2, as shown in Figure 8.42.

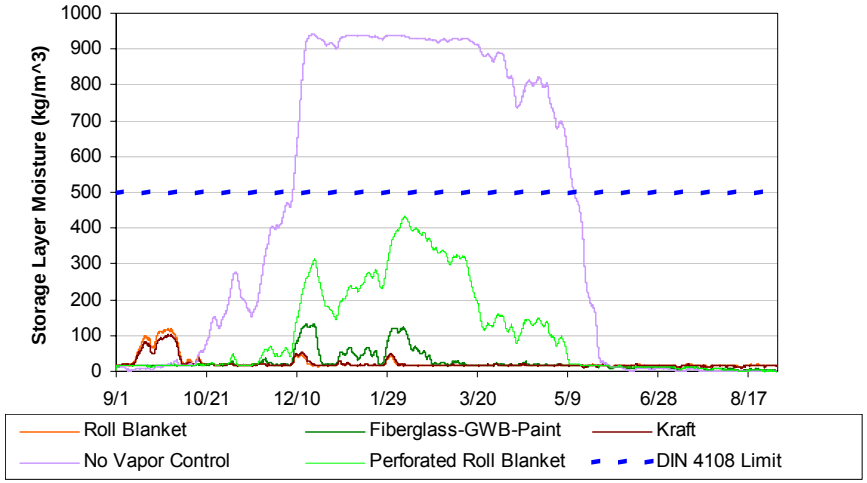

Figure 8.40: Condensation layer MC, Vancouver AG, mid RH

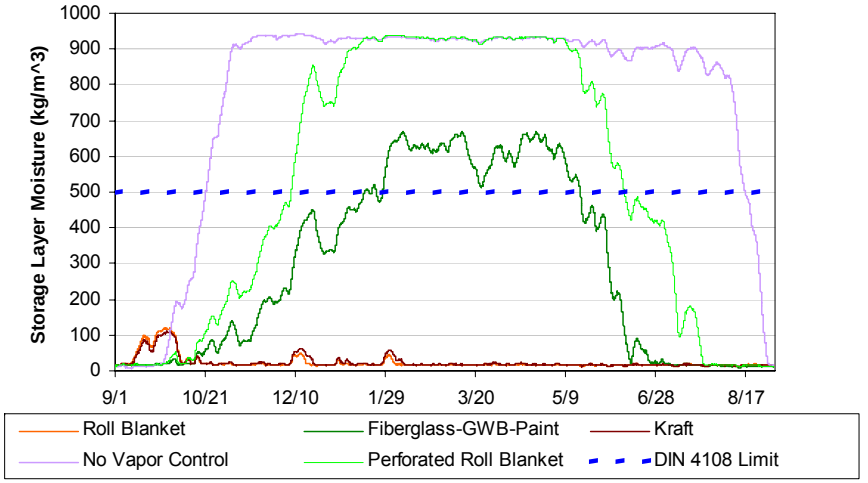

Figure 8.41: Condensation layer MC, Vancouver AG, high RH

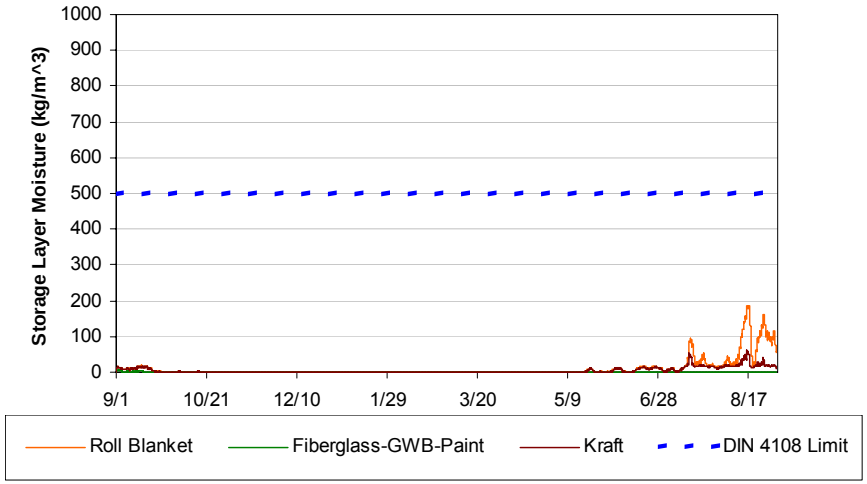

Figure 8.42: Vapor barrier cond. layer MC, Vancouver AG, mid RH

8.2.5.3 St. John's Simulations

The wintertime condensation simulations for St. John's were similar to the Toronto results: the assemblies with a vapor barrier (polyethylene or Kraft) showed little accumulation, while the more vapor permeable options showed moisture accumulation within the wall, increasing with interior humidity and with permeability (see Figure 8.44 through Figure 8.47). The latex paint wall remained below the accumulation threshold only at "low" humidity conditions; all other combinations exceeded this limit.

In the summertime simulations, the results showed insignificant summertime condensation due to inward vapor drive. Peak accumulation at the interior-side condensation layer in the roll blanket assembly was 16 g/m^2, compared to over 700 g/m^2 in Toronto. This can be explained by comparing the cooling loads of these two climates: 58 CDD 18° C in St. John's, compared to 360 CDD 18° C in Toronto.

8.2.5.4 Edmonton Simulations

Edmonton is a substantially colder climate (5708 HDD 18° C) than St. John's (4881 HDD 18° C). Therefore, it is unsurprising that the wintertime condensation performance of the permeable assemblies is even worse: as shown in Figure 8.43, even the fiberglass-latex paint assembly under "low" humidity conditions has significant hours over the 500 g/m^2 threshold. Many of the walls demonstrate an unstable wetting cycle over the first year; they do not dry down to their original moisture content over the course of the summer. The walls with a vapor barrier (polyethylene and Kraft paper) both show acceptable performance.

In addition, Edmonton has essentially no cooling load, so the inward vapor drive was negligible, as in St. John's. Peak accumulation at the polyethylene condensation layer was 25 g/m^2.

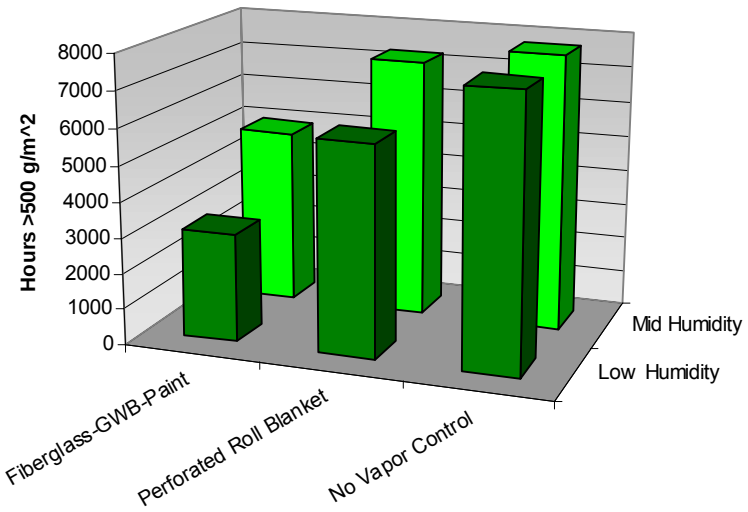

Figure 8.43: Edmonton AG condensation layer hours over 500 g/m^2

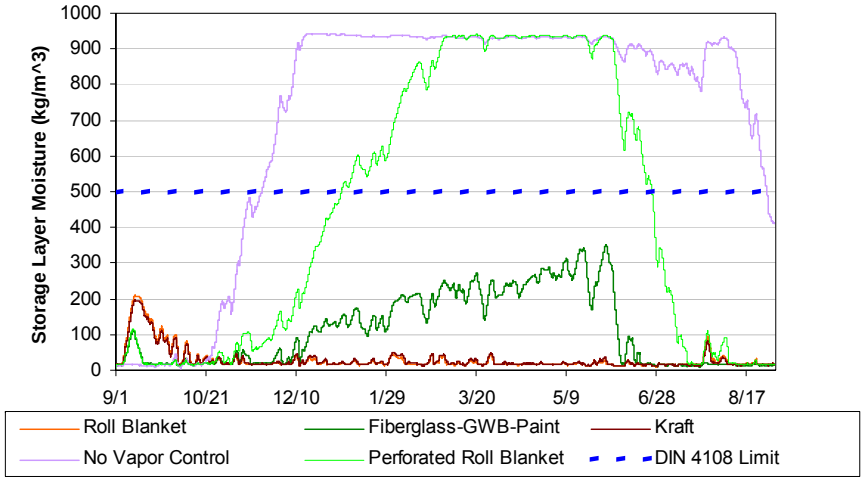

Figure 8.44: Condensation layer MC, St. John's AG, low RH

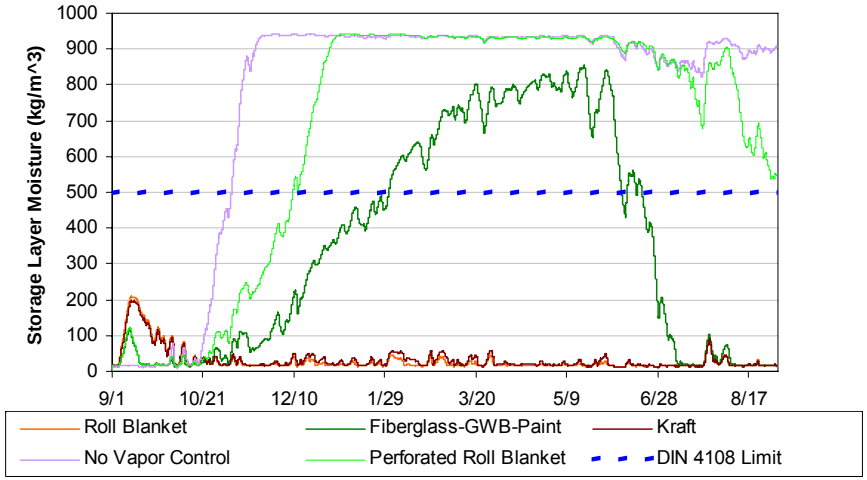

Figure 8.45: Condensation layer MC, St. John's AG, mid RH

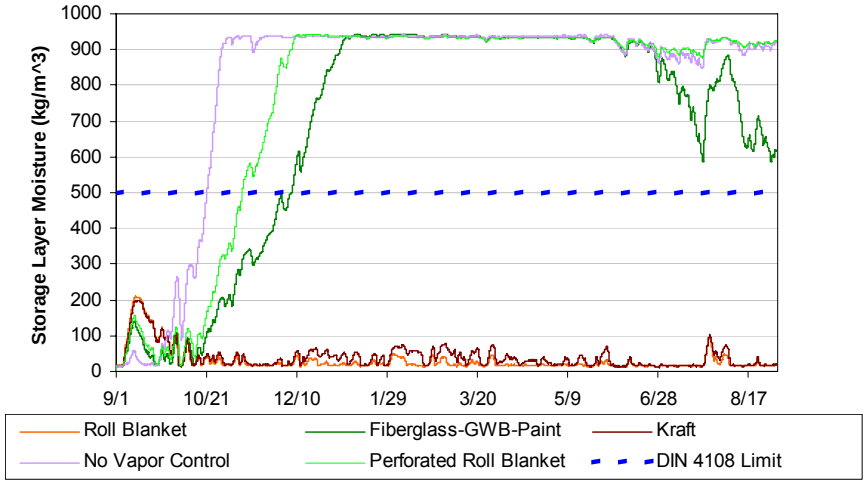

Figure 8.46: Condensation layer MC, St. John's AG, high RH

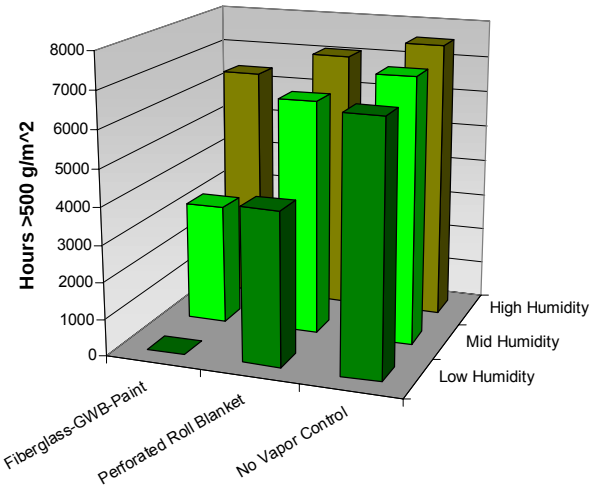

Figure 8.47: St. John's AG condensation layer hours over 500 g/m^2

8.2.6 Below-grade Extrapolations

The first step for the below-grade extrapolations was to narrow the focus on the most informative cases to model. As per previous cases, the interior relative humidity was varied, and several interior insulation assemblies were used. However, it is notable that the worst case below grade situations will typically be at the "lowest" location: it has the greatest thermal lag, and therefore the coldest temperatures (and greatest chances of condensation) under summertime high dewpoint conditions. Any wintertime issues seen at the "middle" height would occur in worse form at the "upper" or above grade location. Therefore, the first set of simulations uses the "lowest" boundary conditions for the Kitchener field site, and varies interior RH and assemblies.

In addition, the synthesized "Edmonton" soil conditions (as described in Section 8.2.3.2) were used as a second set of boundary conditions. Edmonton was the coldest climate in the selection, so it is used as a "bounding" condition. The applicability of an extensive set of simulations in all climates would be questionable, given that they would all be synthesized below-grade conditions, simply offset by the difference in average annual temperature, without regard for amplitude changes.

Finally, given the lack of moisture accumulation seen in the Kitchener simulation, additional simulations were run.

8.2.6.1 Simulations Using Kitchener Boundary Conditions

The first cursory analysis was to plot the interior and exterior boundary conditions (temperature and dewpoint) over the year, as shown in Figure 8.48. It is notable that the interior temperature is always higher than the lower wall temperature, showing an outward thermal gradient throughout the year. Second, the exterior boundary conditions (100% RH at the "Wall T Lower" temperature) are at a higher dewpoint (absolute moisture content) than interior for almost all of the year, demonstrating a largely inward vapor gradient. Even though the concrete is not entirely at 100% RH, it is at 90% RH or higher through most of its thickness; we can infer that drying of the concrete to the interior will occur. There appears to be close to no chance of interior moisture condensing on the concrete surface; there is a minimal overlap in late winter.

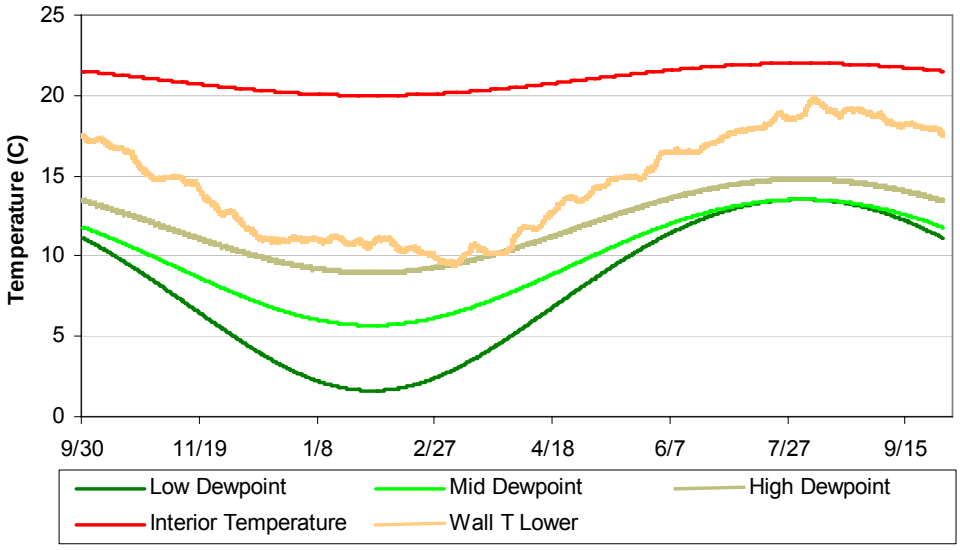

Figure 8.48: Interior dewpoint extrapolation conditions, and lower wall temperature

After examining the initial results of the hygrothermal simulations, it was necessary to create criteria to interpret and compare them. The results were first compared using the "condensation layer" approach used at the above grade simulations, as shown in Figure 8.49. The simulations were run over a period of six years at the "high" relative humidity condition; the plot shows the condensation layer at the concrete-insulation interface. All of the walls except for the roll blanket show minimal accumulation, with the Kraft paper wall showing a small rise during the winter seasons. However, the polyethylene roll blanket shows a seasonally ratcheting pattern of increasing accumulation due to movement of moisture from the concrete into the fiberglass batt space. Although the polyethylene peaks increase towards the 500 g/m^2 limit, it does not reach the limit during the six years simulated here. These results show that thermal and moisture drives in the below-grade environment are less powerful and dynamic than the above-grade portion.

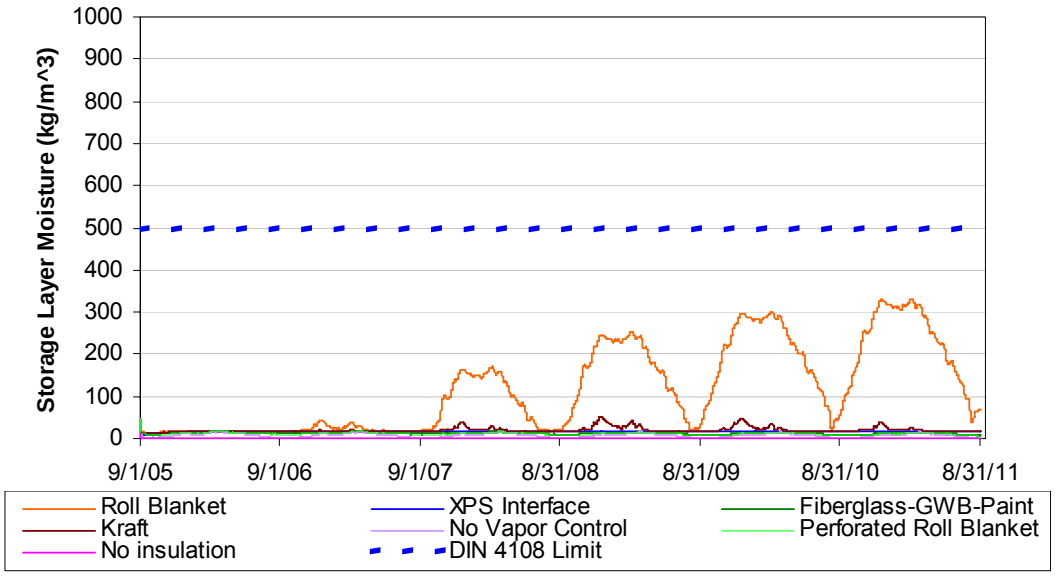

Figure 8.49: Condensation layer accumulation for lower location, "high" relative humidity

Since the condensation layer approach does not differentiate the assemblies well, the isopleths at the concrete-insulation interface were compared, as shown for the least and most permeable assemblies (roll blanket and no vapor control; Figure 8.50 and Figure 8.51). Although the roll blanket wall shows much higher sustained moisture levels, both of these assemblies remain above LIM_{Bau} II for the majority of the year. Although the more permeable option could be considered "better" (drying below the LIM_{Bau} II state for part of the year), this method provides insufficient differentiation between assemblies.

Since the interface conditions are not at condensation, but are at sustained high relative humidity levels, another approach was considered.

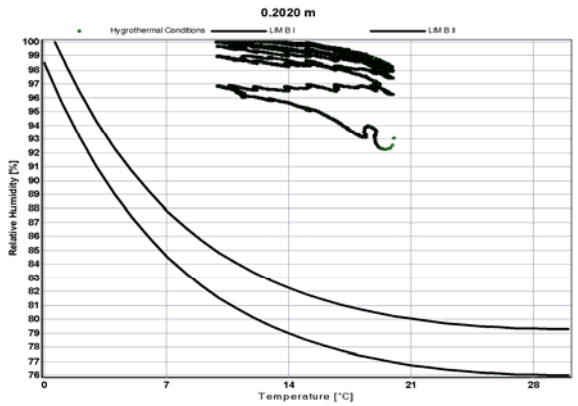

Figure 8.50: Roll blanket isopleth at concrete-insulation interface, "mid" humidity

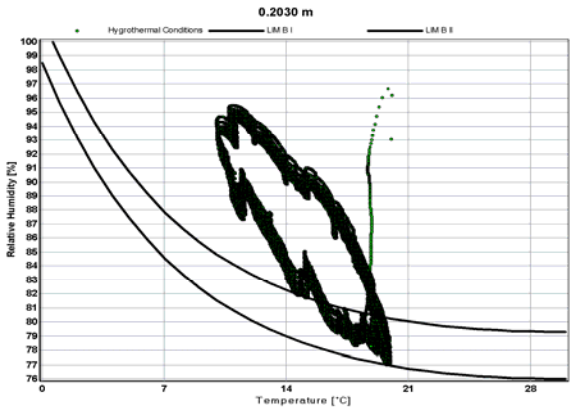

Figure 8.51: No vapor control isopleth at concrete-insulation interface, "mid" humidity

Another way to compare these assemblies was to record the drying of the concrete to the interior. The water content of the concrete wall is plotted in Figure 8.52 ("low" humidity conditions) and Figure 8.53 ("high" humidity conditions). As one might expect, the drying of the concrete increases with greater permeability of the interior insulation, given that the dampproofing prevents drying to the exterior. One option simulated was to leave the concrete bare (i.e., no interior insulation); as expected, it shows the fastest drying, but is only slightly faster than the most permeable options (no vapor control and perforated roll blanket). In addition, lower interior relative humidity increases the drying rate for the more permeable assemblies, but not by a large margin.

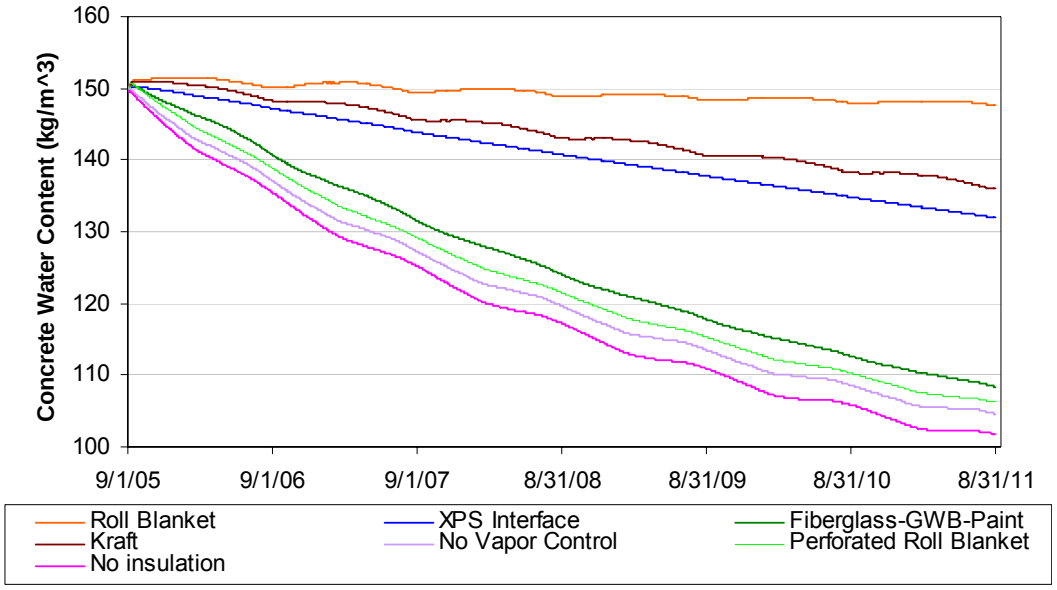

Figure 8.52: Concrete water content, "low" humidity conditions

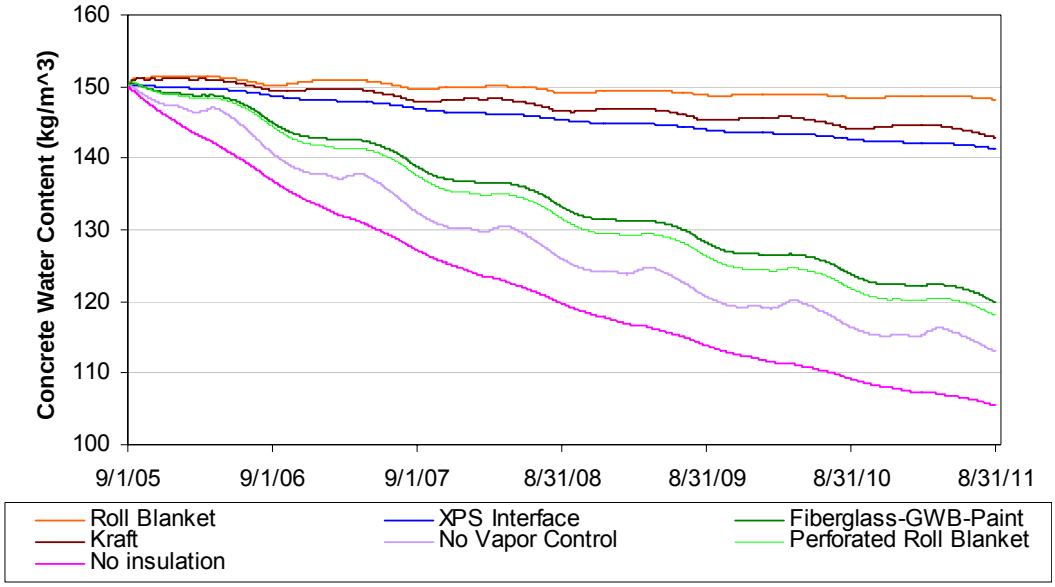

Figure 8.53: Concrete water content, "high" humidity conditions

It can be argued that the drying of the concrete has little relevance to actual performance, given that even the most permeable options show high relative humidity levels at the concrete-insulation interface, even after several years of drying (as per Figure 8.51). However, the least permeable material (polyethylene) shows rising humidity levels at the interface heading towards condensation (Figure 8.50), which is a much more dangerous condition for mold growth than high RH levels. If nothing else, faster-drying assemblies will be at lower risk levels sooner.

One traditional argument for low permeance materials at the below-grade portion of the wall is to reduce moisture flux into the basement, thus preventing higher interior humidity levels and mold. The moisture introduced from drying of the concrete can be compared with typical interior moisture generation rates, to understand the relative magnitudes. Over the six year simulation, the greatest drying is seen in the "no insulation" option, drying from 150 to 100 kg/m^3. For the 0.20 m (8") concrete wall and a 30 by 40 foot (9.1 m x 12.2 m) basement with 8-foot (2.4 m) high walls, this gives an average rate of 0.5 liters/day. Note that this is a rough estimate, ignoring the differences at the above-grade part of the wall, which dries to interior and exterior. This rate can be compared to average moisture generation rates of a family of four, at 10-15 liters/day (Straube and Burnett 2005). Seasonal desorption effects are listed at 3-8 liters/day (depending on house construction). As another comparison point, a person generates 0.75 to 1.2 liters/day (from sedentary to average). So although the drying of the concrete construction moisture can add noticeable total amounts of water, it is not a large increase in the moisture generation rate, which would result in substantially higher interior humidity levels by itself. It is more of a concern in terms of the moisture accumulation within interior insulation assemblies, where it can cause much greater damage.

Note that the calculated moisture release rate only includes drying of the concrete's construction moisture, as opposed to vapor transmission from the soil through the concrete: the impermeable

exterior dampproofing prevents this from occurring in the simulation. Separate WUFI simulations were run comparing vapor diffusion with capillary transport through an 8" concrete wall at isothermal conditions in Chapter 3: Thermal and Moisture Physics of Basements. The moisture transport rate due to capillary transport (i.e., exterior precipitation conditions every hour) was over an order of magnitude higher than the rate with the exterior at 100% relative humidity. Assuming the basement dimensions used above, the calculated rates were 3.2 liters/day for capillarity, and 0.4 liters/day for vapor diffusion only. This demonstrates the vital importance of bulk water drainage and capillary separation between the soil and the concrete wall.

8.2.6.2 Simulations Using Edmonton Simulated Boundary Conditions

Below grade simulations were run using the "synthesized" Edmonton soil conditions; i.e., the Kitchener temperature profile, offset by the mean annual temperature difference between the two climates. These boundary conditions are shown in Figure 8.54. As per the above-grade runs, only "low" and "mid" humidity levels were used.

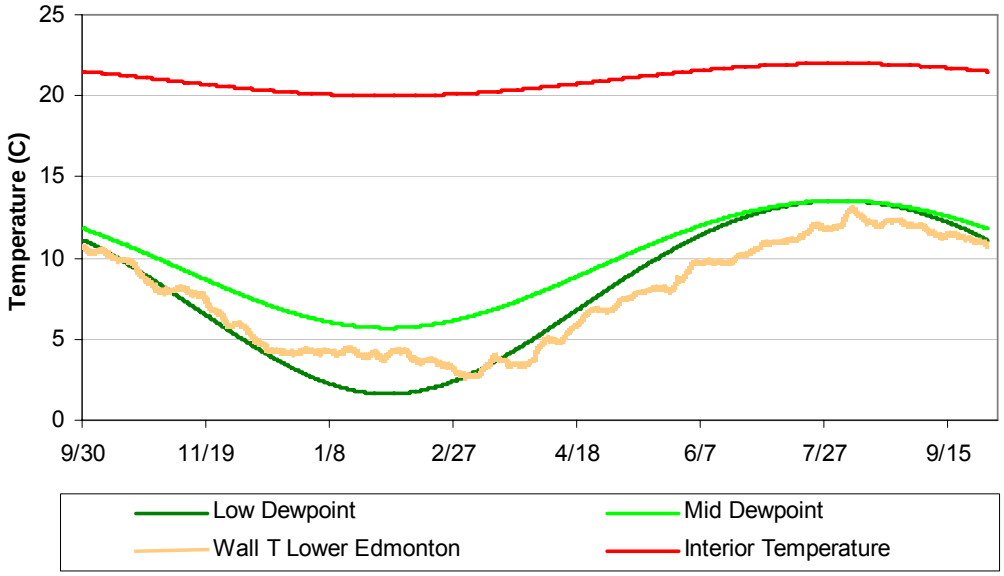

Figure 8.54: Interior dewpoints and lower wall T for Edmonton extrapolation

Again, the thermal gradient is always outward. But in contrast with the Kitchener relationships, the interior dewpoint is higher than the exterior or concrete dewpoint for most or all of the year. These conditions would cause wetting or condensation on the concrete, as opposed to the drying seen in the Kitchener simulations.

The simulations were first examined using the condensation layer at the concrete-insulation interface; results are shown for "low" (Figure 8.55) and "mid" (Figure 8.56) humidity conditions. In the "low" humidity simulation, the higher permeability options (no vapor control, perforated facer, latex paint) quickly accumulate moisture and rise above the 500 g/m^2 limit. However, the vapor control options (polyethylene, Kraft paper, XPS) also show a ratcheting rise towards this limit. The

only option that does not show condensation/accumulation at the interface is the “no insulation” option, which leaves that surface open to the interior.

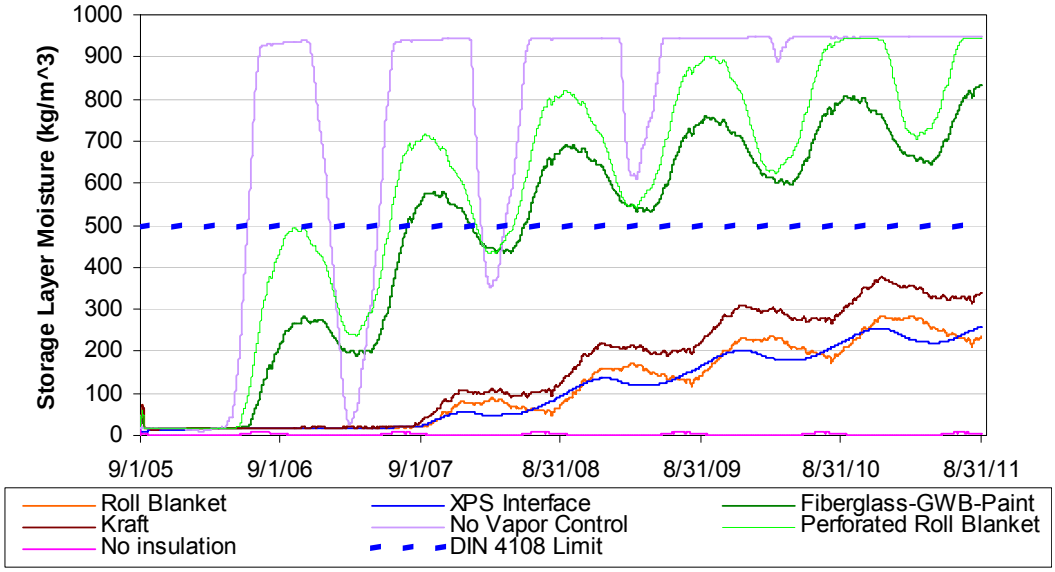

Figure 8.55: Accumulation at storage layer, Edmonton extrapolation, "low" humidity

Running the simulations at “mid” humidity levels result in an even faster failure for all of the walls, except for the “no insulation” option, which remains dry.

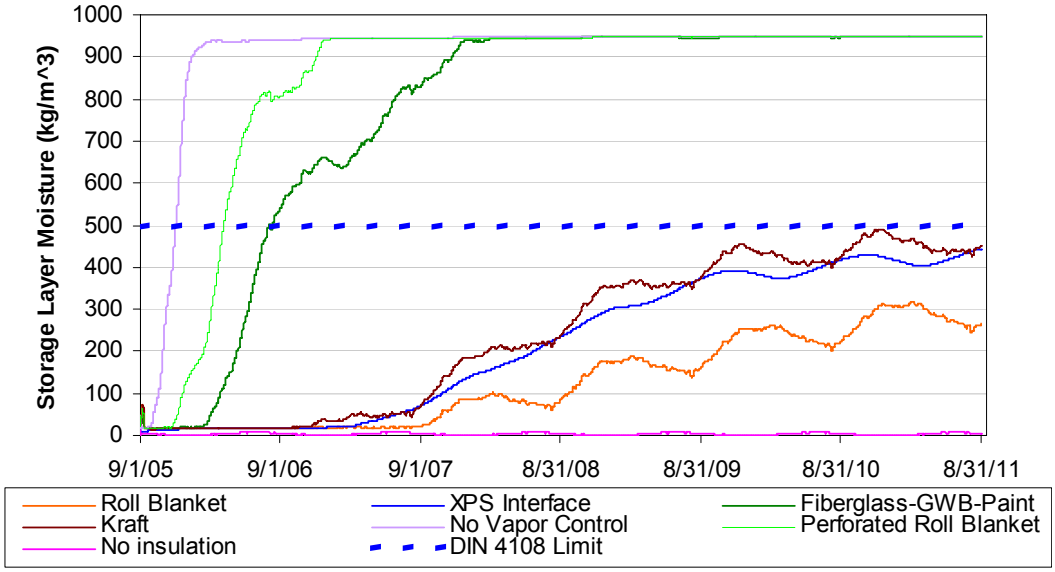

Figure 8.56: Accumulation at storage layer, Edmonton extrapolation, "mid" humidity

The difference in behavior of Kitchener and synthesized Edmonton conditions is shown in another form in Figure 8.57. When the interior dewpoint and the exterior boundary condition temperatures are plotted in Figure 8.48 and Figure 8.54, the difference between the two could be "integrated" into a dewpoint degree-hour total for the year. For instance, when the "low" humidity condition is compared with the Edmonton exterior condition, it will dry the wall part of the year, and wet it for the remainder: this calculation demonstrates the net effect over the year.

As shown in the plot, the Kitchener boundary conditions always result in drying of the wall, with a smaller drying potential at higher interior relative humidity. In contrast, in the synthesized Edmonton conditions, there is always a net wetting potential over the course of the year.

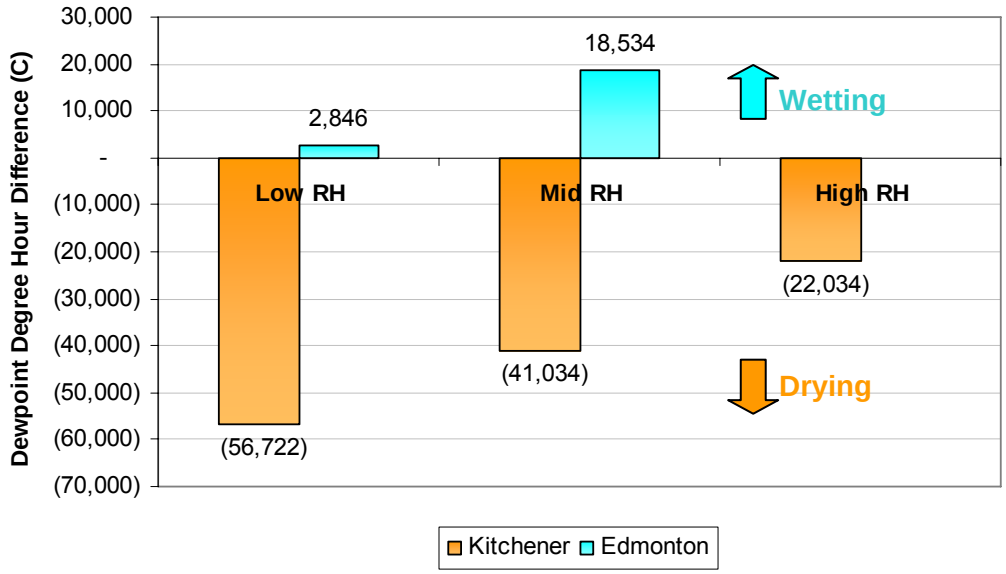

Figure 8.57: Dewpoint degree hour differences between concrete & interior conditions

As a final comparison, the concrete moisture content over the six year modeled period is shown in Figure 8.58 for the "low" humidity conditions. All of the higher permeability options (no vapor control, perforated facer, latex paint) demonstrate notable moisture accumulation in the concrete. The vapor control options (polyethylene, Kraft) show a small rise, but appear to be stable. The only option that shows drying is the "no insulation" option.

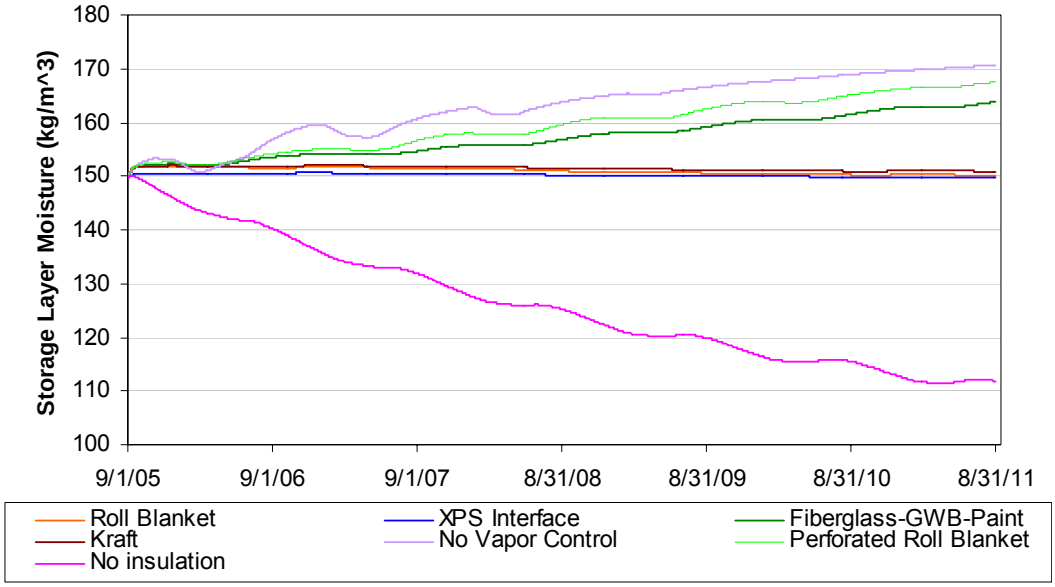

Figure 8.58: Concrete water content, "low" humidity conditions

However, these simulations should be viewed with some skepticism. Widespread failures of the below-grade portions of walls in extremely cold climates such as Edmonton are not known to be an issue. There are several explanations that might be acting alone or in combination.

First, the below grade boundary conditions were synthesized from a best estimate; it is quite possible that actual below grade conditions have a different temperature regime. Second, it is possible that relative high relative humidity levels are being experienced in these assemblies, but levels are not high enough to cause widespread problems. Third, Edmonton has an extremely dry climate; a modified version of the dewpoint-temperature comparison (Figure 8.54) is shown with average Edmonton weather exterior dewpoints (Figure 8.59).

It shows that the summertime exterior dewpoint is well below the “low” and “mid” humidity levels used in simulations. During the winter, interior dewpoints are expected to be higher than exterior due to moisture generation by occupancy, humidification, and an air sealed building enclosure. However, during the summer, operation of windows for ventilation and cooling is more likely, resulting in similar inside and outside dewpoints. If anything, monitored data typically shows lower interior dewpoints than exterior during the summer, due to dehumidification from running a cooling system.

In the graph below, it is notable that these exterior dewpoints are below the wall surface temperatures; as a result, a drying potential would exist, like the Kitchener simulations. Therefore, it seems unreasonable to assume that no drying potential for the wall to the interior would exist for the entire year.

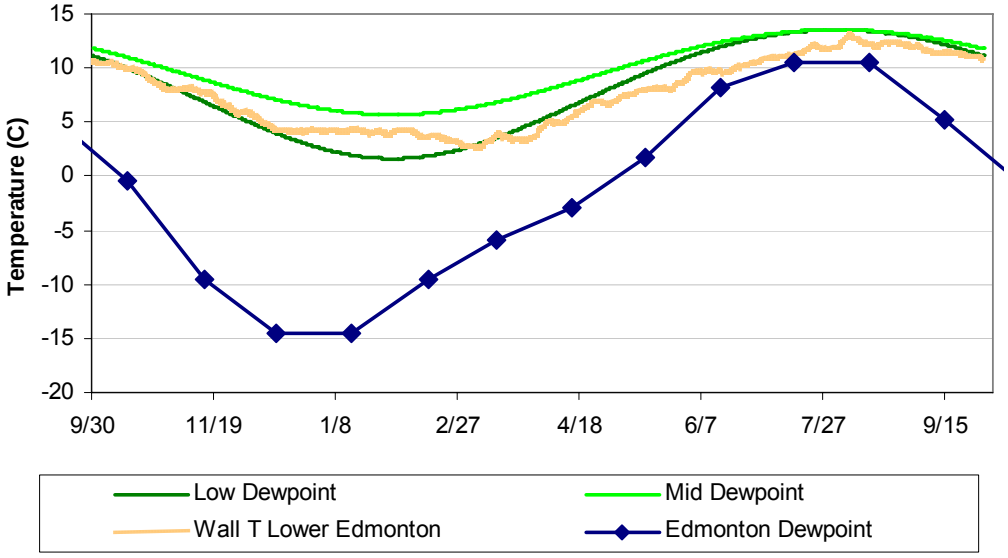

Figure 8.59: Interior dewpoint, lower wall temperature, and Edmonton exterior dewpoint

8.2.6.3 Simulations Using High Summertime Interior Relative Humidity

Additional simulations were run to examine situations that might cause condensation at the lower part of the wall using the Kitchener boundary conditions. Summertime interior conditions are typically drier than exterior conditions due to air conditioning; infiltration of exterior air would raise interior dewpoints. Therefore, the worst likely scenario is interior air at exterior dewpoint conditions.

Exterior dewpoint is plotted with the temperature of the lower portion of the wall in Kitchener in Figure 8.60. Unlike previous simulations of the lower Kitchener wall, this dewpoint rises above the wall surface temperature (compare with Figure 8.48), as seen in the summertime spikes.

Therefore, these conditions were simulated by using an interior climate file with temperatures as per monitored conditions, but with dewpoints identical to exterior for the summer months. When the dewpoint went over interior air temperature, humidity was set to 100%. The assemblies tested in previous work were compared using these conditions; the results are plotted in terms of accumulation at the fictional condensation layer, as shown in Figure 8.61.

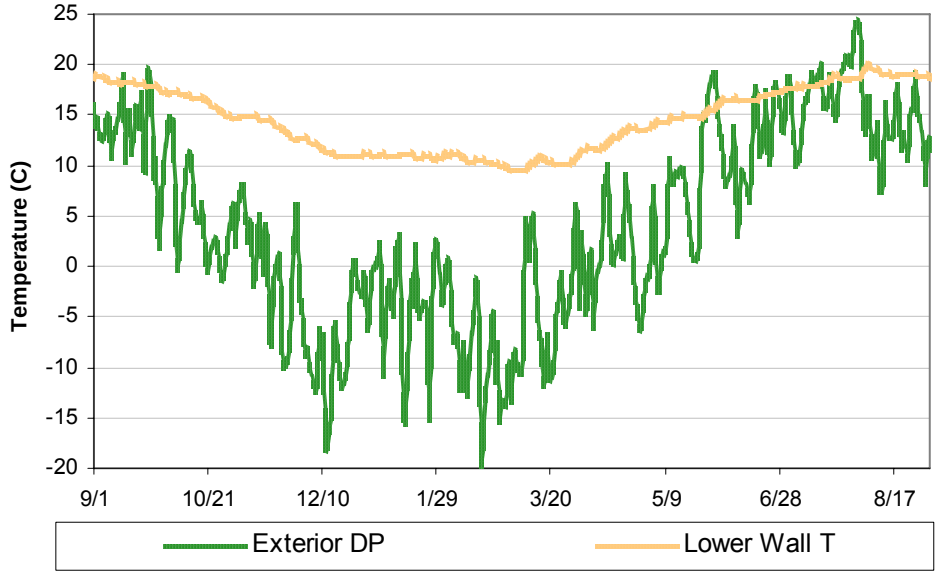

Figure 8.60: Exterior dewpoint and lower wall temperature from Kitchener data

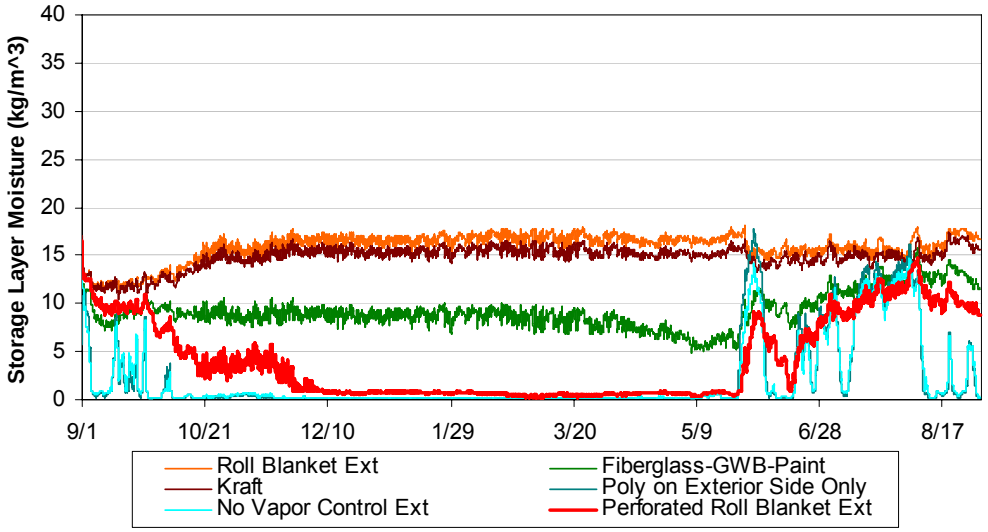

Figure 8.61: Results of Kitchener simulation with elevated summertime interior humidity

This plot shows that accumulation is minimal: it is nowhere near the 500 g/m^2 rundown limit described earlier. This zoomed-in plot shows that the less permeable assemblies (polyethylene and Kraft paper) have slightly greater accumulation levels; the more permeable assemblies show summertime spikes, but are able to dry quickly. XPS is not included in this analysis, given the lack of danger seen in previous simulations.

The question then becomes whether or not these boundary conditions are realistic or representative of typical conditions. For further comparison, the exterior dewpoint and lower wall temperature are plotted for the Huntley site for 2004 and 2005, in Figure 8.62. It shows a similar behavior pattern:

exterior dewpoint exceeds the wall temperature in discontinuous spikes, although Huntley shows longer periods of condensation risk.

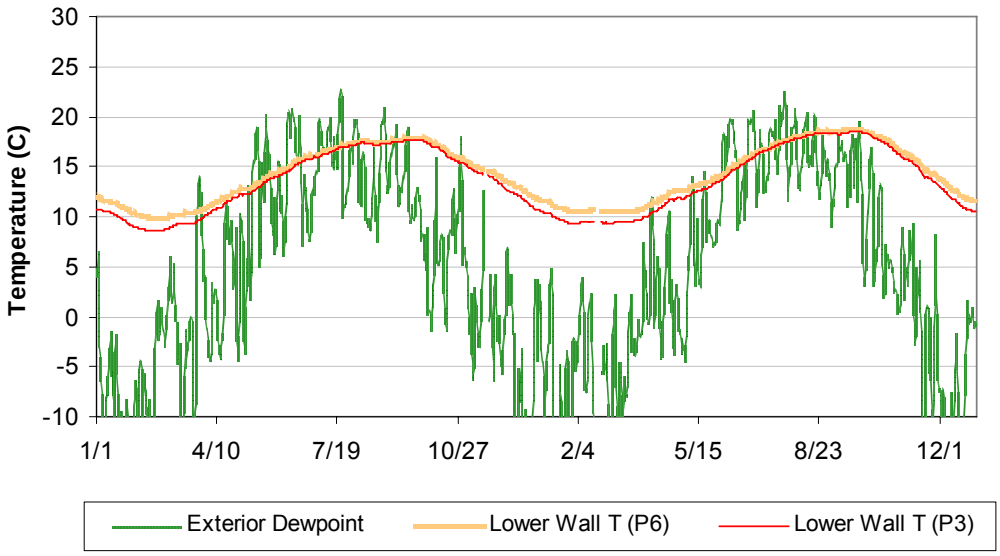

Figure 8.62: Exterior dewpoint and lower wall temperature from Huntley data

This analysis is not meant to imply that that high humidity levels could not cause condensation at the lower portion of the wall, due to soil thermal lag effects. A set of simulations was run with much higher interior dewpoint levels; sinusoidal conditions were set up with a peak condition of 80% RH at 26° C in early August. These conditions resulted in dewpoints above wall temperature for a large portion of the year (roughly April through October). Simulations showed moisture accumulation above the rundown limit in all of the vapor permeable assemblies, and minimal accumulation in the polyethylene and Kraft assemblies, similar to the Edmonton results.

However, these conditions are very unlikely, since they would require significant summertime moisture generation to raise interior dewpoints this far above exterior conditions, not to mention summertime heating of the basement to reach that temperature. Note that to some degree, condensation on the lower portion of the wall is somewhat self-protecting due to climate relationships. Climates that have high summertime exterior dewpoints are also likely to have warmer temperatures at the lowest portion of the wall, therefore reducing the risk. Likewise, locations with colder temperatures at the bottom of wall will likely have lower summertime dewpoints.

Note that none of these simulations account for air transport: it seems quite possible that summertime condensation issues at the lower portion of the wall could be related to the absence of an air barrier.

8.3 Conclusions from Extrapolation Simulations

8.3.1 Above Grade Simulations

8.3.1.1 Wintertime Condensation Issues

The initial interpretation of the above-grade extrapolation simulations would suggest the necessity of an interior vapor control layer to prevent wintertime condensation at the concrete-insulation interface, at most boundary conditions. However, there are several caveats to this interpretation, noted below.

Creating a pass/fail criterion will always be somewhat subjective; estimating mold risk by examining hours over given humidity or humidity/temperature thresholds seemed to show strong risk for all examined walls. However, use of a "condensation accumulation/rundown" limit of 500 g/m^2 at the interface did a reasonable job of differentiating the options.

Using this metric, assemblies with polyethylene or Kraft paper had wintertime accumulation peaks well below this level. The extruded polystyrene (XPS) wall showed excellent performance, due to its combination of vapor resistance and insulating value. More permeable assemblies, such as latex paint/gypsum wallboard, a perforated facer, or no vapor control, showed increasingly worse performance with colder climates, higher interior humidity levels, and increasing permeability. For instance, the latex paint/gypsum board assembly showed accumulation below the limit in some climates (Toronto, St. John's) at "low" relative humidity levels, or even "mid" humidity levels with a sufficiently mild winter (Vancouver). In all cases, using no interior vapor control resulted in accumulation over the 500 g/m^2 limit.

There was a stark difference in behavior between materials considered to be vapor barriers (i.e., below 57 ng/(s·m^2·Pa)/1 perm) and more permeable options. As would be expected, the walls with low permeance interior layers were minimally affected by changes in interior RH, as they are effectively decoupled from the interior. However, further simulation work may be worthwhile to explore the middle ground between assemblies such as Kraft paper, at 17-34 ng/(s·m^2·Pa)/0.3-0.6 perms, and the more permeable latex paint/gypsum board, at 200-1000 ng/(s·m^2·Pa)/3-18 perms. Recent BEG work suggests that latex paint may have a higher dry cup permeability in practice, reducing the wintertime safety margin of this assembly.

All of the wintertime condensation simulations were run using a north facing orientation and a "cold" year for a given climate (when available).

However, some important caveats must be noted when interpreting these simulations. First, as shown by the temperature comparison between in the monitored and simulated performance of the above-grade portion (see 8.1.1.4), the concrete-insulation interface remains much warmer than one-dimensional above-grade simulations predict. This was attributed to the effects of the two-dimensional geometry, specifically the tempering effect of the moderate soil temperatures. The difference was much more pronounced during the winter; summertime interface temperatures matched more closely. Hence, the wintertime condensation risk is expected to be much lower than predicted by the simulations.

In addition, field data suggests that assemblies with higher permeability interior layers can work under conditions that are shown to fail in these simulations. For instance, a field survey of 42 houses in Minnesota with and without interior vapor control (Robert W. Anderson and Associates 1989) showed framing wood moisture content levels well within safe ranges for both types of walls. In contrast, simulations of vapor open assemblies in Minneapolis show moisture accumulation well above the limit, as shown in Figure 8.63. This suggests the simulations are overly conservative. Similarly, anecdotal reports and monitored data from the Chicago area indicate that roll blankets with perforated facers give acceptable performance.

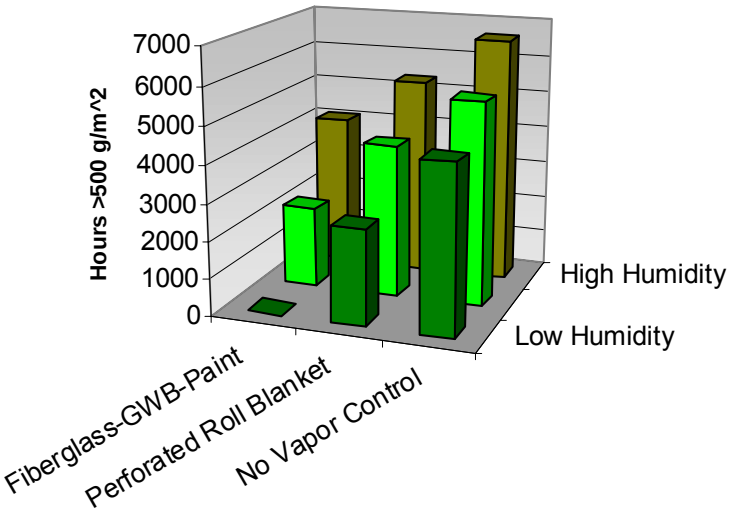

Figure 8.63: Minneapolis AG condensation layer hours over 500 g/m^2

This information suggests that one-dimensional simulations of the above-grade portion are not the best method to determine interior vapor control requirements. The acceptable performance of these more permeable systems might be caused by a combination of several factors, including low interior relative humidity levels, the tempering effect of soil/two-dimensional thermal effects, and possibly the ability of the assemblies to dry between wintertime accumulation seasons (as demonstrated in simulations).

8.3.1.2 Summertime Condensation Issues

In comparing results for four geographic locations, simulations indicated that summertime condensation at the interior vapor control layer due to inward vapor drive is only a problem in climates with significant cooling loads. In order for this problem to occur, a notable portion of the year must have an inward thermal gradient. Climates with negligible cooling loads, such as Vancouver, St. John's, or Edmonton showed minimal accumulation in simulations. Note that the risk factor is an inward thermal gradient; it does not mean the climate must be cooling dominated: problems were noted in heating-dominated climates such as Toronto, ON, Waterloo, ON, and Minneapolis, MN (as shown below in Figure 8.64).

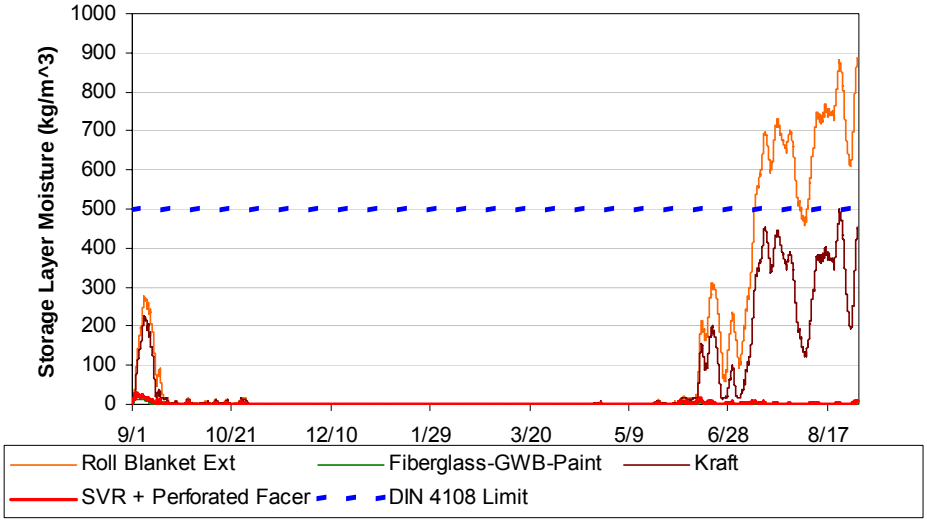

Figure 8.64: Vapor barrier condensation layer MC, Minneapolis above grade, mid RH

In all of these climates, significant problems were only seen with polyethylene. In contrast, Kraft paper, which has an order of magnitude higher permeability (3.4 vs. 17-34 ng/(s·m^2·Pa)), demonstrated accumulation, but below the rundown limit stated above. An additional simulation was run using a variable-permeability polyamide-6 (PA-6) membrane (colloquially known as a "smart vapor retarder"/SVR). This material has permeability that can change between 43-700 ng/(s·m^2·Pa) or 0.8-12 perms, dry/wet cup. Simulations had excellent summertime performance, with negligible accumulation at the exterior side of the membrane, showing the "flow-through" properties of this material at high relative humidity.

Some sources have raised concerns that eliminating the impermeable layer (such as polyethylene) would allow moisture accumulation and damage to the gypsum wallboard interior finish during this summertime inward vapor drive. Although the gypsum board shows a seasonal rise in moisture content over the summer, it is a stable cycle, becoming drier every year (due to the drying of the concrete moisture source). The maximum relative humidity experienced by the gypsum layer is approximately 90%: it does not experience condensation conditions, as found in the polyethylene assembly. This behavior is matched by observations made during disassembly of the Kitchener field site: no indication of mold growth was seen on the exterior side of the gypsum board after the first year of operation. The situation could be considered analogous to a dammed or undammed river: moisture only begins to accumulate at that location when it can no longer travel through the system; otherwise, it flows through without causing damage. The moisture damage only occurs because of the presence of the "dam," or impermeable layer.

All summertime simulations were the south-facing orientation, with a "warm" year for a given climate. The simulations were run using concrete that had dried for six months prior to the installation of insulation. In contrast to the winter simulation, temperatures at the concrete-insulation interface had a reasonable match between monitored data and simulation in the summer.

8.3.2 Below Grade Simulations

A simple analysis of the boundary conditions used in the Kitchener below grade simulations showed that there is only an inward drying potential for the construction moisture of the concrete wall. In addition, the dewpoint relationships showed that there was a minimal chance of condensation of interior moisture on the concrete. The hygrothermal modeling provided the same conclusions: the only situation heading towards condensation was the polyethylene roll blanket. That wall had a ratcheting increase in moisture content at the concrete-insulation interface due to the impermeable layer eliminating drying to the inside. Levels were approaching (but did not exceed) the condensation accumulation limit after six years. However, all walls had sustained periods over 80% RH and the LIM_{Bau} II isopleth: conditions considered favorable for mold growth. Drying of the concrete through the interior insulation is proportional to the permeability of the assembly and inversely proportional to the interior relative humidity (although this is a weaker effect).

However, these simulations must be viewed with some skepticism: the results are for assemblies that have a "perfect" air seal, with no airflow between the interstitial spaces and the interior. In reality, this type of air leakage can increase the drying and/or reduce accumulation in the less permeable systems; small construction defects can easily cause air leakage that will effectively negate extremely low permeance materials such as polyethylene (TenWolde 1998). Further evidence is the comparison between the monitored and simulated data in below grade locations (Sections 8.1.2.4 and 8.1.2.5). The monitored data was consistently drier than the simulation results, possibly because of incidental air leakage.

Simulations using a "synthesized" Edmonton exterior condition ("lower" measured wall conditions shifted by the average annual temperature difference between Kitchener and Edmonton) showed strongly different results. The simple dewpoint temperature comparison showed that interior conditions would have a tendency to cause condensation at the wall over the course of the year. This was supported by the hygrothermal modeling: condensation over the 500 g/m^2 limit was seen for the more permeable options (no vapor control, perforated facer, and latex paint). Also, the less permeable options (polyethylene, Kraft, XPS) showed increasing moisture accumulation headed towards this limit. The only option that showed consistently acceptable performance was the uninsulated bare concrete wall option.

However, these simulations should be viewed with some skepticism. Widespread failures of the below-grade portions of walls in extremely cold climates such as Edmonton are not known to be an issue. Reasons proposed for these differences included the lack of realism of below grade boundary conditions, and the dry climate of Edmonton, resulting in drier interior conditions than used in the model.

Further simulations were run using the Kitchener below-grade boundary conditions and interior air with a dewpoint equal to exterior conditions. This dewpoint only exceeded lower wall temperatures during brief summertime spikes; as a result, minimal moisture accumulation was seen in assemblies. Some simulations were run at very high interior summertime relative humidity levels; the insulation assemblies demonstrated condensation, but these boundary conditions were found to be quite unrealistic. Instead, the climate has a self-limiting or self-protecting nature: high summertime

dewpoints are usually seen in climates that have moderate winters, and therefore, warmer temperatures at the lower wall.

8.3.3 Other Concerns and Observations

Simulations were used to estimate initial moisture content of the concrete wall; they indicated that concrete remains very wet for long periods of time. For instance, even after a year of drying with no insulation or vapor barrier, the majority of the thickness of the wall is still over 90% relative humidity; concrete stores roughly 100 kg/m^3 of water at this condition. An important comparison point is the storage capacity of air, which is much smaller: 17 g/m^3 (0.017 kg/m^3) at 100% RH at 20° C. Therefore, this stored moisture can easily cause high relative humidity conditions in assembly cavities. This behavior may explain why summertime condensation issues at polyethylene can be seen even with walls that have been allowed to dry for several years, as mentioned anecdotally by Swinton and Karagiozis (1995). Note that these results are contingent on the material properties used in the simulations. Concrete with a water/cement ratio of 0.5 was used in simulations; a w/c of 0.7 is more typical for residential basements. A higher w/c ratio yields concrete with higher vapor permeability, faster liquid water uptake, and more built-in moisture. All of these properties would likely change the drying simulations.

In addition, in both above-grade and below-grade simulations, the conditions at the concrete-insulation interface remained at sustained high relative humidity levels, typically above the LIM_{Bau} II level. This behavior was noted by Timusk (1997) in discussing internal basement insulation:

> … the outer layers of the insulation are, at all times, close to the one hundred percent relative humidity line. The region between the one hundred percent and the eighty percent relative humidity lines represents a region where many organic materials and metals are prone to decay. This "danger zone" must be recognized since it can lead to serious deterioration and indoor air quality problems if it is not considered in the design process.

To some degree, this points out the risk of using moisture-sensitive materials such as wood framing or batt insulation in contact with the concrete surface. However, in reality, extensive mold and rot does not always occur at this interface. Several mechanisms are likely at work. First, wood framing has a considerable safe storage volume. Second, imperfections in the assembly will likely results in air leakage, which in most cases will tend to dry the assembly. Finally, the thresholds for mold growth set by the isopleth might be too stringent; work by Doll (2002) and Black (2006) show that the presence of liquid water causes much more rapid mold amplification than sustained high relative humidity levels.

As mentioned in section 8.2.6.1, one concern with eliminating a vapor control layer in the below-grade environment is that moisture sourced from the concrete will increase interior relative humidity. Calculations indicated that drying of concrete construction moisture in a typical house would release roughly 0.5 liters/day, which can be compared with typical interior generation rates for a family of four of 10-15 liters/day. This is not a significant loading in terms of increasing relative humidity, but

is important when that moisture is localized and "trapped" behind impermeable finishes. Simulations were run to gauge the effects of the moisture transport mechanisms of vapor diffusion and liquid capillarity through a concrete wall. They showed that capillarity is far more important, transporting water at a rate an order of magnitude higher than vapor diffusion (from a 100% RH environment); this demonstrates the vital importance of liquid water drainage and capillary isolation of the basement walls from the soil.

One common assembly used in Ontario and Minnesota is a "double polyethylene" stud wall, as discussed in Chapter 2. There is a layer of polyethylene at the concrete-insulation interface, intended as a "moisture barrier," protecting the vulnerable components from concrete-sourced moisture. This moisture barrier typically runs from the slab level to grade. In addition, there is an interior full height polyethylene vapor barrier; however, this assembly was not simulated. The reason for the failures seen in the field is a lack of drying capacity of this assembly when imperfections or incidental wetting result in moisture entry into the stud bay. In simulations, given the "perfect" conditions, this assembly would likely show dry and safe conditions in the stud bay. In reality, it has been shown to be an assembly that is vulnerable to moisture damage.

One quick simulation was run to examine the moisture accumulation behind the outer "moisture barrier" layer. The behavior at the concrete-polyethylene (or concrete-insulation) interface is shown in Figure 8.65, in terms of the condensation layer moisture content and relative humidity. Results are shown both for the double polyethylene wall, as well as the single polyethylene (roll blanket) wall, as a comparison point.

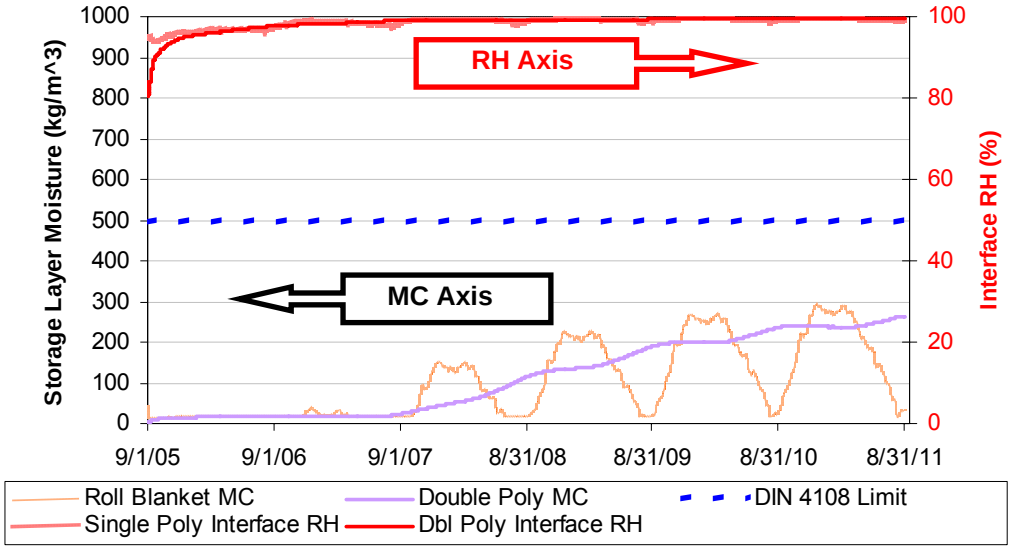

Figure 8.65: Roll blanket and double polyethylene interface condensation layer MC and RH

The results show that as would be expected, moisture accumulates behind the polyethylene at the double polyethylene wall. Although the condensation layer does not show accumulation above the DIN 4108 limit, the relative humidity at that location rises to a consistent 99.5% after six years. In comparison, in the roll blanket wall, the relative humidity is close to this level, but shows more

variation. The moisture content of the condensing layer increases continuously though the simulation; although it might reach the 500 g/m^2 limit, it also seems likely that incidental air leakage might cause some drying in reality. However, it is important to remember that these simulations only include the drying of construction moisture, as opposed to capillary or vapor state moisture coming from the soil.

Chapter 9
Conclusions and Recommendations

The conclusions drawn from this thesis combine the results of field monitoring, hygrothermal simulations, and the literature survey. The first section is a summary of the behavior seen in the experimental walls, followed by a section that examines certain phenomena in detail. The final section provides general recommendations for basement wall insulation assemblies. Some of the important conclusions included the following:

- Air leakage played a large role in the behavior of assemblies: performance could not be predicted simply by the permeability of the assembly, or its least permeable layer.
- The validation of the model was relatively weak: the simulations typically captured relative performance between walls and general seasonal patterns, but failed to accurately predict absolute magnitudes. In general, the simulations typically overpredicted the moisture levels in the assemblies
- The response of the walls to the wetting system was not what was originally expected: the wetting pattern was strongly influenced by details at the concrete-insulation interface and material properties at the interface. As a result, the wetting response was a function of both the amount of water that was originally retained in the system, the location of the wetting plume relative to the sensors, and then the wall performance itself.
- Wintertime condensation or frost formation at the upper portions of the concrete-insulation interface was not observed in any of the monitored walls. Disassembly of the walls showed no damage or evidence of condensation on the exterior side of the stud bay.
- Summertime inward vapor drive resulting in condensation at the polyethylene vapor barrier was conclusively demonstrated at the Kitchener site. It was seen in both the polyethylene roll blanket and frame-polyethylene walls, but was notably worse in the former wall. The summertime condensation was clearly tied to the interior to exterior temperature gradient.
- The monitored data showed that the below-grade portions of the basement walls exhibited temperatures that make interior vapor control unnecessary. Also, the monitored results showed that the basement concrete wall is a source of moisture, even after several years of drying.
- Two general recommendations were noted when considering this research in aggregate. First was the importance of controlling bulk/liquid water, and its overwhelming effect relative to available drying mechanisms. Second, the concrete-insulation interface often remained at high relative humidity levels, suggesting that use of moisture-insensitive materials at this interface is a good way to lower the risk of these assemblies.

9.1 Analysis of Installed and Monitored Assemblies

In neither the Huntley, IL nor the Kitchener, ON monitoring locations did any walls experience conditions that would be considered a moisture-related failure. Neither site had leakage of bulk liquid water from the exterior: the results suggest that if this moisture source is eliminated, many types of interior assemblies can succeed. However, the monitored data and simulations indicated which walls have higher and lower risks.

The "composite" foam walls (25 mm/1" of extruded polystyrene with stud framing and fiberglass or cellulose insulation) were seen as assemblies with a higher first cost, but excellent moisture tolerance. Monitored performance showed that this was the case: concrete-sourced moisture could dry slowly through the semi-vapor permeable foam; as a result, the relative humidity at the foam-concrete interface did not rise to levels linked to mold risks. This drying occurred without moisture accumulation in the vulnerable stud bay cavity. The wetting event had a similar response: even though there was a humidity spike at the concrete-foam interface, moisture levels in the stud bay remained relatively constant, and within safe levels.

The assembly using thicker (50 mm/2") extruded polystyrene foam showed similar performance to the previous walls, when not loaded with moisture. However, when moisture loading from the concrete was higher, such as during wetting events (in Huntley) or when drying construction moisture (in Kitchener), the permeability of the foam was low enough that sustained high relative humidity levels were seen at the concrete-insulation interface. It is not clear whether or not this behavior poses any substantial risk in installed assemblies. For instance, although this data seemed to point out the risk of increasing the thickness of this foam insulation, no mold growth was observed at this interface during the Huntley disassembly.

The single and double polyethylene walls installed in Huntley site had similar behavior to each other in their stud bays; wood moisture contents remained in the safe range. However, in the double polyethylene wall, the relative humidity at the concrete-outer polyethylene interface quickly rose to 95% or higher and remained at this level. This shows the accumulation of concrete-sourced moisture that occurs, even with a concrete wall that had dried for over two years. Therefore, this interface should be detailed with the knowledge that this location has a high mold risk (i.e., air sealing from the interior). After the wetting event, the double polyethylene wall remained at higher relative humidity levels for longer periods, showing the lack of drying available in this assembly. However, wetting system response was a combination of the wall response and the moisture load added to the wall, which in turn was a function of wall construction and geometry.

The stud frame/polyethylene and stud frame/latex paint assemblies were compared at the Kitchener site. Their performance was mostly similar; the lack of a difference might be partially ascribed to installation details. However, the frame-polyethylene wall demonstrated summertime inward vapor drive condensation at the above-grade portion, and had higher wood moisture content levels at the lower portion of the wall (albeit within safe levels), demonstrating inhibited drying. In contrast, the frame-latex paint wall was generally dryer; the above-grade framing had elevated wintertime moisture contents (within safe levels), but they dried over the summer. These results match the findings of the Minnesota study by Robert Anderson and Associates (1989); they found similar wood moisture contents in assemblies with and without polyethylene. These results indicate that polyethylene was not necessary, assuming the boundary conditions of the experimental site. Although

vapor control might be necessary at the above grade portion under other boundary conditions, the vapor resistance of polyethylene is an order of magnitude less permeable than what simulations would require to control wintertime condensation.

The polyethylene roll blanket in Kitchener demonstrated several of the problems predicted with an impermeable assembly, including the inward vapor drive mentioned above, and accumulation of concrete-sourced moisture at the lower portion of the wall. Both of these problems were of a higher magnitude than in the frame/polyethylene wall.

In contrast, the perforated roll blanket wall used in Huntley showed excellent performance, drying to a dewpoint almost identical to interior conditions. However, acceptable performance was contingent on low interior humidity levels; at higher humidity levels (winter or summer), the permeability of this assembly could result in moisture accumulation at the concrete-insulation interface. However, construction moisture and wetting events have a much higher ability to dry with this assembly. Simulations showed that wintertime condensation risks at the upper portion of the wall were higher with colder exterior climates and higher interior humidity levels.

The performance of the foil-faced polyisocyanurate wall was dominated by air leakage due to installation details. Similarly to the perforated roll blanket wall, this resulted in drying at the interior conditions of the Huntley basement, but could pose some risks at higher humidity levels. When the wall was reinstalled without an air gap, moisture began to accumulate at the concrete-insulation assembly, as would be expected given the low permeability of the insulation. However, it did not reach exceptionally high levels.

The polyamide-6 (PA-6) “smart vapor retarder” assembly did not show the superior drying performance that was expected, given its material properties. Its behavior, both with and without wetting events, was closer to patterns seen in the less permeable extruded polystyrene foam walls. The permeance of the PA-6 facer (with the laminated perforated scrim) was calculated, based on the average humidity conditions on both sides of the membrane. The predicted permeance ranged from 120-450 ng/(s·m^2·Pa) (2 to 8 US perms) over the course of the year (higher permeability in the summer). This is more permeable than any of the XPS assemblies: given the drying seen in the very permeable assemblies (e.g., perforated roll blanket), it should have resulted in greater drying.

9.2 General Observations

9.2.1 Air Leakage

One pattern seen repeatedly at both experimental sites was that air leakage played a large role in the behavior of assemblies: performance could not be predicted simply by the permeability of the assembly, or its least permeable layer. This phenomenon was demonstrated in plots of the dewpoint of the assembly with the interior dewpoint. Close correlation between the two dewpoints demonstrated air leakage from interior to the wall cavity; the gap behind the polyisocyanurate wall was an extreme example. Some weaker examples would be the single and double polyethylene stud frame walls in Huntley: dewpoints were much lower than would be expected, given the low permeance of the assembly. In the monitored cases, this air leakage almost always provided drying,

since interior dewpoint was typically lower than assembly dewpoint. It is possible that this air leakage from the interior could cause wetting at higher indoor humidities.

9.2.2 Modeling Correlation

On a related topic, the simulations typically overpredicted the moisture levels in the assemblies, compared to monitored data from the Kitchener site. This was seen in several assemblies, and at all vertical locations in the wall. One example was the comparison between the roll blanket and frame-polyethylene wall. The walls had different behavior patterns, even though the one-dimensional cross section was essentially identical. Possible causes included air leakage, vapor diffusion through the stud frame (in the case of the frame-polyethylene wall), and concrete that was drier than predicted in simulations.

The validation of the model was relatively weak: the simulations typically captured relative performance between walls and general seasonal patterns, but failed to accurately predict absolute magnitudes. However, the higher moisture levels mean that the simulations could be used as a conservative worst case for comparing basement wall assemblies, as long as these limitations are acknowledged.

9.2.3 Wetting System Response

The response of the walls to the wetting system was not what was originally expected. Although the system accurately metered equal amounts of water to the test walls in Huntley, the rundown patterns and distribution of water were a strong function of the individual wall details, and therefore differed between panels. The wetting plume was strongly influenced by small details at the concrete-insulation interface, for instance, following surface cracks, form seams, and instrumentation wires in non-uniform manners. In addition, the material properties played a function: in the double polyethylene wall, the water quickly ran down the polyethylene-insulation interface and drained from the wall, while in the single polyethylene wall, a repeatable wetting plume formed beneath the injector. As a result, the wetting response of the Huntley walls was a function of both the amount of water that was originally retained in the system, the location of the wetting plume relative to the sensors, and then the wall performance itself. Therefore, in future experiments introducing water to assemblies, we would recommend the use of a wetting system, as demonstrated by Van Straaten (2003).

Looking at the overall dewpoint response of the walls over three years (with and without wetting), it appears that the volume of water introduced during wetting events was not overwhelming to any of the assemblies. None of the walls exhibited substantial failures, either in the wetted or non-wetted years.

9.3 Wintertime Condensation

Wintertime condensation or frost formation at the upper portions of the concrete-insulation interface was not observed in any of the monitored walls. Given the low interior relative humidities in Huntley, this was predicted behavior: interior dewpoint never rose above the temperature of the coldest part of the concrete wall. In the Kitchener walls, the relative humidity at the concrete-

insulation interface rose to high levels (90-100% in the frame-latex and frame-polyethylene walls); however, no evidence of condensation was noted in the framing moisture content sensors (peak wintertime MC of 15% in frame-latex wall). Disassembly of the walls showed no damage or evidence of condensation on the exterior side of the stud bay. In addition, the roll blanket and XPS showed lower wintertime relative humidity levels than the frame walls.

Hygrothermal simulations using an imaginary layer to estimate condensation accumulation suggested that vapor control is often necessary on the above-grade portion of basement walls. The level of accumulation varied depending on simulation parameters: with greater interior permeability, colder climates, or higher interior humidity, hours above condensation limit increased. For instance, in the simulations, latex paint (as a vapor control layer) provided acceptable results at "low" and "mid" humidity levels in Toronto, but clearly failed at "high" humidity. In comparison, the vapor barrier materials (polyethylene and Kraft paper) did not show wintertime condensation.

However, in validating the model against data, it was found that the model significantly underpredicts the wintertime temperature at the "upper" level concrete-insulation interface. This was found to be the case in both the Kitchener and Huntley data; this phenomenon was attributed to the effects of the two-dimensional geometry and the tempering effect of the moderate soil temperatures. These two-dimensional effects occurred even with a relatively large (400 mm/16") section of exposed above-grade basement wall. Also, it is worth noting that the soil temperature, at a depth of only 150 mm (6"), never went below freezing, despite sustained sub-freezing weather. This was attributed to the "protection" provided by the latent heat of fusion.

The effect of the warmer-than-predicted surface temperatures at the above-grade section is that the simulations overpredict condensation at the concrete-insulation interface, and would be too conservative to be a useful design tool. This is corroborated both by monitored data (i.e., the acceptable performance of the latex paint wall in Kitchener) and field examples. For instance, several relatively permeable assemblies (latex paint, or a permeable facer) failed in Minneapolis climate simulations. However, the Robert Anderson & Associates (1989) survey showed safe framing moisture contents in walls with and without polyethylene.

This is not to say that vapor control at the upper portion of the wall can be entirely ignored in all cases. During the wintertime disassembly of vapor-open (Owens Corning) walls tested by Goldberg and Aloi (2002) near Duluth, MN, frost and condensation was noted at the above grade concrete-insulation interface. However, it should be noted that the test building was being run under elevated humidity conditions. Other data from that experiment suggested that this wall was able to readily dry incidental moisture and condensation due to its vapor open nature.

The upper portion of the basement wall is likely to be relatively forgiving in terms of interior vapor control, both due to the interface temperature phenomenon discussed above, and the massive hygric storage available in the concrete wall. Simulations of higher permeability assemblies demonstrated that wintertime condensation could often dry to original moisture levels by spring. The detrimental effect of eliminating this concrete storage was demonstrated in Goldberg and Gatland (2006); the use of polyethylene or an impermeable elastomeric coating at the concrete-insulation interface resulted in notable condensation.

9.4 Summertime Inward Vapor Drive

Summertime inward vapor drive resulting in condensation at the polyethylene vapor barrier was conclusively demonstrated at the Kitchener site. It was seen in both the polyethylene roll blanket and frame-polyethylene walls, but was notably worse in the former wall. Possible reasons for this difference included air leakage, storage in the wood framing, and "flanking" vapor diffusion through the framing. The summertime condensation was clearly tied to the interior to exterior temperature gradient: the insulation-polyethylene interface grew wetter when there was an inward thermal gradient, resulting in inward vapor gradient. When the thermal gradient reversed, this interface dried.

This level of moisture accumulation was not seen in the frame-latex paint or XPS walls: although they showed a slight rise in relative humidity, both of them allowed drying to the interior. Disassembly of the frame-latex paint wall showed that the passage of this water vapor caused no damage to the gypsum board or framing during a year of operation. Instead, condensation and damage are the result of having an impermeable material at this interface; without this material, no accumulation or damage occurs.

However, the actual damage seen to the assemblies did not appear to be serious after a year of operation. The frame-polyethylene wall only showed some minor discoloration of the upper inboard portions of the stud framing. The roll blanket wall does not have moisture-sensitive materials to indicate damage, although some brown discoloration was seen in the fiberglass, reflecting transient moisture accumulation. On the other hand, both of the moisture content surrogate sensors (wafers) located at the fiberglass-polyethylene interface showed notable mold growth. In addition, the condensation was likely visible through the polyethylene: homeowners have historically registered callbacks to builders when they saw this problem.

Simulations were run to estimate condensation accumulation at the insulation-vapor barrier interface. Although simulations showed poor correspondence for temperatures at the concrete-insulation interface in the winter, summertime temperatures matched more closely. The results clearly showed substantial accumulation in the polyethylene case (as matched by the data). Lower accumulation levels were seen in the Kraft paper simulations, although they might raise mold concerns, given the vulnerability of a paper-based material.

Geographic extrapolation simulations showed that problems only occurred in climates with notable cooling loads (although still heating-dominated). Climates with insignificant cooling loads, such as Edmonton, Vancouver, and St. Johns, had minimal periods with inward thermal (and therefore vapor) gradients. Therefore, inward vapor drive problems are not very likely in these locations.

9.5 Vapor Control on Below Grade Walls

The monitored results showed that the basement concrete wall is a source of moisture, even after several years of drying. This was particularly pronounced in the double polyethylene wall in Huntley: the relative humidity behind the exterior polyethylene "moisture barrier" rose to 95%+ within a year of installation, and remained at this level for the remainder of the experiment. Simulations indicate that drying of the below-grade concrete wall can only occur to the interior, especially when an exterior dampproofing layer is used.

The monitored data showed that the below-grade portions of the basement walls exhibited temperatures that make interior vapor control unnecessary; the lowest temperatures of the lower concrete wall were comparable to weather data at locations that have no need (or code requirements) for vapor retarders or barriers.

Monitored data showed that the higher-permeability frame-latex paint wall showed consistently lower relative humidity and wood moisture content levels than the frame-polyethylene wall at the below grade sections. The XPS and roll blanket wall showed consistently high relative humidity levels (90%+) in their lowest locations; this was a source of concern for both walls.

In the monitored installations, air leakage tended to dry assemblies; this was especially true in assemblies that accumulated moisture, such as a polyethylene roll blanket. The builder practice of removing the bottom 150 mm (6") of a roll blanket wall are basically taking advantage of this fact, allowing interior air to communicate with the insulation cavity.

Simulations of the below-grade portions of the basement wall all showed better performance and lower moisture levels with increasing permeability, which allowed greater drying of the concrete. However, all simulations showed extended periods over 80% RH (the ASHRAE Standard 160P failure criterion) and LIM_{Bau} II isotherm level (porous substrates such as mineral building materials and some woods) at the concrete-insulation interface. This suggests some of the risks of using moisture-sensitive materials at this interface. On the other hand, as mentioned earlier, simulations typically showed higher moisture levels than monitored data.

Condensation on the lower portions of the wall (due to summertime thermal lag) was not seen in simulations: this response was expected, given the moderate summertime dewpoint levels. Monitored data shows that exterior dewpoint exceeds the lower wall temperature, suggesting possible condensation risks if the basement were ventilated with exterior air. However, simulations were run with interior air at exterior dewpoint; minimal accumulation was seen in the permeable assemblies. In fact, moisture levels were typically lower than the accumulation seen in the impermeable (polyethylene, Kraft) assemblies that could not dry to the interior.

The below-grade simulations using a synthesized Edmonton boundary condition showed moisture accumulation problems under almost all circumstances. However, these results were viewed with skepticism: widespread failures of below-grade insulation in Edmonton are not reported. Closer analysis revealed that the interior humidity levels used here were not very realistic, given the extreme dryness of the Edmonton climate.

One important conclusion of the simulations was that under all interior relative humidity conditions, there was no risk of moisture accumulation due to lack of vapor control on lower walls. This fact, combined with the monitored observations, strongly suggests that low permeance materials are detrimental at the below grade portions of the basement wall. However, there are likely several objections that would be raised to the removal of the vapor control layer from this portion of the wall.

One issue would be summertime condensation caused by thermal lag, as mentioned above. Large amounts of outdoor air could be introduced to the basement by, for example, a walkout condition (e.g., leaving the door open), or through duct leakage. However, given the lack of problems seen in simulations of this condition, it seems quite possible that an air barrier, as opposed to a vapor barrier, is necessary. An air barrier might reduce the transport rate enough that concrete storage (both

adsorption and surface storage) could safely handle the moisture load, and then allow drying under more favorable conditions.

An argument against eliminating this vapor control layer is that carpets located on basement slabs are well known as a source of mold and poor indoor air quality. Although this issue cannot be dismissed lightly, it is notable that carpets provide insulation, but have an air barrier on the cold side of the assembly. This allows interior air to easily communicate with the coldest surface (bottom layer of the carpet), creating greater condensation risk. Second, carpets are particularly amenable as a food source, being a horizontal surface that traps dust, dirt, food particles, etc. Finally, if a polyethylene vapor retarder is not specified underneath the slab, the concrete can be a significant source of moisture via vapor diffusion or liquid capillarity. The vapor permeance of carpet backer is not known, but it may not be high enough to prevent some accumulation, thus creating conditions favorable for mold growth under the carpet.

One final reason given for vapor control at the lower portion of the wall is that moisture sourced from the concrete will raise interior humidity levels if that layer is eliminated. However, rough calculations were run comparing moisture transport by vapor diffusion and liquid capillarity; they demonstrated that capillarity is far more important, transporting water an order of magnitude faster than vapor diffusion (from a 100% RH environment). The conclusion that can be drawn is that if liquid capillarity can be eliminated, the moisture emission rate becomes negligible. Therefore, it seems more worthwhile to eliminate this moisture source (by measures such as a sub-slab polyethylene vapor barrier, an exterior drainage board, and a capillary break over the footings), rather than to specify a material that will inhibit drying of the assembly. The vapor diffusion rate is not a significant loading in terms of increasing relative humidity, but is important when that moisture is localized and “trapped” behind impermeable finishes. In addition, the emission rate of the drying of concrete construction moisture was estimated; it was comparable to the vapor diffusion rate calculated earlier.

9.6 General Recommendations for Basement Assemblies

One observation consistently noted in studies and field investigations is that the failure of interior basement insulation is strongly linked to bulk water leakage sources—for example, inadequate surface drainage; missing/clogged eavestroughs, downspouts, and footing drains; or foundation cracks, etc., as detailed in Chapter 3. Bulk water often has a dominant effect compared to other moisture transport mechanisms, due to its higher transport rate, and its ability to overwhelm available drying mechanisms. Therefore, the most important consideration in designing moisture-resistant insulated basement assemblies is to control the entry of liquid bulk water.

One location that requires particular attention is the interface between the exterior soil and the basement wall, given that the surrounding earth will be a source of liquid bulk water (e.g., percolating rainwater), capillary moisture, and water vapor diffusion (100% RH soil conditions). Basement walls are typically protected by dampproofing on the exterior, which is meant to control capillarity and vapor diffusion. However, dampproofing cannot be considered a reliable barrier against liquid water. Waterproofing, which is designed to withstand hydrostatic head, can meet this requirement. The use of a robust exterior drainage layer seems to be a clear way to provide effective protection at this interface.

Anecdotal evidence supports the dramatic difference that results from the addition of exterior drainage. The Ontario New Home Warranty Plan tracks customer complaints to builders by subject; after the use of an exterior drainage layer below grade was mandated by code, basement complaints dropped from among the top three complaints to below the top ten level.

Another general recommendation stems from simulation results: in all cases, with both permeable and impermeable assemblies, the insulation-concrete interface stayed at high relative humidity levels for extended periods. In contrast, monitored data showed lower humidity levels than simulations; furthermore, widespread mold growth at this interface is the exception rather than the rule. This fact was attributed to air leakage drying due to imperfections in the assembly. However, these results raise questions as to why one would specify a moisture-sensitive material such as wood framing at this interface; the success of this assembly almost seems dependent on accidental imperfections, instead of correct execution of the design. This provides a strong reason to use moisture-insensitive materials such as plastic foam insulation board at the concrete-insulation interface.

Chapter 10
Recommendations and Future Work

The final items presented here are descriptions of proposed wall assemblies, with a discussion on how they meet the design challenges of interior basement insulation, and recommendations for future research.

10.1 Proposed Wall Assemblies

Two assemblies are proposed here that might warrant further examination with hygrothermal simulation and/or field monitoring; they are based on insights gained from this thesis research.

10.1.1 Thin Foam Composite Wall

The "composite" walls (extruded polystyrene foam and insulated stud frame) showed superior performance: they allowed controlled drying of the concrete without damage to the wood framing. A potentially more economical version of this wall could substitute the 25 mm (1") foam with a thinner layer, such as 12 mm (½"), or possibly even 6 mm (¼"). This assembly retains the use of a moisture-tolerant material at the concrete-insulation interface, protecting the stud framing. This assembly would retain the use of latex paint on gypsum board as the interior vapor control mechanism.

The field monitoring data indicated that above-grade wintertime condensation is much less likely than static one-dimensional thermal calculations would suggest. Therefore, a thinner foam layer would likely control condensation. Thicker foam insulation is needed to control air leakage condensation in colder climates and/or at higher interior humidities.

The thermal gradients at the lower portion of the wall are relatively small, so a thin layer of foam would likely keep the surface temperature above interior dewpoint. However, this material eliminates the safety factor provided by the storage capacity of the concrete wall.

Thinner XPS foam is often manufactured with an impermeable facer; this product should likely be avoided in this application, due to the resulting elimination of drying to the interior.

This assembly would have a lower material cost; whether or not this would result in labor savings is uncertain. The thinner foam has greater physical flexibility, possibly allowing installation by being adhered to the concrete, thus simultaneously addressing air leakage issues.

10.1.2 Hybrid Roll Blanket

Cost-sensitive builders typically insulate basements to meet code requirements, while trying to avoid undue risk. However, many of the high-performance interior basement insulation assemblies are unlikely to meet their cost requirements. Therefore, many builders turn to more cost-effective solutions, such as the roll blanket. However, the data from the Kitchener site demonstrated that the impermeable polyethylene roll blanket was susceptible to summertime above-grade condensation due

to inward vapor drives, and to accumulation of concrete-sourced moisture at the lower portion of the wall.

These results show that there is a need for a low-cost basement insulation system that does not accumulate moisture. The perforated blanket (as tested in Huntley) allowed rapid drying to the interior, given the facer permeability of 700 to 1000 ng/(s·m^2·Pa) (12 to 18 perms). It showed excellent performance during the winter; no condensation risk was noted. However, it is not clear whether vapor control can be entirely eliminated at the above-grade wall in all cases. This vapor control layer should not be polyethylene, at 3 ng/(s·m^2·Pa) (0.06 perms), due to the problems mentioned above. However, simulations showed that inward vapor drive accumulation was greatly reduced when using a Kraft paper vapor control layer, at 17 to 160 ng/(s·m^2·Pa) (0.3 to 3 perms). This material meets code definitions for a vapor barrier, and successfully controlled wintertime condensation in all simulation locations. These bounding conditions suggest that a material on the order of 57 ng/(s·m^2·Pa) (1 perm) would provide wintertime vapor control and avoid summertime inward drive issues.

Therefore, the proposed assembly would use a roll blanket insulation with a facer of roughly 57 ng/(s·m^2·Pa) (1 perm) on the upper portion of the wall. In contrast, the below-grade portion benefits from greater drying and does not need vapor control (although an air barrier might be warranted); a perforated roll blanket would be used on the lower portion of the wall. Of course, both of the facer materials need to meet fire code exposure requirements (i.e., flame spread and smoke developed indices). Also, this material should ideally be a material that is not conductive to mold growth.

The ideal location for a dividing line between the “upper” and “lower” portions is unclear; this research suggests that only small portions of the below grade wall (e.g., 0.3 m/1 foot) would benefit from vapor control. However, roll blankets are currently fabricated in 4 foot widths, which match 8 foot tall basement wall heights; so it is likely that this manufacturing limitation would set this dividing line. The new Ontario Building Code requires full-height basement insulation; therefore, eight-foot roll blankets may be quite practical. This assembly would require an air barrier separating the “upper”and “lower” portions of the blanket, as well as an indication of the correct orientation.

10.2 Further Research Needs

Several topics were uncovered in this research that would benefit from further exploration.

Many of the WUFI hygrothermal models showed a lack of correspondence to monitored data: possible reasons for this issue included incidental air leakage, vapor diffusion flanking, lower initial concrete moisture content, and storage in wood framing. Some of these reasons could be examined with further simulation. For instance, simulations with a lower “effective permeance” of the vapor control layer might show improved correlation to monitored data that includes air leakage. Also, if material properties can be determined for concrete with a higher water to cement ratio (e.g., 0.7), that might improve correlation. Specifically, higher w/c concrete has a higher vapor permeability; this would have increased the speed of initial drying, and potentially reduced the initial moisture load.

One notable lack of correlation between simulations and monitored data was the temperatures of the above-grade simulations. This was ascribed to two-dimensional effects, in particular, the effect of soil temperatures. These interface temperatures were much higher than predicted by static R-value

calculations of the concrete wall. Therefore, two dimensional thermal modeling with packages such as THERM (static), HEAT2 or WUFI 2D (dynamic) might provide better predictions of above-grade interface temperatures. Alternately, some of the existing models that predict ground-coupled heat loss from foundations (Deru 2002) might provide predictions. These results would provide boundary conditions for calculating vapor control requirements for the above-grade portion of the wall.

If such a model were validated, it could be used for several other basement insulation problems. For instance, when using exterior foundation insulation, the thermal bridge created by a brick ledge is a concern. This simulation could gauge the magnitude of this problem, and evaluate proposed solutions. Some have proposed using a hybrid exterior/interior basement insulation system, with exterior insulation to grade, and interior insulation at the above-grade portion. The magnitude of the thermal bridge could be estimated with this model.

The extrapolations simulations of the below grade wall in Alberta indicated moisture accumulation might result; the validity of this result was questionable, given that interior humidity levels were higher than would be expected in reality. However, measurements of temperatures of the below-grade portion of insulated basement walls in colder climates would provide useful boundary conditions to determine whether or not condensation is at all likely.

One topic that was not prioritized in this research was concrete block foundations; both research sites were cast concrete basement walls. Block foundations are known to have issues with thermal looping within their cores, resulting in colder temperatures at the foundation wall-insulation interface. Although codes often require measures to prevent this convective looping, better understanding of these types of foundations would be useful to provide potential worst-case condensation conditions.

One limitation of this thesis research was that interior conditions were not driven to more challenging humidity levels. Increasing wintertime relative humidity and gauging the risk or extent of condensation would have provided valuable limiting cases for these insulation assemblies. In addition, long-term monitoring of this failure case would measure the ability of these assemblies to store moisture (e.g., in the concrete), and then dry without resulting in mold damage to the assembly.

Finally, the Kitchener site is still in operation and collecting data. Data from this upcoming summer can help determine whether or not the extent of the summertime inward vapor drive was purely a function of construction moisture, or if this problem will continue to occur seasonally. The use of an exterior drainage mat eliminates the soil as a moisture source. In addition, measures were taken to reduce air leakage and vapor diffusion flanking in the frame-polyethylene wall; this might result in behavior closer to the polyethylene roll blanket. Moisture accumulation in the lower portion of the extruded polystyrene and roll blanket walls should also continue to be monitored. At the conclusion of the experiment, all walls should be disassembled and examined for damage or mold growth, similar to the Huntley site. This will provide insight into the damage that correlates with monitored data.

Appendix A

Sensors and Data Collection Equipment

The tables below list the instrumentation used in the field monitoring portion of the research. Specification sheets are attached.

Huntley, Illinois Site

The following instruments were used at the Huntley, Illinois (Chicago-area) site.

Instrument	Specification Summary
Data collection	Campbell Scientific CR10X-2M Measurement and Control System (2 MB extended memory)
Outdoor temperature/humidity	Campbell Scientific Temperature and Relative Humidity Probe Model CS500
Temperature	Honeywell (formerly Fenwal) Uni-Curve® Interchangeable Thermistor; 192-103LET-A01 10,000 Ω at 25° C, ±0.2° C tolerance
Relative Humidity	Honeywell Humidity Sensor HIH-3610 Series
Soil moisture content	Model 223 Delmhorst Cylindrical Soil Moisture Block

Kitchener, Ontario Site

The following instruments were used at the Kitchener, Ontario, Canada site.

Instrument	Specification Summary
Data collection	Campbell Scientific CR1000 Measurement and Control System
Temperature	Honeywell (formerly Fenwal) Uni-Curve® Interchangeable Thermistor; 192-103LET-A01 10,000 Ω at 25° C, ±0.2° C tolerance
Relative Humidity	Honeywell Humidity Sensor HIH-3610 Series
Soil moisture content	Model 223 Delmhorst Cylindrical Soil Moisture Block

Outdoor temperature and humidity at this site were measured with the same Honeywell sensors used for interior measurements.

CR10X Specifications

Electrical specifications are valid over a -25° to +50°C range unless otherwise specified; non-condensing environment required. To maintain electrical specifications, Campbell Scientific recommends recalibrating dataloggers every two years.

PROGRAM EXECUTION RATE

Program is synchronized with real-time up to 64 Hz. One channel can be measured at this rate with uninterrupted data transfer. Burst measurements up to 750 Hz are possible over short intervals.

ANALOG INPUTS

NUMBER OF CHANNELS: 6 differential or 12 single-ended, individually configured. Channel expansion provided by AM16/32 or AM416 Relay Multiplexers and AM25T Thermocouple Multiplexers.

ACCURACY: ±0.1% of FSR (-25° to 50°C); ±0.05% of FSR (0° to 40°C); e.g., ±0.1% FSR = ±5.0 mV for ±2500 mV range

RANGE AND RESOLUTION:

Full Scale Input Range (mV)	*Resolution (µV) Differential*	*Single-Ended*
±2500	333	666
±250	33.3	66.6
±25	3.33	6.66
±7.5	1.00	2.00
±2.5	0.33	0.66

INPUT SAMPLE RATES: Includes the measurement time and conversion to engineering units. The fast and slow measurements integrate the signal for 0.25 and 2.72 ms, respectively. Differential measurements incorporate two integrations with reversed input polarities to reduce thermal offset and common mode errors.

Fast single-ended voltage:	2.6 ms
Fast differential voltage:	4.2 ms
Slow single-ended voltage:	5.1 ms
Slow differential voltage:	9.2 ms
Differential with 60 Hz rejection:	25.9 ms
Fast differential thermocouple:	8.6 ms

INPUT NOISE VOLTAGE (for ±2.5 mV range):
Fast differential: 0.82 µV rms
Slow differential: 0.25 µV rms
Differential with 60 Hz rejection: 0.18 µV rms

COMMON MODE RANGE: ±2.5 V

DC COMMON MODE REJECTION: >140 dB

NORMAL MODE REJECTION: 70 dB (60 Hz with slow differential measurement)

INPUT CURRENT: ±9 nA maximum

INPUT RESISTANCE: 20 Gohms typical

ANALOG OUTPUTS

DESCRIPTION: 3 switched, active only during measurement, one at a time.

RANGE: ±2.5 V

RESOLUTION: 0.67 mV

ACCURACY: ±5 mV; ±2.5 mV (0° to 40°C)

CURRENT SOURCING: 25 mA

CURRENT SINKING: 25 mA

FREQUENCY SWEEP FUNCTION: The switched outputs provide a programmable swept frequency, 0 to 2.5 V square wave for exciting vibrating wire transducers.

RESISTANCE MEASUREMENTS

MEASUREMENT TYPES: The CR10X provides ratiometric bridge measurements of 4- and 6-wire full bridge, and 2-, 3-, and 4-wire half bridges. Precise dual polarity excitation using any of the switched outputs eliminates dc errors. Conductivity measurements use a dual polarity 0.75 ms excitation to minimize polarization errors.

ACCURACY: ±0.02% of FSR plus bridge resistor error.

PERIOD AVERAGING MEASUREMENTS

The average period for a single cycle is determined by measuring the duration of a specified number of cycles. Any of the 12 single-ended analog input channels can be used. Signal attentuation and ac coupling are typically required.

INPUT FREQUENCY RANGE:

Signal peak-to-peak[1] *Min.*	*Max.*	*Min. Pulse w.*	*Max Freq.[2]*
500 mV	5.0 V	2.5 µs	200 kHz
10 mV	2.0 V	10 µs	50 kHz
5 mV	2.0 V	62 µs	8 kHz
2 mV	2.0 V	100 µs	5 kHz

[1]Signals centered around datalogger ground
[2]Assuming 50% duty cycle

RESOLUTION: 35 ns divided by the number of cycles measured

ACCURACY: ±0.03% of reading

TIME REQUIRED FOR MEASUREMENT: Signal period times the number of cycles measured plus 1.5 cycles + 2 ms

PULSE COUNTERS

NUMBER OF PULSE COUNTER CHANNELS: 2 eight-bit or 1 sixteen-bit; software selectable as switch closure, high frequency pulse, and low level ac.

MAXIMUM COUNT RATE: 16 kHz, eight-bit counter; 400 kHz, sixteen-bit counter. Channels are scanned at 8 or 64 Hz (software selectable).

SWITCH CLOSURE MODE
Minimum Switch Closed Time: 5 ms
Minimum Switch Open Time: 6 ms
Maximum Bounce Time: 1 ms open without being counted

HIGH FREQUENCY PULSE MODE
Minimum Pulse Width: 1.2 µs
Maximum Input Frequency: 400 kHz
Voltage Thresholds: Count upon transition from below 1.5 V to above 3.5 V at low frequencies. Larger input transitions are required at high frequencies because of input filter with 1.2 µs time constant. Signals up to 400 kHz will be counted if centered around +2.5 V with deviations ≥ ±2.5 V for ≥ 1.2 µs.
Maximum Input Voltage: ±20 V

LOW LEVEL AC MODE
(Typical of magnetic pulse flow transducers or other low voltage, sine wave outputs.)

Input Hysteresis: 14 mV

Maximum ac Input Voltage: ±20 V

Minimum ac Input Voltage: (Sine wave mV RMS)	Range (Hz)
20	1.0 to 1000
200	0.5 to 10,000
1000	0.3 to 16,000

DIGITAL I/O PORTS

8 ports, software selectable as binary inputs or control outputs. 3 ports can be configured to count switch closures up to 40 Hz.

OUTPUT VOLTAGES (no load): high 5.0 V ±0.1 V; low < 0.1 V

OUTPUT RESISTANCE: 500 ohms

INPUT STATE: high 3.0 to 5.5 V; low -0.5 to 0.8 V

INPUT RESISTANCE: 100 kohms

SDI-12 INTERFACE STANDARD

Digital I/O Ports C1-C8 support SDI-12 asynchronous communication; up to ten SDI-12 sensors can be connected to each port. Meets SDI-12 Standard version 1.2 for datalogger and sensor modes.

CR10XTCR THERMOCOUPLE REFERENCE

POLYNOMIAL LINEARIZATION ERROR: Typically <±0.5°C (-35° to +50°C), <±0.1°C (-24° to +45°C).

INTERCHANGEABILITY ERROR: Typically <±0.2°C (0° to +60°C) increasing to ±0.4°C (at -35°C).

CE COMPLIANCE (as of 09/01)

STANDARD(S) TO WHICH CONFORMITY IS DECLARED:
EN55022: 1995 and EN61326: 1998

EMI and ESD PROTECTION

IMMUNITY: Meets or exceeds following standards:
ESD: per IEC 1000-4-2; ±8 kV air, ±4 kV contact discharge
RF: per IEC 1000-4-3; 3 V/m, 80-1000 MHz
EFT: per IEC 1000-4-4; 1 kV power, 500 V I/O
Surge: per IEC 1000-4-5; 1 kV power and I/O
Conducted: per IEC 1000-4-6; 3 V 150 kHz-80 MHz

Emissions and immunity performance criteria available on request.

CPU AND INTERFACE

PROCESSOR: Hitachi 6303

PROGRAM STORAGE: Up to 16 kbytes for active program; additional 16 kbytes for alternate programs. Operating system stored in 128 kbytes Flash memory.

DATA STORAGE: 128 kbytes SRAM standard (approximately 60,000 data values). Additional 2 Mbytes Flash available as an option.

OPTIONAL KEYBOARD DISPLAY: 8-digit LCD (0.5" digits)

PERIPHERAL INTERFACE: 9 pin D-type connector for keyboard display, storage module, modem, printer, card storage module, and RS-232 adapter.

BAUD RATES: Selectable at 300, 1200, 9600 and 76,800 bps for synchronous devices. ASCII communication protocol is one start bit, one stop bit, eight data bits (no parity).

CLOCK ACCURACY: ±1 minute per month

SYSTEM POWER REQUIREMENTS

VOLTAGE: 9.6 to 16 Vdc

TYPICAL CURRENT DRAIN: 1.3 mA quiescent, 13 mA during processing, and 46 mA during analog measurement.

BATTERIES: Any 12 V battery can be connected as a primary power source. Several power supply options are available from Campbell Scientific. The Model CR2430 lithium battery for clock and SRAM backup has a capacity of 270 mAhr.

PHYSICAL SPECIFICATIONS

SIZE: 7.8" x 3.5" x 1.5" - Measurement & Control Module; 9" x 3.5" x 2.9" - with CR10WP Wiring Panel. Additional clearance required for serial cable and sensor leads.

WEIGHT: 2 lbs

WARRANTY

Three years against defects in materials and workmanship.

We recommend that you confirm system configuration and critical specifications with Campbell Scientific before purchase.

CAMPBELL SCIENTIFIC, INC.
815 W. 1800 N. • Logan, Utah 84321-1784 • (435) 753-2342 • FAX (435) 750-9540
Offices also located in: Australia • Brazil • Canada • England • France • South Africa • Spain

CR1000 Specifications

Electrical specifications are valid over a -25° to +50°C range unless otherwise specified; non-condensing environment required. To maintain electrical specifications, Campbell Scientific recommends recalibrating dataloggers every two years.

PROGRAM EXECUTION RATE

10 ms to 30 min. @ 10 ms increments

ANALOG INPUTS

8 differential (DF) or 16 single-ended (SE) individually configured. Channel expansion provided by AM16/32 and AM25T multiplexers.

RANGES and RESOLUTION: Basic resolution (Basic Res) is the A/D resolution of a single conversion. **Resolution of DF measurements with input reversal is half the Basic Res.**

	Input Referred Noise Voltage	
Input Range (mV)[1]	DF Res (µV)[2]	Basic Res (µV)
±5000	667	1333
±2500	333	667
±250	33.3	66.7
±25	3.33	6.7
±7.5	1.0	2.0
±2.5	0.33	0.67

[1]Range overhead of ~9% exists on all ranges to guarantee that full-scale values will not cause over-range.

[2]Resolution of DF measurements with input reversal.

ACCURACY[3]:
±(0.06% of reading + offset), 0° to 40°C
±(0.12% of reading + offset), -25° to 50°C
±(0.18% of reading + offset), -55° to 85°C

[3]The sensor and measurement noise are not included and the offsets are the following:
Offset for DF w/input reversal = 1.5·Basic Res + 1.0 µV
Offset for DF w/o input reversal = 3·Basic Res + 2.0 µV
Offset for SE = 3·Basic Res + 3.0 µV

INPUT NOISE VOLTAGE: For DF measurements with input reversal on ±2.5 mV input range; digital resolution dominates for higher ranges.

250 µs Integration:	0.34 µV RMS
50/60 Hz Integration:	0.19 µV RMS

MINIMUM TIME BETWEEN VOLTAGE MEASUREMENTS: Includes the measurement time and conversion to engineering units. For voltage measurements, the CR1000 integrates the input signal for 0.25 ms or a full 16.66 ms or 20 ms line cycle for 50/60 Hz noise rejection. DF measurements with input reversal incorporate two integrations with reversed input polarities to reduce thermal offset and common mode errors and therefore take twice as long.

250 µs Analog Integration:	~1 ms SE
1/60 Hz Analog Integration:	~20 ms SE
1/50 Hz Analog Integration:	~25 ms SE

COMMON MODE RANGE: ±5 V

DC COMMON MODE REJECTION: >100 dB

NORMAL MODE REJECTION: 70 dB @ 60 Hz when using 60 Hz rejection

SUSTAINED INPUT VOLTAGE W/O DAMAGE: ±16 Vdc max.

INPUT CURRENT: ±1 nA typical, ±6 nA max. @ 50°C; ±90 nA @ 85°C

INPUT RESISTANCE: 20 Gohms typical

ACCURACY OF BUILT-IN REFERENCE JUNCTION THERMISTOR (for thermocouple measurements):
±0.3°C, -25° to 50°C
±0.8°C, -55° to 85°C (-XT only)

ANALOG OUTPUTS

3 switched voltage, active only during measurement, one at a time.

RANGE AND RESOLUTION: Voltage outputs programmable between ±2.5 V with 0.67 mV resolution.

ACCURACY: ±(0.06% of setting + 0.8 mV), 0° to 40°C
±(0.12% of setting + 0.8 mV), -25° to 50°C
±(0.18% of setting + 0.8 mV), -55° to 85°C (-XT only)

CURRENT SOURCING/SINKING: ±25 mA

RESISTANCE MEASUREMENTS

MEASUREMENT TYPES: The CR1000 provides ratiometric measurements of 4- and 6-wire full bridges, and 2-, 3-, and 4-wire half bridges. Precise, dual polarity excitation using any of the 3 switched voltage excitations eliminates dc errors.

RATIO ACCURACY[3]: Assuming excitation voltage of at least 1000 mV, not including bridge resistor error.

±(0.04% of voltage reading + offset)/V_X

[3]The sensor and measurement noise are not included and the offsets are the following:
Offset for DF w/input reversal = 1.5·Basic Res + 1.0 µV
Offset for DF w/o input reversal = 3·Basic Res + 2.0 µV
Offset for SE = 3·Basic Res + 3.0 µV

Offset values are reduced by a factor of 2 when excitation reversal is used.

PERIOD AVERAGING MEASUREMENTS

The average period for a single cycle is determined by measuring the average duration of a specified number of cycles. The period resolution is 192 ns divided by the specified number of cycles to be measured; the period accuracy is ±(0.01% of reading + resolution). Any of the 16 SE analog inputs can be used for period averaging. Signal limiting are typically required for the SE analog channel.

INPUT FREQUENCY RANGE:

Input Range	Signal (peak to peak)[4] Min	Max	Min. Pulse W.	Max[5] Freq.
±2500 mV	500 mV	10 V	2.5 µs	200 kHz
±250 mV	10 mV	2 V	10 µs	50 kHz
±25 mV	5 mV	2 V	62 µs	8 kHz
±2.5 mV	2 mV	2 V	100 µs	5 kHz

[4]The signal is centered at the datalogger ground.

[5]The maximum frequency = 1/(Twice Minimum Pulse Width) for 50% of duty cycle signals.

PULSE COUNTERS

Two 24-bit inputs selectable for switch closure, high frequency pulse, or low-level ac.

MAXIMUM COUNTS PER SCAN: 16.7×10^6

SWITCH CLOSURE MODE:
Minimum Switch Closed Time: 5 ms
Minimum Switch Open Time: 6 ms
Max. Bounce Time: 1 ms open w/o being counted

HIGH FREQUENCY PULSE MODE:
Maximum Input Frequency: 250 kHz
Maximum Input Voltage: ±20 V
Voltage Thresholds: Count upon transition from below 0.9 V to above 2.2 V after input filter with 1.2 µs time constant.

LOW LEVEL AC MODE: Internal ac coupling removes dc offsets up to ±0.5 V.

Input Hysteresis: 16 mV @ 1 Hz
Maximum ac Input Voltage: ±20 V
Minimum ac Input Voltage:

Sine wave (mV RMS)	Range (Hz)
20	1.0 to 20
200	0.5 to 200
2000	0.3 to 10,000
5000	0.3 to 20,000

DIGITAL I/O PORTS

8 ports software selectable, as binary inputs or control outputs. C1-C8 also provide edge timing, subroutine interrupts/wake up, switch closure pulse counting, high frequency pulse counting, asynchronous communications (UART), SDI-12 communications, and SDM communications.

HIGH FREQUENCY MAX: 400 kHz

SWITCH CLOSURE FREQUENCY MAX: 150 Hz

OUTPUT VOLTAGES (no load): high 5.0 V ±0.1 V; low <0.1

OUTPUT RESISTANCE: 330 ohms

INPUT STATE: high 3.8 to 5.3 V; low -0.3 to 1.2 V

INPUT HYSTERISIS: 1.4 V

INPUT RESISTANCE: 100 kohms

SWITCHED 12 V

One independent 12 V unregulated sources switched on and off under program control. Thermal fuse hold current = 900 mA @ 20°C, 650 mA @ 50°C, 360 mA @ 85°C.

SDI-12 INTERFACE SUPPORT

Control ports 1, 3, 5, and 7 may be configured for SDI-12 asynchronous communications. Up to ten SDI-12 sensors are supported per port. It meets SDI-12 Standard version 1.3 for datalogger mode.

CE COMPLIANCE

STANDARD(S) TO WHICH CONFORMITY IS DECLARED: IEC61326:2002

CPU AND INTERFACE

PROCESSOR: Hitachi H8S 2322 (16-bit CPU with 32-bit internal core)

MEMORY: 2 Mbytes of Flash for operating system; 2 Mbytes of battery-backed SRAM for CPU usage, program storage and data storage; 4 Mbytes optional

SERIAL INTERFACES: CS I/O port is used to interface with Campbell Scientific peripherals; RS-232 port is for computer or non-CSI modem connection.

PARALLEL INTERFACE: 40-pin interface for attaching data storage or communication peripherals such as the CFM100 module

BAUD RATES: Selectable from 300 bps to 115.2 kbps. ASCII protocol is one start bit, one stop bit, eight data bits, and no parity.

CLOCK ACCURACY: ±3 min. per year

SYSTEM POWER REQUIREMENTS

VOLTAGE: 9.6 to 16 Vdc

TYPICAL CURRENT DRAIN:
Sleep Mode: ~0.6 mA
1 Hz Scan (8 diff. meas., 60 Hz rej., 2 pulse meas.)
w/RS-232 communication: 19 mA
w/o RS-232 communication: 4.2 mA
1 Hz Scan (8 diff. meas., 250 µs integ., 2 pulse meas.)
w/RS-232 communication: 16.7 mA
w/o RS-232 communication: 1 mA
100 Hz Scan (4 diff. meas., 250 µs integ.)
w/RS-232 communication: 27.6 mA
w/o RS-232 communication: 16.2 mA

EXTERNAL BATTERIES: 12 Vdc nominal; reverse polarity protected.

PHYSICAL SPECIFICATIONS

MEASUREMENT & CONTROL MODULE SIZE: 8.5" x 3.9" x 0.85" (21.6 x 9.9 x 2.2 cm)

CR1000WP WIRING PANEL SIZE: 9.4" x 4" x 2.4" (23.9 x 10.2 x 6.1 cm); additional clearance required for serial cable and sensor leads.

WEIGHT: 2.1 lbs (1 kg)

WARRANTY

Three years against defects in materials and workmanship.

815 W. 1800 N. | Logan, Utah 84321-1784 | USA | phone (435) 753-2342 | www.campbellsci.com
Australia | Brazil | Canada | England | France | Germany | South Africa | Spain | USA (headquarters)

Temperature and Relative Humidity Probe

Model CS500

The CS500 is a modified version of Vaisala's 50Y Humitter. The CS500 measures air temperature with a 1000 ohm platinum resistance thermometer (PRT); RH is measured by a laser-trimmed INTERCAP capacitive chip. The chip is field-replaceable, as needed, and eliminates the downtime typically required for the recalibration process.

Sensor Mounts

When exposed to sunlight, the CS500 must be housed in a radiation shield. If the CS500 is mounted to a CM6/CM10 tripod or a UT10 tower, a model 41303 6-plate radiation shield is used. If the CS500 is mounted on a UT20 or UT30 tower, a UT018 Crossarm and Mounting Bracket and a UT6P 6-plate radiation shield are used.

Ordering Information

CS500-L6	6 ft lead length for use with CM6/CM10 tripods or a UT10 tower.
CS500-L9	9 ft lead length for use with a UT10, UT20 or UT30 tower and a UT018
9598	Replacement chip for the CS500.
UT018	Crossarm and Mounting Bracket; required for mounting the CS500 to a UT20 or UT30 tower

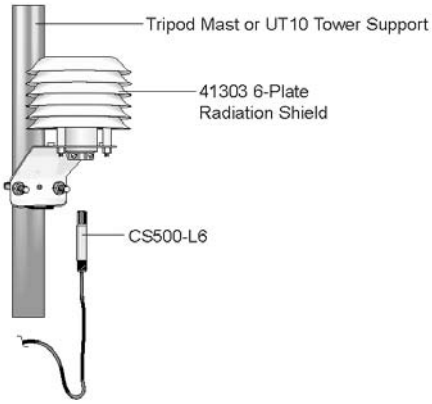

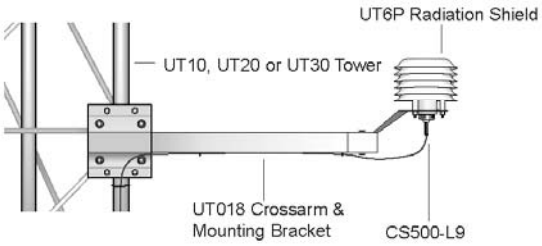

CAMPBELL SCIENTIFIC, INC.
815 W. 1800 N. • Logan, Utah 84321-1784 • (435) 753-2342 • FAX (435) 750-9540 • www.campbellsci.com

Specifications

Relative Humidity

Operating Range: 0 to 100% RH

Accuracy: 0-10% range: unspecified
10-90% range: ±3.0%
90-100% range: ±6.0%

Temperature Dependence of Relative Humidity Measurement:

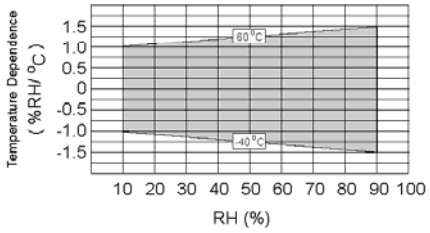

Typical Long-Term Stability: Better than ±1% RH per year

Temperature

Measurement Range: -40° to +60°C

Temperature Accuracy:

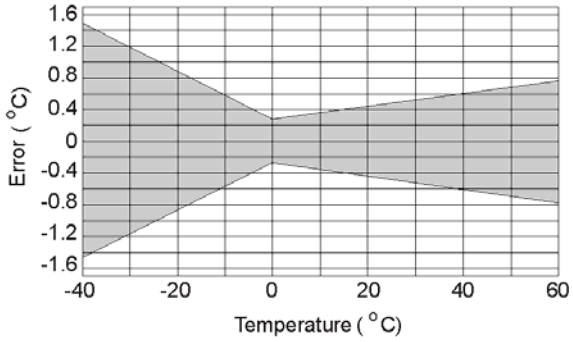

General

Supply Voltage: 7-28 Vdc (typically powered by datalogger's 12 V supply)

Current Consumption: < 2 mA typical

Diameter: 0.47" (12 mm)

Length: 2.66" (67.5 mm)

Housing Material: ABS plastic

CAMPBELL SCIENTIFIC, INC.
815 W. 1800 N. • Logan, Utah 84321-1784 • (435) 753-2342 • FAX (435) 750-9540
Offices also located in: Australia • Brazil • Canada • England • France • South Africa • Spain

Humidity Sensors
Humidity Sensor

HIH-3610 Series

FEATURES
- Molded thermoset plastic housing with cover
- Linear voltage output vs %RH
- Laser trimmed interchangeability
- Low power design
- High accuracy
- Fast response time
- Stable, low drift performance
- Chemically resistant

TYPICAL APPLICATIONS
- Refrigeration
- Drying
- Metrology
- Battery-powered systems
- OEM assemblies

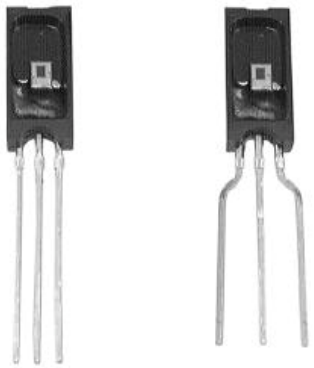

The HIH-3610 Series humidity sensor is designed specifically for high volume OEM (Original Equipment Manufacturer) users. Direct input to a controller or other device is made possible by this sensor's linear voltage output. With a typical current draw of only 200 µA, the HIH-3610 Series is ideally suited for low drain, battery operated systems. Tight sensor interchangeability reduces or eliminates OEM production calibration costs. Individual sensor calibration data is available.

The HIH-3610 Series delivers instrumentation-quality RH (Relative Humidity) sensing performance in a low cost, solderable SIP (Single In-line Package). Available in two lead spacing configurations, the RH sensor is a laser trimmed thermoset polymer capacitive sensing element with on-chip integrated signal conditioning. The sensing element's multilayer construction provides excellent resistance to application hazards such as wetting, dust, dirt, oils, and common environmental chemicals.

⚠WARNING
PERSONAL INJURY
- DO NOT USE these products as safety or emergency stop devices, or in any other application where failure of the product could result in personal injury.

Failure to comply with these instructions could result in death or serious injury.

⚠WARNING
MISUSE OF DOCUMENTATION
- The information presented in this product sheet is for reference only. Do not use this document as system installation information
- Complete installation, operation, and maintenance information is provided in the instructions supplied with each product.

Failure to comply with these instructions could result in death or serious injury.

TABLE 1: PERFORMANCE SPECIFICATIONS

Parameter	Condition
RH Accuracy[1]	±2% RH, 0-100% RH non-condensing, 25 °C, V_{supply} = 5 Vdc
RH Interchangeability	±5% RH, 0-60% RH; ±8% @ 90% RH typical
RH Linearity	±0.5% RH typical
RH Hysteresis	±1.2% RH span maximum
RH Repeatability	±0.5% RH
RH Response Time, 1/e	15 sec in slowly moving air at 25 °C
RH Stability	±1% RH typical at 50% RH in 5 years
Power Requirements	
Voltage Supply	4 Vdc to 5.8 Vdc, sensor calibrated at 5 Vdc
Current Supply	200 µA at 5 Vdc
Voltage Output	$V_{out} = V_{supply}(0.0062(\text{Sensor RH}) + 0.16)$, typical @ 25 °C
	(Data printout option provides a similar, but sensor specific, equation at 25 °C.)
V_{supply} = 5 Vdc	0.8 Vdc to 3.9 Vdc output @ 25 °C typical
Drive Limits	Push/pull symmetric; 50 µA typical, 20 µA minimum, 100 µA maximum
	Turn-on ≤ 0.1 sec
Temperature Compensation	True RH = (Sensor RH)/(1.093-0.0012T), T in °F
	True RH = (Sensor RH)/(1.0546-0.00216T), T in °C
Effect @ 0% RH	±0.007 %RH/°C (negligible)
Effect @ 100% RH	-0.22% RH/°C (<1% RH effect typical in occupied space systems above 15 °C (59 °F))
Humidity Range	
Operating	0 to 100% RH, non-condensing[1]
Storage	0 to 90% RH, non-condensing
Temperature Range	
Operating	-40 °C to 85 °C (-40 °F to 185 °F)
Storage	-51 °C to 125 °C (-60 °F to 257 °F)
Package[2]	Three pin, solderable SIP in molded thermoset plastic housing with thermoplastic cover
Handling	Static sensitive diode protected to 15 kV maximum

Notes:

1. Extended exposure to ≥90% RH causes a reversible shift of 3% RH.
2. This sensor is light sensitive. For best results, shield the sensor from bright light.

FACTORY CALIBRATION

HIH-3610 sensors may be ordered with a calibration and data printout (Table 2). See order guide on back page.

TABLE 2: EXAMPLE DATA PRINTOUT

Model	HIH-3610-001
Channel	92
Wafer	030996M
MRP	337313
Calculated values at 5 V V_{out} @ 0% RH V_{out} @ 75.3% RH	 0.958 V 3.268 V
Linear output for 2% RH accuracy @ 25 °C Zero offset Slope RH	 0.958 V 30.680 mV/%RH (V_{out}-zero offset)/slope (V_{out}-0.958)/0.0307
Ratiometric response for 0 to 100% RH V_{out}	 V_{supply} (0.1915 to 0.8130)

FIGURE 1: RH SENSOR CONSTRUCTION

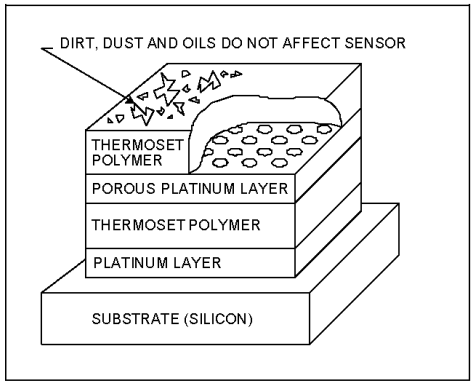

FIGURE 2: OUTPUT VOLTAGE VS RELATIVE HUMIDITY AT 0 °C

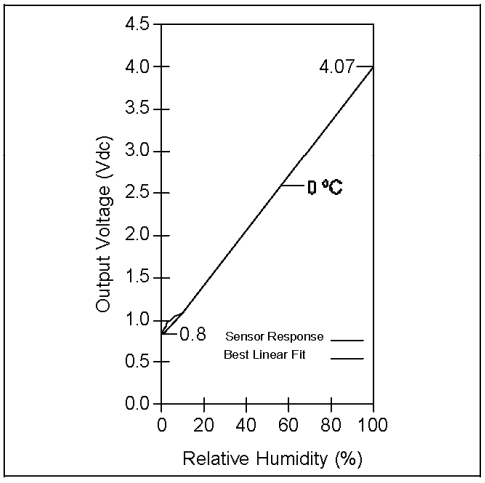

FIGURE 3: OUTPUT VOLTAGE VS RELATIVE HUMIDITY AT 0 °C, 25 °C, 85 °C

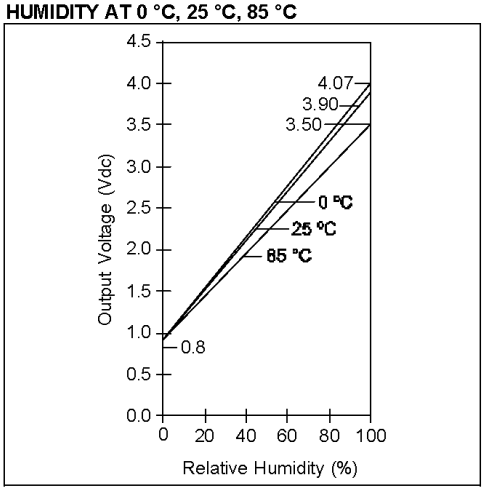

ORDER GUIDE

Catalog Listing	Description
HIH-3610-001	Integrated circuit humidity sensor, 0.100 in lead pitch SIP
HIH-3610-002	Integrated circuit humidity sensor, 0.050 in lead pitch SIP
HIH-3610-003	Integrated circuit humidity sensor, 0.100 in lead pitch SIP with calibration and data printout
HIH-3610-004	Integrated circuit humidity sensor, 0.050 in lead pitch SIP with calibration and data printout

FIGURE 4: MOUNTING DIMENSIONS (for reference only) mm (in)

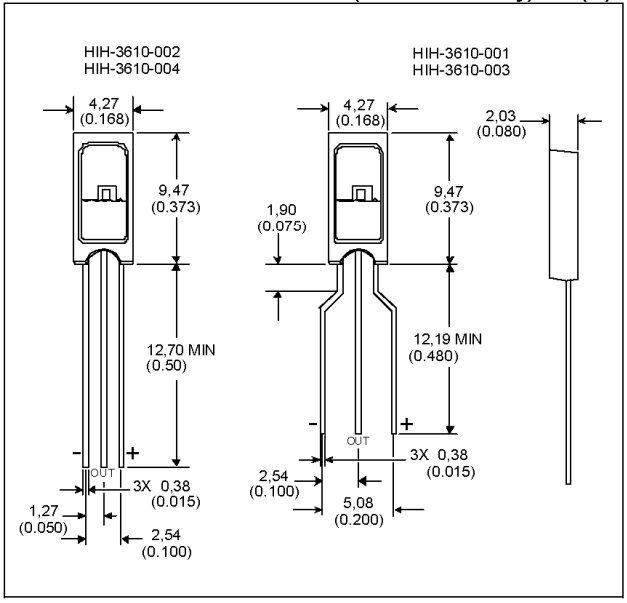

WARRANTY/REMEDY

Honeywell warrants goods of its manufacture as being free of defective materials and faulty workmanship. Contact your local sales office for warranty information. If warranted goods are returned to Honeywell during the period of coverage, Honeywell will repair or replace without charge those items it finds defective. The foregoing is Buyer's sole remedy and is **in lieu of all other warranties, expressed or implied, including those of merchantability and fitness for a particular purpose.**

Specifications may change without notice. The information we supply is believed to be accurate and reliable as of this printing. However, we assume no responsibility for its use.

While we provide application assistance personally, through our literature and the Honeywell web site, it is up to the customer to determine the suitability of the product in the application.

For application assistance, current specifications, or name of the nearest Authorized Distributor, check the Honeywell web site or call:
1-800-537-6945 USA
1-800-737-3360 Canada
1-815-235-6847 International
FAX
1-815-235-6545 USA
INTERNET
www.honeywell.com/sensing
info.sc@honeywell.com

Honeywell

Sensing and Control
Honeywell
11 West Spring Street
Freeport, Illinois 61032

www.honeywell.com/sensing

Printed with Soy Ink on 50% Recycled Paper
009012-2-EN IL50 GLO 501 Printed in USA

192 Series Unicurve®
R-T Matched Interchangeable
NTC Thermistors

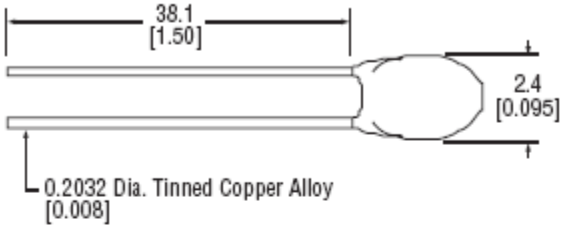

UNI-CURVE® INTERCHANGEABLE THERMISTORS are high quality, low cost resistance temperature matched interchangeable thermistors. They offer additional cost savings by eliminating the need for individual resistance temperature calibration, as well as standardization of circuit components and simplification of design and replacement problems. They are particularly well suited for use in applications such as temperature measurement, indication and control. Other applications include: compensation of ambient temperature effects on copper coils, transistors, integrated circuits and other semiconductor devices.

Features

- Applications: Temperature Measurement, Indication, and Control Accuracy
- High Stability; High Reliability; Long Life
- Small Size
- Epoxy Coated; Lead Material = Tinned Copper Alloy
- Dissipation Constant = 0.75 mW/°C In Still Air Minimum
- Time Constant = 15 Sec. In Still Air Maximum
- Resistance Range = 1K Ohm to 100K Ohm
- Maximum Temperature = 150°C

Stock No.	Mfr.'s Type	Ohms @ 25°C	Tolerance ± °C	Resistance Ratio	EACH
254-0064	192-501DET-A01	500	0.2	6.35	**3.81**
254-0065	192-102DEW-A01	1K	1.0	6.35	**2.58**
254-0066	192-222LET-A01	2.2K	0.2	9.10	**3.81**
254-0067	192-222LEV-A01	2.2K	0.5	9.10	**3.13**
254-0068	192-302LET-A01	3K	0.2	9.10	**2.47**
254-0069	192-502LET-A01	5K	0.2	9.10	**3.81**
254-0070	192-103LET-A01	10K	0.2	9.10	**3.81**
254-0071	192-103LEV-A01	10K	0.5	9.10	**3.13**
254-0072	192-103LEW-A01	10K	1.0	9.10	**2.58**
254-0073	192-103LFW-A01	10K	1.0	9.10	**2.58**
254-0074	192-303KET-A01	30K	0.2	8.72	**3.81**
254-0076	192-303QET-A01	30K	0.2	8.72	**3.81**
254-0075	192-303KET-A02	30K	0.2	8.72	**3.81**
254-0077	192-503QET-A01	50K	0.2	8.72	**3.81**
254-0078	192-104QET-A01	100K	0.2	8.72	**3.81**

Model 223 Delmhorst Cylindrical Soil Moisture Block

1. General Description

The 223 gypsum soil moisture block is configured for use with the AM32 and AM416 Multiplexer. The -L option on the Model 223-L indicates that the cable length is user specified. This manual refers to the sensor as the 223 and applies to the 223-L as well. The Delmhorst cylindrical block is composed of gypsum cast around two concentric electrodes which confine current flow to the interior of the block, greatly reducing potential ground loops. Gypsum located between the outer electrode and the soil creates a buffer against salts which may affect the electrical conductivity. Individual calibrations are required for accurate readings of soil water potential.

The multiplexer that the 223 is connected to leaves the circuit open when no measurements are being made. This blocks direct current flow from the 223 to datalogger ground and prevents electrolysis from prematurely destroying the sensor.

The 223 should not be connected directly to the datalogger. The 227 Delmhorst soil moisture block is available for direct connection and has capacitors in the cable that block direct current flow.

Gypsum blocks typically last for one to two years. Saline or acidic soils tend to degrade the block, reducing longevity. To maximize longevity, gypsum blocks not used during the winter should be removed from the field. Shallow blocks may become frozen and crack, while blocks located below the frost line may not maintain full contact with the soil. Regardless of depth, blocks left in the field over winter are subject to the corrosive chemistry of the soil.

2. Specifications

Approximate Cylinder Dimensions	
Diameter	2.25 cm (0.88")
Length	2.86 cm (1.25")
Material	Gypsum
Electrode Configuration	Concentric cylinders
Center electrode	Excitation
Outer electrode	Ground

Calibration: Measurements are affected by soil salinity, including fertilizer salts. Individual calibrations are required for accurate measurement of soil water potential. The soil water potential versus resistance values in Table 2 are "typical" values supplied by Delmhorst Corporation. Neither Delmhorst or Campbell Scientific make any claim as to the accuracy of these values. The calibration equations in Section 4.5 were fit to the values in Table 2 to allow output of an estimated water potential.

Appendix B

Development and Calibration of Wood Surrogate Sensors

Previous field monitoring work has shown that the currently used relative humidity sensor technology (a thermoset polymer capacitive sensing element) is vulnerable to extended exposure to high relative humidity, especially condensing environments. These conditions have led to sensor failure. In an effort to develop a long-term, low-cost, high-reliability measurement of moisture conditions, several wood moisture content surrogate sensors were developed and deployed at the field monitoring sites.

Two form factors were developed: a cylindrical sensor, intended for post-construction installation in a drilled hole in a solid material, such as masonry or brickwork (referred to as a "plug" sensor), and a flat sensor meant to measure moisture conditions at a planar interface (referred to as a "wafer" sensor). The "plug" sensors were used at the Kitchener site, to estimate soil moisture conditions. The "wafer" sensors were installed on the interior of the Kitchener site, and for a portion of the monitoring period at the Huntley, IL site.

Background

The moisture content of the wood can be measured by electrical resistance; this technique has been well documented (Garrahan 1988, Straube et al. 2002), and can be related to humidity levels (Carll and TenWolde 1996). The relationship between the equilibrium moisture content of a porous medium and the environmental relative humidity is known as the sorption isotherm, as shown in Figure 1.

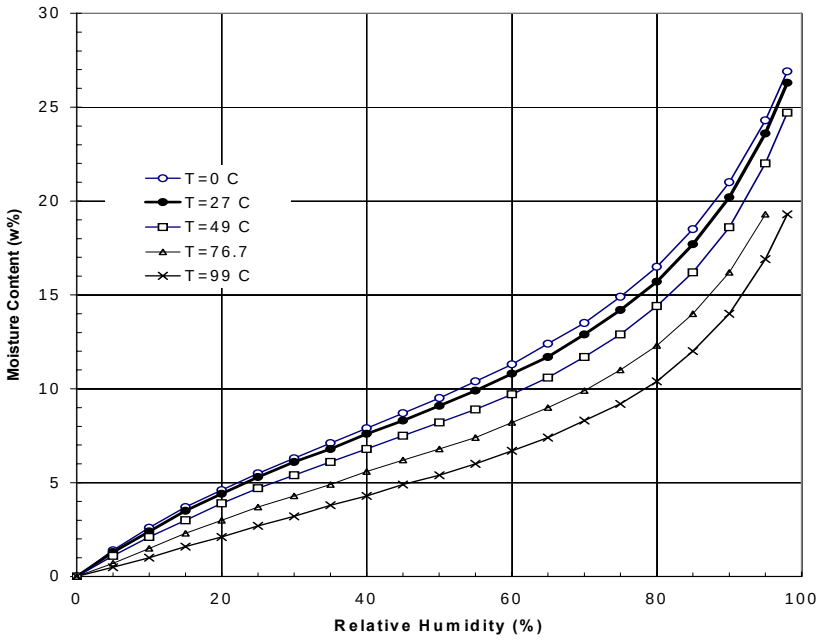

Figure 1: Average sorption isotherm for wood (Straube and Burnett 2005)

Note that at moderate humidity ranges (20-75%), the slope of the isotherm is relatively low; as a result, small errors in MC measurement can result in larger errors in humidity readings. In addition, the sorption isotherm shows some hysteresis behavior, which further impedes accuracy (average isotherm is shown in figure above). Carll and TenWolde (1996) note errors on the order of ±10% RH without pre-screening of sensors.

One advantage of wooden block sensors comes from their material properties. As shown in the sorption isotherm, at high humidity (~98%), moisture content is in the 28-30% range. However, in contact with liquid water (100% RH, by definition), moisture content can rise to two or three times this amount (known as "capillary suction" behavior).

Therefore, the "wafer" sensor would be able to indicate the occurrence of condensation events (resulting in liquid water at the interface), and "plug" sensor might be able to resolve the degree of masonry moisture saturation when embedded. In comparison, humidity sensors would only indicate 100% RH in all of these situations. In order to take advantage of this material property, the sensor must be in direct capillary contact with the porous media; when a sensor is installed in a drilled opening, there is a small air gap between the wood and concrete. Therefore, a capillary active filler material, such as clay, must be used. It will ensure capillary contact, as per its use in pressure plate apparatus tests. Clay has high vapor permeability at the thicknesses used in this research, and should have minimal effect on the humidity response.

However, there is some question to this approach, due to differences in pore size distribution. Liquid water is redistributed in porous media moving from large pores to smaller pores, which have a stronger capillary suction. However, the pore size distribution for wood is generally believed to be larger than most masonry materials (brick, concrete), so it might not draw capillary water from the surrounding masonry, even with a capillary filler.

Plug Sensor Geometry

The sensors were fabricated from Eastern White Pine cylinders 9.5 mm diameter x 29 mm (3/8" x 1-1/8"), as shown in the figures below.

Figure 2: Close-up of completed sensor

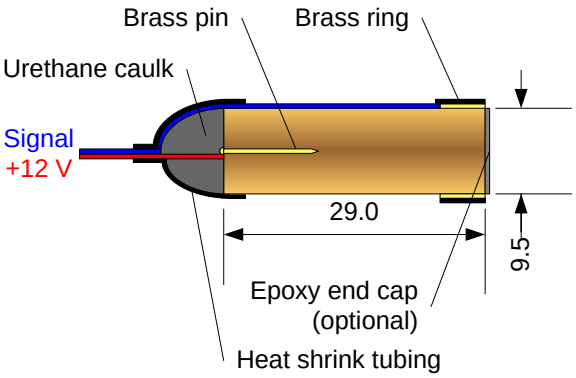

Figure 3: Schematic cross section of sensor (dimensions in mm)

The electrical resistance of the wood is measured to obtain moisture content; a brass pin driven into one end provides +12 volts DC excitation, and signal is measured at a brass ring friction-fit on the other end. Urethane caulk seals the wire exit end, and heat shrink tubing is used at both ends.

Plug Sensor Calibration and Time Constant

Several sensors was acclimated in the test lab, and then moved to a 100% relative humidity enclosure for calibration. The intent of this work was to record the response to a step change of 50% RH to 100% RH, as well as to gauge sensor variability. One sensor was coated with damp clay, as per its use as a capillary filler, to note any effect on sensor response.

In the initial calibration stage, the sensors showed a moisture content value of approximately 11%, which maps to 55% RH, as per the sorption isotherm (Figure 1).

Figure 4: Sensors in 100% humidity calibration enclosure

Actual humidity was 45-50%; moisture content measurements were sporadic, as wood electrical resistance reaches the limit for consistent readings with the logger equipment (1-2 GΩ range). Once placed into the humidity enclosure, moisture content values quickly rose to the 25-28% range (95%-100% RH), as shown in Figure 5. There was some variation in the final moisture content measurements; average value was 27%, ±2%. The clay-coated sensor showed a similar type and speed of response, but with a smoother curve than the bare wood sensors. The non-labeled lines in Figure 5 are the bare sensors.

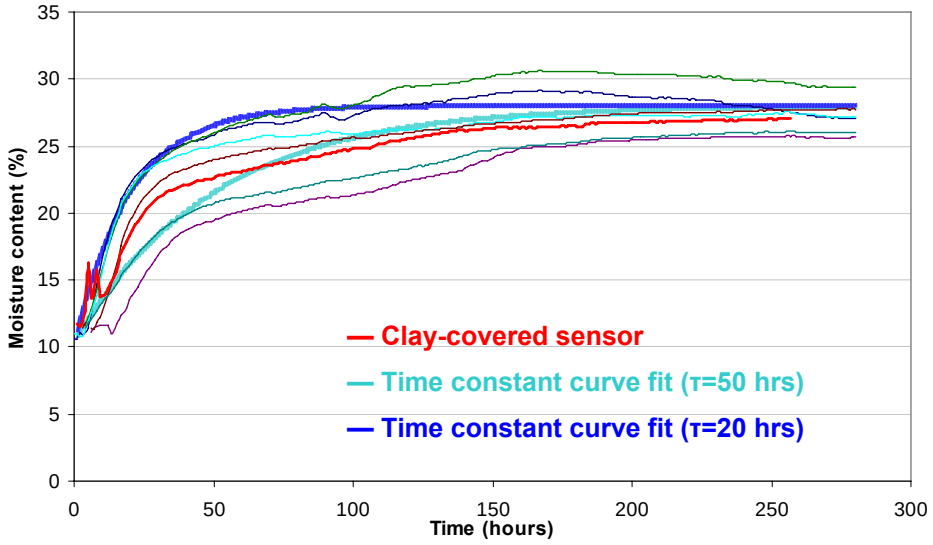

Figure 5: Plug sensor response after placement in humidity enclosure

Trial fits of time constant (τ) values showed that the sensor response curve did not match the expected exponential ($1 - e^{-t/\tau}$) function (Wheeler and Ganji 2004). However, bounding values of τ=20 and τ=50 hours provided curves that roughly match the response of the sensors; at $t=4\tau$, a sensor's output nominally reaches 98.2% of its final value.

In a second calibration test, the desorption or drying response was measured. The sensors were moved from the 100% RH chamber to a 50% RH environment (Figure 6; change at 15 hour mark).

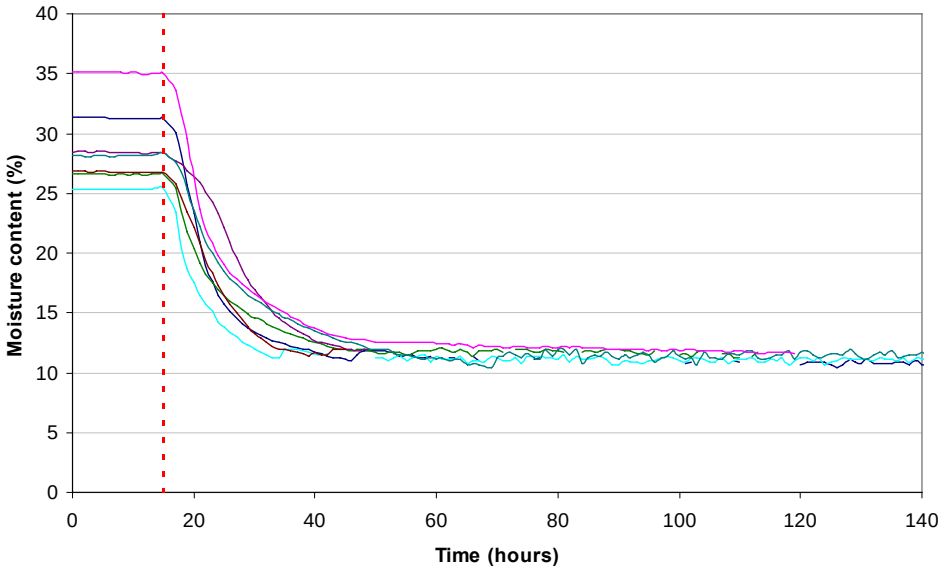

Figure 6: Plug sensor response after removal from humidity enclosure

Two points are noted in this response. First, the drying response is much faster than the wetting response: it reaches its equilibrium condition in approximately 40-50 hours, as opposed to 150-200 hours in Figure 5. It was not initially clear from this data whether this reflects an actual physical response, or an artifact of measuring the moisture content using electrical resistance. This phenomenon was examined in more detail in a later section.

Second, the variability of measurements at 100% RH is much higher than the variability at 50% RH. This might come from the uncertainty of the electrical resistance measurement combined with the non-linear relationship between resistance and moisture content. The formula for uncorrected moisture content of the reference species (Douglas Fir), as stated in Straube et al. (2002) is as follows:

$$\text{Log}_{10}\,(\text{Moisture content}) = 2.99 - 2.113\ \ (\log_{10}(\log_{10}(\text{Resistance}_{\text{wood}}))$$

where moisture content is in mass %, and resistance is in ohms (Ω).

Due to this $\log_{10}(\log_{10})$ relationship, a deviation in resistance measurement has a very small effect at low moisture contents, while it has a much larger effect at higher moisture contents. For instance, at 11% moisture content (MC), a deviation of ±1% MC is equivalent to –120/+350 MΩ. In contrast, at 27% MC, a deviation of ±1% is equivalent to –50/+80 Ω—a sensitivity more than three orders of magnitude larger.

Another calibration test was to immerse six plug sensors in water for 48 hours while simultaneously monitoring moisture content, to determine their response to liquid water (Figure 7). The sensors were then removed from the water and allowed to dry in a 50% RH/20° C environment.

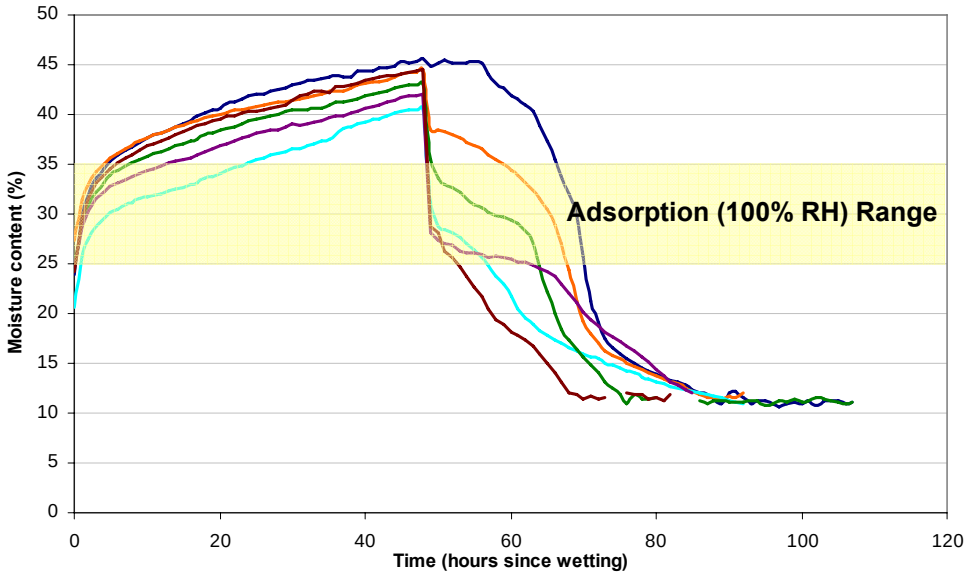

Figure 7: Plug sensor response to water immersion test and drying

The plot shows that measured moisture content goes up to the 40-45% range by the end of the immersion period, and it appears that the sensors have not yet achieved equilibrium. This is well above the 25-35% range for hygroscopic adsorption (100% RH environment) found in previous tests. After removal from water, the samples dry at a variety of rates, but all eventually recover to conditions in equilibrium with a 50% RH environment.

Although this demonstrates that these sensors can distinguish between liquid water wetting events and high humidity environments, absolute moisture contents are not very certain at high levels. The resistance vs. moisture content relationship was developed for the 7-25% range, and extrapolation to 40% seems to provide reasonable results (Straube 2002). However, over 40% MC, the equation will underpredict moisture content.

Wafer Sensor Geometry

The sensors are fabricated from Eastern White Pine blocks 35 mm x 19 mm x 4.75 mm (1-3/8" x 3/4" x 3/16"), as shown in Figure 8, Figure 9, and Figure 10. Two ½" brass pins are predrilled and inserted into the block, at a spacing of 25 mm (1"). The two pins are used to apply the +12 volts excitation current and to measure the wood resistance.

The dimensions of the sensor were chosen to meet the requirements of adequate pin coverage/embedment, fast response (if possible), and minimal disturbance to the building assembly.

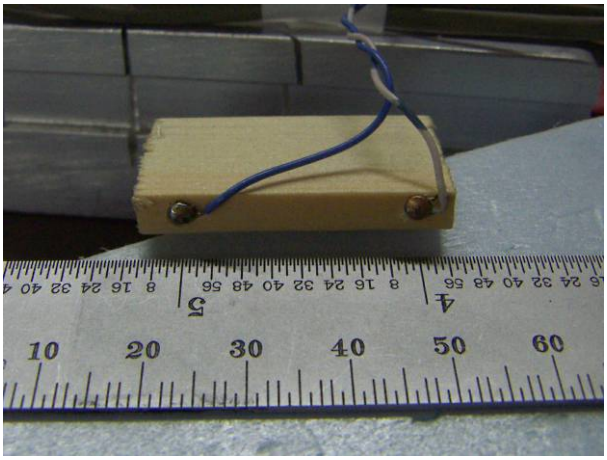

Figure 8: Close-up of completed sensor

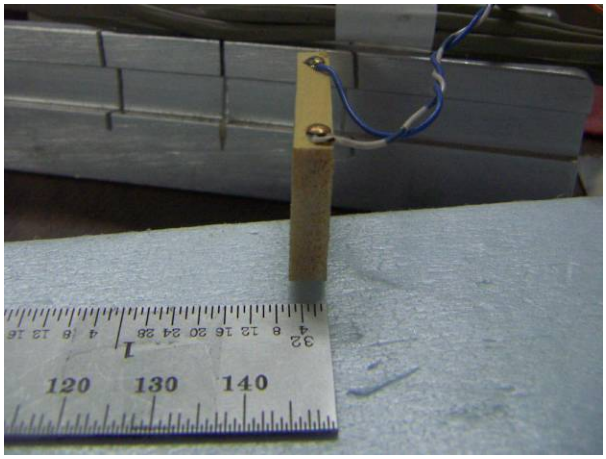

Figure 9: Close-up of completed sensor

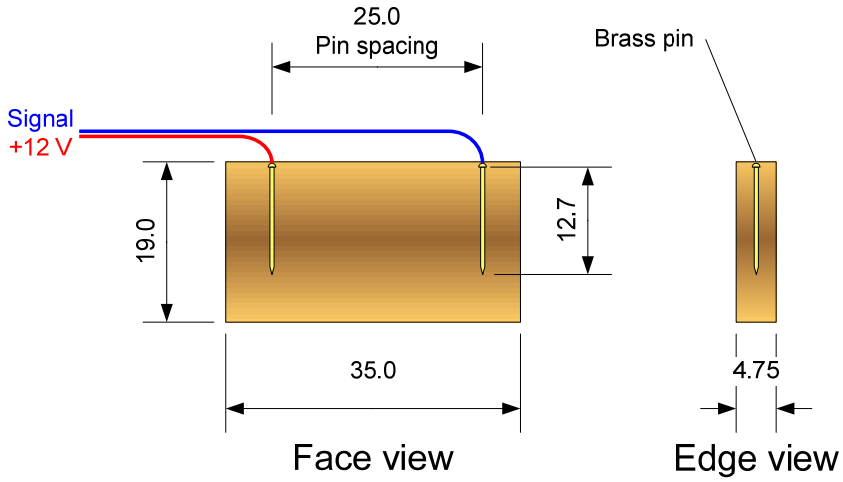

Figure 10: Schematic of wafer sensor (dimensions in mm)

Wafer Sensors: Calibration

The wafer sensors were calibrated using the same methodology as the plug sensors, moving them from a 50% RH 20° C environment to a 100% RH chamber, letting them achieve equilibrium, and then returning them to the 50% environment. The wetting results are shown in Figure 11.

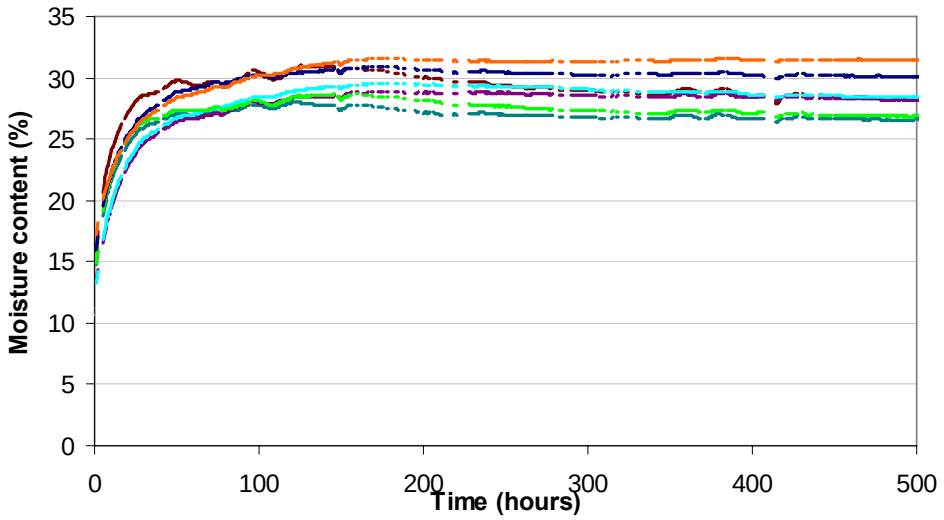

Figure 11: Wafer sensor response after placement in humidity enclosure

The response is similar to the plug sensors: moisture contents quickly rose to 27-32% (slightly higher than the plugs), and final moisture content measurements were in the range of 28%, ±3%.

The drying response is shown in Figure 12 below; note that the timescale is different from Figure 11, covering only 80 hours instead of 500.

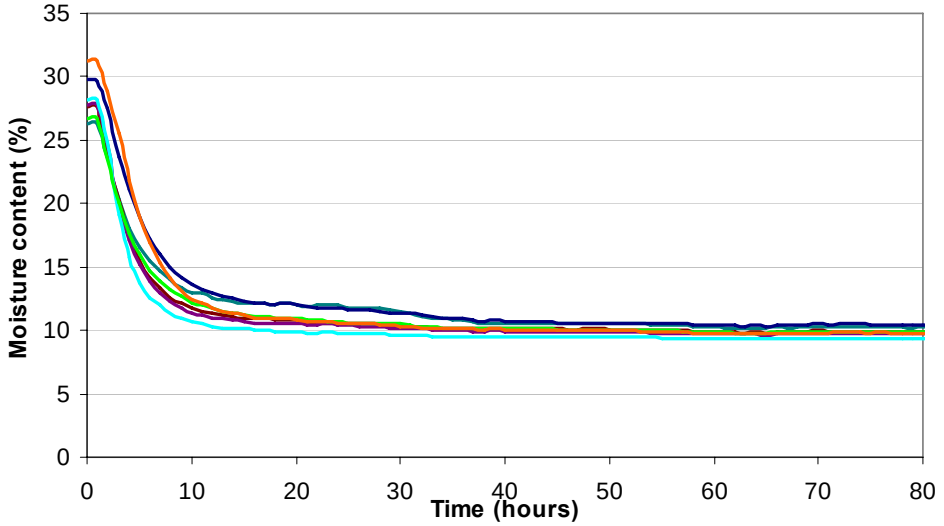

Figure 12: Wafer sensor response after removal from humidity enclosure

As with the plug sensors, the drying response is much faster, reaching equilibrium conditions, coming close to its final value in 24 hours, as opposed to 100-150 hours for wetting.

Wafer Gravimetric Adsorption and Desorption Measurement

The calibration of the plug and wafer sensors suggests that they adsorb and desorb moisture at different rates, even though the absolute vapor pressure difference is the same in both cases. It was important to determine if this is the actual behavior of the wood sensor, or an artifact of the measurement of moisture content using electrical resistance.

A simple experiment was set up to determine the adsorption/desorption response of the wafer stock using gravimetric moisture content. Samples were moved from a 50% RH/20° C controlled environment into a 100% RH chamber, and the weights were periodically measured. After they had achieved their final weight, they were removed from the chamber, and again periodically weighed while desorbing moisture. After returning to equilibrium conditions with 50% RH, the wafers were then oven dried to 0% MC, as per ASTM D 4442-92 (ASTM 2003), to allow back-calculation of gravimetric moisture content through the experiment.

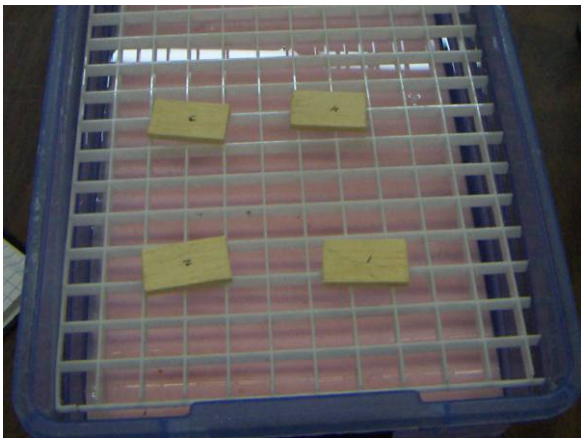

Figure 13: Wafer stock in 100% humidity calibration enclosure

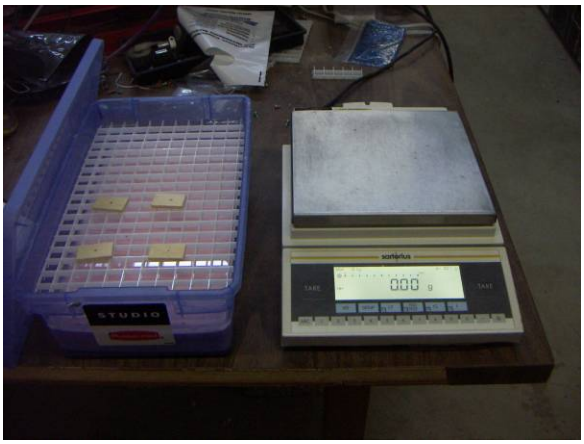

Figure 14: Wafer stock in 100% humidity calibration enclosure with balance

The gravimetric results are shown below: the adsorption response is shown in Figure 15, and the desorption response in Figure 16. The average of the resistance-based moisture content readings are also graphed as a comparison.

The adsorption response clearly shows that the long time response of the sensor is a function of the slow increase in wood moisture content when placed in the 100% RH environment. Both show a slow response, taking 150 to 200 hours to reach final values. However, the ending gravimetric moisture content is consistently higher than the corresponding electrical resistance readings: the former are in the 38-41% range, while the latter are near 30%. As mentioned earlier, the resistance moisture content measurements have more variability at higher levels.

The gravimetric desorption response also closely matches the electrical resistance readings. The curve shows a similar time response (reaching equilibrium with 50% RH in 15-24 hours).

Note that timescales of these two figures are not identical (300 hours vs. 50 hours)

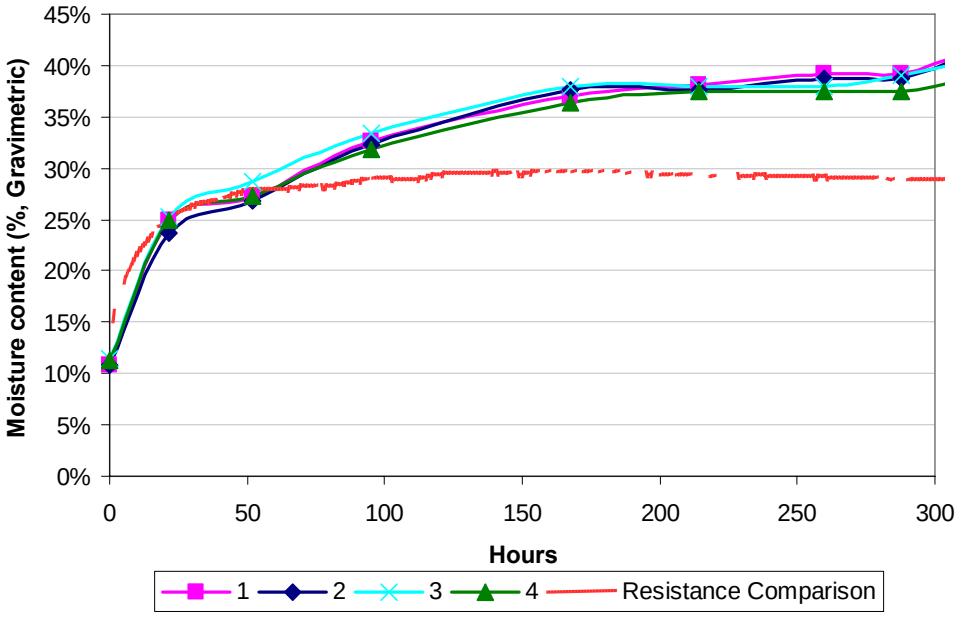

Figure 15: Gravimetric adsorption response of wafers

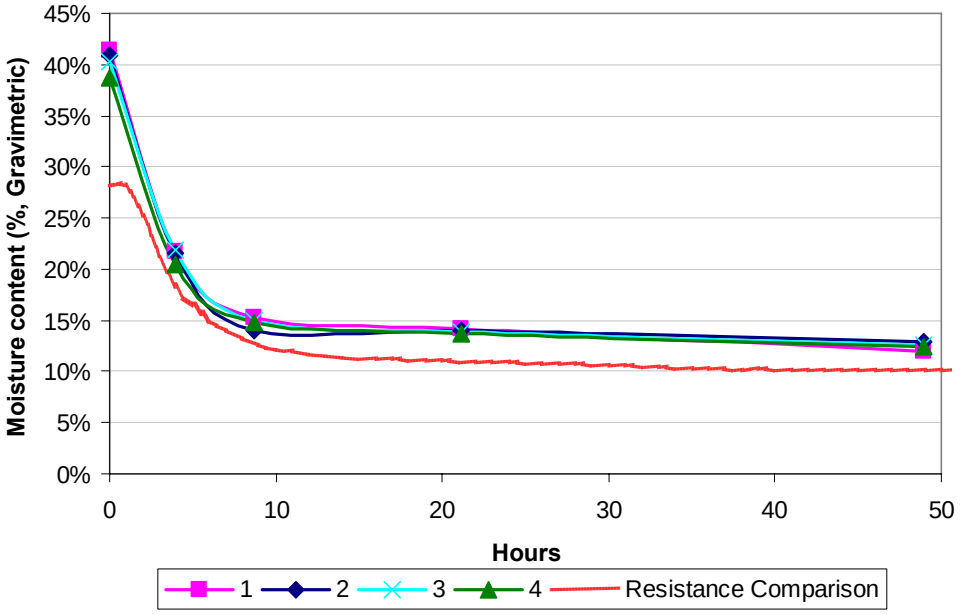

Figure 16: Gravimetric desorption response of wafers

The difference between electrical resistance and gravimetric measurement should not be simply considered an error in this measurement method; it is not certain if the moisture distribution within the wafer is completely uniform. Therefore, the average moisture content of the wafer (which is measured by gravimetric methods) could be higher than the moisture content seen at the electrical resistance pins.

Hygrothermal Simulation of Wafer Sensor Response

To gain some insight into the asymmetric adsorption/desorption response and the related moisture physics, one-dimensional hygrothermal simulations were run using WUFI 4.0. If this behavior is duplicated in the simulation, the material property causing it might be isolated and identified.

A wood layer matching the thinnest dimension of the wafer (4.75 mm) was exposed to step changes similar to the calibration experiments: 20° C, and alternating between 50% and 100%, at 1000-hour intervals. Two wood materials were selected: softwood from the IBP (Institute for Building Physics) database, and "pine transverse direction," taken from NTNU (Norwegian University of Science and Technology) data.

The results for NTNU pine are shown in Figure 17; two tests were run: one cycling between 50-100%, the other 50-99%. A typical sorption isotherm becomes very steep close to 100%, so a small change can result in a large difference in moisture response. However, in this case, there was minimal difference between the two.

The response of the wood is relatively fast: comparisons between adsorption and desorption cannot be discerned on that plot. Therefore, a detail plot (Figure 18) shows both the adsorption and desorption response on the same axis. The two responses seem close to symmetric; they are both on the order of 40-50 hours

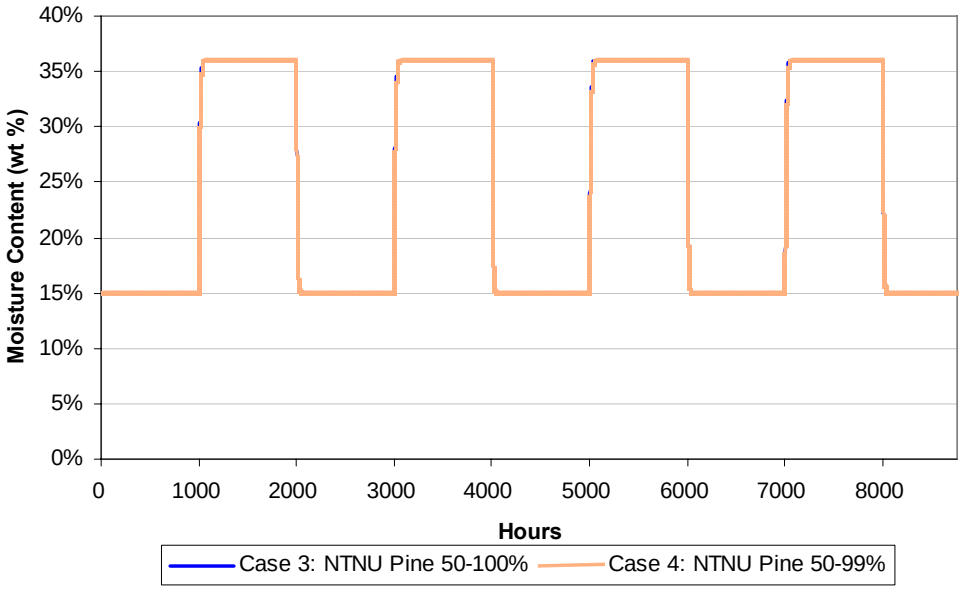

Figure 17: NTNU pine moisture content response to 50-100% and 50-99% RH cycling

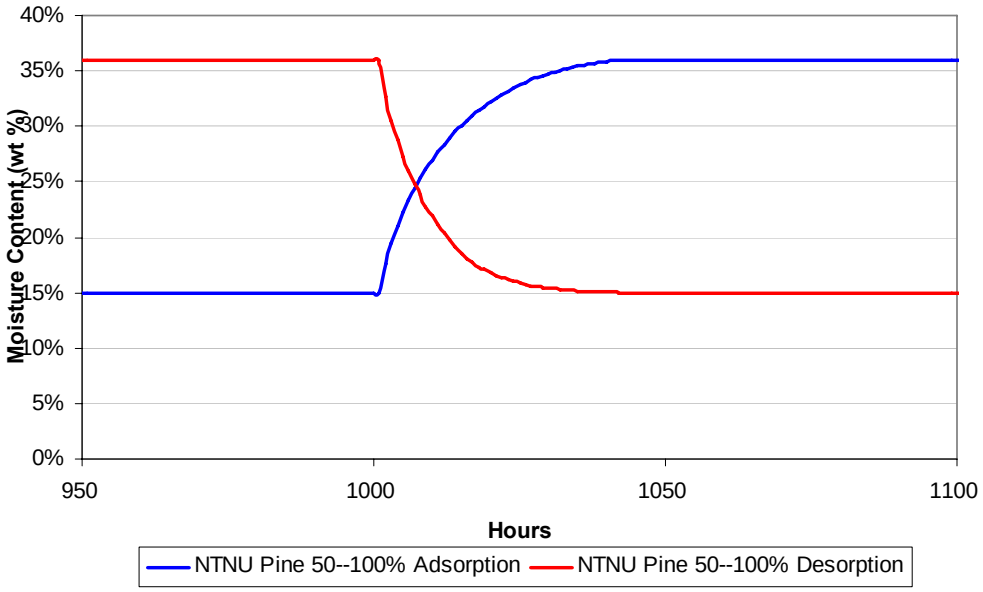

Figure 18: Detail of NTNU pine adsorption/desorption response

The response of the IBP softwood material is very different, as shown in Figure 19. First, the wood rises to a moisture content of 100-140% of dry weight, as opposed to 36% for the NTNU pine. Second, the response time is much longer: even after 1000 hours, the material has not reached equilibrium. It takes roughly 2000 hours to reach equilibrium (as shown by Case 5). Third, the adsorption-desorption response times are distinctly different: desorption is much faster than adsorption, as per lab results. Finally, there is a marked difference between 50-100% and 50-99% humidity cycling, as seen by the difference between Case 1 and Case 2.

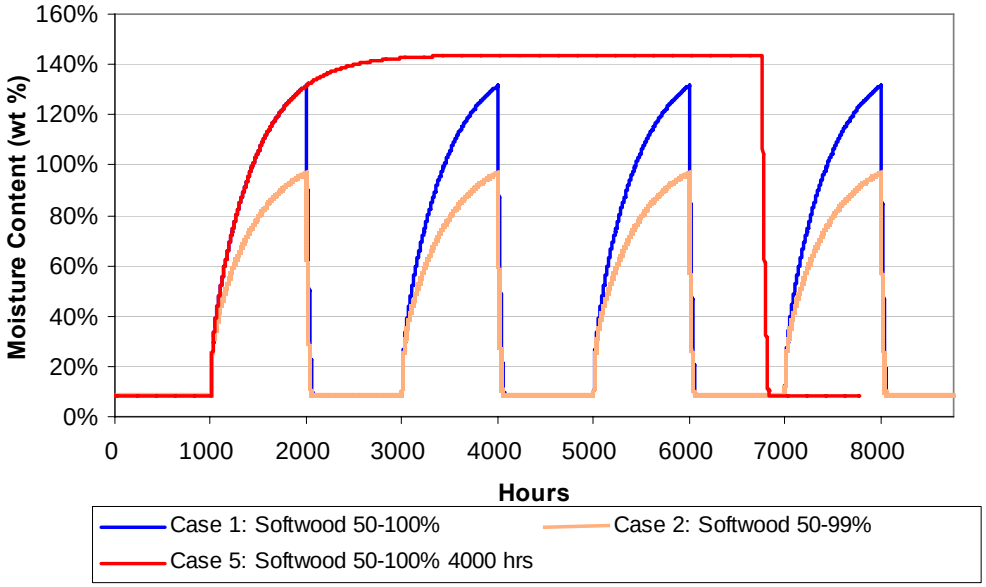

Figure 19: IBP softwood moisture content response to 50-100% and 50-99% RH cycling

The different response of these materials is partially caused by the differences in the sorption isotherm (moisture storage function) material data, plotted in terms of % moisture content in Figure 24 below. The curves are similar below 95% RH; however, the IBP softwood has a sharp "hook" rising from 97 to 100% RH. In all simulations, equilibrium moisture content at 100% RH matches the maximum value supplied in the isotherm (144% and 36%). The long response time of the IBP softwood compared to NTNU pine is partially due to the large amount of water (factor of four difference) that must diffuse through the material to reach equilibrium conditions.

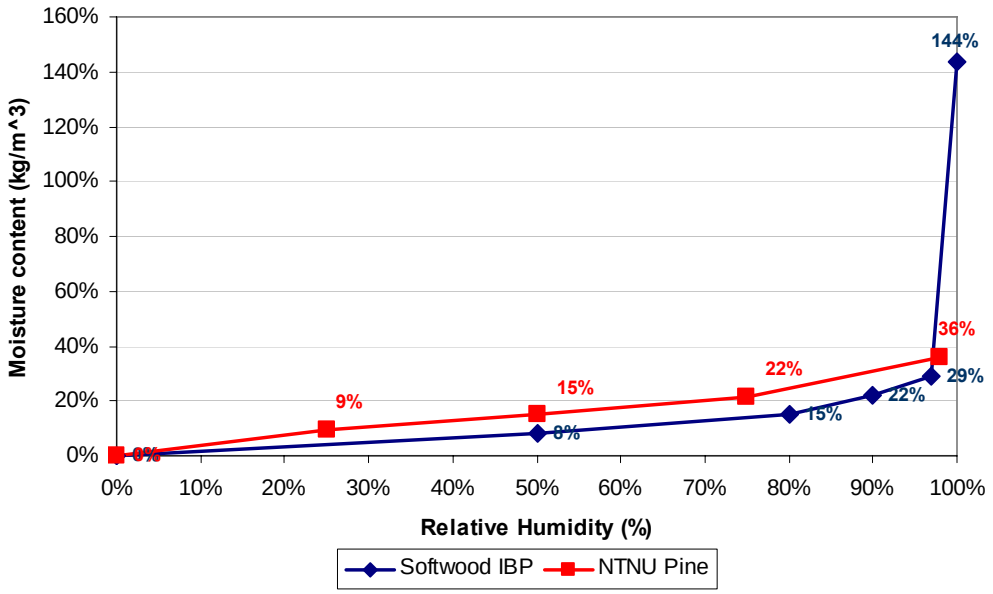

Figure 20: Sorption isotherms for IBP softwood and NTNU pine

The moisture-dependent vapor resistance of the material was examined as a possible cause for the difference in adsorption and desorption response. Both of these materials show a VDRF (vapor diffusion resistance factor) that varies with humidity; these values are plotted in terms of permeability (ng/Pa·m·s) in Figure 21.

The NTNU pine showed a mostly symmetric response, while IBP softwood was noticeably asymmetric. The IBP softwood has a very steep increase in permeability at high humidity, while the NTNU response is flatter; 100% RH conditions have a stronger effect on permeability in the IBP material. It seems that this difference might cause the asymmetric response: at the 50-100% RH step change, the material starts at equilibrium with 50% RH, and has a lower permeability (and therefore slower adsorption). Permeability increases as it comes into equilibrium with 100% RH. At the 100-50% step change, permeability is higher, with a resulting faster desorption. In addition, the exterior surfaces are supplied with moisture from the core of the material, keeping humidity (and permeability) higher.

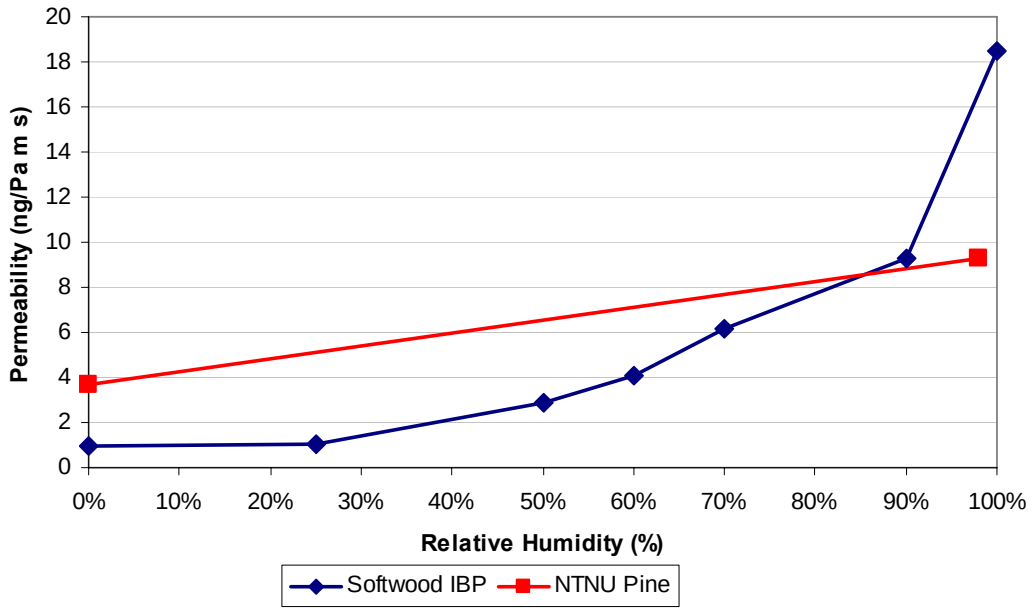

Figure 21: Moisture-dependent permeability data for IBP softwood and NTNU pine

To check this theory, a simulation was run with a modified material, with the moisture-dependent vapor diffusion resistance factor (VDRF) disabled (set to 200, or roughly 1 ng/Pa·m·s), as shown by Case 6 in Figure 22. The baseline (Case 1) is shown for comparison. The adsorption/desorption response is still asymmetric; the amplitude is reduced, due to the reduced vapor transport.

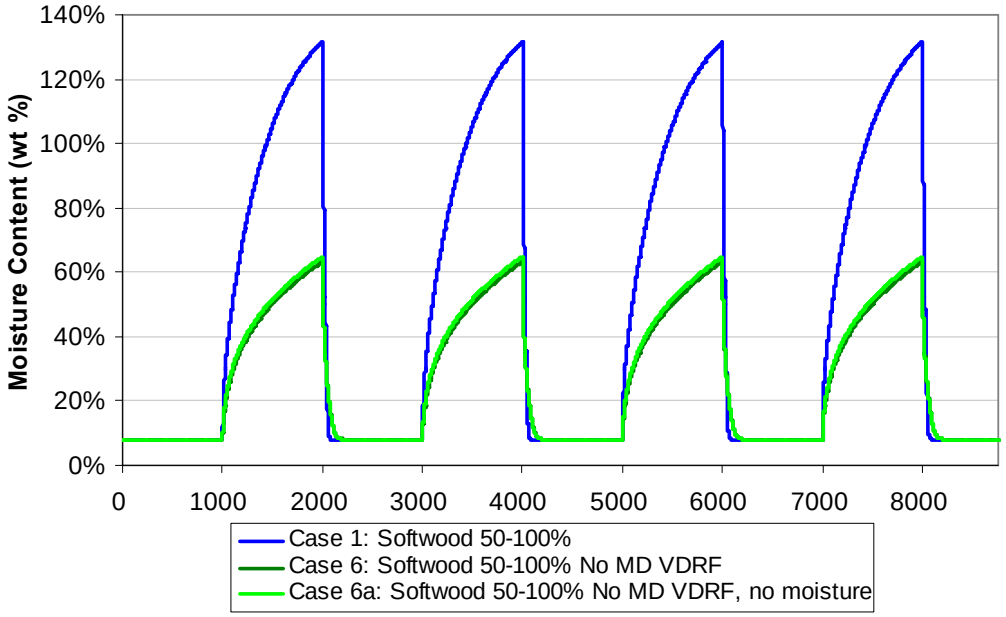

Figure 22: Modified IBP softwood moisture content response to 50-100% RH cycling

Another simulation was run; the hygrothermal options were selected to exclude capillary conduction, and latent heat of evaporation and fusion; the results are shown in Case 6a. These changes had a negligible effect.

The next theory was that the asymmetric response might be a function of the shape of the sorption isotherm, specifically, the steep "hook" at high humidity. The NTNU pine material did not have this feature, and exhibited a mostly symmetric response. A modified version of the NTNU pine was developed, with a similar hook (adding 510 kg/m^3 or 100% MC at 99.5% RH). The results are shown in Figure 23. This simulation shows the asymmetric response: it appears that the sorption isotherm shape causes this behavior.

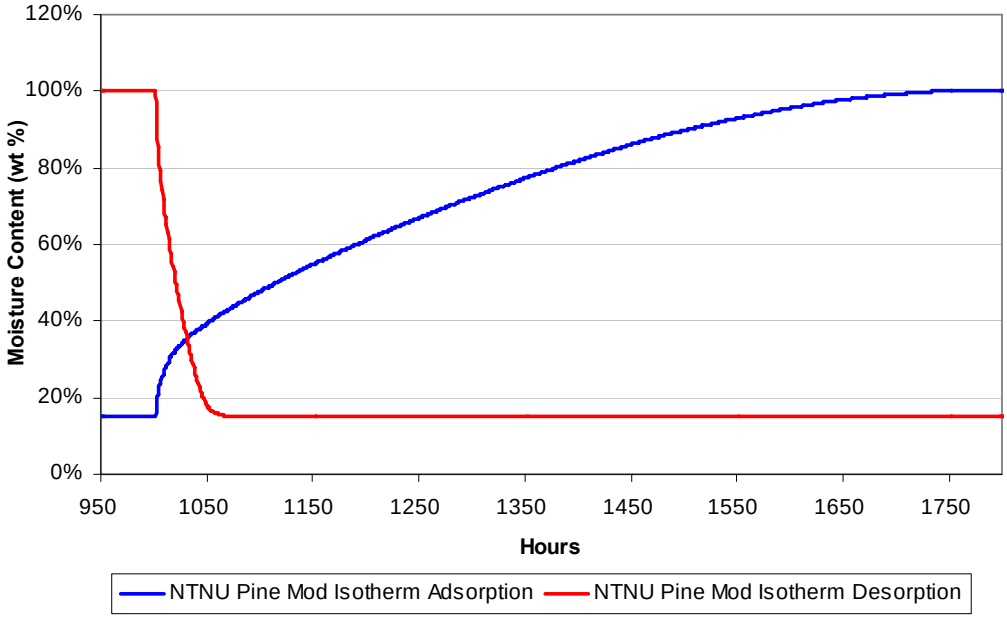

Figure 23: Adsorption and desorption response of modified isotherm NTNU pine material

Wafer Sensors: Field Comparison to Relative Humidity Sensors

Some in-situ data comparing relative humidity measurements with wafer sensors is available from the University of Waterloo BEGHut exposure facility and the Kitchener basement site.

At the BEGHut, wafer sensors were placed in parallel with relative humidity sensors in the brick space ventilation/drainage cavity in six walls (three north, three south), as shown in Figure 24 and Figure 25. This was done to provide redundancy, given the challenging high humidity conditions in the ventilation space.

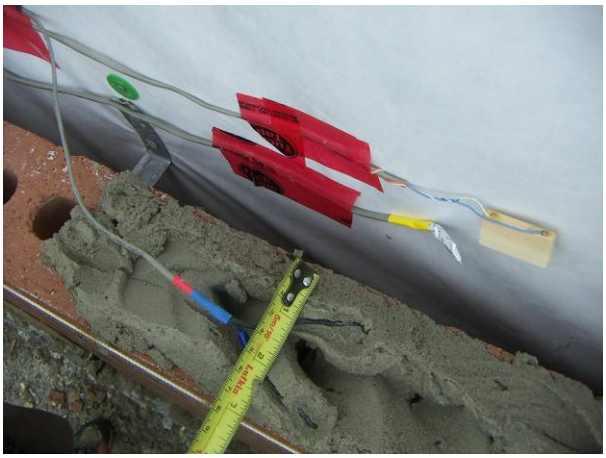

Figure 24: RH sensor and MC wafer in brick space cavity at UW test facility

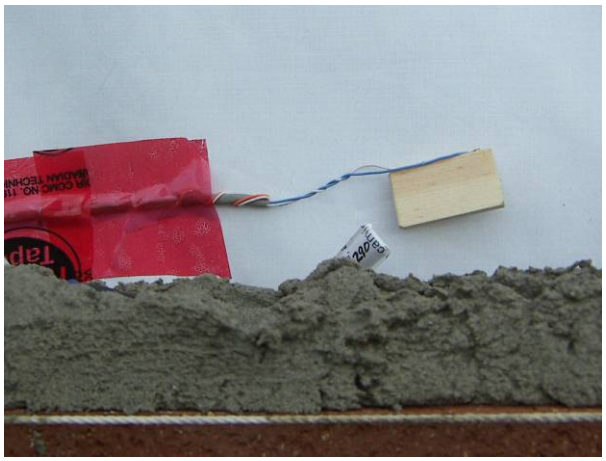

Figure 25: RH sensor and MC wafer in brick space cavity

Data for the wafer response from September 2005 through July 2006 is shown in Figure 26. The general trend is that moisture contents rise over the course of the winter, and then fall through the summer. Some walls are indicated to be wetter than others (N3, N2).

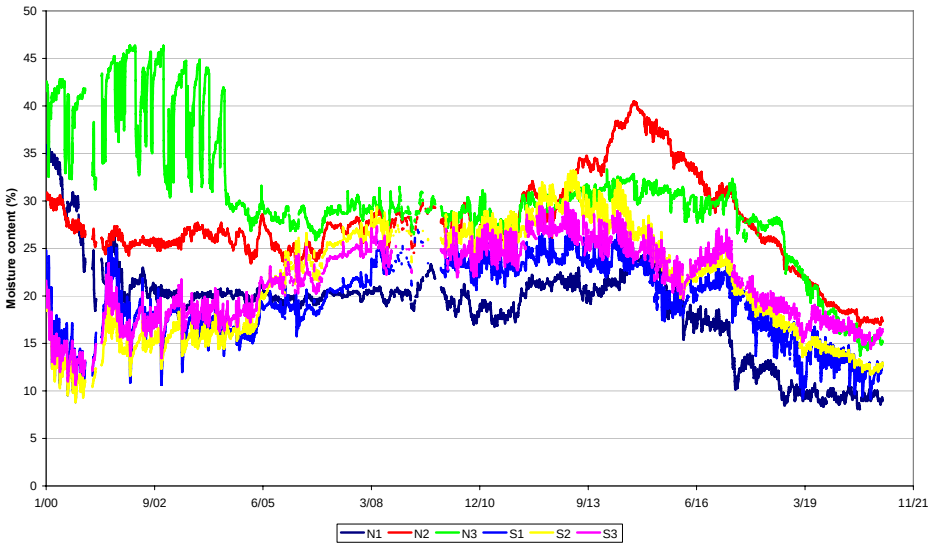

Figure 26: BEGHut brick space wafer moisture content data

That data can be compared with the relative humidity data at the same location. The challenge of using humidity sensors in that high humidity location is evident by the anomalies seen in the data. Sensors N1, N2, and S3 all return anomalous results (e.g., 30-40% RH), for at least a portion of the period. The humidity sensors also show the pattern of N2 and N3 being wetter during the later parts of the summer.

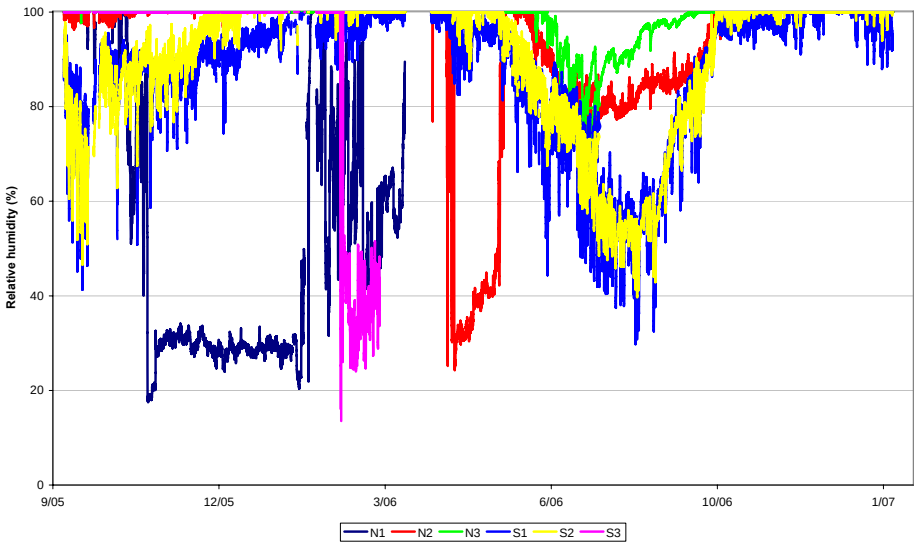

Figure 27: BEGHut brick space relative humidity data

The anomalous relative humidity data was culled, and concurrent moisture content and humidity values were plotted against each other in Figure 28. In addition, the sorption isotherm for wood (from Straube 2002) is also plotted; the behavior should ideally follow this line.

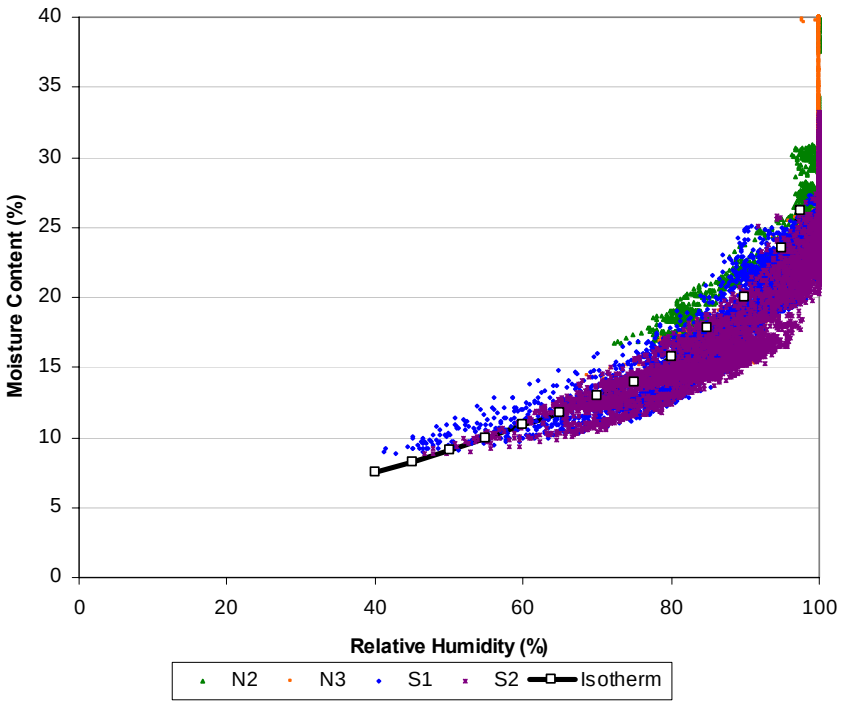

Figure 28: BEGHut relative humidity vs. moisture content, with sorption isotherm

The plot shows relatively good agreement; most data seems to lie within ±5% of the sorption isotherm. This of course assumes that the relative humidity sensors are maintaining their accuracy over time; given the history of damage to RH sensors, it is entirely possible that drift is occurring.

At the Kitchener basement site, RH and wafer sensors were installed in parallel at the concrete-insulation interface, at mid-height, as shown in Figure 29. The results were plotted against each other in Figure 30; one of the four walls had a failed RH sensor, so only three channels are shown.

Figure 29: Mid-height sensors in Kitchener basement

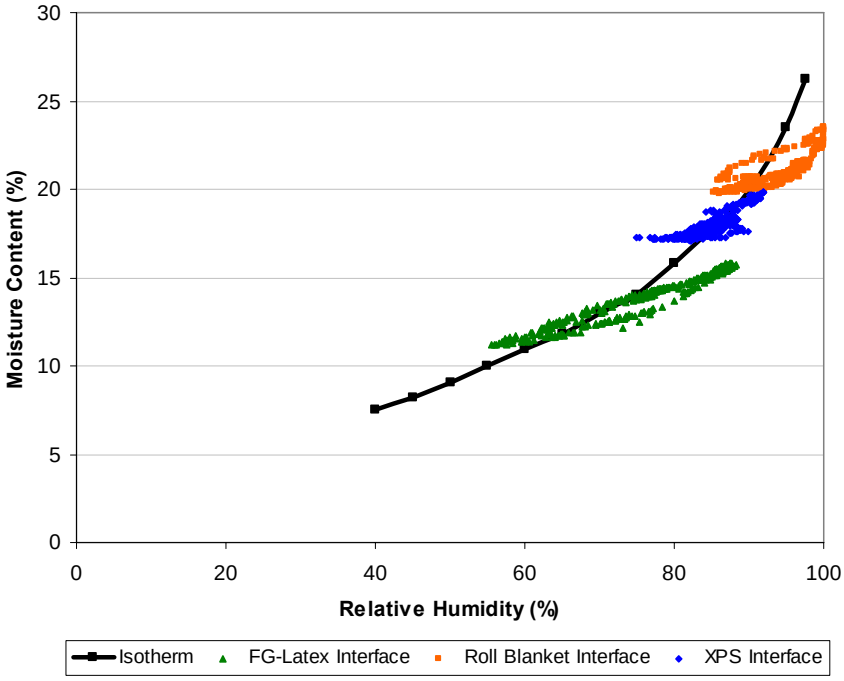

Figure 30: Kitchener site relative humidity vs. moisture content, with sorption isotherm

The Kitchener results have a looser correspondence with the sorption isotherm, however, again, all data falls within ±5% of the sorption curve.

The data shows good agreement between the monitored data and the sorption isotherm. Hysteresis effects are causing some of the deviation from the isotherm values. It would be safe to judge that moisture content measurements can be used to estimate relative humidity measurements within 10%. More importantly, looking at the failure rate (2 out of 6 at one site, 1 out of 4 at the other) and poor data quality of the relative humidity sensors in this location, it seems that wafer sensors provide a

durable and reliable measurement of moisture conditions in severely challenging high humidity environments.

Conclusions

Taking this calibration and field installation work together, several conclusions can be drawn in regards to the use of these wood surrogate moisture content sensors:

- In steady-state calibration measurements, these sensors showed accuracy of ±3% RH at 100% RH. In a dynamic field installation, the results agreed with relative humidity measurements within ±10% RH or better.
- The sensors have a very slow wetting response, responding to a step change from 50% RH to 100% RH over a course of 150-200 hours. However, drying occurs at a much faster rate. This reflects the actual moisture response of the wafer material itself.

  This response suggests that these sensors are not a good indicator of diurnal or more rapid phenomena, and should be instead used to capture longer-term (i.e., seasonal) wetting or drying.
- Simulations suggest that the asymmetric adsorption-desorption response may be due to the steep rise in moisture content at the high end of the sorption isotherm (at 95%$^{+}$ RH).
- Calibration measurements demonstrate that these sensors can distinguish between liquid water wetting events and high humidity environments (adsorbed moisture).
- These sensors showed good reliability and performance in environments challenging for the currently used type of relative humidity sensors.

In field use at the University of Waterloo BEGHut and the Kitchener site, a secondary use for this sensor was noted: during visual inspection of assemblies, the wood will show mold growth on its surface, indicating a history of high moisture levels. Mold growth occurred on wafers at stud bay cavities that did not show any mold growth on the framing. This suggests that condensation occurred at the interface, resulting in liquid water wetting of the wafer, but later safely evaporated, without running down to the framing in any noticeable amount.

Appendix C

Development and Commissioning of Wetting System

The wetting system was developed and installed by Aaron Townsend of Building Science Corporation; the following is a report on the installation and commissioning of the system. Mr. Townsend is the sole author of this report.

Wetting Equipment and Installation

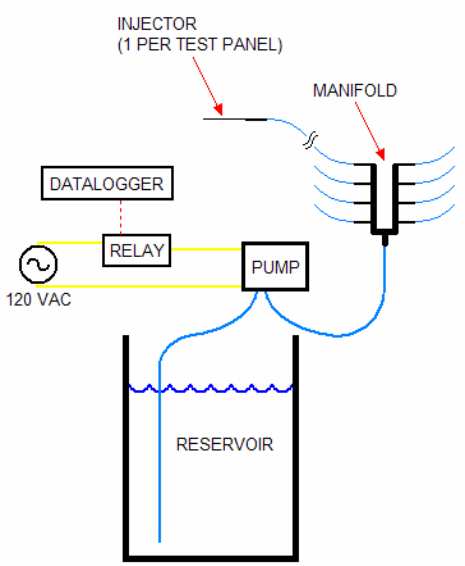

Figure 31: Schematic of wetting system

Figure 31 shows a schematic diagram of the wetting system. The system contains a water reservoir, peristaltic pump, manifold, plastic tubing to each wall, and injectors.

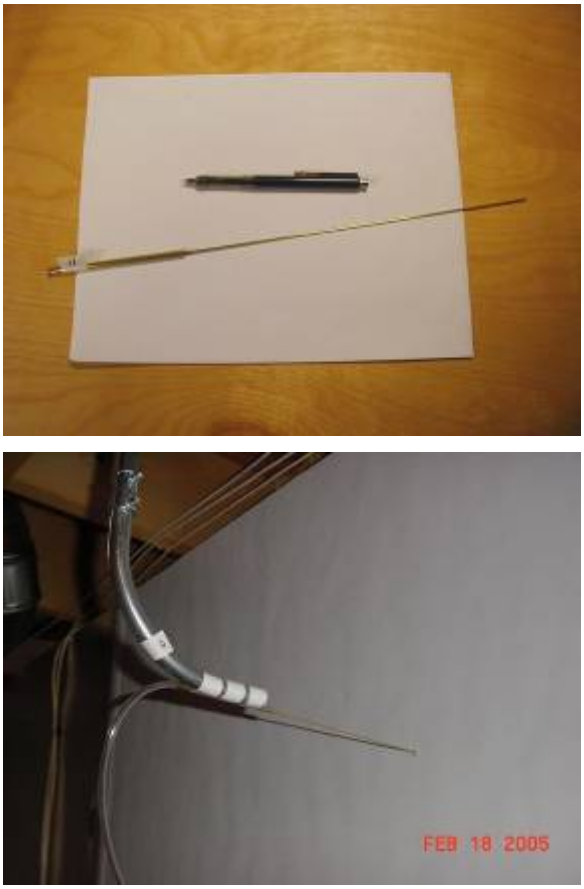

Figure 32: Injector, for size reference and as installed

Figure 32 shows the injector alone and as installed. The injector is made of a 12" piece of 1/16" brass tubing fixed to a short section of 3/16" brass tubing (in order to connect to the ¼" vinyl tubing). The installation is accomplished by drilling a 5/23" hole through the insulation assembly and approximately ¼" into the concrete basement wall. The injector is then inserted into the hole so that the end of the injector is in the hole in the concrete.

Test wall 2 (stud wall with poly both sides) was an exception; for this wall the injector was first placed as the others, then pulled back approximately one inch so that the water will be injected inside

the stud space. For all walls, the injector is fixed in place using ½" metal conduit attached to the joists (as shown in Figure 32). A laser level was used in order to ensure that all the injectors were installed at the same elevation (Figure 33).

Figure 33: Holes were drilled at the same elevation in each wall

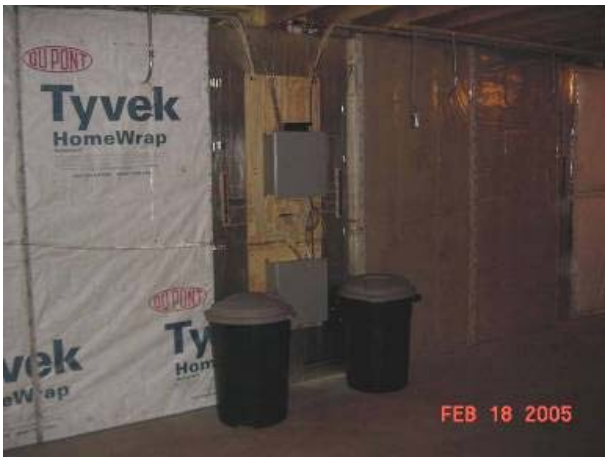

Figure 34: Reservoirs and pump and manifold housing

Figure 34 shows the wetting equipment as installed in the test basement. The lower gray box contains the pump and manifold, and two 32-gallon trash containers serve as the reservoir. ¼" vinyl tubing leaves the manifold and carries water to each injector.

The pump is controlled by the data logger program, through a relay. Figure 35 shows the interior of the pump housing, with the pump (upper left corner), the manifold (lower half), and relay housing (upper right, white electrical outlet). The relay (and therefore the pump) is controlled by the data logger program, which can be changed remotely.

Figure 35: Pump housing

Commissioning

After installation, the system was commissioned. First, the injectors were turned around backwards on their supports, to allow measurement of the flow from each one (see Figure 36). The pump was run until all the air was purged from the tubing and a steady flow was obtained from the injectors.

Tests were then run to ensure that the system would deliver equal amounts of water to each test panel. The pump was run for approximately five minutes, and the resulting flow volume was measured using funnels and 100 mL graduated cylinders (1 per test panel). The average flow rate from each injector, with the pump running, was 18 mL/min. All injectors were within ±10% of this rate; most were within ±5%. Table 1 shows the results of the final commissioning test.

Figure 36: Commissioning

Table 1: Commissioning test results

Panel #	Panel Name	Measured flow (mL)	Difference from Average (%)
1	Standard stud wall	101	5%
2	Diaper wall	90	-7%
3	1.5" Thermax	105	9%
4	2" XPS	92	-5%
5	1" XPS w/ fiberglass stud wall	93	-4%
6	1" XPS w/ cellulose stud wall	92	-5%
7	Rigid Fiberglass w/ SVR	100	3%
8	Vinyl-faced fiberglass batts	100	3%
	Average	97	
	Time (min)	5.37	
	Average flow rate (mL/min)	18	

Appendix D

Vapor Permeability Testing

The hygrothermal behavior for most of the components of the experimental assemblies has been well characterized by manufacturers' data and various standards and testing agencies. However, the permeance of two of the materials used at the Huntley, IL site were not available; therefore, ASTM E96-00 (ASTM 2000) vapor permeability tests were performed on samples taken from the assemblies. The tested samples were the polyamide-6 (PA-6) "Smart Vapor Retarder" material, laminated to a perforated vinyl facer as a fire protection layer from the P7 assembly, and the perforated polypropylene facer on the roll blanket wall P8.

Procedure

The 20 cm x 20 cm (8" x 8") sample was divided into two 20 cm x 10 cm (8" x 4") pieces: one for dry cup (Procedure A/desiccant method) testing, the other for simultaneous wet cup (Procedure B/water method) testing. Indicating Drierite desiccant (anhydrous calcium sulfate, 97% $CaSO_4$/3% $CoCl_2$) was used for the testing; it was regenerated at 200° C for 1 hour immediately prior to the test.

Since both of these samples were sheet goods, the edges were first wrapped with foil tape to provide a defined test area. The samples were then taped to the lids of the test containers; the lid was sealed to the container body with foil tape. The samples were tested with the "finish" (interior) face of the material on the outside of the container, facing the variable humidity environments.

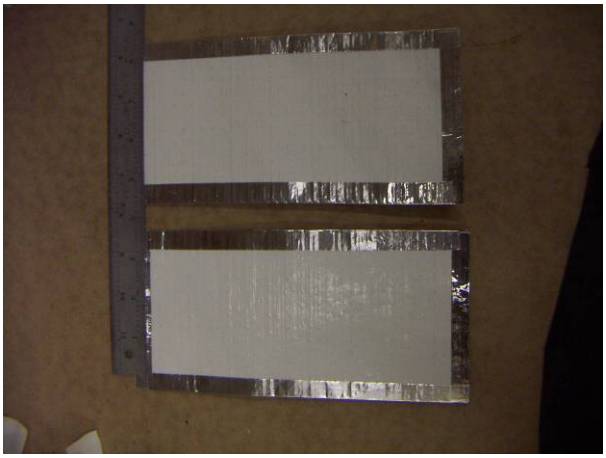

Figure 37: Sample edges wrapped with foil tape

Figure 38: Sample sealed to container lid with foil tape

The samples were run at multiple humidity levels to obtain several points on the permeance vs. relative humidity curve; these included the conditions of approximately 50%, 72%, 87% RH. The samples were held at these conditions for various lengths of time, from 48 hours to 12 days. The 50% RH data was obtained in the 20° C/50% RH climate-controlled test laboratory; elevated humidity levels were run in an environmental chamber.

Figure 39: Testing at 20° C/50% RH in climate-controlled test laboratory

Figure 40: Testing at elevated humidity levels in environmental chamber

Results

The summarized results are shown in below in Table 2, for polyamide-6 with laminated perforated facer (Wall P7) and Table 3, for the perforated vinyl facer (Wall P8). Over the course of the measurements (a total of 42 days), the environmental humidity was ramped upwards and downwards, from approximately 50% to 87%, and then back down. In the tables below, the consecutive tests with similar average RHs are the results of tests at the beginning and end of the measurement period, respectively. Relative humidity control was not as precise as ideal conditions: the standard deviation of the measurements (taken every five minutes) is shown. ASTM E96 calls for humidity control of 50% ± 2% and 90% ± 2%; assuming ±2σ (95% of measured periods), the environmental conditions were kept within ±1.6 to 3.2%

Note that there are several more dry cup tests for the PA-6 facer than the perforated vinyl facer: the desiccant in the more permeable vinyl facer test quickly became saturated, and testing was discontinued when this occurred.

Table 2: Vapor permeability results for polyamide-6 with laminated perforated facer (P7)

	Std. Dev. σ		Test Conditions		Metric perms
Avg. RH (%)	RH (%)	Imp Perms	ΔRH (%)	Test Type	(ng/Pa·m·s^2)
25.1	0.8	1.1	0%/50%	Dry Cup	61
27.5	1.3	1.0	0%/55%	Dry Cup	55
35.6	1.6	1.0	0%/71%	Dry Cup	56
36.0	1.0	1.2	0%/72%	Dry Cup	69
43.7	1.5	1.5	0%/87%	Dry Cup	87
75.1	0.8	8.0	50%/100%	Wet Cup	455
77.5	1.3	9.3	55%/100%	Wet Cup	532
85.6	1.6	10.8	71%/100%	Wet Cup	618
86.0	1.0	11.4	72%/100%	Wet Cup	650
93.7	1.5	13.6	87%/100%	Wet Cup	777

Table 3: Vapor permeability results for perforated vinyl facer (P8)

Avg. RH (%)	Std. Dev. σ RH (%)	Imp Perms	Test Conditions ΔRH (%)	Test Type	Metric perms (ng/Pa·m·s^2)
25.1	0.8	12.6	0%/50%	Dry Cup	720
35.7	1.4	12.3	0%/71%	Dry Cup	702
75.1	0.8	13.9	50%/100%	Wet Cup	793
78.2	1.5	14.9	56%/100%	Wet Cup	849
85.6	1.6	16.4	71%/100%	Wet Cup	932
93.7	1.5	18.2	87%/100%	Wet Cup	1037

These results are the calculated results from the raw data, not accounting for the air layer thickness or surface resistance. However, assuming a distance between the tested membrane and the water surface of 9 mm (3/8”), the permeability would be 18,400 ng/Pa·m·s^2, or 320 Imperial perms, or more than an order of magnitude greater than the tested permeabilities.

These results are plotted below, with previously published data for PA-6 (SVR) material tested in isolation (Gatland 2005; measurements taken by ORNL).

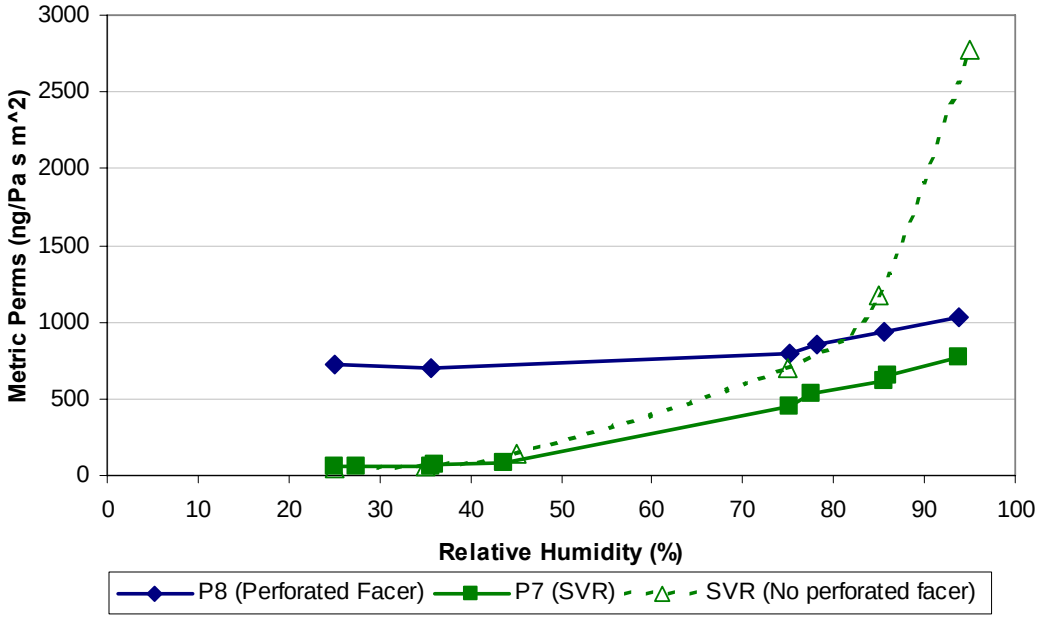

Figure 41: Vapor permeability measurements for materials from walls P7 and P8

The perforated vinyl facer shows a relatively flat response, varying from 720 to 1037 ng/Pa·m·s^2 (13 to 18 Imperial perms). Note that it is a relatively permeable material, falling into the “vapor permeable” category (570 metric/10 Imperial perms or greater, Lstiburek 2002).

In contrast, the PA-6 laminated scrim combination shows a strong response to relative humidity, going from 60-90 ng/Pa·m·s^2 (1.0 to 1.5 Imperial perms) in the dry cup tests, to 450-800 ng/Pa·m·s^2 (8 to 14 Imperial perms) in the wet cup tests. It changes from a borderline Class I to Class II vapor retarder (Lstiburek 2004) to a vapor permeable material. This demonstrates the effect of the polyamide “smart vapor retarder” incorporated into the assembly. However, note that the

permeability does not rise as high as the PA-6 material tested in isolation; this is due to the serial resistance effect of the laminated perforated vinyl facer. Calculations indicate that the perforated facer in isolation has a permeability of roughly 1150 ng/Pa·m·s^2 (20 Imperial perms)

Sample Post-Test Conditions

At the conclusion of the tests, the wet cup samples were disassembled, and the surface exposed to 100% RH was examined for damage and/or microbial growth. The PA-6 laminated scrim from wall P7 appeared to be completely intact; it showed some waviness on its surface, which is its macroscopic response to high humidity levels.

However, the perforated vinyl facer from wall P8 showed apparent mold growth on one side of the sample. Based on the presence of liquid water in the adhered fiberglass insulation, it appears that this damage is the result of liquid water contact with the underside of the sample. The fact that this pattern is limited to one end of the sample (i.e., the container was tipped to one side), as opposed to uniform over the area, suggests that the damage is not solely due to high relative humidity exposure.

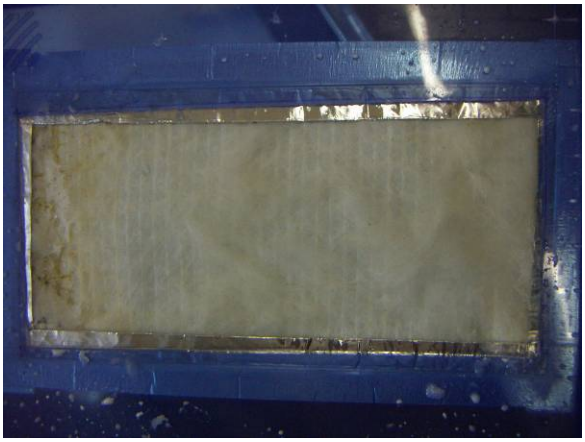

Figure 42: Mold growth on water side of P8 perforated facer sample

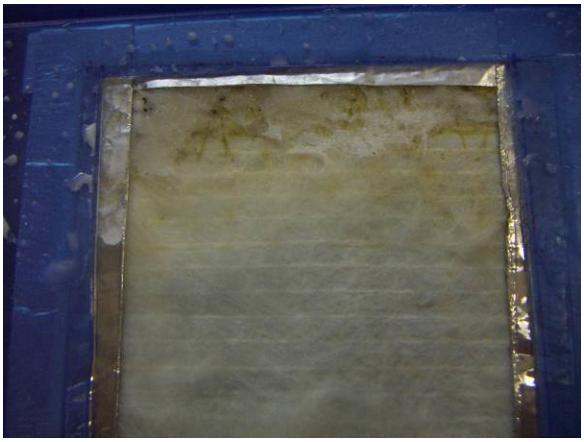

Figure 43: Detail of mold growth, showing water "matting" at one end

This information provides some indication on how these systems respond to sustained high relative humidity or contact with liquid water in field installations.

Equipment

Measurement	Manufacturer	Model #	Specifications
Mass balance	Sartorius	FB12CCE-SOUR	12 kg capacity; 0.01 g readability/resolution
Temperature & humidity	Onset Computer	HOBO Pro H08-032-08	Temperature Accuracy: ±0.2° at 21°C RH Accuracy: ±3% RH; ±4% RH in condensing environments

Appendix E

Foil-faced Polyisocyanurate Permeability Experiment

The following is a research report prepared by Aaron Townsend of Building Science Corporation; the goal of this experiment was to determine if lateral permeability of foil-faced polyisocyanurate could explain some of the data gathered from the polyisocyanurate wall panel at the Huntley test site. In this panel, the dew points at the interface between the concrete wall and the insulation, and within the polyisocyanurate (between the layers of foil facing) tracked the indoor dew point much more closely than expected. This experiment eliminated one of the two remaining explanations: that moisture could diffuse through the edges of the Thermax panel at a fairly fast rate. The experiment showed that polyisocyanurate has low moisture diffusivity. The only remaining explanation that has been identified is that there is significant air leakage behind the insulation, and that the foil tape used to repair the foil facing that separates the mid-insulation sensor from the concrete wall has failed. This explanation is supported by the fact that both sensors responded to the wetting event initiated on September 8, 2005.

Mr. Townsend is the sole author of this report; it was submitted October 10, 2005.

Introduction

This report covers a short experiment intended to qualitatively determine the lateral permeability of polyisocyanurate insulation. The need for this information comes from the basement insulation research BSC is conducting in Chicago. One of the insulation systems being researched in that location is 38 mm (1.5") thick foil-faced polyisocyanurate insulation. One possible explanation of a portion of the data gathered in Chicago requires knowledge of the lateral (or in-plane) moisture diffusivity of polyisocyanurate, which is related to the permeability and the moisture storage function.

Experimental Setup

The experiment was conducted in my home office in Menlo Park, California, using spare equipment from decommissioned data logging projects. I used two Balanced Solutions (BS) T/RH sensors and two Campbell Scientific (CS) CS500 T/RH sensors, as well as a Campbell Scientific CR10X, to perform the data logging.

I purchased the polyisocyanurate used in this experiment from my local Home Depot. I cut a sheet of 38 mm (1.5") thick polyisocyanurate insulation made by Johns Manville into two 0.61 m (2') squares. On both specimens, I cut an access port at the center of the square, inserted a BS sensor, replaced the removed polyisocyanurate, and resealed the foil facing using foil tape. On the first specimen, I used foil tape to seal all four sides of the square. On the second specimen, I made a recess in the polyisocyanurate on one side of the square, inserted a CS sensor, and sealed three sides of the square with foil tape, leaving the side opposite the CS sensor open. Figure 44 shows one of the two test specimens before cutting the access port; Figure 45 shows one of the access ports cut into the center of each specimen; and Figure 46 shows a diagram of the sensor locations in the two test specimens.

Figure 44: View of the 2’ square polyisocyanurate specimens

Figure 45: View of access port cut into center of each specimen

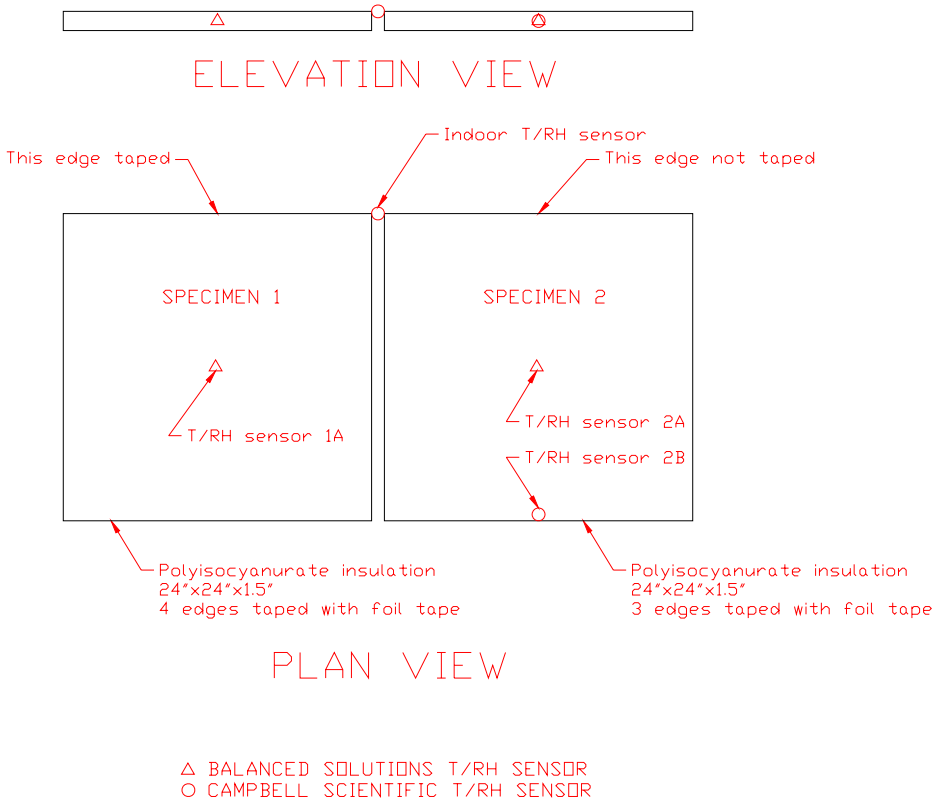

Figure 46: Diagram of polyisocyanurate specimens

After installing the sensors, the two specimens were placed side by side, in a horizontal orientation, on a shelf in my office. As the samples were inside, there was no significant thermal gradient from one side to the other.

Results

The experiment was run for approximately three weeks; however, the second week was lost due to a power failure. The last week of data will be presented here, for ease of reading the graphs. The first week of data is identical to the data presented in terms of the trends noted.

Figure 47 shows the monitored temperature. As would be expected, the indoor temperature swings slightly more than the sensors inside the insulation. The sensor installed in the edge of specimen 2 (sensor 2B) would be expected to show the strongest response of the insulation sensors, as the sensor was only separated from the indoor air by the single layer of foil tape. This is true for the daytime peak temperatures; however at night sensor 2B does not get as cool as any of the other three sensors. The two sensors in the middle of the specimens are nearly identical temperatures, as would be expected since they are in corresponding locations. Overall, the daily temperature is 30 ± 2 °C during the afternoon and falls to between 15 °C and 20 °C at night.

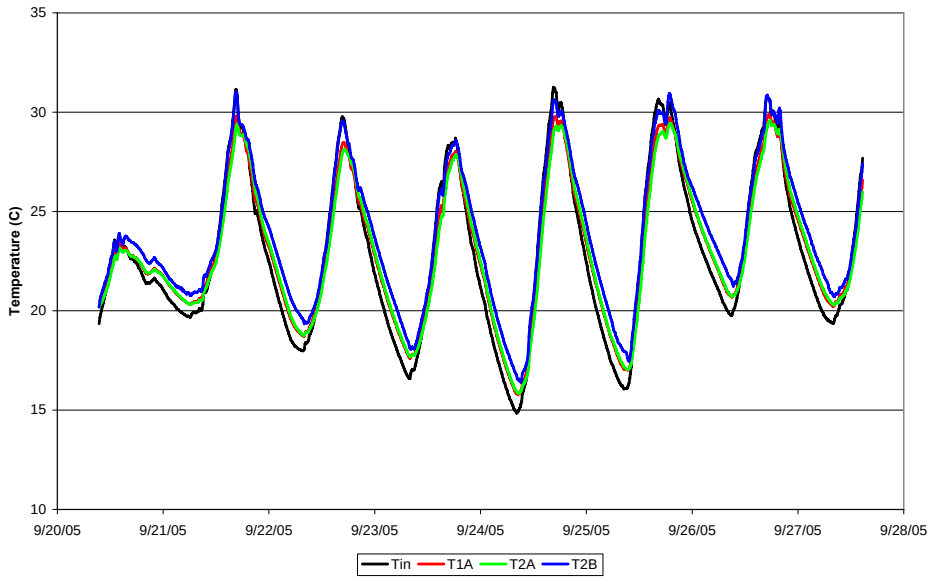

Figure 47: Temperature during final week of experiment

Figure 48 shows the relative humidity data for the last week of the experiment. The daily maximum indoor relative humidity is between 50% and 70%, and daily minimums are between 15% and 35%. The daily relative humidity swing (difference between the daily maximum and minimum) is routinely between 30% and 40%. The relative humidity inside the insulation is very steady, at approximately 35%. The flat relative humidity data, in combination with the above temperature data, indicates that polyisocyanurate is hygroscopic, and the severe suppression of any swings in the relative humidity indicates that the polyisocyanurate material has a large storage capacity in relation to the storage capacity of the gas within the polyisocyanurate.

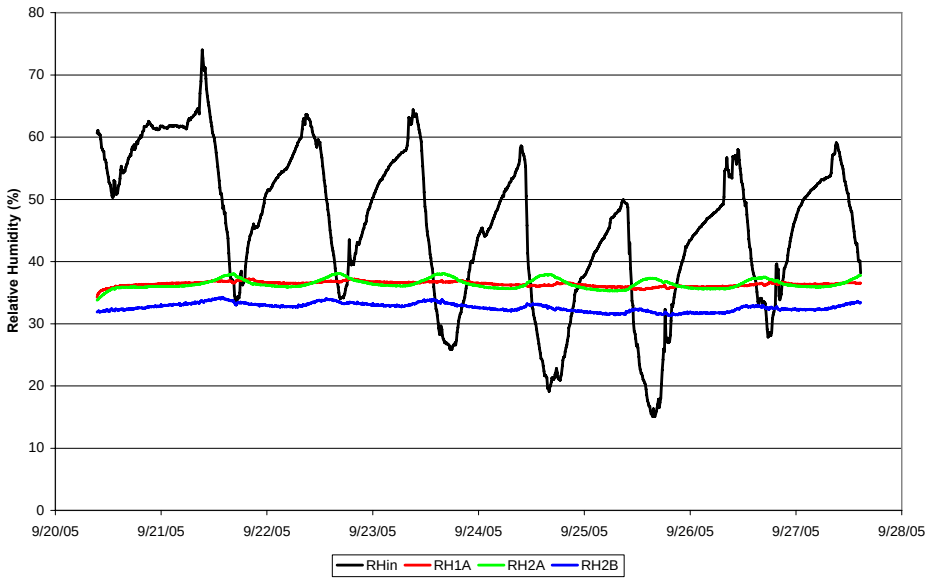

Figure 48: Relative humidity during final week of experiment

Figure 49 shows the dew point data from the final week of the experiment. The indoor dew point declines from about 15 °C at the beginning of the week and approaches 0 °C before increasing to about 12 °C at the end of the week. The dew point inside the polyisocyanurate swings over a consistent range each day, between 0-2 °C and 12-14 °C.

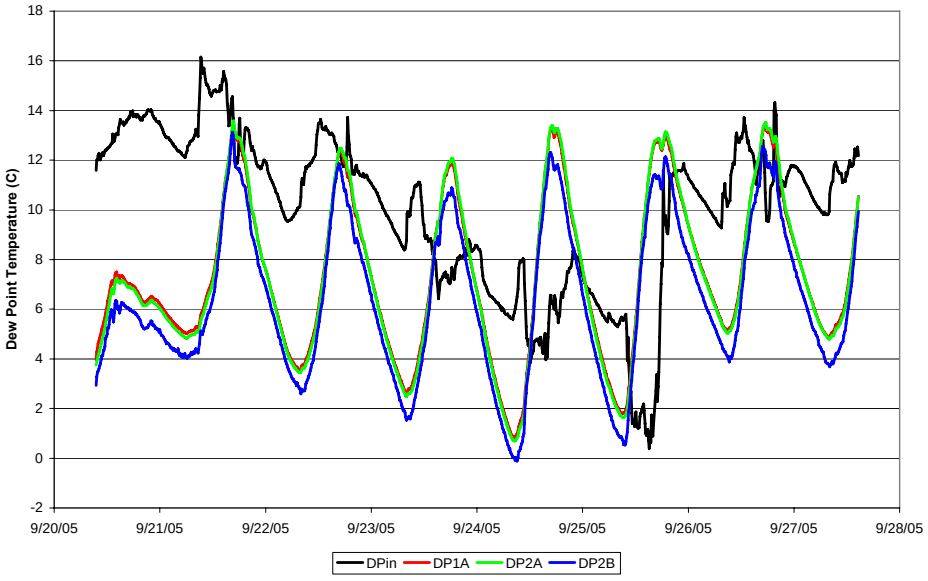

Figure 49: Dew point during the final week of experiment

Conclusions

There is little difference between sensors 1A and 2A. These two were intended to compare the effect of diffusion through the unfaced edge of the polyisocyanurate. The very minor differences indicate that diffusion through the polyisocyanurate is not significant, at least over the time period in this study (3 weeks). This conclusion is supported by comparison of sensors 2A and 2B. The difference between these two sensors is constant, suggesting a sensor zero-offset error instead of an actual moisture gradient in the polyisocyanurate.

Kohta Ueno, Chris Schumacher, John Straube, and I had a debate over the permeability of polyisocyanurate insulation with the foil facers peeled off. At that time the permeability of polyisocyanurate was not readily available in any of the standard sources. In preparing this report (after performing the experiment), I checked the new ASHRAE Fundamentals (2005), which now lists polyisocyanurate permeability at 2.8 to 4.5 perm-in. The middle of a 4' panel of polyisocyanurate would then see a permeance of about 0.1-0.2 perms. Aluminum foil facers have permeance ratings of about 0.01 perms. If the problem were 1-dimensional, the polyisocyanurate permeance would dominate the foil facing permeance, however in the 3-dimensional problem there is approximately 10 times as much area of the foil facing as there is unfaced polyisocyanurate on the edge of the board, resulting in comparable overall moisture transfer from the two paths.

However, even having the permeability would not have been sufficient to answer the question from the basement insulation project. The permeability would be sufficient in a steady-state problem; however in the real world this problem is transient. To solve the transient problem, both the permeability and the moisture storage function are needed. The ratio of the permeability and the moisture storage function give the moisture diffusivity, which determines how quickly a transient pulse of moisture moves through the material. In this experiment, over the course of three weeks the dew point measured inside the polyisocyanurate responded only to the temperature and did not respond to the indoor dew point, indicating that the moisture diffusivity of polyisocyanurate is very low and is not sufficient to explain the phenomena seen in the Huntley polyisocyanurate panel.

By process of elimination, I believe that an examination of the polyisocyanurate panel would find that the foil tape used to reseal the mid-insulation sensor has pulled away from the foil facing, resulting in air communication between the sensor and the concrete wall. Data obtained since the 9/8/05 trip to the Chicago basement supports this conclusion. Figure 50 shows relative humidity data from 9/1/05 through 10/1/05. The wetting system ran on 9/8/05, resulting in the expected spike in relative humidity at the concrete wall (sensor at interface of insulation and concrete RGNM, the green line on the graph); however, in the case of the Thermax wall (P3), **the mid-insulation sensor (RCNM, the black line on the graph) spikes as well**, reaching the same peak relative humidity within a few hours of the concrete wall sensor.

Additionally, I suspect that there was sufficient air leakage behind the polyisocyanurate to explain the apparent connection between the mid-insulation and concrete-side sensor and the indoor air. There is not yet enough data since Kohta sealed the air space between the insulation and the concrete wall to evaluate this.

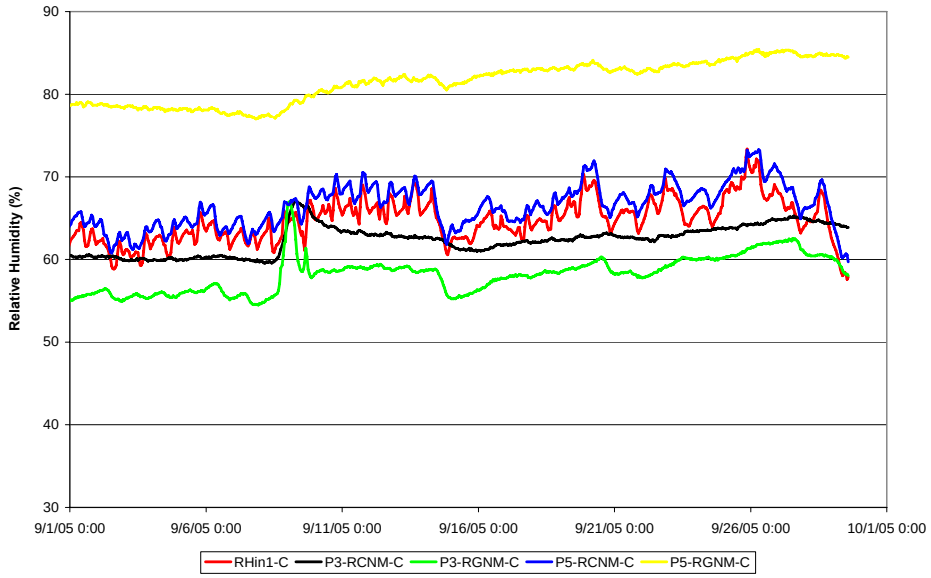

Figure 50: Relative humidity data from Huntley site (Thermax and 1" XPS + fiberglass walls)

Appendix F

Wood Moisture Content Measurements in Cellulose Wall

Moisture content measurements were taken at the Huntley test site in the panel with a stud frame wall and damp-spray cellulose insulation. Early measurements showed some anomalous results: readings of 20-25% MC were noted, while the analogous fiberglass wall had measurements in the 8-12% range. There was no obvious reason why the cellulose wall should be substantially wetter, especially since they started out at the same moisture content levels (i.e., not construction moisture).

The moisture content rose over the summer, and fell during the winter (see Figure 54); in plotting the data, it was shown that it followed the same pattern as the stud bay relative humidity.

Previous research suggested that cellulose insulation has a level of electrical conductivity that could interfere with the wood moisture content measurements, due to the presence of borate or ammonium sulfate salts used as a preservative, antifungal agent, and fire retardant. Based on the observed data, it appeared that the conductivity of cellulose was a function of its humidity and/or moisture content.

The likelihood of electrical shorting through the pins was high, given the lack of insulating material at the heads of the pins, as shown in Figure 51. Therefore, during a field visit in October of 2004, the pins were excavated and painted with a non-conductive coating, as shown in Figure 52.

Figure 51: Original installation of MC pins (unpainted)

Figure 52: MC pin painting with non-conductive coating, 10/04

This measure immediately brought the apparent moisture content of the upper stud measurements down to levels similar to the XPS-fiberglass wall (under 10%). However, the lower moisture content measurements did not demonstrate a similar drop. Therefore, during a later trip (September 2005), these pins were insulated a second time, using electrical tape (see Figure 53).

Figure 53: Wrapping pins with electrical tape, 9/05

However, it appears that this second repair attempt had little impact; the effect of these two repairs on apparent moisture content is shown in Figure 54.

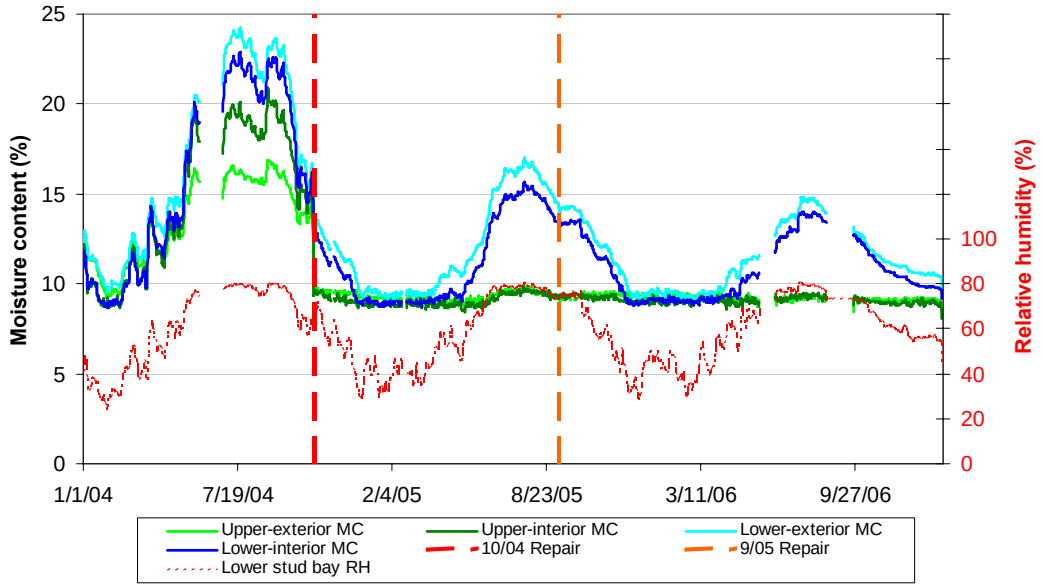

Figure 54: Framing moisture content measurements in XPS-cellulose wall

It was unknown if these problems were localized to the moisture content pin areas, therefore, measurements of the frame were taken with a handheld Delmhorst wood moisture content meter during a field visit in July 2006. In the XPS-fiberglass wall (panel 5), MCs were 9-10% in the studs and top plate. The sill plate was in the 11-13% range.

However, the XPS-cellulose wall (panel 6) provided different results. The interior faces of the studs were all 10-12% MC; the face of the sill plate was 13-15%. These were locations that were in contact with the SBPO (Tyvek) housewrap. However, other measurements were much higher: the top of the sill plate showed 19%, and the side of the stud showed 15-20% MC (higher at the interface with the XPS). These measurements were all at locations where the wood was in contact with the cellulose.

The concurrent relative humidity measurement at the lower portion of the stud bay was 80% RH, and 72% at the upper portion. Assuming a standard wood sorption isotherm, 80% RH should result in an equilibrium moisture content of 16% MC.

Holes were drilled that cleared the Delmhorst pins, past the surface of the stud (see Figure 55); measurements taken here were noticeably lower than the surface measurement (15% vs. 20%). This suggests that increased conduction at the surface is caused by salt migration from the cellulose insulation into the wood. This would explain why the use of electrical insulation at the pins did not result in a drop in apparent moisture content. However, it is also possible that the interior of the wood is drier than the surface, and has not reached equilibrium.

As an additional test, the cellulose itself was measured with the Delmhorst meter. Although the insulation felt dry to the touch, the meter read ~20% MC.

Figure 55: Holes drilled into test stud for sub-surface MC measurements

Figure 56: Handheld moisture meter measurement of cellulose insulation

These results show that cellulose insulation can affect resistance-based moisture content reading in adjoining wood framing, and that it is important to isolate the moisture content pins from the cellulose insulation.

Although these results suggest that it might be useful to measure moisture content of cellulose with electrical resistance, it will require fairly extensive testing to calibrate the response to humidity changes, and the effect (if any) of different salt chemistry, temperature, and density. For instance, Carll (2006) noted that simply pressing on the cellulose insulation in an open stud bay changed electrical resistance measurements in the adjacent framing, which is likely an effect of the electrical contact between the cellulose and the electrodes.

Appendix G

Data Collection Timeline

The following is a timeline record of the data collection and experimental events at the Huntley and Kitchener field sites.

Huntley, Illinois Site

Date	Event
9/19/2003	Installation of test walls and sensors
1/1/2004	Data started (data collected before this point was lost)
1/8/2004	P7 SVR Wall installed (at blank opening)
5/14/2004	P2 Diaper RGNM failed (6 AM)
5/30/2004	All RH and MC channels die (11 AM)-lightning—disabled multiplexer A
6/30/2004	Aaron & Kohta replaced MUX A (all RH and MC channels); replaced phone line (flat with twisted pair). Repaired following RH sensors: Wall 2 Diaper (RGNM-VP sensor; RCNL-T/RH), Wall 3 Thermax (RGNM-VP sensor), Wall 5 XPS/FG (RGNM-RH sensor), Wall 8 Vinyl batt (RGNM-RH sensor), interior T/RH below logger
10/25/2004	Kohta & Chris applied liquid electrical tape to the MC pins in the cellulose wall (after GTI work)
2/18/2005	Installed wetting apparatus (Aaron & Armin); system run (30 sec per 30 min; 12 hours) 216 ml
2/24/2005	Wetting system run (30 sec per 30 min; 12 hours) 216 ml
2/27/2005	Wetting system run (30 sec per 30 min; 12 hours) 216 ml
4/6/2005	Aaron return trip; unclogged injector nozzle P7 SVR; wetting system run (30 sec per 30 min; 12 hours) 216 ml
4/19/2005	System run (30 sec per 30 min; 12 hours) accidental 216 ml
4/29/2005	System run (30 sec per 30 min; 12 hours) accidental 216 ml
5/13/2005	P7 SVR RGNM Fails
9/8/2005	Aaron & Kohta Repair Trip: Air sealed tops of several walls, ran wetting system 216 ml/wall + second day runs = ~400 ml?, replaced P2 terminal strip with punchdown, replaced P7 RGNM with treated T/RH sensor
1/24/2006	Wetting system run (30 sec per 30 min; 12 hours) 216 ml

1/26/2006	Wetting system run (30 sec per 30 min; 12 hours) 216 ml
7/14/2006	Kohta Solo Repair Trip: P1-P2 Poly: Disassembled, air sealed, moved TD_Ls to TD_Bs (sill plate); condensation sensors replaced with MC wafers; P3: Made polyiso tight caulked installation, Tapcons, RCNM to RGNU position; P4 XPS: Installed 1 GΩ test resistor in place of furring MC; P5-P6: Disassembled walls, verified MCs, installed drywall, primer, and paint; P7 SVR: Replaced condensation sensors with MC wafers; P8 Blanket: Removed facer sample for testing; re-air sealed side; replaced logger, set to local daylight time (was on standard time)
8/28/2006	Mark uploaded new logger program; MC channel data multi-sample and filter
8/30/2006	Added MC columns to condensation gauge data (8 channels); a & b coefficients
9/25/2006	Revised program uploaded by Mark--data storage enabled; lost data 8/21-9/25
10/10/2006	Uploaded revised program: re-added MC filtering subroutine
10/15/2006	Uploaded revised program--corrected T-80 to T-96 memory mapping with CJS
12/17/2006	Uploaded revised program--CJS changed to try to fix condensation gauges
1/18/2007	Started disassembly; ran wetting system periodically through disassembly
1/19/2007	Disassembly complete; experiment decommissioned

Kitchener, Ontario Site

Date	Event
8/22/2005	Basement walls and test equipment installed
8/30/2005	Data collection begins (16:00); soil T/MC sensors
10/6/2005	Uploaded Program R1 (from R0) for gypsum blocks
9/22/2006	Visit to basement; replaced P3-RGNM; inspection
9/23/2006	Added a & b coefficient to all MCs
9/25/2006	New key based on revisions from photos of logger and MUX; P3-TBEM & P3-TDEU reversed P3-MDIU & P3-MDEU reversed P3-MDIL & P3-MDEL reversed
10/4/2006	Multiple sensors failed; Ts, MCs, and 2 RHs
10/28/2006	Download trip; found 10/4 problem occurring; fixed missing P2-MHIL wire
11/3/2006	Field visit: new logger OS uploaded; disconnected RH out--reading 100%+; noted RH 1, 2, 4, 5 are dead: P1-RGNM, RHin1, P2-RCNU, P3-RGNM
1/28/2007	Replaced RHin1, P2-RCNU, P3-RGNM with recovered Huntley sensors

Bibliography

The American Institute of Architects, 2002. *Architectural Graphic Standards (Tenth Edition)*, John Wiley & Sons, New York.

American Society for Testing and Materials. 2003. Standard Test Methods for Direct Moisture Content Measurement of Wood and Wood-Base Materials. ASTM Standard D4442-92. Philadelphia, PA.

American Society for Testing and Materials. 2000. Standard Test Methods for Water Vapor Transmission of Materials. ASTM Standard E96-00. Philadelphia, PA.

ASHRAE, 2005, *ASHRAE Handbook-Fundamentals*, Atlanta, GA: American Society of Heating, Refrigerating and Air-Conditioning Engineers, Inc.

ASHRAE. 2006. *ASHRAE SPC 160P, Design Criteria for Moisture Control in Buildings.* Atlanta, GA: American Society of Heating, Refrigerating and Air-Conditioning Engineers, Inc.

[BETT] Building Energy Technology Transfer. 1982. *Energy Conservation and House Basements: A Research Report ("A Review of the Effects of Energy Conservation Measures on Low-Rise Residential Basements"),* Publication No. 82.01, Energy Conservation and Oil Substitution Branch, Energy, Mines, and Resources Canada.

[BETT] Building Energy Technology Transfer. 1985. *Assessing the Rehabilitation Needs of Foundations: A Research Report ("A Literature Review on Foundation Problems and a Draft Diagnostic Guide for Basement Retrofit Contractors"),* Publication No. 85.02, Energy Conservation and Oil Substitution Branch, Energy, Mines, and Resources Canada.

[BETT] Building Energy Technology Transfer. 1985. *Effects of Insulation on Basement Walls: A Research Report ("A Survey of the Statistical Incidence of Problems, Together with an Evaluation of the Technical Processes"),* Publication No. 85.03, Energy Conservation and Oil Substitution Branch, Energy, Mines, and Resources Canada.

Beausoleil-Morrison, I., G. Mitalas, C. McLarnon. 1995. BASECALC™: New Software for Modelling Basement and Slab-on-Grade Heat Losses. Proceedings of Building Simulation '95: 698-700.

Beausoleil-Morrison, I., G. Mitalas. 1997. BASESIMP: A Residential-Foundation Heat-Loss Algorithm For Incorporating Into Whole-Building Energy-Analysis Programs. Proceedings of Building Simulation '97, Volume 2: 1-8.

Black, Christopher D. 2006. "Mould Resistance of Full Scale Wood Frame Wall Assemblies," MASc Thesis, University of Waterloo, Waterloo, ON.

Bligh, Thomas. 1975, "A Comparison of Energy Consumption in Earth Covered vs. Non-Earth Covered Buildings." *Alternatives in Energy Conservation: The Use of Earth Covered Buildings* (Conference Proceedings, Ft. Worth, TX, July 9-12, 1975), National Science Foundation, US Government Printing Office.

Boileau, G.G. and Latta, J.K. 1968. "Calculation of Basement Heat Losses," Technical Paper 292, Division of Building Research, National Research Council.

Briggs, Robert, Lucas, Robert, Taylor, Z. Todd. 2002. "Climate Classifications for Building Energy Codes and Standards." Technical Paper Final Review Draft. Pacific NW National Laboratory.

Building Science Corporation. 2002. *Basement Insulation Systems*. Report to the U.S. Department of Energy. Westford, Mass: Building Science Corporation.

[CMHC] Canada Mortgage and Housing Corporation. 1992. *Investigating, Diagnosing, & Treating Your Damp Basement*, Canada Mortgage and Housing Corporation.

[CMHC] Canada Mortgage and Housing Corporation. 1996. "Molds in Finished Basements." In *Research and Development Highlights 96-203*. Ottawa, ON: Canada Mortgage and Housing Corporation.

[CMHC] Canada Mortgage and Housing Corporation. 1999. "Basement Walls That Dry Quickly." *Research Highlights Technical Series 99-109*. Ottawa, ON: Canada Mortgage and Housing Corporation.

Carmody, J. Christian, J., Labs, K. 1991. "Builder's Foundation Handbook" Report to Oak Ridge National Laboratory ORNL/CON-295, Oak Ridge, TN.

Canadian Home Builders' Association. *R-2000 Builders' Manual*. Energy, Mines, and Resources Canada. 1984.

Canadian Home Builders' Association. *Canadian Home Builders' Association Builders' Manual.* Ottawa, ON 2001.

Carll, C. and TenWolde, A. 1996. “Accuracy of Wood Resistance Sensors for Measurement of Humidity,” *Journal of Testing and Evaluation*, JTEVA, Vol. 24, No. 3, May 1996, pp. 154-160.

Carll, Charles. 2006. Personal communication on field monitoring of cellulose-insulated stud frame walls at U.S. Forest Products Laboratory, April 2006.

Cheple, M. and Huelman, P. 2001. Why we need to know more about basement moisture. *Thermal Performance of the Exterior Envelopes of Whole Buildings VIII.* American Society of Heating, Refrigerating and Air-Conditioning Engineers, Inc.

Crocker, C.R. 1974. NRC-IRC (Institute for Research in Construction) Canadian Building Digest CBD-161. "Moisture and Thermal Considerations in Basement Walls," Ottawa, ON: National Research Council of Canada.

Deru, M.; Judkoff, R.; Neymark, J. 2002. Whole-Building Energy Simulation with a Three-Dimensional Ground-Coupled Heat Transfer Model: Preprint; NICH Report No. CP-550-32690

Deru, M. 2003. “A Model for Ground-Coupled Heat and Moisture Transfer from Buildings.” NREL/TP-550-33954, National Renewable Energy Laboratory, Golden, CO.

Deutsches Institut für Normung. 1999. *Wärmeschutz und Energie Einsparung in Gebäuden, Teil x: Vermeidung von Schimmelpilzen (Heat Protection and Energy Saving in Buildings, Part X: Prevention of Mold Growth)*, 4108-3 Section 3.2.1.

DeVries, Daniel A. (ed), 1975, *Heat and Mass Transfer in the Biosphere*, “Heat Transfer in Soils,” New York: John Wiley & Sons.

[DOE-EIA] United States Department of Energy, Energy Information Administration. 1999. *A Look at Residential Energy Consumption in 1997*, United States Department of Energy.

Doll, C. S. 2002. *Determination of Limiting Conditions for Fungal Growth in the Built Environment*, Sc.D. Thesis, Harvard School of Public Health.

Garden, C.K. 1969. NRC-IRC (Institute for Research in Construction) Canadian Building Digest CBD-120. “Design and Service Life,” Ottawa, ON: National Research Council of Canada.

Garrahan, Peter. 1988. “Moisture meter correction factors.” *Proceedings of In-Grade Testing of Structural Lumber*, USDA Forest Products Laboratory, Madison, WI.

Gatland, Stanley III. 2005. "Comparison of Water Vapor Permeance Data of Common Interior Building Materials in North American Wall Systems." 10th Canadian Conference on Building Science and Technology. Ottawa, ON: National Building Envelope Council.

Goldberg, L. and Aloi, T. 2002. Owens Corning Basement Insulation System Experimental Evaluation Project. Available online: http://www.buildingfoundation.umn.edu/OCBasementSystem/default.htm. Minneapolis-St. Paul, MN: University of Minnesota.

Goldberg, L. and Gatland, S. 2006. Polyamide-6 Based Interior Foundation Insulation System: Experimental Evaluation. Available online: http://www.buildingfoundation.umn.edu/CT-FTF/default.htm. Minneapolis-St. Paul, MN: University of Minnesota.

Goldberg, L. and Farkas, G. 2004. Icynene Foundation Insulation Project, Available online: http://www.buildingfoundation.umn.edu/IcynenFinalReport/default.htm. Minneapolis-St. Paul, MN: University of Minnesota.

Goldberg, L., and Huelman, P. 2001. Cloquet Residential Research Facility: Rim Joist and Foundation Insulation Project Final Report, Building Physics and Foundations Research Programs, University of Minnesota.

Hagentoft, Carl-Eric and Claesson, Johan. 2006. "Influence of rain water percolation on ground heat losses and temperature for basement foundation." *Third International Conference on Research in Building Physics and Building Engineering*, Montreal, QC, August 2006.

Huelman, P. 2006. Personal communication on the omission of a vapor control layer at the lower portion of basement walls, August 4, 2006.

Hutcheon, N.B. 1964. NRC-IRC (Institute for Research in Construction) Canadian Building Digest CBD-50. "Principles Applied to an Insulated Masonry Wall," Ottawa, ON: National Research Council of Canada.

Hutcheon, N.B. and Handegord, G.O. 1995. *Building Science for a Cold Climate.* Ottawa, ON: National Research Council of Canada.

International Code Council, 2006. *2006 International Building Code*, Country Club Hills, IL: International Code Council, Inc.

Karagiozis, A.N., Künzel, H.M., Holm A. 2001. "WUFI-ORNL/IBP - A North American Hygrothermal Model." *Proceedings from Performance of Exterior Envelopes of Whole Buildings VIII*, Dec. 2-7 2001, Clearwater Beach, Florida.

Kumaran, M.K. et al. 2002. NRC-IRC (Institute for Research in Construction) "A Thermal and Moisture Transport Property Database for Common Building and Insulating Materials," Final Report from ASHRAE Research Project 1018-RP, Ottawa, ON: National Research Council of Canada.

Künzel, H.M. 1998a. "Effect of interior and exterior insulation on the hygrothermal behaviour of exposed walls." *Materials and Structures 31*, H. 206, pp 99-103.

Künzel, H.M. 1998b. "More Moisture Load Tolerance of Construction Assemblies Through the Application of a Smart Vapor Retarder", *Performance of Exterior Envelopes of Whole Buildings VIII*, Clearwater Beach, Florida, December 1998, pp. 1129-132.

Künzel, H. 2002. WUFI® PC-Program for calculating the coupled heat and moisture transfer in buildings. Fraunhofer Institute for Building Physics. Holzkirchen, Germany.

Künzel, H. 1995. "Simultaneous Heat and Moisture Transport in Building Components: One- and Two-Dimensional Calculation Using Simple Parameters," PhD Thesis, Fraunhofer Institute for Building Physics, Holzkirchen, Germany.

Lstiburek J. and Carmody, J. 1996. *Moisture Control Handbook: Principles and Practices for Residential and Small Commercial Buildings.* John Wiley & Sons, New York.

Lstiburek, Joseph. 2002. "Moisture Control for Buildings." *ASHRAE Journal*, February 2002, Atlanta: American Society of Heating, Refrigerating and Air-Conditioning Engineers, Inc.

Lstiburek, Joseph. 2004. "Understanding Vapor Barriers." *ASHRAE Journal*, August 2004, Atlanta: American Society of Heating, Refrigerating and Air-Conditioning Engineers, Inc.

Lstiburek, Joseph. 2004. *Builder's Guide to Cold Climates.* Building Science Press: Westford, MA.

Lstiburek, Joseph. 2006. "Understanding Basements." *ASHRAE Journal*, July 2006, Atlanta: American Society of Heating, Refrigerating and Air-Conditioning Engineers, Inc.

Lstiburek, Joseph. 2006. Personal communication on historical use of basement insulation and assembly types, October 15, 2006.

Makepeace, C. B. and Dennis, B. T. 1998. "PERSIST—Pressure Equalized Rain Screen Insulated Structure Technique—Design Approach", *Thermal Performance of the Exterior Envelopes of Buildings VII*, Clearwater Beach, Florida, pp.767.

McDermott, P. 2001. "Improve Your Bottom Line by Finishing the Basement." *Ontario Homebuilder Magazine*.

National Association of Homebuilders. 2006. "Housing Facts, Figures and Trends." NAHB Public Affairs and NAHB Economics, Washington, DC.

Ontario Ministry of Housing. 1997. *Ontario Building Code.* Section 9.13: Dampproofing, Waterproofing and Soil Gas Control. Ottawa, ON.

[PHRC] Pennsylvania Housing Research Center. 1997. *Research Series Report No. 50: Below-grade Construction: Issues and Needs*. Pennsylvania State University, University Park, PA

[PHRC] Pennsylvania Housing Research Center. 1997. *Research Series Report No. 51: Foundation Wall Systems For Houses*. Pennsylvania State University, University Park, PA

Pressnail, K.D. and Timusk, J. 1987. "Adfreezing of Insulated Residential Basements: An Hypothesis." *Canadian Journal of Civil Engineering*, Volume 14, pp. 708-710.

Roberson, J. 2004. "Effect of Building Airtightness and Fan Size on the Performance of Mechanical Ventilation Systems in New U.S. Houses: A Critique of ASHRAE Standard 62.2-2003," Master of Science in Architecture Thesis, University of California, Berkeley, Berkeley, CA.

Robert W. Anderson and Associates, Inc. 1989. "Final Report: A Survey of Moisture in Minnesota Home Interior Foundation Wall Insulation." Prepared for: Energy Division, MN Department of Public Service, St. Paul, MN.

Rogers, T.S. 1938. *Plan Your House to Suit Yourself*. Charles Scribner's Sons, New York, USA.

Rose, W.B. 2005. *Water in Buildings: An Architect's Guide to Moisture and Mold.* New York: John Wiley & Sons.

Rose, W.B. 1997. "Details for a Dry Foundation," *Fine Homebuilding Magazine*, August/September 1997, Taunton Press: Newtown, CT.

Ruest, K., Fettes, P., Jezerinac, M., Gusdorf, J., Platts, B., Robinson, T., and Parekh, A. 1993. *Field Testing of House Characteristics*. Report to the Canada Mortgage and Housing Corporation. Ottawa, ON.

Sedlbauer, K. 2004. *Prediction of mould fungus formation on the surface of and inside building components*, PhD Thesis, Fraunhofer Institute for Building Physics, 2004.

Smegal, Jonathan. 2006. “Drainage and Drying of Small Gaps in Wall Systems,” MASc Thesis, University of Waterloo, Waterloo, ON.

Straube, John, Onysko, Don, and Schumacher, Christopher. 2002. "Methodology and Design of Field Experiments for Monitoring the Hygrothermal Performance of Wood Frame Enclosures," *Journal of Thermal Env. & Bldg. Sci.*, Vol.26, No.2—October 2002. Thousand Oaks, Calif.: Sage Publications.

Straube, J.F., and Schumacher, C.J, 2003. “Hygrothermal Enclosure Models: A Comparison with Field Data,” *Proceedings of the 2nd International Conference on Building Physics*, Leuven, Belgium, Sept. 14-18, pp. 319-326.

Straube, J.F., and Burnett, E.F.P., 2005. *Building Science for Building Enclosure Design*, Building Science Press: Westford, MA.

Straube, J.F., Burnett, E., Van Straaten, R., Schumacher, C. 2004. Review of Literature and Theory – Report #1. *ASHRAE 1091 – Development of Design Strategies for Rainscreen and Sheathing Membrane Performance in Wood Frame Walls.* University of Waterloo, Building Engineering Group Report for ASHRAE.

Swinton, M.C., and A.N. Karagiozis. 1995. *Investigation of warm weather condensation in new and insulated basement walls.* Thermal Performance of the Exterior Envelopes of Buildings VI. Atlanta, GA: American Society of Heating, Refrigeration, and Air-Conditioning Engineers, Inc.

Swinton, M.C., Bomberg, M.T., Kumaran, M.K., Normandin, N. and Maref, W. 1999. Construction Technology Update No. 36: “Performance of Thermal Insulation on the Exterior of Basement Walls,” Ottawa, ON: National Research Council of Canada.

Swinton, M. and Kesik, T. 2005. “Performance Guidelines for Basement Envelope Systems and Materials: Final Research Report.” Institute for Research in Construction/National Research Council Canada.

TenWolde, A, Carll, C., and Malinauskas, V. 1998. *Air Pressures in Wood Frame Walls.* Thermal Performance of the Exterior Envelopes of Buildings VII. Atlanta, GA: American Society of Heating, Refrigeration, and Air-Conditioning Engineers, Inc.

TenWolde, A. and Walker, I. S. 2001. "Interior moisture design loads for residences", *Proceedings for Performance of Exterior Envelopes of Whole Buildings VIII: Integration of Building Envelopes*, December 2-7, Clearwater Beach, Florida.

Timusk, John, and K.D. Pressnail. 1997. *Another Look at Internally-Insulated Basement Wall*. Proceedings of the Seventh Conference on Building Science and Technology, Durability of Buildings – Design, Maintenance, Codes, and Practices, Toronto, ON: University of Toronto.

Van Straaten, R. 2003. "Measurement of Ventilation and Drying of Vinyl Siding and Brick Clad Wall Assemblies," MASc Thesis, University of Waterloo, Waterloo, ON.

Wheeler, Anthony and Ganji, Ahmad. 2004. *Introduction to Engineering Experimentation.* Pearson Prentice Hall, Saddle River, NJ.

Zuluaga, Marc, Robb Aldrich, and Dianne Griffiths. 2004. *Field Performance of Different Interior Basement Insulation Systems*. *Performance of the Exterior Envelopes of Whole Buildings IX*. Atlanta, GA: American Society of Heating, Refrigeration, and Air-Conditioning Engineers, Inc.